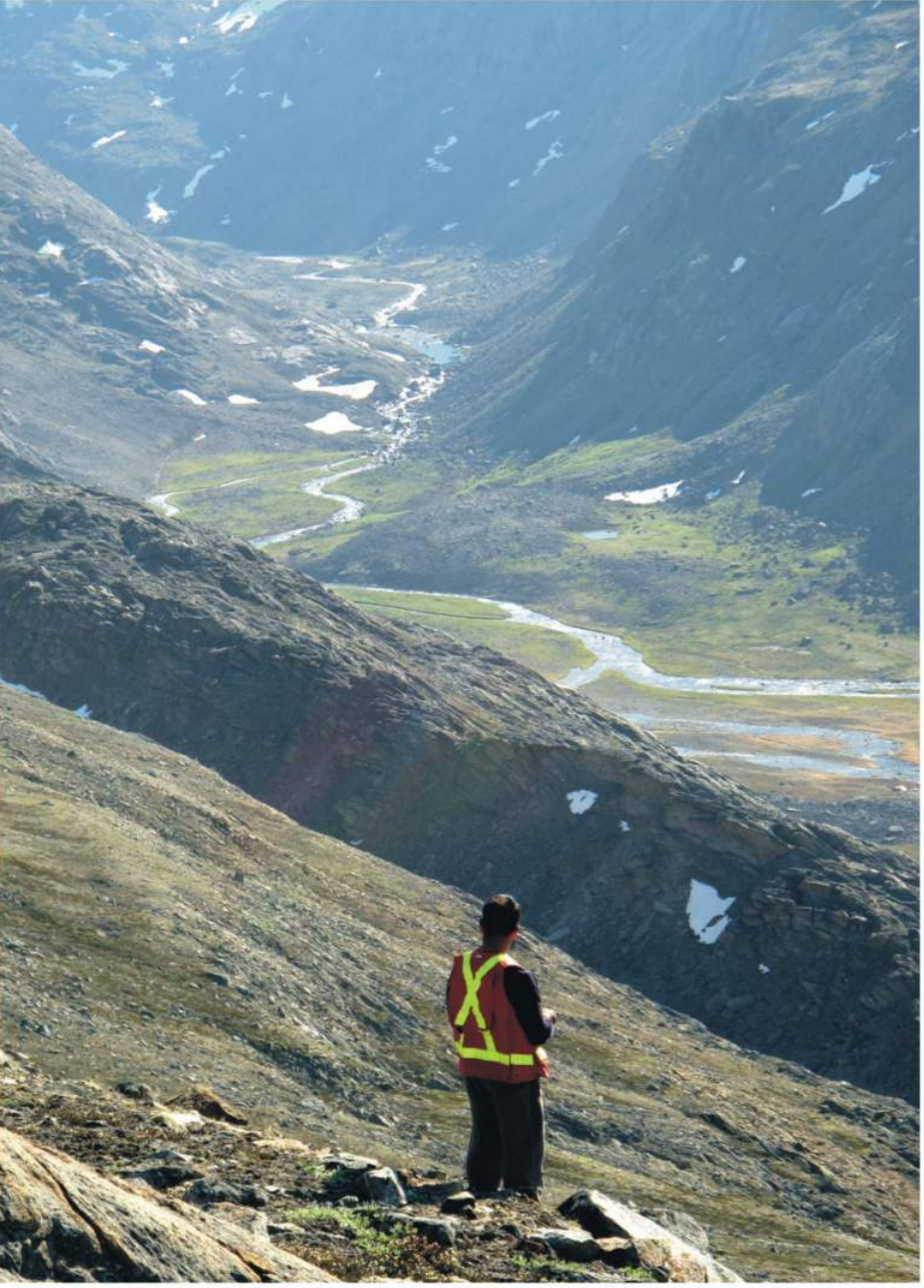

Summary of Activities

2015

CANADA-NUNAVUT GEOSCIENCE OFFICE

ᑲᓇᑕᓄᖅ-ᓄᓇᕗᑦ ᑕᒪᓐᓇᖅᑐᖅᓯᒪᔪᖅ

BUREAU GÉOSCIENTIFIQUE CANADA-NUNAVUT

KANATAMI-NUNAVUMI GEOSCIENCE TITIGAKVIIT

CANADA-NUNAVUT GEOSCIENCE OFFICE

BUREAU GÉOSCIENTIFIQUE CANADA-NUNAVUT

ᑲᓇᑕᒥ-ᓄᓇᕗᑦ ᐅᓴᖅᑲᓂᖅ ᖃᐅᔨᓴᖅᑎᓐᓂᒃ

KANATAMI-NUNAVUMI GEOSCIENCE TITIGAKVIIT

SUMMARY OF ACTIVITIES 2015

This publication is also available, free of charge, as colour digital files in Adobe Acrobat® PDF format from the Canada-Nunavut Geoscience Office website: www.cngo.ca/

Every reasonable effort is made to ensure the accuracy of the information contained in this report, but Natural Resources Canada does not assume any liability for errors that may occur. Source references are included in the report and users should verify critical information.

When using information from this publication in other publications or presentations, due acknowledgment should be given to Canada-Nunavut Geoscience Office. The recommended reference is included on the title page of each paper. The complete volume should be referenced as follows:

Canada-Nunavut Geoscience Office (2015): Canada-Nunavut Geoscience Office Summary of Activities 2015; Canada-Nunavut Geoscience Office, 208 p.

ISSN 2291-1235 Canada-Nunavut Geoscience Office Summary of Activities (Print)
ISSN 2291-1243 Canada-Nunavut Geoscience Office Summary of Activities (Online)

Front cover photo: Sean Noble overlooking a glacially eroded valley, standing among middle Paleoproterozoic age psammitic metasedimentary rocks, nine kilometres west of Chidliak Bay, southern Baffin Island. Photo by Dustin Liikane, Carleton University.

Back cover photo: Iqaluit International Airport under rehabilitation and expansion; the Canada-Nunavut Geoscience Office, Geological Survey of Canada (Natural Resources Canada), Centre d'études nordiques (Université Laval) and Transport Canada contributed to a better understanding of permafrost conditions to support the planned repairs and adapt the infrastructure to new climatic conditions. Photo by Tommy Tremblay, Canada-Nunavut Geoscience Office.

Foreword

I am pleased to introduce the 2015 volume of the Canada-Nunavut Geoscience Office (CNGO) *Summary of Activities*. This is the fourth annual edition of a publication that summarizes both preliminary and final results from projects supported by the CNGO, as well as invited key-research papers from our partners and collaborators. This release is a first-time experience for me, as the new Chief Geologist. During my past 12 years of northern living, I have nevertheless been involved closely with the CNGO and the Summaries of Activities through my work with Indian and Northern Affairs Canada, the Canadian Northern Economic Development Agency (CanNor) and the Government of Nunavut (GN). I am now the fourth Chief Geologist for this tiny, yet industrious office, the first being David Scott (1999–2003), the second being Donald James (2004–2010) and the third being David Mate (2011–2014).

David Mate was the originator, and now strong supporter, of the *Summary of Activities* volumes, while exceptional editorial guidance has been provided by Celine Gilbert—who incidentally has been with the CNGO from its inception in 1999. I look forward to continuing with the releases of this valuable contribution. David Mate put it succinctly last year when he said "each contribution has demonstrated the breadth and quality of research being conducted by the office and its collaborators." By the timely release of observations and data through this publication, we are collectively providing valuable, peer-reviewed information to governments, organizations and industry stakeholders across Nunavut. We feel that the release of this quality geoscience research and dissemination of information are paramount to help land-use decisions and management in Nunavut. Also, individual contributions from previous issues received many citations on a yearly basis, pointing to a lively interest from the scientific community.

When Nunavut became a territory in 1999, more than 70% of it was inadequately mapped and its geology was poorly understood. Informed decisions about land-use planning or exploration could not be made in many cases. To address these deficiencies, the decision was made in 1999 by the federal and territorial governments to open the Canada-Nunavut Geoscience Office. The rationale for the office included spearheading and improving geological research in Nunavut, and helping to coordinate research efforts by geoscientists within the various governments.

The CNGO is co-funded by two federal departments, namely NRCan and Indigenous and Northern Affairs Canada (INAC; formerly Aboriginal Affairs and Northern Development Canada), and the Government of Nunavut, Economic Development and Transportation (GN-EDT). The office is managed with input from a Management Board made up of representatives from NRCan, INAC, GN-EDT and Nunavut Tunngavik Inc. (the latter organization ex officio).

The CNGO's mandate is to 1) develop capacity in geoscience, 2) maintain an accessible geoscience knowledge base, 3) promote sustainable development of Nunavut's mineral and energy resources, and 4) increase awareness of the importance of Earth science for Nunavummiut. To accomplish this mission, the CNGO provides mapping, reports and interpretations on the geological features and resources of Nunavut. In collaboration with an array of geoscience partners, the CNGO aims at engaging the public on key geoscience issues.

The CNGO operates on annual contributions from the funding partners and conducts core-mandate research using Strategic Investments in Northern Economic Development (SINED) funding from CanNor. All work that the CNGO undertakes is conducted collaboratively and in partnerships with other government departments, academia and the general public. Partnered geoscience initiatives were also conducted in 2015 under the second phase of NRCan's Geo-Mapping for Energy and Minerals (GEM-2) program.

The office currently consists of six employees and one postdoctoral Natural Sciences and Engineering Research Council geoscientist, with expertise in Precambrian, Paleozoic and Quaternary geology, GIS and online geoscience-data dissemination.

In 2014, the CNGO received approval for a new two-year geoscience program focused on delivering activities that support responsible natural-resource development, protect investments in infrastructure and disseminate geoscience information. These activities, funded by CanNor under SINED, continued in 2015. Activities focused on three key themes: 1) geoscience for responsible natural-resource development, 2) geoscience for protecting investments in infrastructure and 3) geoscience-data dissemination and public outreach. The latter included a third successful year of the Northern Geoscience Training Program between the CNGO and Dalhousie University.

The CNGO *Summary of Activities 2015* volume presents preliminary results and continues to take advantage of the CNGO Geoscience Data Series as the means for disseminating several new digital datasets that support papers in the volume.

Where appropriate, this series will be referenced in the *Summary of Activities* papers, with links provided to the online repository. This year's volume contains 18 papers, grouped into the following sections: 'Mineral deposit studies', 'Regional geoscience', 'Geoscience for infrastructure', 'Aggregate and industrial minerals', 'Carving stone' and 'Outreach and capacity building'. All papers are available for download at www.cngo.ca.

The 'Mineral deposit studies' section contains three papers. The first paper reports on an assessment of exposed sedimentary rocks of the Elu Basin in the Kitikmeot region to determine the potential for commodities such as uranium, copper, lead and zinc. The second and third papers are both subjects of M.Sc. studies on rocks of southern Baffin Island. The second paper focuses on the distribution, composition and petrogenesis of granitic pegmatites on Hall Peninsula for the purpose of evaluating their metallogenic potential. The third paper provides observations on a suite of mafic, ultramafic and layered mafic-ultramafic sills that occur on Meta Incognita Peninsula. The results will be used to constrain existing regional tectonic models of middle Paleoproterozoic extension in the eastern Trans-Hudson Orogen.

Nine papers in the 'Regional geoscience' section are focused on observations and results from two main areas: 1) southern Baffin Island and 2) western Hudson Bay. All of these projects involve work conducted under SINED programming and new work conducted in collaboration with the Geological Survey of Canada under GEM-2. The focus of these activities is on bedrock and surficial mapping and a range of thematic studies from Hall Peninsula and Meta Incognita Peninsula for south Baffin, and the Tehery Lake–Wager Bay area of western Hudson Bay. New results include bedrock mapping, remote predictive mapping, geochronology, till geochemistry and information about the aeromagnetic survey that was flown over ground north of Iqaluit.

This year's 'Geoscience for infrastructure' section highlights two papers, the first one providing an overview of surficial-geology mapping and compilation in the western Hudson Bay area. The second paper presents results from an ongoing multidisciplinary study conducted in collaboration with NRCan and Université Laval, detailing the results from permafrost-oriented research in Iqaluit.

The 'Aggregate and industrial minerals' section comprises continuing work by the CNGO on the resource potential for industrial, high-calcium limestone on Southampton Island, a project that has involved several years of work. The 'Carving stone' section consists of two papers, the first paper summarizing field observations and deposit evaluations of carving stone sites near Rankin Inlet, south of Pangnirtung on the south shore of Cumberland Sound, and near Arctic Bay. The second paper reports on mineral chemistry from two carving stone sites on southern Baffin Island.

The final paper in this volume discusses 'Outreach, capacity building and data dissemination'. A key part of discovering anything new is to understand what already exists. In order to gain that understanding, all this information and data that has been and is being collected in Nunavut must be readily accessible and publicly available. The NunavutGeoscience.ca website is an open-access data portal to public geoscience information that is available for Nunavut. This paper discusses the status of and updates to NunavutGeoscience.ca and NUMIN, the database within NunavutGeoscience.ca that contains mineral showings and geological metadata for the territory of Nunavut.

Acknowledgments

The CNGO staff thanks all authors of papers in this fourth *Summary of Activities*. Their dedication is greatly appreciated, and is critical in helping the CNGO deliver such a quality product. RnD Technical is also thanked for their technical editing and assembling of the volume. In addition, special thanks are extended to reviewers of papers:

Rob Berman	Geological Survey of Canada
Lesley Chorlton	Geological Survey of Canada
Edward Cloutis	University of Winnipeg
Nicole Couture	Geological Survey of Canada
Bill Davis	Geological Survey of Canada
Keith Dewing	Geological Survey of Canada
Chris Harrison	Geological Survey of Canada
Nancy Joyce	Geological Survey of Canada
Dan Kerr	Geological Survey of Canada
David Mate	Canadian Northern Economic Development Agency
Roger Paulen	Geological Survey of Canada
Tony Peterson	Geological Survey of Canada
David Schneider	University of Ottawa

Tom Skulski	Geological Survey of Canada
Holly Steenkamp	Canada-Nunavut Geoscience Office
Mike Thomas	Geological Survey of Canada
Mike Young	Dalhousie University

Linda Ham
Chief Geologist
Canada-Nunavut Geoscience Office
www.cngo.ca/

Préface

Je suis heureuse de présenter l'édition 2015 du *Sommaire des activités* du Bureau géoscientifique Canada-Nunavut (BGCN). Il s'agit de la quatrième édition de cette publication dans laquelle sont résumés les résultats préliminaires ou finaux de projets ayant reçus l'aval du Bureau ainsi que de projets de recherche importants soumis à notre invitation par nos partenaires et collaborateurs. Il s'agit d'une toute nouvelle expérience pour moi, à titre de géologue en chef récemment nommée à ce poste. Au cours de mes douze années de carrière passées en milieu nordique, j'ai pu cependant suivre de près les travaux du BGCN et la réalisation des sommaires des activités antérieurs par le biais de mes fonctions soit aux Affaires indiennes et du Nord Canada, soit à l'Agence canadienne de développement économique du Nord (CanNor), soit encore lorsque j'œuvrais au sein du Gouvernement du Nunavut. J'occupe maintenant le poste de géologue en chef de ce petit, mais malgré tout industrieux, bureau; j'en suis la quatrième en titre, le premier ayant été David Scott (1999–2003), le second Donald James (2004–2010) et le plus récent, David Mate (2011–2014).

Ce dernier fut celui qui lança, et qui continue de fermement appuyer, la réalisation de ces volumes dont la rédaction a été menée de main de maître par Céline Gilbert — laquelle incidemment fait partie du BGCN depuis sa création en 1999. Je me fais un heureux devoir de respecter la tradition en continuant de publier cette importante contribution scientifique. David Mate a résumé la situation en quelques mots l'an dernier lorsqu'il affirmait que « chaque contribution a su démontrer l'ampleur et la qualité des recherches qui se poursuivent par le biais de nos chercheurs et de nos collaborateurs ». En assurant ainsi la mise en circulation opportune d'observations et de données, nous parvenons collectivement à mettre des renseignements importants, évalués par des pairs, à la disposition des gouvernements, des organismes et des intervenants du domaine industriel de l'ensemble du Nunavut. Nous estimons qu'il est indispensable de faire circuler les résultats de recherches géoscientifiques de haute qualité et de disséminer l'information, susceptibles d'aider à la gestion et à la prise de décisions en matière d'utilisation des terres au Nunavut. En outre, les articles ayant paru dans des éditions antérieures ont été cités dans de nombreuses publications plusieurs fois chaque année, ce qui témoigne de l'intérêt qu'ils suscitent au sein de la communauté scientifique.

Lorsque le Nunavut est devenu un territoire en 1999, plus de 70 % de sa superficie était dépourvue de couverture cartographique adéquate et ses antécédents de nature géologique étaient peu connus. Dans bien des cas, il était impossible de prendre des décisions éclairées en matière de planification au niveau de l'utilisation des terres ou de travaux d'exploration. Afin de pallier à ces carences, la décision fut prise en 1999 par les gouvernements fédéral et territorial de fonder le Bureau géoscientifique Canada-Nunavut. La fonction du BGCN consiste d'une part à diriger et à améliorer les travaux entrepris dans le cadre de la recherche géoscientifique au Nunavut et d'autre part, à contribuer à la coordination des efforts déployés au niveau de la recherche menée par les géoscientifiques œuvrant au sein des divers organismes gouvernementaux.

Le BGCN est subventionné à la fois par deux ministères fédéraux, soit Ressources naturelles Canada et Affaires autochtones et du Nord Canada (autrefois connu sous le nom d'Affaires autochtones et Développement du Nord Canada), et le ministère du Développement économique et des Transports du Gouvernement du Nunavut. Les gestionnaires du BGCN reçoivent un soutien de la part d'un Conseil de gestion constitué de représentants de tous ces organismes gouvernementaux ainsi que de la société Nunavut Tunngavik Incorporated (cette dernière à titre de membre d'office du BGCN).

Le BGCN a pour mandat de 1) renforcer les capacités au niveau des connaissances géoscientifiques; 2) assurer le maintien d'un corpus de connaissances géoscientifiques à la portée de tous; 3) encourager la mise en valeur durable des ressources minérales et énergétiques du Nunavut; et 4) accroître la sensibilisation du public à l'égard de l'importance des sciences de la Terre pour les Nunavummiut. Afin d'accomplir cette tâche, le BGCN réalise des cartes et des rapports, et fournit des interprétations des caractéristiques géologiques et des ressources du Nunavut. En collaboration avec une gamme de partenaires géoscientifiques, le BGCN cherche à encourager l'engagement du public relatif aux questions d'ordre géoscientifique d'importance.

Le BGCN dépend de contributions annuelles reçues de ses partenaires financiers et poursuit des travaux de recherche propres à son mandat principal grâce au financement fourni par le biais du programme Investissements stratégiques dans le développement économique du Nord (ISDEN) dirigé par CanNor. Tous les travaux entrepris par le BGCN sont menés soit en collaboration, soit en partenariat avec d'autres ministères gouvernementaux, le milieu universitaire et le grand public. De telles initiatives géoscientifiques en partenariat ont également été entreprises en 2015 dans le cadre du second volet du programme géocartographie de l'énergie et des minéraux (GEM-2) de Ressources naturelles Canada.

Le BGCN compte actuellement six employés et un boursier de recherches postdoctorales, ce dernier soutenu par le Conseil de recherches en sciences naturelles et en génie du Canada, dont les connaissances spécialisées portent sur la géologie du Précambrien, du Paléozoïque et du Quaternaire, ainsi que sur les systèmes d'information géographique et la diffusion de données géoscientifiques en ligne.

En 2014, le BGCN s'est vu octroyer la direction d'un nouveau programme de deux ans qui portait sur l'élaboration de travaux visant la mise en valeur responsable des ressources naturelles, la protection des mises de fonds dans des projets d'infrastructure et la diffusion de renseignements de nature géoscientifique. Ces travaux subventionnés par CanNor dans le cadre du programme ISDEN se sont poursuivis en 2015 et ont portés sur trois thèmes principaux : 1) les géosciences au service de la mise en valeur responsable des ressources naturelles; 2) les géosciences au service de la protection des mises de fonds dans des projets d'infrastructure; et 3) la diffusion de données géoscientifiques et les activités de sensibilisation du public. Ce dernier volet s'est traduit par la poursuite, pour une troisième année consécutive, du programme de formation nordique en géosciences auquel participent le BGCN et l'université Dalhousie.

La publication *Sommaire des activités 2015* présente des résultats préliminaires et continue d'exploiter l'information disponible grâce à la *Série des données géoscientifiques*, qui permet la diffusion de nouveaux ensembles de données numériques à l'appui des rapports publiés dans le volume. Le cas échéant, la série est citée en référence dans les rapports paraissant dans le *Sommaire des activités* et un lien assure l'accès au dépôt de données électroniques. La présente édition du volume regroupe un total de 18 articles répartis en fonction des sections suivantes : « Études sur les gisements minéraux », « Études géoscientifiques régionales », « Études géoscientifiques liées à l'infrastructure », « Agrégats et minéraux industriels », « Pierre à sculpter » et « Sensibilisation du public et renforcement des capacités ». Tous les articles sont publiés (en anglais seulement, accompagnés de résumés en français) sur Internet et peuvent être téléchargés depuis le www.cngo.ca.

La section « Études sur les gisements minéraux » présente trois articles. Le premier porte sur une évaluation des roches sédimentaires du bassin d'Elu affleurant dans la région de Kitikmeot afin d'établir la possibilité que ces dernières recèlent des produits de base tels que de l'uranium, du cuivre, du plomb et du zinc. Les deux autres rapports se penchent sur des sujets faisant l'objet de travaux entrepris dans le cadre de thèses de maîtrise s'intéressant aux roches de la partie sud de l'île de Baffin. Le second met l'accent sur la répartition, la composition et la pétrogenèse des pegmatites granitiques de la péninsule Hall en vue de cerner leur potentiel métallogénique. Le troisième article offre une série d'observations portant sur une suite de filons-couches mafiques, ultramafiques et mafiques-ultramafiques lités0 qui se retrouvent dans la péninsule Meta Incognita. À partir des résultats obtenus, il sera possible d'apporter des précisions à l'échelle régionale aux modèles tectoniques actuels d'extension de l'orogène trans-hudsonien s'étant produite au Paléoprotérozoïque moyen.

Les neuf rapports réunis dans la section « Études géoscientifiques régionales » mettent l'accent sur les observations et les résultats associés à deux régions principales : 1) la partie sud de l'île de Baffin; et 2) l'ouest de la baie d'Hudson. Il s'agit de projets accomplis dans le cadre du programme ISDEN et de nouveaux travaux entrepris en collaboration avec la Commission géologique du Canada dans le cadre du programme GEM-2. Les travaux ont surtout portés sur la cartographie du substratum rocheux et des matériaux de surface, ainsi que sur toute une gamme d'études thématiques réalisées dans les péninsules Hall et Meta Incognita, en ce qui a trait à la partie sud de l'île de Baffin, et dans la région du lac Tehery et de la baie Wager, en ce qui a trait à la partie occidentale de la baie d'Hudson. Ces travaux ont permis de procéder à la cartographie du substratum rocheux et à des essais de télécartographie prédictive aussi bien que d'obtenir des résultats géochronologiques et d'analyse géochimique des tills, ainsi que des renseignements provenant d'un levé aéromagnétique effectué au-dessus de la région s'étendant au nord d'Iqaluit.

La section « Études géoscientifiques liées à l'infrastructure » met en évidence deux articles, dont le premier offre un aperçu des travaux de restitution et de cartographie des matériaux de surface dans la région ouest de la baie d'Hudson. Le second présente des résultats d'une étude multidisciplinaire en cours entreprise en collaboration avec Ressources naturelles Canada et l'Université Laval, laquelle étude fait état des résultats de recherches portant sur le pergélisol à Iqaluit.

La section « Agrégats et minéraux industriels » rend compte de travaux en cours du BGCN dont l'objet est d'évaluer la possibilité que l'île Southampton recèle des gisements de calcaire à teneur élevée en calcium; il s'agit d'un projet ayant exigé plusieurs années de recherche. La section « Pierre à sculpter » regroupe deux articles, dont le premier résume les observations de terrain et le résultat des évaluations de gisements liés à des emplacements de pierre à sculpter situés près de Rankin Inlet, au sud de Pangnirtung sur la côte sud du détroit de Cumberland, et près de la baie Arctic. Le deuxième article fait état de la chimie des minéraux indicateurs de deux gisements de pierre à sculpter au sud de l'île de Baffin.

Le dernier article du volume relève de la section « Sensibilisation du public et renforcement des capacités ». Il est entendu que toute nouvelle découverte dépend en premier lieu d'une connaissance de ce qui est déjà connu. Afin de posséder ces connaissances, il est essentiel que toutes les données et tous les renseignements dont on dispose présentement et que l'on continue de recueillir au Nunavut soient mis à la disposition d'un public en mesure d'y accéder facilement. Le site Web NunavutGeoscience.ca est un portail de données en libre accès permettant au public de consulter les renseignements de nature géoscientifique portant sur le Nunavut. Le rapport décrit l'état actuel du site Web et les améliorations qui ont été apportées non seulement au portail NunavutGeoscience.ca mais également à NUMIN, la base de données qui se trouve sur le site et qui renferme des renseignements sur les venues minérales et des métadonnées géologiques portant sur le Nunavut.

Remerciements

Le BGCN tient à remercier les auteurs des articles publiés dans cette quatrième édition du *Sommaire des activités*. Leur dévouement est extrêmement apprécié et c'est grâce à eux qu'il est possible de publier un document d'une telle qualité. Merci à RnD Technical d'avoir vu à l'édition technique et à l'assemblage de ce numéro. Nos remerciements s'adressent également aux personnes suivantes, lecteurs critiques des articles :

Rob Berman	Commission géologique du Canada
Lesley Chorlton	Commission géologique du Canada
Edward Cloutis	Université de Winnipeg
Nicole Couture	Commission géologique du Canada
Bill Davis	Commission géologique du Canada
Keith Dewing	Commission géologique du Canada
Chris Harrison	Commission géologique du Canada
Nancy Joyce	Commission géologique du Canada
Dan Kerr	Commission géologique du Canada
David Mate	Agence canadienne de développement économique du Nord
Roger Paulen	Commission géologique du Canada
Tony Peterson	Commission géologique du Canada
David Schneider	Université d'Ottawa
Tom Skulski	Commission géologique du Canada
Holly Steenkamp	Bureau géoscientifique Canada-Nunavut
Mike Thomas	Commission géologique du Canada
Mike Young	Université Dalhousie

Linda Ham
Géologue en chef
Bureau géoscientifique Canada-Nunavut
www.cngo.ca/

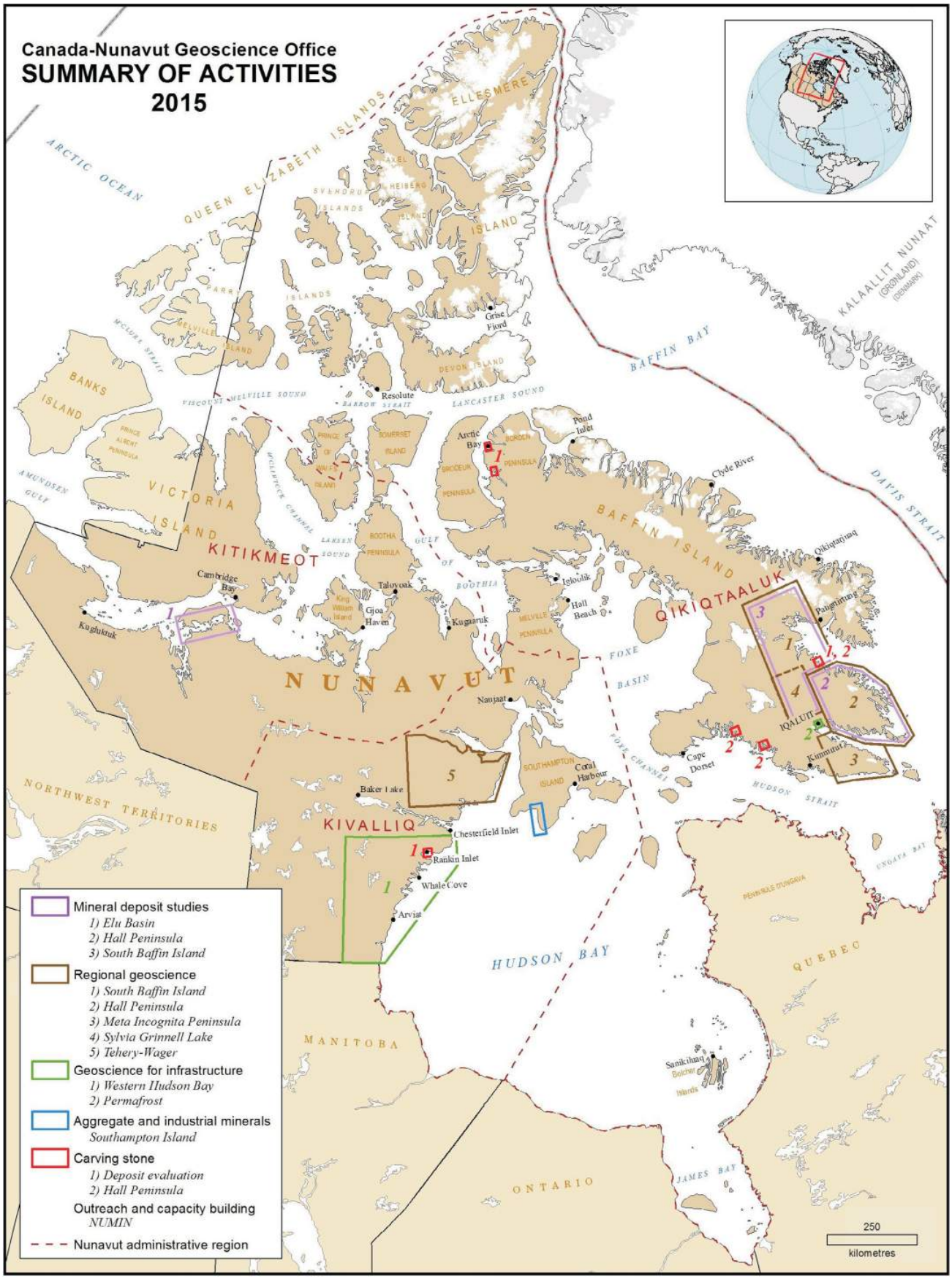
Canada-Nunavut Geoscience Office
SUMMARY OF ACTIVITIES
2015
ARCTIC OCEAN
QUEEN ELIZABETH ISLANDS
ELLESMERE ISLAND
BAFFIN BAY
KALAALLIT NUNAAT (GREENLAND) (DENMARK)
DAVIS STRAIT
BANKS ISLAND
VICTORIA ISLAND
KITIKMEOT
BAFFIN ISLAND
QIKIQTAALUK
NUNAVUT
FOXE BASIN
FOXE CHANNEL
HUDSON STRAIT
HUDSON BAY
KIVALLIQ
NORTHWEST TERRITORIES
MANITOBA
ONTARIO
QUEBEC
JAMES BAY
Resolute
Grise Fiord
Arctic Bay
Pond Inlet
Clyde River
Cambridge Bay
Kugluktuk
Taloyoak
Gjoa Haven
King William Island
Kugaaruk
Igloolik
Hall Beach
Qikiqtarjuaq
Pangnirtung
Iqaluit
Kimmirut
Cape Dorset
Naujaat
Coral Harbour
Baker Lake
Chesterfield Inlet
Rankin Inlet
Whale Cove
Arviat
Sanikiluaq
Mineral deposit studies
1) Elu Basin
2) Hall Peninsula
3) South Baffin Island
Regional geoscience
1) South Baffin Island
2) Hall Peninsula
3) Meta Incognita Peninsula
4) Sylvia Grinnell Lake
5) Tehery-Wager
Geoscience for infrastructure
1) Western Hudson Bay
2) Permafrost
Aggregate and industrial minerals
Southampton Island
Carving stone
1) Deposit evaluation
2) Hall Peninsula
Outreach and capacity building
NUMIN
Nunavut administrative region
250
kilometres

Contents

The 1.9 Ga Kilohigok paleosol and Burnside River Formation, western Nunavut: stratigraphy and gamma-ray spectrometry

A. Ielpi[1,2], R.H. Rainbird[2], J.W. Greenman[3] and C.G. Creason[4]

[1]*Canada-Nunavut Geoscience Office, Iqaluit, Nunavut; with Laurentian University as of January 1, 2016, aielpi@laurentian.ca*

[2]*Natural Resources Canada, Geological Survey of Canada, Ottawa, Ontario*

[3]*Department of Earth Sciences, Carleton University, Ottawa, Ontario*

[4]*College of Earth, Ocean, and Atmospheric Sciences, Oregon State University, Corvallis, Oregon*

This work was part of the second phase of the Geo-mapping for Energy and Minerals (GEM) Program in the Elu Basin area and surroundings. It is being co-led by the Canada-Nunavut Geoscience Office (CNGO) and the Geological Survey of Canada (GSC). The study area comprises National Topographic System map areas 77A, 77B, 76O, 76N. The objective of this work is to improve the sedimentological framework within the Elu Basin and surrounding area, and to explore its economic potential.

Ielpi, A., Rainbird, R.H., Greenman, J.W. and Creason, C.G. 2015: The 1.9 Ga Kilohigok paleosol and Burnside River Formation, western Nunavut: stratigraphy and gamma-ray spectrometry; *in* Summary of Activities 2015, Canada-Nunavut Geoscience Office, p. 1–10.

Abstract

Elu Inlet and Tariyunnuaq (Melville Sound) are located in the Kitikmeot Region of Nunavut (Canada), and are underlain by a succession of Paleo- to Mesoproterozoic sedimentary rocks known as the Elu and Kilohigok basins. This paper focuses on the stratigraphy and gamma-ray spectrometry of the northeastern margin of the Kilohigok Basin, which is exposed along the southern shore, and inland, of Tariyunnuaq. At this location, the Kilohigok Basin is represented by the ca. 1.9 Ga Burnside River Formation, a sandstone-dominated fluvial unit that overlies granitoid and greenstone-belt rocks of the Archean Slave Province. The nonconformable contact between the Slave Province basement rocks and the Kilohigok Basin is characterized by a distinctive paleosol horizon (the 'Kilohigok paleosol'). Stratigraphic and gamma-ray spectrometry data were collected at several sites across the contact, along an ~80 km transect.

The Kilohigok paleosol is developed at the expense of either granitoid basement or greenstone-belt rocks. Well-developed paleosaprolites derived from the granitoid protoliths demonstrate potential for unconformity-related uranium mineralization, whereas poorly developed alteration profiles derived from greenstone-belt rocks are overall less prospective. The overlying Burnside River Formation is composed mainly of laterally continuous sandstone sheets, as well as preserved large foreset bars, channel bodies and eolian dunes. Although radioactivity measurements from the Burnside River Formation yielded uranium levels consistent with background values, local coarse-grained bodies contained within paleovalleys cut into basement rocks host nominally higher uranium concentrations. Similarly, above-background levels of radioactivity were recorded at higher stratigraphic levels, notably in proximity to intrabasin-fill surfaces of the unconformity.

Résumé

Une succession de roches sédimentaires d'âge paléoprotérozoïque et mésoprotérozoïque, connue sous le nom de bassin d'Elu et bassin de Kilohigok, repose sous le passage d'Elu et la collectivité de Tariyunnuaq (détroit de Melville), tous deux situés dans la région de Kitikmeot au Nunavut, au Canada. Le présent rapport met l'accent sur les travaux de stratigraphie et de spectrométrie gamma réalisés en bordure de la marge nord-est du bassin de Kilohigok, lequel se trouve exposé aussi bien le long du littoral sud de Tariyunnuaq que dans l'arrière-pays. À cet endroit, les roches qui constituent le basin Kilohigok font partie de la formation de Burnside River, âgée de 1,9 Ga; il s'agit d'une unité d'origine fluviale, principalement constituée de grès, qui recouvre des roches granitoïdes et des roches de ceintures de roches vertes d'âge archéen appartenant à la Province des Esclaves. À l'endroit où les roches du bassin de Kilohigok reposent en discordance sur les roches de socle de la Province des Esclaves, un horizon de paléosol distinctif s'est formé (« paléosol de Kilohigok »). Des données stratigraphiques et de spectrométrie gamma ont été recueillies à quelques endroits le long d'un transect d'environ 80 km correspondant à la zone de contact.

This publication is also available, free of charge, as colour digital files in Adobe Acrobat® PDF format from the Canada-Nunavut Geoscience Office website: http://cngo.ca/summary-of-activities/2015/.

La formation du paléosol de Kilohigok a impliqué à la fois les roches de socle granitoïdes et les roches de ceintures de roches vertes. Des paléosaprolites bien formés provenant des protolites granitoïdes semblent présenter des signes de minéralisation en uranium liée à la discordance, alors que les profils d'altération peu développés qui caractérisent les ceintures de roches vertes s'avèrent moins prometteurs de façon générale. La formation de Burnside River susjacente est principalement composée d'épaisses unités de grès de grande continuité latérale, ainsi que de barres sableuses de front de delta, d'amas de chenaux et de dunes éoliennes conservés. Bien que des mesures de la radioactivité provenant de la formation de Burnside River aient révélé des niveaux de radioactivité conformes aux valeurs de fond, des amas locaux à granulométrie grossière qui se trouvent au fond des paléovallées entaillées dans la roche de socle affichent des taux de concentration plus élévés d'uranium. Des taux de radioactivité supérieurs aux valeurs de fond ont également été enregistrés à des niveaux stratigraphiques plus élevés, et plus particulièrement à proximité d'aires de remplissage de bassin associées à la discordance.

Introduction

The Kilohigok and Elu basins in the Kitikmeot Region of Nunavut, containing Paleo- to Mesoproterozoic sedimentary rocks (Figure 1), are relatively underexplored compared to other Precambrian sedimentary basins in Canada. During the summers of 2014 and 2015, the Elu Basin Geoscience Project, which was co-led by the Canada-Nunavut Geoscience Office and the Geological Survey of Canada, had the objective of collecting original geological information on the stratigraphy, sedimentology and economic potential of the Elu Basin and the northeastern margin of the adjacent Kilohigok Basin (Ielpi and Rainbird, 2015a). The study area encompasses Elu Inlet, Tariyunnuaq (Melville Sound) and northeastern Kiluhiqtuq (Bathurst Inlet), and is centred roughly on latitude 68°15'N, longitude 107°15'W. This area was the focus of exploratory geological mapping in the late 1970s and early 1980s (Campbell, 1978, 1979; Campbell and Cecile, 1979, 1981); with the exception of a Ph.D. thesis by McCormick (1992), it has received little attention since then. Many of the Proterozoic basins on the Canadian Shield have demonstrated economic viability for uranium, lead-zinc and other metals (Jefferson et al., 2007). The scope of the Elu Basin Geoscience Project therefore includes provision of assessments on the economic potential of the sedimentary basins hosted in the Kitikmeot Region of Nunavut.

In the study area, two Proterozoic clastic units, the Burnside River and Ellice formations, occur in depositional contact with Archean basement rocks (Figure 1) and represent the main targets for unconformity-related uranium mineralization. The Ellice Formation was investigated during the 2014 field season in terms of stratigraphy, sedimentology and gamma-ray spectrometry (Ielpi and Rainbird, 2015a, b). Focusing on the older Burnside River Formation, a similar approach was followed during the 2015 field season. The Burnside River Formation and the underlying alteration profile developed on basement rocks ('Kilohigok paleosol') demonstrate prospectivity for uranium in places, and thus provide the specific target for the stratigraphic and gamma-ray spectrometry analyses presented here. Gamma-ray spectrometry data, reported at targeted stations during the 2014 and 2015 field seasons, are contained in Ielpi et al. (2015)[5].

Geological setting

The Kilohigok and Elu basins underlie the southeastern rim of the younger Amundsen Basin of Arctic Canada (Young, 1981), recording a time span of roughly 300 m.y. (ca. 1.97–1.63 Ga; Bowring and Grotzinger, 1992; Heaman et al., 1992). However, despite their similar stratigraphy, the Kilohigok and Elu basins likely formed under different geodynamic settings. The Kilohigok Basin is a 250 km long by 200 km wide domain of sedimentary rocks that are widely exposed on the western shore, and inland, of Kiluhiqtuq (Figure 1). The basin extends northeastward, where other prominent exposures occur at the boundary between Kiluhiqtuq and Tariyunnuaq (Figure 1), the study area of this research. In this area, the northeastern margin of the Kilohigok Basin is unconformably overlain by deposits of the younger 100 km long by 30 km wide Elu Basin (Ielpi and Rainbird, 2015a).

The geodynamic history of the Kilohigok and Elu basins has been a subject of debate. Based on stratigraphic similarities and structural affinities with the nearby Wopmay Orogen, Hoffman (1973) proposed an aulacogen (i.e., aborted-rift basin) model for the development of the Kilohigok Basin. However, owing to a lack of growth faulting and magmatism, this hypothesis was refined by Campbell and Cecile (1981), who promoted a model of an intracratonic trough related to a hypothetical aulacogen that developed to the north. Yet, ensuing work of Grotzinger and Gall (1986) and McCormick and Grotzinger (1992) refuted the intracratonic-trough model, as a greater amount of field evidence pointed to stratigraphic development and basin evolution consistent with a foreland basin concomitant with the Thelon orogeny (Figure 1; Tirrul, 1985; Tirrul and Grotzin-

[5] *CNGO Geoscience Data Series GDS2015-007, containing the data or other information sources used to compile this paper, is available online to download free of charge at http://cngo.ca/summary-of-activities/2015.*

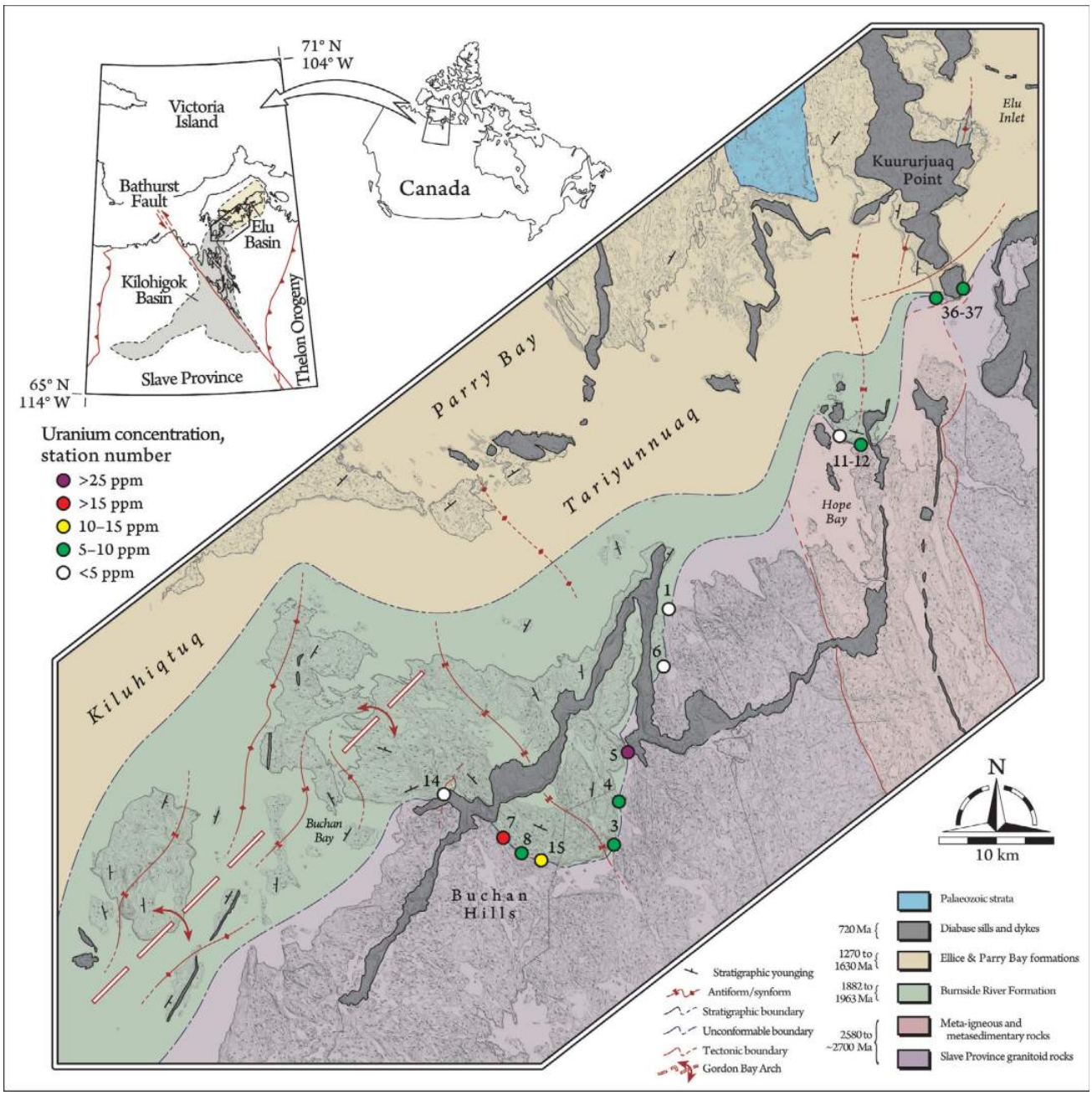

Figure 1: Geological framework of the northeastern margin of the Kilohigok Basin and overlying rocks of the Elu Basin. Modified, in part, from Campbell (1979), Campbell and Cecile (1979) and Ielpi and Rainbird (2015a). Geochronology from Bowring and Grotzinger (1992) and Heaman et al. (1992).

ger, 1990). Similarly, the Elu Basin was first interpreted as the product of rift tectonics (Campbell, 1979), a conjecture revised in favour of an intracratonic-sag model related to thermal insulation (Rainbird et al., 2014). The structural setting of the study area is characterized by gentle folding related to the Gordon Bay Arch (Figure 1; McCormick and Grotzinger, 1992), a regional-scale tectonic feature that probably formed and migrated toward the foreland in response to crustal loading (i.e., thrust stacking) at the front of the Thelon Orogen. Fault structures are subordinate and relate to minor, postdepositional, extensional to strike-slip displacement.

Stratigraphic framework

The basement rocks within the study area are part of the Archean Slave Province, which consists mainly of both weakly deformed granitoid rocks and heavily deformed belts of mafic (meta)volcanic and (meta)sedimentary rocks (Figure 1), the latter composing the north-trending Hope Bay greenstone belt (Sherlock et al., 2012). The Slave

Province is nonconformably covered by Proterozoic deposits that show little deformation, lack evidence of metamorphism and are arranged in three unconformity-bounded sequences with supraregional traceability (Rainbird and Davis, 2007). The Burnside River Formation (Sequence I) is up to 3.5 km thick and consists of crossbedded fluvial sandstone and minor conglomerate. Along the nonconformity with the Slave Province, the Burnside River Formation overlies the Kilohigok paleosol. The Tinney Cove Formation (Sequence II) is a coarse-clastic talus deposit less than 50 m thick. It was developed at the expense of the Burnside River Formation and occurs along cliff exposures at Kuururjuaq Point (Figure 1). The fluvial-eolian to nearshore-marine Ellice and Parry Bay formations (Sequence III) comprise a ≤2 km thick succession of clastic and carbonate rocks that is widely exposed in Elu Inlet and northern Tariyunnuaq (Ielpi and Rainbird, 2015a). These strata are intersected by diabase dykes and sills related to the Franklin igneous event (Heaman et al., 1992) and, in places, covered by clastic rocks of probable Paleozoic age (O'Neill, 1924; Thorsteinsson and Tozer, 1962).

Methods

Helicopter-supported mapping and ground traversing were performed out of the Doris North mining camp of TMAC Resources Inc. and a remote field camp during late June to early July 2015, covering parts of the NTS areas 76O, 76N, 77A and 77B. Observations on the bulk composition and alteration state of paleoweathered basement rocks (Figures 2, 3) were gathered in the field using hand lenses. Estimates on gross mineral abundance were performed using comparative tables. Observations on the stratigraphic development and depositional architecture of the Burnside River Formation (Figure 4) were collected on continuous stepped-cliff exposures, in places up to 3 km along strike and 500 m thick. The sedimentology of the Burnside River Formation was assessed along the same exposures, including paleoflow measurements (n = 1540) from crossbeds. The reconstruction of large-scale depositional architecture was aided by high-resolution satellite imagery, which included RapidEye™ and Pléiades™ imagery with 5.0 m and 0.5 m of ground resolution, respectively.

The radiation of basement rocks and overlying deposits (Figure 5) was assessed using a Radiation Solutions Inc. RS-125 hand-held spectrometer. The database of spectral signatures includes readings of radioactive dose rate (expressed in nanosieverts/hour or nSv/h) and extrapolated abundances of potassium (%), uranium (ppm) and thorium (ppm). Vertical lithological and spectrometry profiles were measured throughout the Kilohigok paleosol at several locations, in conjunction with bulk-rock sampling for future analysis.

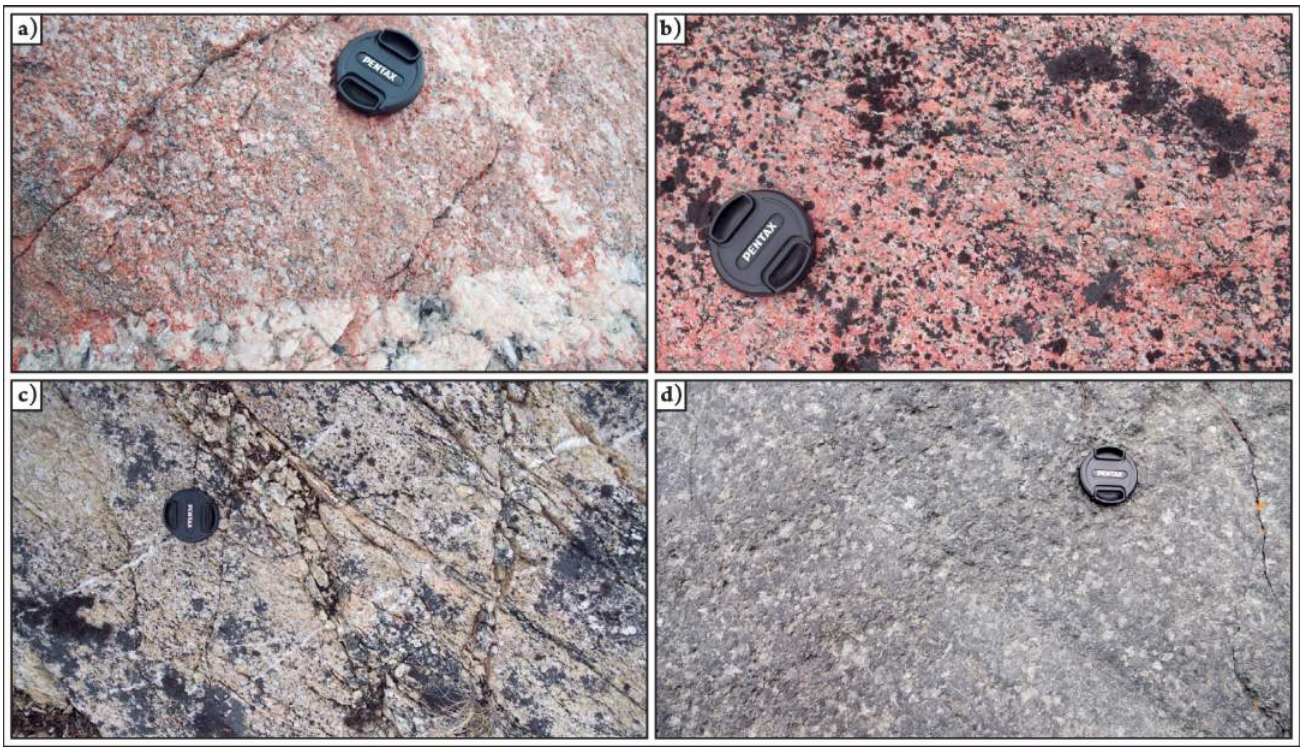

Figure 2: Representative rock types of the Archean Slave Province and derived alteration profile, outcropping mostly in the southwestern part of the study area (Figure 1; lens cap is ~5 cm across): **a)** fresh unaltered syenogranite intersected by quartz veins; **b)** lower saprolite superimposed on (a), showing reddening related to enrichment in hematite; **c)** upper saprolite superimposed on (b), showing intense illitization that resulted in loss of K-feldspar and plagioclase, and sericite crystallization; **d)** gabbro intrusions, although subordinate, occurring in isolated outcrops and locally collected for carving stone.

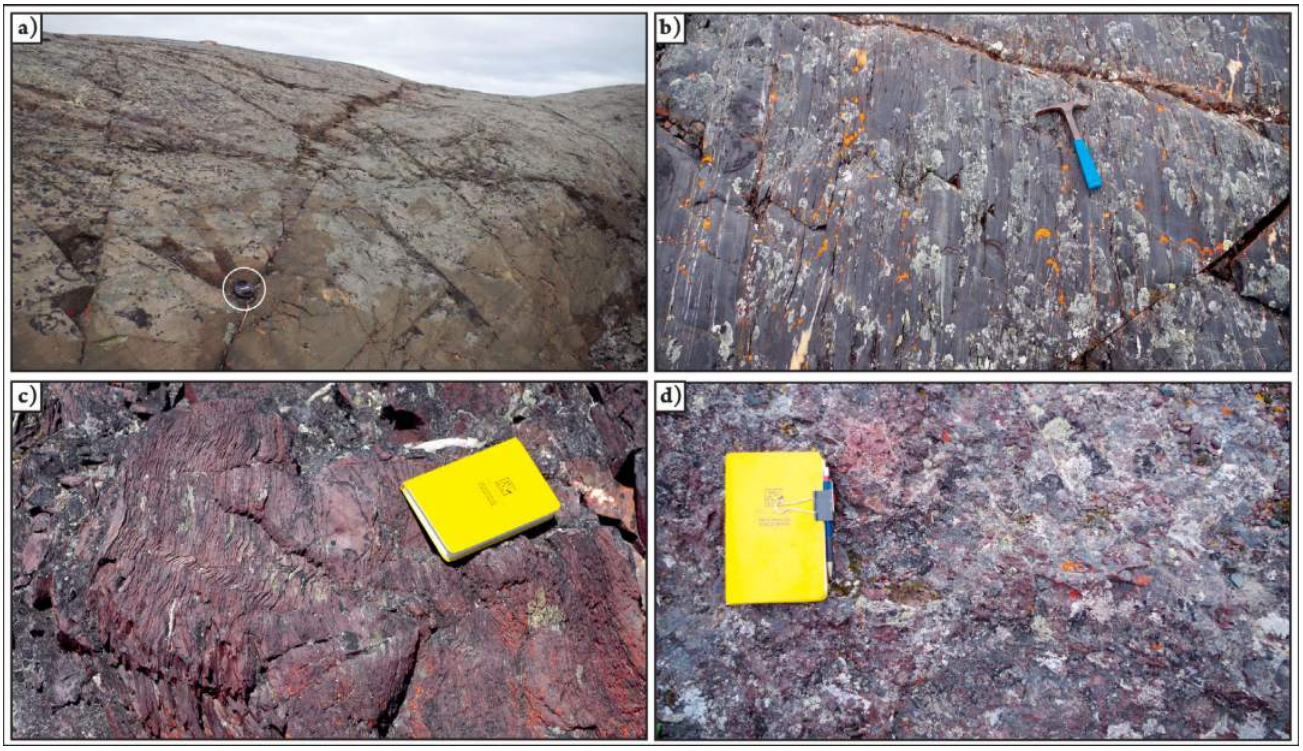

Figure 3: Representative rock types of the Archean Hope Bay greenstone belt and derived alteration profile, outcropping in the northeastern part of the study area (Figure 1): **a)** hydrothermally altered, tholeiitic and iron-rich basalt; lens cape (circled) is ~5 cm across; **b)** greenschist-grade metamorphic rocks derived from pelitic protolith; hammer is ~20 cm long; **c)** hematitic, fine-grained sandstone and siltstone of turbiditic origin; field book is 18 cm tall; **d)** deeply weathered profile superimposed on (a); field book is 18 cm tall.

Field results

Granitoid paleosol

The features of paleosol horizons developed on granitic rocks of the Archean Slave Province were assessed at 10 sites along an ~40 km transect (Figure 1). At these sites, the horizons can be subdivided in three zones, based on texture and bulk petrology. A lowermost horizon consists of relatively unaltered syenogranite (K-feldspar>quartz>plagioclase>muscovite), commonly intersected by decimetre-scale quartz veins (Figure 2a), with gneissic fabric developed in local shear zones. Subordinate gabbro occurs as decimetre to metre-scale xenoliths, or decametre-scale intrusions (Figure 2d), the latter locally collected as carving stone (Beauregard, 2014).

Closer to the contact with the Burnside River Formation, the unaltered granite transitions to a 'lower saprolite' zone, ranging in thickness from 2 to 8 m. The lower saprolite displays moderate fracturing (although no systematic jointing is observed) and is strongly reddened (Figure 2b). The reddening is related to hematization and sericitization (i.e., breakdown of iron and magnesium oxides and reprecipitation of iron on clay minerals derived from plagioclase weathering; cf. Gall, 1994). Accordingly, the bulk mineralogy of the lower saprolite is characterized by quartz, K-feldspar, muscovite, hematite and sericite.

An overlying 'upper saprolite' zone shows extensive textural breakdown and is dissected by centimetre-spaced joints oriented vertically with respect to the contact above. The upper saprolite is a pale yellow-green colour due to extensive sericitization (Figure 2c). This phase contains reduced amounts of plagioclase and K-feldspar as a result of illitization (Rainbird et al., 1990; Fedo et al., 1997), and its mineralogy is dominated by quartz and sericite, with selvages of clay minerals along joints. A horizontally bedded to massive pavement of pebbly sandstone sharply overlies the upper saprolite, which transitions upward over a few tens of decimetres into an iron-oxide–rich, crossbedded quartzarenite. In places, the nonconformity between basement rocks and the Burnside River Formation displays up to 3 m of erosional relief over a distance of 20 m along strike (Figure 4c).

Greenstone paleosol

The features of paleosol horizons developed on the Archean Hope Bay greenstone belt were assessed at three locations along a 20 km transect. At these sites, the Burnside River Formation overlies both mafic volcanic and related highly deformed sedimentary rocks (Figure 3a) that are locally metamorphosed to greenschist facies (Figure 3b, c). Good exposures are located in the headland to the northeast of Hope Bay (Figure 1), where a tectonic assemblage of fractured gabbro and massive, tholeiitic and iron-

rich basalt (clinopyroxene>plagioclase>hematite>olivine) is overlain by, and lateral to, a succession of steeply dipping, folded, Archean metasedimentary rocks. Mafic volcanic products attain a dark green colour related to hydrothermal alteration along the Hope Bay greenstone belt (Sherlock et al., 2012). The Archean sedimentary rocks are fine-grained wacke and mudstone. The paleosol horizon is developed on both basalt and folded sedimentary rocks, and is generally less than 1 m thick. Within this horizon, deeply fractured and weathered basalt is enriched in sericite and chlorite (cf. Rye and Holland, 2000), and hematite is progressively diminished toward the top (Figure 3d).

Physical breakdown occurred in isolated, cobble-sized angular fragments that show a lesser degree of mineralogical alteration, and tight folding in the Archean sedimentary rocks likely favoured the jointing and mechanical breakdown. As a result, the uppermost portion of the paleosol developed on Archean sedimentary rocks consists of a granule- to sand-grained, angular regolith that lacks a significant change in mineralogy with respect to the underlying protolith. The paleosol is sharply overlain by lensoid bodies of rounded-pebble conglomerate locally derived from rocks of the Hope Bay greenstone belt (Figure 4b). This conglomerate is crossbedded and preserved within ero-

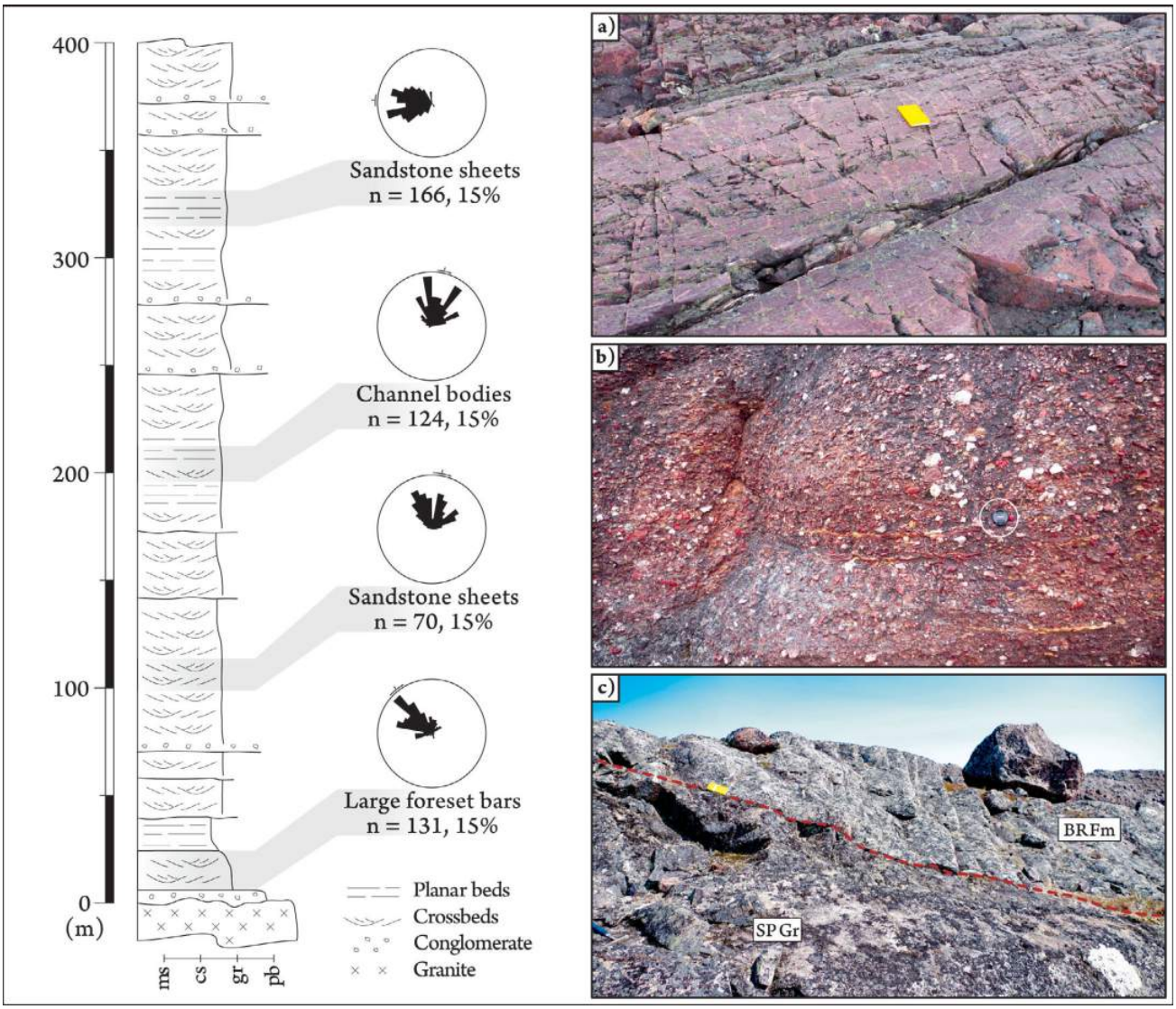

Figure 4: Stratigraphy and field aspect of the Burnside River Formation. The stratigraphic column, is in part, modified from McCormick (1992). Representative paleoflow data collected at different stratigraphic horizons throughout the northeastern Kilohigok Basin are reported in rose diagrams with linear scale, average vector and 95% confidence arc. Abbreviations: ms, medium-grained sand; cs, coarse-grained sand; gr, granules; pb, pebbles. Photographs: **a)** coarse-grained, trough-crossbedded sandstone organized in metre-thick units bounded by erosional contacts; field book is 18 cm tall; **b)** pebble conglomerate derived from the Hope Bay greenstone belt and contained within paleovalleys incised into basement rocks; lens cap (circled), is ~5 cm across; **c)** nonconformity between granite-derived saprolite of the Archean Slave Province (SP Gr) and basal crossbedded sandstone of the Burnside River Formation (BR Fm); field book is 18 cm tall.

sional depressions cut on basement rocks, which represent paleovalleys (Ielpi and Rainbird, 2015a) up to 8 m deep and ~30 m wide. The conglomerate fines upward abruptly into coarse-grained to pebbly, crossbedded sandstone over less than a metre.

Burnside River Formation

In the study area, the most complete succession of Burnside River Formation occurs along Buchan Bay (Figure 1), where a thickness of ~1 km is exposed. The formation is dominated by coarse-grained, iron-oxide–rich arkose, with minor conglomerate and fines. In outcrop, the sedimentary motif exhibits a repetitive character, with strata between 0.5 and 2 m thick and bounded by laterally continuous (>100 m), low relief (<50 cm), planar erosional surfaces. The erosional surfaces are floored by pebble pavements derived mainly from granitoid rocks and rarely from greenstone-belt rocks. Locally, the pavements are composed of flattened, well-rounded pebbles with frosted surfaces, overlain by a similarly frosted, medium-grained quartzarenite.

Strata display trough crossbedding and minor planar crossbedding (Figure 4a), the latter with well-developed soft-sediment deformation and flow-induced shear structures. Minor planar intervals of fine-grained maroon sandstone and siltstone are ripple crosslaminated. Overall, these features are consistent with poorly confined alluvial systems characterized by sustained perennial flow, an assumption based on the lateral continuity of the strata and the predominance of crossbedding over planar stratification (Ielpi, 2012; Rygel et al., 2015). Episodes of wind reworking are evidenced by eolian gravel lags and sheets (frosted pebbles and quartzarenite; Mountney, 2006).

The large-scale depositional architecture of the Burnside River Formation is characterized by four elements: fluvial sand sheets, large foreset bars, channel bodies and eolian dunes. Sandstone sheets represent roughly 70% of the deposits and consist of tabular stacks of strata up to 500 m thick that show little or no change in thickness for up to 5 km along strike. Satellite images show that individual strata within the sandstone sheets attain width:thickness ratios as high as 3000, a feature consistent with sheet-braided fluvial systems (Fuller, 1985). Paleoflow indicators collected on sandstone sheets point to unimodal, focused drainage toward the west-northwest (Figure 4). Large foreset bars account for ~20% of the deposits, and consist of sets of gently inclined (<10°) strata up to 20 m thick that pinch out in less than 50 m downstream. Second-order surfaces (*sensu* Rainbird, 1992) point to accretion consistent with unimodal, northwestward paleoflow (Figure 4). Overall, these features are consistent with large midchannel bars dominated by downstream accretion and generated within deep, open-water channels at high-flood stage (Ielpi and Ghinassi, 2015). Channel bodies represent ~5% of the deposits and consist of scoop-shaped lithosomes that are 500–1200 m wide and up to 12 m thick (width:thickness ratios ranging from 80 to 100). Second-order surfaces within the channel bodies cut each other, and point to accretion consistent with paleoflow indicators. The orientation of these surfaces suggests mildly dispersed, northward sediment paleotransport (Figure 4), a vector roughly perpendicular to that of adjacent sandstone sheets. Eolian dunes form approximately 5% of the deposits and consist of up to 30 m thick sets of steeply inclined cross-strata (>25°) that are laterally continuous for more than 600 m along strike. Second-order surfaces indicate a highly focused, unimodal accretion toward the west-southwest.

The assemblage of fluvial-eolian architectural elements is consistent with a sheet flow–dominated alluvial plain transected locally by mature trunk channels capable of generating large downstream-accretionary bars. These channels had paleoflow inconsistent with that of adjoining sand sheets, thereby suggesting that the Burnside River Formation could have been generated by multiple, interacting alluvial systems with basin-centripetal drainage (Ielpi, 2013). Episodes of eolian reworking of the sediments into dune fields and small draa (Mountney, 2006) point to contemporaneous fluvial shutdown or sand winnowing along interfluves.

Gamma-ray spectrometry

The radioactive properties of basement rocks and sedimentary rocks were investigated in terms of total dose rates, and abundance of potassium, uranium and thorium. Above-background dose rates were recorded in places along the Kilohigok paleosol (~250–450 nSv/h), whereas both basement rocks and sedimentary rocks at different stratigraphic levels yielded only background levels of radiation (<200 nSv/h). Thirteen sites along the Kilohigok paleosol show that the alteration profiles on granitoid rocks have higher prospectivity for uranium than those developed on greenstone-belt rocks (Figure 1).

The highest values of radioactivity were recorded along the Buchan Hills, close to the Gordon Bay Arch, where the nonconformity between the Slave Province granite and Burnside River Formation is folded in a large northwest-trending syncline (Figure 1). At these locations, dose rates of up to 461.8 nSv/h were recorded, corresponding to peak concentrations of uranium and thorium of up to 29.7 and 54.6 ppm, respectively (stations 15-5 and 15-29). A spectrometer profile through the well-developed, granitoid-derived Kilohigok paleosol (type A in Figure 5; station 15-7) demonstrates a strong, direct correlation between dose rate and uranium abundance, yet weaker correlations between dose rate and thorium-potassium abundance. Also, it appears that the uranium mineralization is concentrated along the lower saprolite and in the gravelly pavement flooring

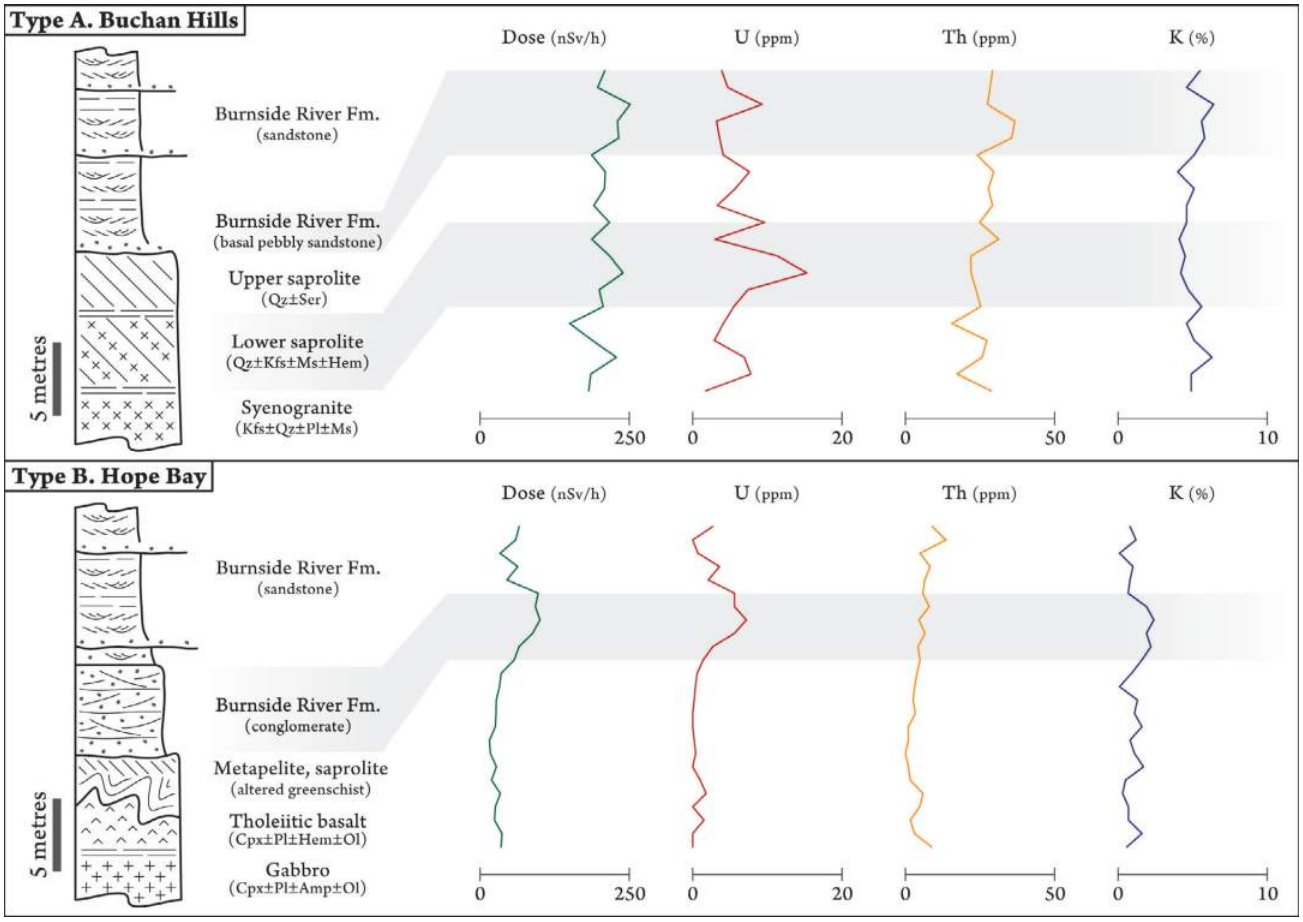

Figure 5: Representative gamma-ray spectrometry profiles of the Kilohigok paleosol. Horizons developed on granitoid rocks (type A) have well-developed saprolite and demonstrate potential for unconformity-related uranium mineralization. Horizons developed on mafic volcanic rocks and associated (meta)sedimentary rocks (type B) have poorly developed saprolite, and lesser concentrations of uranium are found only within basal conglomerate bodies.

the nonconformity between the Slave Province granite and Burnside River Formation (Figure 5). By comparison, granitoid exposures located a few hundred metres away from the Kilohigok paleosol (station 15-8) yielded peak dose rates of 205.4 nSv/h, corresponding to peak concentrations of uranium and thorium of 6.9 and 32.9 ppm, respectively. Exposures of Burnside River Formation at a stratigraphic level ~100 m above the Kilohigok paleosol (station 15-2) yielded peak dose rates of 116.1 nSv/h, corresponding to peak concentrations of uranium and thorium of 5.2 and 18 ppm, respectively.

Lower levels of radioactivity were recorded in the headland east of Hope Bay, where the Kilohigok paleosol is poorly developed over the Hope Bay greenstone belt (type B in Figure 5; stations 14-8, 15-11 and 15-12) and where the nonconformity with the overlying Burnside River Formation is folded in a gentle syncline (Figure 1). There, a peak dose rate of 115.9 nSv/h was recorded, corresponding to peak concentrations of uranium and thorium of 7.2 and 22.7 ppm, respectively. A spectrometer profile through the paleosol and overlying pebble conglomerate of the basal Burnside River Formation reveals a strong positive correlation between dose rate and abundance of uranium and potassium, whereas no apparent correlation exists with the abundance of thorium (Figure 5). By comparison, mafic volcanic products exposed ~50 m below the Kilohigok paleosol (station 14-6) yielded a peak dose rate of 55.6 nSv/h, corresponding to peak concentrations of uranium and thorium of 1.8 and 10.7 ppm, respectively. The unconformable contact between the Burnside River and Tinney Cove formations (~50 m above the Kilohigok paleosol at Kuurujuaq Point; Figure 1; station 14-1) yielded a peak dose rate of 111 nSv/h, corresponding to peak concentrations of uranium and thorium of 5.9 and 24 ppm, respectively.

Discussion and conclusions

During the second year of field activities, the Elu Basin Geoscience Project focused on the stratigraphy and gamma-ray spectrometry of the 1.9 Ga Burnside River Formation exposed in Tariyunnuaq (Melville Sound), and its underlying paleosol developed on granitoid and greenstone-belt rocks of the Archean Slave Province. The field

investigations confirm a stratigraphic subdivision into three unconformity-bounded stratigraphic sequences for both the Elu Basin and the northeastern margin of the underlying Kilohigok Basin. Field-based gamma-ray spectrometry analyses demonstrate a cost- and time-effective method for prospecting for radionuclide mineralization, especially when focused along nonconformable surfaces between crystalline and sedimentary rocks and, to a lesser degree, along intrabasin-fill surfaces of unconformity.

Preliminary investigations on the sedimentology and depositional architecture of the Burnside River Formation depict a sandstone-dominated fluvial system characterized by deposition on wide, unconfined plains subject to sheet flooding. Locally, preservation of large downstream-accretionary bars, large channel bodies and eolian dunes point to major fluvial trunks transecting the alluvial plain, and sided by ephemeral eolian dunes, a possible expression of interfluves (cf. Ielpi and Rainbird, 2015b). The overall northwestward paleodrainage coincides with previous studies on the Burnside River Formation exposed in Kiluhiqtuq (Bathurst Inlet; Campbell and Cecile, 1979, 1981; McCormick and Grotzinger, 1992), suggesting sediment production and routing from the Thelon Tectonic Zone. Local paleoflow dispersion may have responded to the active growth of folds related to the uplift of the Gordon Bay Arch, as suggested by McCormick and Grotzinger (1992). Overall, these features support a depositional setting consistent with a synorogenic, fluvial-dominated foreland basin.

Economic considerations

Unconformity-related deposits are widely considered to be the primary form of uranium mineralization in many Precambrian basins within the Canadian Shield, the most prominent being the high-grade deposits of the Athabasca Basin (Jefferson et al., 2007). As envisaged by Gall (1994), similar styles of mineralization could characterize the basal unconformity of economically underexplored basins such as the Elu and Kilohigok. Investigations on the alteration profile underlying the 1.6 Ga Ellice Formation in the Elu Basin demonstrated only background levels of radioactivity (Ielpi and Rainbird, 2015a). By comparison, field measurements from the 1.9 Ga Kilohigok paleosol yielded above-background concentrations of uranium (up to 30 ppm), especially when it developed on granitoid rocks of the Archean Slave Province and in proximity to large-scale folds. In contrast, those portions of the Kilohigok paleosol derived from rocks of the Hope Bay greenstone belt demonstrated lesser prospectivity. Given these preliminary observations, it is suggested that future exploration focus on the lower portions of granitoid-derived alteration profiles, as well as the conglomeratic bodies directly overlying stratigraphic surfaces of nonconformity or unconformity.

Acknowledgments

The authors thank TMAC Resources Inc. for providing an operational base at their Doris North camp, and particularly for the assistance of A. Buchan, M. McCreadie, N. de Ruyter and S. Hudson. F. Jones and Z. Dippo from Great Slave Helicopters are warmly thanked for safe piloting. K. Vickers and M. McLean from Discovery Mining Services, G. Parsons from the Polar Continental Shelf Program at Resolute and P. Philstone from Air Tindi are thanked for valuable expediting services and logistical support. R. Berman is warmly acknowledged for his insightful reviews.

The Canadian Northern Economic Development Agency's (CanNor) Strategic Investments in Northern Economic Development (SINED) and the Geo-mapping for Energy and Minerals (GEM) programs provided financial support for this work. The senior author is supported by a research grant from the Natural Sciences and Engineering Research Council of Canada (NSERC).

Natural Resources Canada, Earth Sciences Sector contribution 20150337

References

Beauregard, M. 2014: Results from the 2010–2014 carving stone deposit evaluation program; presentation at 2014 Nunavut Mining Symposium, April 7–10, Iqaluit, Nunavut.

Bowring, S.A. and Grotzinger, J.P. 1992: Implications of new chronostratigraphy for tectonic evolution of Wopmay Orogen, northwest Canadian Shield; American Journal of Science, v. 292, p. 1–20.

Campbell, F.H.A. 1978: Geology of the Helikian rocks of the Bathurst Inlet area, Coronation Gulf, Northwest Territories; *in* Current Research, Part A, Geological Survey of Canada, Paper 78-1A, p. 97–106.

Campbell, F.H.A. 1979: Stratigraphy and sedimentation in the Helikian Elu Basin and Hiukitak Platform, Bathurst Inlet–Melville Sound, Northwest Territories; Geological Survey of Canada, Paper 79-8, 19 p.

Campbell, F.H.A. and Cecile, M.P. 1979: The northeastern margin of the Aphebian Kilohigok Basin, Melville Sound, Victoria Island, District of Franklin; *in* Current Research, Part A, Geological Survey of Canada, Paper 79-1A, p. 91–94.

Campbell, F.H.A. and Cecile, M.P. 1981: Evolution of the Early Proterozoic Kilohigok Basin, Bathurst Inlet–Victoria Island, Northwest Territories; *in* Proterozoic Basins of Canada, F.H.A. Campbell (ed.), Geological Survey of Canada, Paper 81-10, p. 103–131.

Fedo, C.M., Young, G.M., Nesbitt, H.W. and Hanchar, J.M. 1997: Potassic and sodic metasomatism in the Southern Province of the Canadian Shield: evidence from the Paleoproterozoic Serpent Formation, Huronian Supergroup, Canada; Precambrian Research, v. 84, p. 17–36.

Fuller, A.O. 1985: A contribution to the conceptual modeling of pre-Devonian fluvial systems; Transactions of the Geological Society of South Africa, v. 88, p. 189–194.

Gall, Q. 1994: The Proterozoic Thelon paleosol, Northwest Territories, Canada; Precambrian Research, v. 68, p. 115–137.

Grotzinger, J.P. and Gall, Q. 1986: Preliminary investigations of early Proterozoic Western River and Burnside River formations: evidence for foredeep origin of Kilohigok Basin, N.W.T., Canada; *in* Current Research, Part A, Geological Survey of Canada, Paper 86-1A, p. 95–106.

Heaman, L.M., LeCheminant, A.N. and Rainbird, R.H. 1992: Nature and timing of Franklin igneous events, Canada: implications for a Neoproterozoic mantle plume and the break-up of Laurentia; Earth and Planetary Science Letters, v. 109, p. 117–131.

Hoffman, P.F. 1973: Evolution of an early Proterozoic continental margin: the Coronation geosyncline and associated aulacogens of the northwestern Canadian Shield; Royal Society of London, Philosophical Transactions A, v. 237, p. 547–581.

Ielpi, A. 2012: Anatomy of major coal successions: facies analysis and sequence architecture of a brown coal-bearing valley fill to lacustrine tract (Upper Valdarno Basin, northern Apennines, Italy); Sedimentary Geology, v. 265–266, p. 163–181.

Ielpi, A., 2013: Frequency-reliant correlative patterns of asymmetric lacustrine-paralic sequences: a genetic approach to the late Miocene Bithynia Marlstones of the southeastern Volterra Basin, Italy; Journal of Sedimentary Research, v. 83, p. 377–394.

Ielpi, A. and Ghinassi, M. 2015: Planview style and palaeodrainage of Torridonian channel belts: Applecross Formation, Stoer Peninsula, Scotland; Sedimentary Geology, v. 325, p. 1–16.

Ielpi, A. and Rainbird, R.H. 2015a: Geological framework of the 1.9–1.6 Ga Elu Basin, western Nunavut: representative sedimentology, gamma-ray spectrometry and lithogeochemistry; *in* Summary of Activities 2014, Canada-Nunavut Geoscience Office, p. 89–96.

Ielpi, A. and Rainbird, R.H. 2015b: Architecture and morphodynamics of a 1.6 Ga fluvial sandstone: Ellice Formation of Elu Basin, Arctic Canada; Sedimentology, v. 62, p. 1950–1977. doi:10.1111/sed.12211

Ielpi, A., Rainbird, R.H., Greenman, J.W. and Creason, C.G. 2015: Data table accompanying "The 1.9 Ga Kilohigok paleosol and Burnside River Formation, western Nunavut: stratigraphy and gamma-ray spectrometry"; Canada-Nunavut Geoscience Office, Geoscience Data Series GDS2015-007, Microsoft® Excel® file.

Jefferson, C.W., Thomas, D.J., Gandhi, S.S., Ramaekers, P., Delaney, G., Brisbin, D., Cutts, C., Portella, P. and Olson, R.A. 2007: Unconformity-associated uranium deposits of the Athabasca Basin, Saskatchewan and Alberta; *in* EXTECH IV: Geology and Uranium EXploration TECHnology of the Proterozoic Athabasca Basin, Saskatchewan and Alberta, C.W. Jefferson and G.D. Delaney (ed.), Geological Survey of Canada, Bulletin 588, p. 23–67.

McCormick, D.S. 1992: Evolution of an early Proterozoic alluvially-dominated foreland basin, Burnside Formation, Kilohigok Basin, N.W.T., Canada; Ph.D. thesis, Massachusetts Institute of Technology, Cambridge, Massachusetts, 547 p.

McCormick, D.S. and Grotzinger, J.P. 1992: Evolution and significance of an overfilled alluvial foreland basin: Burnside Formation (1.9 Ga), Kilohigok Basin, N.W.T., Canada; Basin Research, v. 4, p. 253–278.

Mountney, N.P. 2006: Eolian facies models; *in* Facies Models Revisited, H.W. Posamentier and R.G. Walker (ed.), Society for Sedimentary Geology (SEPM), Special Publication 84, p. 23–88.

O'Neill, J.J. 1924: Geology of the Arctic coast of Canada, west of Kent Peninsula; *in* Report of the Canadian Arctic Expedition 1913–18, v. 11, Geology and Geography, Part A, 107 p.

Rainbird, R.H. 1992: Anatomy of a large-scale braid-plain quartzarenite from the Neoproterozoic Shaler Group, Victoria Island, Northwest Territories, Canada; Canadian Journal of Earth Sciences, v. 29, p. 2537–2550.

Rainbird, R.H. and Davis, W.J. 2007: U-Pb detrital zircon geochronology and provenance of the late Paleoproterozoic Dubawnt Supergroup: linking sedimentation with tectonic reworking of the western Churchill Province, Canada; Geological Society of America Bulletin, v. 119, p. 314–328.

Rainbird, R.H., Ielpi, A., Long, D.G.F. and Donaldson, J.A. 2014: Similarities and paleogeography of late Paleoproterozoic terrestrial sandstone deposits on the Canadian Shield: product of Hudsonian orogenesis; Geological Society of America, Abstract with Programs, v. 46, p. 89.

Rainbird R.H., Nesbitt H.W. and Donaldson, J.A. 1990: Formation and diagenesis of a sub-Huronian saprolith: comparison with a modern weathering profile; The Journal of Geology, v. 98, p. 801–822.

Rye, R. and Holland, H.D. 2000: Geology and geochemistry of paleosols developed on the Hekpoort Basalt, Pretoria Group, South Africa; American Journal of Science, v. 300, p. 85–141.

Rygel, M.C., Lally, C., Gibling, M.R., Ielpi, A., Calder, J.H. and Bashforth, A.R. 2015: Sedimentology and stratigraphy of the type section of the Pennsylvanian Boss Point Formation, Joggins Fossil Cliffs, Nova Scotia, Canada; Atlantic Geology, v. 51, p. 1–43.

Sherlock, R.L., Shannon, A., Hebel, M., Lindsay, D., Madsen, J., Sandeman, H., Hrabi, B., Mortensen, J.K., Tosdal, R.M. and Friedman, R. 2012: Volcanic stratigraphy, geochronology, and gold deposits of the Archean Hope Bay greenstone belt, Nunavut Canada; Economic Geology, v. 107, p. 991–1042.

Thorsteinsson, R. and Tozer, E.T. 1962: Banks, Victoria and Stefansson Islands, Arctic Archipelago; Geological Survey of Canada, Memoir 330, 85 p.

Tirrul, R. 1985: Nappes in the Kilohigok Basin, and their relation to the Thelon tectonic zone, District of Mackenzie; *in* Current Research, Part A, Geological Survey of Canada, Paper 85-1A, p. 407–420.

Tirrul, R. and Grotzinger, J.P. 1990: Early Proterozoic collisional orogeny along the northern Thelon tectonic zone, Northwest Territories, Canada: evidence from the foreland; Tectonics, v. 9, p. 1015–1036.

Young, G.M. 1981: The Amundsen embayment, Northwest Territories: relevance to the upper Proterozoic evolution of North America; *in* Proterozoic Basins of Canada, F.H.A. Campbell (ed.), Geological Survey of Canada, Paper 81-10, p. 203–211.

Preliminary lithogeochemistry and geochronology of pegmatites of the Hall Peninsula, Baffin Island, Nunavut: implications for REE mineralization potential

A. Bigio[1,2] and D. Lentz[2]

[1]*Indigenous and Northern Affairs Canada, Iqaluit, Nunavut, alia.bigio@aandc-aadnc.gc.ca*

[2]*Department of Earth Sciences, University of New Brunswick, Fredericton, New Brunswick*

This work is part of the Hall Peninsula Integrated Geoscience Program (HPIGP), led by the Canada-Nunavut Geoscience Office (CNGO) in collaboration with the Government of Nunavut, Indigenous and Northern Affairs Canada, Dalhousie University, University of Alberta, Université Laval, University of Manitoba, University of Ottawa, University of Saskatchewan, University of New Brunswick, Nunavut Arctic College and the Geological Survey of Canada. It is supported logistically by several local, Inuit-owned businesses and the Polar Continental Shelf Program. The focus is on bedrock and surficial geology mapping (1:100 000 scale). In addition, a range of thematic studies is being conducted, including Archean and Paleoproterozoic tectonics, geochronology, landscape uplift and exhumation, microdiamonds, sedimentary rock xenoliths and permafrost. The goal is to increase the level of geological knowledge and better evaluate the natural resource potential in this frontier area.

Bigio, A. and Lentz, D. 2015: Preliminary lithogeochemistry and geochronology of pegmatites of the Hall Peninsula, Baffin Island, Nunavut: implications for REE mineralization potential; *in* Summary of Activities 2015, Canada-Nunavut Geoscience Office, p. 11–20.

Abstract

A number of granitic pegmatites on the Hall Peninsula were sampled in 2014 as part of an ongoing study to determine their petrogenesis and composition, and to evaluate their metallogenic potential, with a particular focus on rare metals, rare-earth elements and/or gems. To date, whole-rock lithogeochemistry, as well as laser-ablation, multiple-collector, inductively coupled plasma mass–spectrometry, for both spot mineral geochemical analysis and U-Pb geochronology on zircons and monazites, have been completed on various subsets of the more than 70 samples collected as part of the project. This paper presents selected preliminary data available from these analyses to date.

Résumé

Quelques pegmatites granitiques de la péninsule Hall ont été échantillonnées en 2014 dans le cadre d'une étude en cours portant sur la détermination de leur pétrogenèse et de leur composition, ainsi que sur l'évaluation de leur potentiel sur le plan métallogénique, tout particulièrement en ce qui a trait à la présence possible de métaux rares, d'éléments des terres rares et, le cas échéant, de gemmes. À ce jour, des études de litho-géochimie sur roche totale, ainsi que des analyses géochimiques des minéraux et des études géochronologiques par la méthode uranium-plomb sur zircon et monazite ont été réalisées au moyen de l'ablation laser couplée à un spectromètre de masse à source à plasma inductif et collection d'ions multiple sur divers sous-ensembles des plus de 70 échantillons recueillis aux fins de ce projet. Cet article présente des données préliminaires choisies parmi les résultats d'analyses présentement disponibles.

Introduction

The regional geology of the Hall Peninsula can be divided into two major lithological assemblages corresponding to the western and eastern halves of the peninsula (Figure 1). The western half consists of Paleoproterozoic metasedimentary rocks, containing leucogranitic dykes and other granitic intrusions, and supracrustal rocks that are composed mainly of pelite, semipelite and psammite and show evidence of localized partial melting (Dyck and St-Onge, 2014; Skipton and St-Onge, 2014). The eastern half of the peninsula is composed of an Archean orthogneiss complex of alternating tonalite and monzogranite units with minor enclaves of mafic and ultramafic rocks, all of which are crosscut by syenogranite dykes. Supracrustal rocks are also found in the east, structurally above and below the Archean basement (Dyck and St-Onge, 2014; From et al., 2014; Skipton and St-Onge, 2014; Bigio et al., 2015).

Pegmatite bodies are found across the Hall Peninsula. Most of the pegmatites in the study area crosscut the regional metamorphic fabric, although some are foliation-parallel,

This publication is also available, free of charge, as colour digital files in Adobe Acrobat® PDF format from the Canada-Nunavut Geoscience Office website: http://cngo.ca/summary-of-activities/2015/.

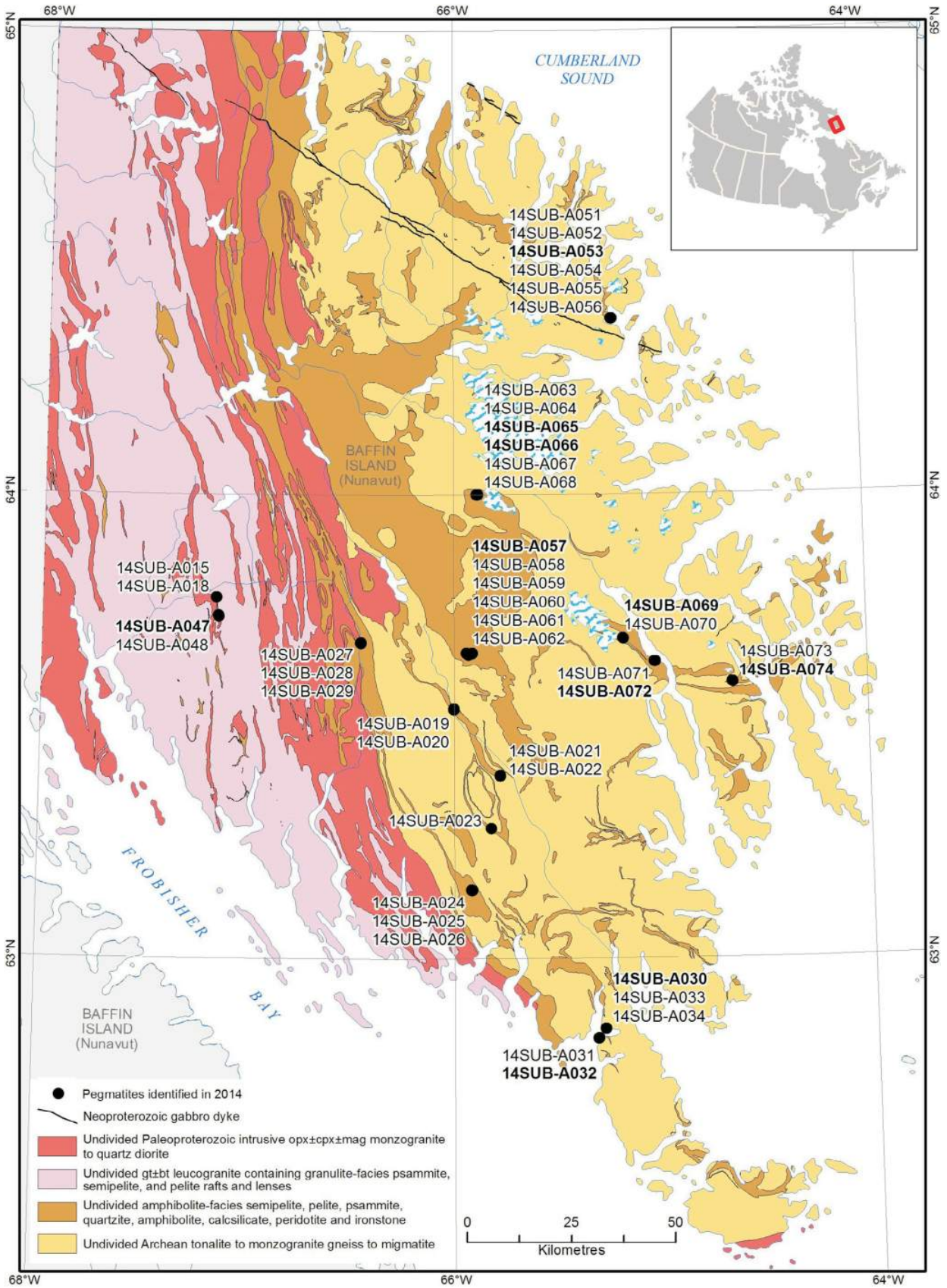

Figure 1: Simplified geology of the Hall Peninsula, Baffin Island, Nunavut. Pegmatites are found in both major geological assemblages. Station numbers indicate locations of pegmatites identified in 2014. Bolded station numbers indicate stations at which whole-rock geochemistry samples were collected (modified after Rayner, 2015).

and all generally appear to have intruded late in the deformational history of the Trans-Hudson Orogen (Skipton and St-Onge, 2014; Bigio et al., 2015). In the eastern half of the study area, locally deformed pegmatites are rarely observed, while in the west, deformation is more common.

To date, whole-rock lithogeochemistry, laser-ablation, multiple-collector, inductively coupled plasma mass–spectrometry (LA-MC-ICP-MS) of micas and feldspars, and U-Pb zircon and monazite geochronology analyses have been performed on samples taken in the 2014 field season (Bigio et al., 2015). This paper describes the analytical methods used, and preliminary results obtained from, these analyses.

Characterization of Hall Peninsula pegmatites

Mineralogy of the pegmatites in the study area varies between K-feldspar and plagioclase feldspar, with quartz, biotite, muscovite, magnetite, graphite, tourmaline, and rare apatite and beryl. The mineral assemblages present allow the pegmatites to be categorized as lithium-cesium-tantalum (LCT)–type pegmatites, based on the classification scheme of Černý and Ercit, (2005) and Černý et al. (2012), and are typically sourced from S-type granites. The pegmatites usually display very coarse grained textures including blocky feldspar crystals, graphic feldspar-quartz intergrowths, and biotite occurring as books or sheets. Graphic texture is observed at both macro- and microscopic scales and shows alkali feldspar with intergrown quartz. Figure 2 is a scanning electron microscope–back-scattered electron (SEM-BSE) image of graphically intergrown K-feldspar and quartz. For a more detailed discussion of the mineralogy and field relationships of pegmatites in the study area, refer to Bigio et al. (2015).

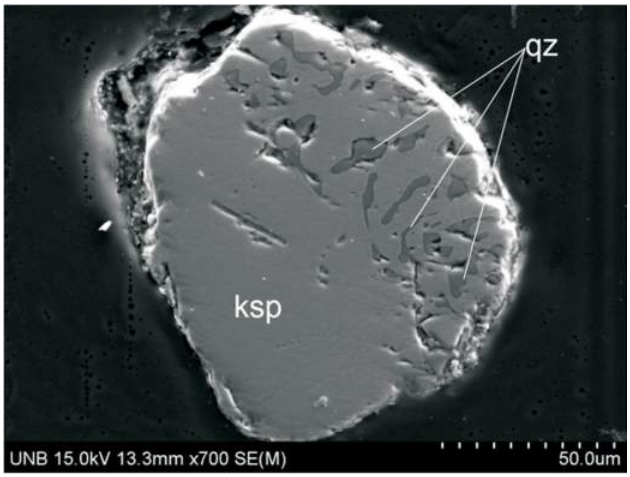

Figure 2: Field-emission scanning electron microscope–back-scattered electron (FESEM-BSE) image of K-feldspar grain from sample 14SUB-A047C01, showing microscopic graphic quartz-feldspar intergrowth texture (Hall Peninsula, Baffin Island, Nunavut). Abbreviations: ksp, K-feldspar (orthoclase); qz, quartz.

Preliminary analytical results

Whole-rock geochemistry

Nineteen pegmatite samples were selected for whole-rock geochemical analysis. To ensure accurate analytical results from the extremely coarse grained pegmatites, it was necessary to analyze between 1 and 4 kg of material from each pegmatite sampled. The analyses were conducted by Activation Laboratories (Actlabs) Ltd. in Ancaster, Ont. The initial analytical package selected for the samples was 4Lithores (Activation Laboratories Ltd., 2015a). Limited funding was available to have 3 of the 19 samples further analyzed using the Ultratrace 6 package, to obtain lighter element quantities not measurable using 4Lithores, in particular Li (see data in Table 1). Lithogeochemical data for the 19 samples analyzed with the 4Lithores method is presented in the CNGO Geoscience Data Series file GDS2015-008[3] (Bigio and Lentz, 2015) and is plotted on Figure 3.

Methods

Actlabs' 4Lithores analytical process involves a lithium metaborate/tetraborate fusion ICP for whole-rock analysis, and trace-element analysis through ICP-MS. Three blanks and five control samples are analyzed per group of samples, and duplicates are inserted after every 15 samples for quality control (Activation Laboratories Ltd., 2015a). None of the additional options were requested as the samples were not expected to be high in base metals, As, Sb, W or Cr (all of which would need more specific analysis).

The Ultratrace 6 process (Activation Laboratories Ltd., 2015b) begins with a 4-acid digestion process involving a sequence of hydrofluoric, nitric, and perchloric acids and aqua regia. Highly resistant minerals such as zircon, monazite, titanite, chromite and barite may only be partially dissolved during the process. After digestion, samples are analyzed through ICP-MS, with one blank per 40 samples, one in-house control per 20 samples, one standard every 80 samples, and a duplicate every 15 samples for quality control.

Trace-element results from whole-rock geochemistry

Sample 14SUB-A074A01 returned the highest rare-earth element (REE) values out of the 19 samples analyzed using the 4Lithores analytical package (Figure 3). The lithogeochemical data are presented in two graphs for clarity, as sample 14SUBA074A01 has some extremely anomalous values in comparison with the rest of the samples that would be over emphasized if all the data were displayed on one plot. Of particular note were the light rare-earth elements (LREE): La (1470 ppm), Ce (3020 ppm), Nd

[3]*CNGO Geoscience Data Series GDS2015-008, containing the data or other information sources used to compile this paper, is available online to download free of charge at http://cngo.ca/summary-of-activities/2015/.*

Table 1: Major- and trace-element analyses using the Ultratrace 6 analytical package for samples 14SUB-A026B01, A053A01 and A065B02 (Hall Peninsula, Baffin Island). Samples were analyzed at Activation Laboratories (Actlabs) Ltd. in Ancaster, Ont.

Analyte:	Li	Na	Mg	Al	K	Ca	Cd	V	Cr	Mn	Fe	Hf	Hg	Ni	Er	Be
Unit:	ppm	%	%	%	%	%	ppm	ppm	ppm	ppm	%	ppm	ppb	ppm	ppm	ppm
Detection limit:	0.5	0.01	0.01	0.01	0.01	0.01	0.1	1	0.5	1	0.01	0.1	10	0.5	0.1	0.1
Analysis method:	TD-MS															
14SUBA026B01	28.5	2.21	0.76	7.68	0.96	1.49	0.2	10	24.8	363	2.41	0.8	< 10	29.4	2.5	23.7
14SUBA053A01	43.2	> 3.00	0.81	8.89	1.7	2.29	0.2	39	26.5	1370	2.37	30	< 10	33.7	6.5	3.3
14SUBA065B02	55.2	1.92	1.26	6.9	3.28	1.01	< 0.1	42	41.2	557	5.32	0.3	< 10	21.6	0.5	5.8

Analyte:	Ho	Ag	Cs	Co	Eu	Bi	Se	Zn	Ga	As	Rb	Y	Sr	Zr	Nb	Mo
Unit:	ppm	ppm	ppm	ppm	ppm	ppm	ppm	ppm	ppm	ppm	ppm	ppm	ppm	ppm	ppm	ppm
Detection limit:	0.1	0.05	0.05	0.1	0.05	0.02	0.1	0.2	0.1	0.1	0.2	0.1	0.2	1	0.1	0.05
Analysis method:	TD-MS															
14SUBA026B01	0.8	0.09	1.61	7.6	1.33	0.04	0.1	52.8	17.5	0.5	31.3	18.4	160	34	1.3	1.58
14SUBA053A01	2.5	0.34	6.9	10.1	0.64	0.06	1.6	53.4	33.9	4.6	31.2	68.6	222	339	6	1.39
14SUBA065B02	0.2	< 0.05	18.5	16.7	0.53	1.8	< 0.1	115	20.3	0.7	181	4.6	79.8	4	0.1	< 0.05

Analyte:	In	Sn	Sb	Te	Ba	La	Ce	Pr	Nd	Sm	Gd	Tb	Dy	Cu	Ge	Tm
Unit:	ppm	ppm	ppm	ppm	ppm	ppm	ppm	ppm	ppm	ppm	ppm	ppm	ppm	ppm	ppm	ppm
Detection limit:	0.1	1	0.1	0.1	1	0.1	0.1	0.1	0.1	0.1	0.1	0.1	0.1	0.2	0.1	0.1
Analysis method:	TD-MS															
14SUBA026B01	< 0.1	< 1	< 0.1	< 0.1	229	24	47.7	5.3	18.8	3.5	3.6	0.5	3.1	46.3	0.2	0.4
14SUBA053A01	< 0.1	1	0.2	< 0.1	145	32.9	106	15.8	68	30.7	33.8	4.4	17.6	33.2	0.4	1
14SUBA065B02	< 0.1	< 1	< 0.1	< 0.1	453	2.2	4	0.4	1.5	0.3	0.5	0.1	0.7	26.3	0.3	< 0.1

Analyte:	Yb	Lu	Ta	W	Re	Tl	Pb	Sc	Th	U	Ti	P	S
Unit:	ppm	ppm	ppm	ppm	ppm	ppm	ppm	ppm	ppm	ppm	%	%	%
Detection limit:	0.1	0.1	0.1	0.1	0.001	0.05	0.5	1	0.1	0.1	0.0005	0.001	0.01
Analysis method:	TD-MS							TD-ICP	TD-MS		TD-ICP		
14SUBA026B01	2.4	0.4	< 0.1	< 0.1	0.017	0.21	19.8	8	9.3	1.9	0.0348	0.028	< 0.01
14SUBA053A01	6.9	1.2	1.2	< 0.1	0.002	0.42	143	12	149	160	0.0847	0.013	0.01
14SUBA065B02	0.7	0.1	< 0.1	< 0.1	0.002	1.24	25.6	18	2.1	9.3	0.0827	0.002	< 0.01

(1230 ppm) and Pr (341 ppm). Thorium (1560 ppm) was also anomalous compared to the rest of the whole-rock samples. As noted above, complete results from the whole-rock lithogeochemistry analysis can be found in GDS2015-008 (Bigio and Lentz, 2015).

After analysis via the Ultratrace 6 method (Activation Laboratories Ltd., 2015b), sample 14SUB-A026B01 returned 24 ppm Be, which is significantly higher than the average crustal abundance (Taylor and McLennan, 1985) and may indicate a partially melted sedimentary source rock. Other results of note include Li values from samples 14SUB-A053A01 and 14SUB-A065B02, which were 43 ppm Li and 55 ppm Li, respectively (Table 1).

The whole-rock samples can be grouped into three categories based on having either a strongly positive, strongly negative, or weakly positive or negative Eu anomaly. Positive Eu anomalies could indicate that Eu fractionated into feldspars (usually plagioclase) as they crystallized out of a melt and which were then picked up by new magma that intruded into host rock as a pegmatite. Alternatively, it could represent an Eu-enriched sedimentary source rock, which partially melted to form the magma that later became the pegmatite. Negative Eu anomalies could indicate a source magma that left its Eu-enriched feldspar crystals behind in the magma chamber when it intruded elsewhere into host rock (Rollinson, 1993).

Laser-ablation, multiple-collector, inductively coupled plasma–mass spectrometry geochemistry

Methods

All of the samples collected in 2014 were analyzed on a Resonetics S-155-LR 193 nm excimer laser ablation system and an Agilent 7700x quadrupole ICP-MS at the University of New Brunswick, using NIST-610, NIST-612 and BCR2G glass standards. Ablation sequences were set up for each group of slides focusing on the contacts between biotite and potassium-feldspar crystals, or muscovite and potassium-feldspar crystals if the sample contained no biotite. Ablation tracks were set to run perpendicular to mica cleavages, and across mica-feldspar grain boundaries where contacts were present between the minerals (Figure 4), in order to determine whether there was any compositional zoning in the micas or any concentration of REEs along mica cleavages or at the edges of the feldspar grains. When present, minerals such as titanite or tourmaline were also ablated to determine if they showed any compositional zoning or areas of REE concentration. The ablations were set to a depth of 60 μm at 30 Hz laser frequency over 60 s.

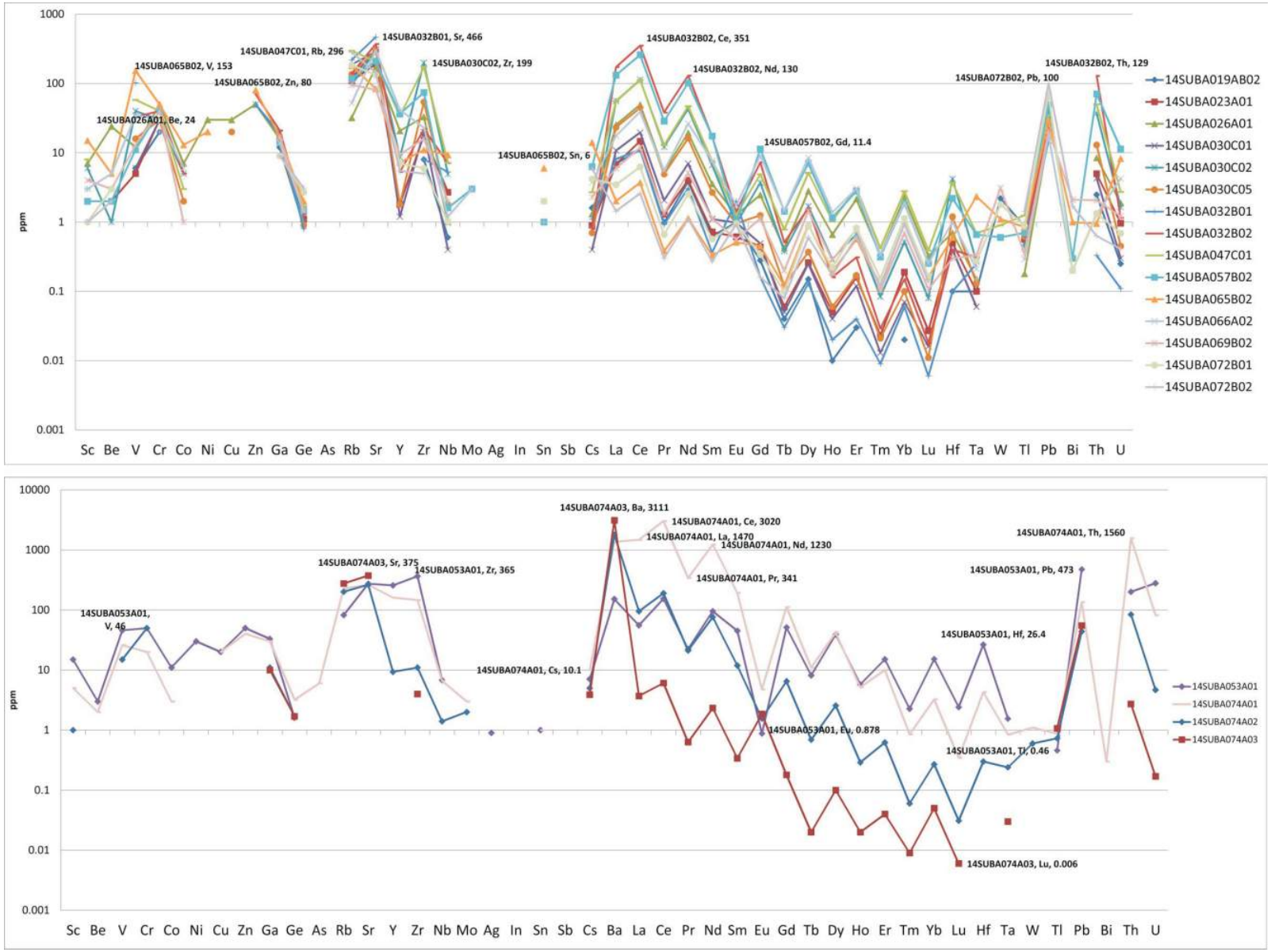

Figure 3: Extended element plots of the 19 whole-rock geochemistry samples (Hall Peninsula, Baffin Island). Elements are on the x axis, while the y axis is in ppm and is logarithmic. Selected high and low values have been labelled. Gaps in the lines indicate that analyses were below the detection limit for that element; detection limits for each element are provided in GDS2015-008 (Bigio and Lentz, 2015).

Data collected during the analyses is being processed and results are pending.

U-Pb geochronology and field-emission scanning electron microscope (FE-SEM) imaging

The crushed reject remainders from seven samples (14SUB-A026B01, A032B02, A047B01, A053B02, A057B02, A065B02 and A074A01) were submitted to Overburden Drilling Management Ltd. (ODM) of Ottawa, Ont., for preparation of heavy mineral separates and corresponding zircon and monazite concentrates. Zircons and monazites were picked from the heavy mineral separates. The remainder of each sample is stored at the University of New Brunswick in case further analysis is needed.

Samples were selected for U-Pb geochronology on the basis of having higher-than-background radioactivity, as determined by the field usage of a GR-135 Plus radioisotope detector (Bigio et al., 2015). Pegmatites with high gamma-ray activity compared to background levels were determined to be good potential sources of minerals suitable for radiometric dating, or possible uranium mineralization. After heavy-mineral picking, samples A053A01 and A057B02 were determined to contain uraninite/thorianite grains in the pan concentrates. From the whole-rock geochemistry (Bigio and Lentz, 2015), A053A01 showed elevated U (279 ppm) and Th (201 ppm), as well as the highest Pb value (473 ppm) of the 19 samples, and was enriched in both LREEs and heavy rare-earth elements (HREEs). Sample A057B02 did not show comparably elevated U, Th or Pb, but was also enriched in REEs; A053A01 had more enrichment in HREEs while A057B02 was more enriched in LREEs.

The monazite grains selected for dating were imaged using a Hitachi SU-70 field-emission scanning electron microscope (FE-SEM) at the University of New Brunswick, to determine if the crystals showed compositional zoning prior to U-Pb geochronology analysis. This process was to ensure that analyses done on individual grains would come from the same compositional zone.

Initial examination of the geochronological data acquired suggests that the dated pegmatites have an approximate age of 1.8 Ga; further detailed analysis of the data is pending.

Discussion and implications for rare element mineralization potential

Initial geochronological data obtained from 7 of the pegmatite samples provide a preliminary age of 1.8 Ga. These data, combined with field relationships, particularly cross-cutting relationships and deformation, suggest that the pegmatites marginally postdate the peak metamorphism in the southern Hall Peninsula region of the Trans-Hudson Orogen, which occurred between 1850 and 1830 Ma (Skipton et al., 2014; Rayner, 2015).

Using the trace-element discrimination diagrams of Pearce et al. (1984) to plot the whole-rock geochemistry data, a syncollisional-volcanic arc (S- to I-type) granitic source for most of the sampled pegmatites is suggested (Figure 5).

Geochemistry results to date indicate that the potential for economic rare-element mineralization in the southern Hall Peninsula region appears to be low. Although many of the whole-rock geochemistry samples did show elevated LREE and/or HREE quantities, only one sample (14SUB-A074) returned ‘showing-level’ REE quantities, using the

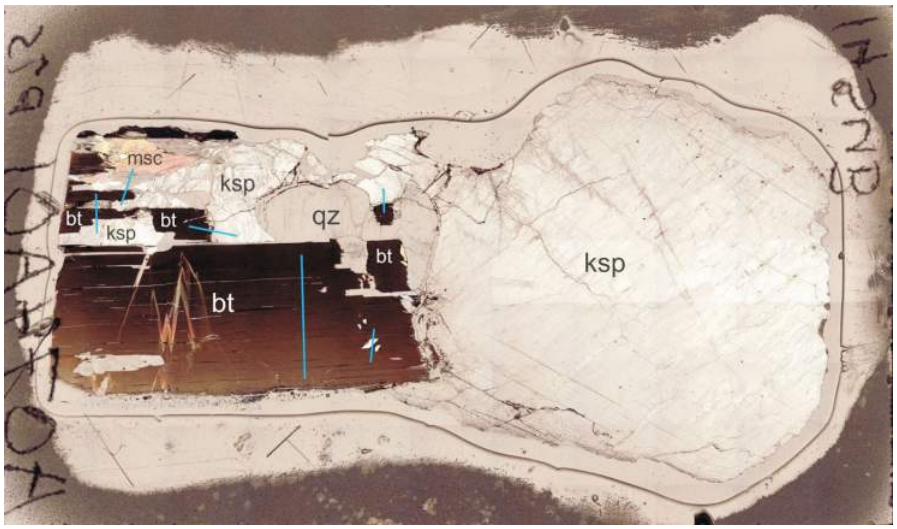

Figure 4: Mosaic image of thin section of sample 14SUB-A074A01 (Hall Peninsula, Baffin Island). Blue lines indicate potential laser-ablation, multiple-collector, inductively coupled plasma–mass spectrometry LA-MC-ICP-MS ablation tracks; not all proposed tracks were used for each sample. Tracks were selected to be perpendicular to mica cleavage and to cross mica-feldspar grain boundaries. Abbreviations: bt, biotite; ksp, K-feldspar; msc, muscovite; qz, quartz. Slide is 26 by 46 mm.

criteria applied for a showing to be considered significant (with a cutoff grade of 0.2% for rare-earth elements and 0.25% for REE oxides) for inclusion in the Nunavut Mineral Occurrence and Reference Database (NUMIN; Markey et al., 2015).

However, occurrences of white beryl, pink tourmaline and green spodumene have been reported from central and northern Baffin Island (Bell, 1992) and elsewhere in the territory, so it is possible that the pegmatites exposed on the southern Hall Peninsula represent the REE-barren zone closest to their parent granite or granites (Selway et al., 2005). It is also possible that these more northern occurrences may be related to different tectonic or petrogenetic processes than the Hall Peninsula pegmatites; but whether

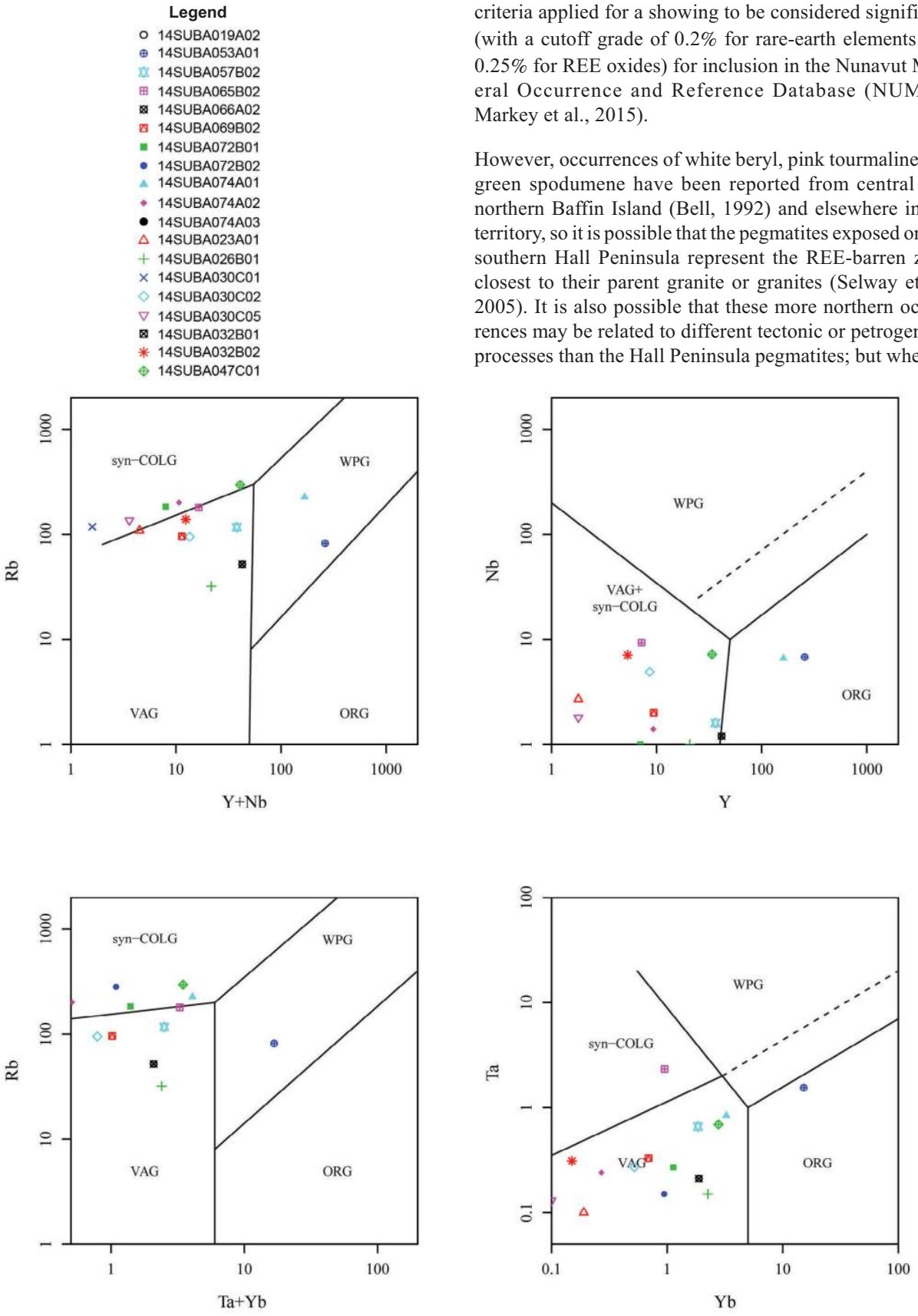

Figure 5: Tectonic discrimination diagram after Pearce et al. (1984). Samples collected from Hall Peninsula, Baffin Island. Abbreviations: VAG, volcanic arc granite; ORG, orogenic granite; WPG, within-plate granite; syn-COLG, syncollisional granite.

the two populations are related or not, there may still be economic pegmatite potential on Baffin Island.

Economic considerations

Pegmatites are major sources of economically significant elements, such as Li, Cs, Ta and Sn, and rare-earth elements (REEs), as well as ceramic-grade feldspar and electronics-grade quartz, and gems such as beryl or gem-quality tourmaline (Bigio et al., 2015).

The global markets for lithium and REEs are currently supplied primarily by Australia, Chile and China. However, the potential for economic deposits of rare-earth elements and rare metals exists in several places in Canada (e.g., Northwest Territories, Ontario, Quebec, Newfoundland, Nova Scotia, Nunavut). Although no REE production or refining is currently taking place in Canada, the investment and political climates are stable and the mining industry has the necessary expertise (House of Commons, Standing Committee on Natural Resources, 2014) to ultimately begin mining REEs for market.

Several companies in Canada are exploring for, or producing, lithium; in particular, Canada Lithium Corp. produced lithium carbonate at its Quebec Lithium property between 2013 and 2015, and Nemaska Lithium Inc. is in the permitting process for its Whabouchi lithium deposit (Met-Chem Canada Inc., 2014), both of which are in Quebec. Demand for REEs and other rare metals and elements is expected to increase worldwide due to increasing demand for advanced electronics products and clean energy applications (CREEN, 2013). Therefore, increased supply of these commodities would be beneficial to the Canadian economy (House of Commons, Standing Committee on Natural Resources, 2014).

Summary

Although rare-metal, REE and gem potential of the southern Hall Peninsula pegmatites appears to be low, further analysis of the LA-MC-ICP-MS data is currently being completed. Reports of REE-bearing minerals from other parts of Baffin Island, including tourmaline and beryl, indicate that such potential may be higher elsewhere on the island.

Detailed analysis of the U-Pb geochronological data is expected to further refine the age of the dated pegmatites, allowing them to be more accurately placed in the tectonic history of the southern Hall Peninsula.

Acknowledgments

The authors would like to thank H. Steenkamp, C. Gilbert and the Canada-Nunavut Geoscience Office for their financial, logistical and technical support of this project; the Canadian Northern Economic Development Agency's (CanNor) Strategic Investments in Northern Economic Development (SINED) program, which also provided funding for the HPIGP; D. Lentz in his capacity as M.Sc. advisor to the corresponding author; B. Boucher and C. MacFarlane with the Laser Ablation-MC-ICP-MS lab at the University of New Brunswick for LA-MC-ICP-MS analysis and U-Pb geochronology; S. Boonsue at the Planetary and Space Sciences Centre at the University of New Brunswick for SEM imaging; P. Budkewitsch, L.J. Ham and M.D. Young for their content review; T. Sifrer with RnD Technical for technical editing; G. Moore at Indigenous and Northern Affairs Canada (INAC) for cartography assistance; and the Nunavut Regional Office of INAC.

References

Activation Laboratories Ltd., 2015a: 4Lithores: lithium metaborate/tetraborate fusion-ICP and ICP/MS; Activation Laboratories Ltd., website, URL <http://www.actlabs.com/list.aspx?menu=64&app=226&cat1=549&tp=12&lk=no> [October 2015].

Activation Laboratories Ltd., 2015b: Ultratrace 6: total digestion-ICP and ICP/MS; Activation Laboratories Ltd., website, URL <http://www.actlabs.com/page.aspx?page=510&app=226&cat1=549&tp=12&lk=no&menu=64 > [October 2015].

Bell, R. 1992: Compilation of lapidary sites of the Northwest Territories: a report done for the Department of Energy, Mines and Petroleum Resources, Government of the Northwest Territories; Department of Indian Affairs and Northern Development, NWT Geology Division, EGS Open File 1992-14, 157 p.

Bigio, A. and Lentz, D. 2015: Data table accompanying "Preliminary lithogeochemistry and geochronology of pegmatites of the Hall Peninsula, Baffin Island, Nunavut: implications for REE mineralization potential"; Canada-Nunavut Geoscience Office, Geoscience Data Series GDS2015-008, Microsoft® Excel® file, URL <http://cngo.ca/summary-of-activities/2015/> [December 2015].

Bigio, A., Budkewitsch, P. and Lentz, D. 2015: Location and characterization of pegmatites in the southern Baffin Island region: field and satellite observations; *in* Summary of Activities 2014, Canada-Nunavut Geoscience Office, p. 1–10.

Boynton, W.V. 1985: Cosmochemistry of the rare earth elements: meteorite studies; *in* Rare Earth Element Geochemistry, Developments in Geochemistry 2, P. Henderson (ed.), Elsevier, Amsterdam. p. 63–114.

Canadian Rare Earth Elements Network (CREEN) 2013: Global REE production; Canadian Institute of Mining, Metallurgy and Petroleum, website, URL <http://www.cim.org/en/RareEarth/Home/GlobalReeProduction.aspx> [October 2015].

Černý, P. and Ercit, T.S. 2005: The classification of granitic pegmatites revisited; The Canadian Mineralogist, v. 43, p. 2005–2026.

Černý, P., London, D. and Novák, M. 2012: Granitic pegmatites as reflections of their sources; Elements v. 8, p. 289–294.

Dyck, B.D. and St-Onge, M.R. 2014: Dehydration-melting reactions, leucogranite emplacement and the Paleoproterozoic structural evolution of Hall Peninsula, Baffin Island,

Nunavut; *in* Summary of Activities 2013, Canada-Nunavut Geoscience Office, p. 73–84.

From, R.E., St-Onge, M.R. and Camacho, A. 2014: Preliminary characterization of the Archean orthogneiss complex of Hall Peninsula, Baffin Island, Nunavut; *in* Summary of Activities 2013, Canada-Nunavut Geoscience Office, p. 53–62.

House of Commons, Standing Committee on Natural Resources 2014: The rare earth elements industry in Canada: summary of evidence, 41st Parliament, Second Session, June 2014; House of Commons, Canada, URL <http://www.parl.gc.ca/Content/HOC/Committee/412/RNNR/WebDoc/WD6669744/412_RNNR_reldoc_PDF/RareEarthElements-Summary-e.pdf> [October 2015].

Markey, A., Budkewitsch, P., Basso, S.L. and Sharpe, S. 2015: NUMIN: online access to information about mineral showings and exploration-project documents at NunavutGeoscience.ca; *in* Summary of Activities 2015, Canada-Nunavut Geoscience Office, p. 201–208.

Met-Chem Canada Inc. 2014: NI43-101 Technical report: feasibility study on the Whabouchi lithium deposit and hydromet plant; prepared for Nemaska Lithium Inc., URL <http://www.nemaskalithium.com/Documents/files/43-101/nemaska-lithium-whabouchi-feasibility-study.pdf> [October 2015].

Rayner, N.M. 2015: New (2013–2014) U-Pb geochronological results from northern Hall Peninsula, southern Baffin Island, Nunavut; *in* Summary of Activities 2014, Canada-Nunavut Geoscience Office, p. 31–44.

Rollinson, H. 1993: Using Geochemical Data: Evaluation, Presentation, Interpretation; Taylor and Francis, New York, 352 p.

Selway, J., Breaks, F.W. and Tindle, A.G. 2005: A review of rare-element (Li-Cs-Ta) pegmatite exploration techniques for the Superior Province, Canada, and large worldwide tantalum deposits; Exploration and Mining Geology, v. 14, p. 1–30.

Skipton, D.R. and St-Onge, M.R. 2014: Paleoproterozoic deformation and metamorphism in metasedimentary rocks west of Okalik Bay: a field template for the evolution of eastern Hall Peninsula, Baffin Island, Nunavut; *in* Summary of Activities 2013, Canada-Nunavut Geoscience Office, p. 63–72.

Taylor, S.R. and McLennan, S.M. 1985: The continental crust: its composition and evolution, Blackwell Scientific Publications, Oxford, 312 p.

Frobisher suite mafic, ultramafic and layered mafic-ultramafic sills, southern Baffin Island, Nunavut

D.A. Liikane[1], M.R. St-Onge[2], B.A. Kjarsgaard[2], N.M. Rayner[2], R.E. Ernst[1,3] and N. Kastek[1]

[1]*Department of Earth Sciences, Carleton University, Ottawa, Ontario, dustinliikane@cmail.carleton.ca*

[2]*Natural Resources Canada, Geological Survey of Canada, Ottawa, Ontario*

[3]*Ernst Geosciences, 43 Margrave Avenue, Ottawa, Ontario*

This work is part of the larger South Baffin mapping project, a partnership between the Canada-Nunavut Geoscience Office (CNGO) and Natural Resources Canada's (NRCan) Geo-mapping for Energy and Minerals (GEM) program on Baffin Island. This particular mapping project is being led by the Geological Survey of Canada (GSC) in collaboration with CNGO, the Government of Nunavut, Nunavut Arctic College, Carleton University and Oxford University. Logistical support is provided by the Polar Continental Shelf Project and several local, Inuit-owned businesses. The study area comprises all or parts of six 1:250 000 map areas north of Iqaluit (NTS areas 26B, C, F, G, J and K). The objective of the work is to complete the regional bedrock mapping for the southern half of Baffin Island and provide a new, modern, geoscience understanding of this part of eastern Nunavut.

Liikane, D.A., St-Onge, M.R., Kjarsgaard, B.A., Rayner, N.M., Ernst, R.E. and Kastek, N. 2015: Frobisher suite mafic, ultramafic and layered mafic-ultramafic sills, southern Baffin Island, Nunavut; *in* Summary of Activities 2015, Canada-Nunavut Geoscience Office, p. 21–32.

Abstract

Presented in this paper, are the 2015 field observations from the Frobisher suite of mafic and mafic-ultramafic sills of southern Baffin Island; geochemical data from mafic/ultramafic samples collected during the 2014 field season on Meta Incognita Peninsula; and U-Pb geochronological results from a leucogabbroic sample of the upper portion of a layered mafic-ultramafic sill. The Frobisher suite sills are emplaced into the psammitic to pelitic metasedimentary strata of the middle Paleoproterozoic Lake Harbour Group. The sills vary in thickness from a few metres to a hundred metres and layering within both mafic and mafic-ultramafic bodies occurs at the centimetre to metre scale. Disseminated sulphides are present in the sills, and in some cases, the adjacent host psammite. Lithologically, the sills vary from pyroxenite/peridotite at the base to gabbro/leucogabbro at the top. Similar sills have been documented throughout southern Baffin Island (including Foxe, Hall and Meta Incognita peninsulas), and a mantle-derived mafic-ultramafic magmatic province of this size may represent the exposed plumbing system of a large igneous province (LIP). Based on major- and trace-element chemistry, the Frobisher suite can be divided into four subgroups. Uranium-lead dating of a leucogabbroic sample from the top of a layered mafic-ultramafic sill was done using the sensitive high-resolution ion microprobe (SHRIMP) and isotope dilution–thermal ionization mass spectrometry (ID-TIMS). A minimum crystallization age of ca. 1900 Ma is suggested based on the preliminary data.

Résumé

Ce document présente les observations de terrain faites en 2015 au sujet des filons-couches mafiques et mafiques-ultramafiques de la suite de Frobisher dans la partie sud de l'île de Baffin; des données géochimiques obtenues à partir d'échantillons mafiques ou ultramafiques recueillis au cours de la campagne de terrain de 2014 dans la péninsule Meta Incognita; et des résultats de datation géochronologique U-Pb sur un échantillon de leucogabbro provenant de la partie supérieure d'un filon-couche lité mafique-ultramafique de la péninsule Meta Incognita. Les filons-couches de la suite de Frobisher ont été mis en place dans les strates psammitiques à pélitiques du groupe de Lake Harbour, datant du Paléoprotérozoïque moyen, et leur épaisseur varie entre quelques mètres à une centaine de mètres. Une stratification d'ordre centimétrique à métrique caractérise les intrusions mafiques et ultramafiques et on a noté la présence de sulfures disséminés aussi bien au sein des filons-couches qu'à certains endroits dans des unités adjacentes de psammite encaissante. La composition des filons-couches varie de la pyroxénite ou péridotite à la base, jusqu'au gabbro ou leucogabbro au sommet. La présence de filons-couches semblables a été remarquée dans la partie sud de l'île de Baffin (y compris les péninsules Foxe, Hall et Meta Incog-

This publication is also available, free of charge, as colour digital files in Adobe Acrobat® PDF format from the Canada-Nunavut Geoscience Office website: http://cngo.ca/summary-of-activities/2015/.

nita) et il se peut qu'une province magmatique mafique-ultramafique d'origine mantellique de cette taille puisse représenter un exemple mis à nu du système d'alimentation à l'origine d'une importante province ignée. En fonction des résultats obtenus des analyses des éléments majeurs et à l'état de traces, la suite de Frobisher peut être divisée en quatre sous-groupes. Les données préliminaires obtenues de la datation géochronologique U-Pb sur un échantillon de leucogabbro provenant du sommet d'un filon-couche mafique-ultramafique au moyen de la microsonde ionique à haute résolution et à haute sensibilité (SHRIMP) et de l'analyse par dilution isotopique et spectrométrie de masse à thermo-ionisation (ID-TIMS) semblent indiquer un âge minimum de cristallisation d'environ 1900 Ma.

Introduction

Presented in this paper is an overview of the characteristics and economic potential of the mafic and mafic-ultramafic sills of the Frobisher suite, based on field observations from the Clearwater Fiord, McKeand River, Sylvia Grinnell Lake, Amittok Lake, Irvine Inlet and Chidliak Bay map areas of southern Baffin Island (Figure 1). In addition, this paper includes geochemical and preliminary geochronological data from samples collected during the 2014 field season on Meta Incognita Peninsula (see St-Onge et al., 2015a for field observations). The geochemical data are used to demonstrate variation within the Frobisher suite sills on Meta Incognita Peninsula, and the preliminary geochronological data provide a first minimum-crystallization age for this suite.

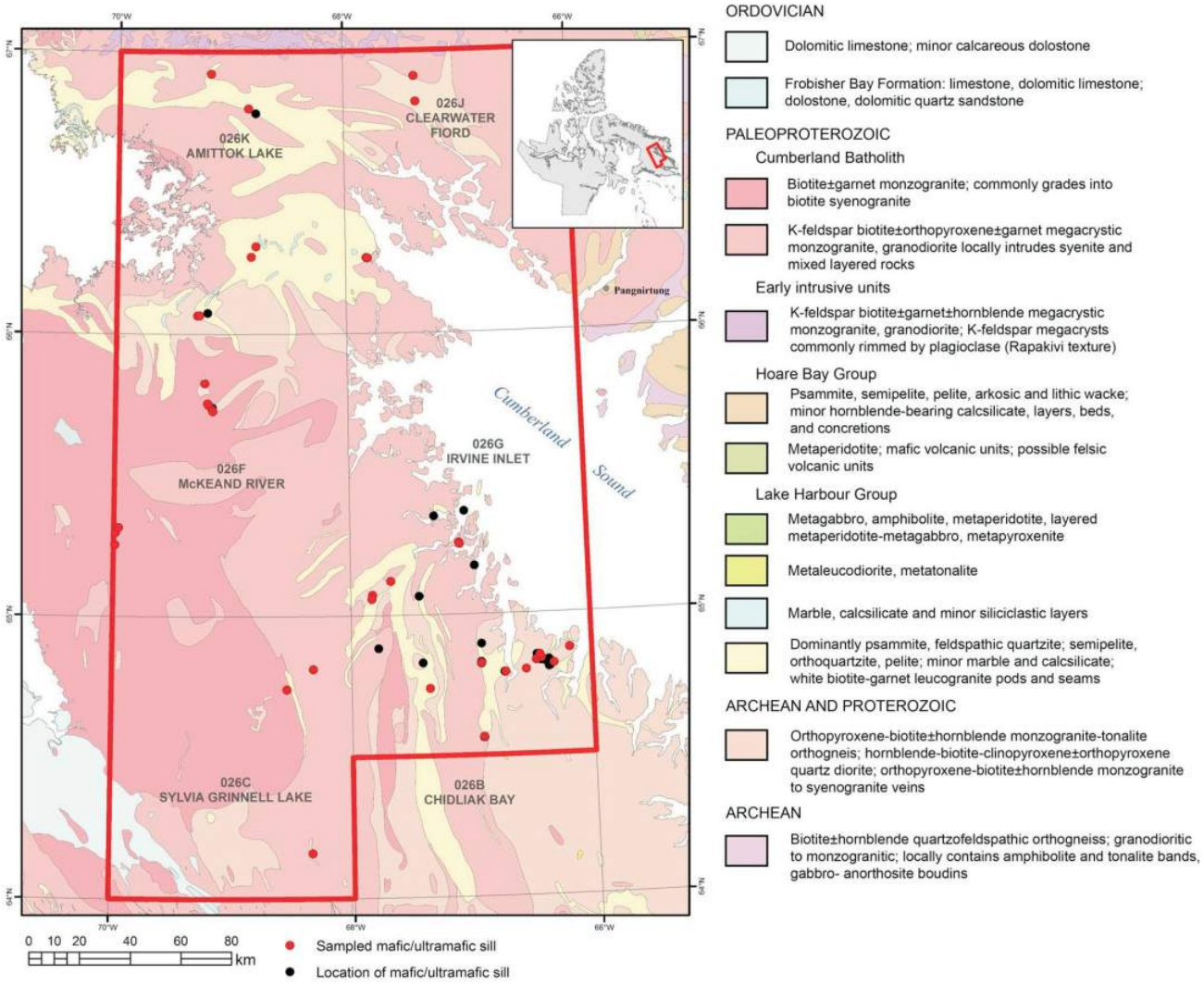

Figure 1: Simplified geological map of the central area of southern Baffin Island, Nunavut, showing locations of mafic and mafic-ultramafic sills. Intrusions sampled for geochemical analyses are shown in red.

Summary of 2015 field observations from the central area of southern Baffin Island

The Geo-mapping for Energy and Minerals (GEM) program, led by Natural Resources Canada (NRCan) in conjunction with the Canada-Nunavut Geoscience office (CNGO) in Nunavut, targeted the central area of southern Baffin Island in 2015, thus effectively completing the regional bedrock mapping for southern Baffin Island (Weller et al., 2015). The fieldwork was carried out between June 21th and August 18th and covered parts of NTS map areas 26B, C, F, G, J and K. The current project is part of the South Baffin project, led by the Geological Survey of Canada (GSC) in collaboration with the Canada-Nunavut Geoscience Office (CNGO), the Government of Nunavut, Nunavut Arctic College, Carleton University and Oxford University.

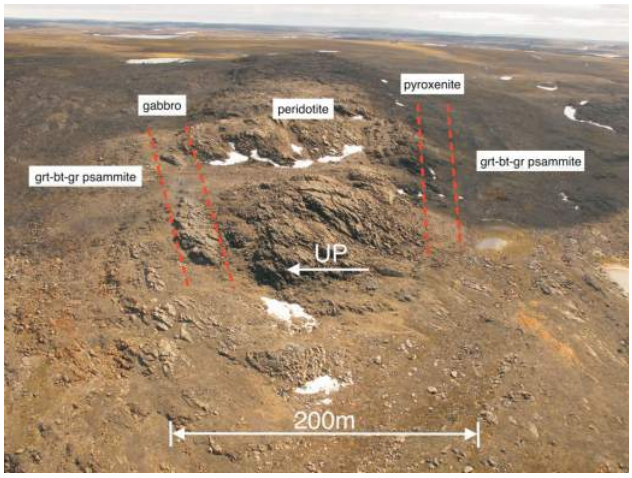

Figure 2: The northern sill (15SAB-L075A–15SAB-L081A), Hall Peninsula, Baffin Island. Detailed sampling was conducted across this structurally overturned layered mafic-ultramafic sill in order to determine the petrogenesis of the Frobisher magmatic suite from a regional perspective. The sill comprises a basal clinopyroxenite, overlain by peridotite, overlain by gabbro and capped by leucograbbro.

Figure 3: Layered metagabbro (15SAB-L080A), Hall Peninsula, Baffin Island. Rhythmic layering is a result of differences in the modal abundances in plagioclase, clinopyroxene and hornblende; hammer is 75 cm in length.

Geological Framework

The metaplutonic and metasedimentary units of the central area of southern Baffin Island form part of the northeastern segment of the Trans-Hudson Orogen; an orogenic belt that extends from northeastern to south-central North America in a broad arcuate shape (Hoffman, 1988; Lewry and Collerson, 1990). This belt comprises tectonostratigraphic packages that were either accumulated on, or accreted to, the northern margin of the lower-plate Paleoarchean to Neoarchean Superior craton during the middle Paleoproterozoic (St-Onge et al., 2006, 2009). Southern Baffin Island can be subdivided into three orogen-scale stacked tectonic elements (St-Onge et al., 2002, 2015b) all separated by major deformation zones. The crustal construct of southern Baffin Island includes the metasedimentary and metavol-

Figure 4: Layered metaperidotite (15SAB-L077A), Hall Peninsula, Baffin Island. Rhythmic layering is a result of differences in the modal abundances of clinopyroxene, orthopyroxene and olivine; hammer is 75 cm in length.

Figure 5: Basal metaclinopyroxenite (15SAB-L076A), Hall Peninsula, Baffin Island; hammer is 75 cm in length.

64°N
63°N
62°N
66°W
68°W
70°W
72°W
Iqaluit
Frobisher Bay
HUDSON STRAIT
14SAB-L017A
Location of mafic/ultramafic sill:
Group A
Group B
Group C
Group D
Not Sampled
0
10
20
40
60
80
km

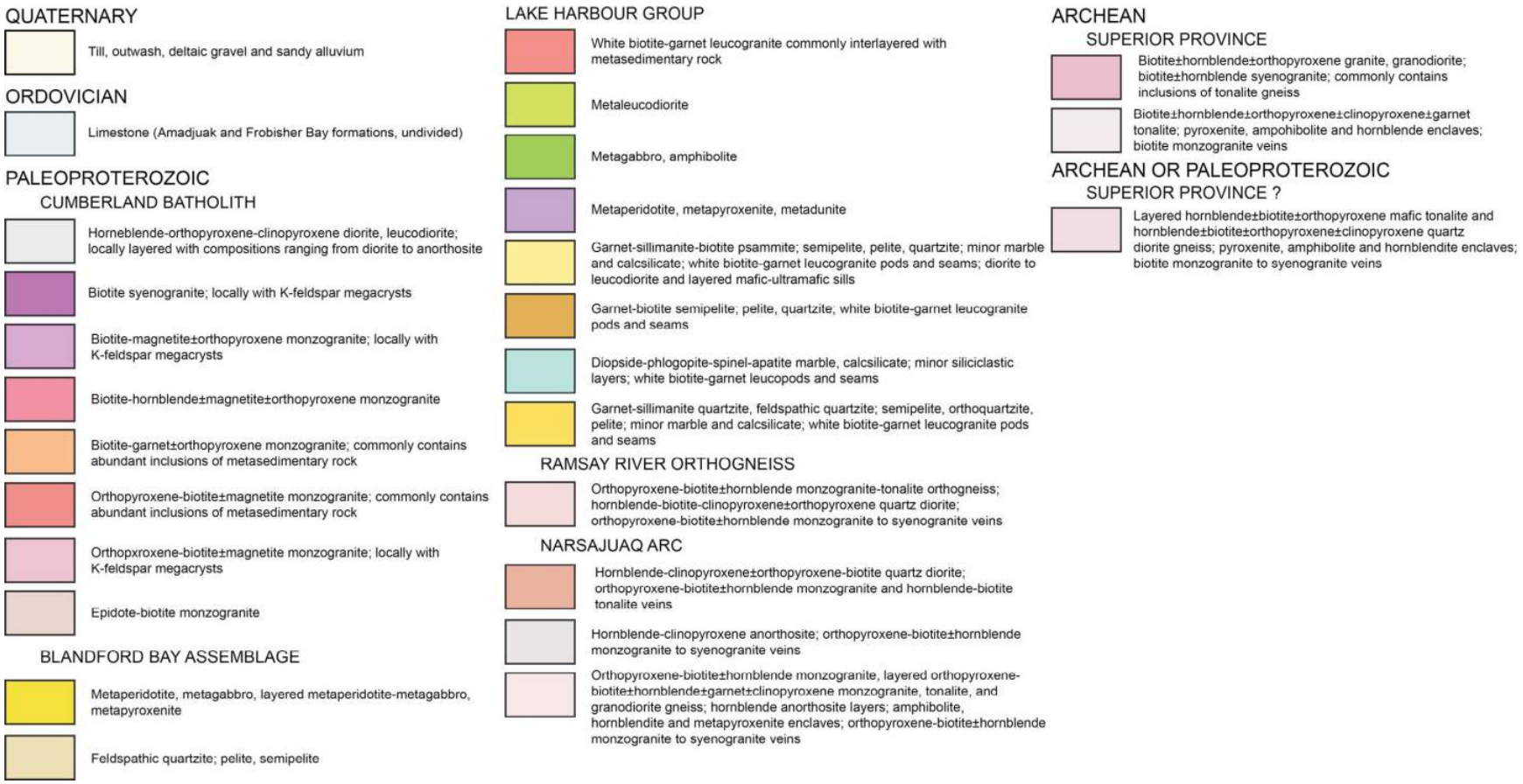

Figure 6 (previous page and this page): Detailed bedrock geology map of on Meta Incognita Peninsula, Baffin Island, showing locations of the mafic, ultramafic and layered mafic-ultramafic sills. Intrusions sampled for geochemical and/or geochronological analysis are shown in their respective group's symbol. Group A (blue star symbols) displays a relatively flat pattern; group B (green triangle symbols) displays a gently sloping pattern; group C (purple cross symbols) displays a steeply sloping pattern, with a significant positive europium anomaly; group D (red cross symbols) is similar to group B, but has a steeper mid to heavy rare-earth element pattern.

canic strata of the Lake Harbour Group (Jackson and Taylor, 1972), and underlying orthogneiss, units that are interpreted as the cover sequence and crystalline basement, respectively, of the accreted middle Paleoproterozoic Meta Incognita microcontinent (St-Onge et al., 2000). The cover and basement units are intruded by various mafic to felsic plutons of the Cumberland Batholith (Whalen et al., 2010).

Lake Harbour Group

The psammite, semipelite, pelite, quartzite, marble and amphibolite rock strata, mapped in the central area of southern Baffin Island, belong to the middle Paleoproterozoic Lake Harbour Group. The supracrustal sequence is volumetrically dominated by garnetiferous psammite and pelite, with graded bedding locally preserved. Southwest of Clearwater Fiord, marble and calcsilicate layers become more prevalent and are characterized by diopside-scapolite-phlogopite, and locally magnetite-rich mineral assemblages. The siliciclastic strata are locally sulphidic.

Frobisher suite

The newly recognized Frobisher suite (informally named after the suite's geographic proximity to Frobisher Bay, Baffin Island, Nunavut) comprises concordant to slightly discordant sheets of variably altered coarse-grained metaperidotite, medium- to coarse-grained metaperidotite-metagabbro, and medium-grained metagabbro emplaced into the siliciclastic strata of the Lake Harbour Group. Commonly, the mafic-ultramafic sills vary lithologically from pyroxenite at the base, overlain by peridotite, and capped by gabbro to leucogabbro at the top (Figure 2); a sequence that provides a way-up indicator, if layering is due to gravity-induced magmatic differentiation. A single mafic-ultramafic gradational sequence is interpreted as due to a single pulse of magma. In map view, the intrusive bodies appear elongate to lensoid in shape, with thicknesses typically ranging from 5 to 20 m—although a few reach 100 m in thickness—and in most cases extend for several kilometres along strike. During the terminal collision of the Trans-Hudson orogeny (1820–1795 Ma; St-Onge et al., 2009), the sills were folded and/or overturned. Metamorphic mineral assemblages indicate that amphibolite- to granulite-facies metamorphic conditions were reached during the Trans-Hudson orogeny (St-Onge et al., 2007b).

Metagabbro

The majority of the mafic intrusions of the Frobisher suite are characterized by faint, to well-defined, centimetre- to metre-scale rhythmic layering (Figure 3) defined by variations in modal abundance of plagioclase, clinopyroxene and hornblende. A minority of the intrusions are homogeneous. The layering is parallel to the intrusive contacts, consistent with emplacement as sills.

Metaperidotite and metapyroxenite

The ultramafic bodies comprise clinopyroxene-orthopyroxene-olivine metaperidotite (Figure 4) and clinopyroxene-orthopyroxene metapyroxenite (Figure 5), and are particularly well layered. In contrast to the homogeneous ultramafic sills that occur on Meta Incognita Peninsula (St-Onge et al., 2015a), the ultramafic units mapped in 2015 are part of layered mafic-ultramafic bodies. Evidence for partial melting or of enclaves of host strata within the sills was not observed. Many intrusions contain disseminated sulphide mineralization—mostly pyrite and/or chalcopyrite, <1 mm in grain size. Deep orange gossans occur in the host psammite adjacent to some of the mafic-ultramafic sills, and commonly contain significant amounts of visible disseminated sulphide minerals.

In addition to the regional sampling of mafic and mafic-ultramafic sills in the project area, detailed sampling was conducted on a structurally overturned layered mafic-ultramafic sill on Hall Peninsula (Figure 2; the 'northern sill' of Steenkamp et al., 2014). Samples were collected starting at the basal contact of the sill, and upward through the internal magmatic stratigraphy to the upper contact. From stratigraphic bottom to top, the sill comprises a basal clinopyroxenite, overlain by peridotite (volumetrically the dominant component), overlain by gabbro and capped by leucogabbro.

Analytical results from 2014 fieldwork on Meta Incognita Peninsula

Geochemistry

Figure 6 indicates the locations of geochemistry samples collected from mafic, ultramafic and mafic-ultramafic sills during the 2014 mapping program (St-Onge et al., 2015b) on Meta Incognita Peninsula, Baffin Island, Nunavut; a subset of sills display evidence of igneous layering. A geochemical data table (see Geochemistry, Liikane et al., 2015[4]) for these samples can be found in the data repository for the 2015 edition of the CNGO Summary of Activities.

The sample suite has MgO ranging from 1 to 30 wt. %. Average Ni (1500 ppm) and Cr (3000 ppm) concentrations are high, and decrease with decreasing Mg# (Figure 7). Based on major- and trace-element chemistry, the Frobisher suite can be divided into four groups, which correlate with modal mineralogy and layering. These can be discriminated using chondrite-normalized rare-earth element (REE) plots (Figure 8).

[4]*CNGO Geoscience Data Series GDS2015-014, containing the data or other information sources used to compile this paper, is available online to download free of charge at http://cngo.ca/summary-of-activities/2015/.*

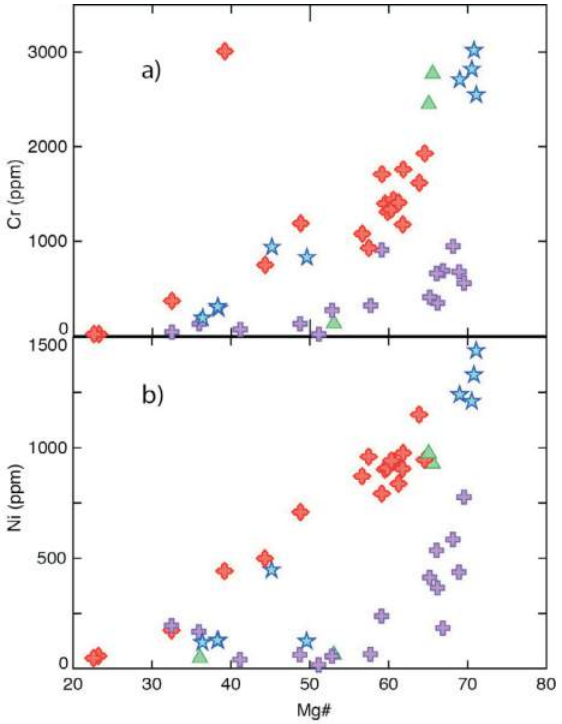

Figure 7: Mafic/ultramafic samples from the Frobisher suite collected from Meta Incognita Peninsula, Baffin Island, showing a decrease in abundance of both a) Cr and b) Ni as Mg# decreases.

Group A (blue star symbols; Figure 8a) exhibits a flat REE pattern, similar to mid-ocean–ridge basalt (MORB), with La/Yb ratios of ~1.8. Group A comprises peridotitic and pyroxenitic units.

Group B (green triangle symbols; Figure 8b) has more enriched light rare-earth element (LREE) patterns, while maintaining a flat heavy rare-earth element (HREE) pattern, with La/Gd ratios of ~2.6 and Gd/Yb ratios of ~1.4. This group includes gabbroic, peridotitic and pyroxenitic units. Samples from group B may simply be crustally contaminated variants of group A, given group B's elevated LREE contents.

Group C (purple cross symbols; Figure 8c) is characterized by an enriched REE pattern, with average La/Gd and Gd/Yb ratios of 7.7 and 2.5, respectively. Also characteristic, is a positive Eu anomaly with Eu/Eu* ranging from 0.72 to 3.24, consistent with accumulated plagioclase. Group C comprises leucogabbroic and peridotitic units. Approximately one half of the samples from group C are spatially associated with samples from group A. Processes such as magmatic differentiation and cumulate precipitation could be the cause of the contrasting REE patterns between the two groups.

Group D (red cross symbols; Figure 8d) shows an enriched REE pattern, with average La/Gd and Gd/Yb ratios of 2.9 and 2.6, respectively. Lithologically, group D includes gabbroic, peridotitic and pyroxenitic units. Group D has a

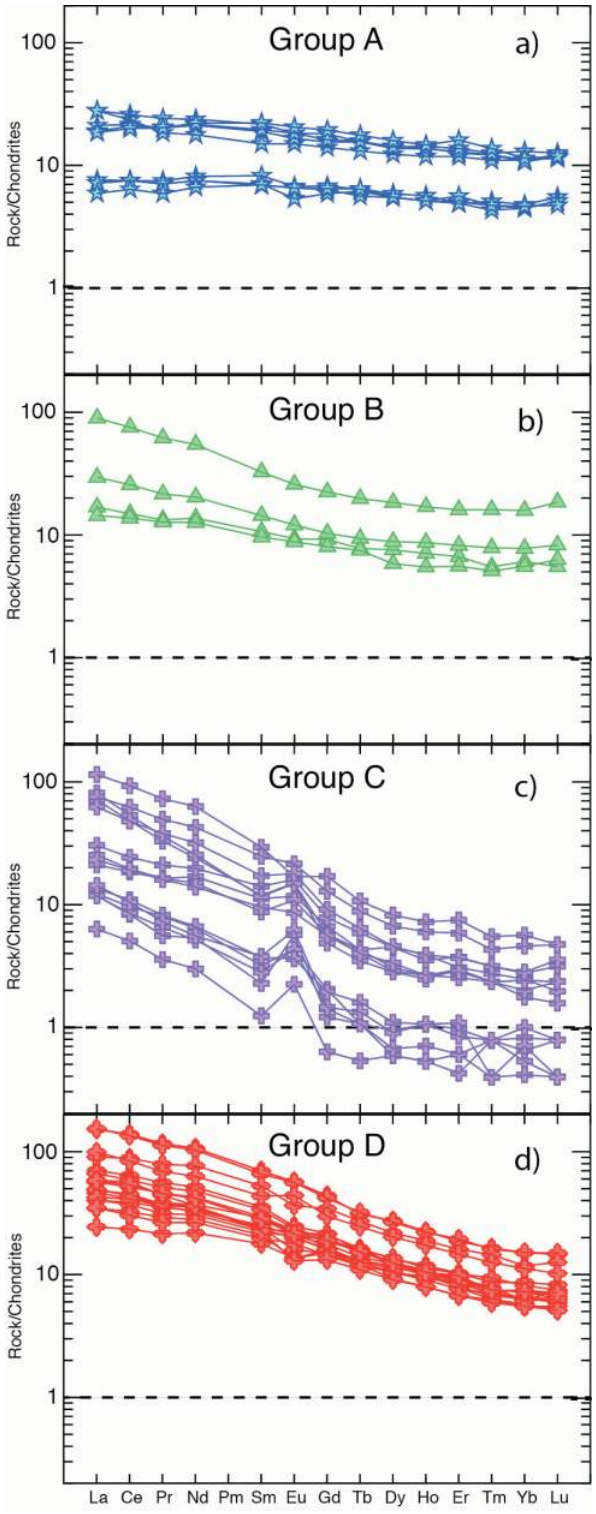

Figure 8: Rare-earth element plots (chondrite-normalization values from Sun and McDonough, 1989), differentiating four distinct groups of rocks from the Frobisher suite on Meta Incognita Peninsula, Baffin Island, Nunavut: **a)** group A (blue star symbols) displays a relatively flat pattern; **b)** group B (green triangle symbols) displays a gently sloping pattern; **c)** group C (purple cross symbols) displays a steeply sloping pattern, with a significant positive europium anomaly; **d)** group D (red cross symbols) is similar to group B, but has a steeper mid to heavy rare-earth element pattern.

variety of trace-element geochemical traits that suggest it is distinctive from group A (Figure 9). Group D has more fractionated REE, and it is relatively enriched in Ti and Th-Nb-Ta. This is illustrated in Figure 9, where two samples from each group are shown, one at 6 wt. % MgO (most evolved) and the other at 22 wt. % MgO contents (least evolved).

Geochronology

To determine the age of the Frobisher suite, a leucogabbroic sample (14SAB-L017A; location shown in Figure 6) from south-central Meta Incognita Peninsula was selected for U-Pb geochronology with the sensitive high-resolution ion microprobe (SHRIMP) and with isotope dilution–thermal ionization mass spectrometry (ID-TIMS), at the Geological Survey of Canada. Abundant, high-quality, clear, colourless zircon grains were recovered from the leucogabbro. The zircon grains are morphologically diverse: anhedral (Figure 10a), prismatic (Figure 10b) or rounded (not shown), and simply zoned (Figure 10c, d) with no apparent core/overgrowths.

Twenty-five analyses, via SHRIMP, of 22 zircon grains encompassing the full morphological range yielded ages ranging from 2004 to 1833 Ma (Figure 10e), with a weighted mean $^{207}Pb/^{206}Pb$ age of 1922 ±12 Ma (2σ, n=25, MSWD = 1.9). Four single-grain ID-TIMS fractions were analyzed, yielding slightly discordant $^{207}Pb/^{206}Pb$ ages between 1876.9 and1896.6 Ma (Figure 10e, inset). The TIMS results indicate some cryptic complexity in the zircon microstructure or U-Pb systematics that only becomes apparent in high spatial resolution analyses. All grains also have Th/U ratios in excess of 1, which is a common attribute of zircon recovered from mafic rocks (Wang, et al., 2011). The concentric oscillatory zoning is consistent with magmatic crystallization (Corfu, 2003) and the high Th/U signature suggests an igneous origin for the zircon (Heaman et al., 1990). Based on the collective data, these preliminary results suggest a minimum crystallization age of ca. 1900 Ma. Results and methods (Table 2, Liikane et al., 2015) can be found in the data repository for the 2015 edition of the CNGO Summary of Activities.

Regional considerations

Middle Paleoproterozoic cover sequences of the northern Superior craton host numerous magmatic nickel–copper–platinum-group element deposits and showings, with the Raglan-type deposits within the eastern Cape Smith Belt in northern Quebec currently supporting active mineral production (see overviews in Green and Dupras, 1999; Lesher, 2007; Northern Miner, 2014). Multiple publications have described the petrology, geochemistry and petrogenesis of these sulphide deposits and their associated platinum-group element (PGE) enrichment (e.g., Miller, 1977; Naldrett, 1981; Barnes et al., 1982, 1997; Lesher, 2007), with a few focusing on the regional, orogen-scale controls

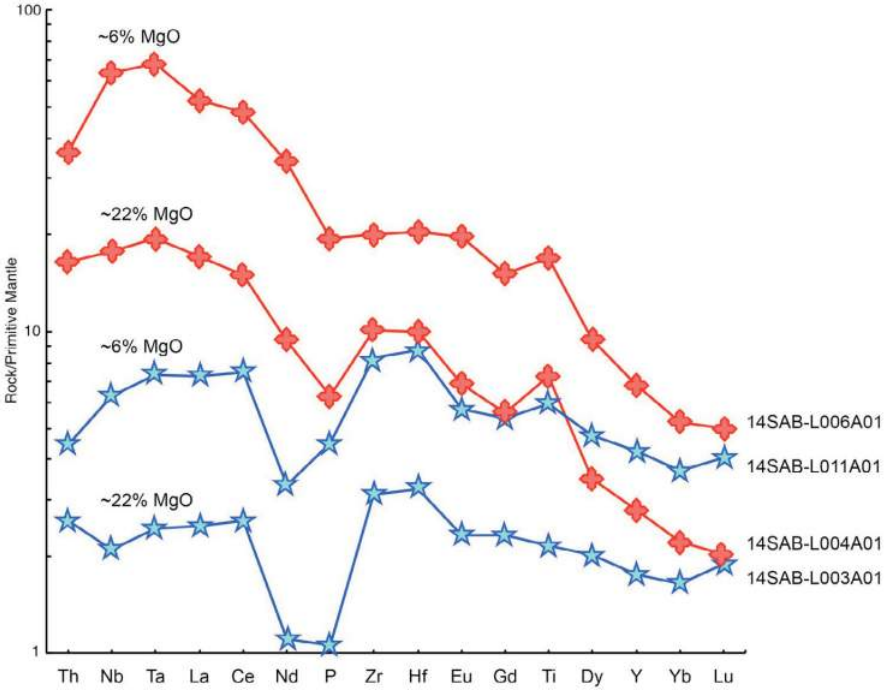

Figure 9: Primitive mantle-normalized rare-earth element plot (primitive mantle-normalization values from Sun and McDonough, 1989), illustrating the differences in the trace-element patterns of groups A (blue stars) and D (red crosses). One representative sample from each group is shown, at both ~6 wt. % MgO and ~22 wt. % MgO concentrations.

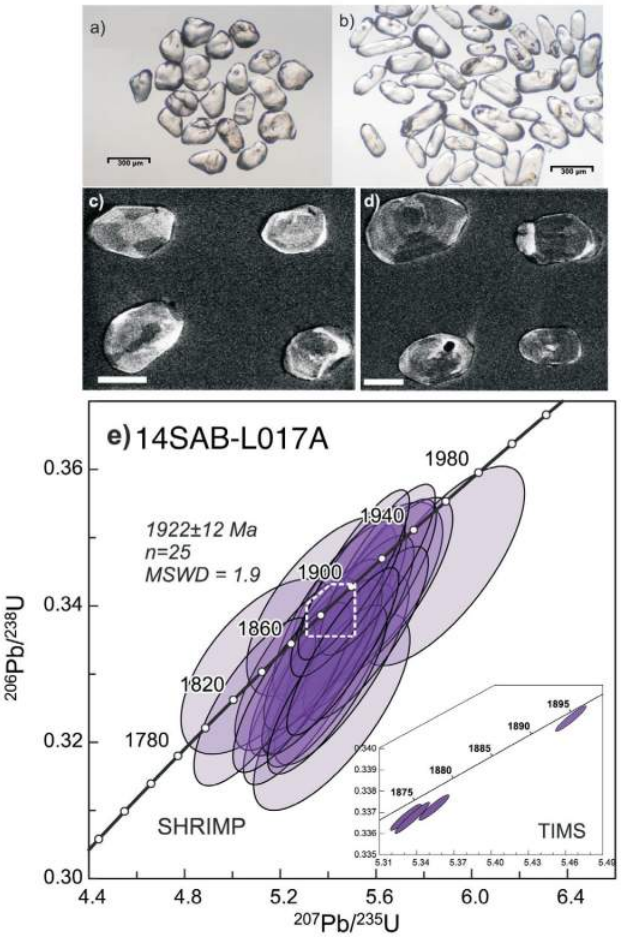

Figure 10: Geochronology for a leucogabbroic sample (14SAB-L017A) collected from a mafic-ultramafic sill on Meta Incognita Peninsula, Baffin Island, Nunavut: **a)** transmitted light photomicrograph of anhedral zircon grains from 14SAB-L017A; **b)** transmitted light photomicrograph of prismatic zircon grains from 14SAB-L017A; **c)**, **d)** cathodoluminescence images of zircon grains prior to SHRIMP analysis. White scale bar is 100 µm; **e)** Concordia diagram of U-Pb sensitive high-resolution ion microprobe (SHRIMP) results from 14SAB-L017A. Ellipses are plotted at the 2σ confidence level, colour was selected to match the coding of the trace-element signature of the sample, white dashed box delineates the outline of the isotope dilution–thermal ionization mass spectrometry (ID-TIMS) concordia diagram. Inset: Concordia diagram of ID-TIMS results from 14SAB-L017A. Ellipses are plotted at the 2σ confidence level.

on the size and distribution of the deposits and showings (Giovenazzo, 1991; St-Onge and Lucas, 1994; Lesher, 2007).

The layered mafic-ultramafic sills of the Frobisher suite have yet to be fully investigated. Following the 2015 fieldwork, it is apparent that these sills potentially represent a previously unrecognized magmatic province extending, discontinuously, from Clearwater Fiord in the east, to Foxe Peninsula in the west, and to Meta Incognita and Hall peninsulas in the south. With an extensional setting and a measured areal extent of >80 000 km^2, the Frobisher mafic-ultramafic magmatic province is being evaluated as the exposed plumbing system of a plume-generated large igneous province (LIP) event (Ernst, 2014). Such a context would allow petrogenetic and metallogenetic comparison with other Ni-Cu-PGE–bearing intrusive suites known to have such a setting, most notably the Norilsk intrusive suite of the Siberian Trap LIP (Ernst and Jowitt, 2013). Other contexts for generating the magmatic suite such as back-arc rifting in an overall convergent context will also be considered.

Economic considerations

During the 2015 systematic and targeted mapping campaign, a number of lithological associations and occurrences with potential economic implications were identified. The tectonostratigraphic/lithological context of the layered mafic-ultramafic sills emplaced in the sulphidic siliciclastic metasedimentary rocks of the Lake Harbour Group is analogous to that hosting Ni-Cu-PGE mineralization elsewhere in the Trans-Hudson Orogen (e.g., Raglan deposits of the eastern Cape Smith Belt of northern Quebec; Lesher, 2007), although metamorphic grade is significantly higher in the Lake Harbour Group (St-Onge et al., 2007b) than in northern Quebec. The ultramafic units of the Frobisher suite have been serpentinized in a number of localities, and as a result might be suitable for carving stone, although no exploitable localities were identified during the 2015 field season.

Future work

The lead author of this field report, a graduate student and field assistant in 2015, is currently conducting an M.Sc. thesis on the petrology, geochemistry and geochronology of the Frobisher suite and its associated mineralization. Through this work, a detailed petrographic analysis of each sample will be done to properly classify the rocks based on their individual mineral assemblages. The characterization of metamorphic mineral fabrics in thin section, and in situ mineral analyses using an electron microprobe, will determine which mineral species are primary igneous phases and which are metamorphic. Olivine can be tested, for example, by comparing Mg# versus Ni content against known compositions of olivine from layered intrusions (e.g., Simkin and Smith, 1970). Further geochemical research is planned to determine to what degree the rocks within each geochemical group differ, or are similar, and whether this difference results in one group having a significantly higher economic potential. This will involve Nd-isotope work, in addition to whole-rock geochemistry, and will hone in on the mantle source for each group. Data obtained from the detailed sample set collected across the northern sill on Hall Peninsula will be used to shed light on the petrogenesis of the Frobisher suite as a whole. Moreover, additional geochronological work is planned to precisely and definitively constrain the timing of Frobisher suite emplacement.

Acknowledgments

Field assistance during the summer was provided by T.C. Chadwick, B. Dyck, O. Weller, A. Ford, S. Noble, T. Rowe and T. Milton. In addition, A. Ford contributed her GIS expertise to help manage the constant influx of data on a daily basis, as well as insuring all the electronic gadgets were kept in good working order. In the kitchen, D. Guilfoyle provided high quality diverse meals daily, which kept the crew fuelled for the eight weeks of fieldwork. The Polar Continental Shelf Program, Universal Helicopters, Kenn Borek and, in particular helicopter pilots G. Nuttall and G. Hartery, are thanked for their care and professionalism whilst providing logistical support to the project. The authors acknowledge N. Shea, S. Dehler, M. Francis and R. Khoun from NRCan for their management and administrative support. Careful and insightful reviews of this paper were provided by T. Skulski (GSC) and T. Peterson (GSC).

Natural Resources Canada, Earth Sciences Sector contribution 20150317

References

Barnes, S.-J., Picard, C., Giovenazzo, D. and Tremblay, C. 1992: The composition of nickel-copper sulphide deposits and their host rocks from the Cape Smith fold belt, northern Quebec; Australian Journal of Earth Sciences, v. 39, p. 335–347.

Barnes, S.-J., Zientek, M. and Severson, M. 1997b: Ni, Cu, Au and platinum-group element contents of sulphides associated with intraplate magmatism: a synthesis; Canadian Journal of Earth Sciences, v. 34, p. 337–351.

Corfu, F., Hanchar, J.M., Hoskin, P.W.O. and Klinny, P. 2003: Atlas of zircon textures; Reviews in Mineralogy and Geochemistry, v. 53, p. 469–500.

Ernst, R.E. 2014: Large Igneous Provinces; Cambridge University Press, Cambridge, UK, 653 p.

Ernst, R.E. and Jowitt, S.M. 2013: Large igneous provinces (LIPs) and metallogeny; Society of Economic Geologists, Special Publication 17, p. 17–51.

Giovenazzo, D. 1991: Géologie et caractéristiques géochimiques des minéralisations Ni-Cu-EPG de la région de Delta, ceinture de Cape Smith, Nouveau Québec; Ph.D. thesis, Université du Québec à Chicoutimi.

Green, A.H. and Dupras, N. 1999: Exploration model for komatiitic peridotite-hosted Ni-Cu-(PGE) mineralization in the Raglan Belt; *in* Komatiitic Peridotite-Hosted Fe-Ni-Cu-(PGE) Sulphide Deposits in the Raglan Area, Cape Smith Belt, New Quebec, C.M. Lesher (ed.), Laurentian University, Mineral Exploration Research Centre, Guidebook Series, v. 2, p. 191–199.

Heaman, L.M., Bowins, R. and Crocket, J., 1990: The chemical composition of igneous zircon suites: implications for geochemical tracer studies; Geochimica et Cosmochimica Acta, v. 54, p. 1597–1607.

Hoffman, P.F. 1988: United Plates of America, the birth of a craton: Early Proterozoic assembly and growth of Laurentia; Annual Reviews of Earth and Planetary Sciences, v. 16, p. 543–603.

Jackson, G.D. and Taylor, F.C. 1972: Correlation of major Aphebian rock units in the northeastern Canadian Shield; Canadian Journal of Earth Sciences, v. 9, p. 1650–1669.

Lesher, C.M. 2007: Ni-Cu-(PGE) deposits in the Raglan area, Cape Smith Belt, New Quebec; *in* Mineral Deposits of Canada: a Synthesis of Major Deposit Types, District Metallogeny, the Evolution of Geological Provinces and Exploration Methods, W.D. Goodfellow (ed.), Geological Association of Canada, Special Publication, v. 5, p. 351–386.

Lewry, J.F. and Collerson, K.D. 1990: The Trans-Hudson Orogen: extent, subdivisions, and problems; *in* The Early Proterozoic Trans-Hudson Orogen of North America, J.F. Lewry and M.R. Stauffer (ed.), Geological Association of Canada, Special Paper 37, p. 1–14.

Liikane, D.A., St-Onge, M.R., Kjarsgaard, B.A., Rayner, N.M., Ernst, R.E. and Kastek, N. 2015: Data tables accompanying "Frobisher suite mafic, ultramafic and layered mafic-ultramafic sills, southern Baffin Island, Nunavut"; Canada-Nunavut Geoscience Office, Geoscience Data Series GDS2015-014, Microsoft® Excel® file, URL <http://cngo.ca/summary-of-activities/2015/> [December 2015].

Miller, A.R. 1977: Petrology and geochemistry of the 2-3 ultramafic sill and related rocks, Cape Smith–Wakeham Bay fold belt, Quebec; Ph.D. thesis, University of Western Ontario, London, Ontario.

Naldrett, A.J. 1981: Nickel sulfide deposits: classification, composition, and genesis; Economic Geology, v. 75, p. 628–685.

Northern Miner, 2014: Canadian & American Mines Handbook 2014–2015; The Northern Miner Group, 83nd edition.

Samis, A.M. and Andersen, E.O. 1980: 1979 year-end report on the Kenty Project: summary of 1979 exploration program? on Ungava permits 567 and 568; Ministère de l'Énergie et des Ressources du Quebec, Document technique, GM 36257.

Simkin, T. and Smith, J.V. 1970: Minor element variation in olivine; Journal of Geology, v. 78, p. 304–325.

Steenkamp, H.M., Bros, E.R. and St-Onge, M.R. 2014: Altered ultramafic and layered mafic-ultramafic intrusions: new economic and carving stone potential on northern Hall Peninsula, Baffin Island, Nunavut; *in* Summary of Activities 2013, Canada-Nunavut Geoscience Office, p. 11–20.

St-Onge, M.R. and Lucas, S.B. 1994: Controls on the regional distribution of iron-nickel-copper-platinum group element sulfide mineralization in the eastern Cape Smith Belt, Quebec; Canadian Journal of Earth Sciences, v. 31, p. 206–218.

St-Onge, M.R., Jackson, G.D. and Henderson, I. 2006: Geology, Baffin Island (south of 70°N and east of 80°W), Nunavut; Geological Survey of Canada, Open File 4931, scale 1:500 000, doi:10.4095/222520

St-Onge, M.R., Rayner, N.M., Liikane, D. and Chadwick, T. 2015a: Mafic, ultramafic and layered mafic-ultramafic sills, Meta Incognita Peninsula, southern Baffin Island, Nunavut; *in* Summary of Activities 2014, Canada-Nunavut Geoscience Office, p. 11–16.

St-Onge, M.R., Rayner, N.M., Steenkamp, H.M. and Skipton, D.R. 2015b: Bedrock mapping of eastern Meta Incognita Peninsula, southern Baffin Island, Nunavut; *in* Summary of Activities 2014, Canada-Nunavut Geoscience Office, p. 105–118.

St-Onge, M.R., Scott, D.J. and Lucas, S.B. 2000: Early partitioning of Quebec: microcontinent formation in the Paleoproterozoic; Geology, v. 28, p. 323–326.

St-Onge, M.R., Van Gool, J.A.M., Garde, A.A. and Scott, D.J. 2009: Correlation of Archaean and Palaeoproterozoic units between northeastern Canada and western Greenland: constraining the pre-collisional upper plate accretionary history of the Trans-Hudson Orogen?; *in* Earth Accretionary Systems in Space and Time, P.A. Cawood and A. Kroner (ed.), The Geological Society, London, Special Publications, v. 318, p. 193–235, doi:10.1144/SP318.7

St-Onge, M.R., Wodicka, N. and Ijewliw, O. 2007b: Polymetamorphic evolution of the Trans-Hudson Orogen, Baffin Island, Canada: integration of petrological, structural and geochronological data; Journal of Petrology, v. 48, p. 271–302, doi:10.1093/petrology/eg1060

Sun, S.-s. and McDonough, W.F. 1989: Chemical and isotopic systematics of oceanic basalts: implication for mantle composition and processes; Geological Society of London, Special Publication 42, p. 313–345.

Weller, O.M., Dyck, B.J., St-Onge, M.R., Rayner, N.M. and Tschirhart, V. 2015: Completing the bedrock mapping of southern Baffin Island, Nunavut: plutonic suites and regional stratigraphy; *in* Summary of Activities 2015, Canada-Nunavut Geoscience Office, p. 33–48.

Wang, X., Griffin, W.L., Chen, J., Huang, P. and Li, X. 2011: U and Th contents and Th/U ratios of zircon in felsic and mafic magmatic rocks: improved zircon-melt distribution coefficients; Acta Geologica Sinica, v. 85, p. 164–174.

Whalen, J.B., Wodicka, N., Taylor, B.E. and Jackson, G.D. 2010: Cumberland batholith, Trans-Hudson Orogen, Canada: petrogenesis and implications for Paleoproterozoic crustal and orogenic processes; Lithos, v. 117, p. 99–118, doi: 10.1016/j.lithos.2010.02.008

Completing the bedrock mapping of southern Baffin Island, Nunavut: plutonic suites and regional stratigraphy

O.M. Weller[1], B.J. Dyck[2], M.R. St-Onge[3], N.M. Rayner[3] and V. Tschirhart[3]

[1]*Natural Resources Canada, Geological Survey of Canada, Ottawa, Ontario, owen.weller@canada.ca*

[2]*Department of Earth Sciences, University of Oxford, Oxford, United Kingdom*

[3]*Natural Resources Canada, Geological Survey of Canada, Ottawa, Ontario*

This work is part of the larger South Baffin mapping project, a partnership between the Canada-Nunavut Geoscience Office (CNGO) and Natural Resources Canada's (NRCan) Geo-mapping for Energy and Minerals (GEM) program on Baffin Island. This particular mapping project is being led by the Geological Survey of Canada (GSC) in collaboration with CNGO, the Government of Nunavut, Nunavut Arctic College, Carleton University and Oxford University. Logistical support is provided by the Polar Continental Shelf Project and several, local, Inuit-owned businesses. The study area comprises all or parts of six 1:250 000 map areas north of Iqaluit (NTS areas 26B, C, F, G, J and K). The objective of the work is to complete the regional bedrock mapping for the southern half of Baffin Island and provide a new, modern, geoscience understanding of this part of eastern Nunavut.

Weller, O.M., Dyck, B.J., St-Onge, M.R., Rayner, N.M. and Tschirhart, V. 2015: Completing the bedrock mapping of southern Baffin Island, Nunavut: plutonic suites and regional stratigraphy; *in* Summary of Activities 2015, Canada-Nunavut Geoscience Office, p. 33–48.

Abstract

This paper summarizes the field observations and initial interpretations following eight weeks of regional and targeted bedrock mapping on south-central Baffin Island, Nunavut. The 2015 field campaign completes a two-decade mission to update the geoscience knowledge for the whole of Baffin Island south of latitude 70°N. The bedrock in the area is dominated by a Paleoproterozoic metaplutonic suite, ranging in composition from gabbro to syenogranite, with crosscutting relations indicating a progression from mafic to silicic magmatism. Phase-equilibria modelling reveals that the prevailing upper-amphibolite– to lower-granulite–facies metamorphic conditions overlap the stability limits of magnetite and orthopyroxene for a typical granitoid bulk composition, which is consistent with field observations of the discontinuous presence of both phases throughout the map area. This result is also consistent with regional aeromagnetic data that show complex structures within relatively homogeneous map units, which are primarily attributed to variations in the abundance of magnetite. The granitoid rocks are interpreted as part of the middle Paleoproterozoic Cumberland Batholith.

Metasedimentary rocks, including quartzite, pelite, marble and metagreywacke, are present as enclaves and screens within and between plutonic bodies. An examination of the 'ghost' stratigraphy suggests that the metasedimentary rocks throughout most of the map area can be correlated with the middle Paleoproterozoic Lake Harbour Group, except in the northeast, where the unique presence of greywacke suggests a middle Paleoproterozoic Piling Group affinity. This transition in strata is consistent with the proposal that a middle Paleoproterozoic tectonic suture (the Baffin suture) associated with the Trans-Hudson Orogen runs through Cumberland Sound. Completion of the bedrock mapping in southern Baffin Island indicates that the region offers a world-class exposure of a reworked Paleoproterozoic convergent margin, which affords valuable insight into a variety of magmatic and tectonic processes that can be applied to younger collisional belts.

Résumé

Le présent rapport résume les observations de terrain et les interprétations préliminaires à la suite de huit semaines de cartographie régionale et ciblée de la roche en place dans la partie centre-sud de l'île de Baffin, au Nunavut. La campagne de terrain 2015 achève deux décennies de travaux ayant pour objet la mise à jour des connaissances géoscientifiques pour l'ensemble de l'île de Baffin gisant au sud de la latitude 70°N. Le socle rocheux dans la région est constitué d'une suite métaplutonique d'âge paléoprotérozoïque, dont la composition varie du gabbro au granite syénitique ; les relations de recoupement qui la caractérisent attestent de la progression des épisodes de magmatisme de nature mafique à siliceuse. La modélisation de diagrammes de phases révèle que les conditions métamorphiques du faciès des amphibolites supérieur au faciès des granulites inférieur chevauchent les limites de stabilité typiques de la magnétite et de l'orthopyroxène pour une

This publication is also available, free of charge, as colour digital files in Adobe Acrobat® PDF format from the Canada-Nunavut Geoscience Office website: http://cngo.ca/summary-of-activities/2015/.

composition granitique caractéristique, ce qui concorde avec les observations de terrain et la présence discontinue des deux phases dans l'ensemble de la région à l'étude. Ce résultat est également compatible avec les données aéromagnétiques régionales qui montrent des structures complexes au sein d'unités cartographiques relativement homogènes, structures dont l'identification est principalement attribuable à la présence de quantités variables de magnétite. Les roches granitoïdes sont interprétées comme faisant partie du batholite de Cumberland datant du Paléoprotérozoïque moyen.

Des roches métasédimentaires, y compris du quartzite, de la pélite, du marbre et de la métagrauwacke, sont présents sous forme d'écrans et d'enclaves entre des masses plutoniques et au sein de ces dernières. Un examen de la stratigraphie «fantôme» semble indiquer que les roches métasédimentaires dans presque l'ensemble de la région cartographiée peuvent être mises en corrélation avec celles du groupe de Lake Harbour datant du Paléoprotérozoïque moyen, sauf dans le nord-est, où la présence unique de grauwacke semble indiquer une affinité avec le groupe de Piling, datant lui aussi du Paléoprotérozoïque moyen. Cette transition concorde avec la proposition selon laquelle une suture tectonique datant du Paléoprotérozoïque moyen (la suture de Baffin), associée à l'orogénie Trans-hudsonienne, traverse le détroit de Cumberland. L'achèvement des travaux de cartographie du substratum rocheux dans le sud de l'île de Baffin révèle une région offrant un exemple frappant d'une marge convergente retravaillée d'âge paléoprotérozoïque, susceptible de livrer de précieux renseignements au sujet d'une variété de processus magmatiques et tectoniques qui peuvent être appliqués aux chaînes de collision plus récentes.

Introduction

Natural Resources Canada's (NRCan) Geo-mapping for Energy and Minerals (GEM) program targeted south-central Baffin Island for strategic, helicopter-assisted bedrock mapping in 2015 (red polygon, Figure 1). The GEM program provides modern, publicly available, regional-scale geoscience knowledge of Canada's North, which supports evidence-based exploration for new energy and mineral resources and enables northern communities to make informed decisions about their land, economy and society. The 2015 field campaign was particularly significant as it updates the regional bedrock-mapping coverage for the southern half of Baffin Island (south of latitude 70°N), allowing for a new, modern, geoscience compilation of the area. Fieldwork in the region (parts of NTS map areas 26B, C, F, G, J and K) was led by the Geological Survey of Canada (GSC) in collaboration with the Canada-Nunavut Geoscience Office (CNGO), and also involved participants from Nunavut Arctic College, Carleton University, Oxford University and the Government of Nunavut. This paper presents an overview of the regional geology, and outlines the dominant tectonostratigraphic units and economic potential identified during eight weeks of fieldwork in 2015.

Historical bedrock mapping

Initial reconnaissance geological investigations of Baffin Island south of latitude 66°N were carried out from 1949 to 1965, with the data compiled into a regional bedrock map that covered eighteen 1:250 000 NTS map areas (Blackadar, 1967). This was followed by a series of helicopter-borne operations in central Baffin Island (e.g., Henderson, 1985). More recently, modern geoscience knowledge has been provided by field campaigns featuring helicopter-assisted foot traverses in: southern Baffin Island (1995–1997; green shading in Figure 1), central Baffin Island (2000–2002; orange shading in Figure 1), south-west Baffin Island (2006; yellow shading in Figure 1), Cumberland Peninsula (2009–2011; pale pink shading in Figure 1), Hall Peninsula (2012–2014; blue shading in Figure 1) and Meta Incognita Peninsula (2014; purple shading in Figure 1). Prior to the summer of 2015, only one section remained to finalize the updated coverage of the whole of Baffin Island south of latitude 70°N: south-central Baffin Island in the Clearwater Fiord–Sylvia Grinnell Lake area (red polygon in Figure 1). This area was the focus of the 2015 field campaign and is the subject of this paper.

Geological framework

South-central Baffin Island forms part of the northeastern (Quebec–Baffin) segment of the Trans-Hudson Orogen (THO), which is a collisional belt that extends in a broad arcuate shape from north-eastern to south-central North America (Hoffman, 1988). The THO formed during the final phase of growth of the Nuna supercontinent, and *sensu lato* records the closure of the Manikewan Ocean between the lower Superior and upper Churchill plates from 1.92 to 1.80 Ga. In detail, the THO is a composite collision zone that involved a series of short-duration tectonothermal events, which encompass specific accretionary phases within a much larger orogenic system during 120 m.y. of gradual ocean-basin closure (Corrigan et al., 2009; St-Onge et al., 2009). In the southeastern Baffin region, four orogen-scale stacked tectonic levels have been identified (Figure 2). From lowest to highest structural level, these comprise

1) Archean basement orthogneiss, interpreted as the northern continuation of the Superior craton, and middle Paleoproterozoic supracrustal cover (Povungnituk Group; St-Onge et al., 1996);
2) middle Paleoproterozoic, dominantly monzogranitic and granodioritic orthogneiss, interpreted as a deformed

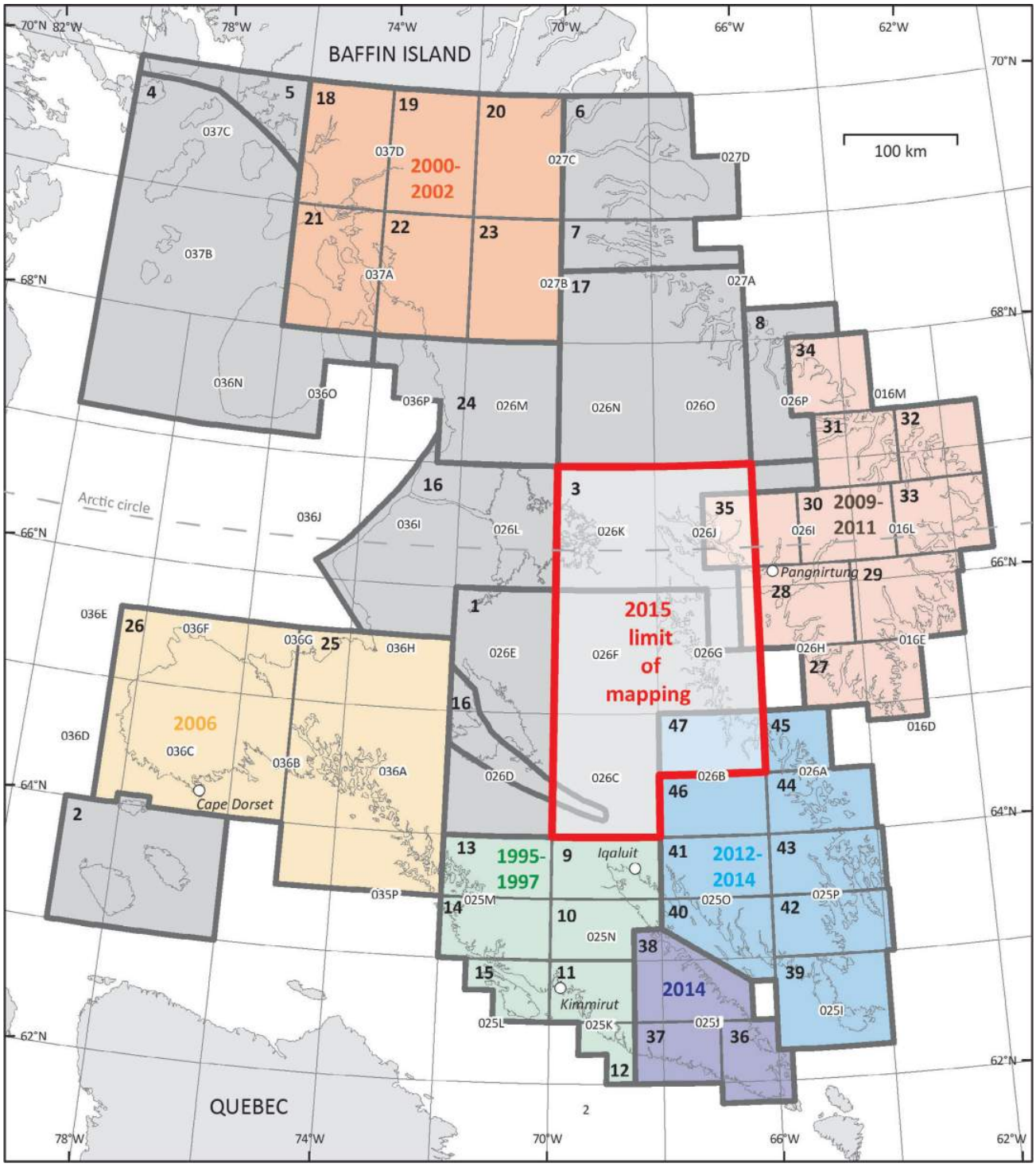

Figure 1: Summary of bedrock-mapping campaigns undertaken on Baffin Island, Nunavut. The location of the 2015 south-central Baffin Island map area is shown as a red polygon, and completes the modern mapping coverage south of 70°N. Bold numbers denote map references in chronological order, which are listed in Appendix 1. Coloured shading highlights areas and year(s) of recent field campaigns, as described in the text. Alphanumeric designators refer to NTS map areas.

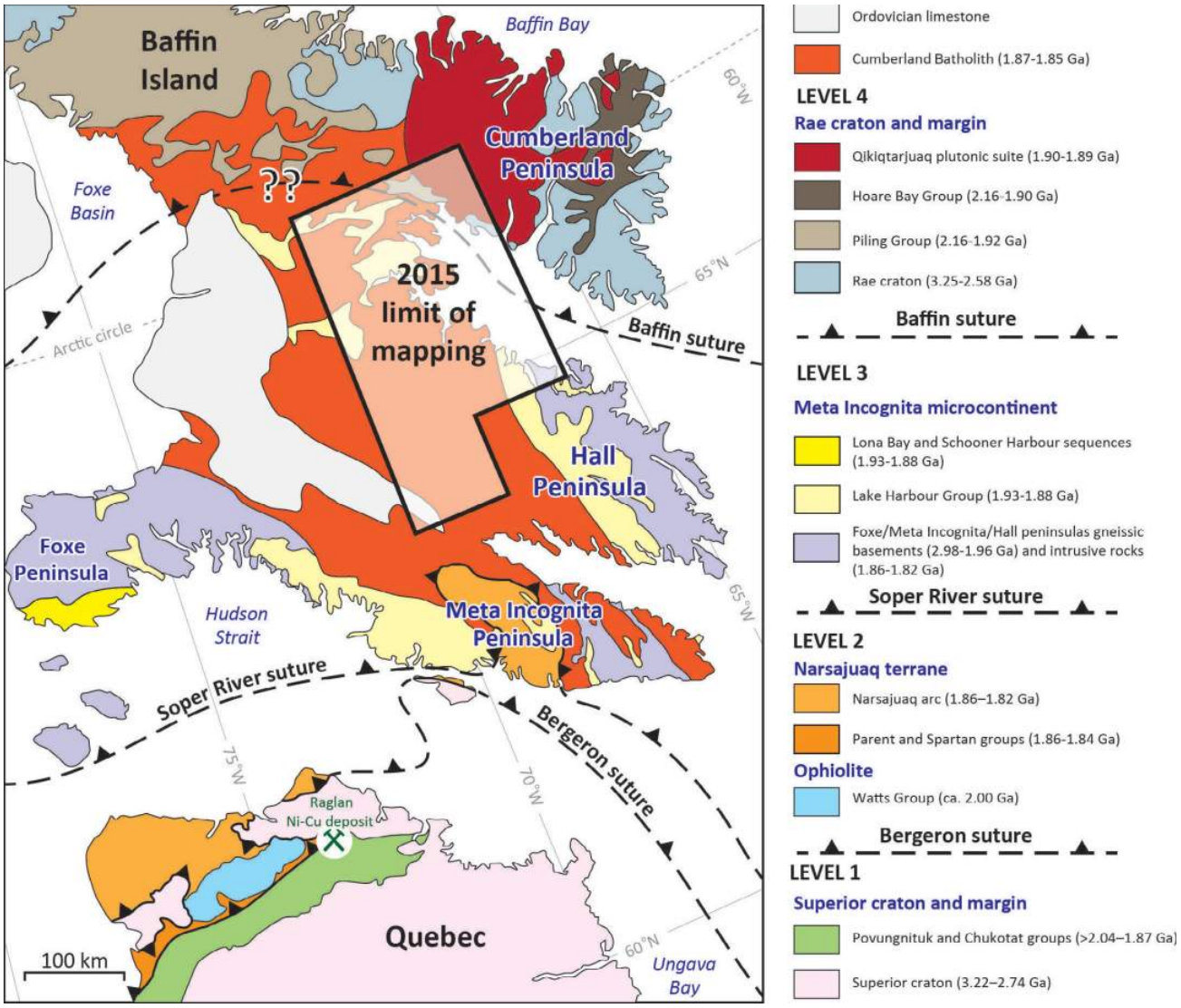

Figure 2: Simplified geological terrane map of the Quebec–Baffin segment of the Trans-Hudson Orogen (modified from St-Onge et al., 2007), showing the four structural levels and three sutures. The map provides a regional tectonic context for the south-central Baffin Island map area, which is outlined in black.

arc-magmatic terrane (Narsajuaq arc; Scott, 1997; St-Onge et al., 2009) or as Narsajuaq-age intrusions in level 3 (Corrigan et al. 2009);

3) Archean basement orthogneiss and middle Paleoproterozoic supracrustal cover (Lake Harbour Group), collectively termed the 'Meta Incognita microcontinent' by St-Onge et al. (2000a), which either represents crust rifted from the Rae or Superior cratons, or is exotic to both; and
4) Archean basement orthogneiss, interpreted as the southern continuation of the Rae craton, and middle Paleoproterozoic supracrustal cover (Piling Group; Wodicka et al., 2014), stratigraphically similar to the Hoare Bay Group on Cumberland Peninsula; both the basement and cover are intruded by a middle Paleoproterozoic felsic plutonic suite (the Qikiqtarjuaq suite; Rayner et al., 2012).

Levels 3 and 4 are pervasively intruded by the Cumberland Batholith, which comprises various granitoid phases dated at ca. 1865–1845 Ma (Whalen et al., 2010). The Cumberland Batholith has been interpreted as an Andean-type batholith (St-Onge et al., 2009), or as the result of post-collisional lithospheric delamination and mantle upwelling (Whalen et al., 2010). All levels are crosscut by ca. 720 Ma basaltic 'Franklin' dykes, which were emplaced during plume magmatism associated with the break-up of the Rodinia supercontinent (Heaman et al., 1992). Levels 3 and 4 are also unconformably overlain by Ordovician limestone strata (Blackadar, 1967).

The four tectonic elements were progressively accreted from the south across a series of north-dipping crustal sutures during long-lived deformation associated with the THO. The oldest of these sutures, the level 3–4 'Baffin suture', is pro-

posed to have resulted from accretion of the Meta Incognita microcontinent to the Rae craton at ca. 1880–1865 Ma (St-Onge et al., 2006). Evidence of this suture is relatively sparse due to postaccretion magmatism engulfing the suture zone, but includes the presence of distinct and opposite-facing stratigraphy in the region (St-Onge et al., 2009). To the north of the proposed suture is the stratigraphically south-facing Piling Group, which comprises a continental margin sequence, characterized by basal shallow-marine continental-margin clastic and carbonate-platform strata, overlain by a volcano-sedimentary rift package that includes iron formations, and capped by foredeep turbidites (Wodicka et al., 2014). To the south of the proposed suture is the north-facing Lake Harbour Group, which also comprises a clastic-carbonate continent- to foredeep-margin sequence but with notable differences, including the presence of a basal orthoquartzite and the absence of iron formation and greywacke. Further evidence for the suture includes thrust imbrication of basement-cover panels in level 3 that predate emplacement of the Cumberland Batholith (St-Onge et al., 2007). As the 2015 map area straddles the proposed Baffin suture, one of the major objectives of the campaign was to further investigate this structure.

The level 2–3 'Soper River' suture records the accretion of the Narsajuaq magmatic arc to the Rae-Meta Incognita continental margin. Formation of the suture is bracketed between ca. 1845 Ma, the age of the youngest intra-oceanic phase in the arc (Dunphy and Ludden, 1998), and ca. 1842 Ma, the age of the oldest Andean-type phase (Scott, 1997). Deformation in the hanging wall of the Soper River suture is both extensive and penetrative, and manifest as a regional synmetamorphic amphibolite- to granulite-facies metamorphic foliation (St-Onge et al., 2007).

The level 1–2 'Bergeron' suture formed during terminal collision of the Superior craton with the amalgamated mosaic of upper-plate terranes (collectively the Churchill plate or peri-Churchill collage), and is bracketed between ca. 1820 Ma, the age of the youngest dated plutonic unit in the hanging wall of the suture (Scott and Wodicka, 1998), and ca. 1795 Ma, the age of a dyke that crosscuts the suture (Wodicka and Scott, 1997). This event resulted in localized retrograde amphibolite-facies metamorphism of granulite-facies rocks in the upper plate of the collision in southern Baffin Island along reactivated Soper River structures and associated fluid-infiltration zones (St-Onge et al., 2000b).

Field observations of 2015

Bedrock mapping of the Clearwater Fiord–Sylvia Grinnell Lake area was completed during eight weeks of strategic, helicopter-assisted fieldwork in the summer of 2015. The bedrock in the area is dominated by a metaplutonic suite ranging in composition from gabbro to syenogranite (Figure 2). Crosscutting relationships define a relative chronology of emplacement for the various phases (e.g., Figure 3a), which can be broadly summarized as a transition from mafic through to more silicic compositions. A suite of samples from the various metagranitoid phases, which are described in their relative age order below, was collected for U-Pb dating to corroborate field crosscutting relationships and the likely correlation with the Cumberland Batholith. Although most of the rocks in the field area are penetratively deformed metamorphic rocks, the prefix 'meta' is omitted from the following lithological descriptions of the metagranitoid units for brevity.

Metasedimentary strata, including quartzite, semipelite, pelite, marble and metagreywacke, occur as enclaves, panels and screens within and between various plutons. Mafic-ultramafic bodies are present as sills within the metasedimentary strata. Field relationships indicate that emplacement of the sills predates emplacement of the metaplutonic suite. Lastly, minor crosscutting Neoproterozoic Franklin dykes (Heaman et al., 1992) and overlying Ordovician limestone (Blackadar, 1967) occur in the map area.

Metagranitoid units

Gabbro

A single, coarse-grained to pegmatitic, kilometre-scale, layered biotite-clinopyroxene-magnetite±hornblende gabbro pluton is present in the northwestern corner of the map area. In places, the pluton contains metre-scale lenses of clinopyroxene-bearing anorthosite.

Quartz diorite

Quartz diorite occurs as a fine-grained, dark-weathering, massive to foliated unit containing the assemblage biotite-clinopyroxene-orthopyroxene±hornblende. It is present as discrete plutons in the western part of the map area and as enclaves within all other metaplutonic units to the east (Figure 3a). Map-scale structural trends indicate that the unit occurs toward the stratigraphic base of the metaplutonic suite.

Biotite granodiorite

Minor, generally massive, biotite±hornblende±magnetite granodiorite is documented in the northwestern part of the map area. The unit is typically dark weathering and medium grained.

K-feldspar–megacrystic biotite monzogranite

Pink- to orange-weathering, medium- to coarse-grained, massive to foliated biotite±orthopyroxene±magnetite±garnet monzogranite, with distinctive K-feldspar megacrysts, occurs throughout large parts of south-central Baffin Island. Potassium-feldspar phenocrysts form augen up to 10 cm wide and locally display rapakivi textures (ovoid alkali feldspar mantled by plagioclase feldspar; Figure 3b). The unit is locally reworked by a kilometre-scale north-dipping

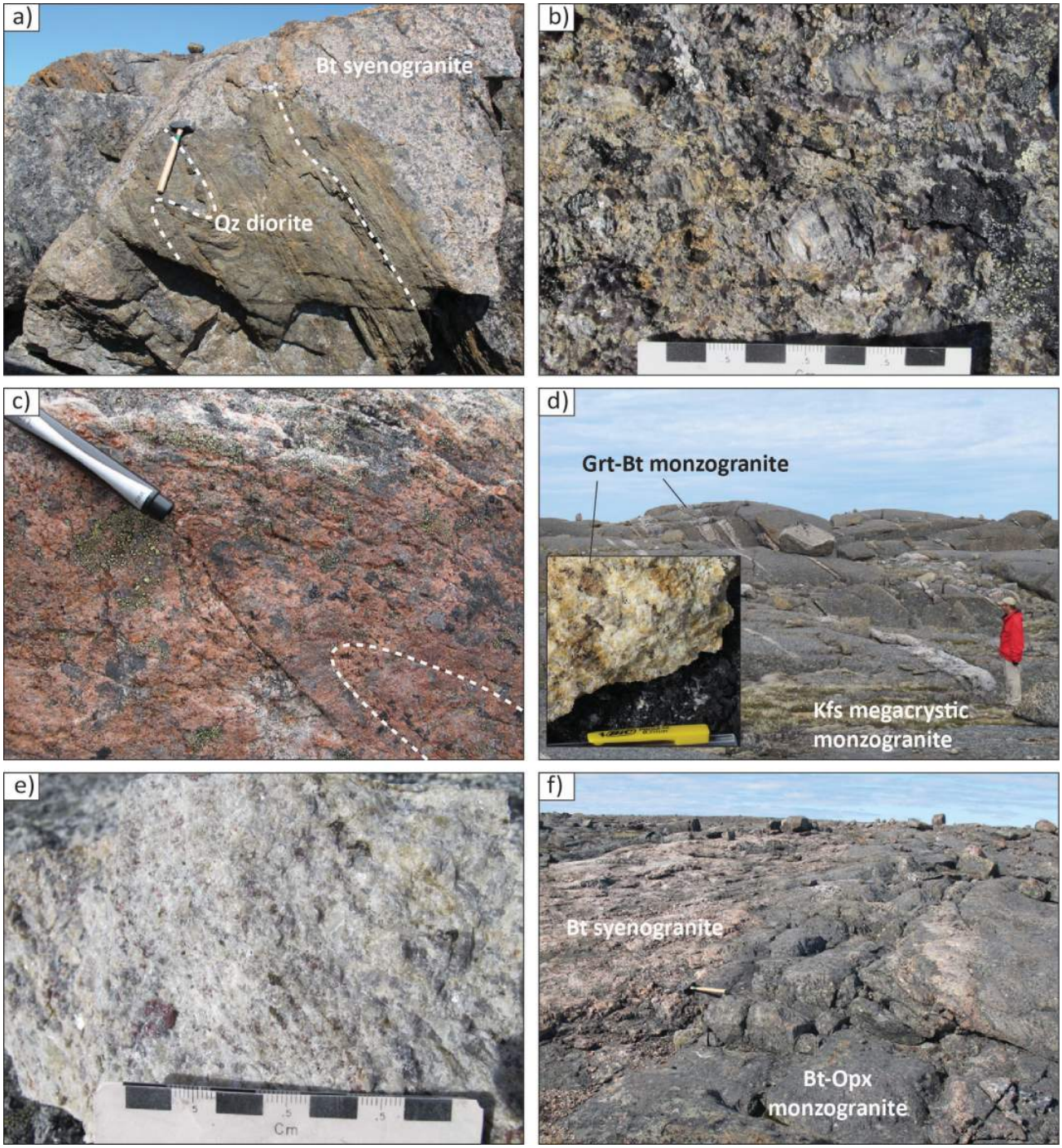

Figure 3: Representative photos of metagranitoid units from southern Baffin Island: **a)** enclave of folded and foliated quartz diorite in massive, coarse-grained biotite syenogranite; **b)** close-up of the K-feldspar–megacrystic monzogranite showing 3–6 cm zoned feldspar augen displaying rapakivi texture; **c)** isoclinally folded biotite-orthopyroxene monzogranite; **d)** massive K-feldspar–megacrystic monzogranite cut by a series of subparallel garnet-biotite monzogranite dykes (geologist for scale is 1.8 m tall); inset: close-up of a garnet-biotite monzogranite sample, showing 1–3 cm burgundy garnet phenocrysts and a weak foliation defined by subparallel biotite flakes; **e)** close-up of a garnet-sillimanite leucogranite, showing abundant pinhead-sized lilac garnet; **f)** massive biotite-orthopyroxene monzogranite cut by a network of anastomosing biotite syenogranite dykes (hammer for scale is 30 cm long). Abbreviations: Bt, biotite; Grt, garnet; Kfs, K-feldspar; Opx, orthopyroxene; Qz, quartz.

shear zone in the northern portion of the map area, with σ-porphyroclasts of K-feldspar defining a top-to-the-south thrust sense of shear.

Biotite monzogranite

Well-foliated biotite±orthopyroxene±magnetite±hornblende±garnet monzogranite underlies large parts of south-central Baffin. The unit is typically medium grained, tan to pink weathering and equigranular. The unit alternates between magnetite-rich and magnetite-free domains, and contains hornblende in the north-western part of the map area. In places, the foliation is observed to be axial planar to isoclinal folding of the unit (Figure 3c), suggestive of widespread shortening across the region.

Garnet-biotite monzogranite

White-weathering, massive to foliated, fine- to medium-grained garnet-biotite±magnetite monzogranite occurs predominantly in the eastern portion of the map area. The unit is present as dykes and sills in the K-feldspar–megacrystic monzogranite (Figure 3d) and forms plutons that intrude the biotite monzogranite. Garnet is present as abundant 2–30 mm burgundy phenocrysts, frequently in association with biotite (inset in Figure 3d).

Garnet-sillimanite leucogranite

Dykes of garnet-sillimanite leucogranite crosscut the garnet-biotite monzogranite in the eastern part of the map area. The unit is typically fine grained, with 1–5 mm lilac garnet phenocrysts and mats of sillimanite (Figure 3e). The presence of sillimanite suggests that the leucogranite is derived from muscovite-dehydration melting of metasedimentary units as documented elsewhere on southern Baffin Island (e.g., Dyck et al., 2015), rather than being a highly fractionated component of the plutonic suite.

Biotite syenogranite

Coarse-grained to pegmatitic, pink-weathering biotite syenogranite forms anastomosing dykes in most units (Figure 3f). In places the syenogranite is foliated, but typically the unit is undeformed and cuts the foliation of the hostrock (Figure 3a). Rarely, the dykes contain phenocrysts of garnet and tourmaline.

Metasedimentary units

Quartzite, psammite, semipelite and pelite

Well-layered and rusty-weathering quartzite occurs as panels up to several hundred metres thick within monzogranite (Figure 4a), and in places is overlain by interbedded psammite, semipelite and/or pelite (Figure 4b). Quartzite layers range in composition from orthoquartzite to feldspathic quartzite, are strongly recrystallized and occasionally contain garnet. Pelite horizons contain the assemblage biotite–garnet–sillimanite–K-feldspar–melt (Figure 4c), and typically occur as subordinate layers within biotite±garnet psammitic or biotite±garnet±sillimanite semipelitic migmatite. The primary assemblages contain up to 20 vol. % coarsened leucosome, interpreted as crystallized melt, with patch to stromatic metatexite textures. The assemblages are devoid of muscovite, consistent with peak metamorphic conditions that exceeded muscovite dehydration (St-Onge et al., 2007; Dyck and St-Onge, 2014). Cordierite is also absent from the metasedimentary assemblages, suggesting paleopressures in excess of 6 kbar. Gossanous horizons are common in the siliciclastic units, which locally host chalcopyrite, graphite and pyrite. Although only seen in restricted windows, the siliciclastic units across most of the map area are lithologically similar to the metasedimentary strata of the contiguous Lake Harbour Group in its type locality (St-Onge et al. 1996, 1998; Scott et al. 1997).

Marble and calcsilicate

Calcareous rocks occur as panels up to 100 m thick within the monzogranite and can be traced for up to 10 km along strike (Figure 4d). The rocks are medium to coarse grained, and locally display compositional layering defined by varying proportions of apatite, calcite, diopside, humite, forsterite, magnetite, phlogopite, scapolite, spodumene, titanite and tremolite (Figure 4e). The calcareous units are considered to represent a structurally higher part of the Lake Harbour Group than the siliciclastic units described above.

Metagreywacke

Metagreywacke was documented in one locality in the north-eastern part of the map area, occurring as enclaves within a biotite monzogranite (Figure 4f). As noted above, greywacke is not a feature of the type Lake Harbour Group stratigraphy, but is a dominant component of the Pilling Group mapped to the north, suggesting a transition in granitoid host stratigraphy.

Other units

Mafic-ultramafic sills

Sheets of medium- to coarse-grained, mafic to ultramafic rocks of the Frobisher suite (Liikane et al., 2015) occur throughout the siliciclastic strata of south-central Baffin Island. Individual bodies are typically 10–20 m thick, although some reach a few hundred metres in thickness, and extend up to several kilometres along strike. The mafic and ultramafic rocks display sharp, concordant margins with their host metasedimentary units, suggesting that they are sills. Larger bodies are compositionally layered, typified by a sequence comprising clinopyroxene-orthopyroxene± hornblende metapyroxenite at the base (Figure 5a), followed by olivine-clinopyroxene-orthopyroxene metaperidotite and metagabbro to metaleucogabbro upsection (Figure 5b). A M.Sc. thesis is currently being completed on the petrology, geochemistry and geochronology of the layered mafic-ultramafic suite and associated mineralization. One of the central questions posed by this thesis is whether the

Figure 4: Representative photos of metasedimentary units on southern Baffin Island: **a)** panel of rusty-weathered quartzite 10 m wide in biotite monzogranite; **b)** well-layered quartzite interbedded with pelite/semipelite (hammer for scale is 30 cm long); **c)** close-up of the pelite/semipelite, showing 1–2 cm garnet porphyroblasts wrapped by biotite and sillimanite, which define a foliation; **d)** enclave of marble within biotite-orthopyroxene monzogranite (hammer for scale is 30 cm long); **e)** left: magnetite horizon in marble (hammer for scale is 30 cm long); right: banding in marble caused by varying amounts of humite, diopside and phlogopite (hammer for scale is 60 cm long); **f)** enclave of metagreywacke in biotite monzogranite (geologist for scale is 1.8 m tall). Abbreviations: Bt, biotite; Di, diopside; Hu, humite; Mag, magnetite; Opx, orthopyroxene; Phl, phlogopite.

suite is correlative with similar layered intrusions in northern Quebec that are associated with the Raglan Ni-Cu deposit (Figure 2). A more complete description of the mafic-ultramafic rocks is given in Liikane et al. (2015).

Basaltic dykes

A suite of minor 1–20 m wide subvertical, fine- to medium-grained basaltic dykes containing 1–2 mm plagioclase phenocrysts are present throughout south-central Baffin Island (Figure 5c). The dykes are relatively magnetic, consistently trend at 110–120° (Tschirhart et al., 2015) and are attributed to the widespread Neoproterozoic (ca. 720 Ma) Franklin dyke suite (Heaman et al., 1992).

Limestone

Shallowly dipping (<10°) limestone (Blackadar, 1967) of the middle Ordovician Amadjuak Formation (Sanford and Grant, 2000) occurs as erosional outliers in the south-western part of the map area (Figure 2). In places, the limestone is juxtaposed against the plutonic suite by northwest-striking normal faults, which were active during Paleocene rifting of the Davis Strait (Clarke et al., 1989). The limestone is typically composed of medium-grey lime mud and is fossiliferous, with the assemblage including Maclurites, gastropods, cephalopods, brachiopods, coral fragments and crinoid stems (Figure 5d).

Phase-equilibria modelling

Phase-equilibria modelling of a representative sample of the Cumberland Batholith was undertaken to investigate the competing effects of pressure, temperature and composition (P, T and X) on the metamorphic mineral assemblage. Phase relationships were calculated across a range of P-T space, centred upon documented regional metamorphic conditions of 6–8 kbar and 700–800°C (St-Onge et al., 2007), with the intent of rationalizing the range of phases documented within the metagranitoid units, rather than refining P-T estimates. All P-T and T-X phase diagrams were constructed using THERMOCALC v3.40 and the internally consistent dataset tc-ds55 updated to August, 2004 (Holland and Powell, 1998). Modelling was performed in the 11 component MnO-Na_2O-CaO-K_2O-FeO-MgO-Al_2O_3-SiO_2-H_2O-TiO_2-Fe_2O_3 system, using the high-temperature solid-solution models considered in Weller et al. (in press). Pressure uncertainties for assemblage-field boundaries are approximately ±1 kbar at the 2σ level (Powell and Holland, 2008; Palin et al., in press). Bulk compositions were calculated by modifying whole-rock X-ray fluorescence data presented by Theriault et al. (2001) for a monzogranite sampled from southern Baffin Island (sample 95-D078B), following the technique of Weller et al. (2013). Modifications included adjusting the CaO total by assuming that all P_2O_5 resided in apatite; applying a value of $XFe^{3+} = Fe^{3+}/\text{total Fe} = 0.1$, using the oxides present as a guide to oxidation state (Diener and Powell, 2010); and setting molar H_2O in the effective bulk composition (MH_2O) at 0.1%, as metagranitoid rocks are relatively anhydrous (Bucher and Frey, 2002). Both of the latter assumptions are explored using relevant T-X diagrams. All bulk compositions are listed in Table 1.

A P-T diagram calculated for a representative monzogranite sample (sample 95-D078B from Theriault et al., 2001; Figure 6a) reveals few reactions between high-variance assemblages across a wide range of P-T space, as is typical of metagranitoid rocks, with only magnetite (blue line) and orthopyroxene (green line) calculated to have limited stability over the considered subsolidus conditions. Of note, both orthopyroxene and magnetite stability limits are encountered within the P-T range of relevance to south-central Baffin Island (white dashed box), consistent with field observations of the discontinuous presence of both phases across the region.

To investigate the effects of H_2O on the assemblage, a T-MH_2O diagram was constructed at a mid-range pressure (7 kbar), with MH_2O varying from 0 to 1 mol% (Figure 6b). This diagram reveals that with increasing H_2O content, the temperature of orthopyroxene-in (green line) rapidly increases from ca. 640°C to 810°C, and conversely the solidus (orange line) decreases from ca. 810°C to 640°C. Given the relevant temperature range of 600–800°C, the presence of orthopyroxene and absence of partial melt textures in the metagranitoid rocks suggest that the assumption of a relatively anhydrous bulk composition (0.1 mol% H_2O, Table 1; white dashed line in Figure 6b) is appropriate. This result is also consistent with the presence of rapakivi textures in the map area (Figure 3b), which are thought to require H_2O-undersatured conditions to form (Nekvasil, 1991). However, the diagram also reveals that for all moderately anhydrous bulk compositions (<0.2 mol% H_2O), over which silicate melt would not be stabilized at <800°C, both orthopyroxene and magnetite (blue line) stability are sensitive to MH_2O. Therefore, in addition to the effects of regional P-T variations discussed above, subtle changes in the water content of a typical granitoid composition at the same P-T condition could also have contributed to the noted discontinuous stability of both phases.

In order to determine the effects of XFe^{3+} on the assemblage, a T-XFe^{3+} diagram was constructed at the same midrange pressure (7 kbar), with XFe^{3+} varying from 0.0 to 0.5 (Figure 6c). This diagram reveals that both magnetite (blue line) and orthopyroxene (green line) stabilities are a strong function of XFe^{3+}, such that variation in XFe^{3+} could also have added to the irregular distribution of both phases. The widespread occurrence of magnetite- and orthopyroxene-bearing metagranitoid rocks suggests that moderate values of $XFe^{3+} = 0.05–0.25$ are the most plausible (a range that includes the assumed value of 0.1; white dashed line in Figure 6c), as both phases are then stabilized within the suggested temperature range.

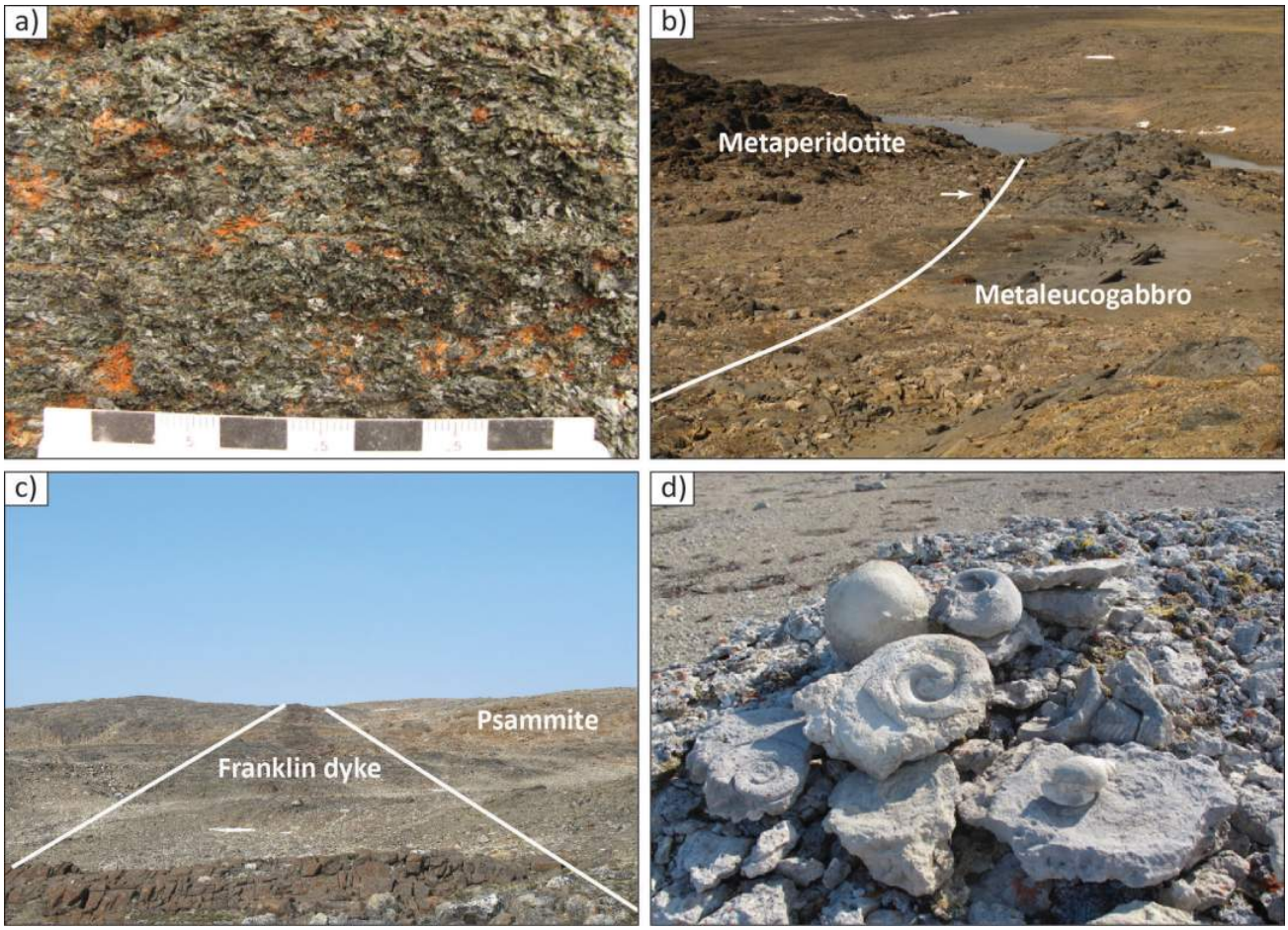

Figure 5: Representative photos of other units on southern Baffin Island: **a)** close-up of metaclinopyroxenite at the base of a layered mafic sill; darker regions correspond to minor retrogression of clinopyroxene to hornblende; **b)** central-upper portion of a layered mafic sill, showing brown-weathering metaperidotite capped by grey-weathering metaleucogabbro (geologist, beside arrow, for scale is 1.8 m tall); **c)** Lake Harbour Group psammite cut by a Franklin dyke, which is approximately 10 m wide and displays columnar jointing in the foreground; **d)** typical knobbly weathered surface of Ordovician limestone, showcasing fossils collected from the wider outcrop; field of view in foreground is 50 cm.

Application to aeromagnetic data

Regional aeromagnetic data show complex variation in the magnetic properties of the bedrock in the project area (e.g., Figure 6d; Kiss and Tschirhart, 2015a, b). Field investigations of the data suggest that the major driver of this variability is the differential abundance of magnetite, typically within otherwise relatively homogeneous plutons (Tschirhart et al., 2015). The phase-equilibria modelling results are consistent with this inference, as they show that subtle changes in P, T and X for a reference granitoid would manifest themselves in complex magnetite (and orthopyroxene) distributions, with all other phases remaining relatively constant.

Regional considerations

The Baffin suture

St-Onge et al. (2007) proposed that a north-dipping, middle Paleoproterozoic suture zone (the Baffin suture of Figure 2) runs through central Baffin Island, approximately along Cumberland Sound, separating the Meta Incognita microcontinent from the Rae craton to the north. Although extensive plutonic activity associated with emplacement of the middle Paleoproterozoic Cumberland Batholith has largely obliterated the older geological record in this locale, two lines of evidence are consistent with the location and vergence of the proposed structure. First, the 'ghost' stratigraphy preserved within the project area changes from dominantly Lake Harbour Group to Piling Group affinity from south to north. On a regional scale, this change in tectonostratigraphic parentage has been previously cited as evidence for an intervening suture zone (St-Onge et al., 2006, 2007). The 2015 field observations thus serve to refine this suggestion, as the most northerly Lake Harbour Group quartzite and southerly Piling Group greywacke constrain a narrow corridor of possible suture-zone loci. Second, a shear zone occurs in the plutonic suite within this corridor, with a top-to-the-south thrust sense of shear. As the emplacement

Table 1: Bulk compositions used to construct all phase-equilibria diagrams in Figure 6 using THERMOCALC (mol %). Two values are provided for Figures 5b and 5c, which represent the end-member compositions of the considered range.

Figure	H_2O	SiO_2	Al_2O_3	CaO	MgO	FeO	K_2O	Na_2O	TiO_2	MnO	O	XFe^{3+}
6a	0.10	79.82	8.79	2.86	0.32	2.14	1.69	3.98	0.16	0.04	0.11	0.1
6b	0.00	79.90	8.79	2.87	0.32	2.14	1.69	3.98	0.16	0.04	0.11	0.1
6b	1.00	79.10	8.71	2.84	0.32	2.12	1.67	3.94	0.16	0.04	0.11	0.1
6c	0.10	79.90	8.80	2.87	0.32	2.14	1.69	3.98	0.16	0.04	0.00	0.0
6c	0.10	79.48	8.75	2.85	0.32	2.13	1.68	3.96	0.16	0.04	0.53	0.5

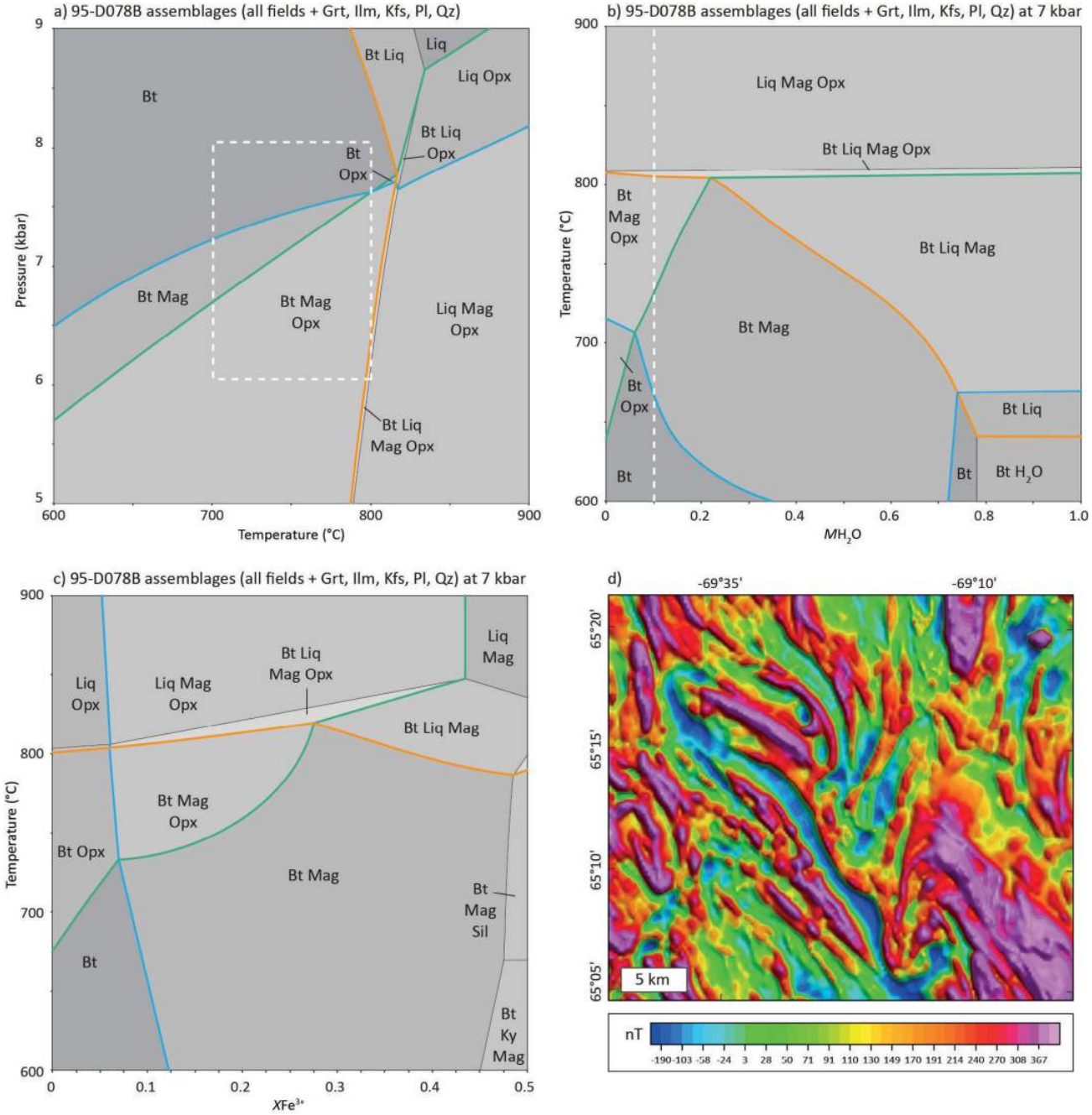

Figure 6: Phase-equilibria modelling of a representative sample of the Cumberland Batholith, southern Baffin Island, exploring metagranitoid amphibolite-granulite facies phase relationships. Phase boundaries (mode = 0 lines) are highlighted for orthopyroxene (green line), magnetite (blue line) and silicate melt (orange line): **a)** P-T diagram; **b)** T-MH_2O diagram; **c)** T-XFe^{3+} diagram; **d)** residual total field over biotite±magnetite±orthopyroxene monzogranite in the western part of the map area. See text for discussion and Table 1 for input bulk compositions. Abbreviations: Bt, biotite; Ky, kyanite; Liq, liquid; Mag, magnetite; Opx, orthopyroxene; Sil, sillimanite.

of the plutonic suite (ca. 1865–1845 Ma; Whalen et al., 2010) postdates the Baffin suture (ca. 1880–1865 Ma; St-Onge et al., 2006), this shear zone could represent reactivation of the suture during prolonged THO deformation.

Future work

Ten new GSC 1:100 000 scale bedrock Canadian Geoscience Map sheets stemming from the 2015 work are currently being prepared for public dissemination in the spring of 2016. The maps, which will feature integrated descriptive notes and a common legend, will complete the modern bedrock-map coverage for Baffin Island south of latitude 70°N.

Planned laboratory work in autumn and winter 2015 includes U-Pb zircon geochronology of the metaplutonic suite from south-central Baffin Island to test correlations with the middle Paleoproterozoic Cumberland batholith and to further constrain the tectonostratigraphic parentage of the host metasedimentary rocks. In particular, detrital zircon will be analyzed from a variety of quartzite samples to establish provenance. All analyses will assist in calibrating the legend of the ten new bedrock maps.

Mineral electron-microprobe analyses and phase-equilibria modelling will document the metamorphic pressure and temperature conditions for samples collected from the map area. The results will be integrated with detailed petrographic studies and in situ monazite geochronology to constrain the tectonometamorphic history of south-central Baffin Island, which will assist in further understanding the evolution of the eastern THO.

Economic considerations

A number of lithological associations and occurrences with potential economic implications were identified during the 2015 field season. This includes several instances of sulphide-bearing gossanous metasedimentary rocks; magnetite and semi-precious minerals in marble, for example gem-quality diopside and apatite; layered mafic-ultramafic sills that may host sulphide mineralization; and several serpentinized ultramafic rocks, which may be suitable as carving stone.

Acknowledgments

Energetic and affable field assistance was provided by T. Chadwick, D. Liikane, T. Milton, S. Noble-Nowdluk, and T. Rowe. C. Gilbert and A. Ford are thanked for their careful management of the project data, with the latter also providing valuable support in the field. The authors are extremely grateful to the camp chef D. Guilfoyle for her many wonderful meals. Universal Helicopters, in particular pilots G. Nuttall and G. Hartery, and Kenn Borek Air are thanked for safe and professional air support. N. Shea, S. Dehler, M. Francis and R. Khoun are acknowledged for their management and administrative support. The Polar Continental Shelf Program (PCSP) provided logistical support (PCSP Project 056-15). Additional financial support of this study was provided by the Strategic Investments in Northern Economic Development (SINED) program delivered by the Canadian Northern Economic Development Agency (CanNor). G. Buller and R. Buenviaje are thanked for processing the archival and new data for south-central Baffin Island. The authors are also are grateful to H. Steenkamp and L. Ham for careful and insightful reviews of this paper.

Natural Resources Canada, Earth Science Sector contribution 20150290

References

Blackadar, R.G. 1967: Geological Reconnaissance, southern Baffin Island, District of Franklin; Geological Survey of Canada, Paper 66-47, 32 p. doi:10.4095/100926

Bucher, K. and Frey, M. 2002: Metamorphism of Granitoid Rocks; *in* Petrogenesis of Metamorphic Rocks, p. 329–334.

Clarke, D.B., Cameron, B.I., Muecke, G.K. and Bates, J.L. 1989: Early Tertiary basalts from the Labrador Sea and Davis Strait region; Canadian Journal of Earth Sciences, v. 26, p. 956–968.

Corrigan, D., Pehrsson, S., Wodicka, N. and de Kemp, E. 2009: the Palaeoproterozoic Trans-Hudson Orogen: a prototype of modern accretionary processes; *in* Ancient Orogens and Modern Analogues, J.B. Murphy, J.D. Keppie and A.J. Hynes (ed.), The Geological Society, London, Special Publications, v. 327, p. 457–479. doi:10.1144/SP327.19

Diener, J.F.A and Powell, R. 2010: Influence of ferric iron on the stability of mineral assemblages; Journal of Metamorphic Geology, v. 28, p. 599–613.

Dunphy, J.M. and Ludden, J.N. 1998: Petrological and geochemical characteristics of a Paleoproterozoic magmatic arc (Narsajuaq Terrane, Ungava Orogen, Canada) and comparisons to Superior Province granitoids; Precambrian Research, v. 91, p. 109–142.

Dyck, B.J. and St-Onge, M.R. 2014: Dehydration-melting reactions, leucogranite emplacement and the Paleoproterozoic structural evolution of Hall Peninsula, Baffin Island, Nunavut; *in* Summary of Activities 2013, Canada-Nunavut Geoscience Office, p. 73–84.

Heaman, L.M., LeCheminant, A.N. and Rainbird, R.H. 1992: Nature and timing of Franklin igneous events, Canada: implications for a Late Proterozoic mantle plume and the break-up of Laurentia; Earth and Planetary Science Letters, v. 109, p. 117–131.

Henderson, J.R. 1985: Geology, McBeth Fiord–Cape Henry Kater, District of Franklin, Northwest Territories; Geological Survey of Canada, Map 1605A, scale 1:250 000.

Hoffman, P.F. 1988: United Plates of America, the birth of a craton: Early Proterozoic assembly and growth of Laurentia; Annual Reviews of Earth and Planetary Sciences, v. 16, p. 543–603.

Holland, T.J.B. and Powell, R. 1998: An internally consistent thermodynamic dataset for phases of petrological interest; Journal of Metamorphic Geology, v. 16, p. 309–343.

Kiss, F. and Tschirhart, V. 2015a: Aeromagnetic survey Amittok Lake area, Baffin Island, Nunavut; Geological Survey of Canada, Open Files 7888–7891, scale 1:100 000.

Kiss, F. and Tschirhart, V. 2015b: Aeromagnetic survey McKeand River area, Baffin Island, Nunavut; Geological Survey of Canada, Open Files 7819–7832, scale 1:100 000.

Liikane, D.A., St-Onge, M.R., Kjarsgaard, B.A., Rayner, N.M., Ernst, R.E and Kastek, N. 2015: Frobisher suite mafic, ultramafic and layered mafic-ultramafic sills, southern Baffin Island, Nunavut; *in* Summary of Activities 2015, Canada-Nunavut Geoscience Office, p. 21–32.

Nekvasil, H. 1991: Ascent of felsic magmas and formation of rapakivi; American Mineralogist, v. 76, p. 1279–1290.

Palin, RM., Weller, O.M., Waters, D.J. and Dyck, B. in press: Quantifying geological uncertainty in metamorphic phase equilibria modelling; a Monte Carlo assessment and implications for tectonic interpretations; Geoscience Frontiers, online version of paper, 17 p. doi:10.1016/j.gsf.2015.08.005

Powell, R. and Holland, T.J.B. 2008: On thermobarometry; Journal of Metamorphic Geology, v. 26, p. 155–179.

Rayner, N.M., Sanborn-Barrie, M., Young, M.D. and Whalen, J.B. 2012: U-Pb ages of Archean basement and Paleoproterozoic plutonic rocks, southern Cumberland Peninsula, eastern Baffin Island, Nunavut; Geological Survey of Canada, Current Research 2012-8, 24 p.

Sanford, B.V. and Grant, A.C.A. 2000: Geological framework of the Ordovician system in the southeast Arctic platform, Nunavut; *in* Geology and Paleontology of the southeast Arctic Platform and southern Baffin Island, Nunavut; Geological Survey of Canada Bulletin 557, p. 13–38.

Scott, D.J. 1997: Geology, U-Pb, and Pb-Pb geochronology of the Lake Harbour area, southern Baffin Island: implications for the Paleoproterozoic tectonic evolution of north-eastern Laurentia; Canadian Journal of Earth Sciences, v. 34, p. 140–155.

Scott, D.J. and Wodicka, N. 1998: A second report on the U-Pb geochronology of southern Baffin Island; *in* Geological Survey of Canada, Current Research 1998-F, p. 47–57.

Scott, D.J., St-Onge, M.R., Wodicka, N. and Hanmer, S. 1997: Geology of the Markham Bay–Crooks Inlet area, southern Baffin Island, Northwest Territories; *in* Geological Survey of Canada, Current Research 1997-C, p. 157–166.

St-Onge, M.R., Hanmer, S. and Scott, D.J. 1996: Geology of the Meta Incognita Peninsula, south Baffin Island: tectonostratigraphic units and regional correlations; *in* Geological Survey of Canada, Current Research 1996-C, p. 63–72.

St-Onge, M.R., Scott, D.J., Wodicka, N. and Lucas, S.B. 1998: Geology of the McKellar Bay–Wight Inlet–Frobisher Bay area, southern Baffin Island, Northwest Territories; *in* Geological Survey of Canada, Current Research 1998-C, p. 43–53.

St-Onge, M.R., Scott, D.J. and Lucas, S.B. 2000a: Early partitioning of Quebec: Microcontinent formation in the Paleoproterozoic; Geology, v. 28, p. 323–326.

St-Onge, M.R. Wodicka, N. and Lucas, S.N. 2000b: Granulite- and amphibolite-facies metamorphism in a convergent plate-margin setting: Synthesis of the Quebec-Baffin segment of Trans-Hudson Orogen; Canadian Mineralogist, v. 38, p. 379–398.

St-Onge, M.R., Searle, M.P. and Wodicka, N. 2006: Trans-Hudson Orogen of North America and Himalaya-Karakoram-Tibetan Orogen of Asia: Structural and thermal characteristics of the lower and upper plates; Tectonics, v. 25, TC4006, 22 p. doi:10.1029/2005TC001907

St-Onge, M.R., Wodicka, N. and Ijewliw, O. 2007: Polymetamorphic evolution of the Trans-Hudson Orogen, Baffin Island, Canada: Integration of petrological, structural and geochronological data; Journal of Petrology, v. 48, p. 271–302. doi:10.1093/petrology/eg1060

St-Onge, M.R., Van Gool, J.A.M., Garde, A.A. and Scott, D.J. 2009: Correlation of Archaean and Palaeoproterozoic units between northeastern Canada and western Greenland: constraining the pre-collisional upper plate accretionary history of the Trans-Hudson orogen; *in* Earth Accretionary Systems in Space and Time, P.A. Cawood and A. Kroner, The Geological Society, London, Special Publications, v. 318, p. 193–235. doi:10.1144/SP318.7

Tschirhart, V., St-Onge, M.R. and Weller, O.M. 2015: Preliminary geophysical interpretation of the McKeand River area, southern Baffin Island, Nunavut: insights from gravity, magnetic and geological data; *in* Summary of Activities 2015, Canada-Nunavut Geoscience Office, p. 49–60.

Thériault, R.J., St-Onge, M.R. and Scott, D.J. 2001: Nd isotopic and geochemical signature of the Paleoproterozoic Trans-Hudson Orogen, southern Baffin Island, Canada: implications for the evolution of eastern Laurentia; Precambrian Research, v. 108, p. 113–138.

Weller, O.M., St-Onge, M.R., Searle, M.P., Rayner, N., Waters, D.J., Chung, S.L., Palin, R.M., Lee, Y.H. and Xu, X.W. 2013: Quantifying Barrovian metamorphism in the Danba Structural Culmination of eastern Tibet; Journal of Metamorphic Geology, v. 31, p. 909–935. doi:10.1111/jmg.12050

Weller, O.M., St-Onge, M.R., Rayner, N., Searle, M.P. and Waters, D.J. in press: Miocene magmatism in the Western Nyainqentanglha mountains of southern Tibet: an exhumed bright spot?; Lithos, online version of paper, 14 p. doi:10.1016/j.lithos.2015.06.024

Whalen, J.B., Wodicka, N., Taylor, B.E. and Jackson, G.D. 2010: Cumberland batholith, Trans-Hudson Orogen, Canada: Petrogenesis and implications for Paleoproterozoic crustal and orogenic processes; Lithos, v. 117, p. 99–118. doi:10.1016/j.lithos.2010.02.008

Wodicka, N. and Scott, D.J. 1997: A preliminary report on the U-Pb geochronology of the Meta Incognita Peninsula, southern Baffin Island, Northwest Territories; *in* Geological Survey of Canada, Current Research 1997-C, p. 167–178.

Wodicka, N., St-Onge, M.R., Corrigan, D., Scott, D.J. and Whalen, J.B. 2014: Did a proto-ocean basin form along the southeastern Rae cratonic margin? Evidence from U-Pb geochronology, geochemistry (Sm-Nd and whole-rock), and stratigraphy of the Paleoproterozoic Piling Group, northern Canada; GSA Bulletin, v. 126, p. 1625–1653. doi:10.1130/B31028.1

Appendix 1 – References cited in Figure 1

1. Blackadar, R.G. 1967: Geology, Cumberland Sound, District of Franklin, Northwest Territories; Geological Survey of Canada, Preliminary Map 17-1966, scale 1:506 880.
2. Blackadar, R.G. 1970: Nottingham, Salisbury, and Mill Islands, District of Franklin, Northwest Territories; Geological Survey of Canada, Preliminary Map 1205A, scale 1:250 000.
3. Jackson, G.D. 1971: Operation Penny Highlands, south-central Baffin Island; Geological Survey of Canada Paper 71-1, Part A, p. 138–140.
4. Trettin, H.P. 1975: Lower Paleozoic geology, central and eastern parts of Foxe Basin and Baird Peninsula, Baffin Island, District of Franklin, Northwest Territories; Geological Survey of Canada, Map 1406A, scale 1:500 000.
5. Morgan, W.C. 1982: Geology, Koch Island, District of Franklin, Northwest Territories; Geological Survey of Canada, Map 1535A, scale 1:250 000.
6. Henderson, J.R. 1985a: Geology, McBeth Fiord-Cape Henry Kater, District of Franklin, Northwest Territories; Geological Survey of Canada, Map 1605A, scale 1:250 000.
7. Henderson, J.R. 1985b: Geology, Ekalugad Fiord-Home Bay, District of Franklin, Northwest Territories; Geological Survey of Canada, Map 1606A, scale 1:250 000.
8. Jackson, G.D. 1998: Geology, Okoa Bay-Padloping Island area, District of Franklin, Northwest Territories; Geological Survey of Canada, Open File 3532, scale 1:250 000.
9. St-Onge, M.R., Scott, D.J. and Wodicka, N. 1999a: Geology, Frobisher Bay, Nunavut; Geological Survey of Canada, "A" Series Map 1979A, 1:100 000 scale. doi:10.4095/210833
10. St-Onge, M.R., Scott, D.J. and Wodicka, N. 1999b: Geology, Hidden Bay, Nunavut; Geological Survey of Canada, "A" Series Map 1980A, 1:100 000 scale. doi:10.4095/210835
11. St-Onge, M.R., Scott, D.J. and Wodicka, N. 1999c: Geology, McKellar Bay, Nunavut; Geological Survey of Canada, "A" Series Map 1981A, 1:100 000 scale. doi:10.4095/210836
12. St-Onge, M.R., Scott, D.J. and Wodicka, N. 1999d: Geology, Wright Inlet, Nunavut; Geological Survey of Canada, "A" Series Map 1982A, 1:100 000 scale. doi:10.4095/210840
13. St-Onge, M.R., Scott, D.J. and Wodicka, N. 1999e: Geology, Blandford Bay, Nunavut; Geological Survey of Canada, "A" Series Map 1983A, 1:100 000 scale. doi:10.4095/210837
14. St-Onge, M.R., Scott, D.J. and Wodicka, N. 1999f: Geology, Crooks Inlet, Nunavut; Geological Survey of Canada, "A" Series Map 1984A, 1:100 000 scale. doi:10.4095/210838
15. St-Onge, M.R., Scott, D.J. and Wodicka, N. 1999g: Geology, White Strait, Nunavut; Geological Survey of Canada, "A" Series Map 1985A, 1:100 000 scale. doi:10.4095/210839
16. Sanford, B.V. and Grant, A.C. 2000: Geological framework of the Ordovician system in the southeast Arctic platform, Nunavut; in Geology and Paleontology of the southeast Arctic Platform and southern Baffin Island, Nunavut; Geological Survey of Canada Bulletin 557, p. 13–38.
17. Jackson, G.D. 2002: Geology, Isurtuq River-Nedlukseak Fiord, Nunavut; Geological Survey of Canada, Open File 4259, scale 1:250 000.
18. St-Onge, M.R., Scott, D.J., Corrigan, D., and Wodicka, N. 2005a: Geology, Ikpik Bay, Baffin Island, Nunavut; Geological Survey of Canada Map 2077A, 1:100 000 scale.
19. St-Onge, M.R., Scott, D.J., Corrigan, D., and Wodicka, N. 2005b: Geology, Flyway Lake, Baffin Island, Nunavut; Geological Survey of Canada Map 2078A, 1:100 000 scale.
20. St-Onge, M.R., Scott, D.J., Corrigan, D., and Wodicka, N. 2005c: Geology, Clyde River, Baffin Island, Nunavut; Geological Survey of Canada Map 2079A, 1:100 000 scale.
21. St-Onge, M.R., Scott, D.J., Corrigan, D., and Wodicka, N. 2005d: Geology, Piling Bay, Baffin Island, Nunavut; Geological Survey of Canada Map 2080A, 1:100 000 scale.
22. St-Onge, M.R., Scott, D.J., Corrigan, D., and Wodicka, N. 2005e: Geology, Straits Bay, Baffin Island, Nunavut; Geological Survey of Canada Map 2081A, 1:100 000 scale.
23. St-Onge, M.R., Scott, D.J., Corrigan, D., and Wodicka, N. 2005f: Geology, Dewar Lakes, Baffin Island, Nunavut; Geological Survey of Canada Map 2082A, 1:100 000 scale.
24. Jackson, G.D. 2006: Geology, Hantzsch River area, Baffin Island, Nunavut; Geological Survey of Canada, Open File 4202, scale 1:250 000.
25. St-Onge, M.R., Sanborn-Barrie, M., and Young, M. 2007a: Geology, Mingo Lake, Baffin Island, Nunavut; Geological Survey of Canada Open File Map 5433, 1:250 000 scale.
26. St-Onge, M.R., Sanborn-Barrie, M., and Young, M. 2007b: Geology, Foxe Peninsula, Baffin Island, Nunavut; Geological Survey of Canada Open File Map 5434, 1:250 000 scale.
27. Sanborn-Barrie, M., Young, M., Whalen, J. and James, D. 2011a: Geology, Ujuktuk Fiord, Nunavut; Geological Survey of Canada, Canadian Geoscience Map 1, (ed. 2, prelim.) 2011; 1 sheet, 1 CD-ROM. doi:10.4095/289237
28. Sanborn-Barrie, M., Young, M. and Whalen, J. 2011b: Geology, Kingnait Fiord, Nunavut; Geological Survey of Canada, Canadian Geoscience Map 2, (ed. 2, prelim.) 2011; 1 , 1 CD-ROM. doi:10.4095/289238
29. Sanborn-Barrie, M., Young, M., Whalen, J., James, D. and St-Onge, M.R. 2011c: Geology, Touak Fiord, Nunavut; Geological Survey of Canada, Canadian Geoscience Map 3 (ed. 2, prelim.), 1 sheet, 1 CD-ROM. doi:10.4095/289239
30. Sanborn-Barrie, M., and Young, M. 2013a: Geology, Circle Lake, Nunavut; Geological Survey of Canada, Canadian Geoscience Map 5 (ed. prelim.), scale 1:100 000; 1 sheet, 1 CD-ROM. doi:10.4095/288929
31. Sanborn-Barrie, M., Young, M., Keim, R., and Hamilton, B.M. 2013b: Geology, Sunneshine Fiord, Nunavut; Geological Survey of Canada, Canadian Geoscience Map 6 (ed. prelim.), scale 1:100 000; 1 sheet, 1 CD-ROM. doi:10.4095/288931
32. Sanborn-Barrie, M. and Young, M. 2013c: Geology, Padle Fiord, Nunavut; Geological Survey of Canada, Canadian Geoscience Map 37 (ed. prelim.), scale 1:100 000, 1 sheet, 1 CD-ROM. doi:10.4095/292014
33. Sanborn-Barrie, M. and Young, M. 2013d: Geology, Durban Harbour, Nunavut; Geological Survey of Canada, Canadian Geoscience Map 38 (ed. prelim.), scale 1:100 000, 1 sheet, 1 CD-ROM. doi:10.4095/292015
34. Sanborn-Barrie, M., and Young, M. 2013e: Geology, Qikiqtarjuaq, Nunavut; Geological Survey of Canada, Canadian Geoscience Map 39 (ed. prelim.), scale 1:100 000, 1 sheet, 1 CD-ROM. doi:10.4095/292016
35. Jackson, G.D. and Sanborn-Barrie, M. 2014: Geology, Pangnirtung Fiord, Nunavut; Geological Survey of Canada,

Canadian Geoscience Map 4 (ed. prelim.), 1:100 000 scale, 1 sheet. doi:10.4095/288928

36. St-Onge, M.R ., Rayner, N.M., Steenkamp, H.M., and Gilbert, C. 2015a: Geology, Terra Nivea, Baffin Island, Nunavut; Geological Survey of Canada , Canadian Geoscience Map 215E (preliminary); Canada-Nunavut Geoscience Office, Open File Map 2015-02E, scale 1:100 000. doi:10.4095/296104
37. St-Onge, M.R., Rayner, N.M., Steenkamp, H.M., and Gilbert, C. 2015b: Geology, Pritzler Harbour, Baffin Island, Nunavut; Geological Survey of Canada, Canadian Geoscience Map 216E (preliminary); Canada-Nunavut Geoscience Office, Open File Map 2015-03E, scale 1:100 000. doi:10.4095/296109
38. St-Onge, M.R., Rayner, N.M., Steenkamp, H.M., and Gilbert, C. 2015c: Geology, Grinnell Glacier, Baffin Island, Nunavut; Geological Survey of Canada, Canadian Geoscience Map 217E (preliminary); Canada-Nunavut Geoscience Office, Open File Map 2015-04E, scale 1:100 000. doi:10.4095/296111
39. Steenkamp, H.M., Gilbert, C., and St-Onge, M.R. 2016a: Geology, Loks Land, Baffin Island, Nunavut, NTS 25-I (part); Geological Survey of Canada, Canadian Geoscience Map 264 (preliminary); Canada-Nunavut Geoscience Office, Open File Map 2016-01, scale 1:100 000. doi:10.4095/297344
40. Steenkamp, H.M., Gilbert, C. and St-Onge, M.R. 2016b: Geology, Ward Inlet (south), Baffin Island, Nunavut,NTS 25-O (south) and 25-J (part); Geological Survey of Canada, Canadian Geoscience Map 266 (preliminary); Canada-Nunavut Geoscience Office, Open File Map 2016-02, scale 1:100 000. doi:10.4095/297349
41. Steenkamp, H.M., Gilbert, C., and St-Onge, M.R. 2016c: Geology, Ward Inlet (north), Baffin Island, Nunavut, NTS 25-O (north); Geological Survey of Canada, Canadian Geoscience Map 265 (preliminary); Canada-Nunavut Geoscience Office, Open File Map 2016-03, scale 1:100 000. doi:10.4095/297348
42. Steenkamp, H.M., Gilbert, C., St-Onge, M.R. 2016d: Geology, Beekman Peninsula (south), Baffin Island, Nunavut, NTS 25-P (south) and 15-M (part); Geological Survey of Canada, Canadian Geoscience Map 267 (preliminary); Canada-Nunavut Geoscience Office, Open File Map 2016-04, scale 1:100 000. doi:10.4095/297351
43. Steenkamp, H.M., Gilbert, C., and St-Onge, M.R. 2016e: Geology, Beekman Peninsula (north), Baffin Island, Nunavut, NTS 25-P (north) and 15-M (part); Geological Survey of Canada, Canadian Geoscience Map 268 (preliminary); Canada-Nunavut Geoscience Office, Open File Map 2016-05, scale 1:100 000. doi:10.4095/297352
44. Steenkamp, H.M., Gilbert, C., and St-Onge, M.R. 2016f: Geology, Leybourne Islands (south), Baffin Island, Nunavut, NTS 26-A (south); Geological Survey of Canada, Canadian Geoscience Map 269 (preliminary); Canada-Nunavut Geoscience Office, Open File Map 2016-06, scale 1:100 000. doi:10.4095/297353
45. Steenkamp, H.M., Gilbert, C., and St-Onge, M.R. 2016g: Geology, Leybourne Islands (north), Baffin Island, Nunavut, NTS 26-A (north); Geological Survey of Canada, Canadian Geoscience Map 271 (preliminary); Canada-Nunavut Geoscience Office, Open File Map 2016-07, scale 1:100 000. doi:10.4095/297355
46. Steenkamp, H.M., Gilbert, C., and St-Onge, M.R. 2016h: Geology, Chidliak Bay (south), Baffin Island, Nunavut, NTS 26-B (south); Geological Survey of Canada, Canadian Geoscience Map 272 (preliminary); Canada-Nunavut Geoscience Office, Open File Map 2016-08, scale 1:100 000. doi:10.4095/297357
47. Steenkamp, H.M., Gilbert, C., and St-Onge, M.R. 2016i: Geology, Chidliak Bay (north), Baffin Island, NTS 26-B (north); Geological Survey of Canada, Canadian Geoscience Map 270 (preliminary); Canada-Nunavut Geoscience Office, Open File Map OFM2016-09, scale 1:100 000. doi:10.4095/297354

Preliminary geophysical interpretation of the McKeand River area, southern Baffin Island, Nunavut: insights from gravity, magnetic and geological data

V. Tschirhart[1], M.R. St-Onge[2] and O.M. Weller[2]

[1]*Natural Resources Canada, Geological Survey of Canada, Ottawa, Ontario, victoria.tschirhart@canada.ca*

[2]*Natural Resources Canada, Geological Survey of Canada, Ottawa, Ontario*

This work was part of the larger South Baffin mapping project, a partnership between the Canada-Nunavut Geoscience Office (CNGO) and Natural Resources Canada's (NRCan) Geo-mapping for Energy and Minerals (GEM) Program on Baffin Island. This particular mapping project is being led by the Geological Survey of Canada (GSC) in collaboration with CNGO, the Government of Nunavut, Nunavut Arctic College, Carleton University and Oxford University. Logistical support is provided by the Polar Continental Shelf Project and several local, Inuit-owned businesses. The study area comprises all or parts of six 1:250 000 map areas north of Iqaluit (NTS 26B, C, F, G, K and J). The objective of the work is to complete the regional bedrock mapping for the southern half of Baffin Island and provide a new, modern, geoscience understanding of this part of eastern Nunavut.

Tschirhart, V., St-Onge, M.R. and Weller, O.M. 2015: Preliminary geophysical interpretation of the McKeand River area, southern Baffin Island, Nunavut: insights from gravity, magnetic and geological data; *in* Summary of Activities 2015, Canada-Nunavut Geoscience Office, p. 49–60.

Abstract

The recently completed McKeand River and Amittok Lake aeromagnetic surveys on southern Baffin Island, Nunavut provide a new high-resolution magnetic dataset over an area with no previous coverage. Complemented by regional gravity data, newly acquired rock-property information and geological-mapping products, the aeromagnetic dataset yields qualitative and quantitative information on the structure and geology of the underlying bedrock. This paper presents a preliminary interpretation of these datasets that delineates three gravimetric and five magnetic domains. The gravity data outline a broad negative anomaly associated with a plutonic-intrusive suite, as well as several isolated gravity highs associated with metasedimentary strata. Magnetic domains are defined on the basis of anomaly amplitude, wavelength and texture, and are correlated to the mapped geology and magnetic properties. Associations between potential-field anomalies, physical properties and mineral occurrences help define the regional distribution of economically significant horizons.

Résumé

Les levés aéromagnétiques récemment réalisés dans la région de la rivière McKeand et du lac Amittok, dans le sud de l'île de Baffin, au Nunavut, fournissent de nouvelles données magnétiques à haute résolution d'une région qui en était auparavant dépourvue. Conjuguées aux données gravimétriques régionales, à l'information nouvellement acquise au sujet des propriétés pétrographiques et aux produits de cartographie géologique, les données aéromagnétiques fournissent des informations de nature qualitative et quantitative sur la structure et la géologie de la roche en place sousjacente. Cet article présente une interprétation préliminaire de ces ensembles de données qui délimitent trois domaines gravimétriques et cinq domaines magnétiques. Les données gravimétriques mettent en relief une grande anomalie négative associée à une suite intrusive plutonique, ainsi que plusieurs anomalies positives isolées associées aux strates de roches métasédimentaires. Les domaines magnétiques sont définis en fonction de l'amplitude, de la longueur d'onde et de la texture de l'anomalie, et sont mis en corrélation avec les unités géologiques cartographiées et les propriétés magnétiques. La relation entre les anomalies gravimétriques et magnétiques, les propriétés physiques et les venues minérales aide à définir la répartition régionale des horizons d'importance économique.

This publication is also available, free of charge, as colour digital files in Adobe Acrobat® PDF format from the Canada-Nunavut Geoscience Office website: http://cngo.ca/summary-of-activities/2015/.

Introduction

Used extensively for bedrock mapping, potential field (gravity and magnetic) maps provide continuous datasets over broad swaths of land. Laterally adjacent, contrasting physical properties (density and magnetic susceptibility) generate potential-field anomalies due to the presence (positive anomaly) or absence (negative or absent anomaly) of dense or magnetic minerals within underlying bedrock units. Subtle compositional differences create textural contrasts and discontinuities on the potential-field maps, and assist in the delineation of distinct geophysical domains that often coincide with distinct map units, lithotectonic domains, geological provinces or terrain boundaries (e.g., Pilkington et al., 2000). Anomaly amplitude and wavelength, and the orientation of magnetic lineaments provide additional information on the structure, geometry and lithology of discrete rock packages. Prospective units identified from outcrop can thus be identified and geophysically characterized for aerially constrained detailed follow-up. Geophysical interpretations supplement the geological knowledge, adding value and precision to the geological interpretation.

On southern Baffin Island, Nunavut, detailed geoscience data were previously lacking, limited to reconnaissance-scale mapping in the mid-1960s (Blackadar, 1967). Informed exploration and development of this region requires modern geoscience knowledge to minimize financial risks and exploration costs associated with focused ground follow-up. The Geo-mapping for Energy and Minerals (GEM) program addressed this knowledge gap through the Southern Baffin Island Mapping Project (Rayner et al., 2015). During eight weeks of fieldwork in 2015, all or parts of six 1:250 000 map areas (NTS 26B, C, F, G, J, K) were mapped at 1:100 000 scale. To support the bedrock mapping and compilation effort, two high-resolution magnetic surveys (Kiss and Tschirhart, 2015a, b) were flown over the study area, generating a continuous magnetic dataset for southern Baffin Island. Geophysical fieldwork, conducted in conjunction with the geological mapping, included sampling of anomalous units to determine the nature of the magnetic properties of the bedrock and to calibrate the magnetic rocks with their respective magnetic anomalies. This paper provides an overview of these investigations and presents the first potential-field interpretive products for the southern Baffin Island region via detailed integration of magnetic, gravity and geological datasets. The geophysical responses of key lithotectonic features are described and provide insight on the spatial distribution of potentially mineralized rock types, including kimberlite pipes, layered mafic–ultramafic intrusions and sulphide-bearing metasedimentary packages. Future analysis characterizing the densities of anomalous units is planned and will further constrain the modelling of regional gravity and a high-resolution ground-gravity transect.

Geological setting

The study area (Figure 1) is underlain by Archean and Paleoproterozoic rocks that have been variably deformed and metamorphosed during the accretionary and continental-collision phases of the Trans-Hudson Orogen (THO). The THO has a broad arcuate shape, extending from northeastern to south-central North America (Hoffman, 1988), and its formation involved the northward subduction of the Superior craton beneath an amalgamation of crustal blocks (Churchill plate) from 1.92 to 1.80 Ga (St-Onge et al., 2006b, 2009). Three orogen-scale, stacked tectonic elements separated by major crustal structures underlie southern Baffin Island (Figure 1; St-Onge et al., 2015).

From east to west, the bedrock in the project area comprises three major crustal entities (Figure 1):

- 2.92–2.80 Ga gneissic rocks of the Hall Peninsula crystalline basement (Scott, 1999; From et al., 2014; Steenkamp and St-Onge, 2014)
- metasedimentary units of the <2.01 to >1.90 Ga Lake Harbour Group, which include quartzite, amphibolite, calcsilicate, semipelite, pelite and psammite, and local mafic-ultramafic metavolcanic sills (St-Onge et al., 2006a; Machado et al., 2013; Steenkamp et al., 2014)
- 1.865–1.845 Ga metaplutonic units of the Cumberland Batholith (CB), comprising voluminous granodiorite to monzogranite (Whalen et al., 2010), that intrude the above units

All of the above are crosscut by ca. 720 Ma basaltic Franklin dykes, trending 110–120° (Heaman et al., 1992).

Geophysical datasets

Magnetic data

The McKeand River (Miles et al., 2015) and Amittok Lake magnetic surveys were acquired from August 5, 2014 to April 5, 2015 along east-west flight lines spaced 400 m apart and flown along a smooth drape surface at a height of 150 m. The surveys were funded jointly by the Canada-Nunavut Geoscience Office (CNGO) and GEM to support the bedrock-mapping program. The study area (Figure 2a) includes five individual surveys (Figure 2b) that were merged to create a continuous magnetic dataset. The regional magnetic data (survey NWT#31, 805 m line spacing; Natural Resources Canada, 2015) in the north were reprocessed to remove corrugations in the flight-line direction and stitched to the Amittok Lake data (Kiss and Tschirhart, 2015a). In the south, the Hall Peninsula survey (400 m line spacing; Dumont and Dostaler, 2010) and the South Baffin area IC survey (805 m line spacing; Natural Resources Canada, 2015) were stitched to the McKeand River data (Kiss and Tschirhart, 2015b). The stitched northern and southern datasets were merged to create a compilation residual total field (RTF) map for southern

Baffin Island (Figure 2a). The datasets are available for download from the Geological Survey of Canada's (GSC) Geoscience Data Repository (http://gdr.agg.nrcan.gc.ca/gdrdap/dap/search-eng.php).

Additional information relevant to geological interpretation was extracted from the RTF grid through the use of source edge detection (SED) processing. The SED routines have been used extensively by geophysicists to provide additional information on the structure and geometry of geological sources associated with magnetic anomalies. They operate by maximizing derivative-based mathematical functions over the magnetic source or source edge, which enhances subtle contrasts in physical properties. An edge, as discussed herein, is presumed to be a boundary that can be stratigraphic, intrusive or tectonic in origin. The first vertical derivative and tilt derivative (Miller and Singh, 1994) grids were calculated from the RTF data. The first vertical derivative accentuates short-wavelength, near-surface features within the upper crust, whereas the tilt derivative acts as an automatic gain-control filter that enhances all features equally (Nabighian et al., 2005). The enhanced magnetic signatures provided in these derivative maps help identify features such as faults, folds and the textural characteristics of magnetic-lithological units.

Magnetic susceptibility was measured on field samples and in outcrop using a Terraplus KT-10 magnetic-susceptibility meter. The values are summarized in Table 1. No magnetic remanence information was available for this study area.

Gravity data

The regional gravity database for southern Baffin Island is based on ground gravity measurements spaced 12–15 km apart, which have been used to derive a 2 km grid using

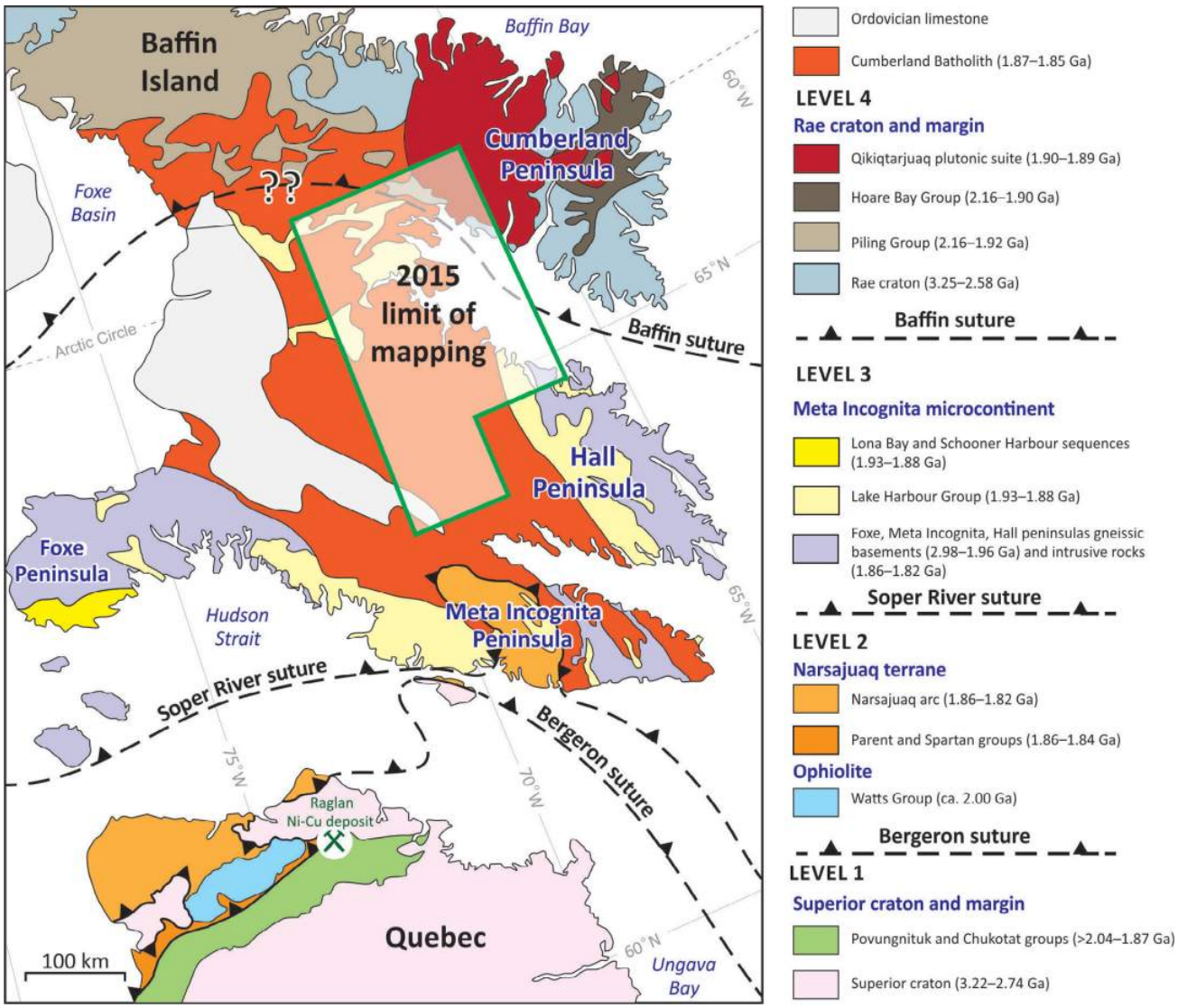

Figure 1: Regional geology of southern Baffin Island, Nunavut.

minimum curvature. The data and grid are available online from the GSC's Geoscience Data Repository (http://gdr.agg.nrcan.gc.ca/gdrdap/dap/search-eng.php). The isostatically corrected Bouguer gravity that was used for the interpretation reflects density variations in Earth's upper and lower crust. The large station spacing only permits resolution of features wider than 25 km; it is therefore useful only for delineating major tectonic or lithological elements and crustal boundaries. At of the time of writing, no density measurements were available for the study area. Gravity anomaly correlations to specific rock types are based on analogous physical-property data (V. Tschirhart, unpublished datasets, 2009–2014).

Interpretation products

Regional gravity anomalies

Within the study area, the Bouguer gravity grid (Figure 3) is dominated by three broad, long-wavelength anomalies:

- an east-southeast-trending low (L1, –53 mGal amplitude) that transects the study area from Cumberland Sound to Foxe Basin

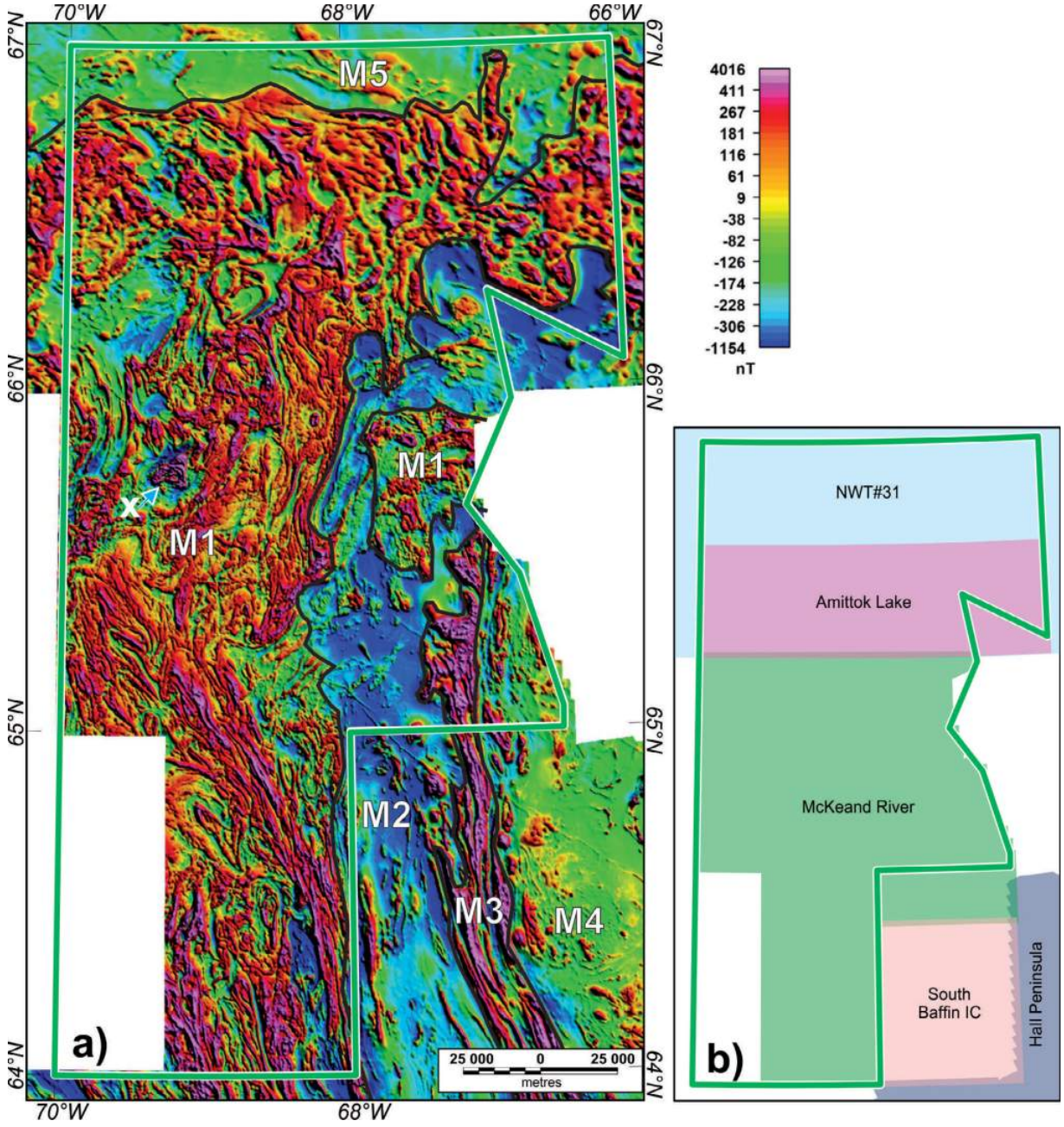

Figure 2: a) Residual total field (RTF) data for the study area (green outline), southern Baffin Island, Nunavut; labels explained in the text. **b)** Location of aeromagnetic surveys within the study area.

Table 1: Magnetic susceptibilities of rocks in the McKeand River area, southern Baffin Island, Nunavut.

	Lithology	Average susceptibility (10^{-3} SI)	Log average susceptibility (10^{-3} SI)	Minimum	Maximum	No. of samples
Felsic (Cumberland Batholith)	Monzogranite	6.86	1.02	0.02	71.37	32
	Granodiorite	10.61	1.99	0.21	36.00	4
	Leucogranite	0.08	0.04	0.00	0.20	4
	Syenogranite	0.39	0.23	0.06	1.31	6
	Tonalite	0.18	0.17	0.15	0.20	2
Intermediate	Diorite	29.70	25.81	15.00	44.40	2
Mafic	Gabbro	15.41	2.53	0.28	96.00	18
	Anothosite	0.20	0.12	0.03	0.47	5
Ultramafic	Peridotite	11.43	11.36	6.29	17.80	2
	Dunite	3.13	1.33	0.21	7.90	2
Metasedimentary rocks (Lake Harbour Group)	Psammite	7.58	0.76	0.02	45.60	15
	Pelite	0.25	0.24	0.20	0.30	3

- north-northwest-trending highs (H1, 20–26 mGal amplitude, and H2, 15 mGal amplitude) that extend from Hall and Meta Incognita peninsulas to the southern margin of the study area, respectively, and taper slightly toward the north-northwest
- a high flanked by steep gradients (H3) in the northeastern corner of the study area

The area of L1 and its neighbouring moderate (–35 to –28 mGal) gravity anomalies is mapped as CB intruding Archean basement and Paleoproterozoic metasedimentary belts. The wavelength and amplitude of L1 suggest the presence at depth of significant volumes of low-density (<2.67 g/cc) rocks, such as CB granitoid rocks, as opposed to denser Archean gneissic basement (>2.70 g/cc; V. Tschirhart, unpublished datasets, 2009–2014). Isolated enclaves and panels of metasedimentary strata mapped at the surface (Figure 3), which have a higher mean density than that of CB granitoid rocks, are of insufficient spatial extent, and presumably thickness, to produce positive gravity responses given the large gravity-station separation.

Rafts of Lake Harbour and Piling Group metasedimentary strata within the CB provide tectonostratigraphic constraints on the location of the Baffin suture (Figure 1; St-Onge et al., 2009; Whalen et al., 2010; Weller et al., 2015), which is interpreted to record the 1.883–1.865 Ga accretion of the upper-plate Meta Incognita microcontinent to the Rae craton (St-Onge et al., 2006b, 2009; Whalen et al., 2010). In many areas, regional gravity data have been used to demarcate cryptic tectonic sutures by identifying paired positive and negative gravity anomalies, where the trace of the suture is at the inflection point between the positive and negative anomalies (Gibb et al., 1983; Thomas, 1992). In the northeastern portion of the study area, the projected location of the Baffin suture follows the southern flank of H3 before angling to the west and crosscutting moderate to low gravity anomalies (Figure 3). However, the exact location of the Baffin suture is obscured by the emplacement of the CB and accompanying widespread crustal melting (Whalen et al., 2010). As the CB intruded after accretion, its negative gravity effect may have modified any pre-existing paired positive and negative anomalies that may have been present.

The H1 gravity high extends north-northwest from western Hall Peninsula, and a parallel high (H2) with a similar amplitude extends north-northwest from Meta Incognita Peninsula (Figure 3). The H1 high coincides with three distinct entities (Figures 2, 4): Archean gneiss, CB, and the Lake Harbour metasedimentary strata, which coincide with the central axis of the high. With a width of >85 km, the anomaly presumably corresponds to a large volume of relatively high density material that apparently differs from the mapped surface bedrock geology. Comprising mainly low-density CB, the peninsulas also include moderately dense metasedimentary strata and Archean gneiss. No large-scale, dense lithogical entities have been mapped at surface, suggesting the high is related to a feature at depth. Layered mafic and ultramafic sills emplaced in the metasedimentary rocks have been documented extensively on both peninsulas (Figure 3; Machado et al., 2013; Steenkamp et al., 2014; St-Onge, et al., 2015) and exhibit Ni-Cu-platinum group element (PGE) potential. If these are contemporaneous, they indicate the presence of intrusive activity on a huge scale. St-Onge et al. (2015) proposed that events of such a size could correspond to a large-igneous-province (LIP) event, which can be associated with significant volumes of high-density crustal bodies (Ernst and Buchan, 1997). Figure 3 shows the location of mafic-ultramafic occurrences (purple dots from St-Onge et al., 2006; Steenkamp et al., 2014; St-Onge et al., 2015) on the gravity map. The majority of occurrences are concentrated on or around the margins of H1 or H2, warranting additional gravity modelling to examine the source of the highs and to determine if there are any links to mafic-ultramafic occurrences. Alternatively, the gravity highs may relate to the juxtaposition of accreted plates and resulting lithospheric flexure from closure of the Baffin suture (Pilkington, 1990), which could also be investigated by modelling.

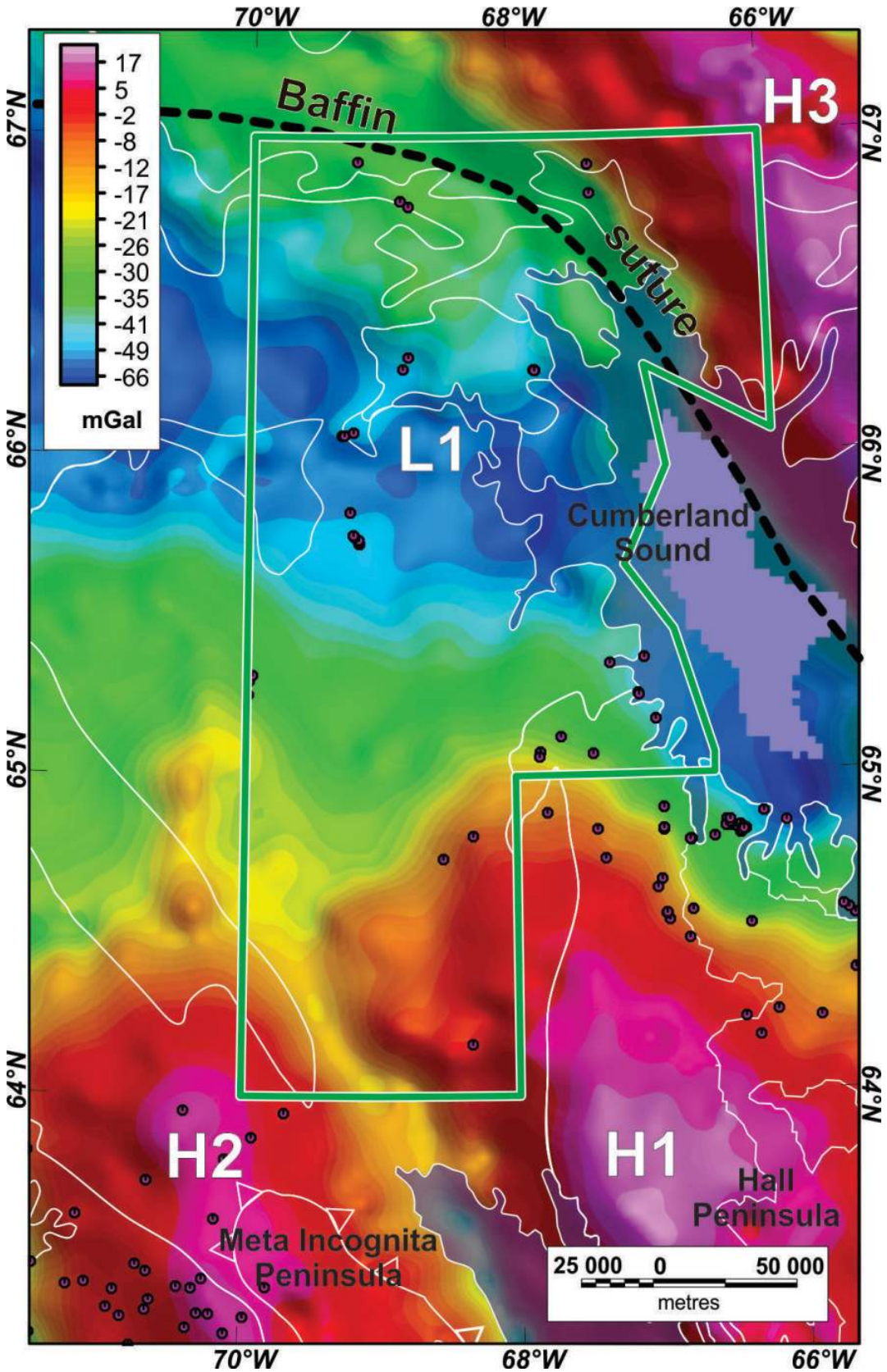

Figure 3: Regional gravity data for the McKeand River study area (green outline; labels as discussed in text); location of mafic-ultramafic occurrences from St-Onge et al. (2006a), Steenkamp et al. (2014) and St-Onge et al. (2015) plotted as purple circles; projected location of Baffin suture (St-Onge et al., 2009) shown by dashed black line and geological contacts from Figure 1 as thin solid white lines.

Magnetic domains

Schetselaar et al. (2013) constructed a remote predictive map for Hall Peninsula, which includes the southeastern limit of the present study area, using remote-sensing imagery, digital elevation models and magnetic data. Map development included subdividing the area into three magnetic domains. In the present study, magnetic texture, amplitude and wavelength are used to subdivide the McKeand River area into five magnetic domains (M1–M5 on Figures 2, 4, 5), M2 generally coinciding with the projected northern extent of the CB domain of Schetselaar et al. (2013), M3 with their high-grade mobile-belt domain and M4 with an Archean gneiss-supracrustal domain.

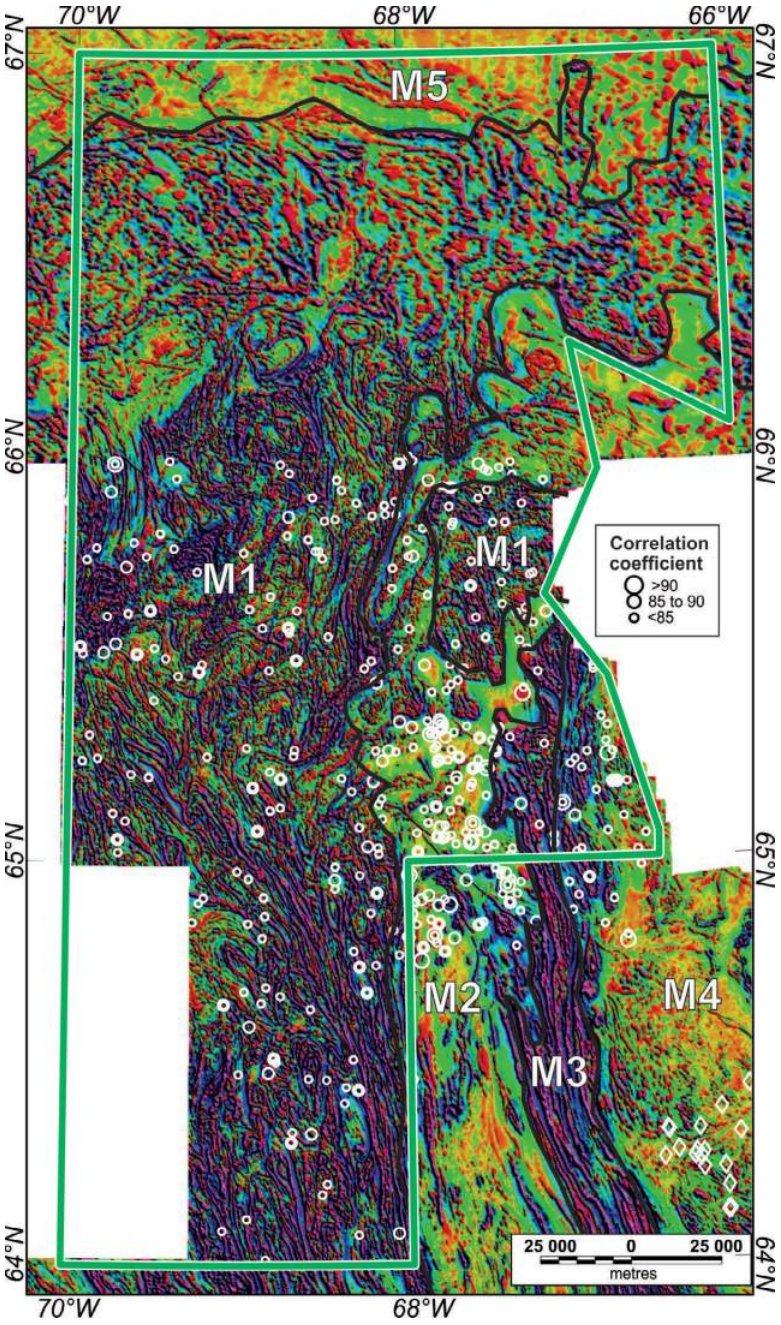

Figure 4: First vertical derivative of the magnetic field over the McKeand River study area (green outline; labels as discussed in text), with known kimberlites plotted as white diamonds (Pell, 2010) and Keating correlation coefficients (Kiss and Tschirhart, 2015b) as white circles scaled to the coefficient values. A high correlation coefficient (>90) indicates a closer match between the observed and modelled magnetic anomalies, with a value of 100 indicating a perfect match.

The largest and most prominent features are in M1, located west of latitude 68°W and extending most of the length of the map area. The anomalies are curvilinear and oriented in a number of directions, and correspond to variably magnetic CB with magnetic susceptibilities ranging from 0.08 to 71.4 × 10^{-3} SI (Table 1). Phase-equilibrium modelling of a representative sample of CB documents competing orthopyroxene and magnetite stability fields (Weller et al., 2015), consistent with field magnetic-susceptibility measurements and remote imagery showing highly variable magnetic properties within individual plutonic bodies. Distinct fold hinges and robust deformation features are visible in the RTF (Figure 2a) and enhanced by the SED data (Figures 4, 5), and correlate with regional structural elements (Figure 2). A distinct gabbroic body is responsible for the largest magnetic anomaly in the study (indicated by a white '×' on Figure 2a; maximum magnetic susceptibility of 96 × 10^{-3} SI, >3500 nT in amplitude). The gabbro is coarse grained and layered, varying in composition from hornblende gabbro to leucogabbro and anorthosite.

The M1 domain is flanked to the east by M2, a north-south belt of nonmagnetic rocks punctuated by circular to elongate magnetic anomalies and moderately magnetic CB curvilinear textures (Figure 2a). The CB monzogranite and Lake Harbour Group psammite have a similar average and range of magnetic susceptibilities (Table 1); however, the most magnetic psammite measured in the field corresponds to thin layers within a more extensive nonmagnetic sequence. This is reflected as a distinct magnetic signature where pronounced, elongate magnetic anomalies in M2 are interpreted to outline bands of magnetic psammite. With the exception of these psammitic strata, rafts of other Lake Harbour Group metasedimentary rocks encountered in the field (e.g., pelite, semipelite and psammite) did not have a pronounced magnetic signature or texture (Figure 2a; Table 1) and, as such, would be magnetically transparent. Within an area of predominantly CB intrusive rocks, it would thus be difficult, if not impossible, to remotely locate discrete packages of Lake Harbour Group metasedimentary rocks on the basis of magnetic signature alone. The subdued magnetic response of M2 relative to the strong magnetic signature of M1 is attributed to extensive Lake Harbour Group metasedimentary strata being present over a larger area.

A pronounced belt (M3) of linear north-south aeromagnetic highs separates the eastern (M2) domain and western (M4) Hall Peninsula gneissic rocks (Machado et al., 2013). The M3 domain is mapped as 1877 Ma magnetite-bearing tonalitic-granodioritic plutons (Scott, 1999; Steenkamp et al., 2014) that intrude both the M2 and M4 domains. In the eastern part of M4, the magnetic texture changes notably across a moderately magnetic background dominated by stippled positive anomalies that lack the pronounced linear north-northwesterly-striking magnetic fabric along the western margin. The Hall Peninsula Archean gneissic rocks host the diamondiferous Chidliak kimberlite field, and several of the stippled anomalies correspond to kimberlite pipes (Figure 4, white diamonds; Pell et al., 2013), which have a characteristic magnetic response as circular positive or negative anomalies, depending on the magnetization direction. Although the flight-line spacing of the southern RTF datasets (South Baffin IC, Hall Peninsula and McKeand River) does not permit discrimination of magnetic kimberlites between lines, the signatures of those along the lines will be recorded by the aircraft sensor (Reed and Witherly, 2007).

To determine if such signatures are present, the Keating correlation coefficient (Keating, 1995) was computed on the vertical derivative of the magnetic field (Kiss and Tschirhart, 2015a, b) prior to the 2015 field season. The Keating correlation coefficient uses a pattern recognition technique that consists of computing, over a moving window, a first-order regression between a vertical cylinder anomaly modelled from a known kimberlite and the gridded magnetic data. As a first-order assessment of the kimberlite potential west of, and for the northern extent of, the Hall Peninsula gneissic rocks, prospective kimberlite anomalies are located on the basis of magnetic signature alone (Figure 4, white circles). Ground follow-up of several magnetic 'pimples' during the 2015 field season either did not identify the magnetic source or located small plugs of magnetic gabbro within Lake Harbour Group metasedimentary strata.

The M5 domain occupies the northernmost section of the study area and is entirely within the area of the low-resolution magnetic data (Figure 2a). With the exception of a number of isolated Lake Harbour Group or Piling Group metasedimentary enclaves, the field observations mapped dominantly CB within the southern limits of M5. More extensive Piling Group metasedimentary outliers, comprising extensive psammite and pelite and mapped immediately north of the study area (St-Onge et al., 2006a), may contribute to the broader, subdued regional magnetic response of M5.

The 720 Ma Franklin dyke swarm is evident in the RTF and SED images as magnetic highs oriented 110–120° and traversing the length of the study area (Figure 5, blue arrows). A smaller unknown set of dykes that is just beyond the resolution limit of the data (Figure 5, green arrow) was mapped in outcrop. Their 040° trend and subdued magnetic response hinder remote identification because phases of the CB are similarly magnetic and oriented. Additional north-northeast-trending nonmagnetic lineaments (Figure 5, yellow arrows) appear to transect the CB plutonic bodies. Although there is little to no evidence for displacement along these crosscutting magnetic lineations, remote-sensing imagery and field observations suggest the nonmagnetic lin-

eaments reflect a network of fractures and normal faults (Weller et al., 2014) related to the opening of Davis Strait and formation of Cumberland Sound during the Paleocene (Clarke et al., 1989).

Future studies and economic considerations

Deposits of Ni-Cu-PGEs are associated with a variety of mafic and ultramafic magmatic rocks, and the tectonostratigraphic context and mineralization styles on Hall and Meta Incognita peninsulas are comparable to those of the Raglan deposit in northern Quebec (Steenkamp et al., 2014; St-Onge et al., 2015). Several new mafic-ultramafic occurrences were documented during the 2015 field season and are being investigated as part of an M.Sc. project (Liikane et al., 2015). Additional planned geophysical modelling will focus on the nature of the regional gravity highs and their relation (if

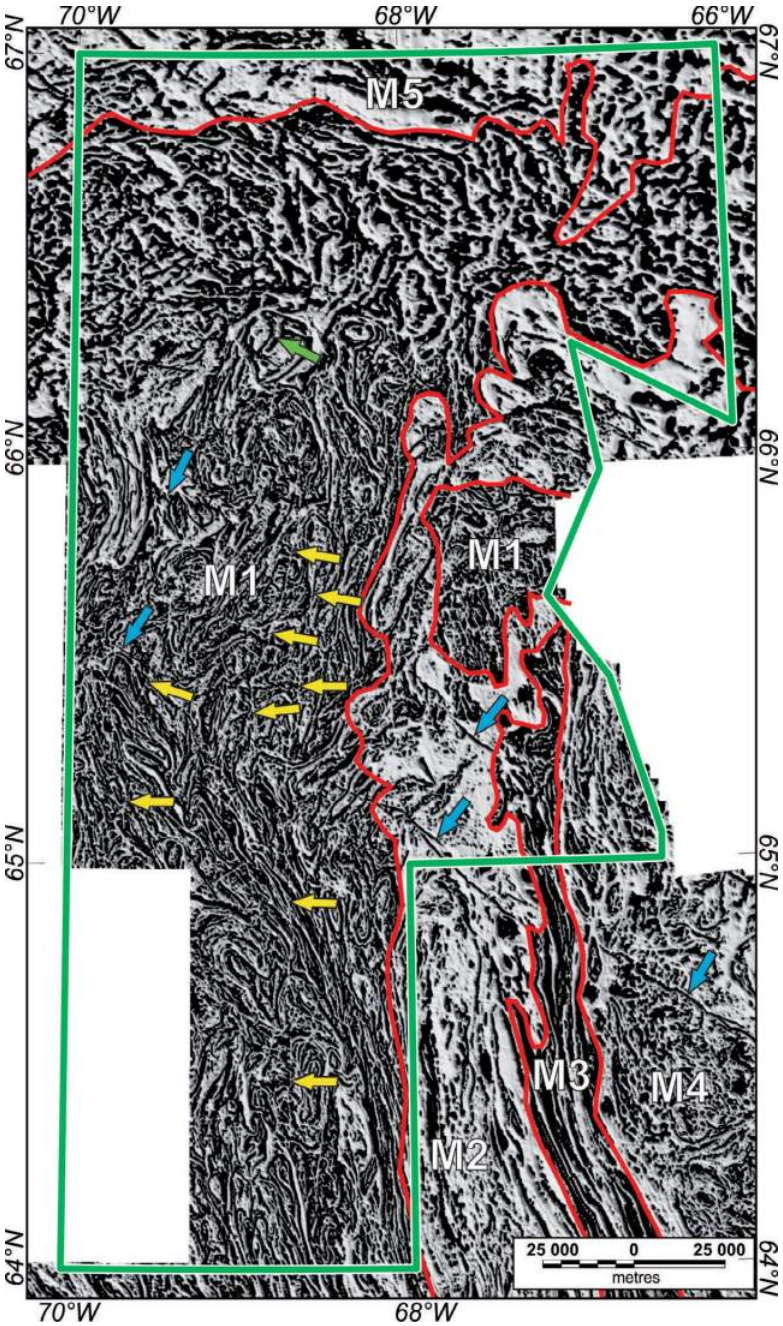

Figure 5: Tilt derivative of the magnetic field over the McKeand River study area (green outline; labels as discussed in text). Black areas show positive tilt (over magnetic source body) and white areas show negative tilt (outside of magnetic source). Magnetic Franklin dykes (blue arrows), the 040° dykes (green arrows) and non-magnetic lineaments (yellow arrows) are labelled.

any) to mafic-ultramafic occurrences. Disseminated semimassive to massive sulphide occurrences are documented within Lake Harbour Group assemblages in the M2 domain (Liikane et al., 2015). The massive sulphides are moderately magnetic (10×10^{-3} SI) with respect to background magnetization values, but the occurrences documented in the field were not sufficiently large (<10 m) to be reflected in the aeromagnetic data.

Diamondiferous kimberlite pipes have been discovered on Hall Peninsula (Pell et al., 2013). The new magnetic surveys provide coverage over the northern extent of the Archean gneissic rocks on Hall Peninsula and to the west. Keating correlation coefficients computed on the first vertical derivative provide a first-order assessment of kimberlite potential (Kiss and Tschirhart, 2015a, b). A detailed gravity transect was conducted during the 2015 field season to further examine the western extension of the Archean gneissic rocks within the project area, and the geometry of the crystalline basement at depth.

Density measurements on selected samples aim to characterize the physical properties of the Hall Peninsula gneissic rocks, Lake Harbour Group supracrustal units and CB intrusive rocks. Provided there is a significant density contrast between the CB and Archean basement rocks, gravity-data inversions offer a method to calculate and then remove the gravity contribution of the CB. The revised data can then be analyzed to determine if gravity anomalies can shed further light on the nature of the Baffin suture.

Acknowledgments

The authors thank N. Rayner, A. Ford, D. Liikane, B. Dyck, T. Chadwick, T. Milton, S. Noble-Nowdluk and T. Rowe for their field assistance and valuable scientific discussion. D. Guilfoyle was responsible for the preparation of many delicious meals. Logistical support was provided by the Polar Continental Shelf Project. S. Dehler, R. Khoun and R. Murphy are thanked for their management and administrative support. The paper benefited from a thorough review by M. Thomas.

Natural Resources Canada, Earth Sciences Sector contribution 20150294

References

Blackadar, R.G. 1967: Geological reconnaissance, southern Baffin Island, District of Franklin; Geological Survey of Canada, Paper 66-47, 32 p. doi:10.4095/100926

Clarke, D.B., Cameron, B.I., Muecke, G.K. and Bates, J.L. 1989: Early Tertiary basalts from the Labrador Sea and Davis Strait region; Canadian Journal of Earth Sciences, v. 26, p. 956–968.

Dumont, R. and Dostaler, F. 2010: Aeromagnetic survey, Hall Peninsula, Nunavut; Geological Survey of Canada, Open Files 6413–6424, scale 1:100 000.

Ernst R.E. and Buchan K.L. 1997: Giant radiating dyke swarms: their use in identifying pre-Mesozoic large igneous provinces and mantle plumes; *in* Large Igneous Provinces: Continental, Oceanic, and Planetary Volcanism, J. Mahoney J. and M. Coffin (ed.), American Geophysical Union, Geophysical Monograph 100, p. 297–333.

From, R.E., St-Onge, M.R. and Camacho, A. 2014: Preliminary characterization of the Archean orthogneiss complex of Hall Peninsula, Baffin Island, Nunavut; *in* Summary of Activities 2013, Canada-Nunavut Geoscience Office, p. 53–62.

Gibb, R.A., Thomas, M.D., Lapointe, P. and Mukhopadhay, M. 1983: Geophysics of proposed Proterozoic sutures in Canada; Precambrian Research, v. 19, p. 349–384.

Heaman, L.M., LeCheminant, A.N. and Rainbird, R.H. 1992: Nature and timing of Franklin igneous events, Canada: implications for a Late Proterozoic mantle plume and the breakup of Laurentia; Earth and Planetary Science Letters, v. 109, p. 117–131.

Hoffman, P.F. 1988: United Plates of America, the birth of a craton: Early Proterozoic assembly and growth of Laurentia; Annual Reviews of Earth and Planetary Sciences, v. 16, p. 543–603.

Keating, P. 1995: A simple technique to identify magnetic anomalies due to kimberlite pipes; Exploration and Mining Geology, v. 4, p. 121–125.

Kiss, F. and Tschirhart, V. 2015a: Aeromagnetic survey, Amittok Lake area, Baffin Island, Nunavut; Geological Survey of Canada, Open Files 7888–7891, scale 1:100 000.

Kiss, F. and Tschirhart, V. 2015b: Aeromagnetic survey, McKeand River area, Baffin Island, Nunavut; Geological Survey of Canada, Open Files 7819–7832, scale 1:100 000.

Liikane, D.A., St-Onge, M.R., Kjarsgaard, B.A., Rayner, N.M., Ernst, R.E. and Kastek, N. 2015: Frobisher suite mafic, ultramafic, and layered mafic-ultramafic sills, southern Baffin Island, Nunavut; *in* Summary of Activities 2015, Canada-Nunavut Geoscience Office, p. 21–32.

Machado, G., Bilodeau, C. and St-Onge, M.R. 2013: Geology, southern part of Hall Peninsula, south Baffin Island, Nunavut; Geological Survey of Canada, Canadian Geoscience Map 135 (preliminary) and Canada-Nunavut Geoscience Office, Open File Map 2013-1, scale 1:250 000. doi:10.4095/292443

Miles, W., Mate, D.J., St-Onge, M.R. and Steenkamp, H.M. 2015: Aeromagnetic survey of the McKeand River area, southern Baffin Island, Nunavut; *in* Summary of Activities 2014, Canada-Nunavut Geoscience Office, p. 97–104.

Miller, H.G. and Singh, V. 1994: Potential field tilt – a new concept for location of potential field sources; Journal of Applied Geophysics, v. 32, p. 213–217. doi.org/10.1016/0926-9851(94)90022-1

Nabighian, M.N., Ander, M.E., Grauch, V.J.S., Hansen, R.O., LaFehr, T.R., Li, Y., Pearson, W.C., Peirce, J.W., Phillips, J.D. and Ruder, M.E. 2005: Historical development of the magnetic method in exploration; Geophysics, v. 70, p. 33ND–61ND. doi.org/10.1190/1.2133785

Natural Resources Canada 2015: Canadian aeromagnetic database; Natural Resources Canada, Earth Sciences Sector, Geoscience Data Repository, URL <http://gdr.agg.nrcan.gc.ca/gdrdap/dap/search-eng.php> [April 2015].

Pell, J. 2010: 2010 technical report on the Chidliak property, 66° 21' 43" W, 64° 28' 26" N, Baffin region, Nunavut: Peregrine Diamonds, unpublished report, 144 p., URL<http://

www.pdiam.com/i/pdf/43-101Chidliak_2010.pdf> [October 2015].

Pell, J., Grütter, H.S., Neilson, S., Lockhart, G., Dempsey, S. and Grenon, H. 2013: Exploration and discovery of the Chidliak kimberlite province, Baffin Island, Nunavut: Canada's newest diamond district; *in* Proceedings of the 10th International Kimberlite Conference, Volume 2, D.G. Pearson, H.S. Grütter, J. W. Harris, B.A. Kjarsgaard, H. O'Brien, N.V. Chalapathi Rao and S. Sparks (ed.), Journal of the Geological Society of India, Special Issue, p. 209–227. doi:10.1007/978-81-322-1173-0_14

Pilkington, M. 1990: Lithospheric flexure and gravity anomalies at Proterozoic plate boundaries in the Canadian Shield; Tectonophysics, v. 176, p. 277–290.

Pilkington, M., Miles, W., Ross, G.M. and Roest, W.R. 2000: Potential-field signatures of buried Precambrian basement in the Western Canada Sedimentary Basin; Canadian Journal of Earth Sciences, v. 27, p. 1453–1471. doi.org/10.1139/e00-020

Rayner, N., St-Onge, M.R., Weller, O. and Tschirhart, V. 2015: 2015 report of activities for completing the regional bedrock mapping of the southern half of Baffin Island, GEM 2 Baffin Project; Geological Survey of Canada, Open File 7953.

Reed, L.E. and Witherly, K.E. 2007: 50 years of kimberlite geophysics: a review; Proceedings of Exploration 07: Fifth Decennial International Conference on Mineral Exploration, p. 679–689.

Schetselaar, E., Harris, J.R. and Lemkow, D. 2013: Remote predictive map, eastern Hall Peninsula, Baffin Island, Canada; Geological Survey of Canada, Open File 7454, 8 p. doi:10.4095/292802

Scott, D.J. 1999: U-Pb geochronology of the eastern Hall Peninsula, southern Baffin Island, Canada: a northern link between the Archean of West Greenland and the Paleoproterozoic Torngat Orogen of northern Labrador; Precambrian Research, v. 93, p. 5–26.

Steenkamp, H.M. and St-Onge, M.R., 2014: Overview of the 2013 regional bedrock mapping program on northern Hall Peninsula, Baffin Island, Nunavut; *in* Summary of Activities 2013, Canada-Nunavut Geoscience Office, p. 27–38.

Steenkamp, H.M., Bros, E.R. and St-Onge, M.R. 2014: Altered ultramafic and layered mafic-ultramafic intrusions: new economic and carving stone potential on northern Hall Peninsula, Baffin Island, Nunavut; *in* Summary of Activities 2013, Canada-Nunavut Geoscience Office, p. 11–20.

St-Onge, M.R., Jackson, G.D. and Henderson, I. 2006a: Geology, Baffin Island (south of 70°N and east of 80°W), Nunavut; Geological Survey of Canada, Open File 4931, scale 1:500 000.

St-Onge, M.R., Rayner, N.M., Liikane, D. and Chadwick, T. 2015: Mafic, ultramafic and layered mafic-ultramafic sills, Meta Incognita Peninsula, southern Baffin Island, Nunavut; *in* Summary of Activities 2014, Canada-Nunavut Geoscience Office, p. 11–16.

St-Onge, M.R., Searle, M.P. and Wodicka, N., 2006b: Trans-Hudson Orogen of North America and Himalaya-Karakoram-Tibetan Orogen of Asia: structural and thermal characteristics of the lower and upper plates; Tectonics, v. 25, p. 1–22.

St-Onge, M.R., Van Gool, J.A.M., Garde, A.A. and Scott, D.J. 2009: Correlation of Archaean and Palaeoproterozoic units between northeastern Canada and western Greenland: constraining the pre-collisional upper plate accretionary history of the Trans-Hudson orogen; Geological Society of London, Special Publications, v. 318, p. 193–235. doi.org/10.1144/SP318.7

Thomas, M.D. 1992: Ancient collisional continental margins in the Canadian Shield: geophysical signatures and derived crustal transects; *in* Basement Tectonics 8: Characterization and Comparison of Ancient and Mesozoic Continental Margins – Proceedings of the 8th International Conference on Basement Tectonics, v. 2, p. 5–25.

Weller, O.M., Dyck, B.J., St-Onge, M.R., Rayner, N.M. and Tschirhart, V. 2015: Completing the bedrock mapping of southern Baffin Island, Nunavut: plutonic suites and regional stratigraphy; *in* Summary of Activities 2015, Canada-Nunavut Geoscience Office, p. 33–48.

Whalen, J.B., Wodicka, N., Taylor, B.E. and Jackson, G.D. 2010: Cumberland batholith, Trans-Hudson Orogen, Canada: petrogenesis and implications for Paleoproterozoic crustal and orogenic processes; Lithos, v. 117, p. 99–118. doi.org/10.1016/j.lithos.2010.02.008

Ptarmigan Fiord basement-cover thrust imbricates, Baffin Island, Nunavut

T.C. Chadwick[1], M.R. St-Onge[2], O.M. Weller[2], S.D. Carr[1] and B.J. Dyck[3]

[1]*Ottawa-Carleton Geoscience Centre, Carleton University, Ottawa, Ontario, timchadwick@cmail.carleton.ca*

[2]*Natural Resources Canada, Geological Survey of Canada, Ottawa, Ontario*

[3]*Department of Earth Sciences, University of Oxford, Oxford, United Kingdom*

This work is part of the larger South Baffin mapping project, a partnership between the Canada-Nunavut Geoscience Office (CNGO) and Natural Resources Canada's (NRCan) Geo-mapping for Energy and Minerals (GEM) program on Baffin Island. This particular mapping project is being led by the Geological Survey of Canada (GSC) in collaboration with CNGO, the Government of Nunavut, Nunavut Arctic College, Carleton University and Oxford University. Logistical support is provided by the Polar Continental Shelf Project and several local, Inuit-owned businesses. The study area comprises all or parts of six 1:250 000 map areas north of Iqaluit (NTS areas 26B, C, F, G, J and K). The objective of the work is to complete the regional bedrock mapping for the southern half of Baffin Island and provide a new, modern, geoscience understanding of this part of eastern Nunavut.

Chadwick, T.C., St-Onge, M.R., Weller, O.M., Carr, S.D. and Dyck, B.J. 2015: Ptarmigan Fiord basement-cover thrust imbricates, Baffin Island, Nunavut; *in* Summary of Activities 2015, Canada-Nunavut Geoscience Office, p. 61–72.

Abstract

The rocks at Ptarmigan Fiord on the Hall Peninsula of Baffin Island underwent midcrustal deformation during the formation of the Paleoproterozoic Trans-Hudson Orogen. The structural style in the region is dominated by imbricate panels of Archean basement orthogneiss and Paleoproterozoic supracrustal strata, interpreted to have been deformed by thick-skinned ductile thrusting. Basement rocks comprise amphibolite-facies metatonalite, metagranodiorite, metaquartz-diorite and metamonzogranite, and cover rocks comprise amphibolite-facies migmatitic pelitic and semipelitic schist, psammitic schist, amphibolite, calcsilicate and quartzite. The S_{1a} penetrative foliation is variably present in basement rocks and consistently present in cover rocks, and is defined by alignment of biotite, sillimanite and leucogranite that formed before and during the thermal metamorphic peak. The S_{1a} foliation was deformed by F_{1b} isoclinal folds with an amplitude of 100 m. These structures are interpreted as forming during a D_1 east-west crustal shortening event. Basement and cover imbrication occurred after the thermal metamorphic peak and is interpreted as D_2 thick-skinned ductile thrusting. Ductile thrust faults at the base of seven basement-cover slices are identified on the basis of repetition of units and strain localization, and are interpreted as predominantly south-to-southeast verging on the basis of shear-sense indicators. There are two structural panels of D_2 thrust imbricates, one in the northwestern part of the map area and one in the eastern part of the map area. Map-scale crosscutting relationships indicate that the northwestern panel overthrusted the eastern panel on a southeasterly T_{2c}-directed thrust fault, following a F_{2b} folding event that folded the T_{2a} basement-cover thrust imbricates in the eastern panel. The Ptarmigan Fiord area contains a world-class exposure of thick-skinned structures as they are spectacularly delineated by belts of distinctive grey-weathering Archean basement rocks and brown- to black-weathering Paleoproterozoic supracrustal rocks.

Résumé

Les roches de Ptarmigan Fiord dans la péninsule Hall de l'île de Baffin documentent des événements de la déformation de la croûte moyenne survenue au moment de l'orogenèse trans-hudsonienne. Le style de déformation dans la région est dominé par des panneaux imbriqués d'orthogneiss du scole archéen et de strates supracrustales du Paléoprotérozoïque, interprétés comme étant le résultat de chevauchements ductiles de couches épaisses. Le socle comprend les unités du faciès des amphibolites suivantes : métatonalite, métagranodiorite, métadiorite quartzique et métamonzogranite ; les roches de couverture du faciès des amphibolites comprennent, elles, du schiste pélitique et semi-pélitique migmatitique, du schiste psammitique, de l'amphibolite, des silicates calciques et du quartzite. Les roches de couverture sont caractérisées par la présence généralisée d'une foliation S_{1a}, tandis que cette dernière ne se manifeste que de façon variable dans les roches du socle. Cette foliation est en outre définie par l'alignement de la biotite, de la sillimanite et du leucogranite, qui se sont formés avant et

This publication is also available, free of charge, as colour digital files in Adobe Acrobat® PDF format from the Canada-Nunavut Geoscience Office website: http://cngo.ca/summary-of-activities/2015/.

pendant le pic de métamorphisme thermique. Des plis isoclinaux F_{1b} ont ensuite imprimé à la foliation S_{1a} une déformation dont l'amplitude atteint 100 m. Ces structures sont interprétées comme étant le résultat d'un événement de raccourcissement crustal D_1 orienté est-ouest. L'imbrication des roches du socle et des roches de couverture s'est produite après le pic de métamorphisme thermique et est interprétée comme étant le résultat d'un chevauchement ductile de couche épaisse D_2. Des failles de chevauchement à la base de sept écailles constituées de roches du socle et de couverture ont été repérées grâce à la répétition d'unités et à la localisation des déformations ; en outre, les indicateurs de sens de cisaillement semblent indiquer que le transport tectonique s'est produit généralement en direction sud à sud-est. Il y a deux domaines structuraux de chevauchements D_2, l'un dans la partie nord-ouest et l'autre dans la partie est de la zone d'étude. Les relations géométriques de recoupement à l'échelle de la carte révèlent que le domaine au nord-ouest a chevauché le domaine à l'est le long d'une faille de chevauchement T_{2c} à vergence sud-est. Le chevauchement T_{2c} s'est produit après un épisode de plissement F_{2b} des panneaux imbriqués T_{2a} de roches du socle et de couverture dans le domaine de l'est. La région de Ptarmigan Fiord est caractérisée par la présence d'affleurements de premier ordre de structures de chevauchement de couches épaisses que délimitent de façon spectaculaire des bandes distinctes de roches du socle d'âge archéen, auxquelles l'altération a conféré une teinte grisâtre, et de roches supracrustales d'âge paléoprotérozoïque, à surface altérée brune et noire.

Introduction

Ptarmigan Fiord is located on western Hall Peninsula, South Baffin Island, Nunavut (Figure 1, inset map). The Hall Peninsula block, the setting of the Ptarmigan study area, is located in the Quebec-Baffin segment of the Paleoproterozoic Trans-Hudson Orogen (THO), a collisional belt that formed during the amalgamation of the supercontinent Nuna (also called Columbia), between 2.0–1.8 Ga (Hoffman, 1988; Lewry and Collerson, 1990; St-Onge et al., 2007; Corrigan, 2012). In the THO, the lower plate comprises the Superior craton whereas the upper plate consists of a collage of Archean crustal fragments, ribbon microcontinents and oceanic arc terranes. The Quebec-Baffin domain is situated in the upper Churchill plate, and includes the Rae craton, Meta Incognita microcontinent and Narsajuaq arc terrane, which were accreted to the southeastern Rae margin between ca. 1.88 and 1.84 Ga (St-Onge et al., 2009). The lower-plate Superior craton terminal collision occurred between ca. 1.82 and 1.80 Ga (St-Onge et al., 2006). The Hall Peninsula block, located east of the Meta Incognita microcontinent (Figure 1), is a section of continental crust composed of tonalitic to monzogranitic Archean basement gneiss and minor supracrustal rocks.

Hall Peninsula was initially mapped by Blackadar (1967), Scott (1999) and in 2012–2014, by the Canada-Nunavut Geoscience Office (CNGO), as part of the Hall Peninsula Integrated Geoscience Project (Steenkamp and St-Onge, 2014). Ptarmigan Fiord was targeted during the summer of 2015, by the Geological Survey of Canada (GSC), as part of a regional bedrock mapping project focused on the central part of Baffin Island (Weller et al., 2015), within the Natural Resources Canada's (NRCan) Geo-mapping for Energy and Minerals (GEM) Program. The purpose of this field-based study is to gain a better understanding of the structural style and tectonic history of the Ptarmigan Fiord area. Mapping at 1:80 000 scale in an approximately 10 by 18 km area forms the basis of the M.Sc. thesis project by the first author at Carleton University. In this paper, results are presented from the 2015 field season that focus on characterizing the tectonostratigraphy, structures and relative timing of structures with respect to metamorphism in the Ptarmigan Fiord area.

Geological setting of Hall Peninsula

The bedrock geology of Hall Peninsula includes Archean crystalline basement orthogneiss nonconformably overlain by middle Paleoproterozoic supracrustal cover strata; in the western peninsula, the supracrustal rocks are intruded by orthopyroxene-bearing diorite to monzogranite (Steenkamp and St-Onge, 2014). The basement orthogneiss comprises dominantly gneissic, migmatitic tonalite to monzogranite with local pods of amphibolite and crosscutting syenogranite dykes (op. cit.; From et al., 2014). A crystalline basement sample of K-feldspar porphyritic monzogranite collected from the southeastern part of Ptarmigan Fiord (R003, Figure 1), yielded a zircon U-Pb age of 2719 ±4 Ma (Rayner, 2014). The supracrustal package is characterized by a larger compositional variation in the eastern part of the peninsula, compared to that in the west (Steenkamp and St-Onge, 2014). The supracrustal rocks consist of upper-amphibolite to lower-granulite facies clastic and pelitic migmatitic schist and gneiss, and compositionally variable amphibolite, calcsilicate and meta-ironstones. The base of the package comprises a blue-grey quartzite, which is overlain by a rusty brown-weathering unit of alternating psammitic, semipelitic and pelitic metasedimentary rocks. Above the basal strata lies a layered unit of semipelitic schist, calcsilicate, meta-ironstone and compositionally variable amphibolite. The amphibolite is interpreted as a sequence of metamorphosed volcaniclastic rocks with minor subaerial mafic volcanic flows (MacKay et al., 2013; MacKay and Ansdell, 2014; Steenkamp and St-Onge, 2014). Approximately 20 km west of Ptarmigan Fiord the

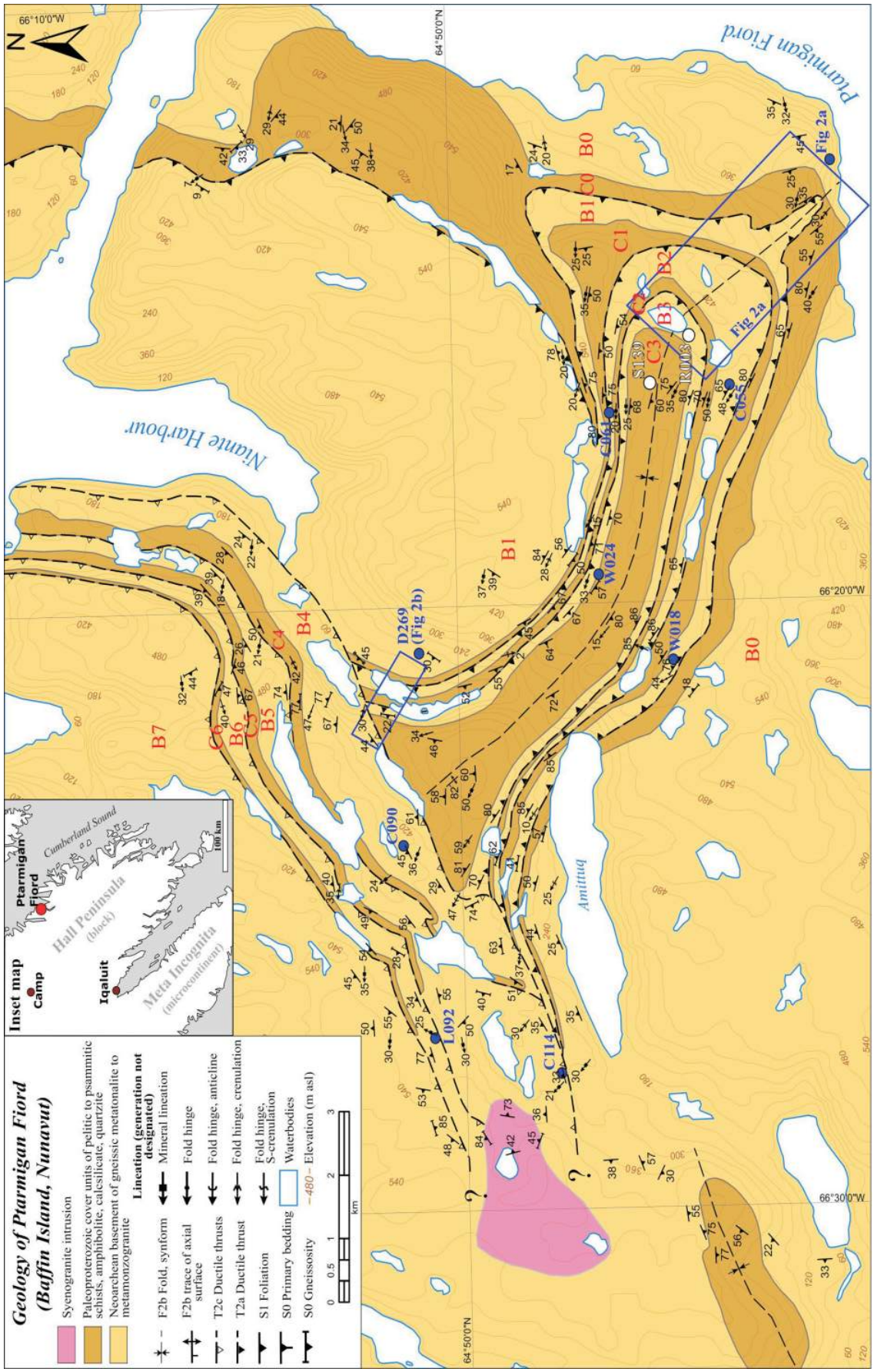

Figure 1: Geology of the Ptarmigan Fiord field area on Hall Peninsula of Baffin Island, southeastern Nunavut (scale 1:80 000), showing folded Archean basement (gold colour, B0-B7) and Paleoproterozoic cover (brown colour, C0-C6) imbrications with late (?) syenogranite intrusion (pink). White circles are geochronology sample locales, and blue station numbers show locations of kinematic indicators and panorama photographs; location of Figure 2a and b also shown. Inset map shows location of the field area.

supracrustal rocks transition to a more homogeneous composition, and comprise dominantly pelitic and psammitic metasedimentary units. The transition from clastic and psammitic-pelitic units with mafic lenses, interpreted as margin-proximal supracrustal units, in the east, to mostly deep-water, distal pelitic units, in the west, has been interpreted as a progressive change in paleodepositional environment of supracrustal rocks now exposed on Hall Peninsula (Steenkamp and St-Onge, 2014). A sample of psammitic schist from Ptarmigan Fiord (S139, Figure 1) yielded a significant population of 1.96 Ga zircon grains, indicating a maximum age of deposition at 1967 ±8 Ma (op. cit.) for that part of the supracrustal package.

Dyck and St-Onge (2014) proposed that three major Paleoproterozoic deformation events characterize the structural and metamorphic evolution of Hall Peninsula, including the Ptarmigan Fiord area. The nature and relative timing of the deformation events are summarized in Table 1.

In the Ptarmigan Fiord area, D_2 thrust repetitions of less than one kilometre thick basement-cover slices dominate the map pattern (Figures 1, 2).

Table 1: Deformation events, structures and metamorphism, Ptarmigan Fiord, Hall Peninsula, Nunavut. Modified after Dyck and St-Onge (2014).

Event	Description
D_0	**Predeformation fabric**
S_0	Gneissic banding in Archean basement rocks Primary bedding
D_1	**East-west crustal shortening (pre-synthermal peak)**
F_{1a}	Isoclinal folding of S_0
S_{1a}	Metamorphic minerals axial planar to F_{1a}
F_{1b}	Isoclinal folding of S_{1a}
S_{1b}	Cleavage axial planar to F_{1b}
D_2	**Southeast-northwest crustal shortening (post-thermal peak)**
T_{2a}	Thick-skinned thrusting in eastern domain
S_2	Shear fabric oriented parallel to T_2 thrust plane
L_2	Mineral stretching and elongate growth
F_{2b}	Upright folding of T_{2a} thick-skinned thrusting
T_{2c}	Thick-skinned thrusting in northwestern domain
D_3	**North-south crustal shortening**
F_3	Open folding of T_{2a} and T_{2c} thick-skinned thrusting

Bedrock geology of Ptarmigan Fiord map area

There are three map units (Figure 1) in the Ptarmigan Fiord area: 1) Neoarchean orthogneiss basement, 2) Paleoproterozoic supracrustal cover rocks, and 3) weakly foliated syenogranite intrusions. Although most of the rocks in the Ptarmigan Fiord area are penetratively metamorphic rocks, the prefix 'meta' is omitted from the following lithological descriptions for brevity.

Neoarchean basement lithology

The Neoarchean crystalline basement at Ptarmigan Fiord comprises multiple phases of variably deformed gneissic to massive tonalite, quartz diorite, granodiorite and monzogranite (Figure 1). Biotite, hornblende±orthopyroxene tonalite is typically fine to medium grained, weathers light to dark grey, and has a flecked salt and pepper grey colour on the fresh surface. In places, the tonalite gneiss contains 20–150 cm thick blocky to banded lenses and folded bands (Figure 3a).

The mafic lenses, blocks and bands consist of biotite, hornblende, garnet±clinopyroxene quartz diorite. Biotite, hornblende±orthopyroxene granodiorite is typically fine to medium grained, weathers a light grey brown, and contains blocky lenses of quartz diorite. The biotite and hornblende-bearing monzogranite is typically reddish-grey to light brown on the weathered and fresh surfaces, medium to coarse grained in areas of lower strain, and generally contains 5–10 mm elongated and rounded K-feldspar porphyroclasts (Figure 3b).

Paleoproterozoic cover lithology

Stratigraphy within the Paleoproterozoic supracrustal cover rocks is disrupted by multiple deformation events, but estimated to be a minimum of ~200 to 500 m thick. From structurally lowest to highest, the cover succession contains pelitic and semipelitic schist, psammitic schist, amphibolite, calcsilicate and quartzite. This sequence has been mapped on the ground in cover slices 'C0' and 'C1' on the northern limb of the syncline in the central part of the area, and marker units are traced across the map area (Figures 1, 2). The majority of the supracrustal successions in the study area are truncated above the amphibolite unit by the crystalline basement hanging wall of the overriding thrust imbricate. Rarely are the calcsilicate and quartzite that lie above the amphibolite observed in the cover slices.

Pelitic and semipelitic schist

The migmatitic garnet–sillimanite–K-feldspar±muscovite pelitic schist and the muscovite-biotite semipelitic schist weather a rusty brown colour and typically occur as 5–20 m thick interlayers within psammite (Figure 3c, d). The sillimanite typically occurs as 1–2 cm long elongate knots with quartz and K-feldspar. In cover sequences 'C3'–'C6' (Figure 1), thin alternating sequences (10–50 cm thick) of pelitic schist and psammitic schist exhibit both sharp and gradational contacts (Figure 3e). These alternating interlayers are interpreted as primary bedding, termed S_0.

In the eastern part of the study area, within the cover sequences 'C0' and 'C1' (Figure 1), 1–3 m wide layers of gar-

net-muscovite-sillimanite schist are studded with 5–20 mm diameter garnets (Figure 3f) and are distinctive marker units. Leucogranite veins and dykes, 1–10 cm thick, occur in the pelitic rocks of cover sequences 'C3'–'C6' (Figure 1b). The leucogranite contains millimetre- to centimetre-sized lilac-coloured garnets with mats of fine sillimanite needles. The leucogranite veins crosscut the dominant S_{1a} foliation and are aligned within the S_{1b} axial-planar surface of F_{1b} isoclinal folds (Figure 3e).

Psammitic schist

Fine- to medium-grained muscovite- and biotite-bearing psammitic schist occurs stratigraphically above the pelitic and semipelitic schist, in 2 to 10 m thick layers. It contains

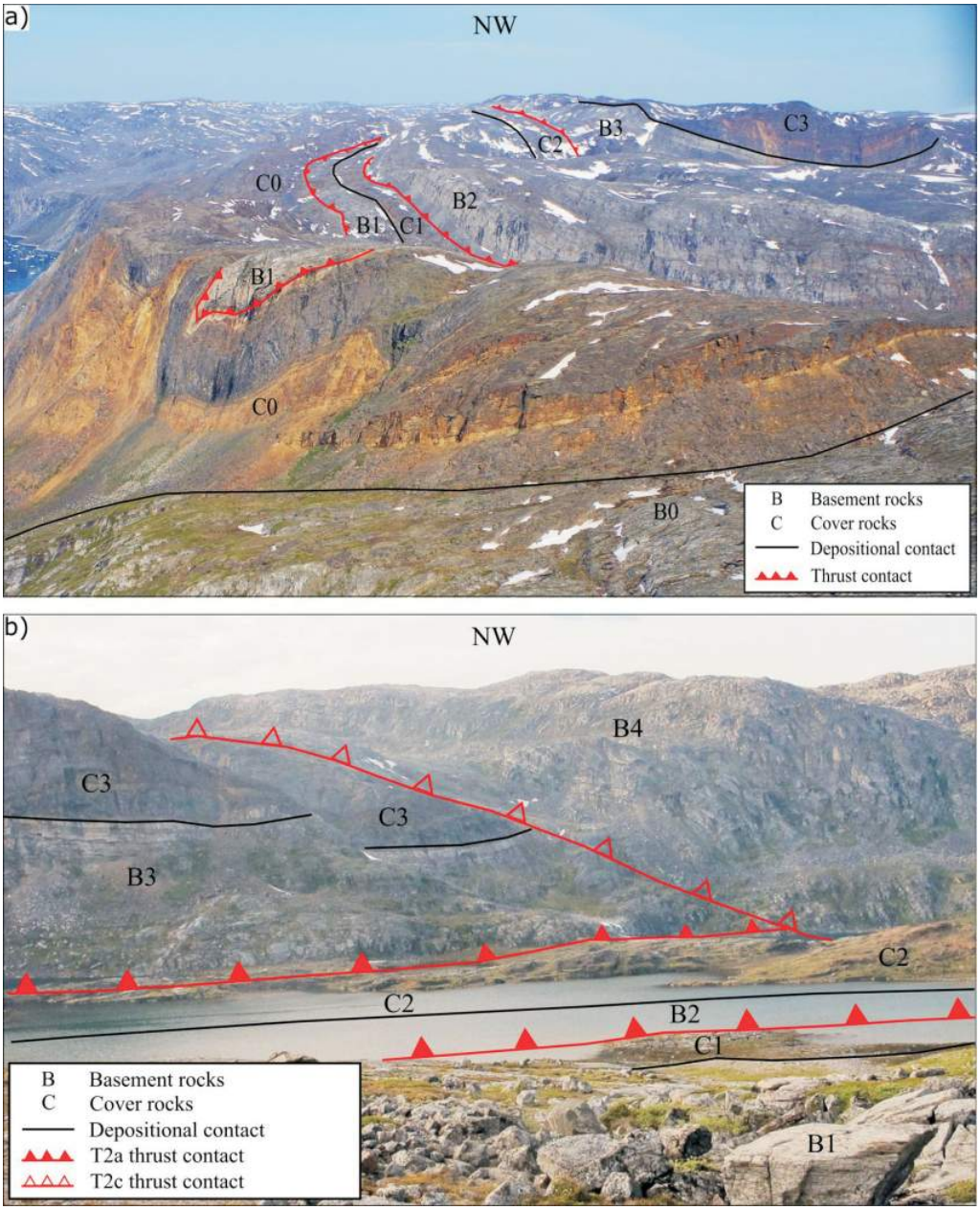

Figure 2: Panoramas of Ptarmigan Fiord geology, Hall Peninsula of Baffin Island. The areas covered by the photographs are delineated on Figure 1: **a)** northwestward view facing ~300° azimuth. The photograph is taken from the helicopter above the station labelled 'Fig 2a' on Figure 1. Basement rocks are grey, metasedimentary clastic and pelitic cover rocks are brown, and metavolcanic rocks are dark grey. Basement-cover imbricates in the far distance ('B3' and 'C3') occur in the southeast closure of an upright syncline (Figure 1); **b)** northwestward view facing ~300° azimuth viewed from station D269 (Figure 1) at the boundary between the northwest structural domain and the eastern domain, where a stack of T_{2c} basement-cover thrust imbricates, with 'B4' at the base, truncates T_{2a} basement-cover imbricates ('B3'+'C3' and 'B2'+'C2') of the eastern domain.

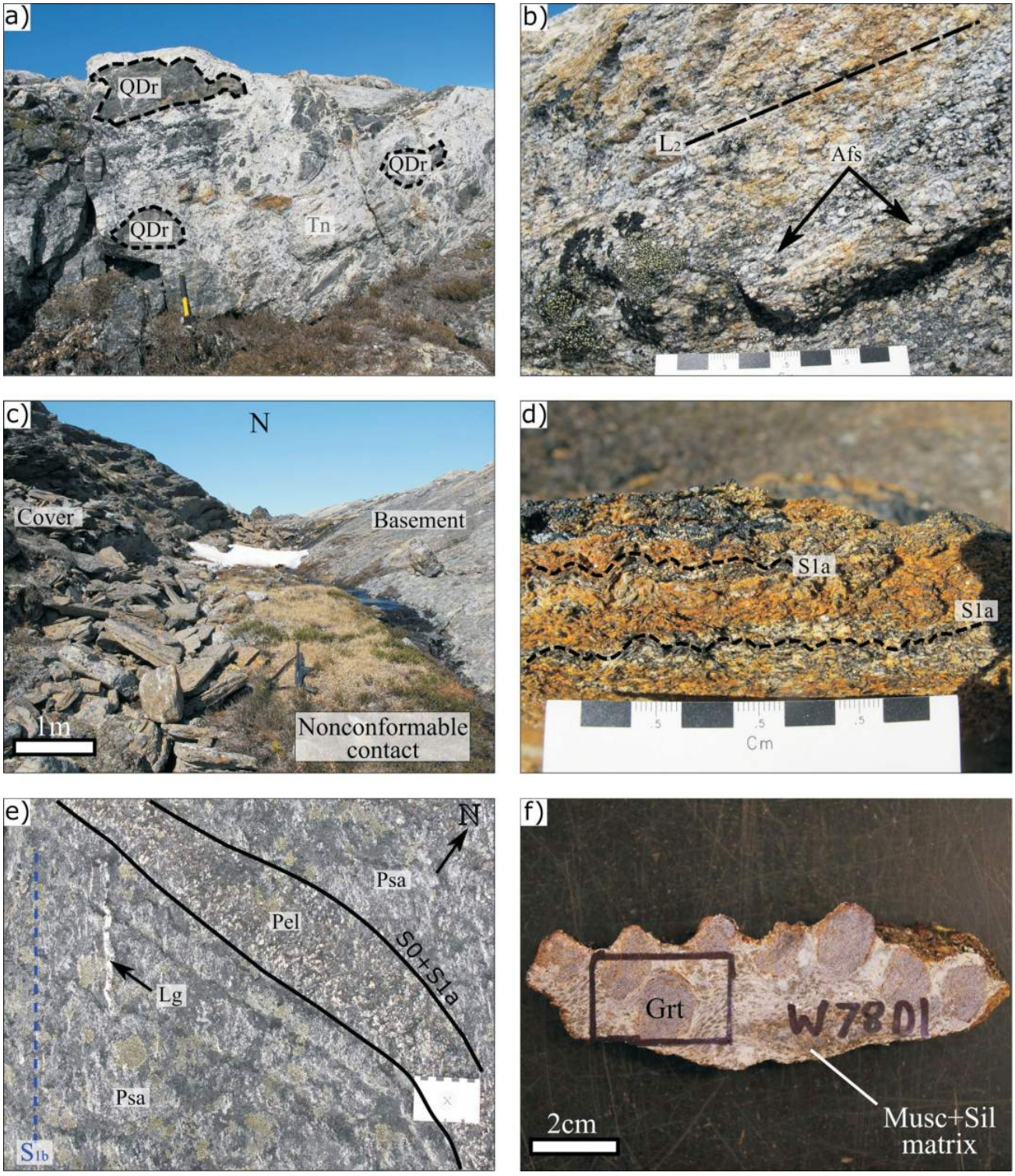

Figure 3: Examples of lithology and structure, Ptarmigan Fiord, Hall Peninsula of Baffin Island: **a)** northward view of Neoarchean basement tonalite with blocks and layers of quartz diorite (note the 30 cm long hammer for scale); **b)** northward view of Neoarchean basement monzogranite with rounded K-feldspar porphyroclasts and L_2 lineation; **c)** northward view of contact between Neoarchean basement (right) and Paleoproterozoic supracrustal rocks (left) interpreted as a nonconformable contact (note the 60 cm long Remington 870 for scale); **d)** muscovite-biotite semipelitic schist with primary compositional layering concordant with S_{1a} is defined by alignment of muscovite and biotite; **e)** psammitic and pelitic garnet–sillimanite–K-feldspar–muscovite schist. Compositional layering, interpreted as primary bedding (S_0), is at a high angle to S_{1b} foliation, parallel to F_{1b} folds, defined by sillimanite and K-feldspar knots, muscovite and biotite minerals and garnet quartzofeldspathic veins; **f)** garnet-muscovite-sillimanite schist studded with 5–-20 mm diameter garnets. Abbreviations: Afs, alkali feldspar; Grt, garnet; Lg, leucogranite veins; Musc, muscovite; Pel, pelitic schist; Psa, psammitic schist; QDr, quartz diorite; Sil, sillimanite; Tn, tonalite.

rare elongate sillimanite–quartz–K-feldspar knots and 1–2 mm sized garnet. The psammitic schist may have interlayers of pelitic schist, with 1 to 3 cm thick gradational contacts.

Amphibolite

A fine- to medium-grained, black– to dark green–weathering garnet-biotite (±quartz, clinopyroxene) amphibolite unit, up to 30 m thick, typically occurs above the pelitic and psammitic schist units. There are calcite and dolomite infills that are interpreted as interflow and/or pillow selvages. The protolith of the amphibolite is interpreted to be mafic volcanic rocks (Figure 4a).

Calcsilicate

Thin, 40–200 cm thick layers of white– to dark grey–weathering calcsilicate overlie the amphibolite. The calcsilicate often contains 2–5 cm size tremolite knots within a dolomitic matrix. Tremolite is aligned within the S_{1a} foliation and within the axial planes of F_{1b} minor isoclinal folds (Figure 4b).

Quartzite

A 3 to 10 m thick, fine- to medium-grained, grey-blue weathering quartzite caps the cover units. Quartzite also occurs as 20–50 cm thick lenses within the psammitic schist. It rarely contains relic heavy-mineral bands that define primary bedding and crossbedding. There are 5–20 mm thick biotite- and amphibole-rich mafic layers interbedded within the quartzite that are interpreted as mafic-volcanic ash layers.

Syenogranite intrusions

A red- to pink-weathering, medium-grained, biotite syenogranite pluton occurs near the western margin of the map area (Figure 1). The weakly foliated syenogranite crosscuts the gneissic foliation within the basement rocks (Figure 4c), and is therefore younger than the basement granitoids and the foliation. One- to two-metre thick syenogranite and pegmatite dykes of this suite also occur within the basement and cover imbricates in the central and eastern part of the map area (‘B1’+‘C1’ to ‘B3’+‘C3’ on Figure 1), but crosscutting relationships involving the intrusions and basement-cover contacts were not observed. The age of the intrusion may provide a timing constraint on the youngest stages of regional deformation.

Structural observations and interpretations from Ptarmigan Fiord

Using the framework developed by Dyck and St-Onge (2014), as summarized in Table 1, structural mapping in the Ptarmigan Fiord area resulted in the identification of three deformation events. There are two structural domains in the map area (Figure 1). The northwestern map domain is characterized by a generally north- to northwest-dipping panel of basement and cover imbricates (‘B4’+‘C4’ to ‘B7’—the structurally highest basement in the map area) separated by T_{2c} thrusts. The map pattern of the eastern domain, between Amittuq and Niante Harbour, is dominated by the keel of a F_{2b} syncline that folds basement-cover T_{2a} thrust imbricates (‘B0’+‘C0’ to ‘B3’+‘C3’), and is readily visible from the air as shown in panorama photo of Figure 2a.

D_1: East-west crustal shortening (pre-synthermal peak)

Early Paleoproterozoic deformation (D_1) resulted in a strong foliation (S_{1a}), axial planar to F_{1a} folds, which is defined by the alignment of muscovite, biotite and sillimanite in pelitic rocks (Figure 3d). This foliation formed during regional F_{1a} isoclinal folding. The F_{1a} folds have ~100 m amplitudes and are generally west-dipping (~180°/65°W) with shallow north- and south-plunging fold axes (Dyck and St-Onge, 2014). Throughout the study area the S_{1a} foliation, primary bedding, leucogranite pods and centimetre-wide leucogranite veins are all folded at the outcrop scale by F_{1b} isoclinal folds (Figure 4d). The F_{1b} folds have approximately northwest-trending (310–340°) fold hinges that plunge ~50°, and have west-dipping axial planes oriented ~140°/75°W. An axial planar cleavage (S_{1b}) is developed as a result of the F_{1b} folding (Figure 4d). The axial planar cleavage is best seen in the folded centimetre-wide leucogranite veins and pods as fine fractures, as well as leucogranite veins oriented parallel to the axial plane of the F_{1b} isoclinal folds (Figure 3e), suggesting that peak metamorphism was syndeformational with this folding event.

D_2: Southeast-northwest crustal shortening (post-thermal peak) and thick-skinned deformation

The 100–800 m thick slices of basement and cover rocks are imbricated (Figures 1, 2). On the map (Figure 1) and panorama photographs (Figure 2), seven basement (‘B’) and cover (‘C’) imbricates are labelled in structurally ascending order from the deepest structural level (‘B1’+‘C1’) to the highest structural level (‘B7’). Figure 2a shows the structurally deepest autochthonous basement and overlying cover in the foreground (‘B0’+‘C0’) structurally overlain by basement-cover pairs (‘B1’+‘C1’ to ‘B3’+‘C3’). Figure 2b shows the boundary between basement slice ‘B4’, of the northwestern domain, truncating the ‘B3’+‘C3’ basement-cover pair in the eastern domain.

Variation of D_2 strain in the Ptarmigan Fiord area and strain localization at basement-cover contacts

Large variations in S_2 foliation and lineation are documented in the rocks of the Ptarmigan Fiord area, from areas of relatively low strain where coarse-grained igneous textures and sedimentary structures (such as bedding, see Figure 3e) are preserved, to areas of high strain with strong D_2

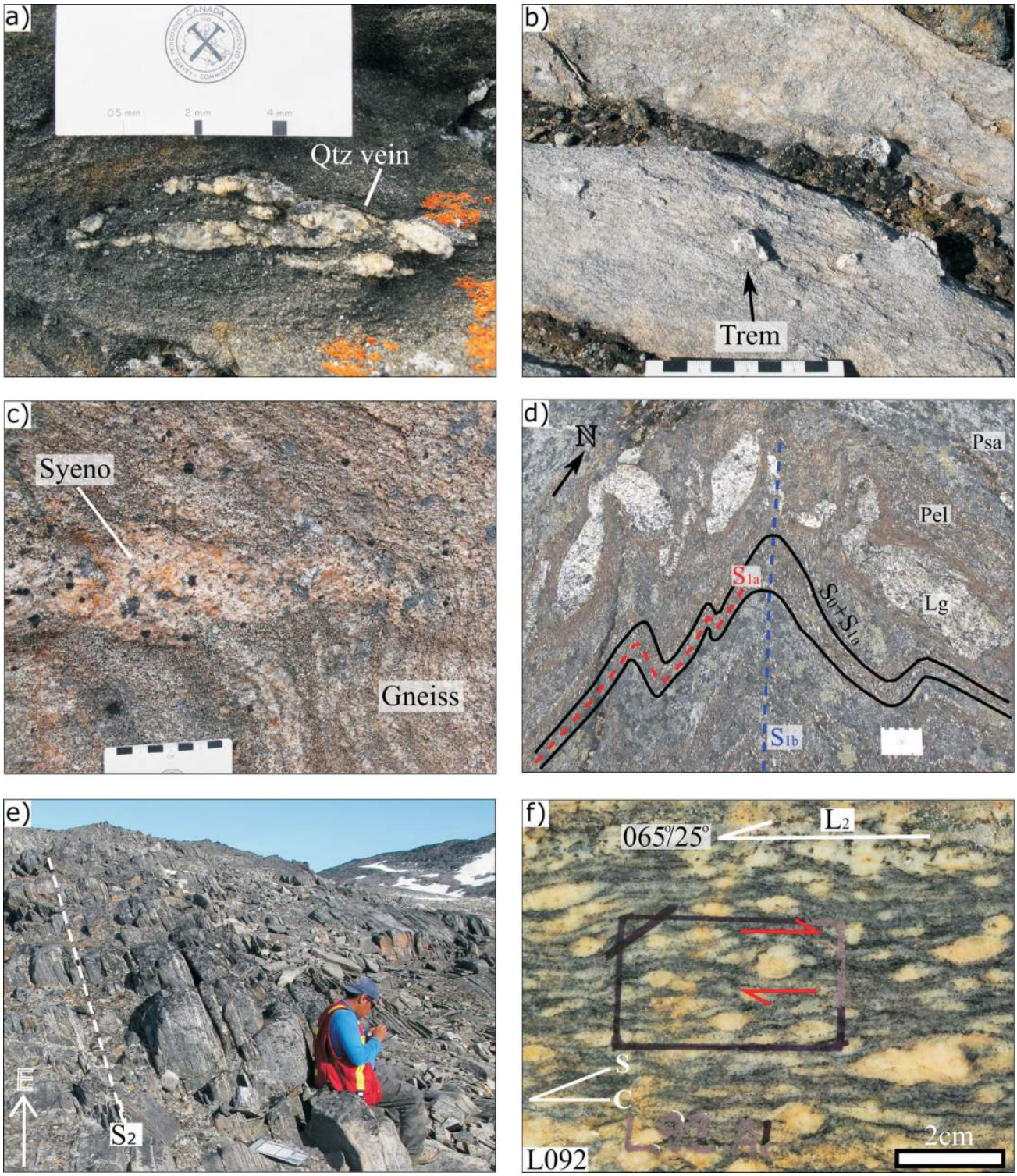

Figure 4: Lithology and structure, Ptarmigan Fiord, Hall Peninsula of Baffin Island: **a)** northwestward view of fine-grained garnet-biotite amphibolite with sheath-folded quartz vein; **b)** eastward view of calcsilicate with 2–5 cm size tremolite knots; **c)** northward view of weakly foliated syenogranite lens that crosscuts gneissic foliation in basement; **d)** S_{1a} compositional layering and foliation with concordant leucogranite or boudinaged veins folded by F_{1b} folds, resulting in the development of S_{1b} foliation; **e)** eastward view of S_2 foliation in granodiorite basement (B1 imbricate); **f)** southeastward view of a slabbed granodiorite basement sample from outcrop L092. View is of the motion plane, cut parallel to L_2 and perpendicular to S_2, exhibiting sigma (σ)-type K-feldspar porphyroclasts inclined to the foliation with top-to-the-southwest sense of shear. Abbreviations: Lg, leucogranite veins; Pel, pelitic schist; Psa, psammitic schist; Qtz, quartz; Syeno, syenogranite; Trem, tremolite; C, C-planes (cisaillement planes); S, S-planes (schistosité planes).

mineral and stretching lineations, and mylonitic textures, in all rock types.

In the eastern domain, autochthonous basement orthogneiss ('B0' in Figure 1), the deepest exposed structural levels in the area, contains large euhedral (~5–15 mm) phenocrysts and the preferred orientation of biotite and muscovite that forms a weak foliation. These are interpreted to be the lowest-strain plutonic rocks in the region and do not contain a visible mineral or stretching lineation, (Figure 3a). However, in the immediate vicinity of the contact with the overlying cover rocks (Figure 3c, 'C0' on Figure 1), platy minerals are aligned in a foliation; and euhedral phenocrysts, especially K-feldspar, occur as elongate porphyroclasts defining a weak stretching lineation (Figure 3b). These structures are interpreted as a strain gradient which may relate to minor shearing at the basement-cover contact. The pelitic and semipelitic rocks at the base of the cover sequence have a S_1 foliation, and although it is aligned parallel to the S_2 foliation in the underlying basement at contact, the rocks are interpreted to be low strain with respect to D_2 deformation (Figure 3c). The basement-cover contact is therefore interpreted as a nonconformable contact between the 'B0' basement and overlying 'C0' supracrustal cover units, with only minor modification of strain.

The plutonic rocks at the base of the first basement imbricate ('B1' in Figure 1), contain a well-developed foliation as shown in Figure 4e. This foliation, interpreted as S_2 in both the basement and 'C1' cover rocks, is defined by the re-alignment of gneissic banding and pre-existing S_1 foliation into parallelism with the basement-cover contact. There appears to be an ~10 to 20% reduction in grain size in all basement units, as well as the development of mylonitic fabrics with shear-sense indicators in the motion-plane parallel to a dominant stretching lineation. Mineral and stretching lineations are penetrative, and are formed by quartz and feldspar rodding and aligned elongate sillimanite–quartz–K-feldspar knots. The strong S_2 foliation, L_2 mineral and stretching lineations and grain-size reduction indicate an increase in strain in the 'B1' basement imbricate, relative to the underlying 'B0' basement. The high-strain contact that separates basement-cover imbricates from the lower strain 'B0' and 'C0' rocks below them, can be interpreted as ductile thrust, where the transport direction was parallel to the mineral and stretching lineations.

At the base of the 'B2' and 'B3' basement imbricates (Figure 1), there is a further reduction in grain size, increase in the percentage of matrix grains and development of protomylonitic fabrics, similar to that of Figure 4f. Shear-sense indicators, in the form of sigma (σ) and delta (δ) K-feldspar porphyroclasts, are used to determine the sense of motion parallel to the stretching lineation (as described in the next section). In finer grained rock types, the S_0 gneissic banding, which is re-aligned into the S_2 shear foliation, shows evidence of extension parallel to the lineation in the form of pulled-apart mafic-mineral and biotite-rich layers (Figure 5a), and boudins.

Evidence for extension also occurs in the pelitic units in the form of large 1–2 m thick rose quartz lineation-parallel boudins. All of these structural observations at base of the 'B2' and 'B3' basement imbricates indicate increases in strain. Based on field observations of the eastern domain of the map area, it can be concluded that the bottom part of the basement slices in the basement-cover imbricates ('B1'+'C1' to 'B3'+'C3') represent moderate to steeply dipping ductile shear zones with T_{2a} thrust movement.

In the northwestern domain, the basement rocks at the base of the thrust imbricates ('B4', 'B5', 'B6' in Figure 1) typically show a further reduction in grain size and increase in the percentage of matrix, resulting in darker colour, and the development quartz- and feldspar-ribbon mylonite textures (Figure 5b). Mylonitic fabrics also occur in the northwestern part of the map area where the cover slices 'C4', 'C5' and 'C6' are truncated or pinched out, and shear zones delineate basement-on-basement contacts at the lower part of basement slice 'B4' and 'B5'(Figures 1, 5b). Northwest-trending sheath folds with ~50° plunges, defined by folded quartz veins, occur in the garnet-biotite amphibolite unit (Figure 4a) at the top of the supracrustal sequence in cover imbricate 'C4' (Figure 1). In cover slices from 'C2' to 'C6', the amphibolite is typically structurally overlain by basement imbricates. Perhaps the top of the relatively competent amphibolite served to localize deformation during overthrusting. Based on an increased percentage of matrix grains, general grain-size reduction and presence of mylonite and sheath folds, these rocks are interpreted to be the highest strain in the study area, and represent discrete ductile shear zones with T_{2c} thrust movement.

Kinematic indicators: transport direction of ductile thrust faults

The strained bases of basement slices within 'B1'+'C1' to 'B6'+'C6' basement-cover imbricates, and at the base of 'B7', are interpreted to represent ductile shear zones (thrust faults); and kinematic indicators are used to determine the sense of motion in the Ptarmigan Fiord area. Sigma (σ) and delta (δ) shaped K-feldspar porphyroclasts within the basement gneiss, and macroscopic shear indicators defined by pulled-apart gneissic banding, are used as kinematic indicators. This section describes a number of shear-sense indicators that, in conjunction with strain variation, provide an explanation for the map patterns. The location of shear-sense indicators are shown on Figure 1 as station numbers in blue font (e.g., W018).

Data in the eastern domain are presented from south to north. Station C055, in 'B2', is located on the southern limb

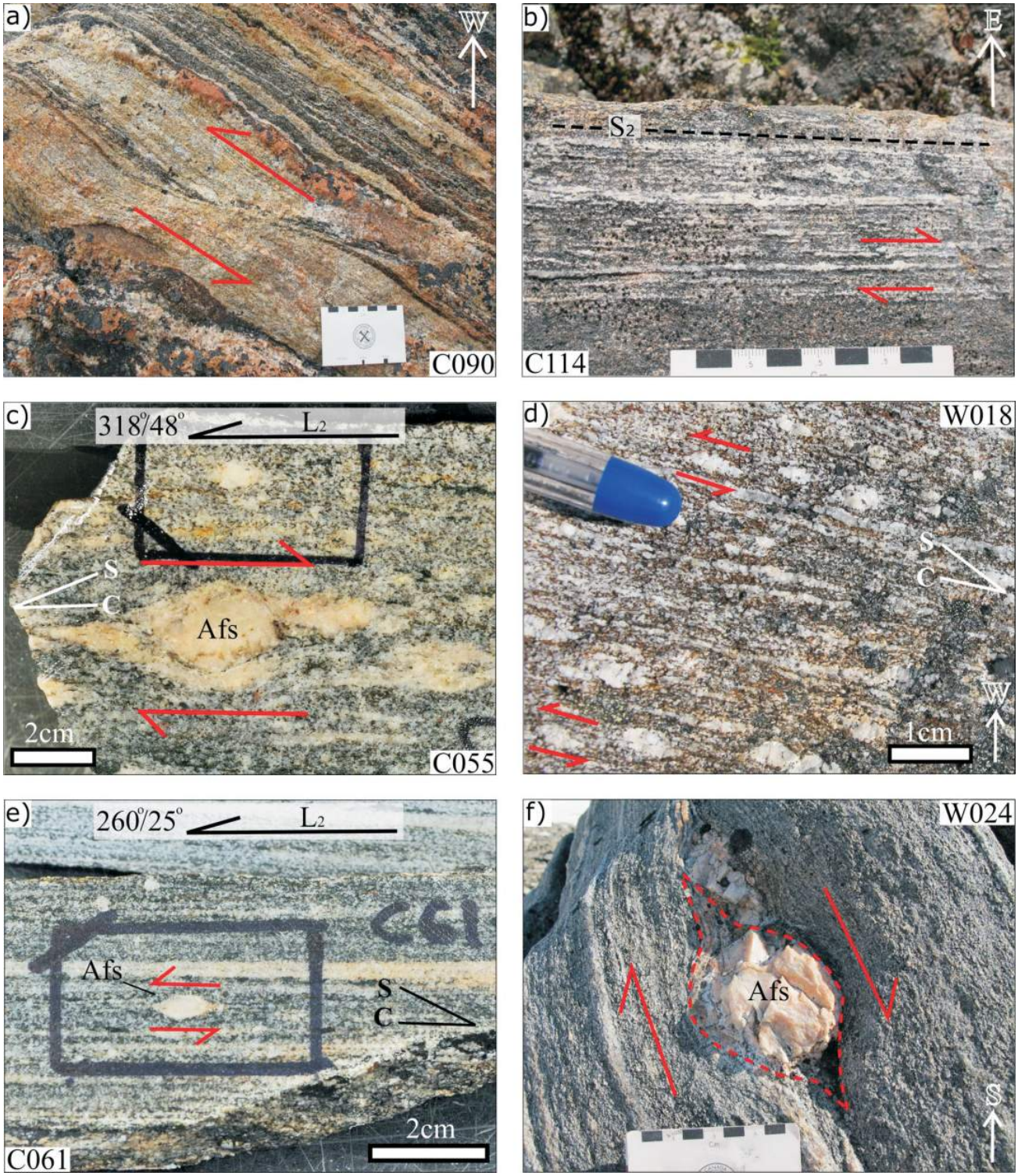

Figure 5: Photographs of structures in the Ptarmigan Fiord area, Hall Peninsula of Baffin Island: **a)** westward view of top-up-to-the-south (reverse shear sense) macroscopic shear-sense indicator defined by extension of a biotite-rich layer in gneissic granodiorite basement, (station C090); **b)** trace of quartz and feldspar ribbons in mylonite in basement-on-basement thrust contact in granodiorite (station C114); **c)** sigma (σ)-type porphyroclast in 'B2' basement granodiorite showing apparent reverse (top-to-the-south) sense of shear (station C055); **d)** sigma (σ)-type porphyroclasts showing apparent reverse (top-to-the-southeast) sense of shear in 'B1' granodiorite basement (station W018, pen parallel to lineation); **e)** sigma (σ)-type porphyroclast within 'B2' basement granodiorite showing apparent normal (top-to-the-west) sense of shear at station C061; **f)** sigma (σ)-type porphyroclast in 'B3' basement granodiorite showing apparent normal (top-to-the-west) sense of shear (station W024).

of the upright F_{2b} synclinal keel. At this station, a basement granodiorite contains a lineation trending northwest and plunging 48°, with σ-type porphyroclast indicating an apparent reverse or top-to-the-southeast sense of shear (Figure 5c). This same shear sense also occurs in a structurally lower basement imbricate ('B1') on the southern limb of the F_{2b} synclinal keel, at station W018. Here, finer grained σ-type porphyroclast shear indicators, aligned parallel to a north-trending lineation with a plunge of 44° also showed a top-to-the-south reverse shear sense (Figure 5d). Based on these two shear indicators from the southern half of the synclinal keel, the inferred direction of thrusting is roughly south, with an apparent reverse sense of shear; this is consistent with interpretations in the region (Dyck and St-Onge, 2014).

In contrast, at station C061 in 'B2', on the northern limb of the upright F_{2b} synclinal keel, the mineral and stretching lineation trends west and plunges shallowly at 20°, with a σ-type porphyroclast indicating a normal, top-to-the-west shear sense (Figure 5e). Farther west, station W024 located on a structurally higher basement imbricate ('B3') also has a west-trending lineation plunging shallowly at ~30°. The shear sense at this station is also top-to-the-west, normal sense of shear, as indicated by a large σ-type K-feldspar porphyroclast within granodiorite (Figure 5f). Based on these two shear indicators from the northern half of the synclinal keel, the inferred direction of transport is roughly west, with an apparent normal sense of shear. One of the primary objectives of the M.Sc. thesis will be to determine the primary orientation of the T_{2a} thrusts by unwinding the S_{2b} folding.

In the northwestern part of the map area, at station C090 in 'B4', a macroscopic shear-sense indicator, defined by the extension of a biotite-rich layer in a gneissic basement unit, is aligned parallel to a roughly north-plunging lineation (Figure 5a). This kinematic indicator represents a top-to-the-south reverse sense of shear. This same shear sense was also recognized in structurally higher thrust imbricates at stations C114 and L092 in 'B4' and 'B5', respectively. Both of these stations have roughly north-plunging lineations, and shear indicators that recorded a top-to-the-south or thrust shear sense. Stations L092 (Figure 4f) and C114 (Figure 5b) are located along high-strain contacts, as described in the previous section, interpreted as basement-on-basement ductile thrusts. Based on these observations, the shear indicators found in the northwestern domain of the map area, at the base of the basement slices in basement-cover imbricates ('B4'+'C4' to 'B7'), represent south-directed thrust faults.

Conclusions

The D_1 event (Table 1), involving east-west crustal shortening (pre-synthermal peak) is manifest in the supracrustal rocks as a strong foliation (S_{1a}) that formed during thermal peak amphibolite-facies metamorphism. The S_{1a} foliation and S_0 primary bedding in metasedimentary rocks were refolded by F_{1b} folds, and a cleavage (S_{1b}) developed axial planar to the F_{1b} folding.

The D_2 event, involving southeast-northwest crustal shortening (post-thermal peak), is recorded in the basement and supracrustal rocks by T_2 thick-skin thrusting with dominantly south- to southeast-directed thrust motion. The T_2 thrust imbricates can be identified on the basis of the following observations and interpretations: 1) the contact between autochthonous basement rocks 'B0' and the cover stratigraphy 'C0' is low-strain and is interpreted as a nonconformable contact, and 2) the contacts between the supracrustal rocks and the structurally overlying basement orthogneiss are higher-strain, and correspond to localized shear zones at the base of each 'B1+C1' to 'B6+C6' basement-cover couplet and at the base of 'B7'. The T_2 ductile shear zones, interpreted as thrusts, were responsible for the development of the L_2 mineral and stretching lineations and S_2 mylonitic foliations. The D_2 deformation can be characterized with respect to an eastern domain and a northwestern domain of the map area, both structurally underlain by autochthonous 'B0+C0' in the south (Figure 1). In the eastern domain, the map pattern is dominated by the keel of an F_{2b} syncline that folds basement-cover T_{2a} thrust imbricates ('B0'+'C0' to 'B3'+'C3'). The map pattern of the northwestern domain is characterized by a generally north- to northwest-dipping panel of basement and cover ('B4'+'C4' to 'B7') imbricates separated by T_{2c} thrusts. At the boundary between the northwestern structural domain and the eastern domain, a stack of basement-cover thrust imbricates (T_{2c}), with 'B4' at the base, truncate T_{2a} basement-cover imbricates ('B3'+'C3' and 'B2'+'C2') of the eastern domain (Figure 2b). The crosscutting relationship implies that the T_{2c} thrust fault at the base of the 'B4' basement imbricate is younger than the T_{2a} thrusts and the F_{2b} fold. This crosscutting relationship implies a two-stage D_2 event involving thrusting of the T_{2a} imbricates first, then folding of the T_{2a} imbricates before truncation by T_{2c} thrust imbricates.

A regional D_3 event (Table 1) has been described in the Hall Peninsula (Steenkamp and St-Onge, 2014; Dyck and St-Onge, 2014). In the Ptarmigan Fiord area, open upright folding (F_3) of the D_2 map-scale patterns is interpreted as D_3. In the northwestern domain, F_3 folding resulted in gentle buckling of the T_{2c} thrust imbricates, while in the eastern domain F_3 folding resulted in a gentle bend of the synclinal keel in the eastern domain of the study area (Figure 1).

The M.Sc. research of T. Chadwick is directed toward detailed petrographic, structural, microstructural and kinematic studies of samples and field data; construction of cross sections; and, map- and regional-scale structural

analysis (e.g., is the thrust at the base of 'B4' an out of sequence thrust?). Goals are to document the geometry and structural evolution of the Ptarmigan Fiord area and to use the results to constrain the geological and structural history of the Hall Peninsula.

Economic considerations

The geological framework and structural evolution of the Ptarmigan Fiord area may have implications for the distribution of mineral resources in the eastern Baffin Island region. Kimberlite pipes, which are geological conduits for transporting diamonds to the Earth's surface, are known to occur in the Archean basement south of Ptarmigan Fiord. This study offers the potential to understand how the emplacement of kimberlite pipes may have been affected by prior imbrication of crystalline basement. A better understanding of the crustal architecture of the Ptarmigan Fiord area could also reveal the full extent of crystalline basement in this part of the eastern Arctic and potentially aid exploration companies in their search for new diamond occurrences in Nunavut.

Acknowledgments

The authors thank D. Liikane, T. Milton, S. Noble-Nowdluk, T. Rowe and A. Ford for providing enthusiastic field assistance and valuable discussions. The Geo-mapping for Energy and Minerals (GEM) program provided financial support for this work. We also thank H. Steenkamp for organizing thin sections for future work through Strategic Investments in Northern Economic Development (SINED) program offered by Canadian Northern Economic Development Agency (CanNor).

Natural Resources Canada, Earth Sciences Sector contribution 20150289

References

Blackadar, R.G. 1967: Geological reconnaissance, southern Baffin Island, District of Franklin; Geological Survey of Canada, Paper 66-47, 32 p.

Corrigan, D. 2012: Paleoproterozoic crustal evolution and tectonic processes: insights from LITHOPROBE program in the Trans-Hudson orogen, Canada; Chapter 4 *in* Tectonic Styles in Canada: The LITHOPROBE Perspective, J.A. Percival, F.A. Cook and R.M. Clowes (ed.), Geological Association of Canada, Special Paper 49, p. 237–284.

Dyck, B.J. and St-Onge, M.R. 2014: Dehydration-melting reactions, leucogranite emplacement and the Paleoproterozoic structural evolution of Hall Peninsula, Baffin Island, Nunavut; *in* Summary of Activities 2013, Canada-Nunavut Geoscience Office, p. 73–84.

From, R.E., St-Onge, M.R. and Camacho A. 2014: Preliminary characterization of the Archean orthogneiss complex of Hall Peninsula, Baffin Island, Nunavut; *in* Summary of Activities 2013, Canada-Nunavut Geoscience Office, p. 47–56.

Hoffman, P.F. 1988: United Plates of America, the birth of a craton: Early Proterozoic assembly and growth of Laurentia; Annual Review of Earth and Planetary Sciences, v. 16, p. 543–603.

Lewry, J.F. and Collerson, K.D. 1990: The Trans-Hudson Orogen: extent, subdivisions and problems; *in* The Early Proterozoic Trans-Hudson Orogen of North America, J.F. Lewry and M.R. Stauffer (ed.), Geological Association of Canada, Special Paper 37, p. 1–14.

MacKay, C.B., Ansdell, K.M., St-Onge, M.R., Machado, G. and Bilodeau, C. 2013: Geological relationships in the Qaqqanittuaq area, southern Hall Peninsula, Baffin Island, Nunavut; *in* Summary of Activities 2012, Canada-Nunavut Geoscience Office, p. 55–64.

MacKay, C.B. and Ansdell, K.M. 2014: Geochemical study of mafic and ultramafic rocks from southern Hall Peninsula, Baffin Island, Nunavut; *in* Summary of Activities 2013, Canada-Nunavut Geoscience Office, p. 85–92.

Rayner, N.M. 2014: New uranium-lead geochronological results from Hall Peninsula, Baffin Island, Nunavut; *in* Summary of Activities 2013, Canada-Nunavut Geoscience Office, p. 39–46.

Scott, D.J. 1999: U-Pb geochronology of the eastern Hall Peninsula, southern Baffin Island, Canada: a northern link between the Archean of West Greenland and the Paleoproterozoic Torngat Orogen of northern Labrador; Precambrian Research, v. 93, p. 5–26.

Steenkamp, H.M. and St-Onge, M.R. 2014: Overview of the 2013 regional bedrock mapping program on northern Hall Peninsula, Baffin Island, Nunavut; *in* Summary of Activities 2013, Canada-Nunavut Geoscience Office, p. 27–38.

St-Onge, M.R., Searle, M.P. and Wodicka, N. 2006: Trans-Hudson Orogen of North America and Himalaya–Karakorum–Tibetan Orogen of Asia: structural and thermal characteristics of the lower and upper plates; Tectonics, v. 25, p. 1–22, doi: 10.1029-2005TC001907

St-Onge, M.R., Wodicka, N. and Ijewliw, O. 2007: Polymetamorphic evolution of the Trans-Hudson Orogen, Baffin Island, Canada: integration of petrological, structural and geochronological data; Journal of Petrology, v. 48, p. 271–302.

St-Onge, M.R., Van Gool, J.A.M., Garde, A.A. and Scott, D.J. 2009: Correlation of Archaean and Palaeoproterozoic units between northeastern Canada and western Greenland: constraining the pre-collisional upper plate accretionary history of the Trans-Hudson orogen; Geological Society, London, Special Publication 318, p. 193–235.

Weller, O.M., Dyck, B.J., St-Onge, M.R., Rayner, N.M. and Tschirhart, V. 2015: Completing the bedrock mapping of southern Baffin Island, Nunavut: plutonic suites and regional stratigraphy; *in* Summary of Activities 2015, Canada-Nunavut Geoscience Office, p. 33–48.

Archean magmatism and metamorphism of eastern Hall Peninsula, southern Baffin Island, Nunavut

R.E. From[1], N.M. Rayner[2] and A. Camacho[3]

[1]*Department of Geological Sciences, University of Manitoba, Winnipeg, Manitoba, jnrfrom@gmail.com*

[2]*Natural Resources Canada, Geological Survey of Canada, Ottawa, Ontario*

[3]*Department of Geological Sciences, University of Manitoba, Winnipeg, Manitoba*

This work is part of the Hall Peninsula Integrated Geoscience Program (HPIGP), led by the Canada-Nunavut Geoscience Office (CNGO) in collaboration with the Government of Nunavut, Indigenous and Northern Affairs Canada, Dalhousie University, University of Alberta, Université Laval, University of Manitoba, University of Ottawa, University of Saskatchewan, University of New Brunswick, Nunavut Arctic College and the Geological Survey of Canada. It is supported logistically by several local, Inuit-owned businesses and the Polar Continental Shelf Program. The focus is on bedrock and surficial geology mapping (1:100 000 scale). In addition, a range of thematic studies is being conducted, including Archean and Paleoproterozoic tectonics, geochronology, landscape uplift and exhumation, microdiamonds, sedimentary rock xenoliths and permafrost. The goal is to increase the level of geological knowledge and better evaluate the natural resource potential in this frontier area.

From, R.E., Rayner, N.M. and Camacho, A. 2015: Archean magmatism and metamorphism of eastern Hall Peninsula, southern Baffin Island, Nunavut; *in* Summary of Activities 2015, Canada-Nunavut Geoscience Office, p. 73–88.

Abstract

Zircon U-Pb geochronology was conducted on six distinct crustal units within a well-constrained study area on eastern Hall Peninsula, Baffin Island. The U-Pb isotopic ages range from ca. 3209 to 2682 Ma[4], outlining a protracted period of Archean magmatic activity and highlighting the previously unrecognized heterogeneity of this orthogneiss suite. Integrating the U-Pb isotopic age data with high-resolution zircon imaging and Th/U ratios, several samples were interpreted to have both an Archean crystallization age and an Archean metamorphic-overprint age. Crystallization ages, characterized by prismatic zircon grains with well-defined oscillatory-growth zoning, range from ca. 2.98 to 2.75 Ga. Archean metamorphic-overprint ages, characterized by rounded zircon grains that are commonly unzoned or sector zoned, or have an irregular internal structure, range from ca. 2.74 to 2.68 Ga. Constraining the timing of Archean crystallization and metamorphism is a key step in fingerprinting the Archean orthogneiss complex of Hall Peninsula. The data can be used for comparison with adjacent Archean terrains, and correlations critical for paleoplate reconstructions for the Baffin Island and subarctic regions can be established.

Résumé

Six unités distinctes de la croûte situées dans une zone d'étude bien délimitée de la partie orientale de la péninsule Hall ont été analysées au moyen de la géochronologie U-Pb sur zircon. Les âges radiométriques obtenus se situent entre environ 3209 et 2682 Ma[5]; ils témoignent d'une période prolongée d'activité magmatique archéenne et mettent en évidence l'hétérogénéité jusqu'à présent non reconnue de cette suite d'orthogneiss. Grâce à la conjugaison des âges radiométriques établis à l'aide de la méthode U-Pb, de l'imagerie à haute résolution des zircons et des rapports Th/U, on a pu établir que certains échantillons font preuve à la fois d'un âge de cristallisation archéen et d'un âge de surimposition archéen. Les âges de cristallisation, laquelle est caractérisée par la présence de grains de zircon prismatiques à zonation oscillatoire bien définie, varient entre environ 2,89 et 2,75 Ga. Les âges correspondant à la surimposition, qui elle se reconnaît à la présence de grains de zircon arrondis, le plus souvent sans zonation ou à zonation en secteurs, ou qui se signale par une structure interne irrégulière, se situent entre environ 2,74 et 2,68 Ga. L'établissement de la plage de temps exact au cours de laquelle se sont produits les épisodes de cristallisation et de métamorphisme constitue une des étapes principales dans la détermination des caractéristiques du complexe d'orthogneiss archéen de la péninsule Hall. Les données recueillies peuvent server à établir non seulement des comparaisons avec des terrains archéens adjacents, mais aussi des corrélations essentielles à la reconstruction des paléoplates-formes des régions subarctiques et de l'île de Baffin.

[4]*When 'ca.' is used before an age range, it applies to both end members of the range.*

[5]*Lorsque « environ » précède un intervalle d'âges, il s'applique aux deux termes extrêmes de l'intervalle*

This publication is also available, free of charge, as colour digital files in Adobe Acrobat® PDF format from the Canada-Nunavut Geoscience Office website: http://cngo.ca/summary-of-activities/2015/.

Introduction

This study is part of the Hall Peninsula Integrated Geoscience Project (HPIGP), led by the Canada-Nunavut Geoscience Office (CNGO) in collaboration with the Geological Survey of Canada (GSC) and a number of Canadian universities. While the broad focus of the HPIGP is the production of bedrock and surficial geological maps, this study targets the Archean geological history of Hall Peninsula.

An overview of the geology of Hall Peninsula can be found in Machado et al. (2013b) and Steenkamp and St-Onge (2014). The Archean rocks of Hall Peninsula are a complex assortment of polydeformed and polymetamorphosed rocks collectively termed "the Archean orthogneiss complex" (From et al., 2013). The Archean orthogneiss complex dominates eastern Hall Peninsula (Figure 1) and is composed mostly of gneissic to migmatitic tonalite to monzogranite with subsidiary components of syenogranite and localized ultramafic pods. Paleoproterozoic metasedimentary units disconformably overlie the Archean orthogneiss complex (Steenkamp and St-Onge, 2014) and are tectonically interleaved in thick-skinned imbricate folds and thrusts as slivers and panels ranging from 20 cm to several kilometres in thickness (Machado et al., 2013).

The Archean orthogneiss complex is very heterogeneous; seven distinct units along a 700 m transect on east-central Hall Peninsula were recognized (Figure 2) and are documented in From et al. (2014). In brief, the study area is dominated by porphyroclastic monzogranite gneiss that intrudes several older orthogneiss units, each with distinct characteristics. Relatively undeformed, coarse-grained syenogranite intrudes all units. Uranium-lead geochronology (presented here) was completed on six of these rock units to determine the time span of Archean magmatism, confirm the field relationships observed in the study area and begin to characterize the Archean orthogneiss complex.

Previous age determinations

Previous reconnaissance-scale U-Pb age determinations of the Archean orthogneiss complex were carried out by Scott (1999) and Rayner (2014a, b, 2015a, b). Scott (1999) analyzed zircon and titanite in four samples of foliated tonalite along the eastern coast of Hall Peninsula and one foliated tonalite along a narrow east-west transect on central Hall Peninsula (Figure 1) using the isotope dilution–thermal ionization mass spectrometry (ID-TIMS) method. The resulting $^{207}Pb/^{206}Pb$ ages of 2920 +8/–6, 2848 ±3, 2844 +6/–5 and 2797 +27/–15 Ma were interpreted as magmatic crystallization ages. In addition, zircon from three separate granitic dykes that intrude the gneisses along the eastern coast gave ages of 2835 ±11, 2768 ±13 and 2820 ±5 Ma. Analyses of titanite from the same granitic dykes returned much younger ages between ca. 1730 and 1842 Ma. Consequently, the Archean zircon from the intrusive granitic dykes is interpreted to have either grown during initial emplacement of the veins or been inherited as xenocrysts within Paleoproterozoic granitic dykes (Scott, 1999).

Subsequent investigations (Rayner, 2014a, b, 2015a, b) used the sensitive high-resolution ion microprobe (SHRIMP) technique to determine the ages of four foliated tonalite gneiss samples and one deformed megacrystic monzogranite collected across central and eastern Hall Peninsula (Figure 1) in order to calibrate the regional geological map legend. The U-Pb isotopic ages of these samples were interpreted to represent crystallization ages between 2701 ±2 and 2841 ±3 Ma (Rayner, 2014a, b, 2015a, b). This work gave an essential understanding of the broad temporal extent of Archean rock emplacement on eastern Hall Peninsula and sets the stage for further, more detailed geochronological investigations.

Hypothesis for further investigation

The crustal provenance of the Archean orthogneiss complex on eastern Hall Peninsula remains enigmatic. Based on lithological similarities, geochronology and aeromagnetic characteristics, these rocks have been previously interpreted to correlate with the Rae craton of northern Baffin Island and western Greenland (Hoffman, 1988), the Meta Incognita microcontinent of southern Baffin Island and northern Labrador (St-Onge et al., 2009), the Aasiaat domain of central western Greenland (Hollis et al., 2006; Thrane and Connelly, 2006; St-Onge et al., 2009) and the Nain craton of northern Labrador (Scott and Campbell, 1993; Scott, 1999; Connelly, 2001; Wardle et al., 2002), and as a unique and distinct microcontinent (Whalen et al., 2010). Uranium-lead geochronology has proven to be an effective method to identify and delineate other unique pieces of crust that may have been tectonically amalgamated in this region during the Trans-Hudson orogeny (e.g., St-Onge et al., 2002; Connelly et al., 2006; Corrigan et al., 2009). Previous reconnaissance-scale geochronology in the Archean orthogneiss complex has targeted mainly the tonalitic gneiss, which was believed to be a significant component of the complex. Recent detailed mapping of a small study area on east-central Hall Peninsula characterized seven distinct units within the Archean orthogneiss complex (From et al., 2014), with monzogranite gneiss being the dominant component. Therefore, further geochronological investigation of the previously unidentified heterogeneity of gneisses within the Archean orthogneiss complex is warranted.

Zircon was selected as the ideal mineral to use with U-Pb isotopes because it is refractory and consequently resistant to most magmatic, metamorphic and erosional processes that may destroy or alter other common U-bearing accessory minerals (Williams, 1992). The closure temperature of Pb in zircon is very high (950 to >1000°C) and is not easily reset (Lee et al., 1997; Möller et al., 2002). Within a single zircon grain, it is not uncommon to observe distinct chemi-

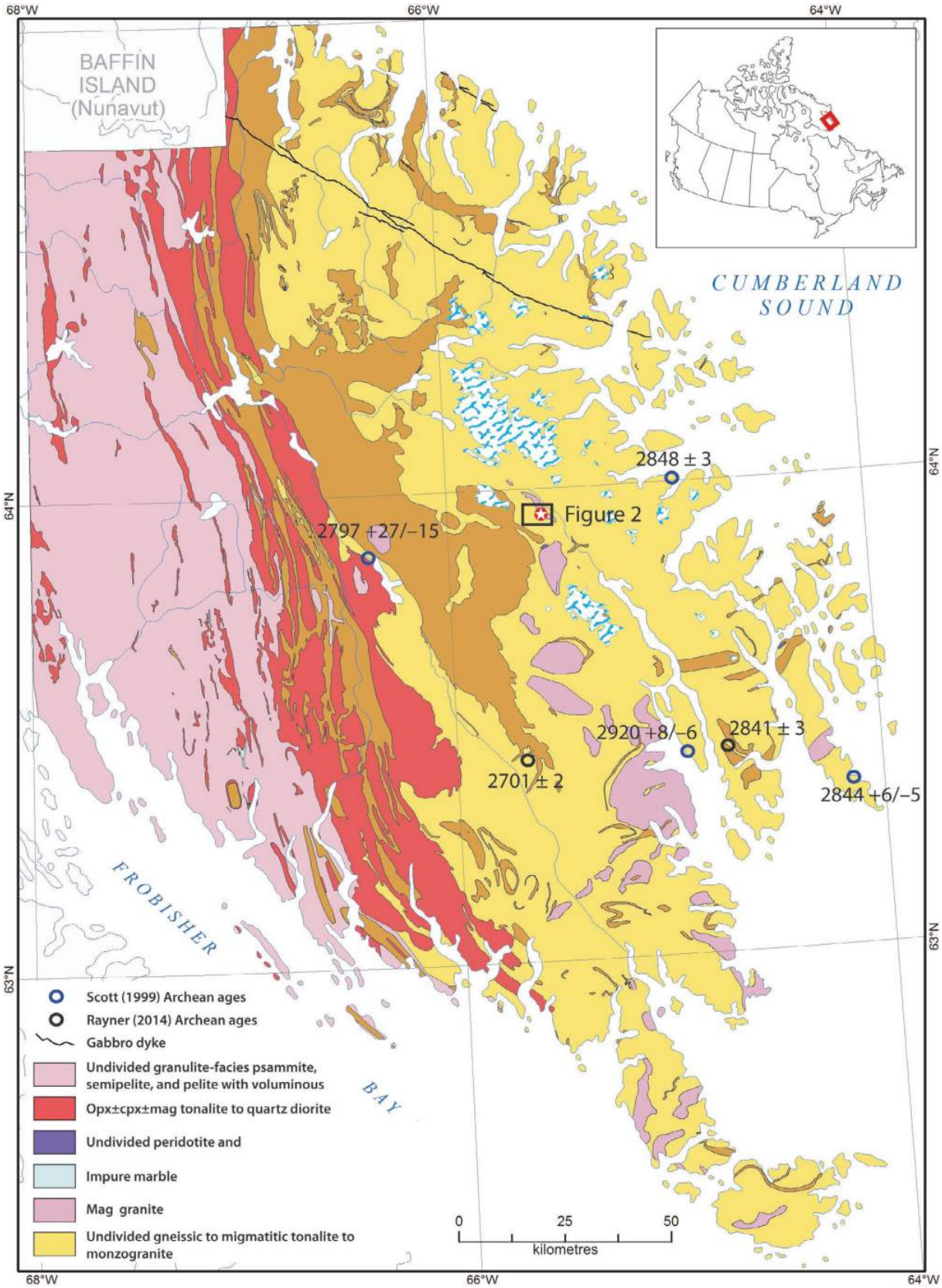

Figure 1: Geology of southern Hall Peninsula, Nunavut from data collected during the 2012 and 2013 field seasons, showing the distribution of the principal units and the locations of previous U-Pb age determinations (modified from Machado et al., 2013). Location of the study area is shown with a red star. Abbreviations: grt, garnet; bt, biotite; mag, magnetite; opx, orthopyroxene; cpx, clinopyroxene.

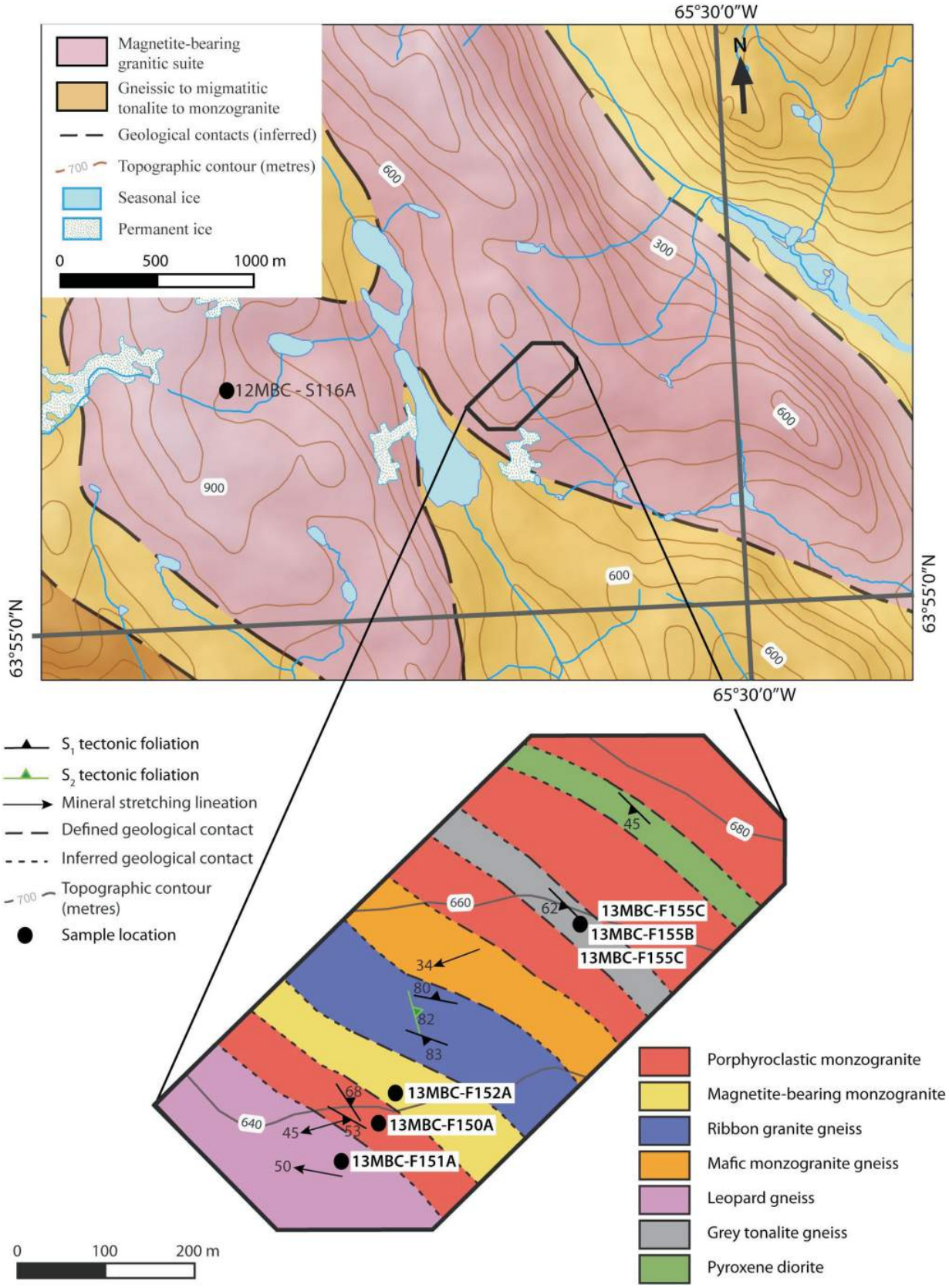

Figure 2: Detailed geology of the study area on east-central Hall Peninsula, Nunavut, with inset schematic map showing the general geology of the surrounding area. The geological unit legend of the study area lists units from oldest to youngest (from top to bottom), as interpreted in From et al. (2014), with black dots and sample numbers indicating the positions of samples analyzed for U-Pb geochronology.

cal and structural domains, each preserving the chemical conditions of a particular period of zircon crystallization. Therefore, both the external morphology and the internal chemical and structural zoning of each zircon grain must be carefully considered when interpreting the relationship between particular domains and specific stages of the rocks' history (e.g., Hanchar and Miller, 1993).

This paper presents SHRIMP U-Pb zircon results for a suite of seven samples from distinct rock types documented within the Archean basement complex, as defined in From et al. (2014). The SHRIMP instrument specializes in isotopic analysis of mineral grains at the micrometre scale and is an ideal tool to help unravel the timing of past geological events in complex and polydeformed rocks, such as those of Hall Peninsula. If the distinct rock units in question are all Archean in age, then they may provide a more detailed age range for the formation of the Archean orthogneiss complex and help to identify any recorded Archean tectonothermal events. Furthermore, refinement of the timing of Archean crustal genesis may provide insight into discriminating different geological processes active during the Archean.

Analytical methods

Seven samples were disaggregated (fine to medium sand size) using standard crushing and pulverizing techniques followed by density separation using a Wilfley table. The crushed material was further separated by density using heavy liquids (methylene iodide) and subsequently a magnetic separator to isolate the zircon separate. Details regarding the procedure, or any deviations from it, are noted in the sections describing specific samples.

The SHRIMP analytical procedures are described in Stern (1997), with reference material and U-Pb calibration methodology following Stern and Amelin (2003). In brief, zircons were set in 2.5 cm diameter epoxy mounts (GSC epoxy mounts #733 and #690) along with fragments of the GSC zircon laboratory standards (z6266 with $^{206}Pb/^{238}U$ age of 559 Ma; z1242 with $^{207}Pb/^{206}Pb$ age of 2679 Ma). The epoxy mounts were polished and cores of the zircons were exposed using 9, 6 and 1 μm diamond polishing compounds. The internal structure and features of the zircons were then characterized in backscattered electron (BSE) mode and cathodoluminescence (CL) mode using a Zeiss Evo® 50 scanning electron microscope. Details of the SHRIMP analytical session, including spot size, number of scans, age/error of standard, calibration error and the application of any intra-element fractionation corrections are given in the footnotes of the data table (From and Rayner, 2015)[6]. The count rates of 11 masses including background were sequentially measured with a single electron multiplier. Offline data processing was accomplished using SQUID2 (version 2.22.08.04.30, revised April 30, 2008). The 1σ external errors of $^{206}Pb/^{238}U$ ratios reported in the data table incorporate the error in calibrating the standard. Common Pb correction used the Pb composition of the surface blank (Stern, 1997). Isoplot version 3.00 (Ludwig, 2003) was used to generate concordia plots and calculate weighted means. The error ellipses on the concordia diagrams and the weighted-mean errors in the text and on the figures are reported at the 2σ uncertainty level.

[6]*CNGO Geoscience Data Series GDS2015-009, containing the data or other information sources used to compile this paper, is available online to download free of charge at http://cngo.ca/summary-of-activities/2015/.*

U-Pb results

A separate section for each sample is presented here, and contains lithology and zircon descriptions, a summary of the geochronological results and a geological interpretation. All analytical results can be found in the accompanying data table (From and Rayner, 2015).

12MBC-S116A – monzogranite gneiss

Sample description

The monzogranite gneiss is typically greyish white on both weathered and fresh surfaces, and is intruded by coarse-grained leucocratic veins. A sample was collected, carefully avoiding the veins, just west-northwest of the detailed study area as part of a larger scale traverse in 2012. The sample is fine grained and has a mineral foliation defined by hornblende and biotite. The mineralogy is 30% quartz, 20% K-feldspar, 20% plagioclase, 20% biotite, 5% titanite and 5% hornblende.

Zircon grains separated from this sample are generally subrounded, prismatic to ovoid, and slightly elongate (aspect ratios up to 3:1; <200 μm long). The zircons show well-defined, fine- to medium-scale oscillatory-growth zoning in BSE and CL images (Figure 3a, b). A few grains have overgrowths that are unzoned or irregularly zoned (Figure 3b).

Results and interpretation

Thirty-two analyses were conducted on 25 separate zircon grains, yielding $^{207}Pb/^{206}Pb$ ages between ca. 2988 and 2716 Ma. A cluster of the thirteen oldest ages, ranging from ca. 2988 to 2969 Ma, is characterized by well-defined, fine-scale growth zonation and has a weighted-mean $^{207}Pb/^{206}Pb$ age of 2976 ±4 Ma (n = 10; mean square of weighted deviates [MSWD] = 2.0; Figure 3c), interpreted as the crystallization age of this monzogranite. The remaining younger ages (n = 11), ranging from ca. 2964 to 2943 Ma, cascade toward three even younger ages of ca. 2901, 2837 and 2716 Ma. Two of these young results (ca. 2901 and 2837 Ma) are from homogeneous overgrowth rims that have relatively high U values (673 to 3834 ppm) and low Th/U values (0.12 to 0.16), compared to the older zircon grains. These dates may be related to non-zero-age Pb loss

(where Pb is leaked from the zircon during open-system behaviour) or perhaps recrystallization of zircon due to tectonothermal activity associated with the emplacement of younger magmatic rocks. The youngest date of ca. 2716 Ma comes from a zircon with a particularly clean core and rim relationship that can be interpreted to represent initial crystallization (core) and subsequent metamorphism (rim) of this sample. However, with only one example of this relationship, an alternative interpretation is that there was Pb loss due to later tectonothermal events (after ca. 2716 Ma)

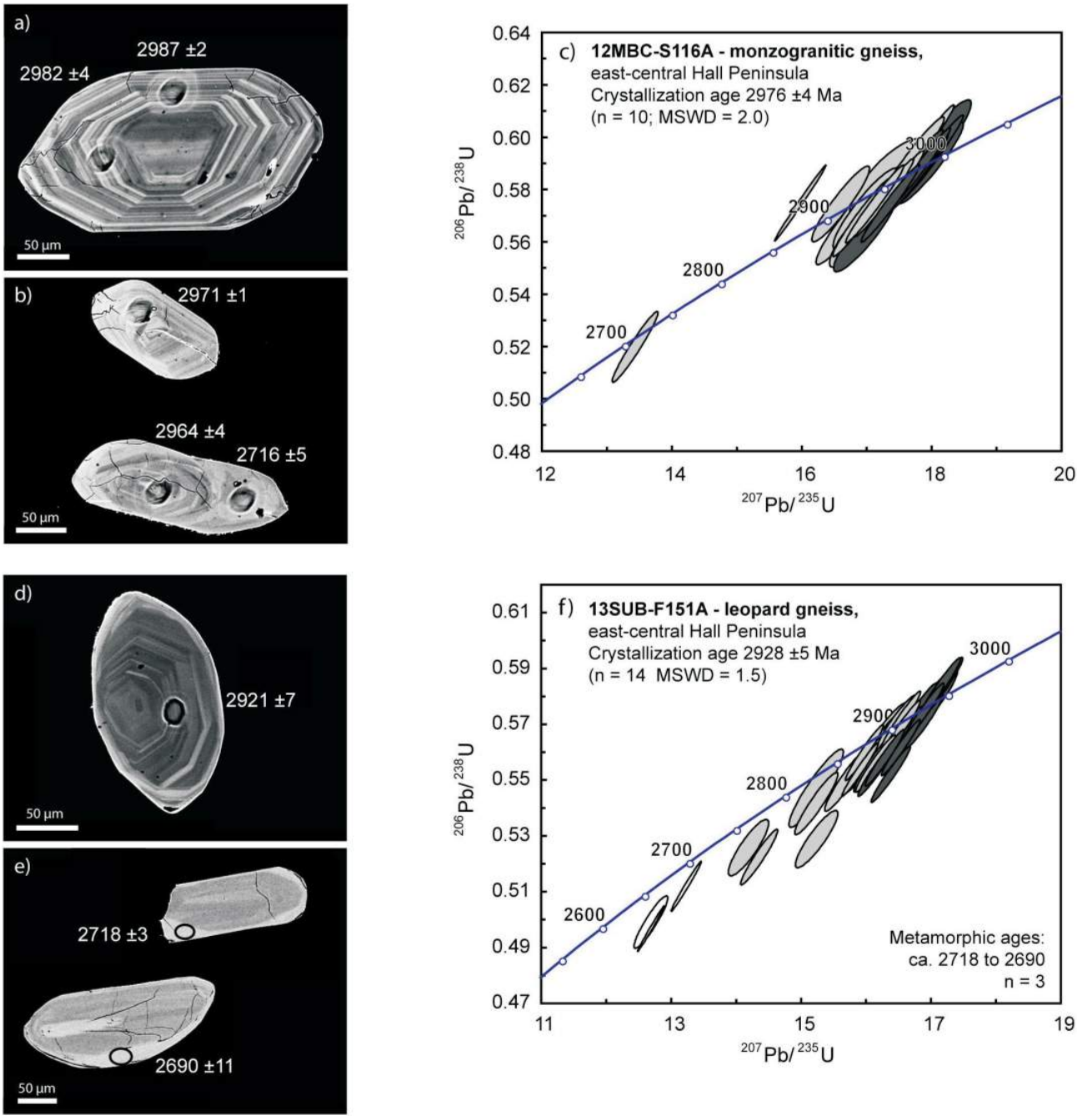

Figure 3: Zircon images (white scale bars all 50 µm) showing spot analyses (correspond to analyses in From and Rayner (2015); errors given at 1σ) and concordia diagrams with plotted ellipses and mean ages reported at the 2σ confidence level: **a)**, **b)** BSE images of representative zircons from sample 12MBC-S116A; **c)** concordia diagram of U-Pb results from sample 12MBC-S116A; dark grey ellipses correspond to ages used to calculate the crystallization age and light grey ellipses are ages excluded from the crystallization-age calculation (see text for discussion); **d)**, **e)** BSE images of representative zircons from sample 13SUB-F151A; **f)** concordia diagram of U-Pb results from sample 13SUB-F151A; dark grey ellipses correspond to ages used to calculate the crystallization age and light grey ellipses are ages excluded from the crystallization-age calculation; unfilled ellipses denote metamorphic ages (see text for discussion). Abbreviation: BSE, backscattered electron.

that may have partially reset the isotope systematics of the older, oscillatory-zoned zircon (e.g., Pb loss through partial recrystallization), resulting in the age scatter.

13SUB-F151A – megacrystic granodiorite gneiss

Rock description

The megacrystic granodiorite gneiss is medium to coarse grained and characterized by a pervasive L-tectonite fabric defined by elongate, relict plagioclase phenocrysts that are commonly surrounded by hornblende. There are fine-grained mafic lenses composed of hornblende+biotite+ epidote quartz diorite. A homogeneous sample without mafic material was collected from the southwestern edge of the detailed study area (Figure 2). The dated sample is medium grained with 40% quartz, 30% plagioclase, 15% hornblende, 10% biotite and 5% titanite.

Zircon grains separated from this sample are dominantly ovoid with rounded grain edges, while only a few grains are elongate and prismatic (aspect ratios 3:1; <200 μm long). Images (BSE and CL) of the zircon show that most grains have fine-scale oscillatory-growth zonation throughout the entire grain (Figure 3d), with a few grains having more diffuse oscillatory zones toward the outer edges. All of the grains have a thin, unzoned, high-U rim (bright in BSE images), but only three of these unzoned rims were large enough for a spot analysis (Figure 3e).

Results and interpretation

Thirty-six analyses were conducted on 31 separate zircon grains, yielding $^{207}Pb/^{206}Pb$ ages between ca. 2945 and 2690 Ma (From and Rayner, 2015). The nine oldest $^{207}Pb/^{206}Pb$ ages, from ca. 2945 to 2917 Ma, were collected in areas of zircon grains with fine-scale oscillatory-growth zoning and are interpreted as the crystallization age of the megacrystic granodiorite gneiss. These data yield a weighted-mean $^{207}Pb/^{206}Pb$ age of 2928 ±5 Ma (n = 14, MSWD = 1.5; Figure 3f). Younger ages (n = 17), from ca. 2913 to 2718 Ma, appear to cascade down to a small cluster of analyses collected from the unzoned overgrowths. The three overgrowths produced ages between ca. 2718 and 2690 Ma, and are characterized by high U (563 to 1497 ppm) and low Th/U (0.07 to 0.18) compared to the analyses with older ages (U concentrations of 55 to 259 ppm and Th/U ratios of 0.39 to 0.73). These three zircon overgrowths are interpreted to have formed during a separate episode of metamorphism and zircon growth. This metamorphic event may have partially reset the isotope systematics of the older, oscillatory-zoned zircon (e.g., Pb loss through partial recrystallization), resulting in the scatter toward younger ages.

13SUB-F155B – grey tonalite gneiss

Rock description

The grey tonalite gneiss is found only as a semicontinuous raft (5 m wide by 25 m long) in monzogranite gneiss (13SUB-F155A) and has a distinct grey weathering surface and a black and white fresh surface. There are local discontinuous mafic lenses (13SUB-F155C) and thin (millimetre-scale) trondhjemitic segregations that define the gneissic foliation. The tonalite gneiss is intruded by centimetre- to metre-scale dykes of the monzogranitic gneiss (13SUB-F155A) concordant to, but locally crosscutting, the gneissic fabric. A homogeneous sample of the grey tonalite gneiss, excluding stringers and other crosscutting components, was collected from the northeastern edge of the detailed study area (Figure 2). The dated sample is fine grained with a mineral foliation defined by hornblende and biotite. The mineralogy is 40% quartz, 30% plagioclase, 15% hornblende, 10% biotite, 3% K-feldspar and 2% apatite.

Zircon grains separated from this sample have varied morphological and zonation characteristics. In general, the majority of grains are mostly ovoid, while a minor population is elongate and prismatic (aspect ratios up to 3:1; <220 μm long). Most of the zircons have fine-scale oscillatory-growth zonation (Figure 4a). These zircons may have cores (Figure 4b) and unzoned overgrowth domains (Figure 4c). There is a separate population of stubby, generally rounded zircon that is unzoned or sector zoned (Figure 4d).

Results and interpretation

Forty-three analyses were conducted on 37 separate zircon grains, yielding $^{207}Pb/^{206}Pb$ ages between ca. 3209 and 2671 Ma (From and Rayner, 2015). The oldest ages, ca. 3209 to 2846 Ma, are from the cores of zircon grains that are overgrown by oscillatory-zoned zircon material (Figure 4d) and are interpreted as inherited cores. A tight cluster of ages, between ca. 2820 and 2806 Ma, with well-defined, fine-scale oscillatory-growth zonation and consistent Th/U values (0.33 to 0.53) are interpreted to represent the crystallization age of the grey tonalite gneiss. These data give a $^{207}Pb/^{206}Pb$ weighted-mean age of 2810 ±3 Ma (n = 6, MSWD = 0.74; Figure 4e). Four younger ages, from ca. 2794 to 2766 Ma, are from oscillatory-zoned zircon with high U and low Th/U values (0.05 to 0.39), and may represent scatter of ages due to Pb loss (see below). The youngest zircon ages, from ca. 2738 to 2671 Ma, are from zircon overgrowth rims and stubby single grains. Many of these zircons are unzoned and have Th/U ratios that are two to four times higher than the Th/U values from all other zircons previously mentioned (0.69 to 1.36). These ages suggest a separate episode of zircon growth with a weighted-mean $^{207}Pb/^{206}Pb$ age of 2727 ±5 (n = 13, MSWD = 2.2). This separate episode of zircon growth is likely from an Archean tectonothermal event that may have partially reset

the isotope systematics of the older, oscillatory-zoned zircon (e.g., Pb loss through partial recrystallization), resulting in the scatter toward younger ages.

13SUB-F155C – mafic lenses

Rock description

The discontinuous hornblende diorite lenses occur within the tonalite gneiss (13SUB-F155B) and are generally elongate parallel to the gneissosity. The mineralogy of these mafic lenses is homogeneous, comprising 55% hornblende, 15% biotite, 15% plagioclase, 10% quartz, and 5% accessory allanite and apatite. Initially, these mafic lenses were thought to be boudins of a nearby pyroxene diorite unit (From et al., 2014), but the mafic lenses within the grey tonalite gneiss do not contain any pyroxene and have a significantly different texture than the pyroxene diorite, based on petrographic analyses, making it unlikely that these mafic lenses are derived from the pyroxene diorite. A sample was collected from the largest mafic horizon (40 cm wide by 80 cm long), observed just a few metres from the grey tonalite gneiss sample (Figure 2).

Zircon grains separated from this sample are ovoid with rounded edges. Images (BSE and CL) show that most of the grains are unzoned, with a few grains containing sector zoning (Figure 4f, g). In several unzoned grains, there are visible internal cores that are darker in BSE images. Several grains have thin, unzoned overgrowth rims that appear dark in BSE images (Figure 4g).

Results and interpretation

Thirty-four analyses were conducted on 22 zircon grains, yielding a range of $^{207}Pb/^{206}Pb$ ages between ca. 2850 and 1825 Ma (From and Rayner, 2015). The four oldest ages, between ca. 2850 and 2777 Ma, are from zircon cores with low Th/U values (0.02 to 0.07); these zircon domains are interpreted as a xenocrystic component. Sixteen $^{207}Pb/^{206}Pb$ ages between ca. 2724 and 2621 Ma are all from the ovoid, unzoned zircon with Th/U values of 0.07 to 0.31. Within this grouping, a cluster of eight analyses gives a $^{207}Pb/^{206}Pb$ weighted-mean age of 2700 ±3 Ma (MSWD = 1.2; Figure 4h). This cluster excludes four outlier ages of ca. 2724 to 2714 Ma. The remaining Archean ages, from ca. 2693 to 2621 Ma, likely represent scatter due to non-zero Pb loss. The seven youngest ages, from ca. 1882 to 1826 Ma, are from the thin, unzoned overgrowth rims, which appear black in BSE images and have distinct, low Th/U values (0.01). These zircon rims are interpreted to have grown due to metamorphism during the Paleoproterozoic Trans-Hudson orogeny (St-Onge et al., 2007), which may have also been the thermotectonic event responsible for the non-zero Pb loss of the slightly older ages.

As these mafic lenses were observed only within the tonalite gneiss, they were inferred in the field to be xenoliths or rafts and consequently older than their host (13SUB-F155B, with a crystallization age of 2810 ±3 Ma). The resulting younger age (2700 ±3 Ma) was unexpected. The revised age relationships among all the samples in the detailed transect will be dealt with in the 'Discussion' section.

13SUB-F155A – porphyroclastic monzogranite gneiss

Rock description

The porphyroclastic monzogranite gneiss is fine grained with greyish-white weathered and fresh surfaces, and commonly contains biotite, hornblende and epidote. There is a characteristic porphyroclastic texture in which K-feldspar porphyroclasts of various sizes (0.5 to 5 cm) are commonly sheared and interconnected by recrystallized bands of finer grained K-feldspar. The porphyroclasts are interpreted to have been derived from the disaggregation of coarse-grained syenogranitic veins. The monzogranite gneiss entrains and intrudes into the tonalite gneiss (13SUB-F155B). A representative sample of homogeneous monzogranite gneiss, with minimal porphyroclastic material and mineral segregations, was collected on the northeastern edge of the detailed study area (Figure 2). The sample is medium to coarse grained with a well-developed mineral foliation defined by biotite and hornblende. The mineralogy is 40% quartz, 35% K-feldspar, 10% plagioclase, 5% biotite, 5% hornblende, 2% epidote, 2% chlorite and 1% magnetite.

Zircon separated from this sample is divided into two morphological groups: elongate prismatic (aspect ratios up to 4:1; <200 μm long) grains and ovoid grains with rounded edges. Images (BSE and CL) show that the elongate prismatic zircon grains have well-defined, fine-scale, oscillatory-zoned cores (Figure 4i) and homogeneous overgrowths (Figure 4i). The population of ovoid, rounded grains is generally unzoned or sector zoned (Figure 4j).

Figure 4: Zircon images (white scale bars all 50 μm) showing spot analyses (correspond to analyses in From and Rayner (2015); errors given at 1σ) and concordia diagrams with plotted ellipses and mean ages reported at the 2σ confidence level: **a)**, **b)**, **c)**, **d)** BSE images of representative zircons from sample 13SUB-F155B; **e)** concordia diagram of U-Pb results from sample 13SUB-F155B; dark grey ellipses correspond to ages used to calculate the crystallization age; light grey ellipses are ages excluded from the crystallization-age calculation; unfilled ellipses denote metamorphic ages used to calculate the weighted-mean age of metamorphism (see text for discussion); **f)**, **g)** BSE images of representative zircons from sample 13SUB-F155C; **h)** concordia diagram of U-Pb results from sample 13SUB-F155C; dark grey ellipses correspond to ages used to calculate the crystallization age; light grey ellipses are ages excluded from the crystallization-age calculation. **i)**, **j)** BSE images of representative zircons from sample 13SUB-F155A.; **k)** concordia diagram of U-Pb results from sample 13SUB-F155A; dark grey ellipses correspond to ages used to calculate the crystallization age; light grey ellipses are ages excluded from the crystallization-age calculation; unfilled ellipses denote ages used to calculate the weighted-mean age of metamorphism (see text for discussion). Abbreviation: BSE, backscattered electron.

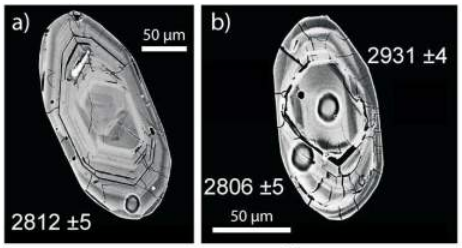
a)
50 µm
2812 ±5
b)
2931 ±4
2806 ±5
50 µm

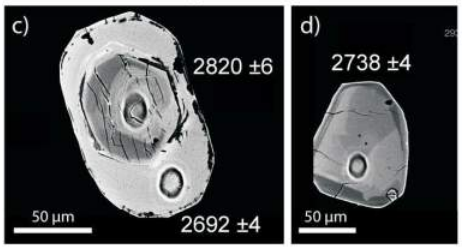
c)
2820 ±6
50 µm
2692 ±4
d)
2738 ±4
50 µm

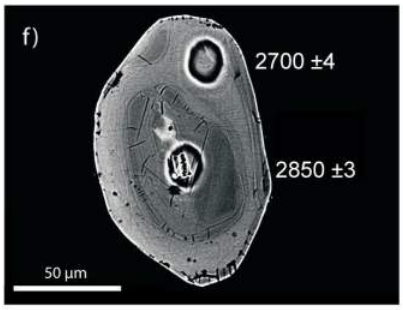
f)
2700 ±4
2850 ±3
50 µm

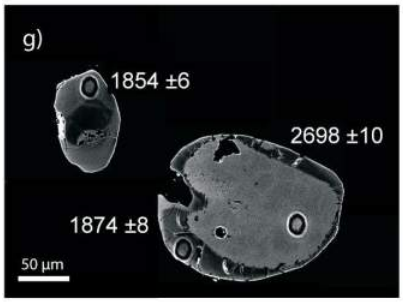
g)
1854 ±6
2698 ±10
1874 ±8
50 µm

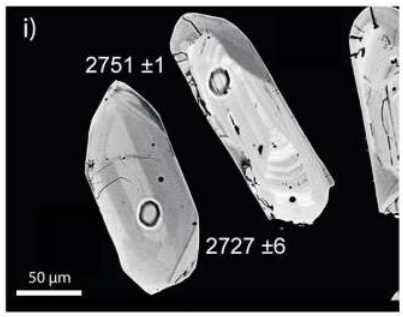
i)
2751 ±1
2727 ±6
50 µm

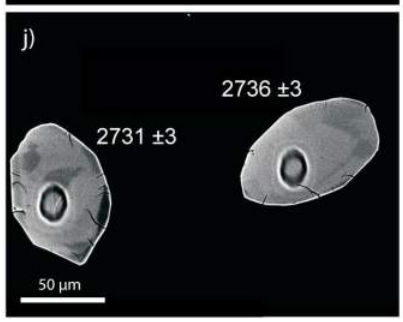
j)
2736 ±3
2731 ±3
50 µm

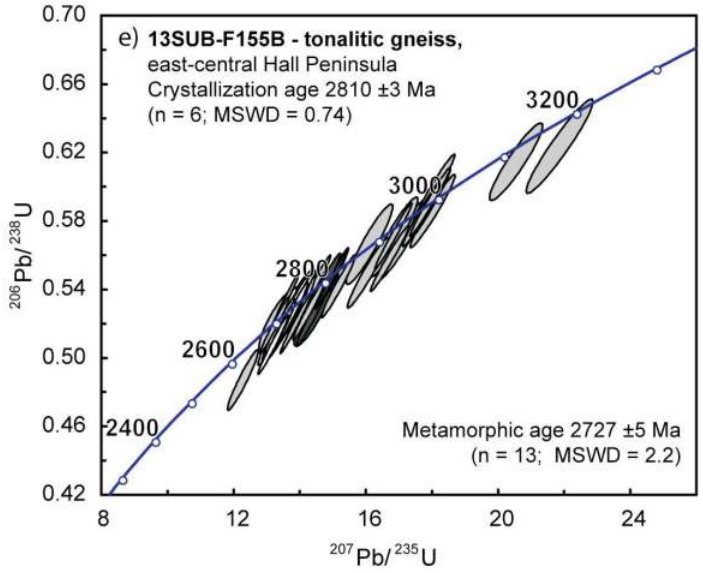
e) 13SUB-F155B - tonalitic gneiss,
east-central Hall Peninsula
Crystallization age 2810 ±3 Ma
(n = 6; MSWD = 0.74)
Metamorphic age 2727 ±5 Ma
(n = 13; MSWD = 2.2)
3200
3000
2800
2600
2400
0.70
0.66
0.62
0.58
0.54
0.50
0.46
0.42
8
12
16
20
24
206Pb/238U
207Pb/235U

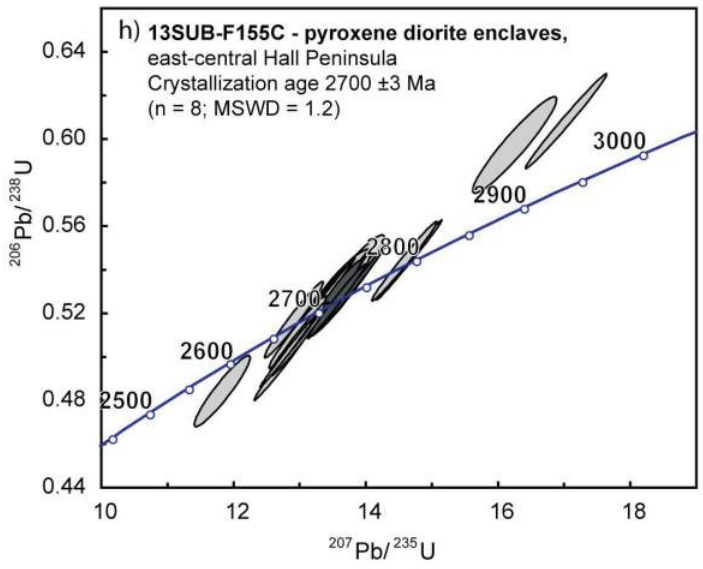
h) 13SUB-F155C - pyroxene diorite enclaves,
east-central Hall Peninsula
Crystallization age 2700 ±3 Ma
(n = 8; MSWD = 1.2)
3000
2900
2800
2700
2600
2500
0.64
0.60
0.56
0.52
0.48
0.44
10
12
14
16
18
206Pb/238U
207Pb/235U

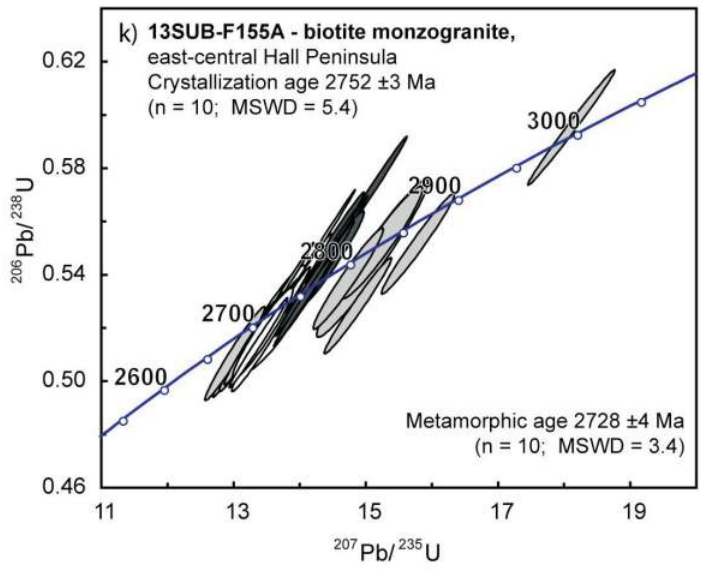
k) 13SUB-F155A - biotite monzogranite,
east-central Hall Peninsula
Crystallization age 2752 ±3 Ma
(n = 10; MSWD = 5.4)
Metamorphic age 2728 ±4 Ma
(n = 10; MSWD = 3.4)
3000
2900
2800
2700
2600
0.62
0.58
0.54
0.50
0.46
11
13
15
17
19
206Pb/238U
207Pb/235U

Results and interpretation

Forty-three analyses were conducted on 37 zircon grains, yielding $^{207}Pb/^{206}Pb$ ages between 2984 and 2687 Ma (From and Rayner, 2015). The six oldest ages, between ca. 2984 and 2810 Ma, were from domains with irregular zonation that are interpreted as xenocrystic components. Ten ages between ca. 2761 and 2742 Ma have well-defined, fine-scale oscillatory-growth zonation and high U concentrations (689 to 3639 ppm), and yield a weighted-mean $^{207}Pb/^{206}Pb$ age of 2752 ±3 Ma (MSWD = 5.4; Figure 4k),

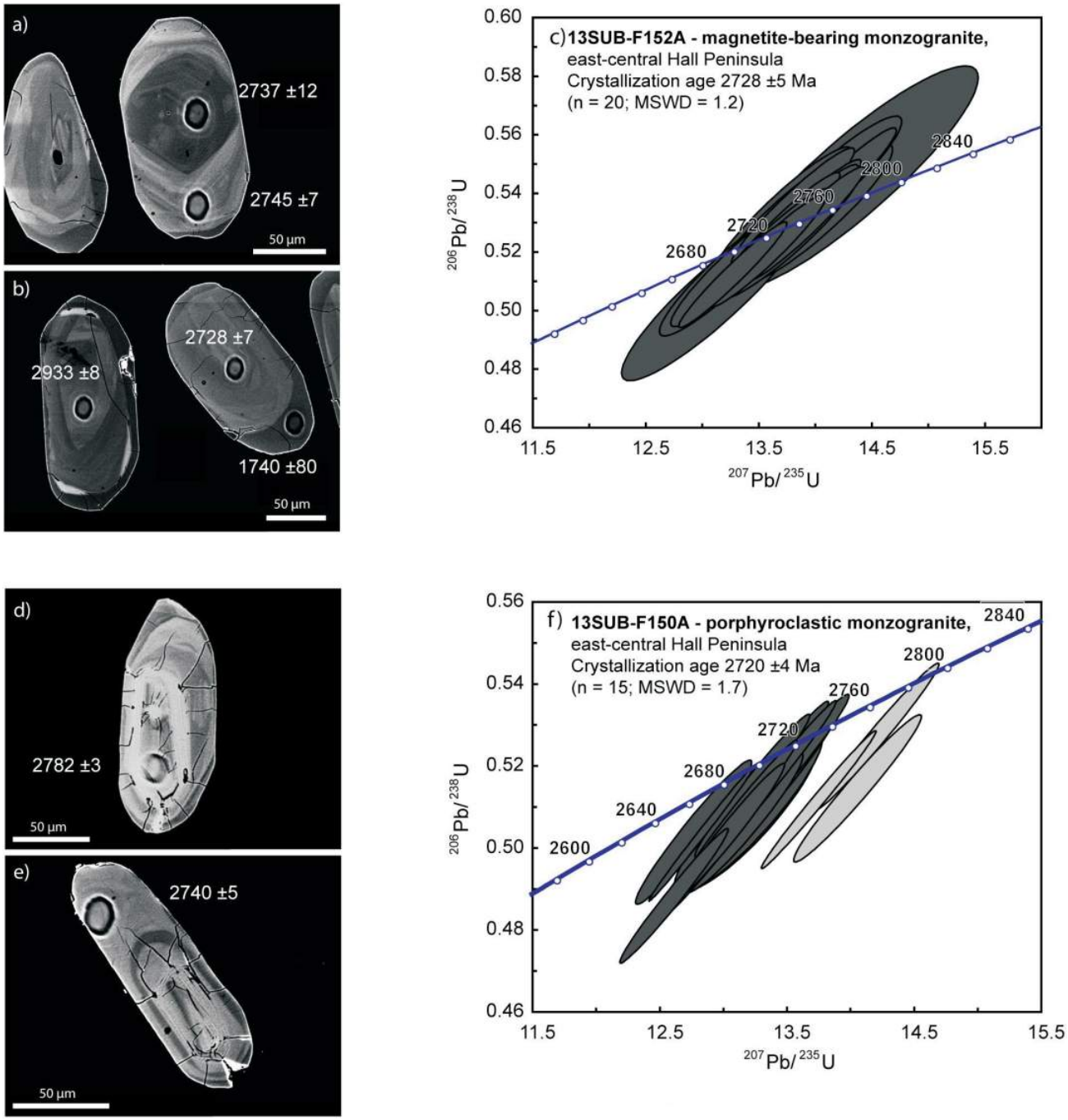

Figure 5: Zircon images (white scale bars all 50 µm) showing spot analyses (correspond to analyses in From and Rayner (2015); errors given at 1σ) and concordia diagrams with plotted ellipses and mean ages reported at the 2σ confidence level: **a)**, **b)** BSE images of representative zircons from sample 13SUB-F152A; **c)** concordia diagram of U-Pb results from sample 13SUB-F152A; dark grey ellipses correspond to ages used to calculate the crystallization age; light grey ellipses are ages excluded from the crystallization-age calculation (see text for discussion); **d), e)** BSE images of representative zircons from sample 13SUB-F150A; f) concordia diagram of U-Pb results from sample 13SUB-F150A; dark grey ellipses correspond to ages used to calculate the crystallization age; light grey ellipses are ages excluded from the crystallization-age calculation (see text for discussion). Abbreviation: BSE, backscattered electron.

interpreted to represent the crystallization age. The remaining younger ages (n = 25), from ca. 2737 to 2687 Ma, have distinctly lower U concentrations, typically between 200 and 650 ppm, and are generally ovoid with sector zoning, or are unzoned. These ages are interpreted to record a separate episode of zircon growth with a weighted-mean age of 2728 ±4 Ma (n = 10, MSWD = 3.4). Several zircons in this youngest cluster (ca. 2737 to 2687 Ma) show oscillatory zonation; therefore, these data are interpreted to be scatter of the oscillatory-zoned zircon population ca. 2761 to 2742 Ma and are not included in the weighted mean of the youngest zircon-growth episode defined by the ovoid, unzoned grains.

13SUB-F152A – magnetite-bearing monzogranite gneiss

Rock description

The magnetite-bearing monzogranite gneiss is medium grained with greyish-white fresh and weathered surfaces. This rock is characterized by abundant melt segregations (leucosomes) that have haloes enriched in mafic minerals (melanosomes). These leucosomes are a prominent feature of this unit, as they locally crosscut the gneissic foliation but are also folded themselves. Magnetite is pervasive throughout the unit, with a slight concentration along leucosome-melanosome boundaries. A homogeneous sample of magnetite-bearing monzogranite gneiss containing minimal felsic material was collected from the central portion of the study area (Figure 2). The sample is medium grained with a mineral foliation defined by hornblende and biotite. The mineralogy is 25% quartz, 20% K-feldspar, 20% plagioclase, 15% biotite, 10% titanite and 10% hornblende.

Zircon grains separated from this sample are dominantly ovoid, with some being prismatic and elongate (aspect ratios up to 4:1; <200 μm long). Images (BSE and CL) show faint and slightly irregular oscillatory-growth zonation, sometimes with internal discontinuities that truncate zonation (Figure 5a, b). All grains have thin, unzoned overgrowth rims (dark in BSE images), but only three of these unzoned rims were large enough for a spot analysis (Figure 5b).

Results and interpretation

Twenty-five analyses were conducted on 20 zircon grains. Twenty analyses yielded $^{207}Pb/^{206}Pb$ ages between ca. 2746 and 2709 Ma (From and Rayner, 2015). These ages are indistinguishable chemically or by zonation characteristics and yield a weighted-mean age of 2728 ±5 Ma (n = 20, MSWD = 1.2; Figure 5c) that is interpreted as the crystallization age of the magnetite-bearing monzogranite. The three youngest ages, between ca. 1838 to 1740 Ma, are preserved in thin, unzoned rims that have low Th/U values (0.01 to 0.12) compared to the Archean zircon (0.33 to 3.52) and are dark in BSE images. These zircon domains are interpreted to have grown due to metamorphism during the Paleoproterozoic Trans-Hudson orogeny (St-Onge et al., 2007).

13SUB-F150A – porphyroclastic monzogranite gneiss

Rock description

The monzogranite gneiss is characterized by a K-feldspar–porphyroclastic texture similar to that of 13SUB-F155A. The gneiss is fine grained with abundant mineral clots of biotite±hornblende±magnetite and local mineral clots consisting of relict orthopyroxene+clinopyroxene+hornblende. A sample was collected with minimal porphyroclastic material and mineral segregations from the western side of the detailed study area (Figure 2). It is fine grained with a moderate foliation defined by biotite. The mineralogy is 30% quartz, 25% plagioclase, 25% K-feldspar, 10% biotite, 5% titanite, 3% apatite and 2% allanite.

Zircon grains separated from this sample are generally elongate (aspect ratios up to 3:1; <200 μm long), with most grains having subrounded rather than prismatic grain edges. There are several ovoid grains. Images (BSE and CL) of the zircon grains show cores with faint, fine-scale oscillatory-growth zoning (Figure 5d, e) and overgrowth rims that are generally unzoned. A few of the rims have faint oscillatory zoning at a broad scale (Figure 5a). There are also several equant to ovoid, single grains that are unzoned.

Results and interpretation

Twenty-seven analyses were conducted on 26 zircon grains, yielding $^{207}Pb/^{206}Pb$ ages between 2810 and 1732 Ma (From and Rayner, 2015). The three oldest ages, between ca. 2810 and 2782 Ma, are from zircon cores, which are interpreted to be xenocrystic components. A cluster of 15 ages between ca. 2731 and 2708 Ma is interpreted as the crystallization age of the monzogranite. These ages have a weighted-mean $^{207}Pb/^{206}Pb$ age of 2720 ±4 Ma (n = 15, MSWD = 1.7; Figure 5f). Two zircon analyses with younger ages of ca. 2695 and 2686 Ma are interpreted to have been the result of non-zero Pb loss (see below). The two youngest results, ca. 1843 and 1732 Ma, are derived from unzoned rims that are dark in BSE images and have low Th/U values (0.05 to 0.08). The rims are interpreted to have grown due to metamorphism during the Paleoproterozoic Trans-Hudson orogeny (St-Onge et al., 2007) and may explain the scattered Archean ages that are interpreted to have experienced non-zero Pb loss.

Discussion

Magmatic versus metamorphic zircon ages

The U-Pb data show that this study area within the Archean orthogneiss complex of Hall Peninsula has a wide range of Archean spot ages: ca. 3209 to 2682 Ma. However, the detailed assessment of zircon morphology and zonation characteristics allows for a more detailed interpretation of magmatic versus metamorphic zircon-growth events.

The ages of all analyses from the study area and two additional Archean orthogneiss samples from eastern Hall Peninsula (12MBC-F105A, 12MBC-F096A; Rayner, 2014a, b) can be grouped based on the zircon domain characteristics as having oscillatory, irregular or no zonation (Figure 6). Analyses from several samples with oscillatory-growth zoning (12MBC-S116A, 13SUB-F151A, 13SUB-F155B, 13SUB-F155A, 13SUB-F150A) provide crystallization ages ranging from 2976 ±4 to 2752 ±3 Ma. Unzoned, and irregular- and sector-zoned zircon ages define a consistent range of ca. 2.74 to 2.68 Ga in every sample (Figure 6). The unzoned zircons are generally ovoid with rounded grain edges and show Th/U values that are anomalous compared to values from the older ages that are generally oscillatory-growth zoned.

Three samples specifically indicate that the Th/U values of the igneous crystallization ages are distinct from the Th/U values of the metamorphic ages. In the tonalite gneiss (13SUB-F155B), the distinct oscillatory-zoned zircons used to interpret the crystallization age had consistent Th/U values (0.33 to 0.53), whereas the irregularly zoned and unzoned zircons show a broad range of Th/U values (0.05 to 1.36), with most of the values greater than 0.53. Typically, zircon that has grown or been modified after initial magmatic crystallization of the rock has a lower Th/U value than magmatic zircon (Pidgeon, 1992). Although zircon with Th/U values <0.1 is usually thought to be melt precipitated after initial crystallization, it has been shown that magmatic zircon can have a large Th/U value range of 0.1 to 1.0 and higher (Rubatto, 2002), precluding interpretations based solely on Th/U values. Therefore, the consistency between the zonation characteristics, Th/U values and $^{206}Pb/^{207}Pb$ ages is critical for identifying the different zircon-growth processes. In the megacrystic granodiorite gneiss (13SUB-F151A), the three unzoned zircons with ages between ca. 2.72 and 2.69 Ga have Th/U values (0.07 to 0.18) that are clearly distinguished from the larger Th/U values (0.39 to 0.73) of the fine-scale oscillatory-growth zoned zircons with ages between ca. 2.95 and 2.79 Ga. In the biotite monzogranite (13SUB-F155A), the zircons displaying fine-scale oscillatory-growth zoning have high U and Th values of 689 to 3639 ppm and 277 to 3477 ppm, respectively. The homogeneous, unzoned zircon rims have distinctly low U and Th values of 206 to 619 ppm and 107 to 620 ppm, respectively, except for two zircons that have U values of 2145 and 3062 ppm, sharing the distinctly high U values of the oscillatory-zoned zircons (From and Rayner, 2015). These two zircons may have initially crystallized with the oscillatory-zoned group at ca. 2752 ±3 Ma but underwent non-zero Pb loss due to recrystallization and yet preserved their initial anomalous U and Th content.

Interestingly, the remaining three samples that do not record multiple Archean zircon-growth events (13SUB-F155C, 13SUB-F152A, 13SUB-F150A) instead record

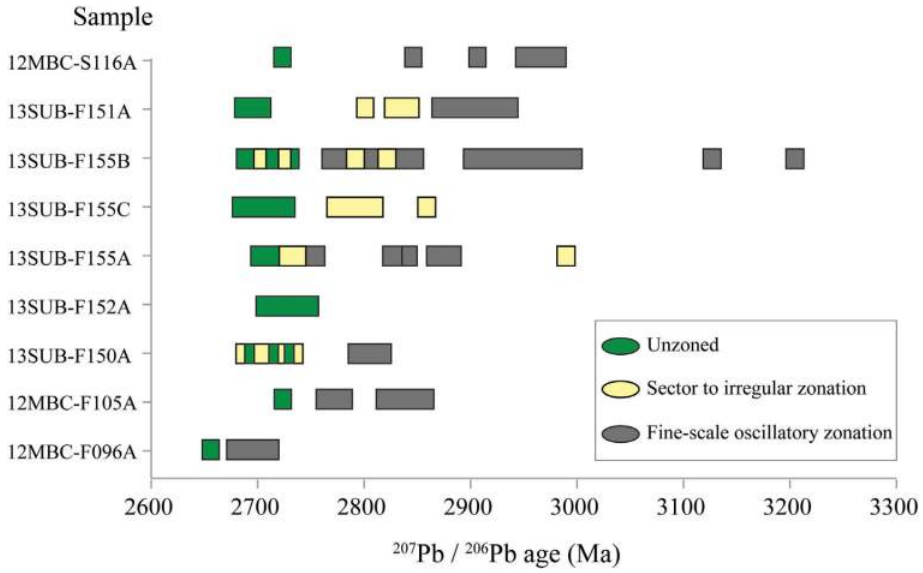

Figure 6: Summary of zircon U-Pb $^{207}Pb/^{206}Pb$ age data for each sample analyzed from the study area and two samples (12MBC-F105A, 12MBC-F096A) from the eastern Hall Peninsula orthogneiss complex dated by Rayner (2014a, b). General zonation characteristics associated with age clusters are shown in the legend.

Paleoproterozoic ages that are synchronous with the terminal collision of the Trans-Hudson orogen, which occurred from ca. 1.88 to 1.80 Ga (St-Onge et al., 2009). All of the Paleoproterozoic zircon ages have low Th/U ratios of 0.01 to 0.12 and are clearly distinguished from the older Archean zircon ages, which have Th/U ratios of 0.21 to 3.52.

Revised age relations between units

Relative emplacement ages of eight rock units were interpreted from field observations in From et al. (2014) based on crosscutting relationships. The new U-Pb ages on six of these units provide absolute constraints on the relationships observed in the field (Table 1). There is an interesting comparison between the absolute ages and the field relationships of the three samples collected from the 13SUB-F155 locality. Here, monzogranitic gneiss (13SUB-F155A) entrains a raft of tonalite gneiss (13SUB-F155B) that has discontinuous mafic lenses (13SUB-F155C). The mafic lenses were observed only within the tonalite gneiss and initially interpreted to be older than the tonalite gneiss. Surprisingly, the U-Pb ages of the mafic lenses cluster around 2700 Ma, which is much younger than the tonalite gneiss that has an interpreted crystallization age of 2810 ±3 Ma. There are two possible interpretations of the data:

- The mafic lenses are older than the tonalite gneiss, crystallizing initially as a coherent plutonic rock. Whole-rock geochemistry of these mafic lenses shows they are silica undersaturated, which has been linked with crystallization of baddeleyite rather than zircon (Allibon et al., 2011). Subsequent interaction between the mafic rock and surrounding country rock during metamorphism caused the breakdown of baddeleyite and produced zircon during a tectonometamorphic event at ca. 2700 Ma.

- The mafic lenses crystallized at ca. 2700 Ma and were subsequently dismembered into discontinuous mafic lenses during the later emplacement of the tonalite gneiss.

The observed field relationship of the monzogranite gneiss (13SUB-F155A) entraining and locally intruding the tonalite gneiss (13SUB-F155B) is confirmed by the U-Pb ages. Ages collected from the fine-scale oscillatory-growth zoning domains of the zircons from the monzogranite gneiss range from ca. 2761 to 2742 Ma. This age range is noticeably absent from the wide spectrum of ages found in the tonalite gneiss. This absence of ages rules out the possibility that those dated zircons are xenocrysts derived from the tonalite gneiss. This also suggests that the younger ages in the tonalite gneiss, ranging from ca. 2738 to 2671 Ma, must be from a later episode of zircon crystallization, interpreted here as an Archean tectonothermal event. This interpretation is further supported by the presence of ovoid, unzoned zircon single grains and overgrowth rims with ages in that same age range from all three of these related units.

Sample 12MBC-S116A, a biotite monzogranite gneiss, was taken just northwest of the study area and has the oldest interpreted crystallization age (2976 ±4 Ma) found so far on Hall Peninsula. This age is most comparable to the megacrystic granodiorite gneiss (13SUB-F151A), which has an interpreted crystallization age of 2928 ±5 Ma, but the lithological characteristics and overall textures of these two rock units are very different. Therefore, the biotite monzogranite gneiss does not correlate with any other rock unit within the study area, and is interpreted as a distinct monzogranite gneiss unit.

This study shows that a small area (700 m transect) within the Archean orthogneiss complex records a complicated and prolonged geological history. Considering the large spatial extent of Archean rocks on eastern Hall Peninsula (>20 000 km^2; Figure 1), there likely remain many more undocumented geological complexities that warrant further, in-depth analysis.

Conclusions

The seven distinct units from within and around the detailed study area on east-central Hall Peninsula delineate

Table 1: Summary of the field relationships presented in From et al. (2014) compared to the zircon U-Pb age data for six samples from the study area.

Sample	Weighted mean $^{207}Pb/^{206}Pb$ age (Ma)	Lithology	Interpreted relative age (From et al., 2014)	Revised age relationship	Figure reference
12MBC-S116A	2976 ±4	Monzogranite gneiss	-	1a	Figure 3
13SUB-F151A	2928 ±5	Megacrystic granodiorite gneiss	3	1b	Figure 3
13SUB-F155B	2810 ±3	Grey tonalite gneiss	2	2	Figure 4
13SUB-F155C	2700 ±3	Mafic lenses	1	6	Figure 4
13SUB-F155A	2751 ±3	Porphyroclastic monzogranite gneiss	5	3	Figure 4
13SUB-F152A	2728 ±5	Magnetite-bearing monzogranite gneiss	4	4	Figure 5
13SUB-F150A	2720 ±5	Porphyroclastic monzogranite gneiss	5	5	Figure 5

the protracted crystallization of Archean rocks at ca. 2.98, 2.97, 2.92 and 2.75 Ga. The timing of these crystallization events corresponds to previous work completed on eastern Hall Peninsula that documented emplacement of Archean units from ca. 2.92 to 2.70 Ga (Scott, 1999; Rayner, 2014). Detailed analyses of zircon morphology, structural and chemical zoning characteristics, and Th/U ratios have elucidated a period of subsolidus zircon modification from ca. 2.74 to 2.68 Ga. Zircon overgrowth domains, and new homogeneous and ovoid zircon grains crystallized during this time period are likely due to metamorphism and are consistent with the observed development of partial melt and migmatization throughout the Archean orthogneiss complex of eastern Hall Peninsula.

Future work

These newly presented U-Pb zircon ages set the stage for further isotopic studies on the same rock units using lutetium-hafnium (Lu-Hf) isotopes. Lutetium-hafnium data can help to provide a more detailed understanding of the magmatic history of the rocks from the detailed study area. Because zircon effectively preserves the initial $^{176}Hf/^{177}Hf$ ratios since the separation of rock-forming magma from the chondritic uniform reservoir, information can be gained about whether 1) all units in the study area were derived from the same magma source, or 2) magma mixing events occurred after the initial extraction (e.g., during partial melting episodes). The same combination of isotopic techniques can then be applied to samples collected from across the Archean orthogneiss complex of Hall Peninsula and the results compared with the dataset from this study.

Economic considerations

The Archean orthogneiss complex of eastern Hall Peninsula is known to host diamondiferous kimberlites, base metals, gem-quality minerals (spinel, apatite and garnet) and carving stone. The ages of Archean magmatism on eastern Hall Peninsula presented here, and the identification of Archean metamorphism allow for a more detailed correlation and paleotectonic reconstruction with nearby crustal blocks that may have other economic commodities yet to be discovered on Hall Peninsula. In addition, information from this study may help minimize investment risk for diamond exploration by defining the spatial extent of Archean rocks and providing further understanding of tectonic reworking during the Paleoproterozoic.

Acknowledgments

The authors thank H. Steenkamp, M. St-Onge, D. Mate, G. Machado and the CNGO staff and crew who made the two fields seasons on Hall Peninsula possible. T. Pestaj, R. Chung, R. Christie and P. Hunt at the GSC are thanked for their assistance with sample preparation, SHRIMP instrumentation and data reduction. Reviews of this paper by D. Schneider greatly improved the content, focus and clarity, and are much appreciated. The Canadian Northern Economic Development Agency's (CanNor) Strategic Investments in Northern Economic Development (SINED) program is also thanked for providing financial support for the HPIGP as a whole.

Natural Resources Canada, Earth Sciences Sector contribution 20150279

References

Allibon, J., Ovtcharova, M., Bussy, F., Cosca, M., Schaltegger, U., Bussien, D. and Lewin, É. 2011: Lifetime of an ocean island volcano feeder zone: constraints from U-Pb dating on coexisting zircon and baddeleyite, and $^{40}Ar/^{39}Ar$ age determinations, Fuerteventura, Canary Islands; Canadian Journal of Earth Sciences, v. 48, p. 567–592.

Connelly, J.N. 2001: Degree of preservation of igneous zonation in zircon as a signpost for concordancy in U/Pb geochronology; Chemical Geology, v. 172, p. 25–39.

Connelly, J.N., Thrane, K., Krawiec, A.W. and Garde, A.A. 2006: Linking the Palaeoproterozoic Nagssugtoqidian and Rinkian orogens through the Disko Bugt region of West Greenland; Journal of the Geological Society, v. 163, p. 319–335.

Corfu, F., Hanchar, J.M., Hoskin, P.W. and Kinny, P. 2003: Atlas of zircon textures; Reviews in Mineralogy and Geochemistry, v. 53, no. 1, p. 469–500. doi:10.2113/0530469

Corrigan, D., Pehrsson, S., Wodicka, N. and De Kemp, E. 2009: The Palaeoproterozoic Trans-Hudson Orogen: a prototype of modern accretionary processes; Geological Society of London, Special Publications, v. 327, p. 457–479. doi: 10.1144/SP327.19

From, R.E. and Rayner, N.M. 2015: Data table accompanying "Archean magmatism and metamorphism of eastern Hall Peninsula, southern Baffin Island, Nunavut"; Canada-Nunavut Geoscience Office, Geoscience Data Series GDS2015-009, Microsoft® Excel® file, URL <http://cngo.ca/summary-of-activities/2015/> [December 2015].

From, R.E., Camacho, A. and St-Onge, M.R. 2013: Preliminary observations on the nature and origin of the eastern orthogneiss complex of southern Hall Peninsula, Baffin Island, Nunavut; *in* Summary of Activities 2012, Canada-Nunavut Geoscience Office, p. 43–54.

From, R.E., St-Onge, M.R. and Camacho, A. 2014: Preliminary characterization of the Archean orthogneiss complex of Hall Peninsula, Baffin Island, Nunavut; *in* Summary of Activities 2013, Canada-Nunavut Geoscience Office, p. 53–62.

Hanchar, J.M. and Miller, C.F. 1993: Zircon zonation patterns as revealed by cathodoluminescence and backscattered electron images: implications for interpretation of complex crustal histories; Chemical Geology, v. 110, p. 1–13

Hollis, J.A., Frei, D., Van Gool, J.A.M., Garde A.A. and Persson, M. 2006: Using zircon geochronology to resolve the Archaean geology of southern West Greenland; Geological Survey of Denmark and Greenland, Bulletin 10, p. 49–52.

Lee, J.K., Williams, I.S. and Ellis, D.J. 1997: Pb, U and Th diffusion in natural zircon; Nature, v. 390, p. 159–162. doi:10.1038/36554

Ludwig, K.R. 2003: User's manual for Isoplot 3.00: a geochronological toolkit for Microsoft® Excel®; Berkeley Geochronology Center, Special Publication 4, 70 p.

Machado, G., Bilodeau, C., Takpanie, R., St-Onge, M.R., Rayner, N.M., Skipton, D.R., From, R.E., MacKay, C.B., Creason, C.G. and Braden, Z.M. 2013: Hall Peninsula regional bedrock mapping, Baffin Island, Nunavut: summary of fieldwork; *in* Summary of Activities 2012, Canada-Nunavut Geoscience Office, p. 13–22.

Möller A., O'Brien P.J., Kennedy A. and Kröner A. 2002: Polyphase zircon in ultrahigh-temperature granulites (Rogaland, SW Norway): constraints for Pb diffusion in zircon; Journal of Metamorphic Geology, v. 20, p. 727–740.

Pidgeon, R.T. 1992: Recrystallization of oscillatory zoned zircon: some geochronological and petrological implications; Contributions to Mineralogy and Petrology, v. 110, p. 463–472.

Rayner, N.M. 2014a: Data table accompanying "New U-Pb geochronological results from Hall Peninsula, Baffin Island, Nunavut"; Canada-Nunavut Geoscience Office, Geoscience Data Series GDS2014-001, Microsoft® Excel® file, URL <http://cngo.ca/summary-of-activities/2013/> [March 2015].

Rayner, N.M. 2014b: New U-Pb geochronological results from Hall Peninsula, Baffin Island, Nunavut; *in* Summary of Activities 2013, Canada-Nunavut Geoscience Office, p. 39–52, URL <http://cngo.ca/summary-of-activities/2013/> [March 2015].

Rayner, N.M. 2015a: Data table accompanying "New (2013–2014) U-Pb geochronological results from northern Hall Peninsula, southern Baffin Island, Nunavut"; Canada-Nunavut Geoscience Office, Geoscience Data Series 2015-002, Microsoft® Excel® file, URL <http://cngo.ca/summary-of-activities/2014/> [March 2015].

Rayner, N.M. 2015b: New (2013–2014) U-Pb geochronological results from northern Hall Peninsula, southern Baffin Island, Nunavut; *in* Summary of Activities 2014, Canada-Nunavut Geoscience Office, p. 31–44 URL <http://cngo.ca/summary-of-activities/2014/> [March 2015].

Rubatto, D. 2002: Zircon trace element geochemistry: partitioning with garnet and the link between U-Pb ages and metamorphism; Chemical Geology, v. 184, p. 123–138.

Scott, D.J. 1999: U-Pb geochronology of the eastern Hall Peninsula, southern Baffin Island, Canada: a northern link between the Archean of West Greenland and the Paleoproterozoic Torngat Orogen of northern Labrador; Precambrian Research, v. 93, p. 5–26.

Scott, D.J. and Campbell, L.M. 1993. Evolution of the Paleoproterozoic Torngat orogen, Labrador, Canada: recent advances using U-Pb geochronology and Nd isotopic systematics (abstract); Geological Society of America, Annual Meeting 1993, Boston, Massachusetts, Program with Abstracts, v. 25, p. A23.

Steenkamp, H.M. and St-Onge, M.R. 2014: Overview of the 2013 regional bedrock mapping program on northern Hall Peninsula, Baffin Island, Nunavut; *in* Summary of Activities 2013, Canada-Nunavut Geoscience Office, p. 27–38, URL <http://cngo.ca/summary-of-activities/2013/> [March 2015].

St-Onge, M.R., Scott, D.J. and Wodicka, N. 2002: Review of crustal architecture and evolution in the Ungava Peninsula–Baffin Island area: connection to the Lithoprobe ECSOOT transect; Canadian Journal of Earth Sciences, v. 39, p. 589–610.

St-Onge, M.R., Van Gool, J.A.M., Garde, A.A. and Scott, D.J. 2009: Correlation of Archaean and Palaeoproterozoic units between northeastern Canada and western Greenland: constraining the pre-collisional upper plate accretionary history of the Trans-Hudson orogen; Geological Society of London, Special Publications, v. 318, p. 193–235. doi:10.1144/SP318.7

St-Onge, M.R., Wodicka, N. and Ijewliw, O. 2007: Polymetamorphic evolution of the Trans-Hudson Orogen, Baffin Island, Canada: integration of petrological, structural and geochronological data; Journal of Petrology, v. 48, p. 271–302.

Stern, R.A. 1997: The GSC sensitive high resolution ion microprobe (SHRIMP): analytical techniques of zircon U-Th-Pb age determinations and performance evaluation; *in* Radiogenic Age and Isotopic Studies: Report 10, Geological Survey of Canada, Current Research 1997-F, p. 1–31.

Stern, R.A. and Amelin, Y. 2003: Assessment of errors in SIMS zircon U-Pb geochronology using a natural zircon standard and NIST SRM 610 glass; Chemical Geology, v. 197, p. 111–146.

Thrane, K. and Connelly J.N. 2006: Zircon geochronology from the Kangatsiaq-Qasigiannguit region, the northern part of the 1.9–1.8 Ga Nagssugtoqidian orogen, West Greenland; Geological Survey of Denmark and Greenland, Bulletin 11, p. 87–99.

Wardle, R.J., James D.T., Scott, D.J. and Hall, J. 2002: The southeastern Churchill Province: synthesis of a Palaeoproterozoic transpressional orogen; Canadian Journal of Earth Sciences, v. 39, p. 639–663. doi:10.1139/E02-004

Whalen, J.B., Wodicka, N., Taylor, B.E. and Jackson, G.D. 2010: Cumberland batholith, Trans-Hudson Orogen, Canada: petrogenesis and implications for Paleoproterozoic crustal and orogenic processes; Lithos, v. 117, p. 99–118.

Williams, I.S. 1992: Some observations on the use of zircon U-Pb geochronology in the study of granitic rocks; Transactions of the Royal Society of Edinburgh: Earth Sciences, v. 83, no. 1-2, p. 447–458. doi:10.1017/S0263593300008129

Multispectral characterization of gossans and iron-oxide–enriched mineral soils using moderate- and high-resolution satellite data from Hall Peninsula, southern Baffin Island, Nunavut

P. Budkewitsch[1] and S. Sharpe[2]

[1]*Indigenous and Northern Affairs Canada, Iqaluit, Nunavut, paul.budkewitsch@aandc-aadnc.gc.ca*

[2]*Indigenous and Northern Affairs Canada, Iqaluit, Nunavut*

This work is part of the Hall Peninsula Integrated Geoscience Program (HPIGP), led by the Canada-Nunavut Geoscience Office (CNGO) in collaboration with the Government of Nunavut, Indigenous and Northern Affairs Canada, Dalhousie University, University of Alberta, Université Laval, University of Manitoba, University of Ottawa, University of Saskatchewan, University of New Brunswick, Nunavut Arctic College and the Geological Survey of Canada. It is supported logistically by several local, Inuit-owned businesses and the Polar Continental Shelf Program. The focus is on bedrock and surficial geology mapping (1:100 000 scale). In addition, a range of thematic studies is being conducted, including Archean and Paleoproterozoic tectonics, geochronology, landscape uplift and exhumation, microdiamonds, sedimentary rock xenoliths and permafrost. The goal is to increase the level of geological knowledge and better evaluate the natural resource potential in this frontier area.

Budkewitsch, P. and Sharpe, S. 2015: Multispectral characterization of gossans and iron-oxide–enriched mineral soils using moderate- and high-resolution satellite data from Hall Peninsula, southern Baffin Island, Nunavut; *in* Summary of Activities 2015, Canada-Nunavut Geoscience Office, p. 89–94.

Abstract

Multispectral satellite data at higher resolution than reconnaissance sensors such as Landsat or ASTER provide relatively high spatial resolution and improved mapping and detection capability that are better suited for identifying exploration targets or other geological features of interest. An analysis of the spectral bands in RapidEye satellite data from Hall Peninsula, southern Baffin Island, was used to highlight the presence of iron oxides and hydroxides commonly associated with gossans or weathered metasedimentary units. In RapidEye data, the presence of iron-oxide minerals causes high reflectance in band 3 and a lower reflectance in band 1. The relationship of this band ratio was examined in comparison to geochemical analyses of rock and weathered material. It was concluded that although all areas of visual iron-oxide staining produce anomalous colouration in satellite images, quantifying the intensity of such colouration using band ratios can correlate to geochemical results, thus providing a method for selecting areas of higher priority for follow-up exploration.

Résumé

Les données satellite multispectrales captées à plus haute résolution que celles fournies par les capteurs de reconnaissance tels Landsat et ASTER se caractérisent par la meilleure qualité de leur résolution spatiale et leur capacité accrue de détection et de captage des éléments cartographiques, se prêtant ainsi mieux aux activités liées à la découverte de cibles d'exploration et autres caractéristiques géologiques intéressantes. Une analyse des bandes spectrales correspondant à des données satellite captées par le système RapidEye au-dessus de la péninsule Hall, dans l'île de Baffin, a permis de mettre en valeur la présence d'oxydes et d'hydroxydes de fer généralement associés aux gossans et aux unités métasédimentaires altérées. Les données obtenues au moyen de RapidEye permettent d'établir la présence de minéraux d'oxyde de fer en comparant la réflectance plus élevée de la bande 3 à celle, moins élevée, de la bande 1. On a comparé la relation du rapport de bandes aux résultats d'analyses géochimiques d'échantillons de roche et de matériaux altérés. Malgré le fait que tous les endroits où l'on avait pu constater des taches de rouille causées par la présence d'oxydes de fer se reconnaissent à la coloration anormale qu'ils affichent sur les images satellitaires, on a conclu qu'en mesurant l'intensité de cette coloration à l'aide du rapport de bandes, il est possible d'établir des corrélations avec les résultats d'analyse géochimique et donc de mettre au point une méthode permettant de choisir des régions cibles susceptibles de présenter plus d'intérêt lors de travaux d'exploration de suivi.

This publication is also available, free of charge, as colour digital files in Adobe Acrobat® PDF format from the Canada-Nunavut Geoscience Office website: http://cngo.ca/summary-of-activities/2015/.

Introduction

The development of a weathered cap of iron-oxide minerals from sulphides present in psammite and semipelite of the Paleoproterozoic Lake Harbour Group exposed at or near the surface is well-documented across southern Baffin Island, from the Foxe Peninsula to the Cumberland Peninsula. Upon investigation, the majority of these ferruginous zones are often of no economic interest; however, some areas, visibly enriched in iron-alteration minerals, reveal the presence of anomalous gold, silver, platinum-palladium, zinc-lead or copper in indicator minerals or sediment analyses from reconnaissance and till-sampling programs (e.g., Pell, 2008). Since not all of these iron-oxide occurrences are barren of precious or base metals, there is value in searching for iron-oxide alteration signatures for further evaluation. Over the years, satellites such as Landsat and ASTER have been used in many areas around the world to provide reconnaissance information in support of mapping efforts and geological exploration. Arctic regions in Canada's North, with their sparse vegetation and extensive outcrop exposures, have provided promising results from these satellite-based research methods.

Although the spectral bands of Landsat and ASTER are suited for identifying some types of mineral alteration, the relatively low resolutions of their datasets is one explanation for the varying degree of success achieved. In order to assess the effectiveness of higher resolution satellite-data products, a series of activities was initiated using Hall Peninsula, southern Baffin Island, as a test case. This paper uses results from RapidEye satellite data to investigate cost-effective methods for identifying iron-oxide mineral-alteration zones in support of mineral exploration and geological mapping.

Priority locations were selected from an analysis of RapidEye data that was acquired over Hall Peninsula during the summer months of 2012 and 2013, in conjunction with the Hall Peninsula Integrated Geoscience program conducted by the Canada-Nunavut Geoscience Office (CNGO). Locations of interest ranged from areas as little as a few tens of square metres to larger zones covering hundreds of square metres. Where possible, areas of interest were validated by field visits and samples were taken for geochemical analysis. Part of the initial work involved collecting samples for testing, the results of which have been published as a CNGO dataset (Steenkamp and Budkewitsch, 2014). A range of geological materials was recognized; however, the most common material was in situ weathered-bedrock material rich in iron-oxide and -hydroxide minerals from metasedimentary units, which could contain disseminated sulphides. Other samples correlated to localized occurrences of ultramafic rock, some of which were previously known and others unmapped due to the relatively small size of the exposure (Budkewitsch et al., 2013).

RapidEye data

Data processing techniques of remotely sensed spectral data to detect the presence of iron-oxide and -hydroxide minerals were first applied over four decades ago (e.g., Hunt et al., 1971; Rowan et al., 1974). These techniques have been successfully applied in many areas owing to the broad-band spectral absorption properties of Fe^{+3} in visible and near-infrared wavelengths. For iron-bearing minerals, particularly hematite, goethite and limonite, strong differences in relative reflectance exist.

Select spectral band ratios from satellite data can be suited to enhancing the contrast between iron-rich targets and all other targets. This technique is often used to search for gossans in mineral exploration. Many of these applications use publicly accessible satellite data such as Landsat or ASTER (Sabins, 1987; Abrams, 2000). Although these datasets have the advantage of covering large areas and are useful for reconnaissance work, the relatively low resolution of these applications (30 m for Landsat, 15 m for ASTER) limits their use to exposed and laterally extensive targets. Since many economic discoveries are comparatively smaller, their detection would benefit from higher resolution sensors.

Several commercial data providers offer multispectral data of 2–4 m resolution. In this paper, the RapidEye data initially examined has an intermediate resolution of 6.5 m and provides wide-area coverage for reconnaissance investigations (RapidEye, 2012) over Hall Peninsula (Figure 1).

The RapidEye mission is a constellation of five satellites (RE1–5) that provides frequent opportunities not only to image the Earth once every 24 hours, but also to cover wide areas in relatively short periods of time. The five spectral band sensors on board each satellite collect data from the visible (0.44 μm) to near-infrared (0.85 μm) wavelength range (Naughton et al., 2011; Chander et al., 2013). The over 90 level 3A data products used for this study were acquired as 25 by 25 km orthorectified tiles resampled to a pixel spacing of 5 m; the data have similar spectral bands to Landsat or ASTER (Figure 2). In this manner, RapidEye datasets offer a practical solution for wide-area coverage at an improved level of resolution.

Data analysis

The presence of iron-oxide minerals in multispectral data can be generally expressed as the ratio of red to blue-green values in the visible bands of the sensor (Sabins, 1987). In the RapidEye data examined over Hall Peninsula, the contrast between the higher reflectance in the visible red level (band 3) and the relatively lower reflectance in the blue (band 1) or green (band 2) portions of the visible spectrum correlates with areas that exhibit strong rust-coloured weathering (i.e., iron-oxide–rich mineral soil or sulphide-

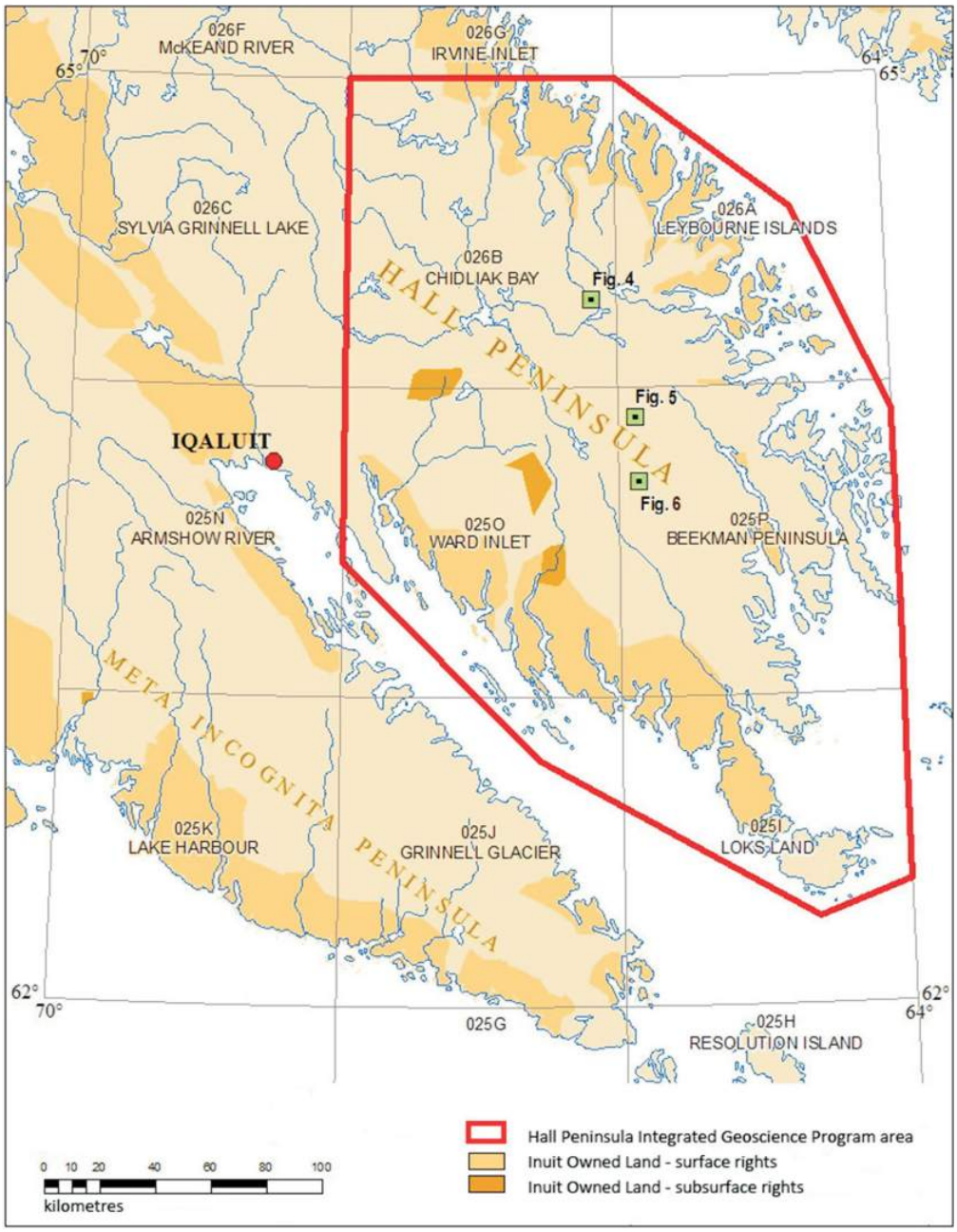

Figure 1: Area covered by the Hall Peninsula Integrated Geoscience project area and location of three sites discussed in this paper.

bearing gossanous zones). Atmospheric scatter is greater in band 1 than in band 2, and better results were obtained using band 2 in the green portion (0.52–0.59 µm) of the spectrum in conjunction with band 3 (0.63–0.685 µm). A simple dark-target subtraction was applied to the data that helped to normalize results from scene to scene collected on different dates, under different atmospheric conditions, and at various solar elevation and azimuth angles. Band 3 and 2 ratios (Figure 3) yielded a relatively consistent index for iron-oxide minerals for several areas across Hall Peninsula. Low- to high-band ratio values were displayed as classified images scaled from blue (low) to red (high) to aid in selecting sites that were then examined in greater detail. Less than 1% of the total map area exhibited band 3 and 2 ratio values >1. Figures 4b, 5b and 6b show examples of these ratios, where pixels in red are ≥1. The highest ratio value encountered was 1.380, with the mean and standard deviation for 51 peak values within discrete target areas in this study being 1.137 ±0.086. Fifty percent of the band-ratio values found lie between 1.00 and 1.11. The distribution of peak

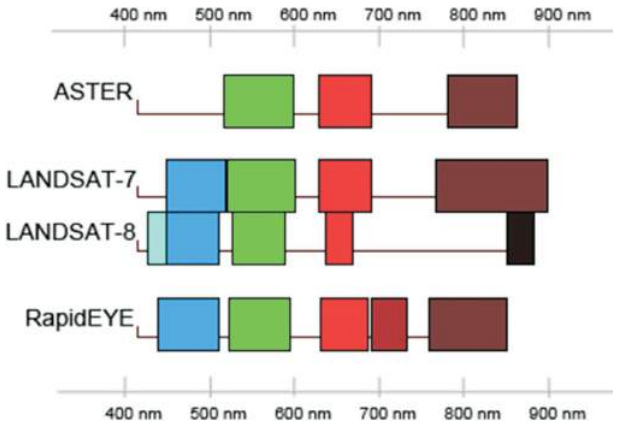

Figure 2: Comparison of spectral bands in the visible to near-infrared between ASTER, Landsat-7 and -8, and RapidEye. Bands for each satellite are numbered sequentially from left (blue) to right (near-infrared).

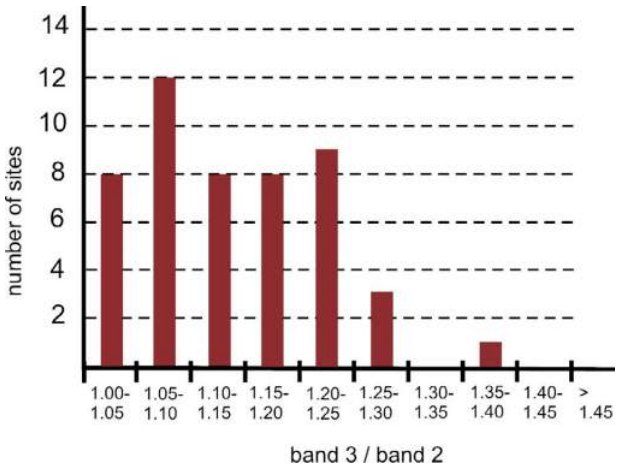

Figure 3: Plot of the distribution of band ratios in RapidEye data for 51 target areas characterized by high concentrations of iron-oxide and -hydroxide minerals on Hall Peninsula.

pixels with the greatest band-ratio intensities is illustrated in Figure 3.

Several areas were examined and sampled in the field during a one-week period in July 2014. Analysis of those results was released as a Geoscience Data Series by Steenkamp and Budkewitsch (2014). Figures 4, 5 and 6 illustrate examples of weathered exposures of psammite and a gossanous exposure exhibiting various iron indices above the threshold of 1 that was applied in this study. These areas in the field correlate to zones exhibiting relatively intensely altered rock (i.e., rust-coloured rock) or mineral soil derived from the weathering of bedrock. Red iron oxides or hydroxides, such as goethite, are more pervasive at the sur-

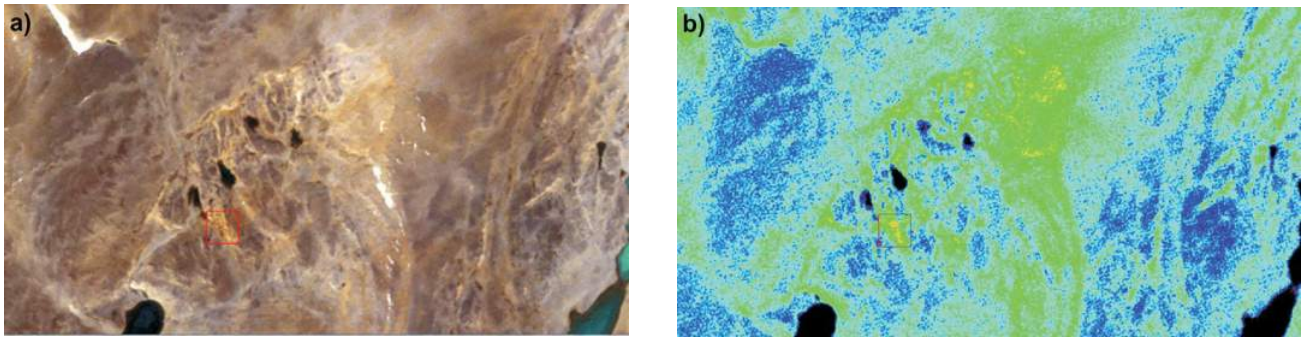

Figure 4: a) Small area of a RapidEye colour image (bands 3, 2 and 1) for a site along a broad zone of supracrustal rock exposures (light brown tones) on Hall Peninsula, with a relatively low intensity of iron-oxide staining. **b)** Corresponding iron-index image derived from the RapidEye multispectral data. Colour scale ranges from low values in blue to high values in red, with a highest value at this location reaching 1.020. Image is 1 by 2 km. Satellite image by BlackBridge.

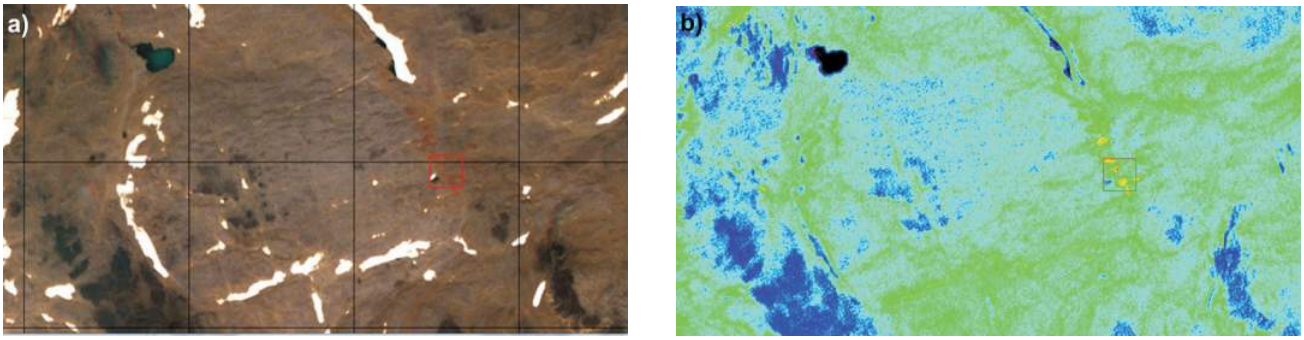

Figure 5: a) Small area of a RapidEye colour image (bands 3, 2 and 1) for a site along a linear trend of supracrustal rock exposures (reddish-brown tones) on Hall Peninsula, with a series of anomalously high-intensity areas of iron-oxide staining. **b)** Corresponding iron-index image derived from the RapidEye multispectral data. Colour scale ranges from low values in blue to high values in red, with the highest value at this location reaching 1.200. Image is 1 by 2 km. Satellite image by BlackBridge.

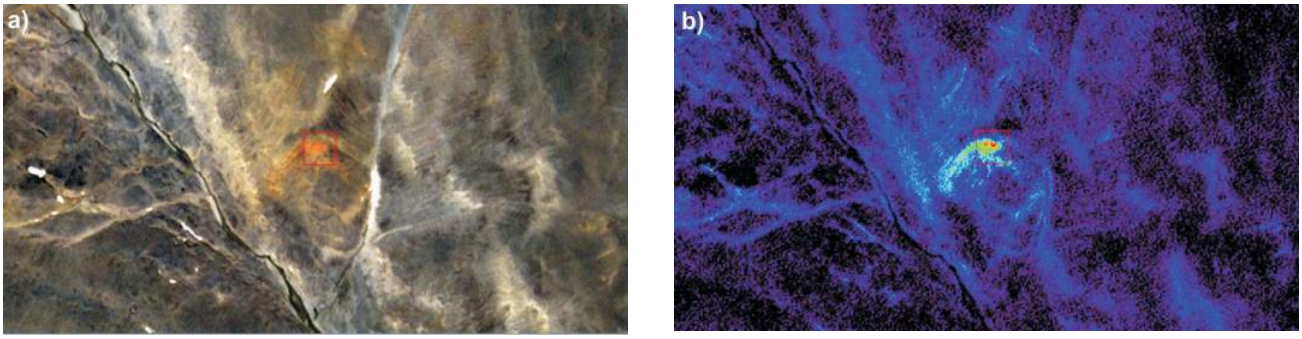

Figure 6: a) Small area of a RapidEye colour image (bands 3, 2 and 1) from Hall Peninsula, illustrating a small gossanous zone (red to orange), with a larger zone of anomalous iron-oxide staining. **b)** Corresponding iron-index image derived from the RapidEye multispectral data. Colour scale ranges from low values in blue to high values in red, with the value of 1.380 reached at this location being the highest encountered among the 51 targets examined. Image is 1 by 2 km. Satellite image by BlackBridge.

face, whereas, few decimetres below the surface, yellowish to ochre limonite is often encountered. At most of the sites examined, no primary sulphide mineralization was identified, which suggests deep weathering and alteration of the hostrock. Geochemical analyses of weathered bedrock collected in situ at seven localities with high band ratios yielded a mean of 8.98 wt. % iron (as Fe_2O_3) for ratio values between 1.090 and 1.230 (mean of 1.164).

Economic considerations

RapidEye and other Earth-observation (remote sensing) data from satellites provide a means to rapidly acquire terrain information imaged over wide areas in a consistent and quantitative manner. Acquisition of higher resolution data is becoming more cost effective, particularly when applied in remote regions, and offers the possibility to better identify exploration target than can lower resolution sensors. The iron-index data described in this paper may help to narrow the search for geological- or mineral-exploration targets of interest.

Geochemical results of collected weathered-bedrock or mineral soil samples exposed at study sites confirm high iron levels at areas with high iron-oxide band ratios. Correlations with other detected metals are less consistent. Analytical results (Steenkamp and Budkewitsch, 2014) show few gold values above 30 ppb and this data did not correlate with higher iron-oxide indices. Zinc values were also low; however, the highest values (170–230 ppm) were returned from weathered rock collected at locations with iron-oxide band ratios of about 1.10. The only significant correlation observed was that rock samples with nickel values >1000 ppm came from areas that had rock exposures with an iron-oxide index on the order of 1.20, which corresponds to some of the highest band ratios encountered in this study.

Conclusions

The results of this study provide supporting evidence that broad-band satellite data with moderate resolution (<10 m) can provide valuable reconnaissance-level surveys for identifying anomalous iron-oxide–rich areas. These results can provide information to enhance geological mapping or preliminary data to assist with targeting prospective areas for mineral exploration.

Vast areas can be quantitatively examined, and field validation of these areas can provide a more reliable geological- and mineral-potential assessment of the region. In conjunction with field validation and supporting geochemical analyses, this technique and resulting information can be used to determine priority areas in which to invest, since it is rarely possible to carry out field examinations of all areas of interest. The simple two-band ratio method based on spectral properties to determine the iron-oxide index from RapidEye data can lead to the identification of a range of field occurrences: from weak, surface iron-oxide staining to the more extensive iron-oxide development associated with the formation of gossans. Work is ongoing to examine the results of the geochemical analyses using more in-depth spectral properties from other high-resolution sensors on these and other exploration targets of interest.

Acknowledgments

The authors would like to acknowledge financial support from Strategic Investments in Northern Economic Development (SINED funding) to the CNGO from the Canadian Northern Economic Development Agency (CanNor) in Nunavut. The funding enabled this program for evaluating new technology in support of resource exploration in remote regions. The authors appreciated thoughtful reviews of the manuscript by E. Cloutis, K. Costello, L. Ham and M. Senkow.

References

Abrams, M. 2000: The Advanced Spaceborne Thermal Emission and Reflection Radiometer (ASTER): Data products for the high spatial resolution imager on NASA's Terra platform; International Journal of Remote Sensing, v. 21, issue 5, p. 847–859. doi:10.1080/014311600210326

Budkewitsch, P., Bilodeau, C. and Senkow, M.D. 2013: Evaluation of iron oxide concentrations from multispectral images for bedrock mapping, Hall Peninsula, Baffin Island.; *in* Summary of Activities 2012, Canada-Nunavut Geoscience Office, p. 85–92, <http://cngo.ca/app/uploads/Summary-of-Activities-2012-P09.pdf> [November 2015].

Chander, G., Haque, M.O., Sampath, A., Brunn, A., Trosset, G., Hoffmann, D., Roloff, S., Thiele, M. and Anderson, C. 2013: Radiometric and geometric assessment of data from the RapidEye constellation of satellites; International Journal of Remote Sensing, v. 34, no. 16, p. 5905–5925. doi:10.1080/01431161.2013.798877

Hunt, G.R., Salisbury, J.W. and Lenhof, C.J. 1971: Visible and near-infrared spectra of minerals and rocks – III, oxides and hydroxides; Modern Geology, v. 2, p. 195–205.

Naughton, D., Brunn, A., Czapla-Myers, J, Douglass, S., Thiele, M., Weichelt, H. and Oxfort, M. 2011: Absolute radiometric calibration of the RapidEye multispectral imager using the reflectance-based vicarious calibration method; Journal of Applied Remote Sensing, v. 5, no. 1, 23 p. doi:10.1117/1.3613950

Pell, J. 2008: Technical report on the Chidliak property, 66° 21' 43" W, 64° 28' 26" N, Baffin region, Nunavut; Peregrine Diamonds Ltd., technical report, 73 p., <http://www.sedar.com/GetFile.do?lang=EN&docClass=24&issuerNo=00023243&fileName=/csfsprod/data94/filings/01357817/00000001/i%3A%5CKKBL%5CSEDAR%5C46784%5C29%5C2008%5CTECHRPT-CH.pdf> [October 2015]

RapidEye AG, 2012: Satellite imagery product specifications; RapidEye AG, Brandenburg, Germany, version 4.1, 44 p., <http://www.rapideye.de/upload/RE_Product_Specifications_ENG.pdf> [November 2012].

Rowan, L.C., Wetlaufer, P.H., Goetz, A.F.H., Billingsley, F.C. and Stewart, J.H. 1974: Discrimination of rock types and detection of hydrothermally altered areas in south-central Nevada by the use of computer-enhanced ERTS images; United States Geological Survey, Professional Paper 883, 35 p.

Sabins, F.F. 1987. Remote Sensing: Principles and Interpretation (2nd ed.); W.H. Freeman, New York, 449 p.

Steenkamp, H.M. and Budkewitsch, P. 2014: Geochemistry and assay results from the 2014 Hall Peninsula Integrated Geoscience Project, Baffin Island, Nunavut; Canada-Nunavut Geoscience Office, Geoscience Data Series GDS2014-005, Microsoft® Excel® file, <http://cngo.ca/cngo-gds/2014-005/> [November 2015].

Uranium-lead geochronology of eastern Meta Incognita Peninsula, southern Baffin Island, Nunavut

N.M. Rayner[1]

[1]*Natural Resources Canada, Geological Survey of Canada, Ottawa, Ontario, nicole.rayner@canada.ca*

The Meta Incognita Peninsula field activity is a part of the larger South Baffin mapping project, a partnership between the Canada-Nunavut Geoscience Office (CNGO) and Natural Resources Canada's (NRCan) Geo-mapping for Energy and Minerals (GEM) Program on Baffin Island (Nunavut). This activity is being led by the Geological Survey of Canada (GSC) in collaboration with the CNGO, Indigenous and Northern Affairs Canada, Nunavut Arctic College, University of Ottawa and Carleton University. It is supported logistically by several local, Inuit-owned businesses. The study area comprises all or parts of four 1:250 000 scale map areas south and east of Iqaluit (NTS areas 025G, J, K and N).

Rayner, N.M. 2015: Uranium-lead geochronology of eastern Meta Incognita Peninsula, southern Baffin Island, Nunavut; *in* Summary of Activities 2015, Canada-Nunavut Geoscience Office, p. 95–106.

Abstract

This paper presents new U-Pb geochronology data from three sedimentary rocks and three plutonic rocks collected during recent bedrock geological mapping of eastern Meta Incognita Peninsula, Baffin Island, Nunavut. A quartzite (sample 14SAB-S013A), contiguous with the type area of the Lake Harbour Group near Kimmirut, is characterized by an exclusively Archean detrital zircon profile, dominated by ca. 2.82 Ga detritus. Calcareous quartzite from the central part of the peninsula (sample 14SAB-O103B) includes detrital ages of 2.7 Ga, 2.6–2.5 Ga, 2.35 Ga, 2.1 Ga and 1.93–1.91 Ga. The maximum age of deposition of the calcareous quartzite is 1913 ±17 Ma. A grey, sandy quartzite horizon (sample 14SAB-R108B), from an outcrop of psammite/leucogranite, is dominated by Orosirian age (2050–1800 Ma) zircon. A component of ca. 1.85 Ga zircon is interpreted to reflect partial melting and emplacement of nearby leucogranite. Given their proximity to the type area, and similar lithological association and geological setting, the metasedimentary rocks on eastern Meta Incognita Peninsula are correlated with the Lake Harbour Group.

A megacrystic biotite-orthopyroxene monzogranite (sample 14SAB-O071A) is interpreted to have crystallized at 1845 ±19 Ma. A megacrystic biotite-magnetite monzogranite (sample 14SAB-R62A) is interpreted to have a crystallization age of 1865 ±10 Ma, with an older 1896 Ma component representing an inherited or possibly autocrystic phase. A pink, sugary-textured biotite-magnetite monzogranite (sample 14SAB-O049A) is cautiously interpreted to have crystallized at 1871 ±4 Ma followed by metamorphism that resulted in resetting of zircon U-Pb systematics. Despite their relatively simple and homogeneous appearance in the field, complex geochronological results made interpretation of the crystallization ages of plutonic phases from Meta Incognita Peninsula challenging. The highest grade, most deformed samples discussed in this paper yielded the youngest ages. This emphasizes the need for careful field observations of crosscutting relationships when establishing a field chronology for plutonic rocks.

Résumé

Le présent article fait état de nouvelles données d'analyses géochronologiques U-Pb effectuées sur trois échantillons de roches sédimentaires et trois échantillons de roches plutoniques recueillis au cours des travaux de cartographie du substratum rocheux de la partie est de la Péninsule Meta Incognita, dans l'île de Baffin, au Nunavut. Une unité de quartzite (échantillon 14SAB-S013A), contiguë à la région type associée au groupe de Lake Harbour près de Kimmirut, se distingue par le profil d'âge exclusivement archéen des zircons détritiques, caractérisé par la présence dominante de débris âgés d'environ 2,82 Ga. Un quartzite calcareux (échantillon 14SAB-O103B) provenant de la partie centrale de la péninsule affiche la gamme d'âges de zircons détritiques suivante: 2,7 Ga, 2,6–2,5 Ga, 2,35 Ga, 2,1 Ga et 1,93–1,91 Ga. L'âge maximum de mise en place du quartzite calcareux est établi à 1913 ±17 Ma. Un horizon gris de quartzite sableux (échantillon 14SAB-R108B), provenant d'un affleurement de psammite et de leucogranite, se caractérise par la présence prédominante d'une population de zircons datant de l'Orosirien (2050–1800 Ma) La présence de quelques populations de zircons dont l'âge se situe à environ 1,85 Ga est associée aux épisodes de fusion partielle et de mise en place d'un leucogranite voisin. En

This publication is also available, free of charge, as colour digital files in Adobe Acrobat® PDF format from the Canada-Nunavut Geoscience Office website: http://cngo.ca/summary-of-activities/2015/.

raison de leur proximité à la région type, ainsi que leur association lithologique et milieu géologique semblables, les roches dans la partie est de la péninsule Meta Incognita sont mises en corrélation avec celles du groupe de Lake Harbour.

On a établi à 1845 ±19 Ma l'âge de cristallisation d'un monzogranite à biotite-orthopyroxène mégacristallin (échantillon 14SAB-O071A), alors que celui d'un monzogranite à biotite-magnétite mégacristallin (échantillon 14SAB-R62A) se situe à 1865 ±10 Ma, bien qu'il présente une composante plus ancienne datant de 1896 Ma, laquelle correspondrait à une phase héritée ou possiblement autocristalline. On estime à 1871 ±4 Ma l'âge de cristallisation d'un monzogranite à magnétite rose à texture saccharoïde, qui aurait été suivi d'un épisode de métamorphisme, lequel aurait entraîné la remise en place isotopique des systèmes U-Pb sur zircon. Malgré leur apparence homogène et peu complexe sur le terrain, la complexité des résultats obtenus des analyses géochronologiques a rendu plus exigeante la tâche d'interpréter les âges de cristallisation des phases plutoniques de la péninsule Meta Incognita. Les échantillons les plus déformés et ayant subi le degré le plus élevé de métamorphisme qui font l'objet du présent rapport ont livré les âges de cristallisation les plus récents. Ce résultat met en évidence le fait qu'il est nécessaire de noter très attentivement les relations de recoupement observées sur le terrain lorsqu'on tente d'établir sur place la chronologie des roches plutoniques.

Introduction

The Geo-mapping for Energy and Minerals (GEM) program is laying the foundation for sustainable economic development in the North. The program provides modern, public geoscience that will set the stage for long-term decision making related to investment in responsible resource development. Geoscience knowledge produced by GEM supports evidence-based exploration for new energy and mineral resources, and enables northern communities to make informed decisions about their land, economy and society. As part of the GEM-Baffin project area, a two-year activity entitled 'Completing the regional bedrock mapping of the southern half of Baffin Island' is being led by the Geological Survey of Canada (GSC) in partnership with the Canada-Nunavut Geoscience Office (CNGO) to provide regional syntheses that encapsulate new knowledge of the bedrock geology and sedimentary basins, including potential zones of mineralization and carving stone.

During the past two decades, modern, systematic and targeted mapping of bedrock geology has been completed for large tracts of southern Baffin Island. Only two gaps remained prior to finalizing the updated coverage of the whole of Baffin Island south of latitude 70°N; Meta Incognita Peninsula east of longitude 68°W, and south-central Baffin Island in the Clearwater Fiord–Sylvia Grinnell Lake area. Available geological information for both areas was limited to low-resolution helicopter reconnaissance work completed in the 1960s. Portions of south-eastern Baffin Island represent some of the last major missing tectonic pieces in the current understanding of Nunavut geology and targeted bedrock tectonostratigraphic, geochronological and structural studies will largely resolve this uncertainty.

In the summer of 2014, helicopter-supported bedrock mapping was carried out on eastern Meta Incognita Peninsula (Figure 1) with the aim of constraining potential vectors to mineralization for a number of mineral commodities including diamonds, Ni, Cu, PGEs, Pb and Zn. In addition, mapping was carried out to define the lateral extent of prospective Lake Harbour Group sedimentary strata and associated layered mafic/ultramafic sills, which provide the most promising carving stone potential in the vicinity of Iqaluit and Kimmirut. This paper presents U-Pb geochronological results stemming from the 2014 fieldwork.

Detailed descriptions of the geology of eastern Meta Incognita Peninsula geology can be found in St-Onge et al. (2015a–e). In brief, metasedimentary units comprising quartzite, marble, psammite, pelite and semipelite were identified, all of which can be correlated with the contiguous middle Paleoproterozoic Lake Harbour Group in the type area north of Kimmirut (Figure 1). The full suite of siliciclastic rock types occurs across all of eastern Meta Incognita Peninsula. The spatial distribution of a suite of layered mafic to ultramafic sills intrusive into the sedimentary strata was also documented and is the focus of further study (St-Onge et al., 2015e; Liikane and St-Onge, 2015). High-grade felsic to intermediate plutonic rocks dominate the bedrock exposures on eastern Meta Incognita Peninsula. The plutonic rocks vary in composition (gabbro/quartz diorite to syenogranite), mineral assemblage (±garnet, orthopyroxene, biotite, hornblende and magnetite) and degree of strain. The plutonic rocks are tentatively interpreted as part of the middle Paleoproterozoic Cumberland Batholith, a hypothesis to be tested by geochronology.

In this paper, zircon U-Pb results from six samples from across eastern Meta Incognita Peninsula are presented. The samples were analyzed using the sensitive high-resolution ion microprobe (SHRIMP) at the Geological Survey of Canada in Ottawa, Ontario. Sample locations are plotted on Figure 1 and UTM locations are included with the geochronology data tables (see Rayner, 2015a[2]). The objective

[2] *CNGO Geoscience Data Series GDS2015-010, containing the data or other information sources used to compile this paper is available online to download free of charge at http://cngo.ca/summary-of-activities/2015/ .*

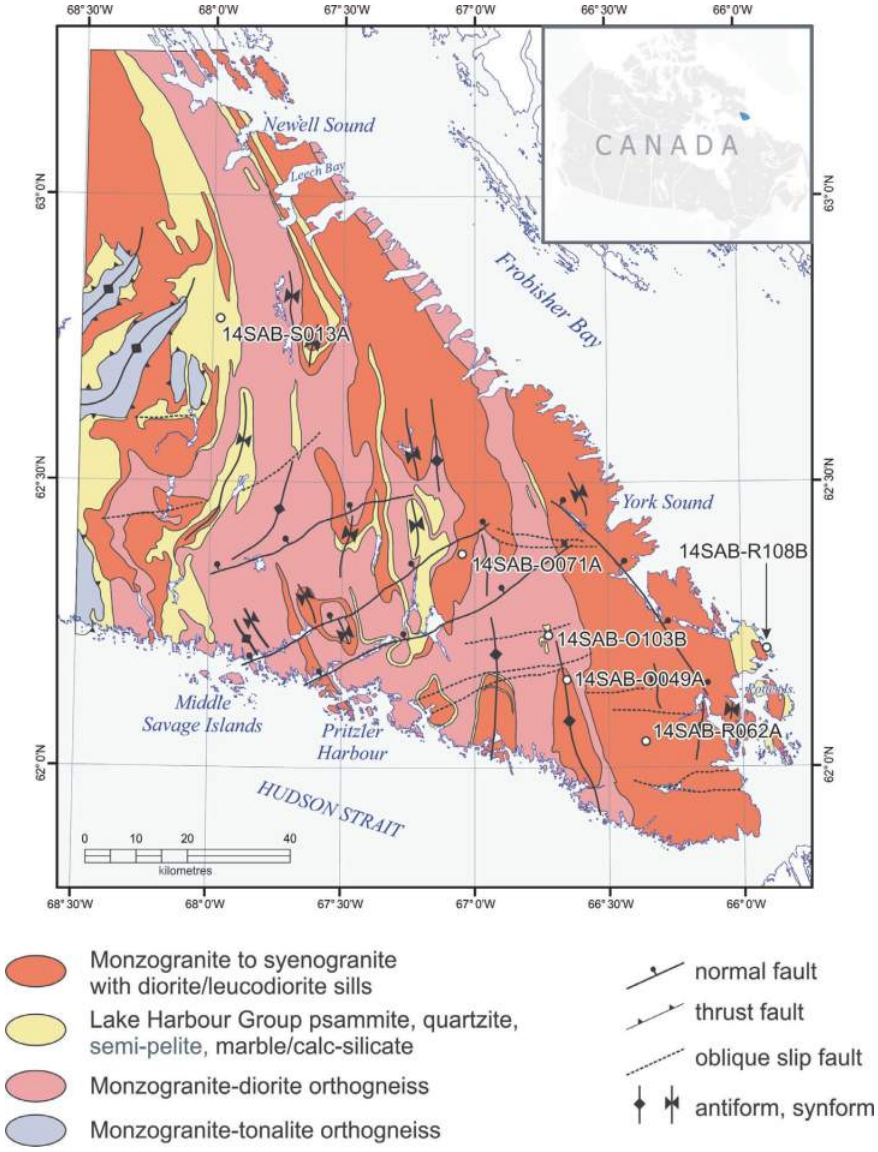

Figure 1: Simplified bedrock geology of eastern Meta Incognita Peninsula, Baffin Island, Nunavut based on 2014 mapping. More detailed geological maps can be found in St-Onge et al., 2015a-c.

of the geochronology research component of the Meta Incognita Peninsula project is to provide temporal pins for the geological observations. The suite of dated samples achieves this objective by 1) constraining the provenance profile and maximum age of deposition of three samples from the extensive metasedimentary assemblage; 2) establishing constraints on the tectonomagmatic evolution of the area through age determinations of three Paleoproterozoic plutonic rocks.

Surface bedrock observations, combined with new geochronological, geochemical, geophysical, and detailed tectonostratigraphic and petrological data, will be synthesized into a new, modern compilation map and geodatabase for the southern half of Baffin Island, including the territorial capital region. This will ultimately lead to an improved understanding of the geological history and Precambrian architecture of the region and its relationship to western Greenland rocks.

Analytical procedures

All samples were disaggregated using standard crushing and pulverizing techniques followed by density separation using a Wilfley table and through the use of heavy liquids (methylene iodide). A magnetic separator was used to isolate a zircon separate.

The SHRIMP analytical procedures followed those described by Stern (1997), with standards and U-Pb error propagation methods following Stern and Amelin (2003).

Briefly, zircons were cast in 2.5 cm diameter epoxy mounts (GSC mounts.744, 756, 762) along with fragments of the GSC laboratory standard zircon (z6266, with $^{206}Pb/^{238}U$ age = 559 Ma). The midsections of the zircons were exposed using 9, 6, and 1 μm diamond compound, and the internal features of the zircons (such as zoning, structures and alteration) were characterized in cathodoluminescence (CL) or back-scattered electron (BSE) mode utilizing a Zeiss Evo® 50 scanning electron microscope. The count rates of 11 masses including background were sequentially measured with a single electron multiplier. Offline data processing was accomplished using SQUID2 (version 2.50.11.10.15, revised 15 October 2011). The 1σ external errors of $^{206}Pb/^{238}U$ ratios reported in the data table incorporate the error in calibrating the standard. Common Pb correction used the Pb composition of the surface blank (Stern, 1997). Details of the analytical session, including spot size, number of scans, calibration error and the application of any intra-element fractionation corrections are given in the footnotes of the data table (Rayner, 2015a). Isoplot v4.15 (Ludwig, 2003) was used to generate concordia plots and calculate weighted means. The error ellipses on the concordia diagrams and the weighted mean errors are reported at 2σ. Probability density diagrams were generated using AgeDisplay (Sircombe, 2004).

Results

Quartzite (sample 14SAB-S013A; GSC lab number z11263)

A 200 m thick, white-weathering quartzite of the Lake Harbour Group was sampled for detrital zircon geochronology from one of the most extensive exposures of Lake Harbour Group rocks in the western part of the map area (Figures 1, 2a). Secondary minerals in the quartzite include garnet, sillimanite and graphite, which define S_1 folds whose axial planes are parallel to the transposition fabric (Figure 2b).

The zircons recovered from the quartzite typically consist of clear, colourless to pale brown cores surrounded by turbid medium-brown overgrowths (Figure 3a, inset). In BSE images these overgrowths are relatively bright, indicating elevated U content. Seventy analyses were conducted on 60 zircon grains (Figure 3a; Rayner, 2015a for data table). Analysis of 12 overgrowths yielded ages between 1779 and 1849 Ma and a weighted mean $^{207}Pb/^{206}Pb$ age of 1806 ±7 Ma (mean square of the weighted deviates; MSWD = 1.9, probability = 0.039). The remaining analyses of zircon cores or single-phase grains yielded ages between 2290 and 2950 Ma. The detrital provenance profile is characterized by a single dominant mode at 2.82 Ga. Many of the younger analyses (2.29–2.67 Ga) are greater than 10% discordant and, therefore, are not reliable indicators of Paleoproterozoic detritus. The youngest reliable concordant zircon yielded an age of 2.67 Ga, which is considered the maximum age of deposition. This extensive quartzite in the western part of the map area is thus characterized by Archean detritus. Basement rocks of that age have not been identified on Meta Incognita Peninsula but are known on Hall Peninsula to the north (Scott, 1999; From et al., 2015; Rayner, 2015b, c).

Calcareous quartzite (sample 14SAB-O103B; GSC lab number 11264)

Exposures of metasedimentary rocks south of York Sound (Figure 1) include a package of clastic and chemical sediments characterized by 10–15 cm interbedded quartzite and calcsilicate/marble (Figure 2c, d). In some cases, the bedding between the silicate and calcareous components is straight or transposed, and in other cases, disharmonic folding is preserved. Elsewhere on the outcrop, garnet-sillimanite leucogranite preserving ghost compositional layers from its source metasedimentary rocks is observed. A sample of calcareous quartzite was collected to evaluate its detrital-provenance signature.

The zircon grains recovered from sample 14SAB-O103B are very similar in appearance (Figure 3b, inset) to those from sample 14SAB-S013A described earlier. They typically consist of clear, colourless to pale brown cores surrounded by medium-brown overgrowths, which appear unzoned and bright in BSE images relative to the cores.

Sixty-two analyses were carried out on 52 separate zircon grains, yielding dates between 1713 and 3002 Ma. Many of the analyses younger than 1900 Ma are from unzoned overgrowths. These are not considered detrital but they do not form a single statistical population as in sample 14SAB-S013A. Other young analyses from zircon cores or single-phase zircon were not reproducible in replicate analyses. The presence of overgrowths and the nonreproducibility of results are consistent with a metamorphic overprint affecting these zircon grains and must be considered when determining the youngest detrital age. When assessing detrital sources, only the oldest analysis from a single grain is considered. Most detrital zircons grains from this calcareous quartzite are younger than 2.7 Ga, with modes at 2.6–2.5 Ga, 2.35 Ga, 2.1 Ga and 1.93–1.91 Ga, with no single mode dominating the profile (Figure 3b). The youngest detrital zircon yielded an age of 1913 ±17 Ma (n = 2 replicates on grain 46, MSWD = 0.13). Replicate analyses on other ca. 1.9–1.93 Ga zircon grains support this as the maximum age of deposition.

Quartzite (sample 14SAB-R108B; GSC lab number z11268)

A grey, sandy, quartz-rich horizon, approximately 30 cm wide, was collected from within an extensive exposure of rusty-weathering garnet-biotite-sillimanite psammite injected with white-weathering leucogranite (Figure 2e, f).

Figure 2: Field photographs and relationships of metasedimentary samples collected for geochronology across eastern Meta Incognita Peninsula, Nunavut (see Figure 1 for sample locations): **a)** outcrop of thick, white quartzite (sample14SAB-S013A), hammer is 40 cm long; **b)** detail of isoclinal folding defined by sillimanite, S_1 axial plane is parallel to regional transposition fabric; **c)** thin horizons of quartzite within a calcsilicate dominated outcrop at sample location 14SAB-O103B, hammer is 40 cm long; **d)** thicker horizon of quartzite (sample14SAB-O103B), hammer for scale (40 cm long) is located just below the 'quartzite' label; **e)** aerial photograph of the general aspect of the outcrop, taken 5 km northwest of sample location 14SAB-R108B; thin white banding on the island is leucogranite, rusty orange rocks are psammite/semi-pelite (scale is approximate); **f)** detail of hand specimen of sample 14SAB-R108B.

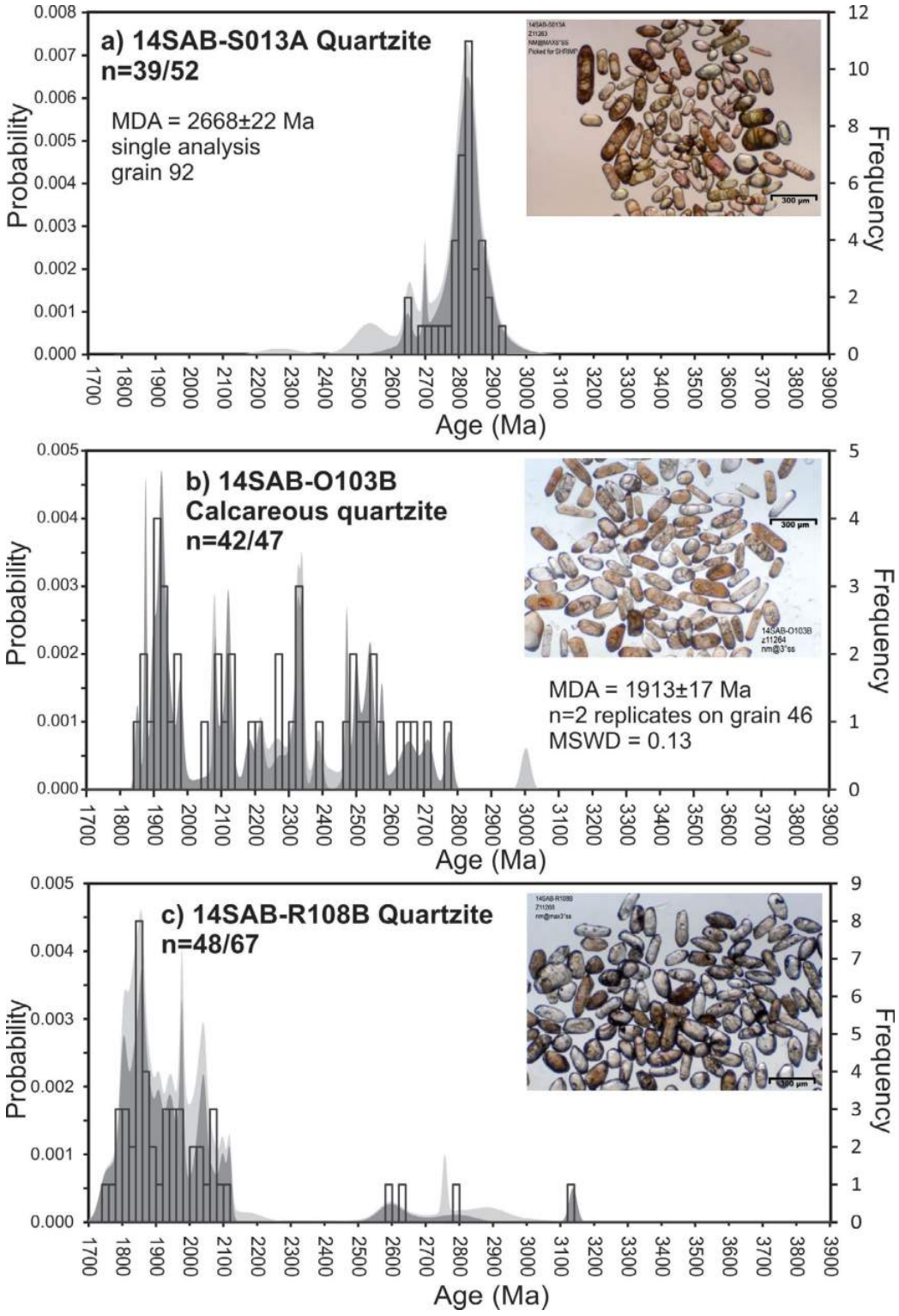

Figure 3: Probability density diagrams and histograms for detrital zircon samples from eastern Meta Incognita Peninsula. Dark grey curves include only data that fall within the ±5% concordance threshold; light grey curves incorporate all data. Replicates and metamorphic overgrowths are not plotted, regardless of concordance. The bin width is 20 m.y. Where applicable, maximum ages of deposition (MDA) are reported at the 2σ confidence level. See text for discussion and Rayner (2015a) for table of results: **a)** results from sample 14SAB-S013A; inset: transmitted light image of the recovered zircons, scale bar is 300 µm. **b)** results from sample 14SAB-O103B; inset: transmitted light image of the recovered zircons, scale bar is 300 µm; **c)** results from sample 14SAB-R108B; inset: transmitted light image of the recovered zircons, scale bar is 300 µm. Abbreviation: MSWD, mean square of the weighted deviates.

Detrital zircon geochronology results from this sample will permit comparisons of the provenance of this easternmost sedimentary unit with that of those further to the west and with the Lake Harbour Group rocks exposed around Kimmirut.

Eighty-five analyses were carried out on 73 individual zircon grains, yielding dates between 1746 and 3137 Ma; notably, only 8 are older than 2.3 Ga. This dominance of Orosirian (2050–1800 Ma) detritus stands in distinct contrast to the other two detrital samples discussed here. Amongst the youngest results (younger than 1.9 Ga), there is no correlation between zoning or grain microstructure, as few zircon grains from this sample contain overgrowths. Many of the ca. 1.85 Ga zircon grains are oscillatory zoned, suggesting a magmatic rather than metamorphic origin, but an interpretation of these zircon grains as detrital would be inconsistent with field relationships. Elsewhere, metasedimentary rocks on southern Baffin Island are intruded by the Cumberland Batholith (1865–1845 Ma, Whalen et al., 2010) or record a metamorphic overprint of similar age and thus must be older. Therefore, it seems likely that many of the ca. 1.85 Ga grains recovered in this sample are from the extensive leucogranite (Figure 2e). Since the ca. 1.85 Ga zircon grains are chemically and morphologically indistinguishable from detrital/inherited zircon, a maximum depositional age cannot be determined. However, the presence of abundant zircon yielding ages less than 2.1 Ga is consistent with an Orosirian age of deposition.

K-feldspar–megacrystic biotite-orthopyroxene monzogranite (sample 14SAB-O071A; GSC lab number 11266)

A sample of strongly foliated and lineated K-feldspar–megacrystic biotite-orthopyroxene monzogranite (unit Pmo, St-Onge et al., 2015b) was collected from a complex outcrop in the central part of the map area (Figure 1). The outcrop consists mainly of megacrystic monzogranite but also includes enclaves of diorite, both of which are cut by syenogranite dykes (Figure 4a, b). Care was taken to avoid either of these components when sampling, Potassium-feldspar–megacrystic biotite-orthopyroxene monzogranite is a common constituent phase of the Cumberland Batholith. The U-Pb results presented here will be used to test the preliminary field interpretation that both this unit and the Cumberland Batholith are related.

Recovered zircon grains are pale to medium brown, with no preserved facets, crystal edges or terminations (Figure 4c). The rounded form of these grains and the high metamorphic grade of the sample, inferred by the presence of orthopyroxene, suggest that the zircons have been partially resorbed. Zoning is very faint to nonexistent in BSE images. Twenty-nine analyses were carried out on 28 zircon grains (Rayner, 2015a). There is a large degree of scatter in the data; however, some individual analyses are relatively imprecise due to low U contents. Due to the highly variable precision of the analyses and given the fairly consistent morphology and zonation of the zircon grains, virtually the entire population of analyzed zircons was grouped together to calculate an age (Figure 4d). Only a single zircon, with distinct U content and sharp oscillatory zoning was excluded from the calculation. A Tukey's biweight mean was used to minimize the effects of weighting particular analyses by their precision. This calculation yielded a $^{207}Pb/^{206}Pb$ age of 1845 ±19 Ma, which is interpreted as the crystallization age of the K-feldspar–megacrystic biotite-orthopyroxene monzogranite. This result is in line with the known ages of the Cumberland Batholith (Whalen et al., 2010).

Biotite-magnetite monzogranite (sample 14SAB-R062A; GSC lab number z11267)

A sample of biotite-magnetite monzogranite was collected from the eastern end of Meta Incognita Peninsula to characterize the age of this regionally extensive unit (unit Pmo, St-Onge et al, 2015a). The sample is medium grained and equigranular, with a greenish cast to the feldspars on a fresh surface consistent with having reached granulite-grade metamorphic conditions (Figure 5a).

The zircons recovered from the biotite-magnetite monzogranite are prismatic, pale brown to pale pink and generally of excellent quality: clear, with few to no fractures or inclusions (Figure 5b). Their CL response is weak, yet broad oscillatory and sector zoning are preserved (Figure 5c, d). Most of the zircon grains appear to comprise an inner and outer component. In some cases, the zoning of the inner component is truncated by the outer component (e.g., Figure 5c, grain no.3), a condition which would suggest that an older core has been overgrown by a younger rim. However, in other instances, the zoning is concentric rather than truncated (e.g., Figure 5c, grain no.1). Across the zircon population there is no consistent difference in the CL response, or the style of zoning between the inner or outer parts of the grains. For example, outer portions of the grains may be brighter or darker than the inner. Since it is not apparent that there is a distinct difference in growth conditions between these two phases, the terms inner and outer will be used rather than core and rim to leave open the possibility that the apparent multicomponent nature of the zoned zircon is a function of changing trace-element composition, rather than a separate zircon-growth event.

Fifty-one analyses were carried out on 39 zircon grains, yielding $^{207}Pb/^{206}Pb$ ages between 1811 and 1934 Ma, which do not form a single statistical population (Figure 6; Rayner, 2015a). When the results are evaluated according to the position of the analytical spot within the zircon (inner versus outer), it is still not possible to resolve two separate, statistically significant groups. Analyses from the inner parts of grains range from 1836 to 1922 Ma, whereas data from the outer parts of grains range from 1828 to 1904 Ma.

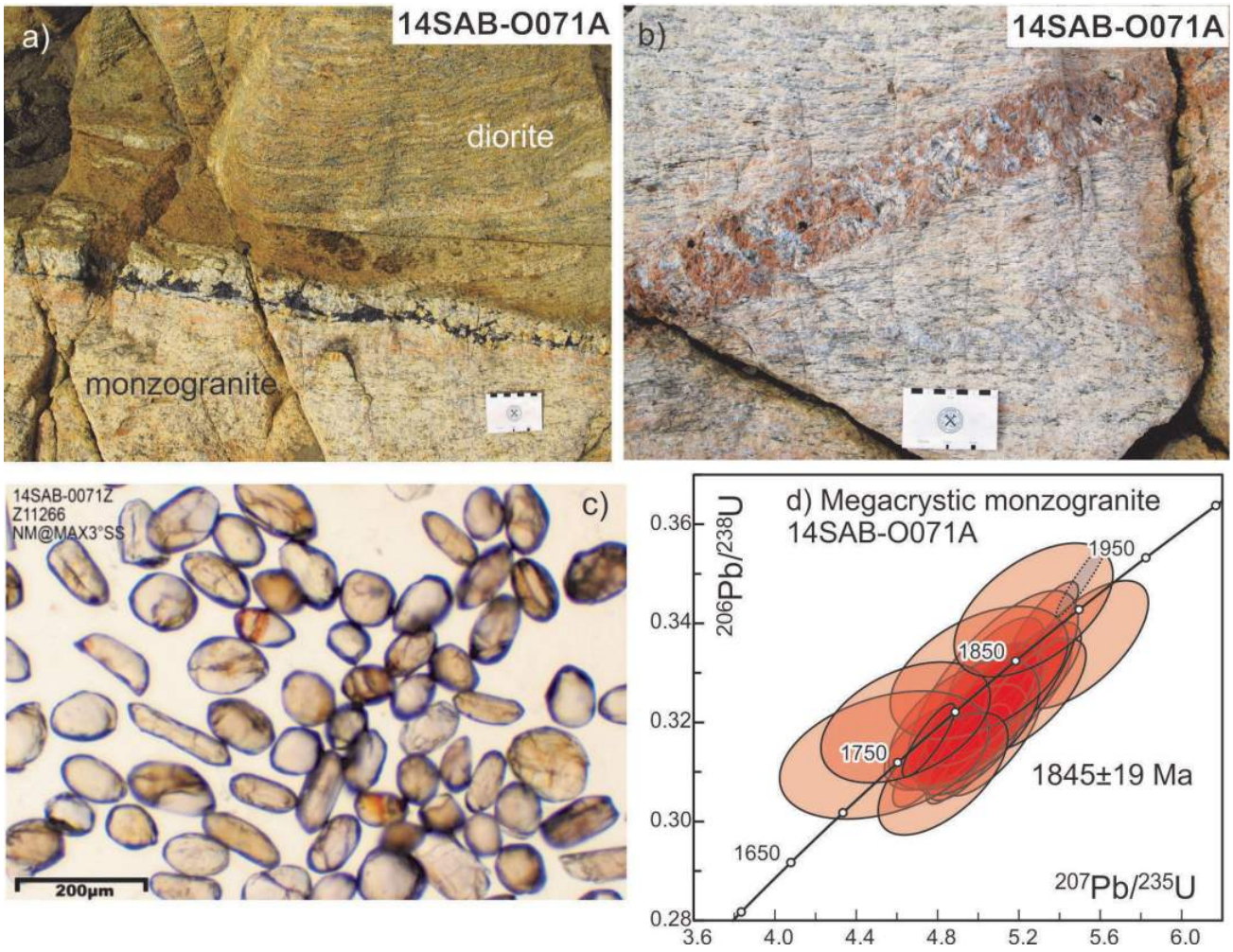

Figure 4: Field relationships, zircon image and concordia diagram of plutonic samples from eastern Meta Incognita Peninsula: **a)** foliated diorite enclave within foliated K-feldspar–megacrystic biotite-orthopyroxene monzogranite; contact between diorite and monzogranite is exploited by late pegmatite; **b)** syenogranite dyke cutting strong fabric in megacrystic monzogranite; **c)** zircon recovered from megacrystic monzogranite, scale bar is 300 µm; **d)** concordia diagram of U-Pb results from sample 14SAB-O071A; dashed line ellipse is excluded from the calculation of the mean; ellipses plotted and mean age reported at the 2σ confidence level.

In order to better evaluate the results, only grains with paired inner and outer analyses, where the relative age relationships are clear, are considered (Figure 6). In the case of 12 analyses from the inner parts of the grains, the weighted mean $^{207}Pb/^{206}Pb$ age is 1896 ±11 Ma (MSWD = 3.5). The weighted mean $^{207}Pb/^{206}Pb$ age from the corresponding outer portions of the same 12 grains is 1865 ±10 Ma (n = 13, MSWD = 1.7).

An alternative treatment of the data utilizes the Unmix function in Isoplot, which deconvolutes a set of data points, whose errors overlap but which are known to consist of more than one age component (Ludwig, 2003; Sambridge and Compston, 1994). The resulting output ages are 1896 ±6 Ma and 1850 ±7 Ma, which are broadly in agreement with the weighted means calculated for the subset of paired analyses. This sample of biotite-magnetite monzogranite from the eastern end of Meta Incognita Peninsula thus contains age components known from the Qikiqtarjuaq plutonic suite (1910–1880 Ma), Cumberland Batholith (1865–1845 Ma; Whalen et al., 2010) and regional metamorphism (1850–1815 Ma: St-Onge et al., 2007), which makes it challenging to equivocally assess its crystallization age. The preferred interpretation is that this rock crystallized at 1865 Ma, with the older component representing an inherited phase or possibly an autocrystic phase from a long-lasting magmatic system. The well-preserved oscillatory zoning observed in the outer parts of many grains is consistent with magmatic growth. One would have expected to see greater intragrain differences in the composition and zoning pattern of the outer portions of the grains if these were related to overgrowths from a regional metamorphic event.

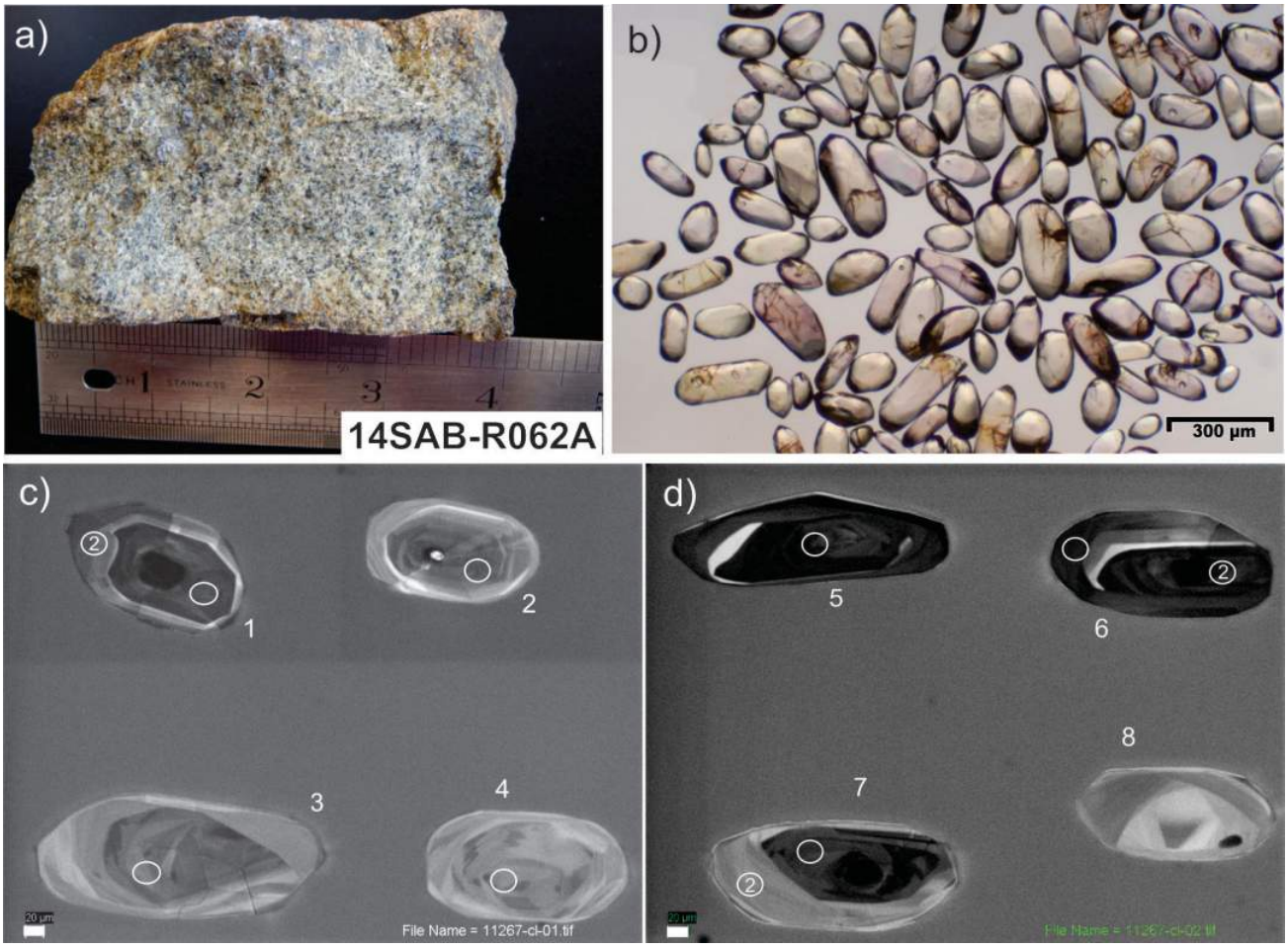

Figure 5: Hand specimen and zircon images of sample 14SAB-R062A collected on eastern Meta Incognita Peninsula: **a)** photograph of hand specimen; note greenish cast on fresh surface; **b)** plane-light photomicrograph of zircon grains recovered from sample 14SAB-R062A; scale bar is 300 µm; **c)** and **d)** cathodoluminescence images of zircon grains illustrating common zoning pattern; white scale bar in lower left is 20 µm. For comparison with data table (Rayner, 2015a), the zircon grain number is indicated in white, the position of analytical spot is indicated by white ellipses and any additional analysis on a given grain is indicated by no.2 within the ellipse.

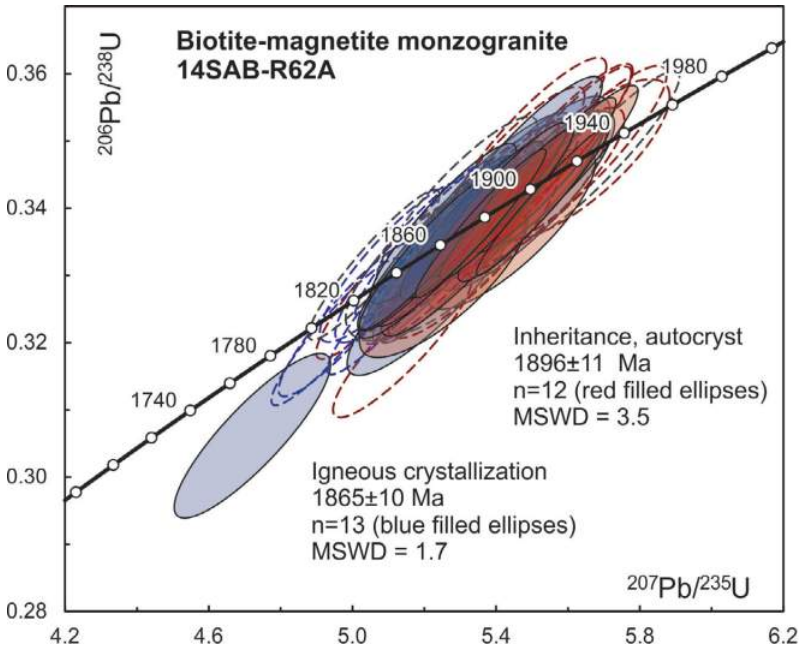

Figure 6: Concordia diagram of U-Pb results from sample 14SAB-R62A collected on eastern Meta Incognita Peninsula. Filled ellipses indicate that pairs of analyses were conducted on both the inner and outer portions of a single grain; unfilled ellipses with dashed outlines indicate that only a single analysis was performed on a given grain. Red ellipses and outlines indicate analyses from the inner parts of zircon grains; blue ellipses and outlines indicate analyses from the outer parts of zircon grains; grey ellipses indicate single phase zircon, where the relative inner or outer position could not be assessed. Ellipses plotted and mean ages reported at the 2σ confidence level. Abbreviation: MSWD, mean square of the weighted deviates.

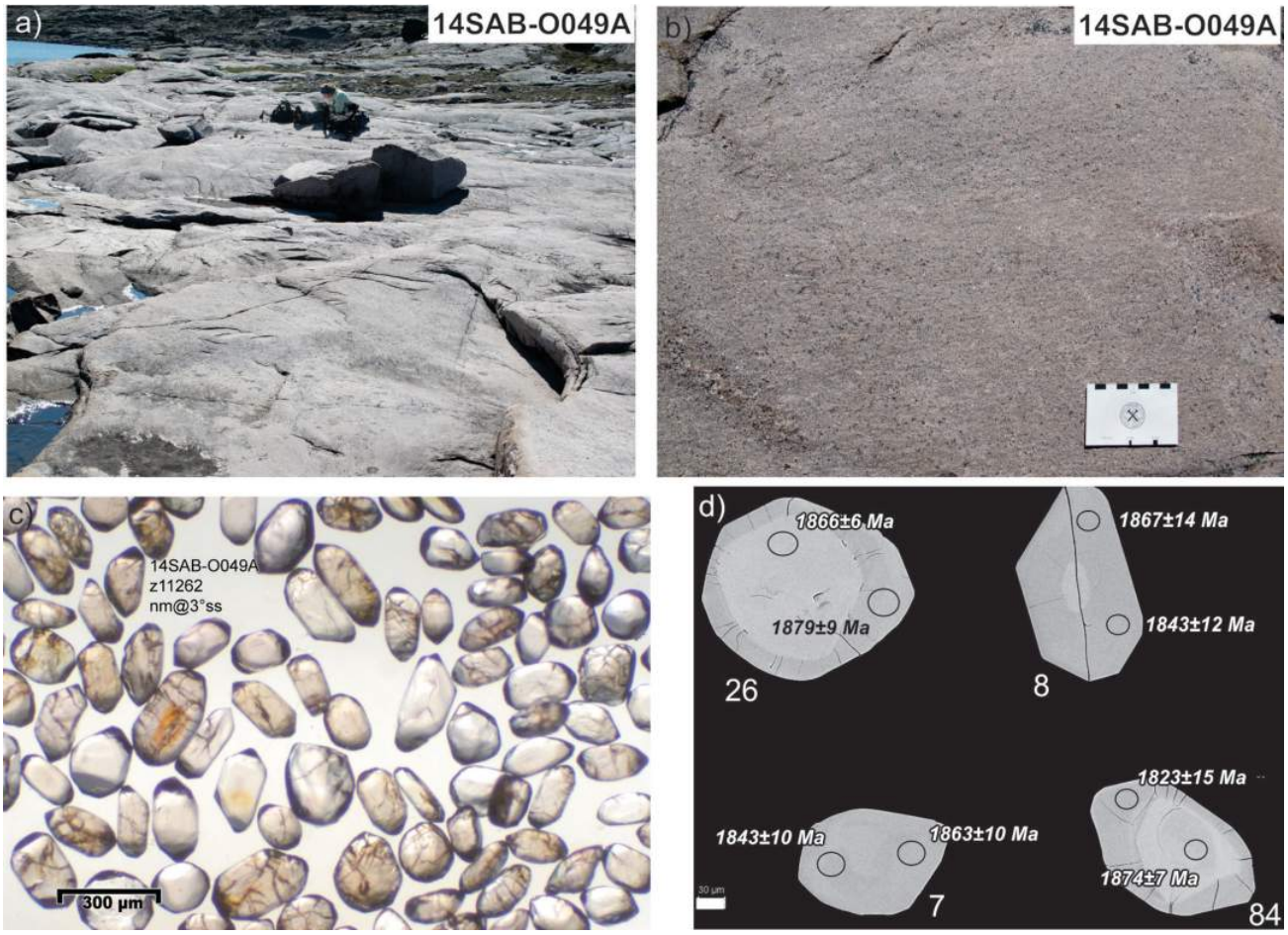

Figure 7: Field relationships and zircon images for eastern Meta Incognita Peninsula plutonic sample 14SAB-O49A: **a)** clean, homogeneous, stream-washed outcrop from which U-Pb sample 14SAB-O049A was collected; seated geologist for scale; **b)** detail of both the fine-grained, equigranular, sugary texture and homogeneity of the biotite-magnetite monzogranite; **c)** plane-light photomicrograph of zircon recovered from sample14SAB-O049A, scale bar is 300 µm; **d)** representative back-scattered electron image of zircons from sample 14SAB-O049A, white scale bar in lower left is 30 µm.

Biotite-magnetite monzogranite (sample 14SAB-O049A; GSC lab number z11262)

A fine- to medium-grained biotite-magnetite monzogranite was collected for geochronology to assess the age range of the common plutonic phases on Meta Incognita Peninsula (unit Pmb St-Onge et al., 2015a). This phase is characterized by pink weathered and fresh surfaces, a sugary texture and moderate foliation. It was sampled in a lichen-free stream bed (Figure 7a) and across the extensive outcrop, this phase is homogeneous, and free of crosscutting veins and enclaves of other material (Figure 7b).

Abundant, prismatic, clear, colourless to pale brown zircons were recovered from the monzogranite (Figure 7c). In BSE images, the zircon grains are unzoned to faintly zoned. Some rare grains consist of a light grey (BSE bright) centre surrounded by a slightly darker overgrowth (Figure 7d). The full range of zoning styles and microstructures was targeted by 37 analyses on 30 grains, yielding dates between 1808 Ma and 1893 Ma (Figure 8a). The combined dataset does not form a single statistical population; however, there is no clear correlation between zoning style (unzoned or faintly zoned), analytical spot position (core or inner versus rim or outer; see Figure 7d) or composition (U content, Th/U). When the data is plotted sequentially, individual point-data values decrease smoothly from 1890 Ma to ca. 1860 Ma then jump to 1850 Ma, at which point they start to decrease incrementally again down to ca. 1820 Ma (Figure 8b). Assuming this jump represents a break into two separate populations, the weighted mean $^{207}Pb/^{206}Pb$ age of the older cluster is 1871 ±4 Ma (n=18, MSWD=1.3), whereas the weighted mean $^{207}Pb/^{206}Pb$ age of the younger cluster is 1838 ±5 Ma (n=19, MSWD=0.95). Output from the Isoplot Unmix function yielded identical ages of 1870 ±4 and 1840 ±5 Ma.

As with sample 14SAB-R062A from the eastern end of Meta Incognita Peninsula, this rock appears to record ages that straddle the younger range of the Qikiqtarjuaq plutonic suite (1910–1880 Ma), the older range of the Cumberland

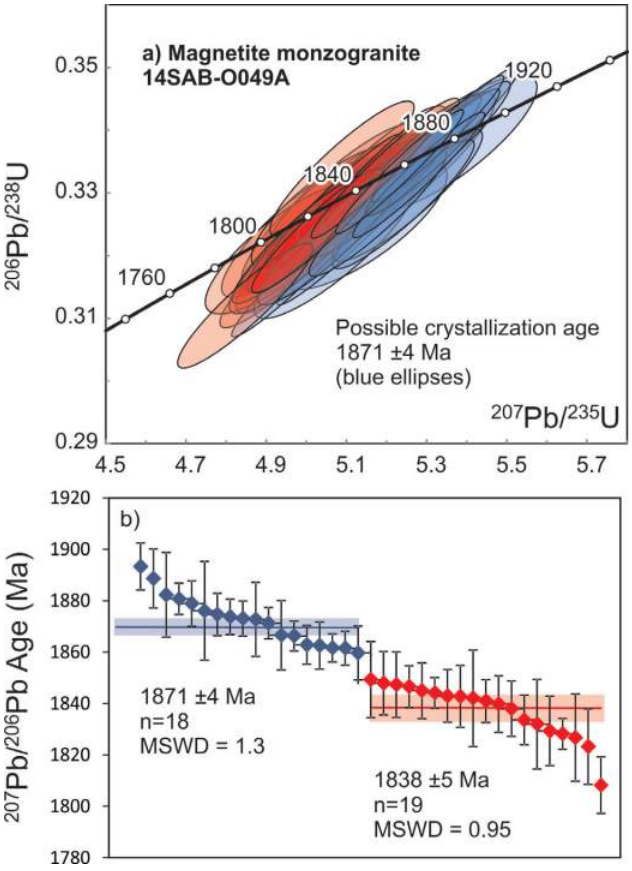

Figure 8: Plots of results for sample 14SAB-O49A from eastern Meta Incognita Peninsula: **a)** concordia diagram of U-Pb results; ellipses plotted at the 2σ confidence level; **b)** individual and $^{207}Pb/^{206}Pb$ ages plotted chronologically. See text for discussion. Blue ellipses and error bars correspond to dates older than 1860 Ma, red ellipses and error bars, to dates younger than 1850 Ma. Mean ages reported at the 2σ confidence level. The weighted means and associated 2σ errors are shown as shaded bars. Abbreviation: MSWD, mean squared weight deviates.

Batholith (1865–1845 Ma; Whalen et al., 2010) and regional metamorphism (1850–1815 Ma: St-Onge et al., 2007). Two interpretations are possible: 1) crystallization at ca. 1840 Ma with an inherited or autocrystic ca. 1870 Ma component or 2) crystallization of the monzogranite at ca. 1870 Ma followed by partial resetting of zircon during metamorphism. Since some grains (e.g., no. 26, Figure 7d) have consistent older ages in both the 'core' and the 'rim', and the younger zircon is chemically indistinguishable from the older zircon, the latter interpretation (crystallization at 1871 ±4 Ma) is preferred. The drift to younger ages is inferred to be the result of Pb loss from the igneous component, not new growth of metamorphic zircon.

Economic considerations

Precise, absolute age constraints are an essential component of modern mapping, as they provide temporal calibration of geological observations, strengthen regional correlations and place time brackets on magmatic and tectonometamorphic events. The continued characterization of the detrital zircon provenance profile of Paleoproterozoic sedimentary rocks across southern Baffin Island advances the study of the origin and evolution of the rocks that host the mafic Frobisher intrusive suite, which has prospectivity for both base metals and carving stone.

Conclusions

This paper presents new U-Pb geochronology data from six samples collected during recent mapping of eastern Meta Incognita Peninsula, Baffin Island, Nunavut. Three samples of quartzite from across the full breadth of the map area were targeted and each one yielded a distinct provenance profile:

- The westernmost sample (14SAB-S013A), contiguous with the type area of the Lake Harbour Group near Kimmirut, is characterized by an exclusively Archean detrital-zircon profile which is dominated by ca. 2.82 Ga detritus.
- Calcareous quartzite is present in an exposure of metasedimentary rocks near the central part of the map area (sample 14SAB-O103B). Most detrital zircons are younger than 2.7 Ga, and include detrital ages of 2.6–2.5 Ga, 2.35 Ga, 2.1 Ga and 1.93–1.91 Ga; however, no single age mode dominates the profile. The maximum age of deposition of the calcareous quartzite is 1913 ±17 Ma.
- The detrital zircon profile of a grey, sandy quartzite horizon (sample 14SAB-R108B), in a dominantly psammite/leucogranite exposure, is dominated by Orosirian age (2050–1800 Ma) zircon. A large component of ca. 1850 Ma zircon is interpreted to reflect partial melting and emplacement of leucogranite.

Notwithstanding these differences in detrital-provenance profile, their lithological association and geological setting support a correlation with the Lake Harbour Group. This correlation will be further tested, and revised or strengthened, through upcoming compilations and comparisons with the detrital-zircon record from across southern Baffin Island.

Despite their relatively simple appearance in the field, interpretation of the geochronological results from plutonic phases from Meta Incognita Peninsula proved challenging. A megacrystic biotite-orthopyroxene monzogranite (sample 14SAB-O071A) is interpreted to have crystallized at 1845 ±19 Ma. A megacrystic biotite-magnetite monzogranite (sample 14SAB-R062A) is interpreted to have a crystallization age of 1865 ±10 Ma, with an older 1896 Ma component representing an inherited phase or possibly an autocrystic phase. A pink, sugary-textured biotite-magnetite monzogranite (sample 14SAB-O049A) is cautiously interpreted to have crystallized at 1871 ±4 Ma, followed by resetting of zircon during metamorphism. It is interesting to

note that the highest grade, most deformed samples discussed in this paper yielded the youngest ages. This emphasizes the need for careful field observations of crosscutting relationships when establishing a field chronology for plutonic rocks.

Acknowledgments

The field observations and relationships, and the development of geological hypotheses to be tested through geochronology, are the result of an engaging and fruitful collaboration with M. St-Onge and the 2014 Meta Incognita bedrock-mapping team. Their careful observations and contributions, both in the field and in the office, underpin this paper. The author is grateful for the support and assistance of the staff of the Geochronology Laboratory of the Geological Survey of Canada. In particular, R. Chung, R. Christie, J. Peressini and T. Pestaj are thanked for their careful efforts and excellent work. P. Hunt provided the necessary high-quality scanning electron microscope images. The manuscript benefited from a thorough review by N. Joyce.

Natural Resources Canada, Earth Sciences Sector contribution number 20150293

References

From, R.E., Rayner, N.M. and Camacho, A. 2015: Archean magmatism and metamorphism of eastern Hall Peninsula, southern Baffin Island, Nunavut; *in* Summary of Activities 2015, Canada-Nunavut Geoscience Office, p. 73–88.

Liikane, D. and St-Onge, M.R. 2015: Frobisher suite mafic, ultramafic, and layered mafic-ultramafic sills, southern Baffin Island, Nunavut; *in* Summary of Activities 2015, Canada-Nunavut Geoscience Office, p. 21–32.

Ludwig, K.R., 2003: User's manual for Isoplot 3.00: a geochronological toolkit for Microsoft Excel®, Berkeley Geochronology Center, Special Publication, 4, 70 p.

Rayner, N.M. 2015a: Data table accompanying "Uranium-lead geochronology of eastern Meta Incognita Peninsula, southern Baffin Island, Nunavut"; Canada-Nunavut Geoscience Office, Geoscience Data Series GDS2015-010, Microsoft® Excel® file, URL <http://cngo.ca/summary-of-activities/2015/> [December 2015].

Rayner, N.M. 2015b: Data table accompanying "New (2013–2014) U-Pb geochronological results from northern Hall Peninsula, southern Baffin Island, Nunavut"; Canada-Nunavut Geoscience Office, Geoscience Data Series 2015-002, Microsoft® Excel® file, URL <http://cngo.ca/summary-of-activities/2014/> [March 2015].

Rayner, N.M. 2015c: New (2013–2014) U-Pb geochronological results from northern Hall Peninsula, southern Baffin Island, Nunavut; *in* Summary of Activities 2014, Canada-Nunavut Geoscience Office, p. 31–44, URL <http://cngo.ca/summary-of-activities/2014/> [March 2015].

Sambridge, M.S. and Compston, W. 1994: Mixture modeling of multi-component data sets with application to ion-probe zircon ages: Earth and Planetary Science Letters, v. 128, p. 373–390.

Scott, D.J. 1999: U-Pb geochronology of the eastern Hall Peninsula, southern Baffin Island, Canada: a northern link between the Archean of West Greenland and the Paleoproterozoic Torngat Orogen of northern Labrador; Precambrian Research, v. 93, p. 5–26.

Sircombe, K.N. 2004: AGEDISPLAY: an Excel workbook to evaluate and display univariate geochronological data using binned frequency histograms and probability density distributions. Computers and Geosciences, v. 30, p. 21–31.

Stern, R.A., 1997: The GSC Sensitive High Resolution Ion Microprobe (SHRIMP): analytical techniques of zircon U-Th-Pb age determinations and performance evaluation: *in* Radiogenic Age and Isotopic Studies, Report 10, Geological Survey of Canada, Current Research 1997-F, p. 1–31.

Stern, R.A. and Amelin, Y., 2003: Assessment of errors in SIMS zircon U-Pb geochronology using a natural zircon standard and NIST SRM 610 glass; Chemical Geology, v. 197, p. 111–146.

St-Onge, M.R., Rayner, N.M., Steenkamp, H. and Gilbert, C., 2015a: Geology, Terra Nivea, Baffin Island, Nunavut; Geological Survey of Canada, Canadian Geoscience Map 215E, (ed. prelim.), 1:100 000 scale, 1 sheet, URL <http://dx.doi.org/10.4095/296105> [September 2015].

St-Onge, M.R., Rayner, N.M., Steenkamp, H. and Gilbert, C., 2015b: Geology, Pritzler Harbour, Baffin Island, Nunavut; Geological Survey of Canada, Canadian Geoscience Map 216E, (ed. prelim.), 1:100 000 scale, 1 sheet, URL <http://dx.doi.org/10.4095/296110> [September 2015].

St-Onge, M.R., Rayner, N.M., Steenkamp, H. and Gilbert, C., 2015c: Geology, Grinnell Glacier, Baffin Island, Nunavut; Geological Survey of Canada, Canadian Geoscience Map 217E, (ed. prelim.), 1:100 000 scale, 1 sheet, URL <http://dx.doi.org/10.4095/296112> [September 2015].

St-Onge, M.R., Rayner, N.M., Steenkamp, H.M. and Skipton, D.R. 2015d: Bedrock mapping of eastern Meta Incognita Peninsula, southern Baffin Island, Nunavut; *in* Summary of Activities 2014, Canada-Nunavut Geoscience Office, p. 105–118.

St-Onge, M.R., Rayner, N.M., Liikane, D. and Chadwick, T. 2015e: Mafic, ultramafic and layered mafic-ultramafic sills, Meta Incognita Peninsula, southern Baffin Island, Nunavut; *in* Summary of Activities 2014, Canada-Nunavut Geoscience Office, p. 11–16.

St-Onge, M.R., Wodicka, N. and Ijewliw, O. 2007: Polymetamorphic evolution of the Trans-Hudson Orogen, Baffin Island, Canada: integration of petrological, structural and geochronological data; Journal of Petrology, v. 48, p. 271–302.

Whalen, J.B., Wodicka, N., Taylor, B.E. and Jackson, G.D. 2010: Cumberland batholith, Trans-Hudson Orogen, Canada: petrogenesis and implications for Paleoproterozoic crustal and orogenic processes; Lithos, v. 117, p. 99–118. doi: 10.1016/j.lithos.2010.02.008

Overview of surficial geology mapping and geochemistry in the Sylvia Grinnell Lake area, Baffin Island, Nunavut

T. Tremblay[1], S. Day[2], R. McNeil[2], K. Smith[3], M. Richardson[3] and J. Shirley[4]

[1]*Canada-Nunavut Geoscience Office, Iqaluit, Nunavut, tommy.tremblay@canada.ca*

[2]*Natural Resources Canada, Geological Survey of Canada, Ottawa, Ontario*

[3]*Department of Geography, Carleton University, Ottawa, Ontario*

[4]*Nunavut Research Institute, Iqaluit, Nunavut*

Tremblay, T., Day, S., McNeil, R., Smith, K., Richardson, M. and Shirley, J. 2015: Overview of surficial geology mapping and geochemistry in the Sylvia Grinnell Lake area, Baffin Island, Nunavut; *in* Summary of Activities 2015, Canada-Nunavut Geoscience Office, p. 107–120.

Abstract

The Sylvia Grinnell Lake area project is a collaborative activity between the Canada-Nunavut Geoscience Office, the Geological Survey of Canada (Geo-mapping for Energy and Minerals program), Nunavut Research Institute and Carleton University. The study area for summer 2015 is located north of Iqaluit, and covers 16 000 km^2 over NTS map areas 25N, 26C and F. The surficial geology results will assist the search for and development of future natural resources, and provide input for infrastructure and environmental studies. Samples of till, stream sediment, lake sediment, stream water and lake water were collected during the summer of 2015 and the results are expected in early 2016. Field observations on surficial sediments and geomorphological processes were documented, and will support the drafting of new 1:100 000 surficial geology maps for the study area. Glaciodynamic settings were mapped as cold-based, intermediate cold-based and warm-based zones from field observations and remote sensing work. The ice-flow history from the last glaciation is divided into two broad phases, ice that flowed toward Foxe Basin, Frobisher Bay and Cumberland Sound, and ice that terminated at terrestrial or grounded ice margins as the glaciers retreated into the highlands.

Résumé

La région du lac Sylvia Grinnell fait l'objet d'un projet de nature collaborative impliquant le Bureau géoscientifique Canada-Nunavut, la Commission géologique du Canada (programme de géocartographie de l'énergie et des minéraux), le Nunavut Research Institute et l'Université Carleton. La région à l'étude au cours de l'été 2015 est située au nord d'Iqaluit et couvre 16 000 km^2 des régions cartographiques 25N, 26C et F du SNRC. Les résultats des travaux géologiques de surface entrepris devraient d'une part contribuer à rendre plus facile le processus d'exploration et de mise en valeur de ressources naturelles futures et, d'autre part fournir les données nécessaires à la poursuite d'études sur les infrastructures et l'environnement. Les résultats d'analyse d'échantillons de till, de sédiments fluviatiles et lacustres, et d'eau de lac et de ruisseau recueillis au cours de l'été 2015 sont attendus au début de 2016. Les observations faites sur le terrain portant sur les sédiments de surface et les processus géomorphologiques ont été documentés et serviront à la réalisation à l'échelle de 1/100 000 de nouvelles cartes de la géologie de surface de la région. Les milieux glaciodynamiques ont également été portés sur carte sous forme de zones à base froide, à base froide intermédiaire et à base tempérée à partir des observations faites sur le terrain et l'interprétation de données de télédétection. Les antécédents de l'écoulement glaciaire datant de la dernière glaciation se répartissent selon deux grandes phases, d'une part la glace qui s'écoulait vers le bassin Foxe, la baie Frobisher et le détroit de Cumberland et, d'autre part la glace qui jouxtait des marges terrestres ou de glace échouée à mesure que les glaciers reculaient en direction des hautes-terres.

This publication is also available, free of charge, as colour digital files in Adobe Acrobat® PDF format from the Canada-Nunavut Geoscience Office website: http://cngo.ca/summary-of-activities/2015/.

Introduction

The Sylvia Grinnell Lake area project is a collaborative activity between the Canada-Nunavut Geoscience Office, the Geological Survey of Canada (Geo-mapping for Energy and Minerals program), Nunavut Research Institute and Carleton University. The Canada-Nunavut Geoscience Office (CNGO) has a mandate to promote mineral exploration in the territory; this includes gathering baseline information about the geochemistry and mineralogy of surficial sediments. This baseline data will potentially help to lower the financial risks of finding new mineral prospects by the exploration industry. Mineral exploration, geotechnical and aggregate resource studies require accurate surficial geology maps and glaciodynamic interpretations. The collection of baseline information about the geochemistry of soils and water is useful, particularly for environmental studies. This project aims to collect geochemical and mineralogical data for surficial sediments from an area north of Iqaluit, on southern Baffin Island, Nunavut, where little or no public data exists. The study area was located north of Iqaluit, and covers 16 000 km^2 over NTS map areas 25N, 26C and F (Figure 1). Currently, the publicly available surficial geology mapping is limited to a national-scale map (Fulton, 1995) and detailed mapping of NTS 25N (Hodgson, 2005).

Regional setting

The topography of the area is displayed using digital elevation modelling (DEM; Natural Resources Canada, 2012; Figure 2). The Sylvia Grinnell River valley is at ~100–200 m asl, with steplike ridges raising up to the plateaus toward the southwest (Meta Incognita plateau, up to 500–600 m asl) and north (McKeand River plateau, adjacent to Hall Peninsula plateau). The undulating McKeand River plateau is the culminating elevation of the study area at about 700 m asl (forming part of the Baffin surface [Bird, 1967]) and gently dips to the northwest to about 400 m asl in the northern part of the study area. This plateau is dissected by deep river valleys, and locally displays a well-formed, subdendritic drainage pattern. The northeastern parts of the study area are slightly more rugged than the plateau, at about 300–500 m asl, and the western part of the study area dips to the west toward the west Baffin lowlands and Foxe Basin, at about 100–400 m asl. The study area's local vegetation is typical of the low-arctic tundra, and lies within the continuous permafrost zone. The observed wildlife consists of sparse caribou, fox, weasel, lemming, snow goose, Canada goose, raven, ptarmigan and small birds (i.e., snow bunting, piper).

The geology of the study area is made up of mainly granitoid rocks associated with the middle Paleoproterozoic Cumberland Batholith (Weller et al., 2015; the granitoid is seen on Figure 3a), which contains screens and enclaves of metasedimentary rocks, including quartzite, pelite, marble and greywacke (Lake Harbour and Piling groups affinities). The area has been affected by amphibolite-grade metamorphism and deformation associated with the Trans-Hudson Orogen (Hoffman, 1988). Weller et al. (2015) mention the presence of sulphide-bearing gossans and layered mafic-ultramafic sills that may host sulphide mineralization. In the southeastern part of study area, Paleozoic carbonate rocks (Figure 3b; limestone, dolomitic limestone and organic-rich black shale) overlie the Paleoproterozoic rocks (Zhang, 2012), and are bounded by either fault zones or unconformities between Ordovician and eroded Paleoproterozoic rocks (Figure 3b).

Previous surficial geology studies

There are currently no surficial geology maps for the Sylvia Grinnell Lake area, except for the area of NTS 25N, which was mapped at 1:100 000 scale by Hodgson (2005). Hodgson (2005) and Manley and Miller (2001) have contributed to a renewed synthesis of ice-flow chronology in the southeastern Baffin area, and Utting et al. (2007) drafted the ice-flow chronology for southwest Baffin Island (around Foxe Peninsula). To the east of study area, further improvements to the knowledge base on ice flow and geomorphology have resulted from the studies from CNGO's Hall Peninsula project (Leblanc-Dumas et al., 2014; Tremblay et al., 2015a, b). Numerous surficial geology works have involved southern Baffin Island (Andrews and Sim, 1964; Matthews, 1967; Miller, 1980, 1985; Andrews, 1989; Utting et al., 2007; Briner et al., 2009; Clements et al., 2009; Vickers et al., 2010; Johnson et al., 2012; Tremblay et al., 2015a), but only a few were conducted directly in the study area.

The study area was covered by the Laurentide Ice Sheet during the last glaciation. During the last glacial maximum (LGM), the ice flowed toward Hudson Strait, Frobisher Bay and Cumberland Sound (Andrews, 1989; Manley and Miller, 2001; Hodgson, 2005; De Angelis and Kleman, 2007). The extent of the Frobisher Bay ice flow during LGM is not defined; some studies propose that the ice flow extended all the way from Foxe Basin (De Angelis and Kleman, 2007), and other studies suggest its extent was limited to the vicinity of Frobisher Bay (Andrews, 1989; Manley and Miller, 2001; Hodgson, 2005). Hodgson (2005) suggests that the carbonate content of till matrix (around 7%) north of Frobisher Bay would have been higher if ice flow from Foxe Basin to Frobisher Bay had been sustained during LGM. Comparatively, on Melville Peninsula and Rae Isthmus to the northwest, the carbonate content of till matrix is typically 25–50%, after a glacial transport distance of approximately 100 km over Precambrian rocks (Dredge, 2000b). Field observations between Amadjuak Lake, to the west of the study area, and Sylvia Grinnell Lake could aid in understanding the history of ice flow between Foxe Basin and Frobisher Bay.

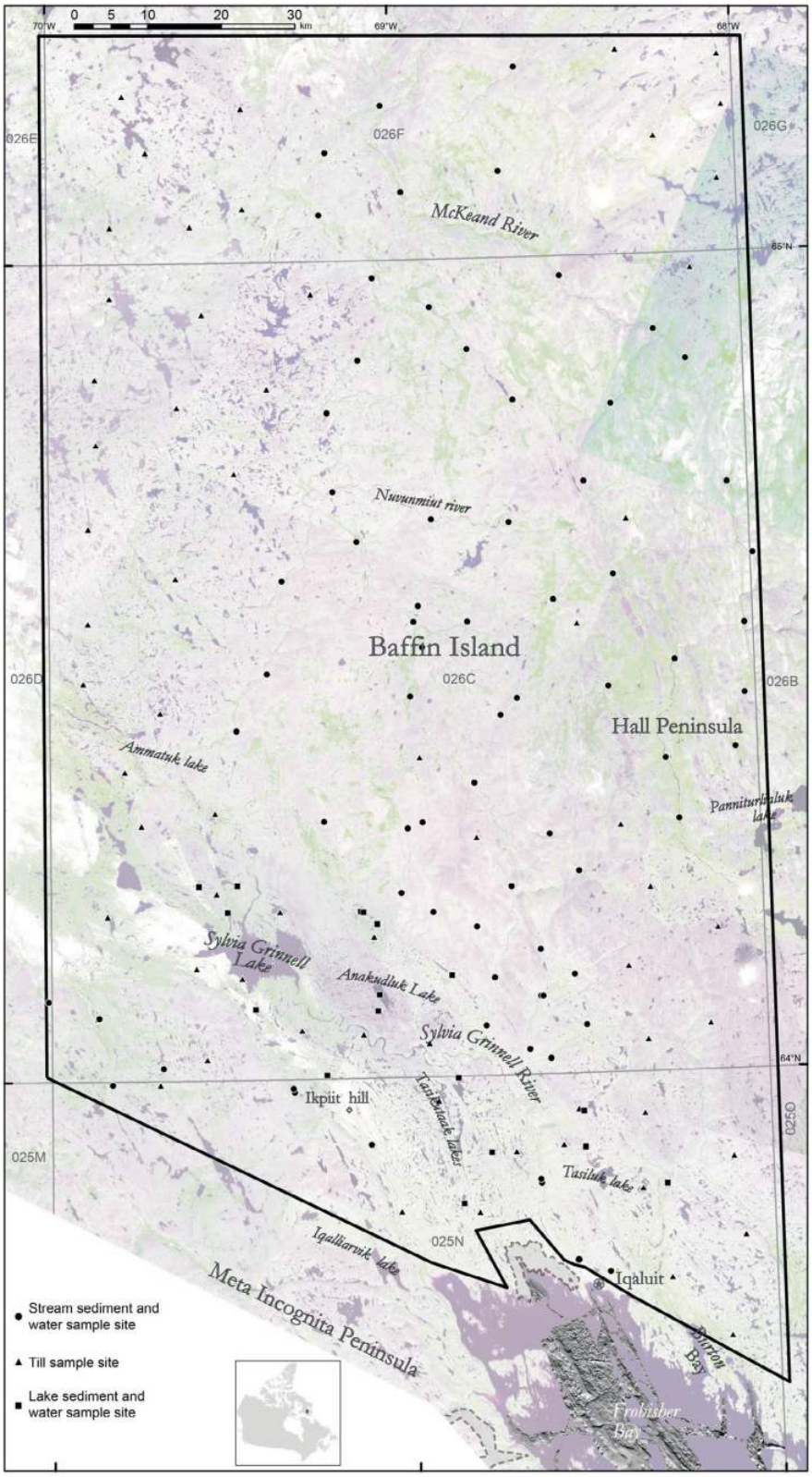

Figure 1: Location map of samples and study area (black outline), Sylvia Grinnell Lake area, Baffin Island, Nunavut. Background imagery is SPOT multispectral (green represents vegetation, pink is boulder diamicton and bedrock, white is vegetation-poor carbonate material and dark grey is water; GeoBase®, 2015). Recently acquired multibeam bathymetric data is shown in Frobisher Bay (Mate et al., 2015; Ocean Mapping Group, 2015). The grey dashed lines delimit the territorial parks, Sylvia Grinnell Park (including Qaummaarviit Park; north of Frobisher Bay) and Katannilik Park (west of Frobisher Bay).

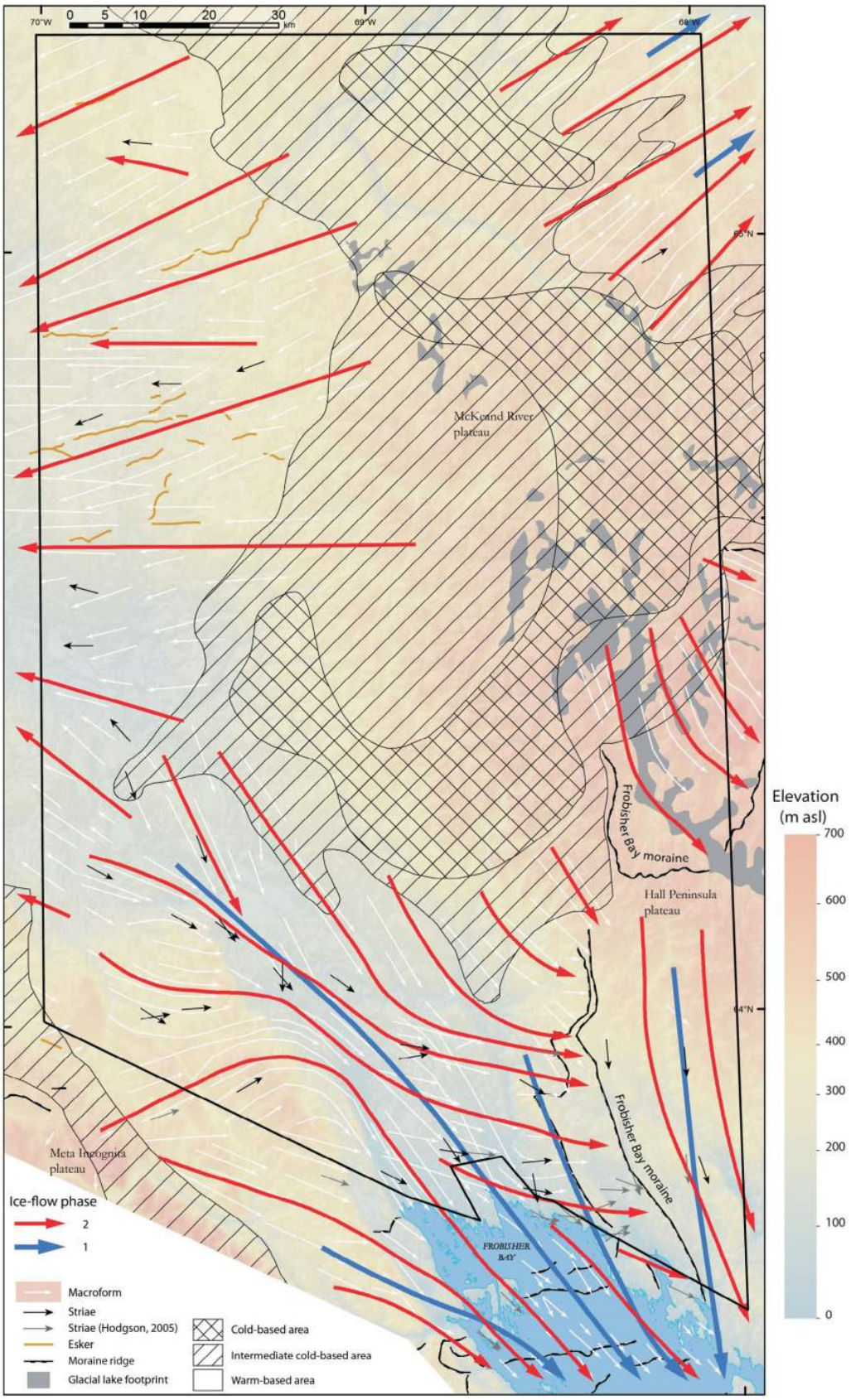

Figure 2: Ice-flow map, with geomorphological features and topographic elevation, Sylvia Grinnell Lake area, Baffin Island, Nunavut. Background image was generated using a CanVec digital elevation model (Natural Resources Canada, 2012).

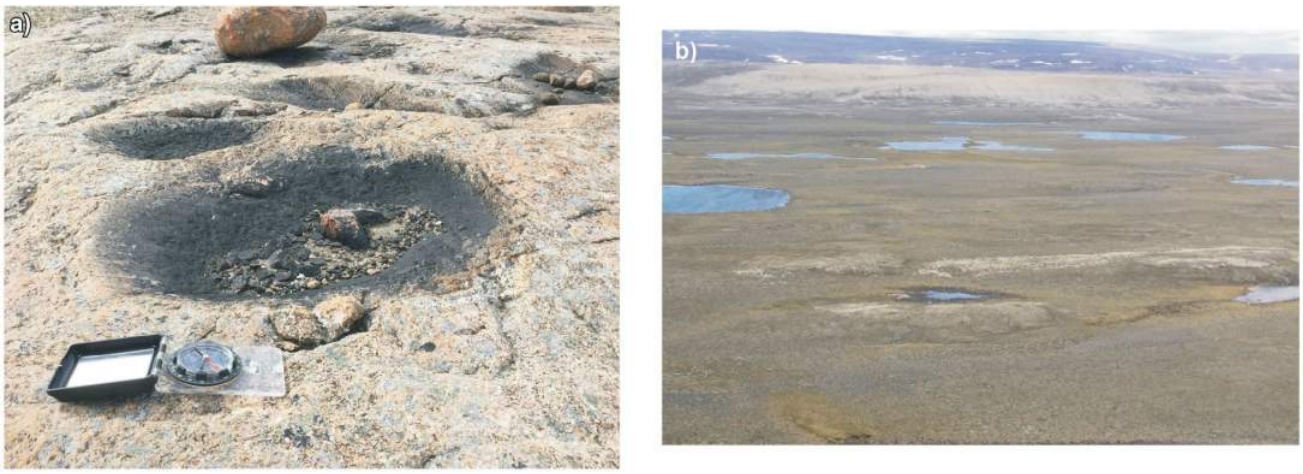

Figure 3: a) Paleoproterozoic granite, exposed at the Ordovician unconformity, showing dissolution pits and black (manganese?) staining, faintly eroded by recent glacial erosion (striae near the compass); **b)** Paleozoic carbonate rocks (background hill), with drumlins and carbonate tills in the foreground, in warm-based glaciodynamic zone.

In Frobisher Bay and Cumberland Sound, ice flows are important as they would have persisted for some time as high-velocity zones of ice flows, or ice streams (Dyke and Morris, 1988; Margold et al., 2015a, b). During deglaciation, an ice stream developed toward Frobisher Bay as evidenced by the ice-flow chronologies and features mapped by numerous authors, including Andrews (1989), Fulton (1995), Manley (1996), Hodgson (2005) and De Angelis and Kleman (2007). The Frobisher Bay moraine (FBM; Figures 2, 4a, b) was deposited around 9 ^{14}C ka (Blake, 1966; Miller, 1980), and the complete deglaciation of Frobisher Bay occurred between 7 and 8 ^{14}C ka (standard Geological Survey of Canada [GSC] dating, uncorrected for marine reservoir effect, all dates below follow this same criteria unless otherwise indicated; Blake, 1966; Dyke et al., 2003; Hodgson, 2005), after the ice retreated from FBM. The decaying ice cap retreated at several terminal positions on the McKeand River plateau where proglacial lakes were dammed in basins (Figure 4d; Miller, 1980; Johnson, 2013; Tremblay et al., 2014, 2015a). The west coast of Baffin Island was deglaciated before 6.8 ^{14}C ka (Blake, 1966; Dyke et al., 2003; Vickers et al., 2010), equivalent to about 6.2 ^{14}C ka with reservoir effect correction (Vickers et al., 2010). The complete deglaciation of the sector is constrained by only one minimum date, 4.5 ^{14}C ka, from a bulk organic sample from a bog deposit near Amadjuak Lake (Blake, 1966), a material subject to reservoir effect frequently older than 1500 yr (Richard et al., 1997; Tremblay, 2008). Prest (1969) suggested that the ice remnants stayed at least until 5.5 ^{14}C ka between Amadjuak Lake and McKeand River.

The southern portion of the study area around Frobisher Bay was inundated by marine waters to levels of 20–40 m asl north of FBM, and 100–120 m asl south of FBM. Glaciomarine deltas are common features at the mouths of rivers in the northern part of Frobisher Bay (Figure 4e; Hodgson, 2005). In the Foxe Basin area, the maximum marine level is 107 m asl (Andrews, 1989; Vickers et al., 2010) but these marine levels were not attained within the study area.

Field methodology

This section presents an overview of the methodology used for geochemical sampling in the study area. Samples were collected from multiple surficial mediums (till, lake sediment, lake water, stream sediment, stream water). Field duplicate samples, laboratory sample splits and certified reference material samples were inserted into the sample populations prior to submission for chemical analyses for the purpose of monitoring, evaluating and ensuring data quality. All samples collected during the 2015 field season have been submitted for sample processing and subsequent mineralogical and geochemical analyses; however, results have not been received yet. Additionally, one sample was collected from marine shells for radiocarbon dating to improve understanding of deglaciation in the study area.

Till sampling

Sixty-six till geochemistry samples (~2 kg) were collected, predominantly in the warm-based glaciodynamic zone, where glacial erosion, transport and depositional processes were most intense (see description below; Figure 2). Inductively coupled plasma–mass spectrometry (ICP-MS) and inductively coupled plasma–emission spectrometry (ICP-ES) will be used to analyze for trace and major elements in the <63 µm till fraction. Fifty-nine till heavy mineral samples (~10 kg) were taken to provide information on kimberlite-indicator minerals (KIMs), base-metal sulphides, platinum, gold, gemstones and other minerals of interest. Spacing between till samples was typically 10–20 km. In addition to till samples, the network of heavy mineral samples was complemented by stream sediment

Figure 4: Aerial field photographs of **a)** Frobisher Bay moraine, with kettles and hummocky till; **b)** Frobisher Bay moraine, with large till ridges separated by elongated lakes; **c)** polygonal soils, typical of till or diamictons in permafrost ground; **d)** glaciolacustrine sediments, including fine-grained sediments (grassy, paler areas in the valley) and glaciolacustrine delta (sandy area in the forefront); **e)** glaciomarine delta by Frobisher Bay; **f)** beaded esker, displaying bulges separated by narrow sections; **g)** glaciofluvial ice-contact terraced sediments, with supraglacial facies, kettles and meltwater channels; **h)** glaciofluvial ice-contact deltaic sediments in glaciolacustrine setting, with kettles; and **i)** glaciofluvial channels on the McKeand River plateau edge.

samples, and collected predominantly in cold-based zones where river networks are well developed and glacial erosion was limited. The Sylvia Grinnell Lake survey is a mixed medium survey, similar to Utting et al. (2008) in the north Baffin Island region, where both till and stream-sediment heavy mineral samples were collected in warm-based and cold-based zones, respectively.

Stream sediment and water sampling

In general, stream sediment and water samples are the preferred sampling media when conducting regional drainage geochemical surveys in areas with a regular network of developed streams (Prior et al., 2009). Stream sediment and water samples collected as part of this study followed the GSC's former National Geochemical Reconnaissance (NGR) program's standards for sample collection and analytical techniques (Friske and Hornbrook, 1991). These standards were used to ensure consistent and reliable results regardless of the area, date of the survey or the analytical laboratory used. Field equipment used and samples collected at a typical bulk stream sediment and water site are illustrated in Figure 5.

Stream sediment and water samples were collected at 76 sites, predominantly from the uplands north of Iqaluit (parts of NTS 25N, 26C, F). Site-specific field observations were recorded at each location. Bulk stream sediment samples were wet sieved on site to obtain ~15 kg of <2 mm sized material from relatively high-energy, gravel-rich sites; these will be processed for heavy mineral contents. Similarly to till samples, the heavy mineral concentrates will be picked to obtain counts for gold grains and platinum group metal (PGM) grains as well as KIMs and metal sulphide-associated minerals. Water samples were collected from the main flowing channel and filtered (0.45 µm) in situ. Chemical analyses of stream waters will involve 67 variables.

Lake sediment and water sampling

In areas of low to moderate topographic relief and abundant lakes, stream networks are typically poorly developed and generally do not provide a suitable sampling media for a broad regional drainage geochemical survey. However, centre-lake sediment and water samples do provide a suitable medium for regional and higher-density geochemical surveys. Seventeen lakes with a surface area smaller than 5 km^2 were targeted and sampled using a torpedo-like grab sampler (routinely used by GSC; Figure 6) for organic-rich lake sediment (gyttia).

After sampling, sediment samples were dried to completion (at <40°C) and sieved to obtain the <177 µm fraction, which was analyzed by 1) aqua-regia digestion followed by ICP-MS analysis, 2) four-acid digestion followed by ICP-MS analysis, and 3) instrumental neutron activation analysis (INAA). Surface water samples (~0.5 m depth) were also collected at each site. Water samples were measured in situ for physical properties (pH, conductivity, dissolved oxygen and redox) and passed through a 0.45 µm filter to be analyzed by ICP-MS, ion chromatography and titration.

Figure 5: a) Field gear used and samples collected at a typical bulk stream sediment and water site: **1)** two 60 ml water samples (filtered with 0.45 µm filter); **2)** YSI Inc. Professional Plus multiparameter water meter; **3)** silt-sized stream sediment sample (~2 kg wet); **4)** #10 mesh (2 mm) sieve; **5)** pan; **6)** steel shovel; **7)** bulk stream sediment sample (>12 kg of ≤2 mm sediment); **8)** bucket lined with prelabelled sample bag (not yet stretched tightly about the bucket opening); and **9)** iPad used for navigation and recording site-specific field observations. **b)** Typical bulk stream sediment and water sampling site.

Figure 6: a) Field gear used for lake sediment and water sampling: **1)** torpedo-like lake sediment sampler, with 30 m rope; **2)** plastic cup for extracting the lake sediment core from the sampler; **3)** cloth bag for sample; **4)** 250 ml sampling bottle–sample is split into two 60 ml water samples (filtered with 0.45 µm filter). Also used for lake sediment and water sampling is the YSI Inc. Professional Plus multiparameter water meter (Figure 5a-2) and the iPad for navigation and recording site-specific field observations (Figure 5a-9). **b)** Helicopter on fixed floats used for lake sediment and water sampling survey.

Chemical analyses of lake sediments and lake waters will yield 90 and 67 variables, respectively.

Microbial water quality indicators

Concentrations of total coliform and *Escherichia coli* (*E. coli,* a subset of coliforms) were measured in surface waters from a subset of sites visited in the 2015 field campaign. These samples will extend the Nunavut Research Institute microbial water quality indicators study already in place around Iqaluit (Apex river watershed). Total coliform and *E. coli* concentrations are used worldwide as indicators of the basic microbial quality of surface waters. The bacteria can be detected rapidly, accurately and with relatively minimal cost and effort. For this project, 11 samples were collected in sterile 120 mL plastic bottles containing a minor quantity of sodium thiosulphate. Water samples for coliform testing were taken immediately after the sediment samples and before any other disturbance to the sample site. Collection bottles were handled with clean nitrile lab gloves to avoid sample contamination. At each site, samples were collected by dipping the sample bottles into the water, just below the surface of the lake or stream sampled. Care was taken to collect samples at a similar depth in an effort to control for variability in the vertical distribution of coliforms in the water column. Following collection, sample bottles were tightly closed and kept as cool as possible for their return to the Nunavut Research Institute lab in Iqaluit.

Upon delivery to the lab, water samples were immediately inoculated with powdered Colilert® reagent (kit from IDEXX Laboratories, Inc.) and incubated for 24 hours at 35°C in heat-sealed disposable 97-well Quanti-Trays®, as per manufacturer's instructions. Total coliform levels were then quantified by enumerating colour change in individual wells of the incubated trays, and *E. coli* levels were quantified based on ultraviolet-fluorescence of the wells. These well counts were then converted to total organism numbers (with 95% confidence) by reference to the most-probable number charts provided by the manufacturer.

Mercury in water

Samples for analysis of mercury in water were collected using a similar methodology as the survey already being undertaken around Iqaluit (Apex river watershed), initiated by the Nunavut Research Institute (NRI) and Carleton University. Prior to disturbance at any sampling site, water samples to test for mercury were collected in 250 mL plastic bottles. These bottles were handled exclusively with clean nitrile lab gloves to avoid contamination and placed in double bags after collection. Thirty-six dip samples were taken from lake or stream water to fill the bottles, after triple rinsing with sample water. Rinse water was discarded away from the dip site (e.g., downstream at stream sites, downwind at lake sites). Stream samples were taken near the water surface, without disturbing the benthos. Lake samples were taken at approximately 30 cm below the water surface. Sample bottles were then kept as cool as possible, in an opaque container to minimize light exposure, for their return to the NRI lab.

As soon as possible upon delivery to the lab, water samples were acidified to 1% by volume with Hg–analytical-grade HCl acid (Optima™, Fisher Chemical), and then refrigerated. These sample bottles were then double-bagged again and shipped in a cooler to Université de Montréal. Total aqueous mercury will be quantified by BrCl oxidation, $SnCl_2$ reduction, two-stage gold amalgamation and gas-phase detection with a Tekran® Instruments Corporation Series 2600 total mercury analyzer with a cold vapour

atomic fluorescence spectrophotometer (CVAFS). Total and/or dissolved methylmercury will be first distilled to remove any matrix interferences and then ethylated with $NaB(C_2H_5)_4$, followed by gas chromatography separation with CVAFS.

Sampling results

Preliminary analytical and mineralogical data will not be available until late 2015, with the complete dataset expected in early 2016. A subsequent publication will contain site-specific field observations, chemical analyses of sediment and water samples, coliform and mercury analysis of water samples, and heavy mineral content data. All results from the sampling will be published in a report following analyses and interpretation of the data.

Preliminary surficial geology results

Surficial geology mapping at a scale of 1:100 000 was undertaken during the summer of 2015 with helicopter support. Field observations, including landforms, surficial cover composition and ice-flow indicators, were compiled using the GSC-developed GanFeld application (Shimamura et al., 2008) and the GSC legend (Cocking et al., 2015). Prior to fieldwork, office-based mapping used an all-digital approach that combined a mosaic of airphotos in an on-screen stereoscopic view and Summit Evolution software (DAT/EM Systems International, 2012). Additionally, the landform mapping processes relied on Landsat (GeoBase®, 2012) and SPOT (GeoBase®, 2015; pan-sharpened to 10 m; Figure 2) satellite imagery and a DEM image (1:50 000 scale) from CanVec data (Natural Resources Canada, 2012). The area covered was approximately 16 000 km^2, of which 14 000 km^2 will be mapped, excluding the previously mapped NTS 25N map area (Hodgson, 2005). Surficial cover composition includes bedrock (Precambrian granitoid rocks and gneiss and Paleozoic carbonate rocks), regolith mixed with till, till (Figure 4a–c), glaciofluvial sediments (Figure 4f–i), glaciolacustrine (Figure 4d) and marine (Figure 4e) sediments, and colluvial and alluvial deposits (Figure 5b). Figure 2 depicts locations of the principal moraines mapped, macroforms (including drumlins, flutings, streamlined glacial features and glacial transport features; Figure 3b), eskers (Figure 4f), striae (new data and from Hodgson, 2005) and glacial lake footprints (Figure 4d, h).

Glaciodynamic zones

Glaciodynamic zone mapping aims to interpret the amount of glacial activity (erosion and transport) that took place during the Quaternary period (Figure 2). A methodology for this mapping was developed after work on Hall Peninsula (Johnson, 2013; Leblanc-Dumas et al., 2015; Tremblay et al., 2015a), and includes procedures from the central Canadian Arctic (Dyke, 1993), Melville Peninsula (Dredge, 2000a; Tremblay and Paulen, 2012) and Baffin Island (Sugden and Watts, 1977; Andrews et al., 1985).

The geomorphological indicators of glacial erosion are summarized as broad classifications of terrain types. The interpretations resulting from this study are based on numerous field observations and interpretation of DEM work, satellite imagery and airphotos. For instance, glacial scouring, as evident from the presence of numerous small lakes and glacially eroded outcrop, is interpreted to represent erosive basal conditions (warm-based ice, Figure 7a). Alternatively, the existence of a mix of thick nonglacial regolith, felsenmeer and till would suggest little or no sliding to have occurred at the glacier bed, and therefore, was covered predominantly by weakly erosive cold-based ice (Figure 7c). The dynamic character of the former ice sheet (cold- versus warm-based) can be inferred from these interpretations and classifications, and can therefore help to understand and outline the nature of glacial transport. The intermediate cold-based zones are interpreted to be areas where glacial erosion gradually became more marked as evidenced by more lakes and bedrock outcrops, and ultimately with the appearance of streamlined outcrops and macroforms (Figure 7b). Cosmogenic samples (Ross et al., 2015) and mineralogical data (Leblanc-Dumas et al., 2015) emphasize the distinction between till from glacially eroded terrain, and regolith and till mixed with regolith in less glacially eroded terrain (Tremblay et al., 2015a). Coverage by cold-based ice sheets during the Quaternary is indicated by locally abundant glaciofluvial channels (Figure 4i) and occasional glacial erratics. Of particular importance, accumulations of glaciofluvial sediments occur across the glaciodynamic boundaries on the southern part of the McKeand River plateau.

Ice-flow chronology

Ice-flow directions and chronology are established using existing geochronological data: striae, glacial landforms and glacial sedimentology (Figure 2). Different phases of ice flow were observed in the field by crosscutting relationships between striae. Interpretation of this ice-flow history is, in part, based on numerous scientific contributions (Prest, 1969; Andrews, 1989; Manley and Miller, 2001; Dyke et al., 2003; Hodgson, 2005; De Angelis and Kleman, 2007; Johnson, 2013; Tremblay et al., 2015a). In this next section, the notion of cold-based ice flow can refer to a momentary physical state of the glacier, occurring over areas described as cold-based, intermediate cold-based and warm-based zones (Figure 2).

Ice-flow phase 1 (marine terminus)

Ice-flow phase 1 involved two important glacial ice outlets that existed during LGM in Baffin Bay, Frobisher Bay (convergent ice flow to the southeast) and Cumberland Sound (northwest ice flow). In Foxe Basin, an ice divide

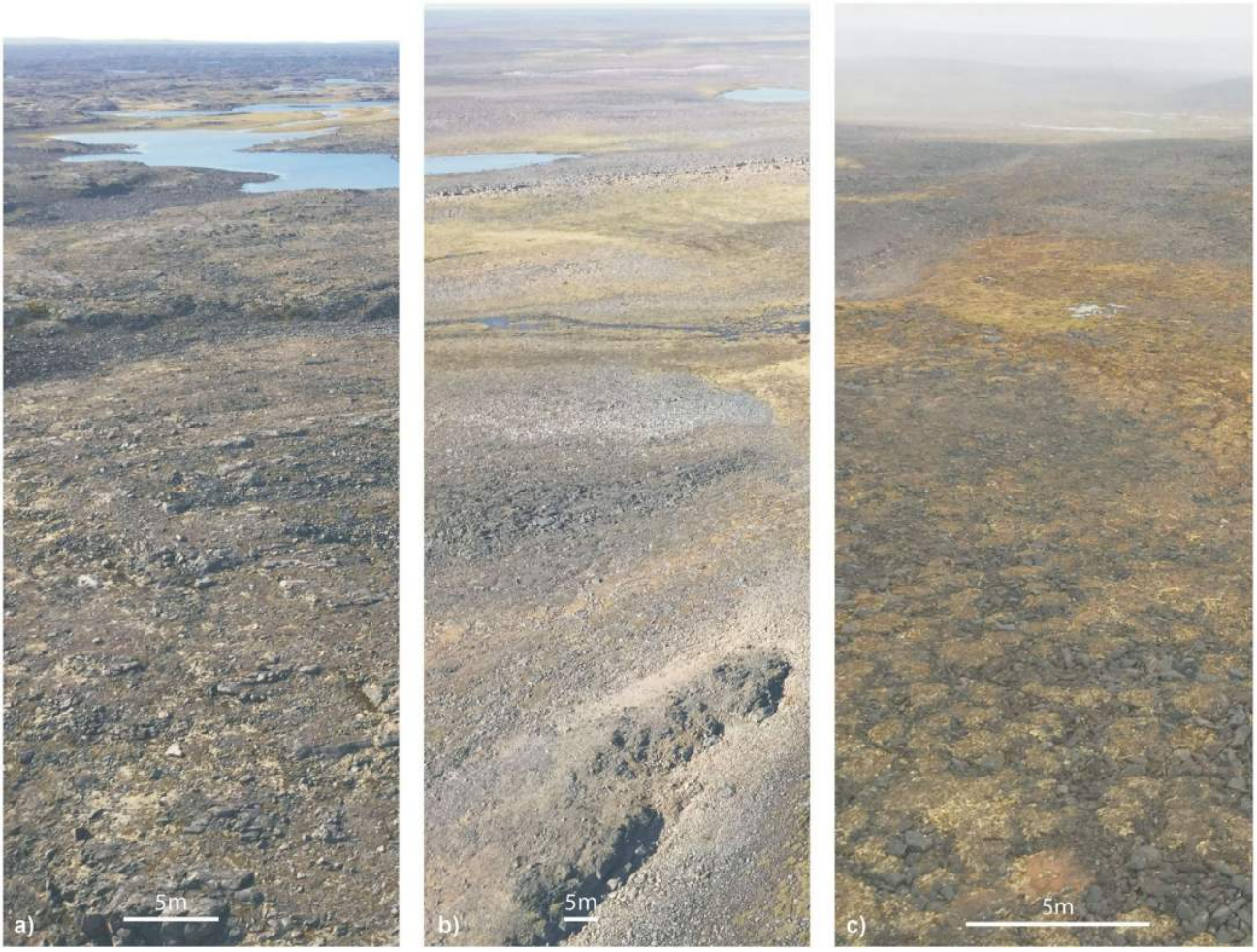

Figure 7: Aerial oblique photographs of **a)** warm-based–zone terrain; **b)** intermediate cold-based–zone terrain; and **c)** cold-based–zone terrain.

was present over the west and central part of study area during LGM (Manley and Miller, 2001; Hodgson, 2005; Utting et al., 2007). Therefore, the ice flow over the west (Amadjuak ice divide), southwest (Meta Incognita ice divide) and central part of study area (Hall Peninsula ice divide) was considered to be briefly cold-based during LGM. The absence of a significant carbonate till dispersal train in the Sylvia Grinnell River valley (Hodgson, 2005), one which is comparable in magnitude to the one on Melville Peninsula, and the presence of intermediate cold-based–zone terrain in the middle portion of the valley between Sylvia Grinnell Lake and Amadjuak Lake, confirm that no strong ice flow from Foxe Basin or Amadjuak Lake area occurred during LGM or at any time during deglaciation. A Frobisher Bay catchment area extending into Foxe Basin, as was suggested in De Angelis and Kleman (2007), is therefore unlikely. A regional glaciological model (Kaplan et al., 1999) illustrates how ice from a cold-based glacier in Foxe Basin (Foxe ice divide) flowed to Cumberland Sound and southwest Baffin Island (south of Amadjuak Lake, as indicated by Utting et al. [2007]) rather than to Frobisher Bay during LGM.

Ice-flow phase 2 (terrestrial terminus)

During early deglaciation, ice streams intensified toward Frobisher Bay and Cumberland Sound as the ice margin approached Baffin Island from a former position in Baffin Bay and Davis Strait (Kaplan et al., 1999; Dyke et al., 2003; Hodgson, 2005). Consequently, the drainage area of the ice streams likely expanded over previously cold-based ice on the McKeand River plateau, the Sylvia Grinnell River valley and Meta Incognita Peninsula. Gradually, as the Hudson Strait ice stream developed and the ice front retreated into Hudson Strait, the Amadjuak River valley ice flow became warm-based and westward ice flow developed toward Foxe Basin, and consequently the Amadjuak ice divide receded northward. In Frobisher Bay, the ice front receded to the FBM position (circa 9.0 ^{14}C ka), and ice flow switched from a convergent pattern to a divergent pattern. This change in pattern is presumed to relate to a significant reduction in output of icebergs at the ice margin as: a) the

Frobisher Bay narrowed as the ice front receded northwest, and therefore the width of the ice shelf was reduced; b) islands in the central part of Frobisher Bay blocked the evacuation of icebergs and obstructed the ice discharge of the ice front; and c) the marine ice shelf became grounded at FBM and this resulted in the formation of significant swaths of moraine ridges in Frobisher Bay (Figures 1, 2; as observed on the multibeam bathymetric map described in Mate et al., 2015). The divergent pattern of ice flow likely extended to the central part of the Hall Peninsula referred to as the Hall Peninsula plateau segment of FBM. However, as seen on Figure 2, FBM is discontinuous between Frobisher Bay and the Hall Peninsula plateau, and no geochronological data exists to support any synchronicity between the FBM segments in Frobisher Bay and on the Hall Peninsula plateau. Proglacial lakes were formed as the ice front retreated against the topographic slope; notably, well-developed proglacial lakes were developed against the FBM position. Circa 7 ^{14}C ka, the ice progressively retreated from Frobisher Bay and Foxe Basin, and subsequent deglaciation of the highlands, suggested to occur after 5.5 ^{14}C ka, occurred progressively (Blake, 1966; Prest, 1969).

Economic considerations

The results and interpretation of this surficial geological mapping and sampling program can be used for mineral exploration, development of natural resources and infrastructure, and aid environmental geochemical studies in the study area—around Nunavut's capital city. Analysis of the geochemical and mineralogical data from the surficial sediment samples will explore the potential regional mineral prospect for diamonds, base metals (copper, nickel, zinc), precious metals (gold, silver, platinum, palladium), rare-earth elements and gemstones. Understanding ice-flow direction and important geomorphological processes (displayed on maps and illustrated in photos) are critical to interpreting the geochemical analyses of and mineralogical data from surficial sediments. The analytical data and mapping outcomes of this project will provide important baseline data for future mineral exploration and possible development in the area, as well as for infrastructure studies (permafrost conditions, granular aggregate sources).

Conclusions

Samples of till, stream sediment, lake sediment, stream water and lake water were collected during the summer of 2015 and analytical results are anticipated in early 2016. Field observations of surficial sediments and geomorphological features (glacial macroforms, proglacial lakes, eskers) were documented, and will support the compilation and drafting of new 1:100 000 surficial geology maps for the study area (excluding NTS 25N, which has already been mapped). The glaciodynamic settings were mapped as cold-based, intermediate cold-based and warm-based zones from both field observations and remote sensing work.

The ice-flow history is divided into two broad phases; phase 1 occurred during the last glacial maximum when Frobisher Bay and Cumberland Sound ice streams were active, and phase 2 took place during deglaciation. In phase 2, the Frobisher Bay and Cumberland Sound ice streams intensified, the Frobisher Bay moraine was established, and ultimately the ice front receded over the McKeand River plateau. The presence of weakly glacially eroded areas (intermediate cold-based zone) between Sylvia Grinnell Lake and Amadjuak Lake does not support the hypothesis that warm-based ice flowed from Foxe Basin directly toward Frobisher Bay during the last glaciation.

Acknowledgments

The Sylvia Grinnell Lake area project is a collaborative undertaking between the Canada-Nunavut Geoscience Office (CNGO), the Geological Survey of Canada (Geo-mapping for Energy and Minerals program [GEM]), Nunavut Research Institute and Carleton University. Funding has been provided by the Canadian Northern Economic Development Agency (CanNor) under the Strategic Investments in Northern Economic Development funding delivered through the Government of Nunavut to CNGO. Polar Continental Shelf Project is thanked for logistical support. Universal Helicopters pilots S. Sande and K. Cashin provided safe and productive flying. Logistical aspects of fieldwork were collaborated on with N. Rayner and M. St-Onge, both from the Geological Survey of Canada and associated with GEM projects. The authors wish to thank Nunavut Research Institute for access to laboratory space and dedicated collaboration with the laboratory staff (J. Peters and students G. Chiasson Poirier and A. Kilabuk). Government of Nunavut, Department of Environment, Fisheries and Sealing division are thanked for sharing summer student M. Kendall with the CNGO during summer 2015. The authors thank D. Mate (CanNor), R. Paulen (GSC) and L. Ham (CNGO) for reviewing this paper.

Natural Resources Canada, Earth Sciences Sector contribution 20150338

References

Andrews, J.T. 1989: Quaternary geology of the northeastern Canadian Shield; *in* Chapter 3, Quaternary Geology of Canada and Greenland, R.J. Fulton (ed.), Geological Survey of Canada, Geology of Canada, no. 1, p. 276–317.

Andrews, J.T. and Sim, V.W. 1964: Examination of the carbonate content of drift in the area of Foxe Basin; Geographical Bulletin, v. 21, p. 44–53.

Andrews, J.T., Clark, P. and Stravers, J. 1985: The pattern of glacial erosion across the eastern Canadian Arctic; *in* Quaternary Environments: Eastern Canadian Arctic, Baffin Bay

and West Greenland, J.T. Andrews (ed.), Allen and Unwin, Winchester, Massachusetts, p. 69–92.

Bird, J.B. 1967: The Physiography of Arctic Canada; Johns Hopkins Press, Baltimore, Maryland, 336 p.

Blake, W.J. Jr. 1966: End moraines and deglaciation chronology in northern Canada with special reference to southern Baffin Island; Geological Survey of Canada, Paper 66-26, 31 p., 1 map, scale 1:2 000 000.

Briner, J.P., Davis, P.T. and Miller, G.H. 2009: Latest Pleistocene and Holocene glaciation of Baffin Island, Arctic Canada: key patterns and chronologies; Quaternary Science Reviews, v. 28, p. 2075–2087.

Clements, B., Pell, J., Holmes, P. and Grenon, H. 2009: Following kimberlite indicator minerals to Chidliak, Baffin Island: Canada's newest diamond district; *in* Workshop B: Indicator Mineral Methods in Mineral Exploration, 24th International Applied Geochemistry Symposium, May 31, 2009, Fredericton, New Brunswick, p. 83–88.

Cocking, R.B., Deblonde, C., Kerr, D.E., Campbell, J.E., Eagles, S., Everett, D., Huntley, D.H., Inglis, E., Laviolette, A., Parent, M., Plouffe, A., Robertson, L., St-Onge, D.A. and Weatherston, A. 2015: Surficial data model, version 2.1.0: revisions to the science language of the integrated Geological Survey of Canada data model for surficial geology maps; Geological Survey of Canada, Open File 7741, 276 p.

DAT/EM Systems International 2012: Summit Evolution software suite; software, DAT/EM Systems International, Anchorage, Alaska.

De Angelis, H. and Kleman, J. 2007: Palaeo-ice streams in the Foxe/Baffin sector of the Laurentide Ice Sheet; Quaternary Science Reviews, v. 26, p. 1313–1331.

Dredge, L.A. 2000a: Age and origin of upland block fields on Melville Peninsula, eastern Canadian Arctic; Geografiska Annaler, v. 82, no. 4, p. 443–454.

Dredge, L.A. 2000b: Carbonate dispersal trains, secondary till plumes, and ice streams in the west Foxe Sector, Laurentide Ice Sheet; Boreas, v. 29, no. 2, p. 144–156.

Dyke, A.S. 1993: Landscapes of cold-centred Late Wisconsinan ice caps, Arctic Canada; Progress in Physical Geography, v. 17, no. 2, p. 223–247.

Dyke, A.S. and Morris, T.F. 1988: Drumlin fields, dispersal trains, and ice streams in Arctic Canada; The Canadian Geographer/Le Géographe canadien, v. 32, no. 1, p. 86–90.

Dyke, A.S., Moore, A. and Robertson, L. 2003: Deglaciation of North America; Geological Survey of Canada, Ottawa, Open File 1574, 2 sheets, 1 CD-ROM.

Friske, P.W.B. and Hornbrook, E.H.W. 1991: Canada's National Geochemical Reconnaissance programme; Applied Earth Sciences, Transactions of the Institution of Mining and Metallurgy, Section B, v. 100, p. B47–B56.

Fulton, R.J. 1995: Surficial materials of Canada/Matériaux superficiels du Canada; Geological Survey of Canada, "A" Series Map 1880A, scale 1:5 000 000.

GeoBase® 2012: Landsat 7 orthorectified imagery over Canada (1999–2003); Natural Resources Canada, URL <http://geogratis.gc.ca/api/en/nrcan-rncan/ess-sst/-/%28urn:iso:series%29canimage-landsat-7-orthoimages-of-canada-150-000?sort-field=relevance> [May 2012].

GeoBase® 2015: GeoBase orthoimage 2005–2010; Natural Resources Canada, URL <http://geogratis.gc.ca/api/en/nrcan-rncan/ess-sst/?q=geobase+orthoimage+nunavut+spot&sort-field=relevance> [August 2015].

Hodgson, D.A. 2005: Quaternary geology of western Meta Incognita Peninsula and Iqaluit area, Baffin Island, Nunavut; Geological Survey of Canada, Bulletin 582, 74 p., 1 CD-ROM.

Hoffman, P.F. 1988: United Plates of America, the birth of a craton: Early Proterozoic assembly and growth of Laurentia; Annual Reviews of Earth and Planetary Sciences, v. 16, p. 543–603.

Johnson, C. 2013: Fingerprinting glacial processes for diamond exploration on Hall Peninsula, Baffin Island; M.Sc. thesis, University of Waterloo, Waterloo, Ontario, 188 p.

Johnson, C., Ross, M. and Tremblay, T. 2012: Glacial geomorphology of north-central Hall Peninsula, southern Baffin Island; Geological Survey of Canada, Open File 7413, 57 p.

Kaplan, M.R., Pfeffer, W.T., Sassolas, C. and Miller, G.H. 1999: Numerical modelling of the Laurentide Ice Sheet in the Baffin Island region: the role of a Cumberland Sound ice stream; Canadian Journal of Earth Sciences, v. 36, p. 1315–1326.

Leblanc-Dumas, J., Allard, M. and Tremblay, T. 2014: Pre or interglacial regolith persistence under non-erosive ice during last glacial maximum in central Hall Peninsula, Baffin Island, Nunavut, Canada; Geological Association of Canada/Mineralogical Association of Canada, Joint Annual Meeting, Program with Abstracts, v. 37, conference CD.

Leblanc-Dumas, J., Allard, M. and Tremblay, T. 2015: Characteristics of a preglacial or interglacial regolith preserved under nonerosive ice during the last glacial maximum in central Hall Peninsula, southern Baffin Island, Nunavut; *in* Summary of Activities 2014, Canada-Nunavut Geoscience Office, p. 69–78.

Manley, W.F. 1996: Late-glacial flow patterns, deglaciation, and postglacial emergence of south-central Baffin Island and the north-central coast of Hudson Strait, eastern Canadian Arctic; Canadian Journal of Earth Sciences, v. 33, p. 1499–1510.

Manley, W.F. and Miller, G.H. 2001: Glacial-geological record on southern Bafin Island reflecting late glacial ice-sheet dynamics in the eastern Hudson Strait region; *in* Marine Geology of Hudson Strait and Ungava Bay, Eastern Arctic Canada: Late Quaternary Sediments, Depositional Environments, and Late Glacial-Deglacial History Derived from Marine and Terrestrial Studies, B. Maclean (ed.), Geological Survey of Canada, Bulletin 566, p. 19–30.

Margold, M., Stokes, C.R. and Clark, C.D. 2015a: Ice streams in the Laurentide Ice Sheet: identification, characteristics and comparison to modern ice sheets; Earth Science Reviews, v. 143, p. 117–146.

Margold, M., Stokes, C.R., Clark, C.D. and Kleman, J. 2015b: Ice streams in the Laurentide Ice Sheet: a new mapping inventory; Journal of Maps, v. 11, no. 3, p. 380–395, doi:10.1080/17445647.2014.912036

Mate, D.J., Campbell, D.C., Barrie, J.V., Hughes Clarke, J.E., Muggah, J., Bell, T. and Forbes, D.L. 2015: Integrated seabed mapping of Frobisher Bay, southern Baffin Island, Nunavut to support infrastructure development, exploration and natural-hazard assessment; *in* Summary of Activities 2014, Canada-Nunavut Geoscience Office, p. 145–152.

Matthews, B. 1967: Late Quaternary marine fossils from Frobisher Bay (Baffin Island, N.W.T., Canada); Palaeogeography, Palaeoclimatology, Palaeoecology, v. 3, p. 243–263.

Miller, G.H. 1980: Late Foxe glaciation of southern Baffin Island, N.W.T., Canada; Geological Society of America Bulletin, v. 91, no. 7, p. 399–405.

Miller, G.H. 1985: Moraines and proglacial lake shorelines, Hall Peninsula, Baffin Island; *in* Quaternary Environments, Eastern Canadian Arctic, Baffin Bay, and Western Greenland, J.T. Andrews (ed.), Allen & Unwin, Boston, Massachusetts, p. 546–557.

Natural Resources Canada 2012: CanVec, topographic reference digital product; Natural Resources Canada, Topographic Information Centre, Sherbrooke, Quebec.

Ocean Mapping Group 2015: Multibeam bathymetric data; University of New Brunswick, URL <http://www.omg.unb.ca/Projects/Arctic/> [September 2015].

Prest, V.K. 1969: Retreat of Wisconsin and recent ice in North America; Geological Survey of Canada, "A" Series Map 1257A, scale 1:5 000 000.

Prior, G.J., McCurdy, M.W. and Friske, P.W.B. 2009: Stream sediment sampling for kimberlite indicator minerals in the Western Canada Sedimentary Basin: the Buffalo Head Hills survey, north-central Alberta; *in* Application of Till and Stream Sediment Heavy Mineral and Geochemical Methods to Mineral Exploration in Western and Northern Canada, R.C. Paulen and I. McMartin (ed.), Geological Association of Canada, Short Course Notes 18, p. 111–124.

Richard, P.J.H., Veillette, J.J., Larouche, A.C., Hétu, B., Gray, J.T. and Gangloff, P. 1997: Chronologie de la déglaciation en Gaspésie: nouvelles données et implications; Géographie physique et Quaternaire, v. 51, p. 163–184.

Ross, M., Johnson, C.L., Gosse, J.C., Tremblay, T., Hodder, T.J., Grunsky, E.C. and Pell, J. 2015: Detrital cosmogenic ^{10}Be of till from contrasting landscapes on Hall Peninsula, Baffin Island; Geological Society of America, Abstracts with Programs, v. 47, no. 3, p. 63.

Shimamura, K., Williams, S.P. and Buller, G. 2008: GanFeld user guide: a map-based field data capture system for geologists; Geological Survey of Canada, Open File 5912, 90 p.

Sugden, D.E. and Watts, S.H. 1977: Tors, felsenmeer, and glaciation in northern Cumberland Peninsula, Baffin Island; Canadian Journal of Earth Sciences, v. 14, p. 2817–2823.

Tremblay, T. 2008: Hydrostratigraphie et géologie du Quaternaire dans le bassin-versant de la rivière Châteauguay, Québec; M.Sc. thesis, Université du Québec, Montréal, Quebec, 224 p.

Tremblay, T. and Paulen, R. 2012: Glacial geomorphology and till geochemistry of central Melville Peninsula, Nunavut; Geological Survey of Canada, Open File 7115, 47 p.

Tremblay, T., Leblanc-Dumas, J. and Allard, M. 2015a: Geochemistry, mineralogy and sedimentology of surficial sediments, Hall Peninsula, southern Baffin Island, Nunavut; *in* Summary of Activities 2014, Canada-Nunavut Geoscience Office, p. 57–58.

Tremblay, T., Leblanc-Dumas, J. and Allard, M. 2015b: Surficial geology, Chidliak Bay, Baffin Island, Nunavut, NTS 26B; Geological Survey of Canada, Canadian Geoscience Map 222 (preliminary) and Canada-Nunavut Geoscience Office, Open File Map 2015-01, scale 1:125 000, doi:10.4095/296407

Tremblay, T., Leblanc-Dumas, J., Allard, M., Ross, M.A. and Johnson, C. 2014: Surficial geology of central Hall Peninsula, Baffin Island, Nunavut: summary of the 2013 field season; *in* Summary of Activities 2013, Canada-Nunavut Geoscience Office, p. 103–114.

Utting, D.J., Gosse, J.C., Hodgson, D.A., Trommelen, M.S., Vickers, K.J., Kelley, S.E. and Ward, B. 2007: Report on ice-flow history, deglacial chronology, and surficial geology, Foxe Peninsula, southwest Baffin Island, Nunavut; Geological Survey of Canada, Current Research 2007-C2, 13 p.

Utting, D.J., Little, E.C., Young, M.D., McCurdy, M.W., Dyke, A.S. and Girard, I. 2008: Till, stream-sediment and bedrock analyses, north Baffin Island, Nunavut (NTS 37E, F, G, H and 47E); Geological Survey of Canada, Open File 5742, 1 CD-ROM.

Vickers, K.J., Ward, B.C., Utting, D.J. and Telka, A.M. 2010: Deglacial reservoir age and implications, Foxe Peninsula, Baffin Island; Journal of Quaternary Research, v. 25, no. 8, p. 1338–1346.

Weller, O.M., Dyck, B.J., St-Onge, M.R., Rayner, N.M. and Tschirhart, V. 2015: Completing the bedrock mapping of southern Baffin Island, Nunavut: plutonic suites and regional stratigraphy; *in* Summary of Activities 2015, Canada-Nunavut Geoscience Office, p. 33–48.

Zhang, S. 2012: Ordovician stratigraphy and petroleum potential of the Hudson Bay and Foxe basins, Nunavut; Geological Survey of Canada, Open File 7199, 25 p.

Overview of bedrock mapping and results from portable X-ray fluorescence spectrometry in the eastern part of the Tehery Lake–Wager Bay area, western Hudson Bay, Nunavut

H.M. Steenkamp[1], N. Wodicka[2], C.J.M. Lawley[2], T.D. Peterson[2] and C. Guilmette[3]

[1]*Canada-Nunavut Geoscience Office, Iqaluit, Nunavut, holly.steenkamp@canada.ca*

[2]*Natural Resources Canada, Geological Survey of Canada, Ottawa, Ontario*

[3]*Université Laval, Québec, Quebec*

This work is part of the Tehery-Wager geoscience mapping activity of Natural Resources Canada's (NRCan) Geo-mapping for Energy and Minerals (GEM) Program Rae project, a multidisciplinary and collaborative effort being led by the Geological Survey of Canada and the Canada-Nunavut Geoscience Office (CNGO), with participants from Nunavut Arctic College and Canadian universities (Dalhousie University, Université du Québec à Montréal, Université Laval, University of New Brunswick and University of Victoria). The focus is on targeted bedrock geology mapping, surficial geology studies, surface and stream sediment sampling, and other thematic studies, which collectively will increase the level of geological knowledge in this frontier area and allow evaluation of the potential for a variety of commodities, including diamonds and other gemstones, base and precious metals, industrial minerals, carving stone and aggregates. This activity also aims to assist northerners by providing geoscience training to college students, and by ensuring that the new geoscience information is accessible for making land-use decisions in the future.

Steenkamp, H.M., Wodicka, N., Lawley, C.J.M., Peterson, T.D. and Guilmette, C. 2015: Overview of bedrock mapping and results from portable X-ray fluorescence spectrometry in the eastern part of the Tehery Lake–Wager Bay area, western Hudson Bay, Nunavut; *in* Summary of Activities 2015, Canada-Nunavut Geoscience Office, p. 121–134.

Abstract

The Tehery-Wager geoscience mapping activity is a four-year initiative conducted by the Geological Survey of Canada and the Canada-Nunavut Geoscience Office. The project aims to gather new geoscience knowledge to create modern bedrock and surficial geological maps, evaluate the economic potential in the area and characterize the tectonic, magmatic, depositional and metamorphic history of the rock units therein. The first of two field seasons of bedrock geological mapping in the Tehery Lake–Wager Bay area, north of Chesterfield Inlet, Nunavut in 2015 focused on better documentation and characterization of rock types and features across the eastern part of the study area. Major lithological units include Archean tonalite to granodiorite gneiss, monzogranite to syenogranite gneiss, K-feldspar–phyric monzogranite (likely correlative with the 2.6 Ga Snow Island suite), presumed Proterozoic supracrustal rocks, undeformed monzogranite to syenogranite (likely correlative with the 1.85–1.81 Ga Hudson suite) and roughly coeval ultrapotassic clinopyroxenite to syenite intrusions. Portable X-Ray fluorescence (pXRF) spectrometry analyses of mafic to intermediate orthogneiss, and amphibolite layers in the tonalite to granodiorite orthogneiss and metasedimentary panels, were collected in the field. The interpreted data suggest that the rocks have diverse, variably metasomatized basaltic to andesitic compositions. Least altered samples range from primitive and mantle-like to more evolved compositions that, coupled with diverging multi-element patterns, point to multiple, chemically distinct subpopulations within the basaltic sample suite. The preliminary results highlight the advantage of in situ, real-time and nondestructive pXRF measurements as a chemostratigraphic tool that can be used in the field to support bedrock mapping.

Résumé

Les travaux de cartographie géoscientifique Tehery-Wager, une initiative menée conjointement par la Commission géologique du Canada et le Bureau géoscientifique Canada-Nunavut, doivent s'échelonner sur quatre ans. Ils ont pour objet d'acquérir de nouvelles connaissances de nature géoscientifique dans le but de permettre la réalisation de cartes géologiques modernes de la surface et du substratum rocheux, l'évaluation du potentiel économique de la région et la caractérisation des antécédents tectoniques, magmatiques, sédimentaires et métamorphiques des unités lithologiques qu'elle renferme. Des deux campagnes de terrain prévues, la première a eu lieu en 2015 dans la région du lac Tehery et de la baie Wager, au nord de Chesterfield Inlet, au Nunavut, et a porté sur la cartographie du substratum rocheux, en mettant plus particulièrement l'accent sur la façon de mieux documenter et caractériser les types et les propriétés des roches dans

This publication is also available, free of charge, as colour digital files in Adobe Acrobat® PDF format from the Canada-Nunavut Geoscience Office website: http://cngo.ca/summary-of-activities/2015/.

l'ensemble de la partie orientale de la région à l'étude. On compte au nombre des unités lithologiques importantes un gneiss de composition tonalitique à granodioritique de l'Archéen, un gneiss de composition monzogranitique à syénogranitique, un monzogranite porphyritique à feldspath potassique (qui peut possiblement être mis en corrélation avec la suite de Snow Island datée à 2,6 Ga), des roches supracrustales présumément d'âge protérozoïque, une unité non déformée dont la composition varie du monzogranite au granite syénitique (qui peut possiblement être mise en corrélation avec la suite de Hudson datant de 1,85 à 1,81 Ga) ainsi que des intrusions ultrapotassiques plus ou moins contemporaines, dont la composition varie de la clinopyroxénite à la syénite. À l'aide d'appareils portatifs de fluorescence à rayons X, on a pu effectuer sur le terrain des analyses spectrométriques de l'orthogneiss de composition mafique à intermédiaire ainsi que des couches d'amphibolite dans les panneaux de roches métasédimentaires et dans l'orthogneiss tonalitique à granodioritique. Les données recueillies semblent indiquer que la composition des roches, plus ou moins métasomatisées, varie de basaltique à andésitique. La composition des échantillons les moins altérés, qui varie de phases minérales d'un type soit primitif, soit mantellique, à un type plus évolué, associée aux configurations en éventail formés par plusieurs éléments indique la présence de nombreuses sous-populations à caractère chimique distinct au sein de la série d'échantillons basaltiques. Les résultats préliminaires témoignent du fait que des mesures non destructives prises sur place et en temps réel à l'aide d'instruments portatifs de fluorescence X s'avèrent un outil chimiostratigraphique avantageux qui peut servir à la réalisation sur le terrain de travaux de cartographie du substratum rocheux.

Introduction

In 2012, the Geological Survey of Canada (GSC) led a two-week reconnaissance survey in the Tehery Lake–Wager Bay study area to evaluate the need for a future, higher resolution mapping campaign in this region. Given the interesting field observations and analytical results from this survey (Day et al., 2013; McMartin et al., 2013), plus the generally insufficient geoscience knowledge in this region, a comprehensive geoscience-mapping project was deemed necessary and a high priority by the GEM-2 program leaders for the Tehery Lake–Wager Bay area.

The current Tehery-Wager geoscience mapping activity is a four-year initiative conducted by the GSC and the Canada-Nunavut Geoscience Office (CNGO) under the GEM-2 program (see also Wodicka et al., 2015). This project aims to increase the level of geoscience knowledge in the area through targeted bedrock and surficial geology mapping and sampling, as well as regional and focused thematic studies. Data and information collected during this project will be used to 1) produce new bedrock and surficial geological maps (1:100 000 Canada Geoscience Maps) for all or parts of eight National Topographic System (NTS) map areas (46E, D, 56A, B, C, F, G, H); 2) characterize and constrain the geological and metamorphic histories of major rock units in the area; 3) provide glacial and postglacial histories and re-evaluate the dispersal and weathering of surficial deposits in the area; and 4) identify locations and lithostratigraphy that may have potential for economic materials, such as base and precious metals, industrial minerals, carving stone, gemstones or aggregate, through bedrock mapping and till and stream–sediment/water surveys.

This paper provides a summary of the initial bedrock-geology findings from the 2015 field season. Presented herein are a simplified geology map, descriptions of field relationships and characteristics of the dominant lithological units, portable X-ray fluorescence (pXRF) data collected in the field for selected rock types and a discussion of areas with economic potential in the eastern part of the Tehery Lake–Wager Bay area.

The study area is approximately 45 000 km^2 and is located on the northwestern coast of Hudson Bay, in the Kivalliq Region of Nunavut (Figure 1). It includes the land south of latitude 65°50'N and the Ukkusiksalik National Park boundary to latitude 64°N, and extends west from the coastline of Roes Welcome Sound to longitude 93°W. Helicopter-supported fieldwork took place between June 30th and August 3rd, 2015, and was focused on the eastern half of the study area. Geological mapping was conducted by setting

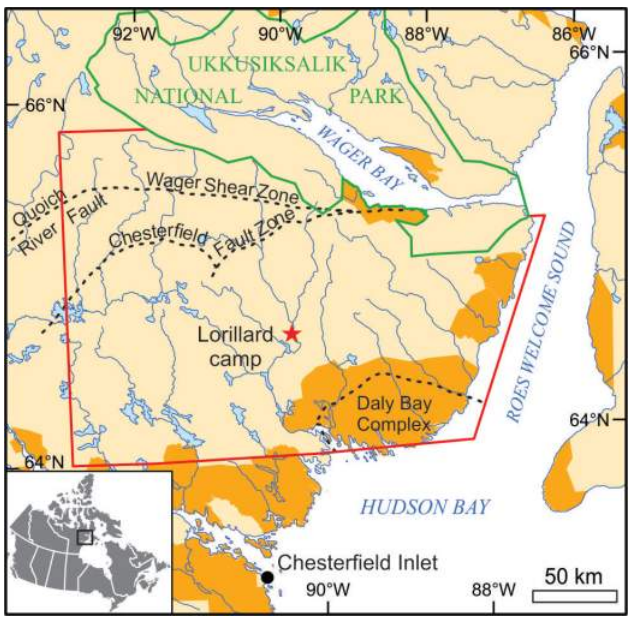

Figure 1: Location of the Tehery-Wager geoscience mapping activity study area (outlined in red) on the western side of Hudson Bay, Nunavut. Inuit-owned land parcels are shown in orange.

out 2–3 teams per day that would each traverse a 6–10 km route, along which geological observations, samples and measurements were collected.

Regional geological background

Reconnaissance-scale (1:1 000 000) bedrock-mapping campaigns in the Tehery Lake–Wager Bay area (Figure 1) were first conducted by the GSC in the 1950s (Wright, 1955, 1967; Lord and Wright, 1967) and 1960s (Heywood, 1967a, b). Since then, further mapping focused around the Daly Bay Complex (Gordon and Heywood, 1987; Gordon, 1988; Hanmer and Williams, 2001) and the Wager Shear Zone (Henderson et al., 1991), and maps have been completed for these areas at scales of 1:250 000 and 1:50 000, respectively. Airborne geophysical surveys have also covered the Tehery Lake–Wager Bay study area (Geological Survey of Canada, 1978, 1998; Keating et al., 2003; Coyle and Kiss, 2012a, b), and remote predictive maps have been interpreted based on all previously collected data (Panagapko et al., 2003).

The Tehery Lake–Wager Bay study area is interpreted as being underlain primarily by Archean and Proterozoic metaplutonic and metasedimentary rocks belonging to the southeastern Rae craton within the western Churchill Province (Hoffman, 1988). The northern part of the study area includes the Wager Shear Zone, a >25 km thick, dextral mylonite zone that parallels the southern shore of Wager Bay (Figure 1; Henderson and Broome, 1990; Henderson et al., 1991). This shear zone is associated with a prominent aeromagnetic anomaly that extends west of Wager Bay for at least another 100 km, where it may merge with the northwest-vergent Quoich River thrust fault (Panagapko et al., 2003; Figure 1). The Chesterfield Fault Zone, also located in the northern part of the study area, is interpreted by Panagapko et al. (2003) as the northeastern extension of a major shear zone that separates amphibolite-facies rocks of the Ketyet River group to the north from high-grade gneiss to the south (Figure 1; Schau, 1983).

The southeastern part of the study area includes the granulite-facies Daly Bay Complex, traditionally interpreted as forming part of the ca. 1.9 Ga Snowbird Tectonic Zone (e.g., Hanmer and Williams, 2001), a major translithospheric fault that represents the cratonic break between the Rae craton and the Chesterfield block to the south (Berman et al., 2007). Interpretation of magnetotelluric and co-located teleseismic survey data collected along a transect perpendicular to this crustal boundary suggests that the Snowbird Tectonic Zone may extend to the northeast from Baker Lake, or may bend east toward Chesterfield Inlet (Jones et al., 2002). Defining the surficial expression of the Snowbird Tectonic Zone would ultimately resolve many long-standing questions regarding the extent, geometry and paleotectonic reconstruction of the Rae-Hearne boundary zone (e.g., Hanmer et al., 1995; Flowers et al., 2006; Berman et al., 2007; Spratt et al., 2014). All large-scale, translithospheric structures mentioned above, and their associated fault networks, are prospective for a range of economic mineral deposits.

Field observations

Observations were collected from 630 bedrock-outcrop locations in the eastern part of the study area. The data include rock and mineral identification, textural descriptions, relative age relationships, structural measurements, magnetic-susceptibility measurements, pXRF data and digital photographs. A preliminary geological map has been prepared to show the major rock types in the Tehery Lake–Wager Bay study area (Figure 2), based on compilation of the new field data and integration of historical data, aeromagnetic data and satellite imagery. Lithological descriptions are provided in this section; classification of rock subdivisions is based primarily on field observations, combined with results from previous geological mapping, lithogeochemistry and U-Pb age data.

Archean tonalite to granodiorite orthogneiss

The Tehery Lake–Wager Bay study area is underlain predominantly by tonalite to granodiorite orthogneiss that is complexly deformed, contains mafic to intermediate bands and is locally heterogeneous. The mafic to intermediate bands may reflect older plutonic or volcanic phases, or transposed dykes that postdate the emplacement of the tonalite and granodiorite protoliths. A dominant mineral L-S fabric in the orthogneiss is defined by biotite and locally hornblende, as well as coarser grained granitic injections and dykelets (centimetre to metre scale) that have been transposed parallel to the dominant foliation (Figure 3a). Locally, clinopyroxenite, amphibolite (±garnet±biotite), metagabbro, chlorite schist, metadiorite and rare metasedimentary rocks (biotite schist, garnetite and calcsilicate) occur as pods and boudins in the orthogneiss that range from centimetres to 500 m in size. Felsic melts occur around some transposed pod and boudin necks, suggesting that, at least locally, fabric development was concomitant with crustal anatexis. Rocks containing these inclusions are also commonly associated with quartz-rich vein networks that cut both the orthogneiss and foliated mafic pods, are subsequently deformed and are cut by a second generation of quartz veins that postdates the main regional fabric. Mafic pods and mafic to intermediate bands were analyzed by pXRF in the field, and these data are discussed below.

Based on the observed field relationships, the tonalite to granodiorite orthogneiss can be correlated with two archived samples collected by Heywood (1967b) and dated by van Breemen et al. (2007) at 2.7 Ga using the U-Pb zircon SHRIMP (sensitive high-resolution ion microprobe) method. Concordant zircon from a foliated hornblende-biotite

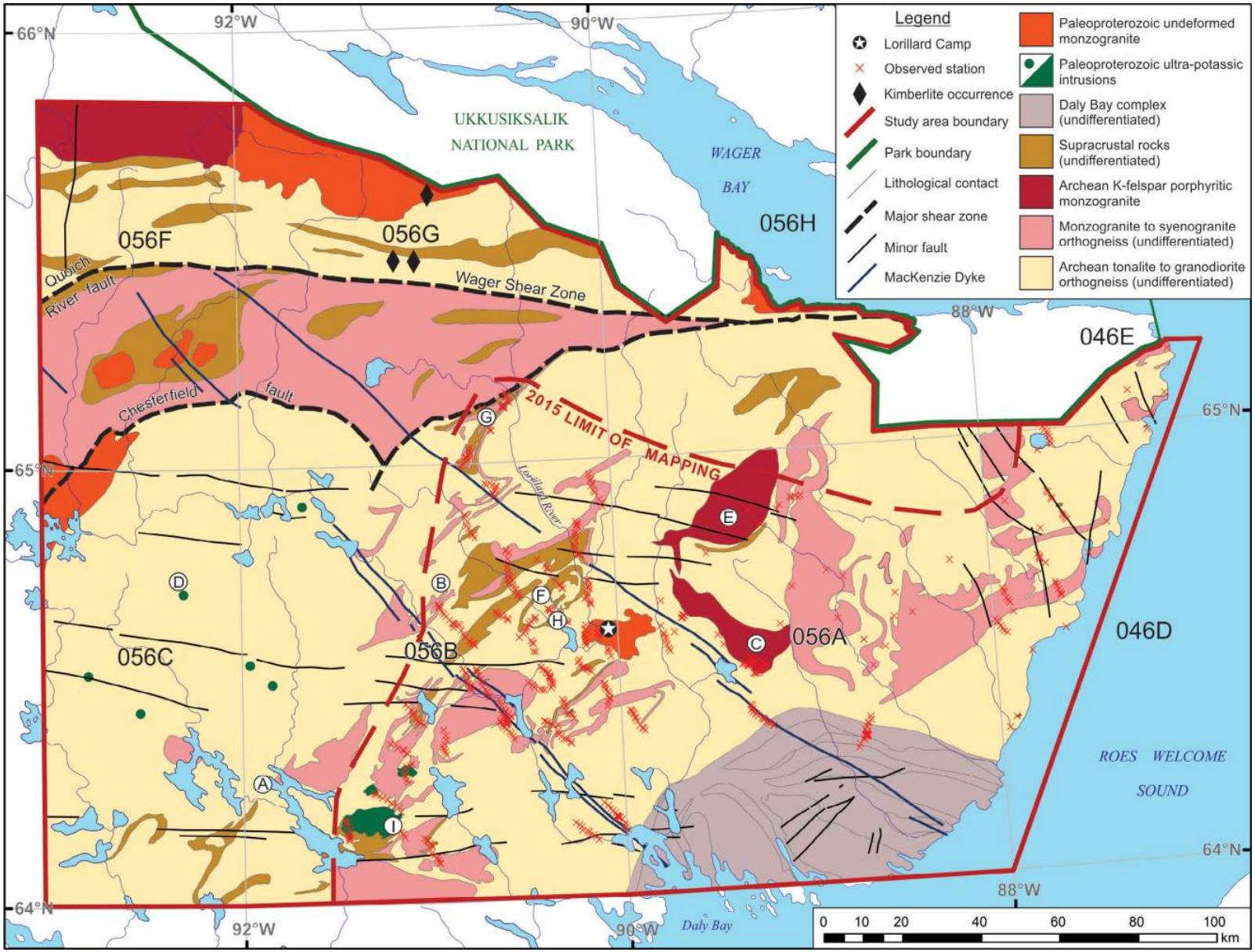

Figure 2: Preliminary geology of the Tehery Lake–Wager Bay study area (outlined in red), based on data collected in 2015 (east of the dashed red line) and remote predictive mapping and 2012 reconnaissance data (west of the dashed red line; after Panagapko et al., 2003). Locations referred to in the paper are indicated with the respective capital letter.

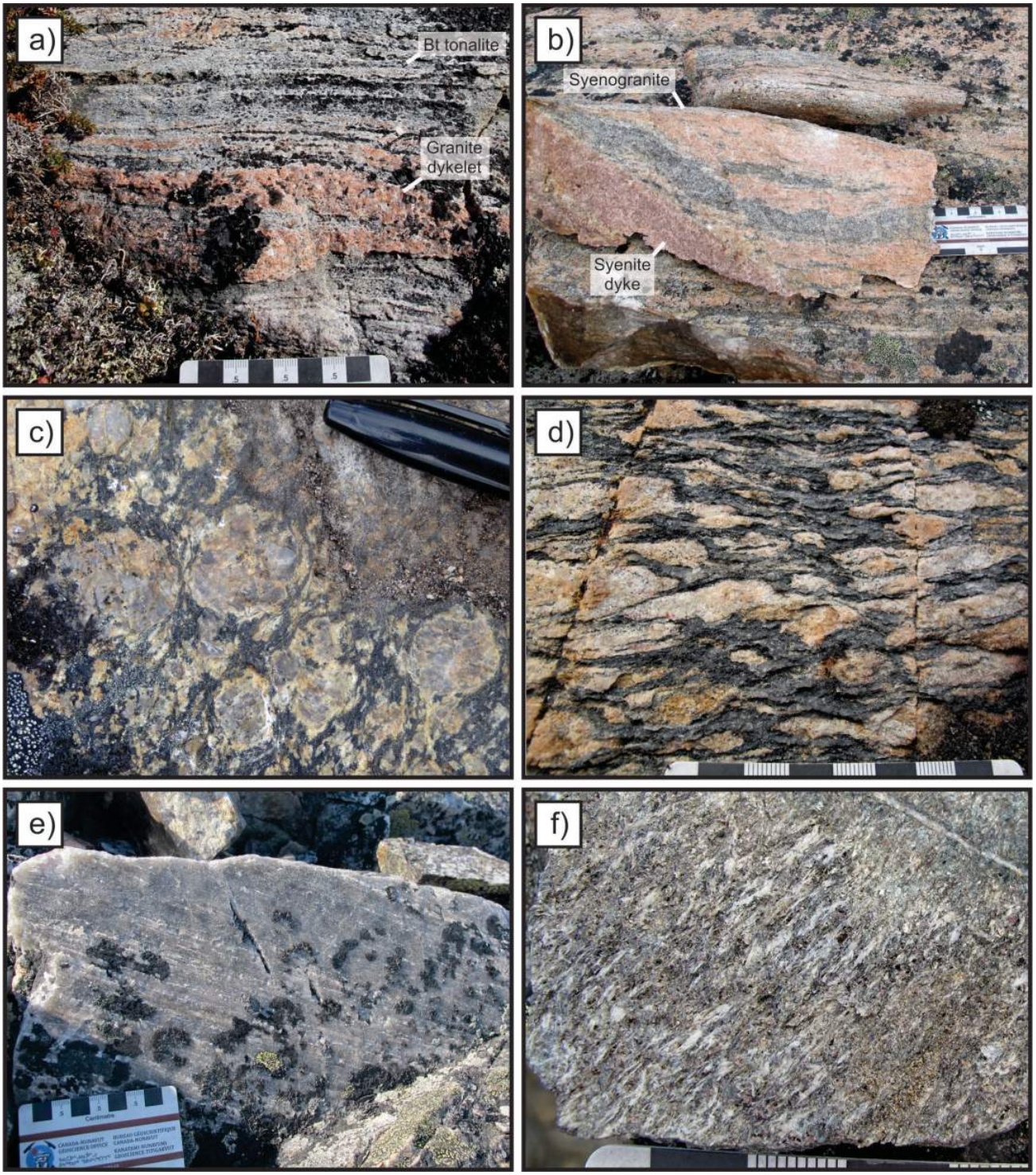

Figure 3: Representative photographs of major lithological units: **a)** biotite tonalite orthogneiss with isoclinally folded granitic dykelets oriented parallel to the main regional fabric; **b)** deformed monzogranite orthogneiss with a crosscutting syenite dyke; **c)** relatively undeformed K-feldspar–phyric monzogranite with thin white rims on K-feldspar phenocrysts, possibly indicating rapakivi texture; **d)** augen texture in deformed K-feldspar–phyric monzogranite near the contact with biotite tonalite orthogneiss (not shown); **e)** grey quartzite with recrystallized white detrital plagioclase defining a lineation fabric; **f)** garnet-sillimanite-biotite-muscovite pelitic gneiss with concentrations of white sillimanite defining a lineation fabric. Abbreviation: bt, biotite.

tonalite located approximately 85 km west of Lorillard camp (Figure 2, location A) yielded a weighted mean $^{207}Pb/^{206}Pb$ crystallization age of 2699 ±11 Ma, and a foliated granodiorite from approximately 35 km southwest of Lorillard camp (Figure 2, location B) has a weighted mean $^{207}Pb/^{206}Pb$ crystallization age of 2701 ±14 Ma, and a weighted mean $^{207}Pb/^{206}Pb$ metamorphic age of 1863 ±14 Ma (van Breemen et al., 2007). Despite the similarity of these two crystallization ages, it is likely that other tonalite-granodiorite plutonic components with different ages are present in the study area, based on the compositionally complex nature of this lithology.

Monzogranite to syenogranite orthogneiss

Large areas of mixed monzogranite to syenogranite orthogneiss were observed throughout the study area. The monzogranite weathers pale pink to white, is generally medium to coarse grained and typically contains biotite and magnetite as mafic phases, and rare muscovite. It has a well-developed foliation fabric defined by biotite, and compositional banding defined by mafic-mineral proportions. The syenogranite weathers dark to pale pink, is fine to medium grained and typically contains <5% biotite and lesser mafic minerals that also define a weak foliation. Fine-grained, homogeneous syenite dykes, up to 1 m thick, are transposed parallel to the main regional fabric and locally cut the foliated syenogranite (Figure 3b), suggesting that these dykes may have intruded during and after the main phase of regional deformation.

The nature of the contact between the monzogranite to syenogranite orthogneiss and the tonalite to granodiorite orthogneiss is unclear due to poor exposure; therefore, the relative timing of emplacement of these units was not accurately interpreted in the field.

Archean K-feldspar–phyric monzogranite

A large body of brown-weathering K-feldspar–phyric monzogranite was identified about 30 km east of Lorillard camp (Figure 2, location C). At the centre of the body, K-feldspar phenocrysts are up to 5 cm wide and rounded, and commonly have white rims, possibly of plagioclase (Figure 3c), a feature typical of rapakivi texture. The matrix is fine grained and contains biotite, plagioclase and quartz.

Within this body, a few scattered positive magnetic anomalies correlate with gabbroic to dioritic phases that locally contain plagioclase phenocrysts. The transition zone from one such phase to the porphyritic monzogranite is marked by a grey, mesocratic, medium-grained matrix containing sparse K-feldspar macrocrysts and likely reflects magma mixing of igneous phases.

Near the contact with the structurally underlying tonalite orthogneiss, the porphyritic monzogranite develops an augen texture, locally with pinhead garnet porphyroblasts (Figure 3d), that transitions to a finely laminated mylonite with K-feldspar porphyroclasts <1 cm wide. At the contact, the underlying tonalite is also mylonitized and contains porphyroclasts of garnet and plagioclase. The textures and relationship suggest that the porphyritic monzogranite body is in tectonic contact with the tonalite orthogneiss; however, the timing of this juxtaposition remains unclear. The remnant igneous textures, the presence of a coeval mafic phase and the interpreted tectonic juxtaposition over Archean tonalite gneiss are similar to descriptions of felsic plutonic rocks of the ca. 2.6 Ga Snow Island suite, which is present across the central Rae domain (Peterson et al., 2015). Within the western part of the Tehery Lake–Wager Bay area (Figure 2, location D), van Breemen et al. (2007) dated a foliated monzonite at 2584 ±22 Ma, which they interpreted as correlative with the Snow Island suite.

A second, kilometre-scale body of K-feldspar–phyric monzogranite occurs farther north (Figure 2, location E), but the presence of mafic phases or augen gneiss near the contact of this body with the surrounding rocks could not be confirmed due to poor exposure.

Smaller intrusions of K-feldspar–phyric monzogranite were identified across the field area as thin sheets associated with presumed Paleoproterozoic supracrustal rocks. Petrography, geochemistry and geochronology will be required to determine if these sheets are related to the larger K-feldspar–phyric monzogranite bodies.

Supracrustal rocks

Several panels of supracrustal rocks were documented in the central part of the Tehery Lake–Wager Bay study area (Figure 2). The panels are 1–800 m wide and continuous for tens of kilometres along strike before they either pinch out or have been eroded away. The nature of the basal contact (i.e., tectonic or depositional) between the orthogneiss units and the supracrustal rocks, and the reason for the apparent repetition of supracrustal panels and orthogneiss layers (i.e., due to thrust imbrication or isoclinal folding) will be the focus of further mapping and thematic studies.

Supracrustal belts comprise a distinct lithological package that includes quartzite, semipelite, garnetite, silicate-facies iron formation, amphibolite, metagabbro, peridotite, calcsilicate and rare marble. Quartzite is a minor lithology observed in several of the metasedimentary panels and is typically at the base of the supracrustal package. In some locations, quartzite is in tectonic contact with the Archean tonalite to granodiorite gneiss. It is generally fine grained, well recrystallized and white, pale pink, pale green or grey (Figure 3e). The quartzite contains metamorphic minerals including muscovite, biotite, sillimanite and garnet. It also locally contains fine-grained, detrital K-feldspar and/or plagioclase grains. Individual layers of quartzite range from 0.1 to 3 m thick and are intercalated with garnetite,

calcsilicate or semipelite layers. A quartzite sample collected in 2012 (Figure 2, location F) has dominantly Archean detrital zircon populations that range in age between ca. 3.7 and 2.55 Ga, and minor Paleoproterozoic ages from low–Th/U zircon overgrowths that may indicate a predepositional metamorphic event (Ferderber et al., 2013)

Layers dominated by semipelite are typically 0.1 to 5 m thick; one location (Figure 2, location G) south of the Chesterfield fault, however, has an approximately 30 m thick layer. Based on the observed metamorphic mineral assemblages, the semipelite locally ranges in composition from highly aluminous or pelitic (i.e., containing 25% sillimanite, 25% biotite, 10% muscovite, 5% garnet and 35% cumulative quartz, feldspars and accessory phases by volume; Figure 3f) to relatively siliceous or psammitic (i.e., containing 35% quartz, 35% feldspars, 15% biotite, 10% garnet and 5% cumulative sillimanite and accessory phases by volume). Foliation fabrics are defined by biotite, sillimanite and muscovite where present, and deflect around garnet porphyroblasts, suggesting that a major deformational event was synchronous with or followed the growth of garnet. Garnet is typically fine grained, but coarser grained examples have rims of biotite and plagioclase, indicating retrograde metamorphism. Foliation-parallel leucosome is documented in multiple locations, which suggests that melting was concomitant with the main phase of deformation.

Garnetite layers 10–250 cm thick comprise primarily garnet, quartz and minor magnetite (Figure 4a), and were commonly found intercalated with 5–30 cm thick magnetite-rich layers that contain green amphibole (likely grunerite), garnet, quartz and graphite. These alternating layers are interpreted as silicate-facies iron formation, and are typically associated with quartzite, calcsilicate, semipelite and amphibolite units within the supracrustal panels. Some sections weather rusty brown and were therefore sampled to evaluate their economic potential.

Mafic to intermediate rocks occur as 1–100 m thick layers intercalated with the metasedimentary successions. The layers are dominated by metagabbro, metadiorite and amphibolite, which are typically compositionally layered into ultramafic, mafic and intermediate components at a smaller scale (Figure 4b). These rocks typically contain clinopyroxene, garnet (Figure 4c) and hornblende porphyroblasts, with minor matrix biotite, plagioclase and quartz. Plagioclase rims on garnet were documented in several locations, suggesting decompression during retrograde metamorphism. A suite of these rocks was analyzed by pXRF in the field (discussed below) to compositionally classify them and evaluate whether or not compositional variations could be used as a tool to accurately subdivide this lithological unit during mapping. A variety of other homogeneous, fine- to medium-grained, dark grey and black mafic units containing garnet, clinopyroxene, orthopyroxene, plagioclase, hornblende and minor magnetite were identified in several of the supracrustal belts. These rocks require further work (i.e., thin-section and geochemical analyses) to classify their protoliths and provide some context for their source and genetic environment.

Lesser ultramafic rocks weather dark orange to brown and are partially recrystallized with amphibolite-facies mineral assemblages. These rocks act as relatively rigid layers within the supracrustal sequence, and have therefore been boudinaged during deformational events but have not developed pervasive internal fabrics. Boudinaged bodies up to 20 m thick are typically surrounded by other highly deformed and melt-saturated supracrustal units. The ultramafic rocks contain clinopyroxene, olivine, magnetite, orthopyroxene, tremolite, actinolite, phlogopite and other minor mafic and ultramafic phases.

Minor amounts of calcsilicate rocks were observed in every supracrustal panel. Centimetre- to metre-scale, bright green calcsilicate pods and boudins are also found intercalated with Archean basement orthogneiss. These rocks contain diopside, wollastonite, hornblende, tremolite, actinolite, apatite, garnet and rare carbonate phases. Marble was documented at three localities and is associated with the calcsilicate rocks (Figure 4d), garnetite and iron formation. Marble is locally intercalated with narrow psammite layers, giving the appearance of rhythmic bedding. The largest occurrence of marble, about 15 km northwest of Lorillard camp (Figure 2, location H), contains approximately 50% carbonate minerals, 40% olivine and 10% cumulative diopside, apatite, wollastonite and other minor phases by volume. The marble weathers grey and is recessive relative to the calcsilicate and other siliceous rock types.

Paleoproterozoic monzogranite

Medium-grained, homogeneous and undeformed monzogranite (Figure 4e) occurs in several locations as small plutons and sills up to about 25 m thick that are oriented parallel to the regional fabric within strongly deformed Archean granitoid and supracrustal rocks. The monzogranite contains equigranular K-feldspar, plagioclase and quartz, with minor, finer grained biotite, magnetite and rare fluorite. Partially assimilated biotite tonalite and supracrustal xenoliths, ranging from tens of centimetres to 1 m wide, occur within the nonfoliated monzogranite. The largest known plutonic body of monzogranite within the eastern part of the Tehery Lake–Wager Bay area surrounds Lorillard camp (Figure 2, Lorillard camp).

Also associated with this rock type are granitic pegmatite dykes that range from 0.2 to 75 m in width. Similar dykes are ubiquitous throughout the Tehery Lake–Wager Bay study area and cut all older rock types and deformation fabrics. On the basis of field relationships and lithological charac-

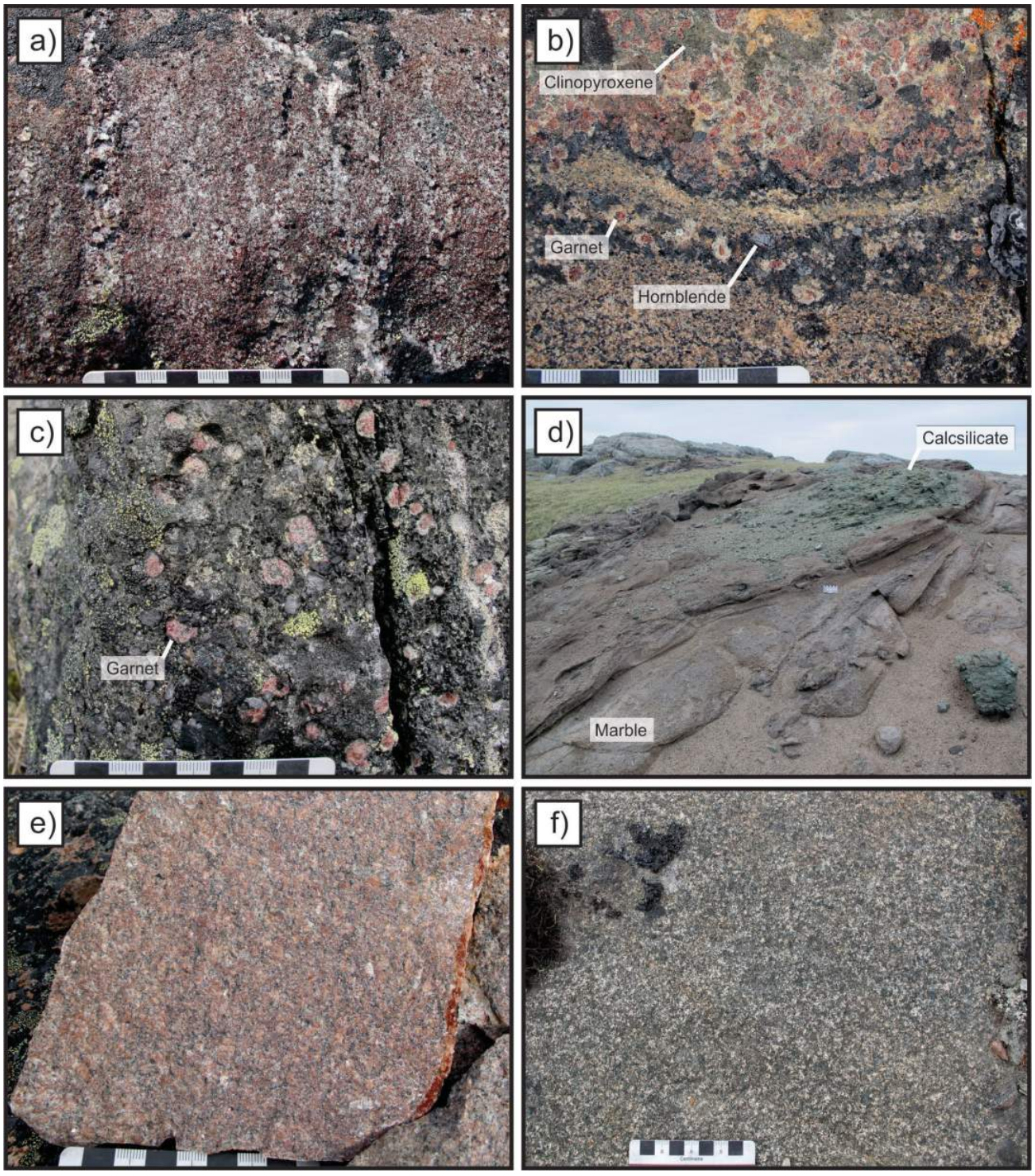

Figure 4: Representative photographs of major lithological units: **a)** supracrustal garnetite comprises mostly garnet and quartz; **b)** metagabbro to metadiorite layers within a supracrustal belt are rich in clinopyroxene or amphibole, and have garnet porphyroblasts rimmed with plagioclase, suggesting retrograde metamorphism; **c)** pyroxenite within a supracrustal belt contains pale pink garnet porphyroblasts that have visible inclusions but minimal retrograde reaction rims; **d)** the largest exposure observed in 2015 of impure marble (grey) contains pods and lenses of green calcsilicate rocks, and is associated with white wollastonite (forming the outcrop in the background); **e)** homogeneous, undeformed monzogranite is believed to be correlative with postorogenic granite of the intrusive Hudson suite (Peterson et al., 2002); **f)** homogeneous pyroxene-rich syenite is likely correlative with ultrapotassic intrusive Martel syenite of the Christopher Island formation (Peterson et al., 2002).

teristics, the monzogranite and granitic dykes are interpreted as correlative with 1.85–1.81 Ga felsic intrusive rocks of the Hudson suite (van Breemen et al., 2005). West of Hudson Bay, the Hudson granite forms large voluminous bodies that are interpreted as mid- to shallow-crustal, postorogenic plutons associated with continental-collision environments (Peterson et al., 2002).

Paleoproterozoic ultrapotassic intrusive rocks

Well-exposed, coarse-grained ultrapotassic plutons were identified in the southern part of the study area (Figure 2). The plutons cut the Archean tonalite to granodiorite gneiss and are typically cut by Hudson granitic dykes. The plutons appear to be zoned bimodal intrusions and display a net-veined complex at their margins, suggesting a mafic to felsic intrusive sequence. The most mafic rock observed within an ultrapotassic pluton is a phlogopite clinopyroxenite with sparse interstitial alkali feldspar (Figure 4f), and this grades into a biotite-pyroxene syenite. The most felsic phase was observed within an intrusive contact zone of a pluton located approximately 80 km southwest of Lorillard camp (Figure 2, location I). The contact zone was found to be only 10 m thick and composed of leucosyenite with partly resorbed rafts of clinopyroxene-rich melasyenite. The internal portion of this body is dominated by syenite, which has about 5–10% mafic minerals in a matrix dominated by alkali feldspar and is remarkably homogeneous in texture and mineralogy. A single 2 m wide minette dyke that cuts Archean granodiorite was observed in the same area as the ultrapotassic plutons.

Within a large portion of the central and southern Rae and Hearne cratons, the Hudson suite is coincident in time and space with a felsic to mafic ultrapotassic (minette to lamproite) suite of dykes and volcanic rocks known as the Christopher Island formation (CIF; Peterson et al., 2002). The lower felsic volcanic rocks are compositionally similar to mixed minette-granite intrusive rocks (Martell syenite), which can be recognized by their intermediate compositions and heterogeneous mixing textures (Scott et al., 2015). It is believed that the ultrapotassic rocks recognized in the Tehery Lake–Wager Bay area are correlative with the CIF and Martell syenite rocks.

Mesoproterozoic Mackenzie dykes

A series of southeast-trending diabase dykes cuts all rock types and deformation fabrics in the study area. These dykes are about 25 m thick, mostly continuous and subvertical, and interpreted as correlative with the 1267 ±2 Ma Mackenzie dyke swarm that radiates throughout northern Canada (LeCheminant and Heaman, 1989; Ernst and Baragar, 1992).

pXRF data

Amphibolite and mafic to intermediate gneiss occur as pods and layers intercalated with metasedimentary panels and granitoid gneiss throughout the Tehery Lake–Wager Bay map area (Figure 2). Fine- to medium-grained examples of these rocks were targeted for pXRF analysis to test its usefulness as a chemostratigraphic tool and to help identify probable precursor rock types. A full description of the methodology and specific instrumentation used, as well as the complete dataset collected in the field, are provided in Lawley et al. (2015a)[4]. Semiquantitative pXRF results are presented in Figure 5.

Results and discussion

Most published rock-classification and tectonic-discrimination diagrams rely on immobile trace elements with concentrations that are significantly below the analytical detection limit of the pXRF (e.g., Nb, Yb, Y, Th, Ta; e.g., Pearce, 1996). To address this issue and to construct pXRF-compatible rock-discrimination indices, the authors compiled a diverse suite of volcanic-rock lithogeochemical data from the GEOROC database (http://georoc.mpch-mainz.gwdg.de/georoc/; Sarbas and Nohl, 2008). Least altered samples from this database (classified using the total alkalis versus silica and Pearce classification diagrams; Le Bas et al., 1986; Pearce, 1996) acted as a training set to construct rock-discrimination fields using elements with concentrations that are routinely above the analytical detection limit of the pXRF device. This approach is not effective for discriminating alkalic-rock suites, which require major and trace elements that are not routinely collected during pXRF analyses (e.g., Na_2O, Nb, Y).

Two examples of rock-discrimination diagrams using this approach are presented in Figure 5. Mafic (amphibolite and mafic orthogneiss) to intermediate (metadiorite) samples that occur as pods and layers intercalated with granitoid gneiss and metasedimentary panels plot primarily within the basaltic field and extend toward lesser andesitic compositions (Figure 5a). Rhyolite classifications are spurious and reflect sample heterogeneity that is not captured by the relatively small analytical window of the pXRF device for these coarser grained and/or heterogeneous samples. In contrast, fine-grained samples tend to yield compositions that are in good agreement with conventional whole-rock lithogeochemistry (Lawley et al., 2015b). Samples that plot to the right of the three rock fields are likely metasomatized (i.e., the metasomatized field is based on the approximate limit of the least altered training set; Figure 5a). As a result, real-time and nondestructive pXRF analyses can be used to

[4]*CNGO Geoscience Data Series GDS2015-011, containing the data or other information sources used to compile this paper, is available online to download free of charge at http://cngo.ca/summary-of-activities/2015/.*

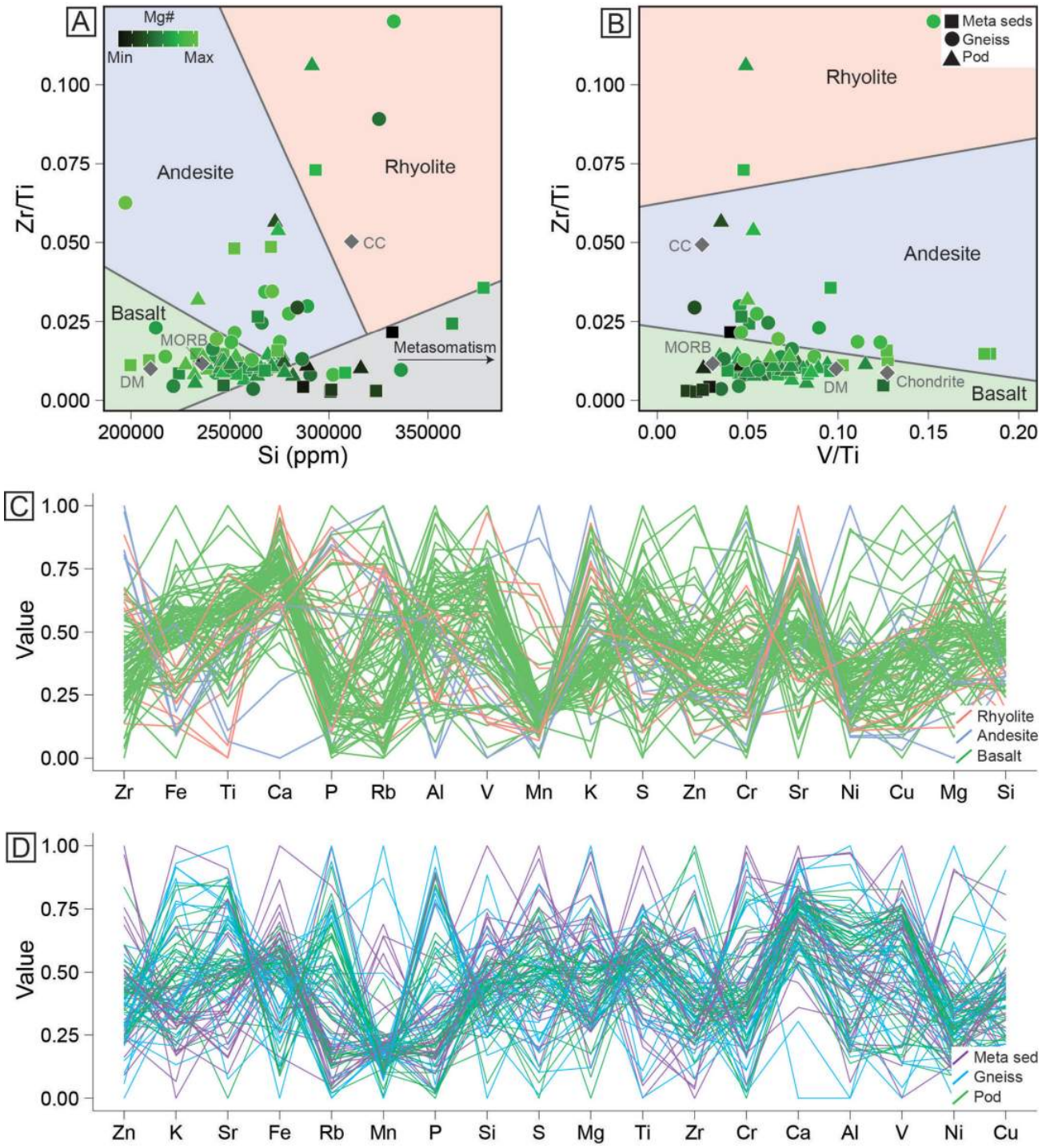

Figure 5: a) Modified pXRF-based rock-discrimination diagram colour coded to Mg enrichment [Mg / (Mg + Fe)]. Rock fields are based on the classified training set (GEOROC, n = 54 946) and logistic regression in R (R Core Team, 2015). Abbreviations reflect the samples' setting: Gneiss, mafic layers intercalated with tonalite-granodiorite gneiss; Meta seds., mafic layers intercalated with metasedimentary panels; Pod, pod hosted entirely within tonalite-granodiorite gneiss. Combining mobile and least mobile elements can identify metasomatized samples and be used to target sampling for conventional lithogeochemistry; **b)** Modified pXRF-based rock-discrimination diagram colour coded to Mg enrichment. Seven anomalous superchondritic Ti/V ratios for andesitic and rhyolitic samples were excluded for plotting purposes; **c–d)** Parallel co-ordinate plot of log-ratio (clr)–transformed element concentrations colour coded to rock type (c) and geological setting (d). Elements are ordered according to variance between groups, following the approach of Schloerke et al. (2014). Diverging patterns highlight geochemical subpopulations between rock types and geological settings: Chondrite (McDonough and Sun, 1995); CC, continental crust (Rudnick and Gao, 2003); DM, depleted mantle (Salters and Stracke, 2004); MORB, mid-ocean-ridge basalt (Gale et al., 2013).

help identify least altered samples and guide sample selection for conventional whole-rock lithogeochemistry.

Least altered basaltic samples yielded a range of Ti/V ratios (Ti/V mean = 18 ±2) that vary between relatively primitive (Ti/V mean = 10; Salters and Stracke, 2004) and more evolved basaltic (MORB; Ti/V mean = 32; Gale et al., 2013) compositions (Figure 5b), along with lesser superchondritic compositions (Ti/V mean = 8; McDonough and Sun, 1995). Primitive, mantle-like samples are also relatively rich in Mg, Cr and Ni (Figure 5b). Therefore, the sample suite likely comprises a range of basaltic compositions and possible precursor rocks that were not clear from field relationships and modal mineralogy. Diverging multi-element patterns also suggest that multiple, chemically distinct subpopulations are included within the basaltic sample suite (Figure 5c). Each basaltic subpopulation is represented as distinct clusters on the parallel co-ordinate plot (e.g., Fe, Ti, Rb, Al, K, S, Cr, Sr, Cu, Mg), whereas other elements (e.g., Zr, Ca, P, V, Mn, Ni, Si) yield relatively unimodal but skewed concentrations for each basaltic subpopulation (Figure 5c). Rhyolitic samples are clearly anomalous and define unique multi-element patterns (see above; Figure 5c). Andesitic samples are also distinct and yield relatively depleted Fe-Cr concentrations that, along with relative K-Sr enrichment, are consistent with their more geochemically evolved compositions.

Multi-element comparisons between geological settings (i.e., pods and layers intercalated with tonalite to granodiorite orthogneiss versus layers intercalated with metasedimentary panels) for the analyzed rocks are presented in Figure 5d. Amphibolite and mafic to intermediate orthogneiss layers intercalated with metasedimentary panels yield relatively depleted element concentrations (K, Sr, Rb, P) in comparison with mafic to intermediate pods and layers intercalated with tonalite to granodiorite gneiss (Figure 5d). The relatively depleted incompatible trace-element pattern for metasedimentary-hosted samples, coupled with Ti/V ratios that tend to plot closer to basaltic compositions (metasedimentary Ti/V mean = 19 ±6; gneissic Ti/V mean = 18 ±2; enclave Ti/V mean = 17 ±2; Figure 5b), point to systematic geochemical differences between each setting (e.g., Figure 5d). Whether these primitive to more evolved basaltic samples represent volcanic flows intercalated with metasedimentary panels requires further geochemical and isotopic analysis. Nevertheless, pXRF analyses provide a geochemical framework for correlating basaltic horizons within tectonized and dismembered metasedimentary stratigraphy.

Economic considerations

Based on the results of the fieldwork carried out in 2015, several rock types with favourable associations and mineral assemblages are being evaluated for their economic potential. The mafic and ultramafic rock layers in the supracrustal sequences may have potential for base or precious metals, such as Ag, Au, Pt or Ni, and have been sampled to investigate this. Similarly, rusty weathered (gossanous) layers of supracrustal rocks, such as quartzite, garnetite and iron formation, have been sampled to establish their metal content. Till and stream-sediment samples collected within and near one of the supracrustal belts (Figure 2, location G) contain elevated concentrations of Ag, Cu, Bi, Au and Co-Fe–arsenide minerals (Day et al., 2013; McMartin et al., 2013). Detailed mapping and sampling of this supracrustal belt is a major component in a Ph.D. thesis project that focuses on the economic potential and metamorphic history of supracrustal rocks throughout the Tehery Lake–Wager Bay study area.

The ultrapotassic plutons mapped in the southern part of the study area will be analyzed in detail using geochemical and isotopic methods, as similar rocks from the central Churchill Province contain elevated concentrations of rare earth elements (Miller and Blackwell, 1992).

Conclusions

The first field season of the Tehery-Wager geoscience mapping activity focused on the eastern part of the study area and led to a better documentation and characterization of rock units and features in the area. Rocks presumed to be correlative with Snow Island suite porphyritic monzogranite, Hudson granite and Martell syenite found elsewhere in the western Churchill Province were identified and will be analyzed to confirm their relationships. Supracrustal belts, previously mapped only at reconnaissance scale, have been delineated, described and sampled, and will be further analyzed to determine their depositional age and environment, the conditions and timing of metamorphic and deformational events they experienced, and their economic potential.

The results obtained this field season highlight that in situ, real-time and nondestructive pXRF analyses provide a powerful chemostratigraphic tool in support of bedrock-mapping programs. The authors demonstrated that pXRF analytical accuracy and precision, following the standard-sample-standard bracketing approach (Lawley et al., 2015b), is sufficient to differentiate disparate rock types that were unclear from field observations alone, and to identify metasomatized samples by combining mobile and least mobile pXRF element concentrations.

A second field season of regional bedrock- and surficial-geology mapping in the western part of the Tehery Lake–Wager Bay study area will be conducted during the summer of 2016. The sum of the collected data and samples will be used to produce higher resolution regional-geology maps, evaluate economic potential and characterize the regional tectonic and metamorphic histories of the major crustal

blocks in the area. This information will be helpful for paleotectonic reconstructions, minimizing investment risk associated with natural-resource exploration and assisting organizations that require geoscience knowledge to make fully informed land-use decisions regarding future economic development in the area.

Acknowledgments

The authors gratefully acknowledge I. McMartin, S. Day, E. Girard, R. Buenviaje, J. Beales, B. Garrison, K. Hatogina, I. Randour and J. Byatt for their cheerful determination, skillful assistance and dedication in the field. L. Levesque and R. Issaluk are thanked for keeping the field crews nourished and happy with their delicious meals and bubbly attitudes. The Hamlet of Chesterfield Inlet provided tremendous logistical and organizational assistance, and the authors thank the staff at the Hamlet Office and the people in Chesterfield Inlet for their welcome. Professional aviation support was provided by Prairie Helicopters and Ookpik Aviation through the Polar Continental Shelf Program (Project 053-15). Financial support for this project is provided by the Geo-mapping for Energy and Minerals program, Phase 2 (GEM-2) of the Geological Survey of Canada and the Strategic Investments in Northern Economic Development (SINED) program delivered by the Canadian Northern Economic Development Agency (CanNor). This paper benefited from a thorough and thoughtful review by W. Davis.

Natural Resources Canada, Earth Sciences Sector contribution number 20150328

References

Berman, R.G., Davis, W.J. and Pehrsson, S. 2007: Collisional Snowbird tectonic zone resurrected: growth of Laurentia during the 1.9 Ga accretionary phase of the Hudsonian orogeny; Geological Society of America Bulletin, v. 35, no. 10, p. 911–914. doi:10.1130/G23771A

Coyle, M. and Kiss, F. 2012a: Residual total magnetic field, aeromagnetic survey of the Tehery Lake area, Nunavut; Geological Survey of Canada, Open Files 7203–7206.

Coyle, M. and Kiss, F. 2012b: First vertical derivative of the magnetic field, aeromagnetic survey of the Tehery Lake area, Nunavut; Geological Survey of Canada, Open Files 7207–7210.

Day, S.J.A., Wodicka, N. and McMartin, I. 2013: Preliminary geochemical, mineralogical and indicator mineral data for heavy mineral concentrates and waters, Lorillard River area, Nunavut (parts of NTS 056 A, B and G); Geological Survey of Canada, Open File 7428, 11 p.

Ernst, R.E. and Baragar, W.R.A. 1992: Evidence from magnetic fabric for the flow pattern of magma in the Mackenzie giant radiating dyke swarm; Nature, v. 356, p. 511–513.

Ferderber, J., Kellett, D.A. and Wodicka, N. 2013: Exploring the Tehery region: correlating supracrustal sequences using detrital zircon geochronology, Rae Craton, Nunavut; Geological Survey of Canada, Open File 7424. doi:10.4095/292709

Flowers, R.M., Bowring, S.A. and Williams, M.L. 2006: Timescales and significance of high-pressure, high-temperature metamorphism and mafic dike anatexis, Snowbird tectonic zone, Canada; Contributions to Mineralogy and Petrology, v. 151, p. 558–581. doi:10.1007/s00410-006-0066-7

Gale, A., Dalton, C.A., Langmuir, C.H., Su, Y. and Schilling, J.G. 2013: The mean composition of ocean ridge basalts; Geochemistry, Geophysics, Geosystems, v. 14, p. 489–518. doi:10.1029/2012GC004334

Geological Survey of Canada 1978: Airborne gamma ray spectrometric map, Armit Lake, District of Keewatin, Northwest Territories; Geological Survey of Canada, Geophysical Series, Map 35256G, scale 1:250 000.

Geological Survey of Canada 1998: Western Churchill NATMAP Project region, decorrugated residual total field magnetics, colour shaded relief; Geological Survey of Canada, scale 1:1 000 000.

Gordon, T.M. 1988: Precambrian geology of the Daly Bay area, District of Keewatin; Geological Survey of Canada, Memoir 422, 21 p.

Gordon, T.M. and Heywood, W.W. 1987: Geology, Daly Bay area, District of Keewatin, Northwest Territories; Geological Survey of Canada, Map 1652A, scale 1:250 000.

Hanmer, S. and Williams, M.L. 2001: Targeted field work in the Daly Bay Complex, Hudson Bay, Nunavut; Geological Survey of Canada, Current Research 2001-C15, 10 p.

Hanmer, S., Williams, M.L. and Kopf, C. 1995: Striding-Athabasca mylonite zone: implications for Archean and Early Proterozoic tectonics of the western Canadian Shield; Canadian Journal of Earth Sciences, v. 32, p. 178–196. doi:10.1139/e95-015

Henderson, J.R. and Broome, J. 1990: Geometry and kinematics of Wager shear zone interpreted from structural fabrics and magnetic data; Canadian Journal of Earth Sciences, v. 27, p. 590–604.

Henderson, J.R., Jefferson, C.W., Henderson, M.N., Coe, K. and Derome, I. 1991: Geology of the region around Wager Bay, District of Keewatin (parts of 46E and 56H); Geological Survey of Canada, Open File 2383.

Heywood, W.W. 1967a: Geology of northeastern District of Keewatin and southern Melville Peninsula, Districts of Franklin and Keewatin; Geological Survey of Canada, Open File 1, scale 1:506 880. doi:10.4095/100310

Heywood, W.W. 1967b: Geological notes northeastern District of Keewatin and southern Melville Peninsula, District of Franklin, Northwest Territories (parts of 46, 47, 56, 57); Geological Survey of Canada, Paper 66-40, 20 p.

Hoffman, P.F. 1988: United plates of America, birth of a craton – Early Proterozoic assembly and growth of Laurentia, Annual Review of Earth and Planetary Sciences, v. 16, p. 543–603.

Jones, A.G., Snyder, D.B., Hanmer, S., Asudeh, I., White, D., Eaton, D. and Clarke, G. 2002: Magnetotelluric and teleseismic study across the Snowbird Tectonic Zone, Canadian Shield: a Neoarchean mantle suture?; Geophysical Research Letters, v. 29, no. 17, p. 10-1–10-4.

Keating, P.B., Pilkington, M. and Miles, W.F. 2003: Colour shaded relief of the residual total magnetic field with Keating correlation coefficients, NTS 56 B, C, F, G, Nunavut, Canada; Geological Survey of Canada, Open File 4489, scale 1:500 000.

Lawley, C.J.M., Steenkamp, H.M. and Wodicka, N. 2015a: Portable X-ray fluorescence geochemical results from the Tehery Lake–Wager Bay area, western Hudson Bay, Nunavut; Canada-Nunavut Geoscience Office, Geoscience Data Series 2015-011, Microsoft® Excel® file, URL <http://cngo.ca/summary-of-activities/2015/> [December 2015].

Lawley, C.J.M., Dubé, B., Mercier-Langevin, P., Kjarsgaard, B., Knight, R. and Vaillancourt, D. 2015b: Defining and mapping hydrothermal footprints at the BIF-hosted Meliadine gold district, Nunavut, Canada; Journal of Geochemical Exploration, v. 155, p. 33–55. doi:10.1016/j.gexplo.2015.04.001

Le Bas, M.J., Le Maitre, R.W., Streckeisen, A. and Zanettin, B. 1986: A chemical classification of volcanic rocks based on the total alkali-silica diagram; Journal of Petrology, v. 27, no. 3, p. 745–750.

LeCheminant, A.N. and Heaman, L.M. 1989: Mackenzie igneous events, Canada: Middle Proterozoic hotspot magmatism associated with ocean opening; Earth and Planetary Science Letters, v. 96, no. 1, p. 38–48.

Lord, C.S. and Wright, G.M. 1967: Geology, southeastern Barren Grounds, District of Keewatin–District of Mackenzie; Geological Survey of Canada, Map 1216A, scale 1:1 000 000 scale. doi:10.4095/108854

McDonough, W.F. and Sun, S.S. 1995: Composition of the Earth; Chemical Geology, v. 120, p. 223–253.

McMartin, I., Wodicka, N., Bazor, D. and Boyd, B. 2013: Till composition across the Rae craton south of Wager Bay, Nunavut: results from the Geo-Mapping Frontiers' Tehery–Cape Dobbs project; Geological Survey of Canada, Open File 7417, 31 p. doi:10.4095/293307

Miller, A.R. and Blackwell, G.W. 1992: Petrology of alkaline rare earth element–bearing plutonic rocks, Enekatcha Lake (65E/15) and Carey Lake (65L/7) map areas, District of Mackenzie; Geological Survey of Canada Open File 2428, p. 129–134.

Panagapko, D.A., Pehrsson, S., Pilkington, M. and Currie, M. 2003: Geoscience data compilation: Tehery Lake–Wager Bay area, Nunavut (NTS 56 B, C, F, and G), part 1 – base data themes; Geological Survey of Canada, Open File 1809. doi:10.4095/214767

Pearce, J.A. 1996: A user's guide to basalt discrimination diagrams; *in* Trace Element Geochemistry of Volcanic Rocks: Applications for Massive Sulphide Exploration, D.A. Wyman (ed.), Geological Association of Canada, Short Course Notes, v. 12, p. 79–113.

Peterson, T.D., Jefferson, C.W. and Anand, A. 2015: Geological setting and geochemistry of the ca. 2.6 Ga Snow Island Suite in the central Rae Domain of the western Churchill Province, Nunavut; Geological Survey of Canada, Open File 7841. doi:10.4095/296599

Peterson, T.D., van Breemen, O., Sandeman H. and Cousens, B. 2002: Proterozoic (1.85–1.75 Ga) igneous suites of the western Churchill Province: granitoid and ultrapotassic magmatism in a reworked Archean hinterland; Precambrian Research, v. 119, p. 73–100.

R Core Team 2015: R: a language and environment for statistical computing; R Foundation for Statistical Computing, Vienna, Austria. URL <https://www.R-project.org/> [November 2015].

Rudnick, R.L. and Gao, S. 2003: Composition of the continental crust; *in* The Crust, R.L. Rudnick (ed.), Elsevier, p. 1–64.

Salters, V.J.M. and Stracke, A. 2004: Composition of the depleted mantle; Geochemistry, Geophysics, Geosystems, v. 5. doi:10.1029/2003GC000597

Sarbas, B. and Nohl, U. 2008: The GEOROC database as part of a growing geoinformatics network; *in* Geoinformatics 2008: Data to Knowledge, S.R. Brady, A.K. Sinha and L.C. Gundersen (ed.), United States Geological Survey, Scientific Investigations Report 2008-5172, p. 42–43.

Schau, M. 1983: Baker Lake map sheet (56D); Geological Survey of Canada, Open File 883, scale 1:125 000.

Schloerke, B., Crowley, J., Cook, D., Hofmann, H., Wickham, H., Briatte, F., Moritz, M. and Thoen, E. 2014: GGally: extension to ggplot2; The Comprehensive R Archive Network, URL <https://cran.r-project.org/web/packages/GGally/index.html> [November 2015].

Scott, J.M.J., Peterson, T.D., Davis, W.J., Jefferson, C.W. and Cousens, B.L. 2015: Petrology and geochronology of Paleoproterozoic intrusive rocks, Kiggavik uranium camp, Nunavut; Canadian Journal of Earth Sciences, v. 52, no. 7, p. 495–518. doi:10.1139/cjes-2014-0153

Spratt, J.E., Skulski, T., Craven, J.A., Jones, A.G., Snyder, D.B. and Kiyan, D. 2014: Magnetotelluric investigations of the lithosphere beneath the central Rae craton, mainland Nunavut, Canada; Journal of Geophysical Research, Solid Earth, v. 119, p. 2415–2439. doi:10.1002/2013JB010221

van Breemen, O., Pehrsson, S. and Peterson, T.D. 2007: Reconnaissance U-Pb SHRIMP geochronology and Sm-Nd isotope analyses from the Tehery–Wager Bay gneiss domain, western Churchill Province, Nunavut; Geological Survey of Canada, Current Research 2007-F2, 17 p.

van Breemen, O., Peterson, T.D. and Sandeman, H.A. 2005: U-Pb zircon geochronology and Nd isotope geochemistry of Proterozoic granitoids in the western Churchill Province: intrusive age pattern and Archean source domains; Canadian Journal of Earth Sciences, v. 42, p. 339–377.

Wodicka, N., Steenkamp, H.M., Lawley, C.J.M., Peterson, T.D., Guilmette, C., Girard, É. and Buenviaje, R. 2015: Report of activities for the bedrock geology and economic potential of the Tehery-Wager area: GEM-2 Rae Project; Geological Survey of Canada, Open File 7970, 14 p.

Wright, G.M. (1955): Geological notes on central District of Keewatin, Northwest Territories; Geological Survey of Canada, Paper 55-17, 21 p., URL <http://geoscan.nrcan.gc.ca/starweb/geoscan/servlet.starweb?path=geoscan/downloade.web&search1=R=101294> [November 2015].

Wright, G.M. (1967): Geology of the southeastern Barren Grounds, parts of Mackenzie and Keewatin, Operations Keewatin, Baker, Thelon; Geological Survey of Canada, Memoir 350, 91 p.

Mapping of surficial materials south of Wager Bay, southern Nunavut, using RADARSAT-2 C-band dual-polarized and Landsat 8 images, a digital elevation model and slope data: preliminary map and summary of fieldwork

J. Byatt[1], A. LaRocque[1], B. Leblon[2], I. McMartin[3] and J. Harris[3]

[1]*Faculty of Forestry and Environmental Management, University of New Brunswick, Fredericton, New Brunswick*

[2]*Faculty of Forestry and Environmental Management, University of New Brunswick, Fredericton, New Brunswick, bleblon@unb.ca (corresponding author)*

[3]*Natural Resources Canada, Geological Survey of Canada, Ottawa, Ontario*

This work is part of the Tehery-Wager geoscience mapping activity of Natural Resources Canada's (NRCan) Geo-mapping for Energy and Minerals (GEM) program Rae project, a multidisciplinary and collaborative effort being led by the Geological Survey of Canada and the Canada-Nunavut Geoscience Office (CNGO), with participants from Nunavut Arctic College and Canadian universities (Dalhousie University, Université du Québec à Montréal, Université Laval, University of New Brunswick and University of Victoria). The focus is on targeted bedrock geology mapping, surficial geology studies, surface and stream sediment sampling, and other thematic studies, which collectively will increase the level of geological knowledge in this frontier area and allow evaluation of the potential for a variety of commodities, including diamonds and other gemstones, base and precious metals, industrial minerals, carving stone and aggregates. This activity also aims to assist northerners by providing geoscience training to college students, and by ensuring that the new geoscience information is accessible for making land-use decisions in the future.

Byatt, J., LaRocque, A., Leblon, B., McMartin, I. and Harris, J. 2015: Mapping surficial materials south of Wager Bay, southern Nunavut, using RADARSAT-2 C-band dual-polarized and Landsat 8 images, a digital elevation model and slope data: preliminary map and summary of fieldwork; *in* Summary of Activities 2015, Canada-Nunavut Geoscience Office, p. 135–144.

Abstract

The Canadian Arctic is currently the focus of increased mapping activities, which aim to provide better knowledge to assist in making informed decisions for sustainable minerals and energy development and land-use management. One of the maps that is needed is a surficial materials map.

This paper presents preliminary results of a surficial materials mapping research activity within the Tehery-Wager geoscience mapping activity for the Rae project area of Natural Resources Canada's Geo-mapping for Energy and Minerals program, a collaborative project co-led by the Geological Survey of Canada and the Canada-Nunavut Geoscience Office. The study area is located south of Wager Bay in Nunavut (NTS map areas 46D, E, 56A, H) and covers targeted areas that have not been mapped or mapped only at a reconnaissance scale. A preliminary surficial materials map with 15 classes was produced from a combination of images from RADARSAT-2 in the C-band (with horizontal-horizontal polarization and horizontal-vertical polarization) and from Landsat 8 Operational Land Imager with a digital elevation model and slope data. This paper also presents field observations that were made in the summer of 2015 and will be used as ground control points to validate the map.

Résumé

L'Arctique canadien fait actuellement l'objet d'un niveau accru d'activité dans le domaine de la réalisation de documents cartographiques, qui ont pour but de fournir de meilleures connaissances susceptibles de contribuer à la prise de décisions éclairée en matière de développement énergétique et d'aménagement des terres. Parmi tous les types de cartes requises, la réalisation d'une carte des matériaux de surface s'impose.

Cet article présente les résultats préliminaires du projet de recherche en cartographie des matériaux de surface Tehery-Wager entrepris dans le secteur couvert par le projet Rae qui lui-même s'inscrit dans le cadre du programme de géocartographie de l'énergie et des minéraux de Ressources naturelles Canada; il s'agit d'un programme de nature collaborative

This publication is also available, free of charge, as colour digital files in Adobe Acrobat® PDF format from the Canada-Nunavut Geoscience Office website: http://cngo.ca/summary-of-activities/2015/.

mené de front par la Commission géologique du Canada et le Bureau géoscientifique Canada-Nunavut. La zone cartographiée est située au sud de Wager Bay, au Nunavut (cartes 46D, E, 56A, H du SNRC). Elle correspond à une région ciblée qui n'est toujours pas cartographiée ou qui a été cartographiée uniquement à une échelle de reconnaissance. Une carte préliminaire regroupant 15 classes de dépôts de surface a été produite à partir d'images recueillies par RADARSAT-2 dans la bande C (en fonction d'une polarisation horizontale-horizontale et d'une polarisation horizontale-verticale) et par le capteur Operational Land Imager installé sur le satellite Landsat 8, lesquelles sont combinées avec un modèle altimétrique numérique de terrain et des données de pente. Les auteurs présentent également les observations de terrain qui ont été faites au cours de l'été 2015 et qui serviront à valider la carte.

Introduction

The Canadian Arctic is currently the focus of increased mapping activities, which aim to provide better knowledge to assist in making informed decisions for sustainable resource and infrastructure development, and land-use management. This study is part of the surficial geology component of the Tehery-Wager geoscience mapping activity for the Rae project of Natural Resources Canada's (NRCan) Geo-mapping for Energy and Minerals (GEM) program, a collaborative project led by the Geological Survey of Canada (GSC) and the Canada-Nunavut Geoscience Office (CNGO). The overall objective of this activity is to provide new geological knowledge on the nature and composition of surficial materials for sustainable management and development (McMartin et al., 2015). Remote interpretation of surficial materials provides first-order assessment of the unconsolidated sediment covering the study area, guides geological mapping field activities (both surficial and bedrock), assists in interpretation of the surficial geology between field sites, and provides a regional context for the surficial materials.

Northern Canada presents challenges for geological mapping because the land area is vast and difficult to access. Mapping has traditionally been done at a regional scale and accomplished by expensive and logistically challenging field programs. Remote predictive mapping (RPM) is a technique that can be used to map vast areas in a time-efficient manner and at a relatively low cost (Harris, 2008). Satellite images, such as those provided by RADARSAT-2 and Landsat, offer the advantages of extensive regional coverage, no disturbances to the area being mapped and a method of acquiring data in less accessible areas on a regular and cost-effective basis. Remote predictive mapping can be performed using optical imagery (Harris et al., 2011), such as those acquired by Landsat or SPOT satellites; however, optical images cannot be acquired at night or during cloudy conditions. Such limitations do not exist with synthetic aperture radar (SAR) images, such as those acquired by RADARSAT-2 (e.g., Schetselaar et al., 2007; LaRocque et al., 2012). Combining RADARSAT and Landsat imagery offers several advantages because both image types are complementary (Mei and Paulen, 2009; LaRocque et al., 2012). RADARSAT-2 images are sensitive to surface texture by providing information on scattering mechanisms that are related to surface roughness and moisture content (Harris et al., 2008; LaRocque et al., 2012). Landsat images are sensitive to surficial reflective properties that are generally governed by surface chemistry, vegetation and surface moisture content (Brown et al., 2008).

As part of a GEM-1 (2008–2013) project north of Wager Bay, Campbell et al. (2013) produced a surficial materials map with 12 classes using a maximum likelihood classifier applied to Landsat 7 images. The resulting RPM map had an accuracy of 25.6%, when classes were compared to the available GPS field data acquired at GEM-1 field stations. For the same area and using the same GPS field data, J. Byatt, A. LaRocque, B. Leblon, I. McMartin and J. Harris (unpublished data, 2015) achieved a mapping accuracy of 81.4% by classifying a combination of Landsat 8 optical images and RADARSAT-2 SAR images in the C-band with horizontal transmit and horizontal receive polarization (C-HH) and with C-band horizontal transmit and vertical receive polarization (C-HV) with a digital elevation model (DEM) and slope data using the Random Forest™ (RF) classifier (Breiman, 2001, 2003). For this project, the latter method will be used to map 15 surficial materials classes in an area located south of Wager Bay in the frame of the GEM-2 Tehery-Wager mapping activity. Besides the preliminary surficial materials map, this paper also presents the field data that were acquired during the summer of 2015, which will be used to validate the map.

Study area

The study area is located south of Wager Bay, Nunavut, on the western side of Hudson Bay (east of 90°W longitude), and includes parts of Ukkusiksalik National Park (Figure 1). It covers the NTS map areas 46D, E, 56A and H. Elevations range from sea level along Wager Bay and Hudson Bay to 550 m asl in the northwestern part of the study area. The area is characterized by streamlined, thin and thick till extending southeast from a major ice divide zone (Keewatin Ice Divide), from which ice flowed radially during the last glaciation (McMartin and Dredge, 2005). The former Keewatin Ice Divide zone, centred in the uplands southwest of Wager Bay, is now dominated by a mixture of till blankets and veneers, felsenmeer and weathered bed-

rock (McMartin et al., 2013, 2015). This glacial landscape is interspersed by a complex system of subglacial meltwater corridors and proglacial channels. Between these corridors, till surfaces show no sign of glaciofluvial erosion or reworking. The limit of postglacial marine submergence increases from 119 m asl south of Wager Bay to about 145–160 m asl west of Roes Welcome Sound. Lowlands that skirt the coasts of Roes Welcome Sound and Chesterfield Inlet, to the south, show evidence for postglacial marine erosion and reworking of thin glacial and glaciofluvial sediments. Marine veneers are sandy and occur as scattered deposits between rock ridges or glacial landforms.

Materials

Four RADARSAT-2 Scan SAR Wide-A C-band dual-polarized (HH and HV) imagery taken in August of 2014 were used for this study. They were acquired with an incidence angle that varied between 20 and 49.3°. Two SAR images were acquired with the ascending orbit and two with the descending orbit (Table 1). Two images were acquired during dry conditions and two during wet conditions, as Byatt (2014) showed that the best mapping accuracy is achieved when combining images acquired over dry and wet conditions. Each imagery file had two images: the HH polarized image and the HV polarized intensity image. All the images were checked visually to ensure the ground was free of snow and ice cover.

The Landsat 8 data acquired by the Operational Land Imager (OLI) sensor comprises three images taken in 2013 (Table 2), which were mosaicked together to cover the entire study area. Like the RADARSAT-2 images, they were visually checked to ensure that the ground was free of ice and snow. As well, these images do not include any clouds. The Landsat 8 images were georeferenced in a NAD83 format (UTM Zone 16, Row W) and have eight bands: B1 (0.43–0.45 µm), B2 (0.45–0.51 µm), B3 (0.53–0.59 µm), B4 (0.64–0.67 µm), B5 (0.85–0.88 µm), B6 (1.57–1.65 µm), B7 (2.11–2.29 µm) and B8 (0.50–0.68 µm).

Ancillary data used included a DEM mosaic (Natural Resources Canada, 2015), which is composed of several 1:50 000 DEM tiles that were used for terrain correction when georeferencing the SAR images and to take into account the topographic effects in the classification. The DEM has a resolution of 16.1 m in the x direction, 23.3 m in the y direction and 1 m in the z direction. Ground elevations are recorded in metres relative to mean sea level (MSL), based on the NAD83 horizontal reference datum.

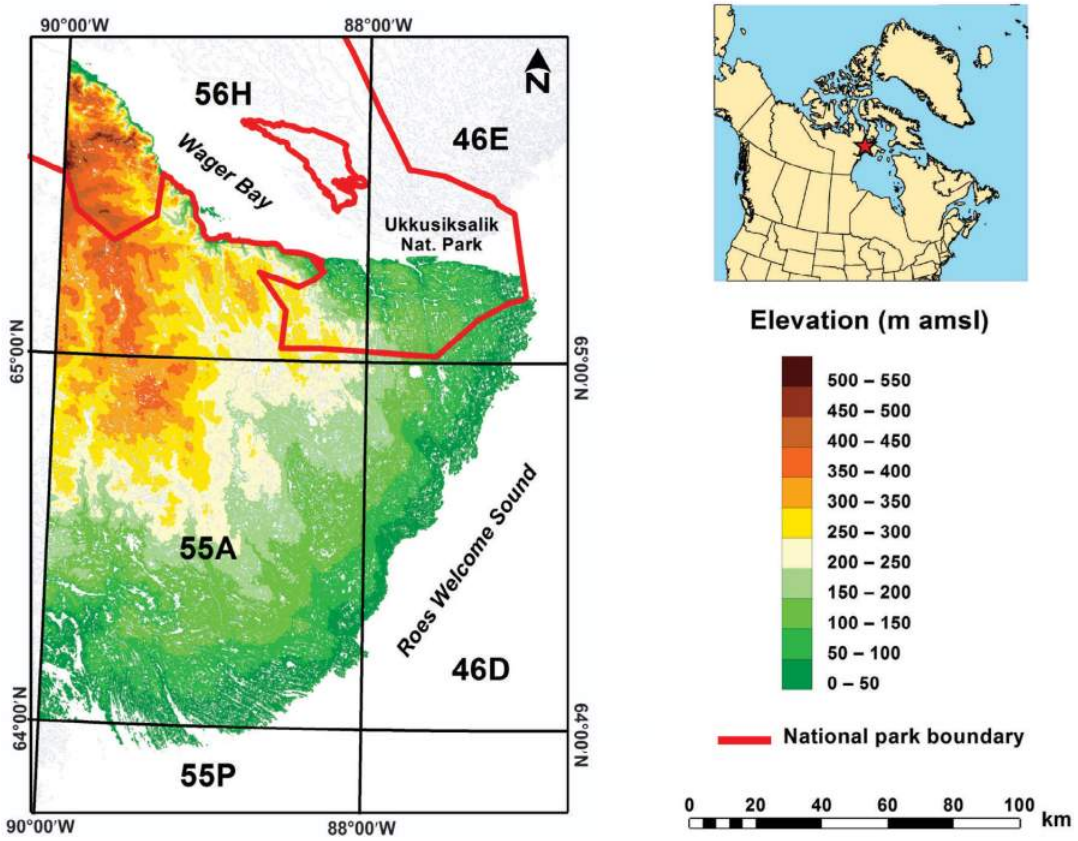

Figure 1: Location and digital elevation model (Natural Resources Canada, 2015) for the study area located south of Wager Bay, Nunavut. Abbreviations: amsl, above mean sea level; Nat., national.

Table 1: Characteristics of the RADARSAT-2 C-band horizontal transmit and horizontal receive (C-HH) and C-band horizontal transmit and vertical receive (C-HV) synthetic aperture radar (SAR) images used for the study in the southern Wager Bay area, Nunavut.

Image ID	Orbit	Date	Local time	Precipitation[1] (mm)
RS2_20140815_SCWA_A	Ascending	2014-08-15	18 h 21 min	2.04
RS2_20140825_SCWA_A	Ascending	2014-08-25	18 h 30 min	0.22
RS2_20140814_SCWA_D	Descending	2014-08-14	12 h 19 min	6.06
RS2_20140824_SCWA_D	Descending	2014-08-24	12 h 27 min	0.18

[1]Mean total precipitation during the three days prior to image acquisition as recorded at the following climatic stations: 1) Baker Lake (lat. 64°17'56"N, long. 96°04'40"W); 2) Rankin Inlet (lat. 62°48'00"N, long. 92°54'00"W); 3) Kugaaruk (lat. 68°32'26"N, long. 89°47'50"W); 4) Gjoa Haven (lat. 68°38'08"N, long. 95°51'01"W); and 5) Hall Beach (lat. 68°46'33"N, long. 81°14'33"W).

Field observations were also collected at selected GPS sites to assess the mapping errors and validate or eventually correct the preliminary RPM map, which has the 15 classes described in Table 3. Two types of field data were collected during a five-day period in the summer of 2015: field observations at 45 visited sites and aerial photographs of the terrain between visited sites (Figure 2). The visited sites were located in 10 areas of interest that represent the surficial material diversity of the study area (Figure 2).

The surficial material and landform features at each visited site were described, with an attempt to assign the site to one of the 15 surficial material classes of the map (Table 4). For each visited site, additional recorded observations included the geographic co-ordinates, photos of the site (surface and material) and photos of the area surrounding the site (Table 4).

The data collected during fieldwork is still being processed. The photographs taken from the helicopter have all been geolocated and sorted by time and date of capture. Both the GPS field observations and aerial photographs will be used to further refine the preliminary RPM map and to assess its mapping accuracy by determining the percentage of GPS sites correctly mapped over the RPM map per surficial material class.

Methods

Image processing

The majority of the image processing was performed in PCI Geomatica 2015 software. The DEM tiles were first imported and then mosaicked together using PCI OrthoEngine. The digital numbers of the Landsat 8 OLI images were first converted into top of atmosphere (TOA) reflectance values, following the method described in the Landsat 8 users handbook (United States Geological Survey, 2015). Such a conversion also removes some of the atmospheric interferences.

The RADARSAT-2 C-HH and C-HV images were filtered for removing speckle, using a Gaussian filter (with a standard deviation of 1.6) developed by Grunsky et al. (2009), and applied by LaRocque et al. (2012). Speckle can be considered as a noise and its intensity must be attenuated in order to enhance fine details on SAR images (Goodman, 1976). Each individual image was then orthorectified with the RADARSAT-2 Rational Function math model of the PCI OrthoEngine module, using the DEM and ground control points (GCPs). About 20 GCPs were extracted from the orthorectified Landsat 8 data for geocorrection, which was achieved with an mean accuracy of less than one pixel in both x and y axes. The georeferenced images were then mosaicked together to cover the entire study area. A mask created using a combination of Landsat 8 B8 and RADARSAT-2 C-HV images was applied to both SAR and optical images to remove lakes, rivers and other water bodies.

Image classification

Representative training areas of each the 15 material classes were delineated from photo interpretation of the orthorectified Landsat 8 and RADARSAT-2 imagery. The surficial material classes were defined based on the 12

Table 2: Characteristics of the Landsat 8 optical images acquired with the Operational Land Imager (OLI) sensor and used for the study in the southern Wager Bay area, Nunavut.

Image ID	Date	Time (UTC)	Cloud cover (%)	Sun elevation (°)	Sun azimuth (°)
LC80310142013207LGN00	2013-07-26	17 h 19 min	0.71	43.4	167.48
LC80310142013223LGN00	2013-08-11	17 h 19 min	2.35	39.23	168.42
LC80330142013221LGN00	2013-08-09	17 h 31 min	0.01	39.81	166.26

Abbreviation: UTC, Co-ordinated Universal Time.

Table 3: Description of the 15 surficial material classes used in the remote predictive mapping (RPM) map of the southern Wager Bay area, Nunavut.

Class code	Material class	Description
R	Bedrock	Bedrock outcrops of various rock types; >50% of the surface cover; surfaces range from rough and weathered to glacially polished and striated; patches of boulders and thin drift cover; may be lichen-covered outcrop.
B	Boulders	Includes exposed and lichen-covered felsenmeer (broken bedrock) and boulder fields; boulders cover >50% of the surface; rare discontinuous till and bedrock.
bT	Bouldery till	Silty-sand to sandy bouldery till; abundant lichen-covered boulders on surface; includes thin (<1 m) veneers and thick (>1 m) deposits of streamlined till, bouldery till blankets, eroded/modified till and/or wave-washed (winnowed) till.
T/R	Thin till	Thin cover of silty-sand till, interspersed with bedrock outcrops; till thickness commonly <1 m; bedrock outcrops may be present but are <50% of the surface; may have some boulders; little vegetation.
T	Thick till	Thick silty-sand to silty-clay till; grass- and lichen-covered; includes blanket and streamlined till; commonly soliflucted; thickness commonly >1 m.
sT	Sandy till	Sandy till, including eroded till; found with undifferentiated glaciofluvial sediments in meltwater corridor complex; thickness commonly between 2 to 5 m; hummocky topography interspersed with eroded till features; grass- and/or lichen-covered.
TV	Thick till with vegetation	Silty-sand to silty-clay till covered by short but dense vegetation; includes blanket and streamlined till; commonly soliflucted; thickness commonly >1 m; grass-covered.
SG	Sand and gravel	Sand and gravel, exposed or lichen-covered; proglacial deltas, eskers, outwash terraces, ice-contact glaciofluvial deposits.
SGV	Sand and gravel with vegetation	Sand and gravel, covered with short vegetation; proglacial deltas, eskers, outwash terraces, ice-contact glaciofluvial deposits.
Ms	Marine sand	Marine and minor silt deposit; sediments locally wave-washed or winnowed; thick (>1 m) marine or glaciolacustrine deposits; may include eolian dunes, beaches and intertidal flats.
MsV	Marine sand with vegetation	Marine sand and minor silt; covered with short but dense vegetation; material locally wave-washed or winnowed; thick (>2 m) marine or glaciolacustrine deposits; may include vegetated eolian dunes and raised beaches.
Ms/R	Thin marine sand	Thin marine sand and minor silt; material locally wave-washed or winnowed; thin (<1 m) marine or glaciolacustrine deposits; bedrock outcrops may be present but are <50% of the surface.
O	Organic	Water saturated thin organic sediments; poor drainage; shallow sedge fens and sphagnum bogs.
At	Alluvial terrace	Exposed sand and minor silt; mostly dry; alluvial terraces, former deltas and fans.
Ap	Alluvial plain	Alluvial sands and minor silts, exposed; periodically water-saturated sediment; alluvial plains, recent deltas and fans.

classes of Campbell et al.'s (2013) report from the GEM-1 Wager Bay study region. Because the GEM-2 study area's southern region is composed of different materials, some changes were made and new classes were defined in order to take into account the influence of vegetation cover (Table 3).

The classifier used in this study is a nonparametric decision-tree–type classifier (RF), which does not assume normal distribution of the input data (Breiman, 2001, 2003). The algorithm used for this study was the one developed in R programming language (R Development Core Team, 2012), which had recently been successfully employed in a study on surficial material mapping in the Hudson Bay Lowland (Ou et al., in press). The RF classifier has two versions, known as all-polygon and subpolygon. The all-polygon version uses all of the pixels within all of the training-area polygons to define class training areas, whereas the subpolygon version randomly selects a user-determined number of training area pixels from each class. For this study, the all-polygon version was only used as it has the advantage of taking into account the actual class size. The mtry variable in the RF classifier refers to the number of variables randomly sampled as candidates at each split of every node. The default values of mtry for a classification are calculated as the square root of p, where p is the number of variables in x, which is the matrix of predictors for the classification. Such default values lead to a setting that includes all input features, that is, all pixels are randomly sampled as candidates at each split of every node.

The RF classifier uses two-thirds of the input training-area data, referred to as in-bag data, for calibration. The remaining third of the data is then referred to as out-of-bag data

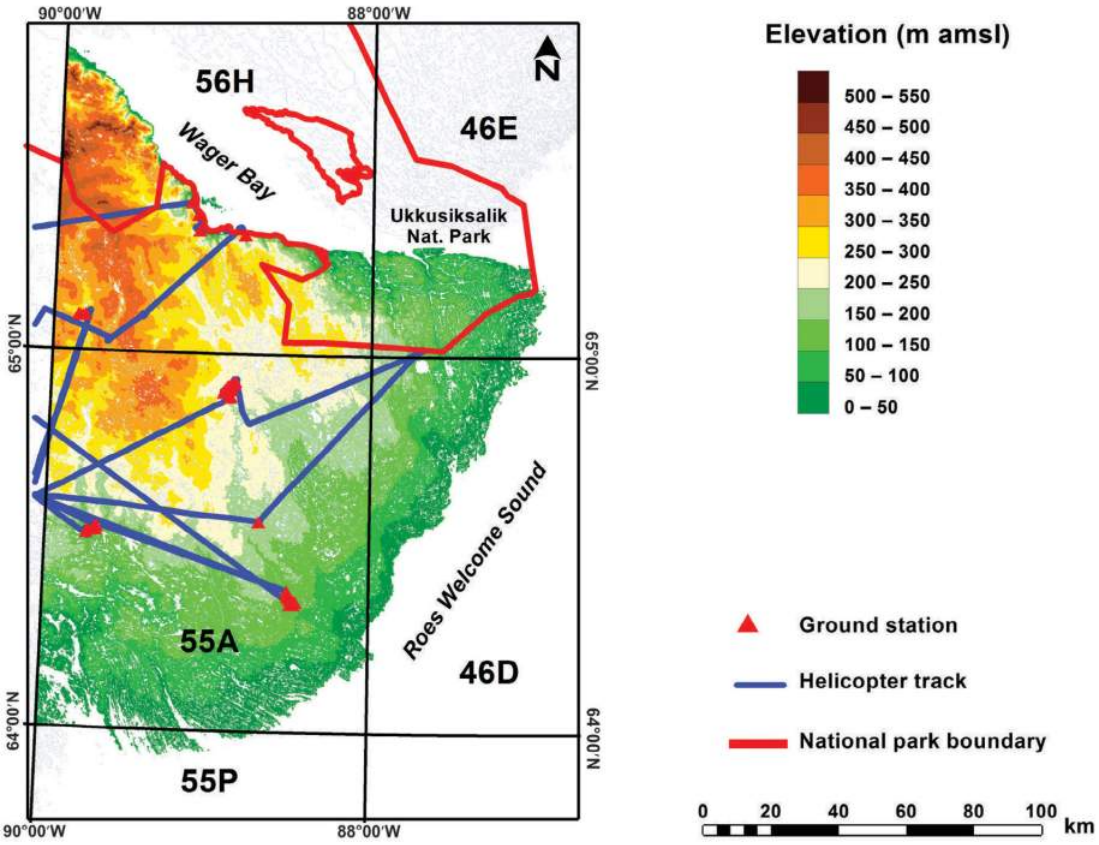

Figure 2: Location of the GPS sites and the aerial surveys, southern Wager Bay area, Nunavut. Background image was generated using a Canadian digital elevation model mosaic (Natural Resources Canada, 2015). Abbreviations: amsl, above mean sea level; Nat., national.

and is used to test or validate the resulting classification. In-bag data are used to create the 500 individual decision trees, which are applied to produce independent classifications. These independent classifications are then combined into the final classification map (Waske and Braun, 2009). When there are relatively limited training data in some classes, the RF classifier allows bootstrap aggregating of the in-bag data to increase the number of training pixels. In this study, each class within the study area had enough training sites, so bootstrapping was not required. The RF classifier is not sensitive to noise or overclassifying and can estimate the importance of the individual input variables (Gislason et al., 2006; Waske and Braun, 2009). Indeed, the RF classifier produces a mean decrease accuracy plot that ranks the variable importance of the input data as a function of the degree of usefulness of the input images in the classification. The higher the input data is on the mean decrease accuracy y axis, the more useful the data was in performing the classification (Strobl et al., 2008; Louppe et al., 2013).

The RF classifier outperforms a widely used classification method, known as the maximum likelihood classifier (MLC; Mather and Tso, 2003). For the same combination of input data, the RF classifier consistently gives a better overall accuracy than MLC, as shown in several land-cover mapping studies (Waske and Braun, 2009; Ozdarici-Ok et al., 2012; LaRocque et al., 2013; A. LaRocque, B. Leblon, L.L. Bourgeau-Chavez, N. French and R. Woodward, unpublished paper, 2015). The reason for the better accuracy is that the RF classifier is a nonparametric classifier, which is able to handle various types of input data (optical, SAR, DEM), whatever the data distribution, whereas MLC can only handle Gaussian-distributed data. Another advantage of the RF classifier over the MLC classifier is that the RF classifier can handle as many input data as is desired, so all optical, SAR and DEM data used in this study can be inputted into the classifier. Additionally, in contrast to MLC, the RF classifier allows the assessment of the variable importance of each input data used in the classification.

Accuracy assessment

Classification accuracy can be assessed by comparing the training areas with the equivalent classified land use in the satellite imagery. However, this method only gives an assessment of the classified image accuracy, which is different than the true mapping accuracy (Alexanderson, 2000). A more robust and independent accuracy assessment is to compare the resulting classified image with an independent set of field observation data acquired over validation sites

Table 4: Global Positioning System (GPS) co-ordinates and classes associated with the 45 visited field sites in the southern Wager Bay area, Nunavut.

Site no.	Site ID	Material class	Class code	Latitude (N)	Longitude (W)
1	20150714001	Boulders	B	65°23'58.7"	089°09'47.7"
2	20150714002	Bedrock	R	65°23'56.7"	089°09'34.4"
3	20150714003	Bouldery till	bT	65°22'01.7"	089°06'42.7"
4	20150714004	Sand and gravel	SG	65°19'28.6"	089°06'10.2"
5	20150714005	Bouldery till	bT	65°19'29.2"	089°06'00.1"
6	20150714006	Bedrock	R	65°18'59.2"	088°48'42.1"
7	20150714007	Bouldery till	bT	65°18'55.9"	088°48'39.8"
8	20150714008	Sand and gravel	SG	64°20'30.9"	088°28'51.0"
9	20150714009	Organic/marine sand	O/Ms	64°20'17.6"	088°28'58.6"
10	20150714010	Marine sand	Ms	64°20'15.6"	088°28'50.5"
11	20150715011	Marine sand with vegetation	MsV	64°20'20.4"	088°27'38.5"
12	20150715012	Marine sand	Ms	64°20'43.7"	088°26'56.5"
13	20150714013	Marine sand with vegetation	MsV	64°20'55.6"	088°27'51.9"
14	20150714014	Bouldery till	bT	64°21'10.0"	088°28'52.7"
15	20150714015	Organic	O	64°21'25.1"	088°28'53.9"
16	20150714016	Boulders	B	64°21'31.0"	088°29'30.0"
17	20150714017	Bouldery till	bT	64°21'38.5"	088°29'46.8"
18	20150714018	Thin till	T/R	64°22'00.0"	088°30'06.8"
19	20150714019	Thin marine sand	Ms/R	64°22'28.4"	088°30'08.0"
20	20150714020	Sandy till	sT	64°55'38.8"	088°51'05.1"
21	20150714021	Thin till	T/R	64°55'19.6"	088°51'39.2"
22	20150714022	Thick till	T	64°55'04.2"	088°51'53.5"
23	20150714023	Alluvial plain	Ap	64°55'02.1"	088°52'03.6"
24	20150714024	Organic	O	64°54'57.7"	088°52'40.1"
25	20150714025	Alluvial terrace	At	64°54'54.4"	088°52'55.4"
26	20150714026	Alluvial terrace	At	64°54'55.0"	088°53'17.0"
27	20150714027	Bouldery till	bT	64°54'46.0"	088°53'53.2"
28	20150714028	Thin till	T/R	64°54'42.6"	088°54'05.5"
29	20150714029	Thick till	T	64°54'15.5"	088°54°56.5"
30	20150714030	Thick till with vegetation	TV	64°53'56.6"	088°55'12.1"
31	20150714031	Sand and gravel with vegetation	SGV	64°53'49.5"	088°55'13.1"
32	20150714032	Alluvial plain	Ap	64°53'01.5"	088°53'10.3"
33	20150716033	Organic/thick till	O/T	64°53'11.5"	088°52'31.2"
34	20150716034	Sand and gravel	SG	64°33'22.5"	088°41'05.6"
35	20150717035	Bedrock	R	64°32'04.5"	089°41'04.8"
36	20150717036	Bouldery till	bT	64°32'05.6"	089°40'53.6"
37	20150717037	Organic	O	64°32'00.1"	089°41'37.1"
38	20150717038	Marine sand	Ms	64°31'31.2"	089°41'21.9"
39	20150717039	Marine sand	Ms	64°31'28.4"	089°42'31.5"
40	20150717040	Marine sand	Ms	64°31'32.3"	089°44'14.9"
41	20150717041	Bouldery till	bT	64°31'00.5"	089°44'43.7"
42	20150718042	Thick till with vegetation	TV	65°05'40.1"	089°50'52"
43	20150718043	Marine sand with vegetation	MsV	65°05'39.1"	089°50'20.1"
44	20150718044	Alluvial plain	Ap	65°05'31.6"	089°49'17.1"
45	20150718045	Organic/marine sand	O/Ms	65°05'41.3"	089°48'18.2"

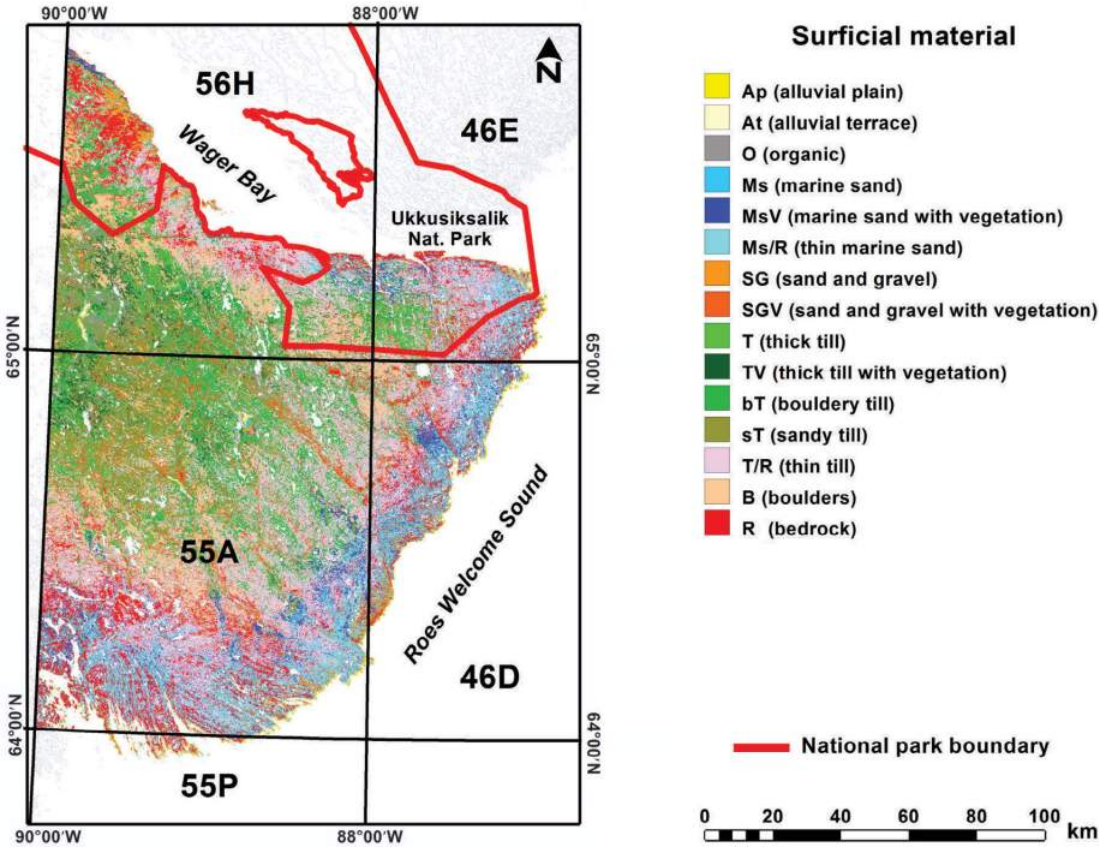

Figure 3: Remote predictive surficial materials map for the southern Wager Bay area produced by the Random Forest™ classifier applied to a combination of Landsat 8 images and RADARSAT-2 C-band images (with horizontal transmit and horizontal receive [HH] and horizontal transmit and vertical receive [HV] polarization) with a digital elevation model (Natural Resources Canada, 2015) and slope data. Abbreviation: Nat., national.

that have a GPS location. If the image returns the same class as observed at the validation sites, then the map is considered correct and the pixels related to this validation site are associated to a value of one. If it is not the case, then the value is zero. A percentage of correct identifications can then be computed as a function of the total number of validation sites.

Results

A preliminary RPM map with the 15 classes was established for the southern part of Wager Bay based on training areas that were delineated from photo interpretation (Figure 3).

The variable importance produced by the RF classifier (Figure 4) shows that the most influential variables are the Landsat 8 near-infrared (B5) and shortwave infrared (B6, B7) bands, the DEM, slope data and the HV image acquired in the descending mode in dry conditions. The other RADARSAT-2 images are more important in the classification than the Landsat 8 visible bands (B1, B2, B3, B4, B8). For the RADARSAT-2 images, the dry images are always more important than the wet images, whatever the polarization and the orbit.

Economic considerations

This report describes an innovative approach to classifying surficial materials using a combination of various Earth observation data from satellites, DEM and slope data. The resulting map will be compared to targeted field data acquired south of Wager Bay in 2015. The resultant predictive map will provide information on the nature, distribution and texture of the surficial materials and, therefore, help to minimize any risk associated with surface mineral exploration and infrastructure development. Furthermore, the remote predictive mapping of materials with increasingly higher accuracy will enhance traditional surficial geology mapping compilation methods, which use fieldwork, sampling and photo interpretation. As shown here, RPM is a technique that can be used to map vast areas in a time-efficient manner and at a relatively low cost. Thereby, it will allow researchers to maximize future fieldwork efforts, both for bedrock and surficial geology research purposes, which are very costly (e.g., Wodicka et al., 2015; McMartin et al., 2015).

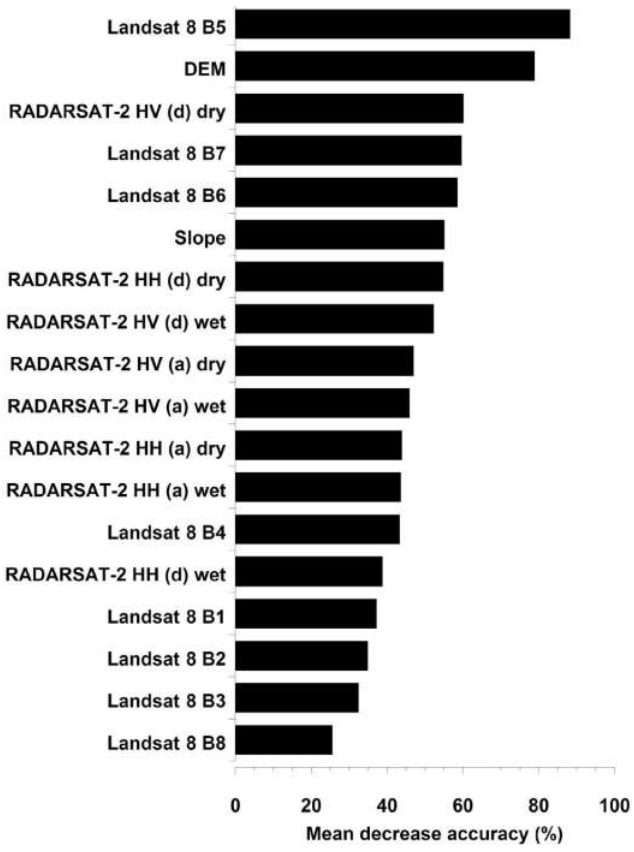

Figure 4: Variable importance of input data for the Random Forest™ classifier applied to a combination of Landsat 8 images and RADARSAT-2 C-band images (with horizontal transmit and horizontal receive [HH] and horizontal transmit and vertical receive [HV] polarization) with a digital elevation model (DEM) and slope data. Abbreviations: a, ascending; B, band; d, descending.

Conclusions

This paper presents preliminary results of a surficial materials mapping project within the southern Wager Bay area. A preliminary map with 15 surficial materials classes was produced from a combination of RADARSAT-2 C-band images with horizontal transmit and horizontal receive polarization and with horizontal transmit and vertical receive polarization and Landsat 8 Operational Land Imager images with a digital elevation model and slope data. The study area was in a region that has not been mapped and/or mapped only at a reconnaissance scale. Field observations and aerial photographs were acquired during a five-day period in the summer of 2015 and will be used to further refine the preliminary remote predictive mapping map and to assess its mapping accuracy. This accuracy will be expressed as a percentage of GPS sites correctly mapped on the remote predictive mapping map for each surficial material class.

Acknowledgments

Scholarships from the National Sciences and Engineering Research Council (postgraduate), New Brunswick Innovation Foundation and Association of Canadian Universities for Northern Studies support the work of J. Byatt. Field travel of J. Byatt was supported by a Northern Scientific Training Program grant awarded to J. Byatt and a National Sciences and Engineering Research Council Discovery Grant awarded to B. Leblon. Logistics were provided through the Tehery-Wager geoscience mapping activity led by N. Wodicka (Natural Resources Canada, Geological Survey of Canada) and H. Steenkamp (Canada-Nunavut Geoscience Office). The RADARSAT-2 images were provided to the authors by the Canadian Space Agency through the Geological Survey of Canada.

Natural Resources Canada, Earth Sciences Sector contribution 20150292

References

Alexanderson, J.H. 2000: Landsat mapping of ice-marginal features on the Taymyr Peninsula, Siberia: image interpretation versus geological reality; Geological Quarterly, v. 44, no. 1, p. 15–25.

Breiman, L. 2001: Random forests; Machine Learning, v. 45, no. 1, p. 5–32.

Breiman, L. 2003: Manual of setting up, using and understanding random forests, V4.0.; University of California Berkeley, Berkeley, California, 33 p., URL <http://www.stat.berkeley.edu/~breiman/Using_random_forests_v4.0.pdf> [November 2015].

Brown, O., Harris, J.R. and Utting, D. 2008: Case study 6: surficial mapping of northern Baffin Island using Landsat and topographic data; *in* Remote Predictive Mapping: An Aid for Northern Mapping, J.R. Harris (ed.), Geological Survey of Canada, Open File 5643, p. 225–232.

Byatt, J. 2014: Influence of environmental conditions on surficial deposit mapping using LANDSAT-5 TM and RADARSAT-2 polarimetric SAR images; B.Sc. (honour) thesis, University of New Brunswick, Fredericton, New Brunswick, 24 p.

Campbell, J.E., Harris, J.R., Huntley, D.H., McMartin, I., Wityk, U., Dredge, L.A. and Eagles, S. 2013: Remote predictive mapping of surficial earth materials: Wager Bay north area, Nunavut - NTS 46-E (N), 46-K (SW), 46-L, 46-M (SW), 56-H (N), 56-I and 56-J (S); Geological Survey of Canada, Open File 7118, 42 p.

Gislason, P., Benediktsson, J. and Sveinsson, J. 2006: Random forest for land cover classification; Pattern Recognition Letters, v. 27, p. 294–300.

Goodman J.W. 1976: Some fundamental properties of speckles; Journal of Optical Society of America, v. 66, no. 11, p. 1145–1150.

Grunsky, E., Harris, J.R. and McMartin, I. 2009: Predictive mapping of surficial materials, Schultz Lake area (NTS 66 A), Nunavut, Canada; Reviews in Economic Geology, v. 16, p. 177–198.

Harris, J.R. 2008: What is RPM: chapter 1; *in* Remote Predictive Mapping: An Aid for Northern Mapping, J.R. Harris (ed.), Geological Survey of Canada, Open File 5643, p. 1–4.

Harris, J.R., Grunsky, E. and Singhroy, V. 2008: Radar remote sensing; *in* Remote Predictive Mapping: An Aid for Northern Mapping, J.R. Harris (ed.), Geological Survey of Canada, Open File 5643, p. 135–160.

Harris, J.R., Wickert, L., Lynds, T., Behnia, P., Rainbird, R., Grunsky, E., McGregor, R. and Schetselaar, E. 2011: Remote predictive mapping 3. Optical remote sensing – a review for remote predictive mapping in northern Canada; Geoscience Canada, v. 38, p. 49–83.

LaRocque, A., Leblon, B., Harris, J.R., Jefferson, C.W., Tschirhart, V. and Shelat, Y. 2012: Surficial materials mapping in Nunavut, Canada, with multi-beam RADARSAT-2 dual-polarization C-HH and C-HV, Landsat-7 ETM+, and DEM data; Canadian Journal of Remote Sensing, v. 38, p. 281–305.

LaRocque, A., Yue, B., Leblon, B., Haddadi, A., Harris, J., Jefferson, C. and Shelat, Y. 2013: A comparison of supervised classifiers applied to RADARSAT-2 polarimetric SAR and Landsat-7 ETM+ images for mapping surficial materials in Nunavut; 34th Canadian Remote Sensing Symposium, August 27–29, 2013, Victoria, British Columbia, Program with Abstracts, abstract.

Louppe, G., Wehenkel, L., Sutera, A. and Geurts, P. 2013: Understanding variable importances in forests of randomized trees; Advances in Neural Information Processing Systems, v. 26, p. 431–439.

Mather, P. and Tso, B. 2009: Classification Methods for Remotely Sensed Data (2nd edition); CRC Press, Boca Raton, Florida, 376 p.

McMartin, I. and Dredge, L.A. 2005: History of ice flow in the Shultz Lake and Wager Bay areas, Kivalliq Region, Nunavut; Geological Survey of Canada, Current Research 2005-B2, 10 p.

McMartin, I., Byatt, J., Randour, I. and Day, S. 2015: Report of 2015 activities for regional surficial mapping, till and stream sediment sampling in the Tehery-Wager GEM 2 Rae project area; Geological Survey of Canada, Open File 7966, 14 p.

McMartin, I., Wodicka, N., Bazor, D. and Boyd, B. 2013: Till composition across the Rae craton south of Wager Bay, Nunavut: results from the Geo-mapping Frontiers' Tehery-Cape Dobbs project; Geological Survey of Canada, Open File 7417, 27 p.

Mei, S. and Paulen, R.C. 2009: Using multi-beam RADARSAT-1 imagery to augment mapping surficial geology in northwest Alberta, Canada; Canadian Journal of Remote Sensing, v. 35, p. 1–22.

Natural Resources Canada 2015: Canadian digital elevation data, level 1; Natural Resources Canada, URL <http://geogratis.gc.ca/api/en/nrcan-rncan/ess-sst/C40ACFBA-C722-4BE1-862E-146B80BE738E.html> [April 2015].

Ou, C., LaRocque, A., Leblon, B., Zhang, Y., Webster, K. and McLaughlin, J. in press: Modelling and mapping permafrost at high spatial resolution using Landsat and Radarsat-2 images in northern Ontario, Canada. Part 2 regional mapping; International Journal of Remote Sensing.

Ozdarici-Ok, A., Akar, O. and Gungor, O. 2012: Evaluation of random forest method for agricultural crop classification; European Journal of Remote Sensing, v. 45, p. 421–432.

R Development Core Team 2012: R: a language and environment for statistical computing; software development tools, R Foundation for Statistical Computing, Vienna, Austria, URL <http://www.R-project.org/> [November 2015].

Schetselaar, E.M., Harris, J.R., Lynds, T. and de Kemp, E.A. 2007: Remote predictive mapping 1. Remote predictive mapping (RPM): a strategy for geological mapping of Canada's north; Geoscience Canada, v. 34, p. 93–111.

Strobl, C., Boulesteix, A.L., Kneib, T., Augustin, T. and Zeileis, A. 2008: Conditional variable importance for random forests; BMC Bioinformatics, v. 9:307, 11 p.

United States Geological Survey 2015: Landsat 8 (L8) data users handbook; Sioux Falls, South Dakota, EROS, June 2015, 9 p., URL <https://landsat.usgs.gov/documents/Landsat8DataUsersHandbook.pdf> [November 2015].

Waske, B. and Braun, B. 2009: Classifier ensembles for land cover mapping using multi-temporal SAR imagery; ISPRS Journal of Photogrammetry and Remote Sensing, v. 64, p. 450–457.

Wodicka, N., Steenkamp, H., Lawley, C., Peterson, T., Guilmette, C., Girard, E. and Buenviaje, R. 2015: Report of activities for the bedrock geology and economic potential of the Tehery-Wager area - GEM 2 Rae project; Geological Survey of Canada, Open File 7970, 14 p.

Overview of the surficial geology map compilation, RapidEye land-cover mapping and permafrost studies for infrastructure in the western Hudson Bay area, Nunavut

T. Tremblay[1], M.S. Kendall[2], A.-M. LeBlanc[3], N. Short[3], O. Bellehumeur-Génier[3], G.A. Oldenborger[3], P. Budkewitsch[4] and D.J. Mate[5]

[1]*Canada-Nunavut Geoscience Office, Iqaluit, Nunavut, tommy.tremblay@canada.ca*

[2]*Department of Geography, Memorial University of Newfoundland, St. John's, Newfoundland and Labrador*

[3]*Natural Resources Canada, Geological Survey of Canada, Ottawa, Ontario*

[4]*Indigenous and Northern Affairs Canada, Iqaluit, Nunavut*

[5]*Canadian Northern Economic Development Agency, Iqaluit, Nunavut*

Tremblay, T., Kendall, M.S., LeBlanc, A.-M., Short, N., Bellehumeur-Génier, O., Oldenborger, G.A., Budkewitsch, P. and Mate, D.J. 2015: Overview of the surficial geology map compilation, RapidEye land-cover mapping and permafrost studies for infrastructure in the western Hudson Bay area, Nunavut; *in* Summary of Activities 2015, Canada-Nunavut Geoscience Office, p. 145–160.

Abstract

The Western Hudson Bay project is a Canada-Nunavut Geoscience Office–led geoscience project collecting and compiling geoscience data for infrastructure. Significant new infrastructure is being considered in the Kivalliq region of Nunavut, including a proposed Manitoba-Nunavut road corridor, in order to support natural resource and community development. Western Hudson Bay lies in the continuous permafrost zone, where 90–100 % of the ground surface is underlain by permafrost. A lack of compiled regional geoscience knowledge in this region is a hindrance in helping advance informed decision-making to build this type of infrastructure. This paper presents 1) the new digital compilation of surficial geology for the area, from various maps published in the 1970s and 1980s; 2) a methodology for interpreting land cover from RapidEye images to enhance the location of some potential aggregate sources (gravel deposits), bedrock outcrops, bouldery tills, freshly eroded sediments, vegetation and water surfaces; 3) a bibliographical summary of till and lake-sediment geochemical samples and of bedrock geology synthesis maps, and of the location of mineral occurrences; and 4) a summary of the existing literature on the permafrost conditions. This paper also presents ongoing and possible future work on 1) the integration of modern and traditional knowledge on permafrost conditions, 2) the assessment of ground surface displacement using a remote sensing method, and 3) new bedrock geology mapping to complete the coverage of the study area.

Résumé

Dans le cadre du projet géoscientifique de l'ouest de la baie d'Hudson dirigé par le Bureau géoscientifique Canada-Nunavut, on a procédé à la cueillette et à la compilation de données géoscientifiques relatives aux infrastructures. Le but d'importants nouveaux projets d'infrastructure à l'étude dans la région de Kivalliq, au Nunavut, notamment le corridor routier proposé reliant le Manitoba et le Nunavut, est de contribuer aussi bien au développement communautaire qu'à celui des ressources naturelles. La partie ouest de la baie d'Hudson se situe dans une zone de pergélisol continu où presque la totalité (90 à 100%) de la région en question repose sur du pergélisol. Des lacunes au niveau des connaissances géoscientifiques au sujet de cette région s'avèrent une entrave à l'amélioration du processus de prise de décisions éclairée lorsqu'il s'agit de construire ce type d'infrastructure. Le présent article porte sur 1) la nouvelle restitution numérique de données géologiques de surface de la région, établie à partir de diverses cartes publiées au cours des années 1970 et 1980; 2) la méthodologie adoptée afin d'interpréter la couverture des terres à partir d'images captées par le système RapidEye de façon à mieux faire ressortir l'emplacement de certaines sources possibles d'agrégats (dépôts de gravier), d'affleurements de la roche en place, de tills pierreux, de sédiments fraîchement érodés et de surfaces couvertes par de la végétation ou de l'eau; 3) l'élaboration d'un répertoire bibliographique d'échantillons géochimiques provenant de tills ou de sédiments lacustres ainsi que de cartes de synthèse de la géologie du substratum rocheux et de l'emplacement des venues minérales; et 4) un sommaire des ouvrages publiés relatifs aux conditions propres au pergélisol. L'article porte également sur des travaux

This publication is also available, free of charge, as colour digital files in Adobe Acrobat® PDF format from the Canada-Nunavut Geoscience Office website: http://cngo.ca/summary-of-activities/2015/.

en cours ou éventuels ayant trait: 1) à l'intégration des connaissances actuelles et du savoir traditionnel au sujet du pergélisol; 2) à l'évaluation du niveau de perturbation de la surface du sol au moyen de méthodes de télédétection; et 3) à de nouveaux travaux cartographiques de la géologie du substratum rocheux entrepris en vue de compléter la couverture de la région à l'étude.

Introduction

Significant new infrastructure, including a proposed Manitoba–Nunavut road corridor, is being considered in the Kivalliq region of Nunavut (Figure 1) in order to support natural resource and community development. In 2006, Nishi-Khon/SNC-Lavalin Limited produced a foundational report, *Building Lasting Infrastructure: Nunavut-Manitoba Route Selection Study*, which aimed to identify and evaluate a series of routes for a proposed road corridor that linked Rankin Inlet, Nunavut, with an existing all-weather road network in northern Manitoba (Nishi-Khon/SNC-Lavalin Limited, 2006, 2007, 2010a, b). A lack of compiled regional geoscience knowledge in this region is a hindrance to advancing informed decision-making to build this type of infrastructure.

In order to address this knowledge gap, the Canada-Nunavut Geoscience Office (CNGO) in collaboration with the Geological Survey of Canada (GSC) has implemented a two-year project (2014–2016) guided by geoscience priorities developed through a commissioned report (Levson, 2014). These priorities include 1) regional mapping of potential sources of granular material and aggregate quality evaluations; 2) identification and detailed evaluation of specific, large-volume and high-quality sources of granular material; 3) detailed permafrost and ground-ice studies within the proposed corridor; 4) 1:50 000 scale surficial geology mapping in areas where granular material is particularly scarce and where ground-ice conditions are expected to be particularly problematic; 5) detailed (e.g., 1:5000 scale) terrain hazard analysis at major stream crossings or other problematic areas; and 6) identification of areas with relatively high mineral prospectivity within the proposed corridor.

The objective of this CNGO-GSC project is to compile all existing aggregate, mineral potential, surficial and permafrost data for a corridor approximately 100 km wide and extending from the Manitoba border to Rankin Inlet (NTS map areas 55D–F, J–L, N, O, 65A, H), along the western Hudson Bay coastline. Expected results from this work include 1) a newly compiled surficial geology dataset for the area, 2) regional identification of aggregate resources and mineral potential, and 3) reports on permafrost characteristics and terrain sensitivity. Compilation of geoscience information in this region, for infrastructure development purposes, has never been completed and addresses a significant knowledge gap for decision-makers. It is expected that results from this project will help direct more detailed geoscience research in the area in the future.

This paper will provide an update on existing or new permafrost, geomorphology, mineral potential and surficial geology compilations and assessment work being conducted in the study area. The following specific objectives and results are presented in this paper:

- compilation and conversion of existing surficial geology paper maps (1:125 000 scale) to digital format, using new GSC legend;
- enhancement of the resolution of some units on the surficial maps with satellite image interpretation (RapidEye, multispectral 5 m resolution), with the goal of finding and detailing gravel sources, and identifying thaw-sensitive areas;
- compilation of existing data and knowledge on climate and permafrost in the study area; and
- examination of the need for new permafrost studies required to enhance knowledge, including field measurements (borehole measurements, thermistors or geophysical surveys) and satellite image observations (RADARSAT, differential interferometric synthetic aperture radar [DInSAR]).

Regional settings

The study area (Figure 1) lies within the Kivalliq region of Nunavut, in the informal general geographic area previously known as Keewatin in former maps and reports. The general topography is a slightly undulating plain generally under 200 m above sea level (asl), and mostly under 100 m asl, with one isolated elevated hill south of Chesterfield Inlet (331 m asl). A mostly parallel, tight network of medium-sized rivers drains the area to the southeast toward Hudson Bay, interrupted by several large lakes (Kaminak Lake, South Henik Lake, Maguse Lake). Small lakes abound, forming in depressions related to bedrock basins, till landforms, eskers and a few rounded depressions that could be associated with thermokarst terrain. Flat plains, underlain by thick marine sediments, strand across the coastline in the vicinity of Arviat. The narrow Chesterfield Inlet leads to the Baker Lake area, and is mostly surrounded by lower elevation, rocky terrain. Most of the study area is covered with tundra vegetation typical of the low-arctic region (mosses, herbaceous plants, shrubs, alpine-arctic plants). The treeline is in the southwestern part of study area, with short trees (e.g., *Picea mariana*) sparsely distributed in isolated pockets.

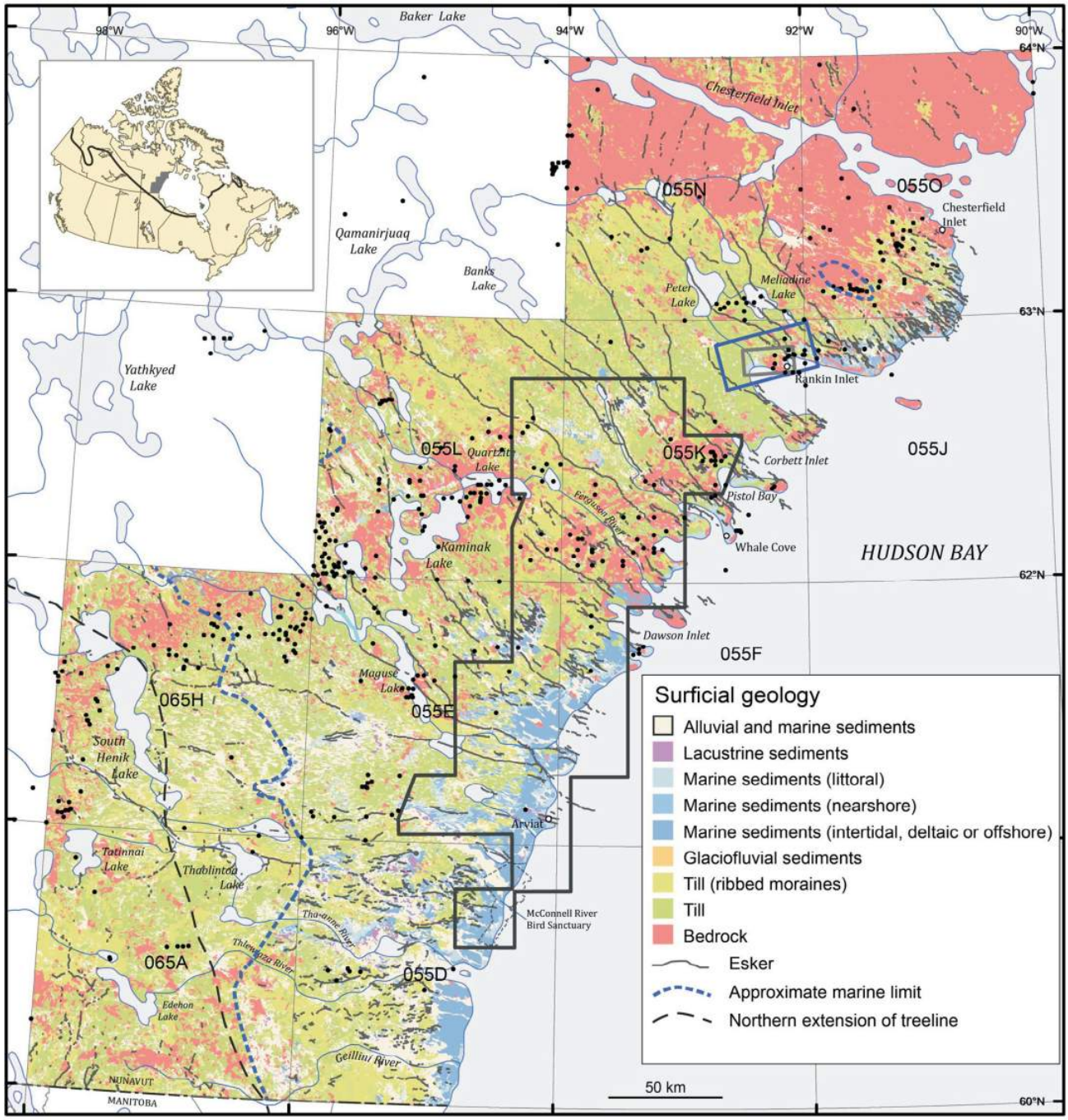

Figure 1: Surficial geology map of western Hudson Bay area, Nunavut. The black outline shows the RapidEye 5 m resolution multispectral data coverage, the blue outline is the RADARSAT 1 m resolution coverage and the grey outline is the RADARSAT 3 m resolution coverage. The black dots represent the mineral occurrences (NunavutGeoscience.ca, 2015). The inset map shows the location of the study area (grey area) within Canada, and the black line corresponds to the southern limit of continuous permafrost.

The bedrock is principally formed of gneiss terranes, supracrustal belts and associated plutons of the Western Churchill Province (Hearne domain). These Archean and Paleoproterozoic rocks were deformed during Paleoproterozoic times (Paul et al., 2002; Tella et al., 2007).

The history of ice flows (Shilts, 1973; Dyke and Dredge, 1989; Fulton, 1995; McMartin and Henderson, 2004a) indicates that the main ice flow direction is to the southwest in the study area, emanating from the Keewatin Ice Divide during the last glaciation and deglaciation. This ice flow is associated with most streamlined tills, ribbed moraines and the general direction of eskers in the study area (Aylsworth and Shilts, 1989). An earlier ice flow to the southwest is also detected from the striations record (McMartin and Henderson, 2004a).

Most of the study area, except the area around South Henik and Edehon lakes, was inundated by the Tyrell Sea after deglaciation (Dyke and Dredge, 1989; Dyke et al., 2003). The maximum marine limit is between 150 and 190 m asl. Deglaciation occurred between 8 and 6.5 ^{14}C ka.

Data compilation and results

Surficial geology maps

The existing 1:125 000 scale surficial maps were recently digitized by the Geological Survey of Canada (Wright, 1967; Boydell, 1974; Shilts et al., 1976; Arsenault et al., 1981a–c; Aylsworth et al., 1981a–c, 1986a–c, 1990; McMartin, 2002; McMartin and Henderson, 2004b; Dredge et al., 2013). The newly converted maps will soon be available online in digital format (Canadian Geoscience Maps series), whereas the original maps are currently available only in .pdf format online at Natural Resources Canada's bibliographic database (http://geoscan.nrcan.gc.ca).

During the digital conversion of the original source maps, the new GSC legend (surficial data model, version 2.1; Cocking et al., 2015) was applied to all of the maps. The main generalized surficial geology units are presented on Figure 1; on the final maps, each of these generalized units is subdivided into one or more surficial geology units (indicated by letters) as described in the next sections. Unless otherwise stated, the following description of surficial geology units was modified from Shilts et al. (1976).

Till

The most frequently represented till units are till blanket (Tb; including zones with drumlins and flutings) and ridged till (Tr; till [ribbed moraines] unit on Figure 1); the later delimits areas of ribbed moraines, and includes mostly Rogen moraines and De Geer moraines along the coastline (Shilts et al., 1976). Undifferentiated tills (T), moraine tills (Tm) and hummocky tills (Th) are present in a few places in the study area, but are mapped along with Tb in Figure 1 (till unit). Thin veneer (<1 m discontinuous till cover over bedrock) is mapped along with bedrock (R) on Figure 1. From multiple samples taken in a variety of till types, the grain size of tills averages 53% sand, 45% silt and 2% clay around the Rankin Inlet and Kaminak Lake areas (McMartin, 2000; McMartin and Henderson, 2004b). The till is described as having a liquid limit of 8–18% and plasticity indices of 0–8%, and is susceptible to liquefaction under loading, and during heavy rains or spring thaw (Shilts et al., 1976). In the study area, tills frequently contain significant amounts of Dubawnt Supergroup clasts in dispersal trains, which are rich in silt and clay and depressed in metal trace elements (Shilts, 1973). Multiple tills are seen in the Kaminak Lake area and along the Kazan River (west of the study area) with significant contrast in texture and composition (Shilts, 1971), generally corresponding to varying amounts of the Dubawnt Supergroup clasts in the tills. Supraglacial tills and ribbed moraines are likely to be more bouldery and rougher at the surface than drumlinized tills, presumably because more ground-ice is present (Nishi-Khon/SNC-Lavalin Limited, 2007). Drainage, ice content and peat cover is expected to have an important effect on the susceptibility of tills to freeze-thaw movement. Sedimentological and geochemical data on tills will be compiled from existing publications in future reports.

Till geochemical and heavy mineral analyses are available within 11 different GSC reports listed in the Canadian Geochemical Survey Database (http://geochem.nrcan.gc.ca) and available in digital format (Hornbrook and Jonasson, 1971; Dilabio and Shilts, 1977; Dilabio, 1979; Coker and Ellwood, 1981; Coker et al., 1981; Shilts and Wyatt, 1989; Shilts and Coker, 1995; Henderson, 2000; McMartin, 2000, 2009; McMartin et al., 2001, 2003; McCurdy et al., 2012a, b; Scott et al., 2012). All of these reports contain data from till and lake-sediment sample work from the last 50 years using different analytical methods and variable background levels.

Other sediment types

Glaciofluvial sediments (GF; all mapped as glaciofluvial sediments on Figure 1) form diverse types of landforms, composed of a wide range of sediments, deposited by the action of glacial meltwaters. The most prominent unit is sand and gravel deposited in contact with ice (GFc) and this unit includes eskers and fan-deltas. Below the marine limit, sand and silt were deposited over the base of eskers and are mapped as GFf (Shilts et al., 1976). Above the marine limit, subaerial outwash plains (GFp) were deposited from the main esker tunnels into the valleys, and remain in flat, hummocky and terraced sand and gravel deposits juxtaposing the previously deposited esker ridges (Shilts et al., 1976). Eskers are abundant and of different sizes (commonly >30 m high) with up to four orders of tributaries, and can be associated with fans or can be beaded (Aylsworth and Shilts, 1989). In some places, eskers crosscut drumlinoids at sharp angles, and Aylsworth and Shilts (1989) concluded that the eskers were not formed at the same time or under the same conditions as the drumlinoids, but in a later phase of deglaciation and close to the ice margin. Rarely, short eskers are grouped and parallel, and likely were deposited close to the ice margin (e.g., in the area east of Maguse Lake).

The map unit Mo represents mainly offshore marine sediments, composed of silty sand and clayey silt, that were deposited below wave action, which commonly display as mudboils and have a mottled appearance on satellite images. Marine deltas (Md) and marine intertidal sediments (Mi) are mapped along with Mo on Figure 1 (marine sediments [intertidal, deltaic or offshore] on Figure 1). The Mo sediments are thicker and more prominent below 60 m asl and along main river valleys. Map unit Mr (marine sedi-

ments [littoral] on Figure 1) represents mostly marine littoral sediments with beach crests, and is found over diverse types of terrain (till, Mo, esker). The Mn map units (marine sediments [nearshore] on Figure 1) represent nearshore sediments, deposited by different processes, and are commonly composed of coarse sediments.

Unit A (alluvial and marine sediments on Figure 1) generally consists of undifferentiated alluvium overlying the M unit (undifferentiated marine sediments). Unit A/M occurs below the marine limit, and unit A/GF is found above the marine limit. The A/M complex unit consists mainly of sand and silt that has been reworked by wave action in the nearby marine shoreline environment, or deposited from the sedimentary load of glaciofluvial streams, or left in place from the action of alluvial streams. The A/GF unit is described as sorted silt, sand, gravel or cobbles deposited in glaciofluvial channels generally above the marine maximum limit. Along major rivers and streams, a cover of silt, sand and gravel is mapped as alluvial floodplain sediments (Ap). Lacustrine sediments (L; lacustrine on Figure 1) consist of a mixture of fine-grained sediments and organic material, and are usually found where a lake dried up or catastrophically drained.

Land-cover interpretation with RapidEye satellite images

Satellite images of Earth are in the public domain or are available commercially. These datasets provide recent image information and have the advantage of covering large areas and are, therefore, useful for reconnaissance work. The relatively low resolution offered by Landsat (30 m) or ASTER (15 m), however, limits observations of the details of small landscape features, which are necessary for the interpretation of landforms associated with glacial surface deposits. Several commercial data providers offer multispectral satellite data with 2 or 4 m resolution, but the high cost for wide area coverage has made using this multispectral data beyond the scope of this work. For this work, the authors chose to employ a set of data products, with an intermediate resolution and similar spectral bands, from RapidEye (RapidEye AG, 2012). These datasets offer a practical commercial solution for covering wide areas with improved resolution over Landsat or ASTER.

RapidEye is a constellation of five satellites (RE1–5), which permits once-per-day imaging opportunities and collects data in five discrete spectral bands from 0.44 to 0.85 µm representing the visible to near infrared range of the electromagnetic spectrum (Naughton et al., 2011). Data collected from the same seasonal period and under similar environmental conditions are especially important for the interpretation of terrain as maturation of the vegetation cover changes over time. These changes affect the spectral characteristics of the image, as do wet or dry conditions on more sparsely vegetated soils or surficial deposits. The RapidEye data covered 16 250 km^2 (26 scenes) of the study area from two 80 km wide passes on July 24 and 26, 2014. The resolution or ground sampling distance of RapidEye is approximately 6.5 m. Level 3A data products, acquired for this study, have a pixel spacing of 5 m. Various near-true colour and false colour images were created from the five available bands, including the red edge band (BlackBridge, 2013), which is ideally positioned to capture vegetation vigour due to the high reflectance in the infrared from the mesophyll in healthy internal leaf structure. Vegetation cover is commonly associated with the type of mineral soil substrate and was used in this study to assist with the identification and interpretation of surficial deposit types. A number of surficial cover types were successfully identified and mapped using a supervised classification technique; this is described in more detail below.

The process of RapidEye land cover interpretation is similar to remote predictive mapping for surficial sediments in that both consist of classification of satellite images (and other data) to obtain information about the surficial materials from a remote sensing perspective (e.g., Harris et al., 2012; Campbell et al., 2013; Wityk et al., 2013). However, with RapidEye land-cover interpretation, the results are given in terms of observed physical composition of the images (e.g., vegetation, water, lichen-covered boulders, lichen-covered rock, fresh sediment) rather than inferred geological units (till, marine sediments, alluvial sediments). The rationale for this particular methodology is that some applications might require precision in the mapping of specific features that are observable on the images, whereas other details might not be so significant or easy to see on the images from the classification. The RapidEye land-cover interpretation process is illustrated on Figure 2.

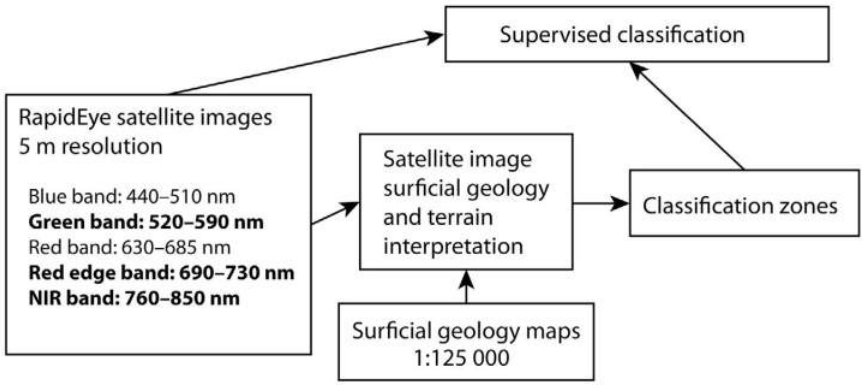

Figure 2: Land cover classification workflow diagram, using RapidEye satellite images and surficial geology maps. The bold letters indicate the RapidEye bands used for classification. Abbreviation: NIR, near infrared.

Previously, land-cover maps were produced at 30 m resolution from Landsat images (Natural Resources Canada, 2015), however not with the specific objective of providing information for surficial sediments mapping. The Landsat land-cover maps will be compared with the new RapidEye land-cover maps in future publications from the Western Hudson Bay project.

The software used for the image classification is SAGA (System for Automated Geoscientific Analyses, version 2.1.4; Conrad et al., 2015), within the supervised classification module. Classification zones with specific land-cover attributes were delimited to drive the classification process (Figure 2), based on the surficial sediments map and geological interpretation of the 5 m RapidEye satellite image. The operation was repeated for each of the 26 satellite image scenes. The land-cover interpretation was classified from RapidEye images, with bands 2 (green), 4 (red edge) and 5 (near infrared, or NIR). These colours were selected because they provide suitable contrast in the vegetation type and moisture content of the ground, which in turns reflects the underlying surficial material. The amount and type of mineral material (bedrock, sand, silt, till), as well as the roughness and lichen cover, are also important factors that are well-represented by these three bands. Figure 3 shows the satellite image classification, which is expressed in a contrasting colour scheme that reflects the main units, and is easy to read for most users, including nonspecialists. The interpretation map is focused on important geological features that will assist in the design of infrastructure, from both engineering and environmental aspects.

The RapidEye images proved useful at finding gravel sources, due to the red edge and near infrared combination that allows one to find subtle contrasts within different types of terrain, depending on moisture, vegetation colour, lichen, rock and sand cover (Figure 3; see Tremblay et al. [2015][6] for full-definition georeferenced image). On the land-cover map, gravel sources are defined by a combination of black (mostly gravel and vegetation), white (general mixture of sediments and vegetation), purple (mostly lichen-covered boulders) and yellow (mostly freshly exposed sediments). Black is the most specific indicator of gravel, associated with dry vegetation, however black is also found in other settings, including some specific bedrock units east of Maze Lake. Esker ridges, beaded eskers, fans and kames are common landforms that display black and indicate mostly gravel, however, some of these do not display as black. The parts of beach ridges (Mr) that are commonly deposited from the reworking of glaciofluvial sediments can also appear as black. In some localities, the RapidEye interpretation allows the identification of gravel deposits (sector A, Figure 4a–c) as being mainly eskers and beaches, and this increases the precision of the surficial maps. In addition, the RapidEye allows one to map some gravel (eskers) deposits that were not mapped in the surficial geology maps (sector B, Figure 4d–f).

Coarse and rocky terrain, such as bedrock and ribbed moraine areas, were identified in detail by zones of purple (lichen-covered bedrock and boulders). North of Kakiakturjuaq lake, there are good examples of areas of coarse ribbed moraines delimited by purple (Figure 3). Another area of coarse ribbed moraines is evident in the northeast corner of sector A (Figure 4d). Coarse ribbed moraines differ from the bedrock areas, as interpreted from the RapidEye images, as the latter displays geometrical fractures and the former is more irregular and diffuse (Figure 4d).

Zones with wet vegetation cover (green; thick vegetation, peat) were identified with detail using the RapidEye image interpretation. Thick and wet vegetation cover (vegetation C and D, dark green) is found in depressions in the till cover and/or in fine-grained sediments (marine, lacustrine, alluvial). These zones are more likely to contain more ground-ice and to be thaw-sensitive, although this interpretation needs to be confirmed by field observations. Vegetation A and B (pale green) are variable and may consist of vegetated soils without thick peat cover. Notably, the pale green areas have several identified drumlinoids, except that the top section of the drumlinloids are dominantly white (indicating a general mix of sediments and vegetation). Figure 4a shows that vegetation C and D are mapped in detail, and are found over almost every unit of the surficial map but dominantly over Tb, A (which corresponds to alluvial sediments in Figure 4b) and L.

Yellow units indicate some freshly exposed sediments, of different granulometry, with little vegetation or lichen on the sediments. These sediments occur on top of eskers, in intermittent or recently drained lakes, on raised beaches, near the seashore or on river banks. In some localities, the sediments of the paler yellow unit (A) are thought to be wetter or slightly more vegetated, than the sediments of the darker yellow unit (B).

White units represent three different classification categories: till, various fine marine sediments and nearshore or beach sediments. These sediments were grouped into one category because they overlap significantly in RapidEye images. In general, the areas depicted by white display variable amounts of mudboils and some vegetation, and are believed to be relatively well-drained. However, this needs to be confirmed in future fieldwork.

[6] *CNGO Geoscience Data Series GDS2015-015, containing the data or other information sources used to compile this paper, is available online to download free of charge at http://cngo.ca/summary-of-activities/2015.*

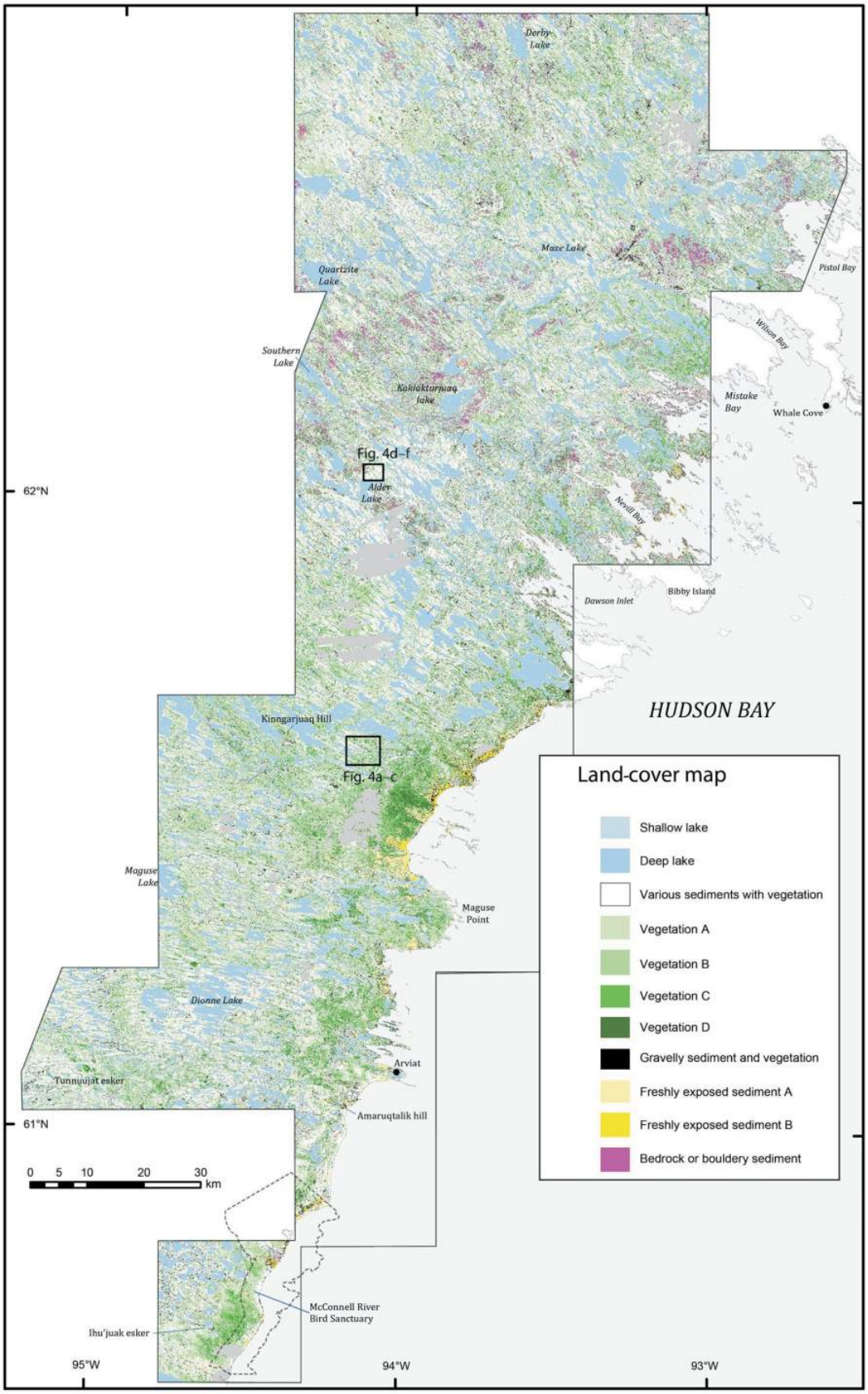

Figure 3: Land-cover map from RapidEye classification. Clouds and shadows are shown as grey areas. Full-resolution image is available in Tremblay et al. (2015).

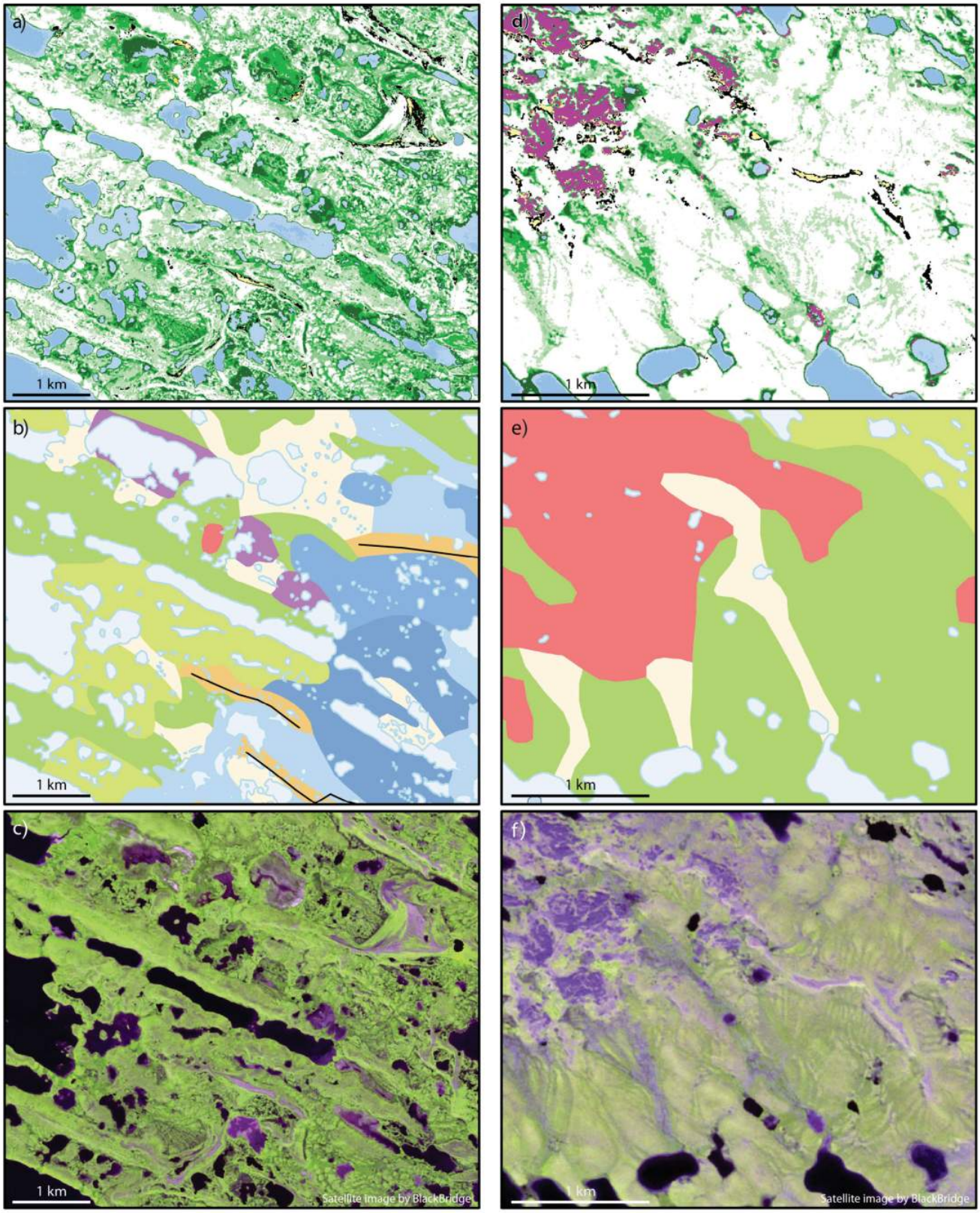

Figure 4: Comparison of RapidEye land-cover maps (see Figure 3 for legend), surficial geology maps (see Figure 1 for legend) and RapidEye images (band 4 is red, band 3 is blue, band 5 is green; copyright 2015© BlackBridge) for sectors A and B (see Figure 3 for locations): **a)** sector A, RapidEye land-cover map; **b)** sector A, surficial geology map; **c)** sector A, RapidEye image; **d)** sector B, RapidEye land-cover map; **e)** sector B, surficial geology map; and **f)** sector B, RapidEye image.

The following items could be assessed in order to improve the quality and usefulness of the RapidEye land-cover interpretation for western Hudson Bay area:

- Complete the RapidEye image coverage during the early summer of 2016. The existing 2014 coverage was marginally increased by images collected in the summer of 2015, and will be processed in 2016.
- Conduct fieldwork to ground-truth permafrost, surficial geology and RapidEye land-cover map features.
- Classify land cover using RADARSAT images. In particular, the mapping of zones of gravel (including eskers) could be examined. Also, the overall roughness of the terrain can be observed in the RADARSAT data, and the delineation of terrain differences could be of particular interest for infrastructure projects.
- Compare the Landsat land-cover maps (Natural Resources Canada, 2015) with the new RapidEye land-cover maps.

Permafrost conditions

Permafrost is defined as ground that remains at or below 0°C for at least two consecutive years (French, 2007). Western Hudson Bay lies in the continuous permafrost zone, where 90–100% of the ground surface is underlain by permafrost (French, 2007). The limit between discontinuous permafrost (being defined as 50–90% of the surface underlain by permafrost) and continuous permafrost is located 50 km south of the study area, as displayed on the inset map of Figure 1 (Brown et al., 2002). In the continuous zone, permafrost is interspersed with layers of taliks, which are layers of ground that remain unfrozen yearround; they are usually found under bodies of water affecting the thermal regime of the soil (French, 2007). Certain conditions are propitious to ice-rich ground, and ground ice is normally found in low-lying marine sediments. At those locations, numerous periglacial features such as ice-wedge polygons, patterned ground and mudboils can be found (Figure 5; McMartin, 2002). Some retrogressive thaw flows were also mapped in the area of Rankin Inlet (McMartin, 2002). In the vicinities of Rankin Inlet and Baker Lake, high salinity levels are reported ranging from 2.5 to 30 ppt with the salinity originating from marine submergence by higher sea levels during glacial retreat (Hivon and Sego, 1993). Elevated soil salinity increases the unfrozen water content and decreases the strength of the soil (Hivon and Sego, 1995), which could have an impact on the performance of infrastructure.

In the western Hudson Bay region, the thickness of the active layer (the top layer of soil that undergoes seasonal thaw and freeze) is highly variable and depends greatly on site-specific conditions (Brown, 1978; French, 2007). Active layer thickness in the region was initially assessed by Brown from 1974 to 1976 near Rankin Inlet and Baker Lake using thermistor cables in bedrock, eskers, till and marine sediments. In these terrain units, the active layer thicknesses ranged from 30 cm in sand and gravel to 400 cm in bedrock (Brown, 1978). More recently, active layer thickness data derived from borehole thermistors were also provided for a site in coarse gravel and sand near Baker Lake (Smith et al., 2005, 2010, 2013). The active layer thickness varied from 125 to 229 cm between 1997 and 2007. The thickness of the permafrost has been estimated to be 200–300 m near Rankin Inlet, and 500 m in the Baker Lake area (Brown, 1978).

The mean annual air temperature (MAAT) for 1981–2014 calculated using Environment Canada climate station data (Environment Canada, 2015), is –11.7°C for Baker Lake and –10.3°C for Rankin Inlet. During the same time period, the MAAT rose 2°C at an average rate of 0.068°C/yr, indicating a progressive warming of the climate in the region (Figure 6). Climate warming is observable throughout the western Hudson Bay area, with similar trends observable at Arviat, Chesterfield Inlet and Whale Cove climate stations. Although a network of climate station exists in the region, boreholes for monitoring the permafrost thermal regime are sparse. Brown (1963) was the first to provide ground ther-

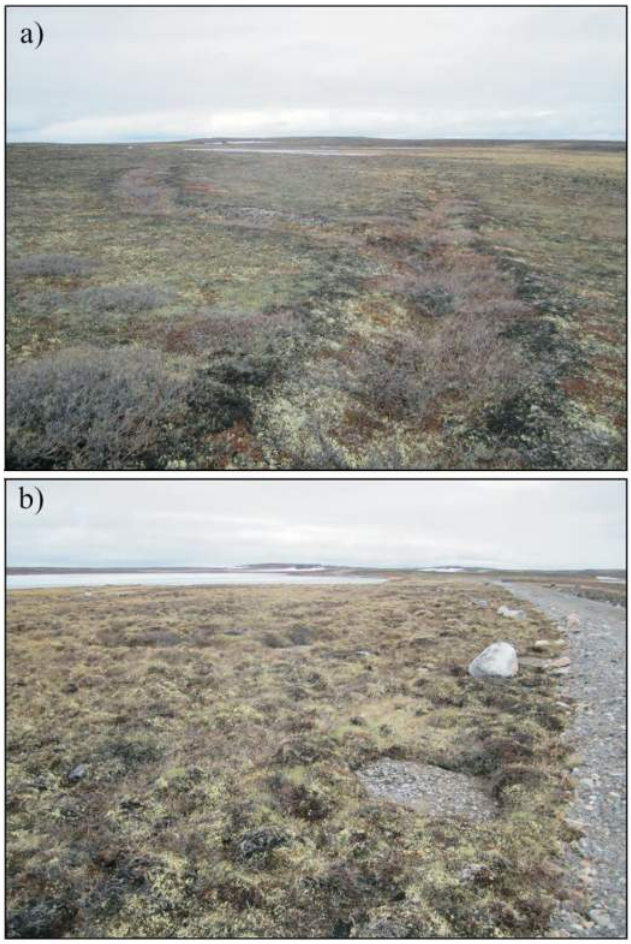

Figure 5: a) Ice wedge polygons and **b)** mudboils in the vicinity of a road infrastructure, near Rankin Inlet.

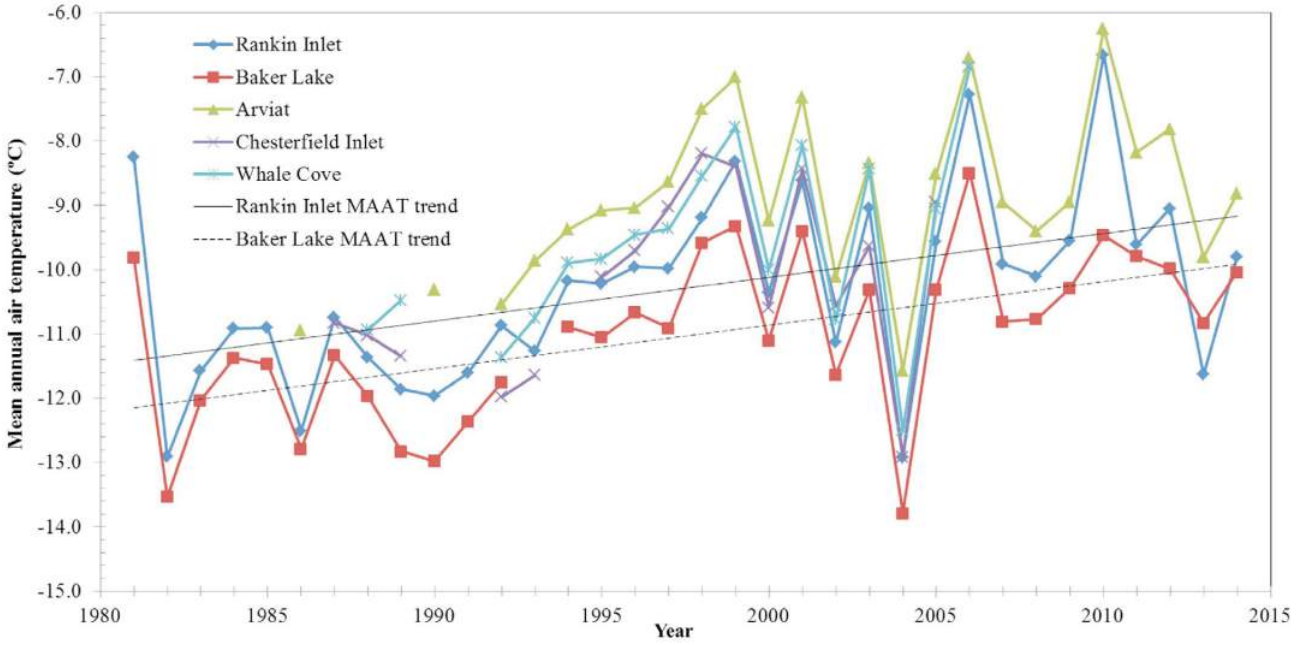

Figure 6: Mean annual air temperatures (MAATs) at five stations located in Nunavut in the western Hudson Bay region. Data were acquired from Environment Canada (Environment Canada, 2015); data gaps represent years where the data quality was judged insufficient to be included. The black lines represent the MAAT trend for Rankin Inlet (solid) and Baker Lake (dashed).

mal data for the Rankin Inlet area with the mean annual ground temperature (MAGT) varying from –8 to –9°C at a 30 m depth in 1960. Further investigations were conducted by Brown between 1974 and 1976 in the Rankin Inlet and Baker Lake areas (Brown, 1978). Near Rankin Inlet, borehole depths ranged from 4 to 14 m and the MAGT at the bottom of the boreholes was –6.4 to –7.9°C (Brown, 1978). In Baker Lake, the boreholes were significantly deeper, ranging from 61 to 130 m deep and the MAGT at the bottom of the boreholes ranged from –4.2 to –5.2°C (Brown, 1978). Two decades later, similar ground temperatures were reported by Dyke (1998) in Rankin Inlet: –7 to –8°C at a depth of 16 m in undisturbed terrain. The borehole with the longest continuous dataset is located in Baker Lake with ground thermal data being collected from 1997 to 2007 with a MAGT of –7.6°C at a depth of 3 m (Smith et al., 2010; Throop et al., 2012). Despite these historical ground temperatures, contemporary borehole monitoring in communities along western Hudson Bay is rare. Furthermore, ground temperature data are being collected at developing mine sites, such as Agnico Eagle Mines Limited's Meadowbank and Meliadine sites, but these data are commonly limited in the length of the recording period, or are not publicly accessible beyond data released in environmental assessment reports (e.g., Smith et al., 2013).

Recent studies have projected changes in the region in response to contemporary climate change that could have important impacts on the permafrost distribution, ecology and the infrastructure sustainability in the region. Two studies have modelled the permafrost response to climate change in the region: a) Tam (2014) concentrated his efforts on modelling the possible distribution of permafrost for the 21st century under climate warming scenarios along a south–north transect in Canada, including Rankin Inlet as a field site; and b) Zhang (2013) projected changes in permafrost from 2010 to 2200 in the northwestern area of the Hudson Bay Lowland, a region characterized by different permafrost zones, such as continuous, extensive discontinuous, sporadically discontinuous and isolated permafrost zones. Both authors suggest that the continuous permafrost in the Hudson Bay region will undergo a transition between continuous permafrost conditions to discontinuous permafrost, but they do not agree on the timing of this change. Tam (2014) states that by 2040 the permafrost in the Rankin Inlet region will change from continuous to discontinuous permafrost, whereas Zhang (2013) predicts a more gradual change with discontinuous conditions reached during the 22nd century. Both researchers agree that the majority of the predicted climate warming will occur during the 21st century.

Although permafrost is a well-known phenomenon in Canada, the understanding of permafrost conditions in the western Hudson Bay region remains limited and calls for further research. A network of functional climate stations exists in the region; however, continuous ground thermal monitoring data is scarce to nonexistent and the available data were collected more than a decade ago. The thermal response of permafrost to recent climate warming (Figure 6) is difficult to establish from available ground temperature records, thus limiting the capacity to understand the

changes in the permafrost conditions under climatic variations. Finally, future climate change effects are projected to also alter the current permafrost conditions.

Local landscape and permafrost knowledge

In order to assess modern and traditional knowledge of permafrost, discussions were conducted in Rankin Inlet with the Kivalliq Inuit Association (KIA) and the Hunters and Trappers Organization (HTO) in the summer of 2015 with the goal of putting new permafrost geoscience observations into an historical and traditional context. The discussions lead to an agreement to conduct community engagement activities in the winter of 2015–2016. One of the major activities will be a mapping and information workshop with the participation of elders and experienced local land users. The goals will be to 1) identify areas that have undergone or are undergoing landscape change (related to permafrost degradation); 2) identify areas that are sensitive or critical to traditional ways of life, such as culturally significant areas, wildlife zones, or areas where access may become limited due to permafrost and climate change; and 3) identify areas with high potential risk to infrastructure. Traditional knowledge will be used as input to scientific planning and will be incorporated with scientific observations, such as surficial geology, ground-ice occurrences and satellite imagery, to form a unified understanding of permafrost conditions.

Ground surface displacement

Ground surface displacement can be derived from DInSAR using repeat satellite radar observations. The ground displacement is captured in the phase differences between the radar acquisitions. Interferometric processing allows these phase differences to be exploited to produce extensive coverage maps of ground displacement. In a permafrost environment, the ground displacement may be seasonal, due to changes in the active layer, or long-term due to changes in the permafrost. Based on positive results in other Nunavut locations (Short et al., 2012a, b), DInSAR data over Rankin Inlet was acquired in 2015. Radar data were acquired using the Canadian RADARSAT-2 satellite with C-band SAR and horizontal transmit and horizontal receive (HH) polarization. Data were collected in two modes (Table 1), one high-resolution spotlight (1 m resolution, 18 by 18 km coverage) to replicate the high resolution results at other locations, and the other in ultra-fine wide mode, which has a lower resolution (3 m) but covers a larger area (50 by 50 km). This mode will be used to explore if the lower resolution data can still deliver useful terrain stability information. The DInSAR results will also be interpreted in conjunction with local and geoscience knowledge.

Table 1: The RADARSAT modes and acquisition dates (2015), western Hudson Bay area, Nunavut.

Spotlight (1 m resolution) SLA-23 descending orbit	Ultra-fine wide (3 m resolution) U18W2 ascending orbit
May 29	May 22
June 22	June 15
July 16	July 09
Aug 09	Aug 02
Sep 02	Aug 26
Sep 26	Sep 19

Mineral occurrences and new bedrock geology fieldwork

Mineral occurrences were compiled from NUMIN (NunavutGeoscience.ca, 2015), the online repository of mineral occurrences in Nunavut. The complete dataset for the study area is online, and includes 693 occurrences (Figure 1), of which 137 were recently compiled from newly released mining and exploration companies' assessment reports. In collaboration with the Western Hudson Bay project, new mapping fieldwork was conducted this past summer (Steenkamp et al., 2015); the reported results of this work will lead to a greater knowledge of bedrock and regional mineral potential.

Economic considerations

This surficial work focuses on the compilation of geoscientific data in the western Hudson Bay area, where a proposed road construction project could potentially impact the local economy. Four coastal communities are located in the study area and along the proposed road corridor, and may benefit from all-year access to the national roadwork system. The mining potential of the area is also substantial, with one gold mine in operation and several more potential mines advancing to development. These exploration and mining projects could also be favourably impacted by the new road corridor. Gravel sources are essential for building roads; these sources can be outlined using the newly compiled 1:125 000 scale surficial geology map, and delineated with the detailed land-cover map interpreted from the RapidEye images. The land-cover map shows many more potential gravel sources and at finer details locally than the regional surficial compilation map. Environmental impact studies can also benefit from this RapidEye land-cover map as various terrains (eskers, river terraces, grasslands) that are key habitats for wildlife might be identified. Various surficial geochemistry studies are also referenced as part of this work, which could be useful for mineral potential assessment and environmental studies. The RapidEye land-cover map also identifies areas that are wetlands (peatlands) or covered with specific vegetation; these areas are likely to be underlain by fine sediments or contain important ground ice—factors that might pose risks of thaw movement, information critical for infrastructure planning. Permafrost-sensitive areas will be assessed based on the surficial geology map compilation and the RapidEye land-cover map; ground surface displacement will be derived from RADARSAT-2 coverage (DInSAR). New thermistors ca-

bles and other field observations/surveys (geophysics, permafrost coring) are recommended to gather permafrost data that are currently lacking spatially and over a longer time period. Traditional knowledge is also being gathered in Rankin Inlet to assess landscape change related to permafrost degradation around the community, and to identify sensitive areas with potential risk to infrastructure development and to cultural/traditional activities. Overall, this permafrost knowledge update will assist engineers in evaluating potential routes and preparing cost assessments related to design and construction of new roads.

Conclusion

The Western Hudson Bay project aims at providing compilations of existing and new geoscience data for infrastructure planning. An important outcome to date, and to be released shortly, is the digital compilation of surficial geology for the area, derived from various maps published during the 1970s and 1980s. Furthermore, some of these maps were refined locally by the use of RapidEye image land-cover interpretation (5 m resolution), which delimited the locations of some gravel deposits, bedrock outcrops, bouldery tills, freshly eroded sediments and vegetation. Further fieldwork will permit the examination of detailed aspects of the RapidEye land-cover interpretation, notably for the location of gravel sources and the identification of thaw-sensitive areas based on the mapping of vegetation areas. Additionally, the study provides a bibliographical summary of till and lake-sediment geochemical samples and of bedrock geology synthesis maps, and of the location of mineral occurrences. New bedrock geology mapping is being undertaken to complete the coverage of the study area. Finally, a compilation of the knowledge on permafrost is underway, including a summary of the existing literature. Future work will include the integration of traditional knowledge with modern geoscience data, ground surface displacement as measured with DInSAR (RADARSAT data) and proposed new permafrost observations sites in key locations.

Acknowledgments

The authors thank S. Eagles, D. Kerr and L. Robertson from the GIS services at the Geological Survey of Canada for the valuable assistance they provided to this project in completing the surficial geology map compilation. Also, A. Markey (Aboriginal Affairs and Northern Development Canada) and S. Basso (Canada-Nunavut Geoscience Office) collaborated on this project by updating the most recent mineral occurrence data on NunavutGeoscience.ca in the study area. The Kivalliq Inuit Association (KIA), the Hunter and Trappers Association (HTO) of Rankin Inlet, and J. Shirley from the Nunavut Research Institute (NRI) are thanked for collaborating in the initial discussions about the community engagement activities. The permafrost component of this research is part of the Natural Resources Canada Climate Change Geoscience Program. Financial support of this study was provided by the Strategic Investments in Northern Economic Development (SINED) program delivered by the Canadian Northern Economic Development Agency (CanNor). The authors thank D. Kerr and L. Ham for reviewing this paper.

Natural Resources Canada, Earth Sciences Sector contribution 20150327

References

Arsenault, L., Aylsworth, J.M., Cunningham, C.M., Kettles, I.M. and Shilts, W.W. 1981a: Surficial geology, Eskimo Point, District of Keewatin; Geological Survey of Canada, Preliminary Map 8-1980, scale 1:125 000, doi:10.4095/119389

Arsenault, L., Aylsworth, J.M., Kettles, I.M. and Shilts, W.W. 1981b: Surficial geology, Dawson Inlet, District of Keewatin; Geological Survey of Canada, Preliminary Map 9-1979, scale 1:125 000, doi:10.4095/109700

Arsenault, L., Aylsworth, J.M., Kettles, I.M. and Shilts, W.W. 1981c: Surficial geology, Kaminak Lake, District of Keewatin; Geological Survey of Canada, Preliminary Map 7-1979, scale 1:125 000, doi:10.4095/109686

Aylsworth, J.M. and Shilts, W.W. 1989: Bedforms of the Keewatin Ice Sheet, Canada; Sedimentary Geology, v. 62, p. 407–428.

Aylsworth, J.M., Boydell, A.N. and Shilts, W.W. 1981a: Surficial geology, Marble Island, District of Keewatin; Geological Survey of Canada, Preliminary Map 10-1980, scale 1:125 000, doi:10.4095/109704

Aylsworth, J.M., Boydell, A.N. and Shilts, W.W. 1981b: Surficial geology, Tavani, District of Keewatin, Northwest Territories; Geological Survey of Canada, Preliminary Map 9-1980, scale 1:125 000, doi:10.4095/109695

Aylsworth, J.M., Boydell, A.N. and Shilts, W.W. 1986a: Surficial geology, Chesterfield Inlet, District of Keewatin, Northwest Territories; Geological Survey of Canada, Preliminary Map 1-1985, scale 1:125 000, doi:10.4095/121054

Aylsworth, J.M., Boydell, A.N. and Shilts, W.W. 1986b: Surficial geology, Gibson Lake, District of Keewatin, Northwest Territories; Geological Survey of Canada, Preliminary Map 1-1984, scale 1:125 000, doi:10.4095/120461

Aylsworth, J.M., Cunningham, C.M. and Shilts, W.W. 1981c: Surficial geology, Hyde Lake, District of Keewatin; Geological Survey of Canada, Preliminary Map 8-1979, scale 1:125 000, doi:10.4095/109688

Aylsworth, J.M., Cunningham, C.M. and Shilts, W.W. 1990: Surficial geology, Edehon Lake, District of Keewatin, Northwest Territories; Geological Survey of Canada, Preliminary Map 10-1990, scale 1:125 000, doi:10.4095/130945

Aylsworth, J.M., Cunningham, C.M., Kettles, I.M. and Shilts, W.W. 1986c: Surficial geology, Henik lakes, District of Keewatin, Northwest Territories; Geological Survey of Canada, Preliminary Map 2-1985, scale 1:125 000, doi:10.4095/121055

BlackBridge 2013: The RapidEye red edge band; BlackBridge, 6 p., URL <http://www.blackbridge.com/rapideye/upload/Red_Edge_White_Paper.pdf> [June 2014].

Boydell, A.N. 1974: Surficial geology, Marble Island, Tavani, MacQuoid Lake, Gibson Lake, Chesterfield Inlet, District of Keewatin; Geological Survey of Canada, Open File 192, 5 maps, scale 1:125 000, doi:10.4095/129313

Brown, R.J.E. 1963: Relation between mean annual air and ground temperatures in the permafrost region of Canada; *in* Proceedings Permafrost International Conference, Lafayette, Indiana, November 1963, p. 241–246.

Brown, R.J.E. 1978: Influence of climate and terrain on ground temperatures in the continuous permafrost zone of northern Manitoba and Keewatin district, Canada; *in* Proceedings of the Third International Conference on Permafrost, Edmonton, Alberta, July 1978, v. 1, p. 15–21.

Brown, J., Ferrians, O., Heginbottom, J.A. and Melnikov, E. 2002: Circum-Arctic map of permafrost and ground-ice conditions, version 2; National Snow and Ice Data Center, Boulder, Colorado, data set ID: GGD318, URL <https://nsidc.org/data/ggd318> [August 2015].

Campbell, J.E., Harris, J.R., Huntley, D.H., McMartin, I., Wityk, U., Dredge, L.A. and Eagles, S. 2013: Remote predictive mapping of surficial earth materials: Wager Bay North area, Nunavut - NTS 46-E (N), 46-K (SW), 46-L, 46-M (SW), 56-H (N), 56-I and 56-J (S); Geological Survey of Canada, Open File 7118, 42 p., doi:10.4095/293158

Cocking, R.B., Deblonde, C., Kerr, D.E., Campbell, J.E., Eagles, S., Everett, D., Huntley, D.H., Inglis, E., Laviolette, A., Parent, M., Plouffe, A., Robertson, L., St-Onge, D.A. and Weatherston, A. 2015: Surficial data model, version 2.1.0: revisions to the science language of the integrated Geological Survey of Canada data model for surficial geology maps; Geological Survey of Canada, Open File 7741, 276 p.

Coker, W.B. and Ellwood, D.J. 1981: National geochemical reconnaissance, northern Manitoba, southeastern Northwest Territories and northeastern Saskatchewan (54L, M; 64I, J, K, N, O, P and parts of 64L, M; 65A, B, C); Geological Survey of Canada, Open File 742, 23 p.

Coker, W.B., Ellwood, D.J. and Maurice, Y.T. 1981: National geochemical reconnaissance, Baker Lake, Northwest Territories (55M, 65P); Geological Survey of Canada, Open File 739, 20 p.

Conrad, O., Bechtel, B., Bock, M., Dietrich, H., Fischer, E., Gerlitz, L., Wehberg, J., Wichmann, V. and Böhner, J. 2015: System for Automated Geoscientific Analyses (SAGA) v. 2.1.4; Geoscientific Model Development, v. 8, p. 1991–2007, doi:10.5194/gmd-8-1991-2015

DiLabio, R.N.W. 1979: Drift prospecting in uranium and base-metal mineralization sites, District of Keewatin, Northwest Territories, Canada; *in* Prospecting in Areas of Glaciated Terrain 1979, Institution of Mining and Metallurgy, London, p. 91–100.

DiLabio, R.N.W. and Shilts, W.W. 1977: Detailed drift prospecting in the southern District of Keewatin; *in* Report of Activities, Geological Survey of Canada, Paper 77-1A, p. 479–483.

Dredge, L.A., McMartin, I. and Campbell, J. 2013: Reconnaissance surficial geology, Daly Bay (south) and Cape Fullerton (north), Nunavut, NTS 56-A south and 55-P north; Geological Survey of Canada, Canadian Geoscience Map 146 (preliminary version), scale 1:100 000, doi:10.4095/293045

Dyke, L. 1998: The freezing of reclaimed tailings at Rankin Inlet, Nunavut, Canada; Geological Survey of Canada, unpublished internal report, 11 p.

Dyke, A.S. and Dredge, L.A. 1989: Quaternary geology of the northwestern Canadian Shield; *in* Quaternary Geology of Canada and Greenland, R.J. Fulton (ed.), Geological Survey of Canada, Geology of Canada, no. 1, p. 189–214.

Dyke, A.S., Moore, A. and Robertson, L. 2003: Deglaciation of North America; Geological Survey of Canada, Open File 1574, 2 sheets.

Environment Canada 2015: Canadian climate normals; Environment Canada, <http://climate.weather.gc.ca/climate_normals/index_e.html> [August 2015].

French, H.M. 2007: The Periglacial Environment (3rd edition); John Wiley and Sons, New Jersey, 458 p.

Fulton, R.J. comp. 1995: Surficial materials of Canada; Geological Survey of Canada, Map 1880A, scale 1:5 000 000.

Harris, J.R., Parkinson, W., Dyke, A., Kerr, D., Russell, H., Eagles, S., Richardson, M. and Grunsky, E. 2012: Predictive surficial geological mapping of Hall Peninsula and Foxe Basin Plateau, Baffin Island using LANDSAT and DEM data; Geological Survey of Canada, Open File 7038, 22 p., doi:10.4095/291820

Henderson, P.J. 2000: Drift composition and surficial geology, MacQuoid Lake area, (NTS 55 M/7 and 55 M/10), Kivalliq region, Nunavut; a guide to drift prospecting; Geological Survey of Canada, Open File 3944, 189 p.

Hivon, E.G. and Sego, D.C. 1993: Distribution of saline permafrost in the Northwest Territories, Canada; Canadian Geotechnical Journal, v. 30, p. 506–514.

Hivon, E.G. and Sego, D.C. 1995: Strength of frozen saline soils; Canadian Geotechnical Journal, v. 32, p. 336–354.

Hornbrook, E.H.W. and Jonasson, I.R. 1971: Mercury in permafrost regions: occurrence and distribution in the Kaminak Lake area, Northwest Territories; Geological Survey of Canada, Paper 71-43, 13 p.

Levson, V.M. 2014: Assessment of geoscience priorities along the proposed Nunavut-Manitoba highway corridor; Canada-Nunavut Geoscience Office, unpublished internal report, 26 p.

McCurdy, M.W., Day, S.J.A., McNeil, R.J. and Pehrsson, S.J. 2012a: Regional lake sediment and water geochemical data, Baker Lake area, Nunavut (NTS 55M and 65P); Geological Survey of Canada, Open File 6985, 12 p.

McCurdy, M.W., McNeil, R.J., Day, S.J.A. and Pehrsson, S.J. 2012b: Regional lake sediment and water geochemical data, Nueltin Lake area, Nunavut (NTS 65A, 65B and 65C); Geological Survey of Canada, Open File 6986, 13 p.

McMartin, I. 2000: Till composition across the Meliadine trend, Rankin Inlet area, Kivalliq region, Nunavut; Geological Survey of Canada, Open File 3747, 330 p.

McMartin, I. 2002: Surficial geology, Rankin Inlet, Nunavut; Geological Survey of Canada, Open File 4116, scale 1:50 000, doi:10.4095/213219

McMartin, I. 2009: Till composition along the Meliadine trend near Rankin Inlet, Nunavut: applications to gold exploration in permafrost terrain; *in* Application of Till and Stream Sediment Heavy Mineral and Geochemical Methods to Mineral Exploration in Western and Northern Canada, R.C. Paulen and I. McMartin (ed.), Geological Association of Canada, Short Course Notes 18, p. 14–18.

McMartin, I. and Henderson, P.J. 2004a: Evidence from Keewatin (central Nunavut) for Paleo-ice divide migration; Géographie physique et Quaternaire, v. 58, no. 2–3, p. 163–186.

McMartin, I. and Henderson, P.J. 2004b: Ice flow history and glacial stratigraphy, Kivalliq Region, Nunavut (NTS 55-J, K, L, M, N, O; 65-I and P): complete datasets, maps and photographs from the Western Churchill NATMAP Project; Geological Survey of Canada, Open File 4595, 8 maps, scales 1:200 000 and 1:500 000.

McMartin, I., Hall, G.E.M., Kerswill, J.A., Douma, S., Goff, S.P., Sangster, A.L. and Vaive, J.A. 2001: Environmental geochemistry of the Kaminak Lake area, Killiq region, Nunavut; Geological Survey of Canada, Open File 4089, 242 p.

McMartin, I., Henderson, P.J., Kjarsgaard, B.K. and Venance, K. 2003: Regional distribution and chemistry of kimberlite indicator minerals, Rankin Inlet and MacQuoid Lake areas, Kivalliq region, Nunavut; Geological Survey of Canada, Open File 1575, 109 p.

Natural Resources Canada 2015: Circa-2000 northern land cover of Canada, NTS 055E, 055L and 055K (1999); Natural Resources Canada, URL <http://geogratis.gc.ca/api/en/nrcan-rncan/ess-sst/-/(urn:iso:series)circa-2000-northern-land-cover-of-canada> [September 2015].

Naughton, D., Brunn, A., Czapla-Myers, J., Douglass, S., Thiele, M., Weichelt, H.A. and Oxfort, M. 2011: Absolute radiometric calibration of the RapidEye multispectral imager using the reflectance-based vicarious calibration method; Journal of Applied Remote Sensing, v. 5, no. 1, 23 p., doi:10.1117/1.3613950

Nishi-Khon/SNC-Lavalin Limited 2006: Building lasting infrastructure, Nunavut-Manitoba route selection study, milestone report A; unpublished report prepared for Nunavut Department of Economic Development and Transportation and Manitoba Infrastructure and Transportation, 34 p. plus appendices.

Nishi-Khon/SNC-Lavalin Limited 2007: Building lasting infrastructure, Nunavut-Manitoba route selection study, milestone report B; unpublished report prepared for Nunavut Department of Economic Development and Transportation and Manitoba Infrastructure and Transportation, 44 p. plus appendices.

Nishi-Khon/SNC-Lavalin Limited 2010a: Building lasting infrastructure: the case for the Nunavut-Manitoba highway (Nunavut-Manitoba all-weather road business case); unpublished report prepared for Nunavut Department of Economic Development and Transportation and Manitoba Infrastructure and Transportation, 60 p., URL <http://www.gov.nu.ca/sites/default/files/Nunavut_Manitoba_Road_Business_Case.pdf> [November 2015].

Nishi-Khon/SNC-Lavalin Limited 2010b: Building lasting infrastructure: the case for the Nunavut-Manitoba highway (Nunavut-Manitoba all-weather road business case, executive summary); unpublished report prepared for Nunavut Department of Economic Development and Transportation and Manitoba Infrastructure and Transportation, 12 p., URL <http://www.gov.nu.ca/sites/default/files/Nunavut_Manitoba_Business_Case_executive_summary.pdf> [November 2015].

NunavutGeoscience.ca 2015: Nunavut mineral occurrences database (NUMIN); Canada-Nunavut Geoscience Office, Aboriginal Affairs and Northern Development Canada, Government of Nunavut, Natural Resources Canada and Nunavut Tunngavik Incorporated, URL <http://nunavutgeoscience.ca/pages/en/numin.html> [September 2015].

Paul, D., Hanmer, S., Tella, S., Peterson, T.D. and LeCheminant, A.N. 2002: Compilation, bedrock geology part of the western Churchill Province, Nunavut-Northwest-Territories; Geological Survey of Canada, Open File 4236, scale 1:1 000 000.

RapidEye AG 2012: Satellite imagery product specifications, version 4.1; RapidEye AG, 44 p., URL <http://www.rapideye.de/upload/RE_Product_Specifications_ENG.pdf> [November 2012].

Scott, J.M.J., Peterson, T.D. and McCurdy, M.W. 2012: U, Th, REE occurrences within Nueltin granite at Nueltin lake, Nunavut: recent observations; Geological Survey of Canada, Current Research 2012-1, 11 p., doi:10.4095/289393

Shilts, W.W. 1971: Till studies and their application to regional drift prospecting; Canadian Mining Journal, v. 92, p. 45–50.

Shilts, W.W. 1973: Drift prospecting; geochemistry of eskers and till in permanently frozen terrain: District of Keewatin, Northwest Territories; Geological Survey of Canada, Paper 72-45, 34 p.

Shilts, W.W. and Coker, W.B. 1995: Mercury anomalies in lake water and in commercially harvested fish, Kaminak Lake area, District of Keewatin, Canada; *in* Mercury as a Global Pollutant, D.B. Porcella, J.W. Huckabee and B. Wheatley (ed.), Water, Air, & Soil Pollution, v. 80, no. 1, p. 881–883.

Shilts, W.W. and Wyatt, P.H. 1989: Gold and base metal exploration using drift as a sample medium, Kaminak Lake-Turquetil Lake Area, District of Keewatin; Geological Survey of Canada, Open File 2132, 168 p.

Shilts, W.W., Kettles, I. and Arsenault, L. 1976: Surficial geology of Eskimo Point [55E], Dawson Inlet [55F], Kaminak Lake [55L], Henik lakes [65H], District of Keewatin; Geological Survey of Canada, Open File 356, 27 p., 4 maps, scale 1:125 000, doi:10.4095/129461

Short, N., LeBlanc, A.-M., Sladen, W.E., Allard, M. and Mathon-Dufour, V. 2012a: Seasonal surface displacement derived from InSAR, Iqaluit, Nunavut; Geological Survey of Canada, Canadian Geoscience Map 66 (preliminary version), scale 1:15 000, doi:10.4095/289606

Short, N., LeBlanc, A.-M., Sladen, W.E., Carbonneau, A.-S. and Allard, M. 2012b: Seasonal surface displacement derived from InSAR, Pangnirtung, Nunavut; Geological Survey of Canada, Canadian Geoscience Map 67 (preliminary version), scale 1:5000, doi:10.4095/289607

Smith, S.L., Burgess, M.M. and Riseborough, D. 2005: Recent trends from Canadian permafrost thermal monitoring network sites; Permafrost and Periglacial Processes, v. 16, p. 19–30.

Smith, S.L., Riseborough, D.W., Ednie, M. and Chartrand, J. 2013: A map and summary database of permafrost temperatures in Nunavut, Canada; Geological Survey of Canada, Open File 7393, 20 p.

Smith, S.L., Romanovsky, V.E., Lewkowicz, A.G., Burn, C.R., Allard, M., Clow, G.D., Yoshikawa, K. and Throop, J. 2010: Thermal state of permafrost in North America: a contribution to the International Polar Year; Permafrost and Periglacial Processes, v. 21, p. 117–135.

Steenkamp, H.M., Wodicka, N., Lawley, C.J.M., Peterson, T.D. and Guilmette, C. 2015: Overview of bedrock mapping and results from portable X-ray fluorescence spectrometry in the

eastern part of the Tehery Lake–Wager Bay area, western Hudson Bay, Nunavut; *in* Summary of Activities 2015, Canada-Nunavut Geoscience Office, p. 121–134.

Tam, A. 2014: The impacts of climate change on potential permafrost distributions from the subarctic to the high arctic regions in Canada; Ph.D. thesis, University of Toronto, Toronto, Ontario, 168 p., URL <http://hdl.handle.net/1807/68103> [November 2015].

Tella, S., Paul, D., Berman, R.G., Davis, W.J., Peterson, T.D., Pehrsson, S.J. and Kerswill, J.A. 2007: Bedrock geology compilation and regional synthesis of parts of Hearne and Rae domains, western Churchill Province, Nunavut – Manitoba; Geological Survey of Canada, Open File 5441, scale 1:550 000, doi:10.4095/224573

Throop, J., Lewkowicz, A.G. and Smith, S.L. 2012: Climate and ground temperature relations at sites across the continuous and discontinuous permafrost zones, northern Canada; Canadian Journal of Earth Sciences, v. 49, p. 865–876.

Tremblay, T., Kendall, M.S., Bellehumeur-Génier, O., LeBlanc, A.-M., Oldenborger, G.A., Budkewitsch, P. and Mate, D.J. 2015: Preliminary RapidEye land-cover map for Western Hudson Bay area, Nunavut; Canada-Nunavut Geoscience Office, Geoscience Data Series GDS2015-015, georeferenced .tif file.

Wityk, U., Harris, J.R., McMartin, I., Campbell, J.E., Ross, M. and Grunsky, E. 2013: Remote predictive mapping of surficial materials west of Repulse Bay, Nunavut (NTS 46M-SW, 46L-W and -S, 46K-SW); Geological Survey of Canada, Open File 7357, 24 p., doi:10.4095/292578

Wright, G.M. 1967: Surficial geology, southeastern Barren Grounds, District of Keewatin and District of Mackenzie; Geological Survey of Canada, Map 1217A, scale 1:1 000 000.

Zhang, Y. 2013: Spatio-temporal features of permafrost thaw projected from long-term high-resolution modeling for a region in the Hudson Bay Lowlands in Canada; Journal of Geophysical Research, v. 118, p. 542–552.

Ground temperatures and spatial permafrost conditions in Iqaluit, Baffin Island, Nunavut

A.-M. LeBlanc[1], G.A. Oldenborger[2], N. Short[3], W.E. Sladen[2], M. Allard[4] and V. Mathon-Dufour[4]

[1]*Natural Resources Canada, Geological Survey of Canada, Ottawa, Ontario, anne-marie.leblanc@canada.ca*

[2]*Natural Resources Canada, Geological Survey of Canada, Ottawa, Ontario*

[3]*Natural Resources Canada, Canada Centre for Mapping and Earth Observation, Ottawa, Ontario*

[4]*Centre d'études nordiques, Université Laval, Québec, Quebec*

LeBlanc, A.-M., Oldenborger, G.A., Short, N., Sladen, W.E., Allard, M. and Mathon-Dufour, V. 2015: Ground temperatures and spatial permafrost conditions in Iqaluit, Baffin Island, Nunavut; *in* Summary of Activities 2015, Canada-Nunavut Geoscience Office, p. 161–170.

Abstract

Iqaluit is an important city for the social and economic development of Nunavut. However, until recently, only sparse data and knowledge on the permafrost conditions in Iqaluit were publicly available. To support informed decision-making and the development of adaptation strategies to cope with the impacts of climate change, a joint study was launched in 2010 between the Canada-Nunavut Geoscience Office, Natural Resources Canada and Université Laval's Centre d'études nordiques to investigate permafrost conditions in Iqaluit. Results from the multidisciplinary study indicate that permafrost conditions in Iqaluit, such as ice-rich soils, are highly variable spatially and with depth. Ground temperatures at three active monitoring sites (2010–2015) and one abandoned site (1988–2004) show that permafrost has warmed at depth and active layer thickness has likely increased since monitoring was first established in Iqaluit in 1988. The warming is about 3.7°C at 5 m depth, and active layer thickness has increased by approximately 30 cm. Thick snow cover is a major influence on the thermal regime of Iqaluit permafrost, increasing the ground temperature at 10 m depth by at least 2°C.

Résumé

La ville d'Iqaluit est un pôle de développement social et économique important pour le Nunavut. Cependant, jusqu'à tout récemment, il y avait peu de données et de connaissance accessibles publiquement sur les conditions du pergélisol à Iqaluit. Afin de fournir une aide à la prise de décisions éclairées et à l'élaboration de stratégies d'adaptation en vue de composer avec les impacts des changements climatiques, une étude conjointe a été lancée en 2010 regroupant les efforts du Bureau géoscientifique Canada-Nunavut, Ressources naturelles Canada et le Centre d'études nordiques de l'Université Laval dans le but d'examiner les conditions du pergélisol à Iqaluit. Les résultats de cette étude multidisciplinaire ont révélé que les conditions propres au pergélisol à Iqaluit, telles que les sols riches en glace, varient grandement aussi bien en fonction de leur étendue que de leur profondeur. Les températures du sol à trois sites de surveillance en service (de 2010 à 2015) et à un ancien site (de 1988 à 2004) indiquent que le pergélisol s'est réchauffé en profondeur et que l'épaisseur de la couche active a probablement augmenté depuis l'établissement du premier site de surveillance en 1988. Ce réchauffement est de l'ordre de 3,7°C à 5 m de profondeur alors que l'épaisseur de la couche active a augmenté d'environ 30 cm. Les résultats démontrent la grande influence qu'un manteau de neige épais peut avoir sur le régime thermique du pergélisol puisqu'il peut entraîner une augmentation de la température d'au moins 2°C à 10 m de profondeur.

Introduction

Iqaluit is an important city for the social and economic development of Nunavut. Various federal and territorial governmental departments and industry sectors have established activities and services in Iqaluit, and the city is the main air transportation hub for the eastern Arctic. Until recently, publicly available geoscience knowledge on permafrost conditions in Iqaluit and its immediate surroundings was sparse. To overcome the lack of permafrost data and

This publication is also available, free of charge, as colour digital files in Adobe Acrobat® PDF format from the Canada-Nunavut Geoscience Office website: http://cngo.ca/summary-of-activities/2015/.

support the socioeconomic development of the region, a joint study was initiated in 2010 between the Canada-Nunavut Geoscience Office (CNGO), Natural Resources Canada (NRCan) and Université Laval's Centre d'études nordiques (CEN) to examine permafrost sensitivity and terrain conditions in the Iqaluit area. Today, not only is new knowledge available, but innovative research has been carried out in the areas of remote sensing, geophysics, modelling and integrative approaches for permafrost characterization. During the first year of this project, ground temperatures monitoring sites were established in three locations. Although temperature data from these sites were made publicly available via the CEN data clearinghouse Nordicana D (http://www.cen.ulaval.ca/nordicanad/), the data were never subjected to further analysis. The objectives of this paper are to 1) direct readers to the literature produced during this joint study, with specific regard to the spatial permafrost conditions that are linked to the surficial geology and the surface conditions; 2) present the current variability (2010–2015) of the ground thermal regime at the three monitoring sites; and 3) put the contemporary ground temperatures and active layer thicknesses (2010–2015) within the context of a longer timescale (since 1988).

Study site

Iqaluit is located on southeastern Baffin Island at the head of Frobisher Bay (latitude 63°45'N, longitude 68°33'W) in the zone of continuous permafrost. The city's older neighbourhoods and the airport are built on flat terrain surrounded by hills and rocky plateaus of the Precambrian shield (St-Onge et al., 2006), whereas more recently built neighbourhoods tend to be located on rocky hill slopes and plateaus. Main roads are built on embankment material covered with a paved surface, whereas buildings rest on piles, fill material or a combination of the two. Low-growing tundra vegetation is generally continuous, except on exposed bedrock. The dominant vegetation is willow and heath, with extensive areas of grass, sedges and moss, depending on moisture conditions (Short and Jacobs, 1982). Climate normals of mean monthly air temperatures for 1981–2010 range from 8.2°C in July to –27.5°C in February, with an annual mean temperature of –9.3°C, and annual precipitation of 404 mm, 49% of which occurred as rain (Environment Canada, 2015).

Permafrost conditions from earlier studies

Since 2010, the joint NRCan/CNGO/CEN collaboration has resulted in a number of publications that characterize permafrost conditions, including maps, reports and scientific papers. Many of the publications concern the Iqaluit airport (LeBlanc et al., 2013, 2015a; Mathon-Dufour, 2014; Oldenborger et al., 2014, 2015; Short et al., 2014; Masoumeh et al., 2015; Mathon-Dufour et al., 2015; Oldenborger and LeBlanc, 2015), but their results can be extrapolated to other areas of town.

Surficial geology was mapped by Allard et al. (2012) at a scale of 1:15 000 for the greater Iqaluit area, and at 1:8000 for the airport area (Figure 1). The map includes a short description of periglacial features, such as ice-wedge networks. A more detailed version of the surficial geology for the airport is provided by Mathon-Dufour et al. (2015). Based on the surficial geology map, field observations and discussions with two of the authors, the Government of Nunavut's Department of Environment published a modified map in *A Homeowner's Guide to Permafrost in Nunavut* (Government of Nunavut, 2013), highlighting geology and the likely distribution of ice-rich permafrost. This simplified map shows that ice-rich permafrost occurs in various surficial geology units, from till blanket to marine sediment, mostly in association with silty soils.

Borehole data provided additional information to characterize not just the surficial geology, but the underlying material as well. Several deep (~15 m) and shallow (<4 m) boreholes were drilled, with permafrost cores being recovered from many of them (Mathon-Dufour, 2014; Mathon-Dufour et al., 2015). The cores made it possible to better understand the Quaternary stratigraphy, which provides important constraints on the spatial variability and depth distribution of permafrost conditions. For example, glaciomarine delta deposits representing up to four depositional environments were found underneath the airport infrastructure, resulting in different ground-ice conditions. Near Frobisher Bay, fine-grained and saline sediments, which are dominated by interstitial and segregated ice, were observed at depth. There, as well as in other locations, sand and gravel, which is dominated by interstitial ice, was observed nearer the ground surface (Mathon-Dufour et al., 2015). Several of the boreholes were instrumented with thermistor cables, and ground temperatures for three sites are presented below in the 'Ground thermal regime analysis' section. Additional ground temperatures are presented in Mathon-Dufour (2014) and Mathon-Dufour et al. (2015). These complementary results show that permafrost temperatures generally increase once embankments and paved roads are built. Permafrost under paved surfaces in Iqaluit is approximately 1.5°C warmer at 10 m depth in comparison to natural terrain, and it has a thicker active layer (Mathon-Dufour et al., 2015).

In addition to the borehole observations and temperature measurements, various geophysical methods were used to characterize the permafrost, including ground penetrating radar (LeBlanc et al., 2013; Mathon-Dufour, 2014), as well as electrical and electromagnetic surveys (Oldenborger and LeBlanc, 2013a, b, 2015; Oldenborger et al., 2014, 2015). In particular, Oldenborger and LeBlanc (2015) and Oldenborger et al. (2015) show that 1) different surficial

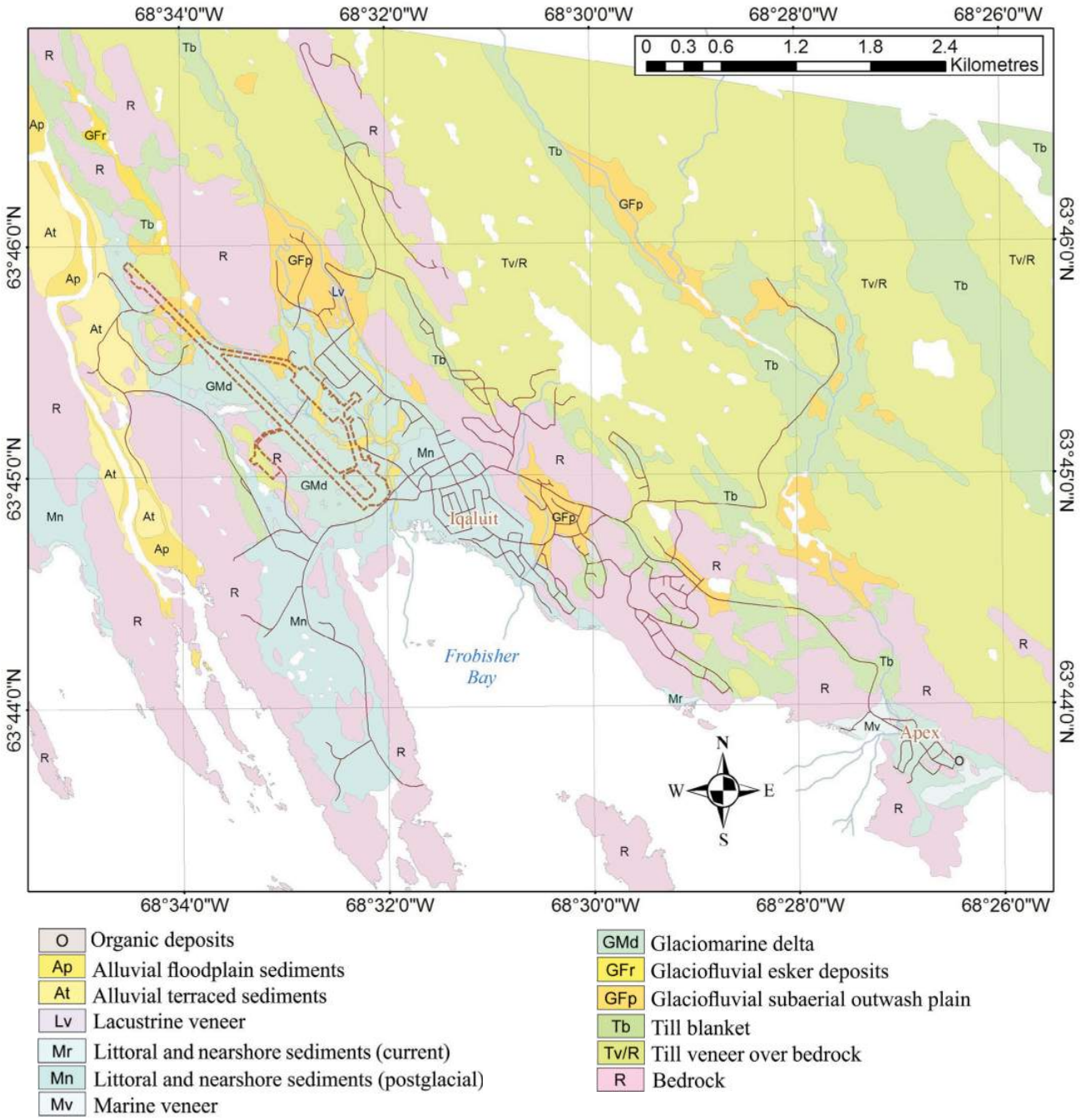

Figure 1: Surficial geology map of Iqaluit, Nunavut (modified from Allard et al., 2012; Mathon-Dufour et al., 2015).

geology units, including ice-rich permafrost and ice wedges, were associated with unique geophysical signatures; and 2) some anomalously conductive material that differs from the surficial geology was observed at depth beneath areas with localized settlement problems. Such conductivity observations would typically be attributed to unfrozen ground in other climatic conditions, but thermistor measurements confirm this is cryotic and, therefore, the material is interpreted as having a significant unfrozen water content. In other words, both resistive (ice-rich permafrost, ice wedges) and conductive ground (frozen, but with significant unfrozen water content) were spatially identified in the area of Iqaluit and are associated with settlement problems. These findings can support the interpretation of similar surveys conducted elsewhere in Iqaluit or in other coastal communities, and may help identify problematic ground for development. Permafrost mapping was further supported by the use of differential interferometric synthetic aperture radar (DInSAR), a remote sensing method used to detect seasonal ground surface displacement. This method was used over several summers and the results mainly relate to seasonal changes in active layer thickness

(Short et al., 2012, 2014; LeBlanc et al., 2013, 2015b, c). Results show that low values of displacement are associated with bedrock and coarse sediments. Finer sediments are more likely to be ice-rich and show higher values of displacement. Medium to high displacement values, in the range of 2–8 cm, were mainly associated with glaciomarine deposits (under airport infrastructure and in the Apex neighbourhood), nearshore sediments (under the older part of Iqaluit and on the west side of Frobisher Bay) and till blanket (in both natural terrain and under builtup areas). In fact, there is good correlation between the DInSAR maps and the map produced by the Government of Nunavut (2013) showing the likelihood of ice-rich permafrost. However, in addition to ground ice, other factors can explain some displacement patterns, such as water flowing within the active layer, which can induce accelerated thaw at the permafrost table and remove fine sediments (Short et al., 2014). Changes in surface water level may also be seen as displacement (LeBlanc et al., 2015b); in such a case, the phenomenon is not related to seasonal settlement of ice-rich soils. These findings are useful for guiding DInSAR applications, especially for infrastructure management and planning.

Finally, the permafrost thermal regime was modelled to 1) determine the impacts of infrastructure (embankments) and future climate warming (LeBlanc et al., 2015a), and 2) assess the coupled impacts of groundwater flow and heat transfer in the context of future climate changes (Masoumeh et al., 2015). In LeBlanc et al. (2015a), estimations of permafrost thermal regimes were presented for the period 1946–2044 using potential warming trends of 0.5 and 1°C per decade. The model was validated using the permafrost conditions at thermistor cable IQAV2TC (see 'Permafrost monitoring sites and ground temperatures' section below). The results highlight the difference in ground temperatures that arise under various surface conditions (e.g., water flow, the presence of embankments, thick or thin snow conditions) and how the permafrost thermal regime for each of these surface conditions may change due to climate warming. For example, for contemporary conditions, permafrost temperatures at 15 m depth can vary from –5.6°C under natural terrain with thin snow cover to –2.7°C under thick snow cover. For the same depth, potential climate warming could induce a ground temperature increase of 0.7 to 1.3°C under thin snow cover (depending on the climate warming trend used), with a smaller increase under thick snow cover (LeBlanc et al., 2015a). In Masoumeh et al. (2015), changes in surface conditions are also modelled for natural terrain, unpaved areas and paved embankments. The results of both studies can be extrapolated as a first-order assessment to other areas around Iqaluit, or other northern coastal communities with surface and subsurface conditions similar to those modelled.

Data for thermal analysis

Climatic data

Data from Environment Canada weather stations in Iqaluit (Iqaluit UA, Iqaluit CLIMATE or Iqaluit A) are available from 1946 to the present. Data from 1946 to 2011 were homogenized into one dataset by Vincent et al. (2012), and climate data from 2011 to the present were obtained directly from the Environment Canada website (Environment Canada, 2015). Daily values were used to calculate the mean annual air temperature (MAAT) for each calendar year. A cooling trend of about 0.03°C/yr occurred between 1946 and 1992, followed by a warming trend of about 0.09°C/yr between 1993 and 2014 (Figure 2). However, if the steplike increase in air temperature between 1993 and 2000 is excluded, the warming trend for the last 15 years is approximately 0.03°C/yr (Figure 2).

From 1997 to 2004, Environment Canada also maintained another weather station near a radio facility along the road to Apex, on the east side of Iqaluit (Figure 3a). This station is at a higher elevation (109 m asl) than the other Environment Canada weather stations (between 21.5 and 33.5 m asl). Complete years of data for this alternate station are only for 1998, 1999, 2002 and 2003, and these data are shown in Figure 2 for comparison.

Permafrost monitoring sites and ground temperatures

Between 1988 and 2004, Environment Canada also maintained a permafrost thermal monitoring site (HT-02) near the high-elevation weather station, in collaboration with the Geological Survey of Canada (Throop et al., 2012). The thermistor cable (YSI Inc. model; unknown specification)

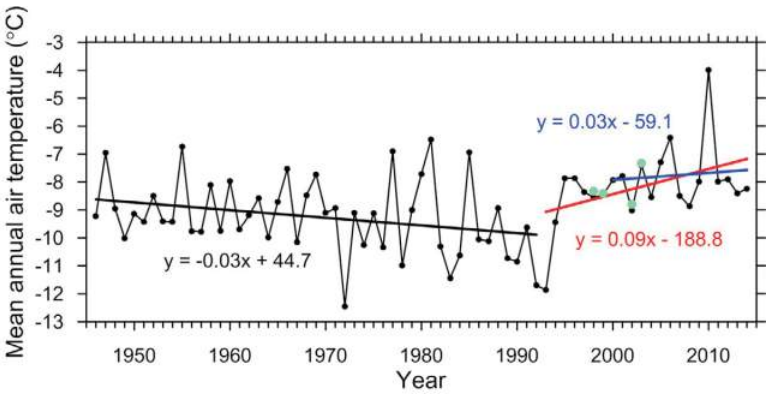

Figure 2: Mean annual air temperature (MAAT) recorded at Environment Canada weather stations from 1946 to 2015, Iqaluit, Nunavut. Green dots are from the high-elevation Environment Canada weather station located at 109 m asl, on the east side of Iqaluit.

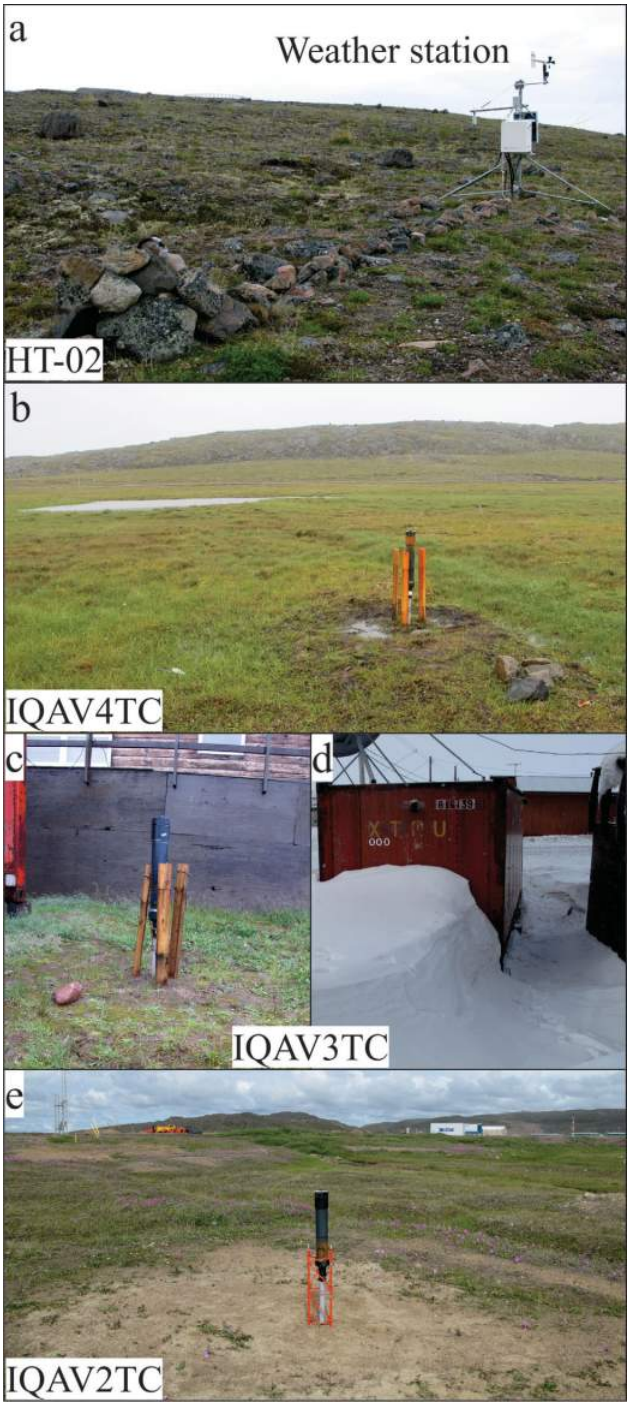

Figure 3: Permafrost monitoring sites, Iqaluit, Nunavut: **a)** HT-02 in till veneer over bedrock, weather station in foreground; **b)** IQAV4TC in poorly drained marine littoral and nearshore sediments; **c)** IQAV3TC in dry marine littoral and nearshore sediments; **d)** IQAV3TC in winter under 100 cm of snow; and **e)** IQAV2TC in well-drained glaciofluvial sediments.

was connected to a Campbell Scientific, Inc. CR10 logger to record ground temperatures every three hours at seven depths between 0.5 and 5 m. The overall error of measurement is on the order of ±0.2°C. The site is characterized by sparse vegetation over till veneer on bedrock (Figure 3a). Snow depth, measured in winter 2003–2004 by an acoustic snow depth sensor (Campbell Scientific, Inc. SR50), was <10 cm on average. In 2010, as part of the collaboration between CNGO, NRCan and CEN, three boreholes were instrumented with thermistor cables (YSI Inc. model YSI-44033) from a depth of 0.25 m to depths of 3.3, 14.7 and 15 m (IQAV4TC, IQAV3TC, IQAV2TC, respectively; Allard et al., 2014). Each cable was connected to a data logger (RBR Ltd. model XR-420) recording hourly temperatures with a resolution of ±0.01°C. In addition, single-channel temperature loggers (Onset Computer Corporation HOBO® Water Temp Pro v2), located within a few centimetres of each of the thermistor cables and 2–5 cm below the ground surface, measured hourly near-surface temperatures with a resolution of ±0.03ºC (IQAV4HO, IQAV3HO, IQAV2HO; Allard et al., 2014). The borehole sites are located in distinct areas, but are all at relatively low elevations (<25 m asl) compared to HT-02. Site IQAV4TC/IQAV4HO is located within the Sylvia Grinnell Territorial Park adjacent to the airport (Figure 3b). This area of the park is low-lying, undisturbed, wet and vegetated with cotton grass and sedges. The thermistor cable is located <1 m from an ice wedge in poorly drained marine littoral and nearshore sediments. Snow cover measured in March 2012 and 2013 was 20 and 40 cm, respectively. Site IQAV3TC/IQAV3HO is located in town, close to a house, in relatively dry marine littoral and nearshore sediments (Figure 3c). Snow drifts typically accumulate to a height of approximately 100 cm (Figure 3d). Site IQAV2TC/IQAV2HO is located near the Iqaluit airport runway, <6 m from an ice wedge, in well-drained glaciofluvial sediments (Figure 3e). Snow cover is typically <2 cm. Detailed soil descriptions for sites IQAV4TC and IQAV2TC can be found in LeBlanc et al. (2015c).

Ground thermal regime analysis

Data processing

Mean annual ground temperatures (MAGT) were calculated at each depth using daily averages from the thermistor cables. A climatic year (October to September) was used instead of the calendar year in order to include one complete freezing and thawing season. The 2014–2015 year is incomplete and ends in mid-June. Furthermore, at the end of the summer of 2014, about 2 m of sand was deposited in the area around IQAV2TC. New temperature sensors were placed in this added material.

Active layer thickness (maximum summer thaw depth) was estimated by linear interpolation of the temperature profile close to 0°C (Riseborough, 2008). The accuracy is approximately 7 cm when the active layer thickness is <100 cm (thermistor spacing of 25 cm), and about 14 cm when the active layer is >100 cm (thermistor spacing of 50 cm).

The earlier ground temperature records (1988–2004) and the recent ones from this study (2010–2015) were not collected in similar terrain, which makes direct comparison difficult. For example, HT-02 is located in till over bedrock (with the maximum summer thaw depth likely reached in bedrock) and IQAV2TC is located in sand. However, HT-02 and IQAV2TC do share common surface conditions of sparse vegetation and very thin snow cover. Furthermore, although the elevations are different, air temperatures recorded at, or close to, the two sites are similar (Figure 2). Therefore, long-term interpretation (1988–2015) is possible if observed data at HT-02 are compared to simulated data for permafrost conditions at IQAV2TC prior to 2010 (LeBlanc et al., 2015a).

Results and discussion

The MAGT profiles for climatic years 2010–2011, 2011–2012, 2012–2013, 2013–2014 and 2014–2015 (incomplete year) are shown in Figure 4 for the thermistor cables IQAV4TC, IQAV3TC and IQAV2TC. These plots show the temporal variability in ground temperatures due to changes in interannual climate. Temporal variability decreases with depth as the ground attenuates the atmospheric signal. At the dry sites (IQAV2TC and IQAV3TC), ground temperatures for the year 2010–2011 were the warmest of the five years mainly due to the high MAAT of 2010 (Figure 2). At site IQAV4TC, the wet surface could explain why this site is not exactly following the same ground-temperature trends as the two other sites (i.e., ground temperatures for the year 2012–2013 are slightly higher than for the year 2010–2011). Except for IQAV2TC, the shallow temperatures in the year 2014–2015 appear lower compared to other years due to the fact that summer temperatures were not included in the data collection. For IQAV2TC, the addition of fill material warmed the ground below the original surface despite the missing summer temperatures.

Spatial variability between the three permafrost sites is mainly due to local surface conditions as sediment type is similar among sites (silty sand to sand). The MAGT at IQAV3TC is clearly affected by the thick snow cover that insulates the ground in winter. Ground temperature for IQAV3TC at 10 m depth is 2.05°C (2010–2011) to 2.43°C (2013–2014) warmer than at IQAV2TC (Figure 5). The MAGT at depths below the bottom thermistor at IQAV4TC are likely more similar to IQAV2TC than IQAV3TC. However, the wet and often flooded surface at IQAV4TC influences the shallow temperatures (Figure 5) and possibly the temperature at depth.

The more recent period of observations show a decreasing trend in ground temperatures at 5 m depth, with 2010–2011 being the warmest year and 2013–2014 being the coldest (Figure 6a). However, at the same depth, comparison of sites HT-02 and IQAV2TC indicates that permafrost temperatures have increased since the first borehole was instrumented in 1988 (Figure 6a). Simulated monthly data at IQAV2TC for the year 1992–1993 (LeBlanc et al., 2015a) correspond well to the observed ground temperatures at HT-02, although the range of simulated annual ground temperature is less for IQAV2TC due to the difference in sediment type (sand versus bedrock). The MAGT from the simulated data is slightly higher at –9.2°C compared to the –9.9°C observed at HT-02. Based on this validation of simulated results for IQAV2TC, the increase in MAGT at 5 m depth

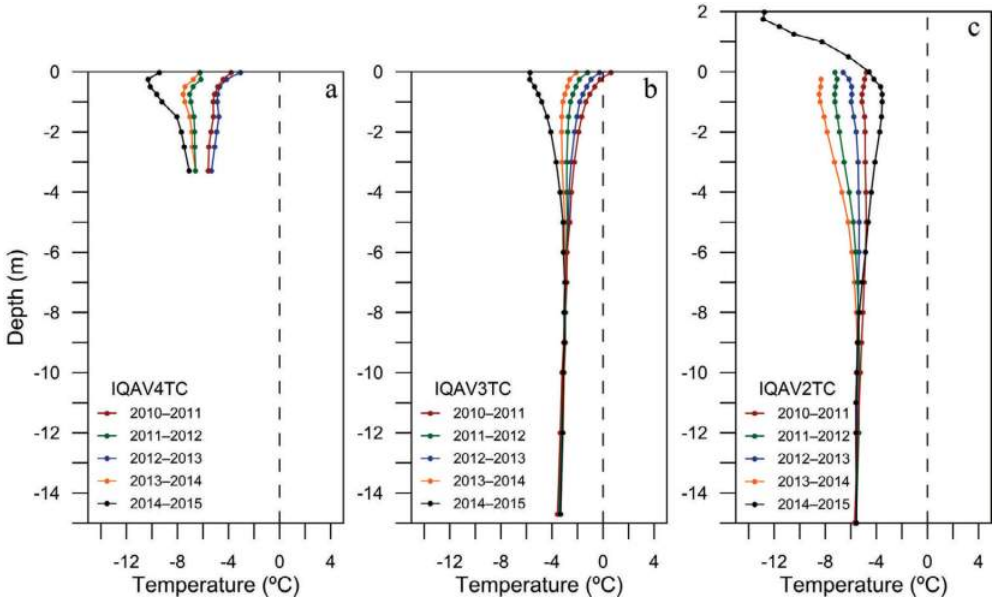

Figure 4: Mean annual ground temperatures (MAGT) profiles by permafrost monitoring site for five climatic years at **a)** IQAV4TC, **b)** IQAV3TC and **c)** IQAV2TC, Iqaluit, Nunavut.

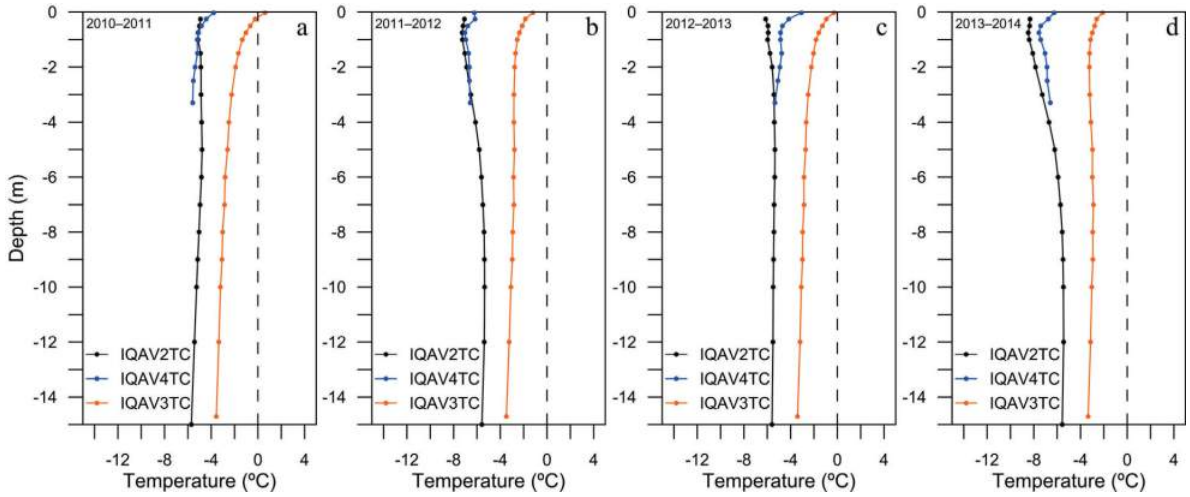

Figure 5: Mean annual ground temperatures (MAGT) profiles by year for each permafrost monitoring site, Iqaluit, Nunavut: **a)** 2010–2011, **b)** 2011–2012, **c)** 2012–2013 and **d)** 2013–2014.

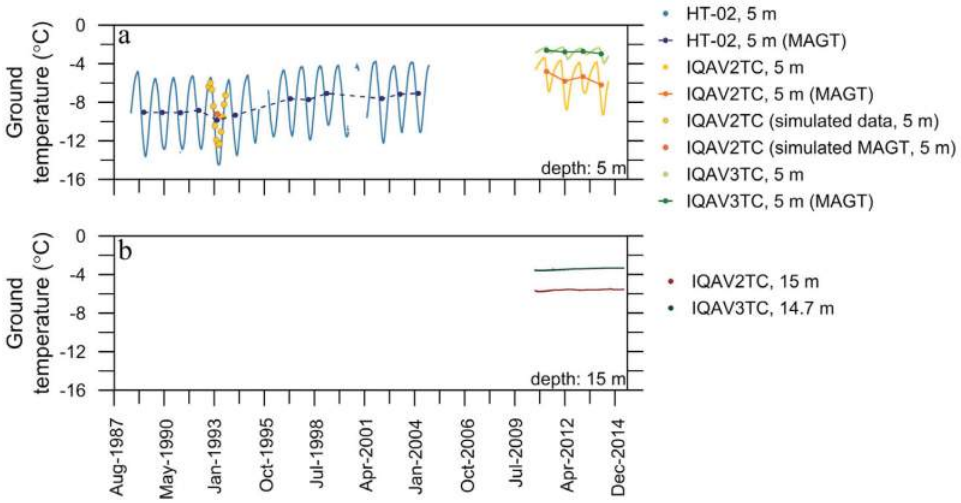

Figure 6: Ground temperatures from 1988 to 2015 at permafrost monitoring sites HT-02, IQAV2TC and IQAV3TC, Iqaluit, Nunavut: **a)** 5 m depth and **b)** 15 m depth. Abbreviation: MAGT, mean annual ground temperature.

between the 1992–1993 year (–9.2°C) and the period 2010–2015 (–5.5°C) is about 3.7°C. This increase could be extrapolated for the period 1988 to 2010–2015 since the ground temperature remained similar between 1988 and 1992–1993.

Whereas recent ground temperatures at 5 m depth have decreased, ground temperatures at 15 m depth have increased very slightly from 2010 to 2015 (Figure 6b). The increases at IQAV2TC and IQAV3TC are 0.04 and 0.06°C/yr, respectively. These observations are in good agreement with the temperature increase of 0.04°C at 15 m depth observed at Igloolik, the smallest increase observed by Ednie and Smith (2015) in a study of various Nunavut communities.

From 2010 to 2014, the maximum summer thaw depths (active layer thickness) decreased at IQAV2TC and IQAV3TC, and increased at IQAV4TC (Figure 7). The decreases are 19 and 14 cm, respectively, at IQAV2TC and IQAV3TC, whereas the increase is about 17 cm at IQAV4TC. These results are close to the accuracy of the thaw depths interpolated for this study. However, for IQAV2TC and IQAV3TC, trends in active layer thickness follow the general cooling in air temperature during the same period (Figure 2). The interpolation of active layer thickness from ground temperature data does not take into account the settlement that usually accompanies thawing. LeBlanc et al. (2015c) found that readings from a thaw tube located near IQAV2TC indicate that yearly settlement for the area is minimal, about 1 or 2 cm per summer. Settlement is unknown at IQAV3TC. For the area around IQAV4TC, yearly

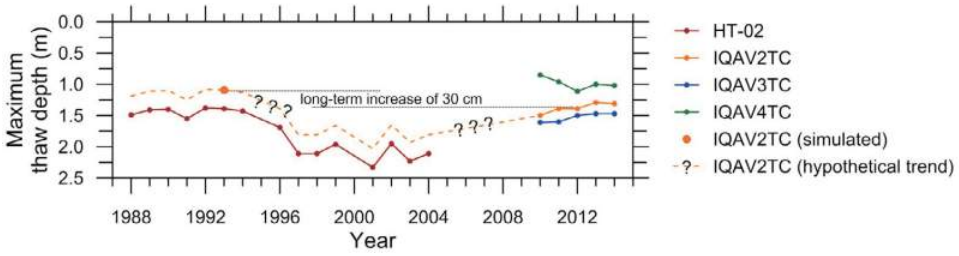

Figure 7: Maximum thaw depth (active layer thickness) from 1988 to 2015 at permafrost monitoring sites HT-02, IQAV2TC, IQAV3TC and IQAV4TC, Iqaluit, Nunavut.

settlement is about 8–12 cm (LeBlanc et al., 2015c). The fact that active layer thickness decreased at IQAV2TC and IQAV3TC and increased at IQAV4TC might be explained by the surface moisture conditions. Wet ground could enhance the thickening of the active layer despite the general cooling in air temperature. For all three sites, the maximum active layer thicknesses were reached between mid-August and about September 10 of all years (2010–2014).

Between 1988 and 2004, active layer thickness increased at HT-02 (Figure 7). The simulated 1993 active layer for IQAV2TC is approximately 30 cm thinner than that for HT-02 and the authors have made the assumption that the active layer at IQAV2TC followed the same trend as at HT-02 (although the more efficient heat transfer of the bedrock at HT-02 might cause the offset to get slightly larger with time). If this assumption is correct, then by 2004, the active layer at IQAV2TC would have been slightly thicker or of the same thickness as today, which is not surprising given that the air temperatures are similar. This allows the authors to place the recent 2010–2014 observations into a long-term context, indicating that despite seeing a slight decrease in the active layer over the last few years, over the long term, it appears to have increased in thickness. This increase is approximately 30 cm.

Economic considerations

The joint study between NRCan/CNGO/CEN has generated useful knowledge and data on spatial and temporal permafrost conditions. These publicly available results contribute to informed decision-making and provide geoscience information to land-use planners, while supporting the development of adaptation strategies to cope with the impacts of climate change. The findings can be used to identify areas of ice-rich permafrost (thaw-sensitive ground) and other ground that is problematic for development; site-specific geotechnical studies are needed for further planning and design. The recently installed ground monitoring sites provide current thermal permafrost conditions, facilitating the assessment of the impact of future climate change. Urban development of Iqaluit, homeowner's practices for houses in Nunavut, and the rehabilitation of the Iqaluit International Airport are known examples where the results of this study have played a role in decision-making.

Conclusions

The ground temperature data presented in this paper, along with knowledge gathered in the region through the duration of this study, demonstrate that spatial permafrost conditions in Iqaluit are highly variable. The spatial distribution of ice-rich ground is strongly related to the surficial geology. Ground ice was observed in boreholes in areas experiencing thaw settlement. Frozen ground with significant unfrozen water content was also identified from geophysical data in regions with settlement problems. Even when subsurface conditions are similar, the permafrost thermal regimes can be different if the surface conditions, such as water flow, paved embankments and thick snow cover, induce warmer ground at depth. At the permafrost monitoring site located under thick snow cover, the ground is approximately 2–2.4°C warmer at 10 m depth.

In addition to spatial permafrost conditions, temporal variability in ground temperature was also assessed. Short-term changes in ground temperatures at 5 m depth occurred over the 2010–2015 period, with the decreasing ground temperatures likely due to decreasing air temperatures. However, based on past ground temperature data along with temperature simulations, it is concluded that permafrost temperatures at 5 m depth increased by about 3.7°C between 1988 and the 2010–2015 period. There was no clear trend in active layer thickness between 2010 and 2015, and any changes seemed to depend on site-specific conditions. Long-term change in active layer thickness between 1988 and the 2010–2015 period is estimated to be about 30 cm.

Acknowledgments

The authors thank J. Graham, J. Hawkins, K. Henderson and Sintra Inc. (T. De Lustrac) for site access and co-operation at the Iqaluit International Airport. Special thanks go to D. Mate (formerly of the Canada-Nunavut Geoscience Office and now with Canadian Northern Economic Development Agency) for his initial collaboration on this project. Thanks also go to M. Horlink, T. Irniq, J. Davidee and

G. Nobles (Nunavut Arctic College students), J. Shirley (Nunavut Research Institute), S. Holzman (Government of Nunavut), C. Duchesne (Natural Resources Canada, Geological Survey of Canada), A.-S. Carbonneau, P. Gosselin, J. Doyon and C. Falardeau-Marcoux (Université Laval) and T. Tremblay (Canada-Nunavut Geoscience Office) for their help in the field throughout the years (2010–2015) as well as E. L'Hérault (Université Laval, Centre d'études nordiques) for his collaboration and S. Smith (Natural Resources Canada, Geological Survey of Canada) for sharing the data from the Environment Canada weather and permafrost stations. The authors also want to thank the Canada-Nunavut Geoscience Office for in-kind contributions. The Canadian Northern Economic Development Agency's (CanNor) Strategic Investments in Northern Economic Development (SINED) program provided financial support for this work. Additional resources were provided by the Canadian Space Agency through the Government Related Initiatives Program and by Transport Canada through contributions to Université Laval, Centre d'études nordiques. This project is part of the Natural Resources Canada Climate Change Geoscience Program. Helpful comments and a thorough review were provided by N. Couture (Natural Resources Canada, Geological Survey of Canada).

Natural Resources Canada, Earth Sciences Sector contribution 20150333

References

Allard, M., Doyon, J., Mathon-Dufour, V., LeBlanc, A.-M., L'Hérault, E., Mate, D., Oldenborger, G.A. and Sladen, W.E. 2012: Surficial geology, Iqaluit, Nunavut; Geological Survey of Canada, Canadian Geoscience Map 64 (preliminary version), scale 1:15 000.

Allard, M., Sarrazin, D. and L'Hérault, E. 2014: Borehole monitoring temperatures in northeastern Canada, v. 1.2 (1988–2014); Nordicana D8, doi:10.5885/45291SL-34F28A9491014AFD

Ednie, M. and Smith, S.L. 2015: Permafrost temperature data 2008–2014 from community based monitoring sites in Nunavut; Geological Survey of Canada, Open File 7784, 18 p.

Environment Canada 2015: Canadian climate normals; Environment Canada, URL <http://climate.weather.gc.ca/climate_normals/index_e.html> [March 2015].

Government of Nunavut 2013: A homeowner's guide to permafrost in Nunavut; Government of Nunavut Department of Environment, URL <http://climatechangenunavut.ca/en/resources/news/homeowners-guide-permafrost-nunavut-just-released> [April 2013].

LeBlanc, A.-M., Oldenborger, G., Short, N., Sladen, W., Allard, M., Mathon-Dufour, V. and L'Hérault, E. 2013: Permafrost study at the Iqaluit airport, Nunavut, in support of decision-making and future planning; *in* Summary of Activities 2012, Canada-Nunavut Geoscience Office, p. 131–142.

LeBlanc, A.-M., Oldenborger, G.A., Sladen, W.E. and Allard, M. 2015a: Infrastructure and climate warming impacts on ground thermal regime, Iqaluit International Airport, Nunavut; *in* Summary of Activities 2014, Canada-Nunavut Geoscience Office, p. 119–132.

LeBlanc, A.-M., Short, N., Mathon-Dufour, V., Allard, M., Tremblay, T., Oldenborger, G.A. and Chartrand, J. 2015b: DInSAR seasonal surface displacement in built and natural permafrost environments, Iqaluit, Nunavut, Canada: *in* Proceedings of GEOQuébec 2015, Québec City, September 20–23, 2015, paper 455, 8 p.

LeBlanc, A.-M., Short, N., Mathon-Dufour, V. and Chartrand, J. 2015c: DInSAR seasonal surface displacement in permafrost terrain, Iqaluit, Nunavut; Geological Survey of Canada, Open File 7874, 36 p.

Masoumeh, S.G., Therrien, R., Molson, J. and Lemieux, J.-M. 2015: Numerical simulations of coupled groundwater flow and heat transport incorporating freeze/thaw cycles and phase change in a continuous permafrost environment; *in* Proceedings of GEOQuébec 2015, Québec City, September 20–23, 2015, paper 720, 8 p.

Mathon-Dufour, V. 2014: Caractérisation du pergélisol en vue de la réfection et de l'adaptation aux changements climatiques de l'aéroport d'Iqaluit, Nunavut; M.Sc. thesis, Université Laval, Québec, Quebec, 279 p.

Mathon-Dufour, V., Allard, M. and LeBlanc, A.-M. 2015: Assessment of permafrost conditions in support of the rehabilitation and adaptation to climate change of the Iqaluit airport, Nunavut, Canada; *in* Proceedings of GEOQuébec 2015, Québec City, September 20–23, 2015, paper 146, 8 p.

Oldenborger, G.A. and LeBlanc, A.-M. 2013a: Capacitive resistivity inversion using effective dipole lengths for line antennas; Journal of Applied Geophysics, v. 98, p. 229–236.

Oldenborger, G.A. and LeBlanc, A.-M. 2013b: Capacitively coupled resistivity inversion using effective dipole lengths; Geological Survey of Canada, Technical Note 6, 7 p.

Oldenborger, G.A. and LeBlanc, A.-M. 2015: Geophysical characterization of permafrost terrain, Iqaluit International Airport, Nunavut; Journal of Applied Geophysics, v. 123, p. 36–49, doi:10.1016/j.jappgeo.2015.09.016

Oldenborger, G.A., LeBlanc, A.-M. and Sladen W.E. 2014: Geophysical monitoring of permafrost conditions at Iqaluit International Airport, Nunavut; *in* Summary of Activities 2013, Canada-Nunavut Geoscience Office, p. 129–138.

Oldenborger, G.A., LeBlanc, A.-M. and Sladen W.E. 2015: Electrical and electromagnetic data for permafrost characterization at Iqaluit International Airport, Nunavut; Geological Survey of Canada, Open File 7750, 43 p.

Riseborough, D. 2008: Estimating active layer and talik thickness from temperature data: implication for modeling results; *in* Proceedings of the Ninth International Conference on Permafrost, D.L. Kane and K.M. Hinkel (ed.), Institute of Northern Engineering, University of Alaska Fairbanks, Fairbanks, Alaska, p. 1487–1492.

Short, S.K. and Jacobs, J.D. 1982: A 1100 year paleoclimatic record from Burton Bay–Tarr Inlet, Baffin Island; Canadian Journal of Earth Sciences, v. 19, no. 3, p. 398–409.

Short, N., LeBlanc, A.-M., Sladen, W.E., Allard, M. and Mathon-Dufour, V. 2012: Seasonal surface displacement derived from InSAR, Iqaluit, Nunavut; Geological Survey of Canada, Canadian Geoscience Map 66 (preliminary version), scale 1:15 000.

Short, N., LeBlanc, A.-M., Sladen, W., Mathon-Dufour, V., Oldenborger, G. and Brisco, B. 2014: RADARSAT-2 D-InSAR for ground displacement in permafrost terrain, vali-

dation from Iqaluit Airport, Baffin Island, Canada; Remote Sensing of Environment, v. 141, p. 40–51.

St-Onge, M.R., Jackson, G.D. and Henderson, I. 2006: Geology, Baffin Island (south of 70°N and east of 80°W), Nunavut; Geological Survey of Canada, Open File 4931, scale 1:500 000.

Throop, J., Lewkowicz, A.G. and Smith, S.L. 2012: Climate and ground temperature relations at sites across the continuous and discontinuous permafrost zones, northern Canada; Canadian Journal of Earth Sciences, v. 49, no. 8, p. 865–876.

Vincent, L.A., Wang, X.L., Milewska, E.J., Wan, H., Yang, F. and Swail, V. 2012: A second generation of homogenized Canadian monthly surface air temperature for climate trend analysis; Journal of Geophysical Research., v. 117, issue D18110, doi:10.1029/2012JD017859

Resource potential for industrial limestone on southwestern Southampton Island, Nunavut: mineable intervals and area

S. Zhang[1]

[1]*Canada-Nunavut Geoscience Office, Iqaluit, Nunavut, shunxin.zhang@canada.ca*

Zhang, S. 2015: Resource potential for industrial limestone on southwestern Southampton Island, Nunavut: mineable intervals and area; *in* Summary of Activities 2015, Canada-Nunavut Geoscience Office, p. 171–182.

Abstract

The data collected in 2013 indicated that high-calcium limestone is present in the Lower Silurian Ekwan River Formation south of Manico Point on western Southampton Island. Following the industrial limestone project in 2013, more detailed fieldwork was carried out in 2014 in the expanded prospective area, approximately 320 km^2 between Manico Point and Nalugalaarvik Point on western Southampton Island. A total of 106 samples were collected along six creeks in this area; all samples were analyzed using X-ray fluorescence. Based on the CaO content, the field observations and the distribution pattern of Paleozoic strata on the island, the mineable intervals with high- and very high calcium limestone have been identified, and a map of limestone purity distribution has been made for the project area.

Résumé

Les données recueillies en 2013 ont indiquées que la formation d'Ekwan River du Silurien inférieur, et située au sud de la pointe Manico dans la partie ouest de l'île Southampton, renferme du calcaire à forte teneur en calcium. Dans la foulée du projet de 2013 portant sur le calcaire industriel, des travaux sur le terrain plus précis ont été réalisés en 2014 dans la zone prometteuse élargie, soit quelque 320 km^2 s'étendant entre la pointe Manico et la pointe Nalugalaarvik dans la partie ouest de l'île Southampton. Un total de 106 échantillons a été recueilli le long de six ruisseaux sillonnant la zone en question; tous les échantillons ont été analysés par fluorescence à rayons X. Les intervalles se prêtant à l'exploitation et renfermant du calcaire à teneur élévée et très élevée en calcium ont été identifiés à partir de l'examen du contenu en CaO, d'observations de terrain et de la configuration de la répartition des strates paléozoïques dans l'île, lesquels renseignements ont permis de dresser une carte de la répartition du niveau de pureté du calcaire de la zone ciblée dans le cadre du projet.

Introduction

Quicklime (CaO) is a product of thermal decomposition of limestone. Limestone containing >97% calcite ($CaCO_3$), or >54.3% CaO, classified as high purity or very high purity (Table 1), is ideal for producing such a product. Quicklime as a chemical reagent has many uses in the mining industry. With the projected growth of the mining industry in the Kivalliq Region of Nunavut alone, 4 000, 4 700 and 4 000–10 000 tonnes of quicklime would be required annually at the Meadowbank mine (gold) and the proposed Kiggavik (uranium) and Meliadine (gold) mines, respectively.

Table 1: Classification of limestone by purity (after Harrison et al., 1998).

No	Percentage of		Category
	$CaCO_3$	Equivalent CaO	
1	>98.5	>55.2	Very high purity
2	98.5–97.0	55.2–54.3	High purity
3	97.0–93.5	54.3–52.4	Medium purity
4	93.5–85.0	52.4–47.6	Low purity
5	<85.0	<47.6	Impure

Finding limestone resources suitable for quicklime on Southampton Island could potentially meet mining-industry needs, reduce transportation costs for mine operators and provide significant opportunities for economic development and local employment in the Kivalliq Region. Since 2009, the Canada-Nunavut Geoscience Office (CNGO) has been conducting a research project to evaluate the industrial-limestone potential in the Upper Ordovician sequence (Zhang et al., 2011), and then in the Lower Silurian sequence (Zhang et al., 2014) on Southampton Island (Figure 1). In 2013, the data collected from a creek (creek 2 of this study; Figure 2) south of Manico Point suggested that high-calcium limestone (CaO >54.3%) occurs in the Lower

This publication is also available, free of charge, as colour digital files in Adobe Acrobat® PDF format from the Canada-Nunavut Geoscience Office website: http://cngo.ca/summary-of-activities/2015/.

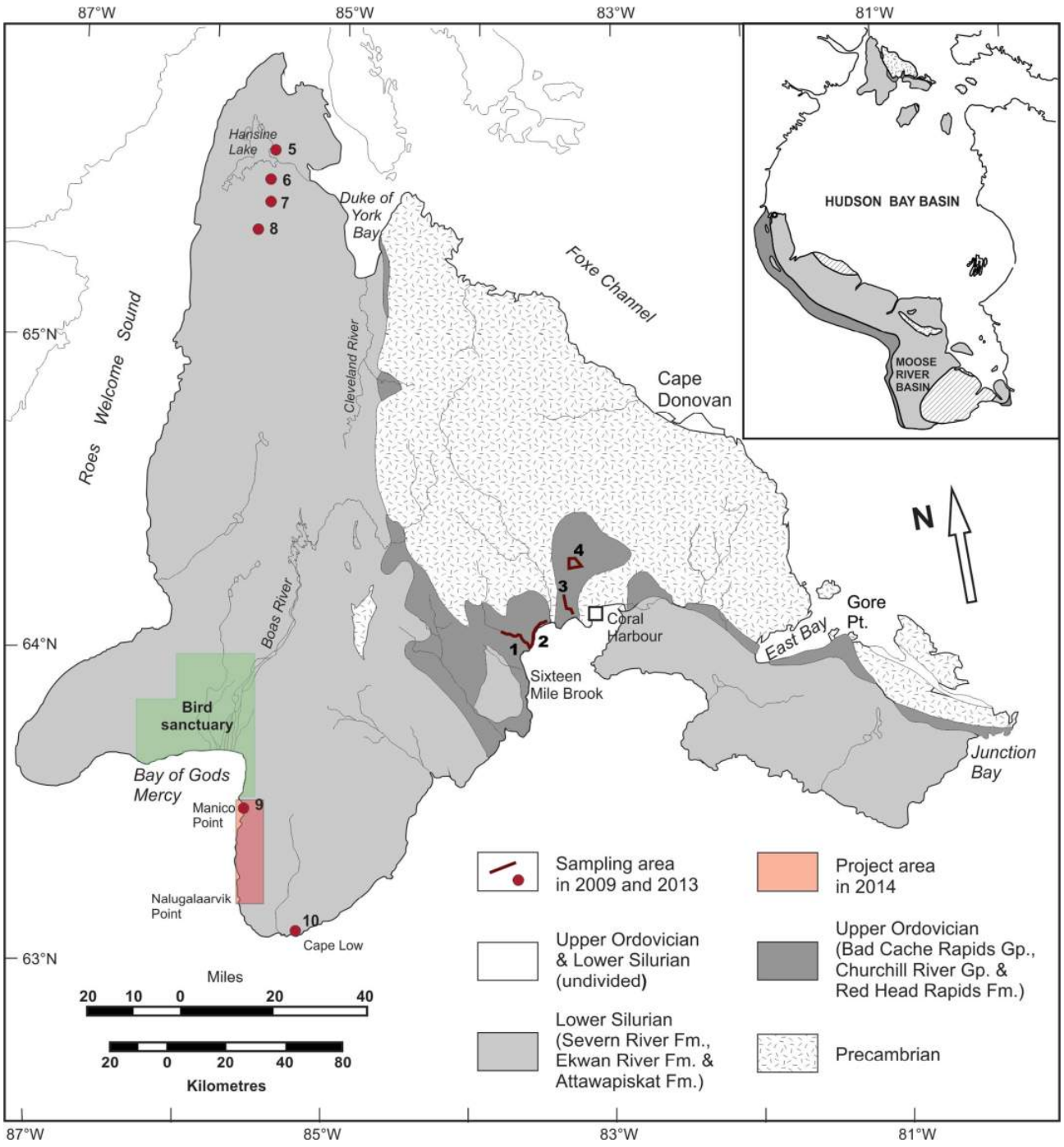

Figure 1: Simplified geology of Southampton Island, eastern Kivalliq Region, Nunavut, modified from Heywood and Sanford (1976) and Zhang (2008), with sample locations. Areas 1–4 and 5–10 were sampled in 2009 (see Zhang et al., 2011) and 2013 (see Zhang et al., 2014) respectively; the area sampled during this study is highlighted by the pink rectangle.

Silurian Ekwan River Formation on western Southampton Island.

A new study was initiated by the CNGO and the Government of Nunavut's Department of Economic Development and Transportation in 2014 between Manico Point and Nalugalaarvik Point on western Southampton Island (Figures 1, 2) to

- better understand the stratigraphic and geographic distribution of relatively pure Silurian limestone intervals of the Ekwan River Formation on Southampton Island,
- provide an assessment of limestone purity based on detailed geochemical data,
- and identify potential quarry locations based on limestone thickness and lateral continuity.

Figure 2: A total of 28 localities (27 represented by red dots in 2014; 1 by a black dot in 2013) along six creeks in the area between Manico Point and Nalugalaarvik Point.

The reasoning behind the expansion of the project area from Manico Point to Nalugalaarvik Point is mainly based on the fact that the Paleozoic strata on Southampton Island are almost horizontally distributed; therefore, the rocks exposed in this area are generally at the same stratigraphic level. This paper summarizes 2014 fieldwork and X-ray fluorescence (XRF) data, and identifies the mineable intervals in the project area.

Lower Paleozoic stratigraphy on Southampton Island

During the Paleozoic, Southampton Island was located on the northern margin of the Hudson Bay Basin somewhere close to the paleo-equator. Thick Paleozoic carbonate rocks were deposited in the Hudson Bay Basin, and this geological record is exposed on Southampton Island today. The lower Paleozoic strata on Southampton Island (Figure 3) include the Upper Ordovician Bad Cache Rapids and Churchill River groups and the Red Head Rapids Formation, and the Lower Silurian Severn River, Ekwan River and Attawapiskat formations (Heywood and Sanford, 1976). They are composed entirely of carbonate rocks with minor shale and distributed throughout the southern and western parts of Southampton Island (Figure 3). Across broad areas, these carbonate rocks are almost horizontally distributed, undeformed and unmetamorphosed; therefore, they are exposed as subcropping rubble, although layered outcrops are commonly found along rivers and creeks. For a detailed introduction to lower Paleozoic stratigraphy on Southampton Island, see Heywood and Sanford (1976), Zhang and Barnes (2007) and Zhang (2011). This paper will describe the Lower Silurian Ekwan River Formation that is the focus of the current study.

The Ekwan River Formation conformably overlies the Severn River Formation, and it consists of well-bedded, fine-grained and fossiliferous limestone. Fossil corals,

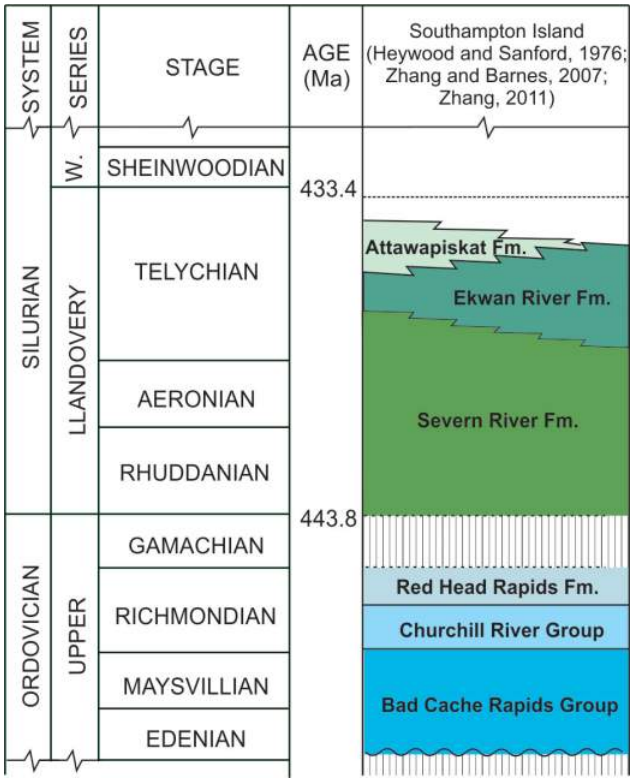

Figure 3: Paleozoic stratigraphy on Southampton Island. Ages are from Cooper and Sadler (2012) and Melchin et al. (2012).

stromatoporoids and brachiopods are common. In the lower part of the formation, light grey or white-coloured chert or dolomite nodules occur locally; stromatolitic dolostone is rare. The upper part of the formation passes laterally into the Attawapiskat Formation, a reef-bearing carbonate unit with algal and stromatoporoid bioherms, which can be seen in the Cape Low area (Zhang et al., 2014). The Ekwan River Formation was divided into three units by Sanford (Heywood and Sanford, 1976), mainly based on the outcrops on Coats and Mansel islands, but the three units are not distinguishable in the study area on Southampton Island. The Ekwan River Formation is not exposed in a complete section in the Hudson Bay area; according to Sanford (Heywood and Sanford, 1976), the formation probably has a composite thickness of approximately 91 m. Based on the horizontal distribution pattern of the Paleozoic strata on Southampton Island, the elevation data and detailed sampling in the area between Manico Point and Nalugalaarvik Point during the current study, this formation has a total thickness of more than 100 m. On Southampton Island, the formation is confined to the western part of the island, rising to form the bedrock surface from Cape Low in the southwestern part of the island and extending northward along the east side of Roes Welcome Sound to the vicinity of Hansine Lake (Figure 1). The outcrops of the formation are scattered along the creeks flowing westward into Roes Welcome Sound. The creeks tend to be more meandering and shallower as one goes from north to south in the project area, so more outcrops of the Ekwan River Formation were found in the northern part than in the southern part of the project area.

Samples and sampling locations

According to Zhang et al. (2014), analyses from samples collected from the Ekwan River Formation in a creek south of Manico Point (creek 2 in Figure 2) indicated the potential for high-calcium limestone with CaO content above 54.3% in 10 out of 12 samples (Zhang et al., 2014). To expand the potential area, the field study targeted an area of approximately 320 km^2 between Manico Point and Nalugalaarvik Point (Figure 2) in summer 2014. Because the Paleozoic rocks on Southampton Island are almost horizontally distributed, the selection of the potential area is based on the following assumptions:

- the rocks dispersed in the target area are at the same stratigraphic level and they belong to the same stratigraphic unit, the Ekwan River Formation;
- the same elevation represents the same stratigraphic level and can be used to estimate the thickness; and
- if the facies does not change significantly laterally, the rocks distributed at the same elevation should contain a similar percentage of CaO.

More than 10 dry creeks run nearly east-west in the area between Manico Point and Nalugalaarvik Point, but outcrops of the Ekwan River Formation were only found in six creeks (Figure 2). Along the six creeks, a total of 106 samples weighing 3 kg were collected from 28 localities. These six creeks are numbered 1–6 from north to south; creek 2 was sampled in 2013 (Zhang et al., 2014).

Results of whole-rock major- and trace-element analysis by XRF

A total of 106 samples were sent to Acme Analytical Laboratories Ltd. (Vancouver, British Columbia) for whole-rock major- and trace-element geochemical analysis. Each sample weighed approximately 3 kg. The entire sample was crushed to 80% passing 10 mesh, and then a 1000 g portion was pulverized to 85% passing 200 mesh. The samples were analyzed by XRF (Acme method 4X01), with total S and C determined by LECO carbon-sulphur analyzer. The results for major oxides are summarized in Table 2 and complete geochemical data are presented in Zhang (2015[2], sheet 1). Application of the British Geological Survey scheme for the classification of limestone by purity (percentage of CaO; Table 1; Harrison et al., 1998) was used in this study to evaluate the limestone sampled in the target area.

Creek 1

Creek 1 is immediately south of Manico Point, where two outcrops (localities 9 and 10) were found. A total of seven samples were collected from these two outcrops; all samples but one contain CaO >54.3% in rocks at an elevation between 50 and 70 m. On average, three samples at locality 9 and four samples at locality 10 contain 54.8 and 54.5% CaO, respectively (Figure 4).

Creek 2

Creek 2 was sampled in 2013 (Zhang et al., 2014) and again in 2014. During the 2013 field season, only two outcrops were sampled along this creek; one is close to the mouth of the creek (green dots in Figure 5) and the other is in the upper reaches of the creek (locality 4 in Figure 5). A total of 35 samples collected from this creek in 2014, plus the eight samples collected from an outcrop near the mouth of the creek in 2013, allow an identification of two intervals of high-purity limestone; one is approximately 10 m of strata, close to the coast at an elevation of 10 m and below, and the other is approximately 35 m of strata distributed at elevations between 65 and 100 m. On average, a total of eight samples from the former locality contain 55% CaO. The latter includes three localities (locality 4, 5 and 6), where four, three and five samples were collected; on average, they contain 55.4, 55.1 and 54.9% CaO, respectively.

[2]*CNGO Geoscience Data Series GDS2015-012, containing the data or other information sources used to compile this report, is available online to download free of charge at http://cngo.ca/summary-of-activities/2015/.*

Table 2: Results for major oxides in carbonate samples collected from 28 localities along six creeks in the area between Manico Point and Nalugalaarvik Point, western Southampton Island.

Creek	Locality	Sample	SiO_2 (%)	CaO (%)	MgO (%)
1	9	SZ14-09-01F	1.14	54.7	0.4
		SZ14-09-02F	1.26	54.68	0.37
		SZ14-09-03F	0.61	54.95	0.37
	10	SZ14-10-01F	0.07	55.47	0.45
		SZ14-10-02F	0.07	55.27	0.67
		SZ14-10-03F	0.13	52.48	2.91
		SZ14-10-04F	0.26	54.89	0.55
2	24 (2013)	SZ13-09-05	0.4	55.54	0.39
		SZ13-09-06	0.07	55.99	0.38
		SZ13-09-07	0.18	55.69	0.4
		SZ13-09-08	0.84	54.76	1.16
		SZ13-09-09	3.8	53.69	0.52
		SZ13-09-10	1.18	55.03	0.8
		SZ13-09-11	3.44	53.89	0.42
		SZ13-09-12	0.93	55.21	0.74
	8	SZ14-08-01F	2.05	53.99	0.53
		SZ14-08-02F	2.5	53.58	0.51
		SZ14-08-03F	1.31	54.55	0.5
		SZ14-08-04F	1.35	54.23	0.51
		SZ14-08-05F	1.98	54.17	0.49
		SZ14-08-06F	1.02	54.86	0.39
		SZ14-08-07F	1.75	54.41	0.39
		SZ14-08-08F	1.71	53.41	1.57
		SZ14-08-09F	1.04	54.93	0.37
	7	SZ14-07-01Fa	10	49.67	0.45
		SZ14-07-01Fb	0.19	55.34	0.5
		SZ14-07-02F	0.18	55.33	0.36
	6	SZ14-06-01F	0.28	54.66	0.8
		SZ14-06-02F	0.24	55.03	0.41
		SZ14-06-03F	0.36	55.11	0.44
		SZ14-06-04F	0.29	54.7	0.71
		SZ14-06-05F	0.35	54.79	0.65
	5	SZ14-05-01F	0.25	55	0.5
		SZ14-05-02F	0.2	55.04	0.51
		SZ14-05-03F	0.23	55.22	0.49
	4	SZ14-04-01F	0.12	55.25	0.43
		SZ14-04-02F	0.04	55.72	0.38
		SZ14-04-03F	0.05	55.49	0.38
		SZ14-04-04F	0.04	55.4	0.43
		SZ14-04-05F	0.08	55.3	0.47
		SZ14-04-06F	0.15	55.26	0.53
	3	SZ14-03-01F	0.32	53.85	1.82
		SZ14-03-02F	0.17	53.56	1.9
		SZ14-03-03F	0.36	53	1.94
		SZ14-03-04F	0.09	55.01	0.49
		SZ14-03-05F	0.11	55.47	0.42
	2	SZ14-02-01F	0.04	53.92	1.4
		SZ14-02-02F	0.02	55.51	0.38
	1	SZ14-01-01F	0.12	41.07	12.77
		SZ14-01-02F	0.13	55.02	0.64
N/A	25	SZ14-25-01F	0.27	55.06	0.45
		SZ14-25-02F	0.4	54.95	0.48
3	18	SZ14-18-01aF	1.48	54.29	0.49
		SZ14-18-01bF	0.32	56.01	0.51
		SZ14-18-01F	0.43	54.8	0.54
		SZ14-18-02F	0.17	51.07	4.09
		SZ14-18-03F	0.52	55.03	0.44
		SZ14-18-04F	0.42	54.93	0.49
	18	SZ14-18-05F	0.11	51.76	3.36
		SZ14-18-06F	0.42	55.09	0.45
	19	SZ14-19-01F	0.44	47.32	7.28
		SZ14-19-02F	0.27	54.22	1.14
	20	SZ14-20-01F	0.14	31.53	21.08
3	21	SZ14-21-01F	0.25	54.8	0.54
		SZ14-21-02F	0.27	55.09	0.57
		SZ14-21-03F	0.52	54.92	0.54
		SZ14-21-04F	0.29	54.87	0.49
		SZ14-21-05F	0.18	55.26	0.51
		SZ14-21-06F	0.24	55.53	0.45
		SZ14-21-07F	0.32	54.98	0.48
	22	SZ14-22-01F	0.05	55.86	0.43
		SZ14-22-02F	0.02	55.61	0.32
4	23	SZ14-23-01F	0.73	52.62	2.27
		SZ14-23-02F	0.25	55.01	0.4
		SZ14-23-03F	0.41	54.81	0.68
		SZ14-23-04F	0.23	55.05	0.49
		SZ14-23-05F	5.45	50.76	0.85
		SZ14-23-06F	0.44	54.88	0.49
		SZ14-23-07F	0.26	55.12	0.45
		SZ14-23-08F	0.4	55.15	0.46
	24	SZ14-24-01F	0.21	55.15	0.39
		SZ14-24-02F	0.18	55.87	0.4
5	14	SZ14-14-01F	5.88	46.75	5.71
		SZ14-14-02F	2.01	52.81	1.48
		SZ14-14-03F	2.37	47.22	5.93
		SZ14-14-04F	1.36	48.22	5.97
		SZ14-14-05F	0.2	55.46	0.38
	13	SZ14-13-01aF	0.85	54.51	0.56
		SZ14-13-01bF	0.38	55	0.55
		SZ14-13-01F	0.61	54.74	0.55
		SZ14-13-02F	0.59	54.73	0.54
		SZ14-13-03F	0.95	54.56	0.53
		SZ14-13-04F	1.04	52.52	2.75
		SZ14-13-05F	1.06	51.14	3.72
	15	SZ14-15-01F	0.25	55.54	0.37
		SZ14-15-02F	0.21	54.96	0.42
		SZ14-15-03F	0.19	54.92	0.45
		SZ14-15-04F	0.16	55.21	0.45
	17	SZ14-17-01F	0.24	54.95	0.5
		SZ14-17-02F	0.08	55.17	0.44
		SZ14-17-03F	0.14	55.23	0.7
	16	SZ14-16-01F	1.37	53.77	0.89
		SZ14-16-02F	2.12	52.56	1.75
		SZ14-16-03F	1.3	54	1.1
		SZ14-16-04F	0.86	52.99	2.69
		SZ14-16-05F	0.63	52.64	2.27
6	11	SZ14-11-01F	0.43	48.24	6.39
		SZ14-11-02F	0.34	47.65	7.04
		SZ14-11-03F	0.49	42.2	12.09
		SZ14-11-04F	0.57	42.69	11.4
	12	SZ14-12-01F	27.06	40.15	0.36
		SZ14-12-02F	19.12	44.4	0.41
		SZ14-12-03F	0.15	55.19	0.36
		SZ14-12-04F	0.14	55.24	0.38

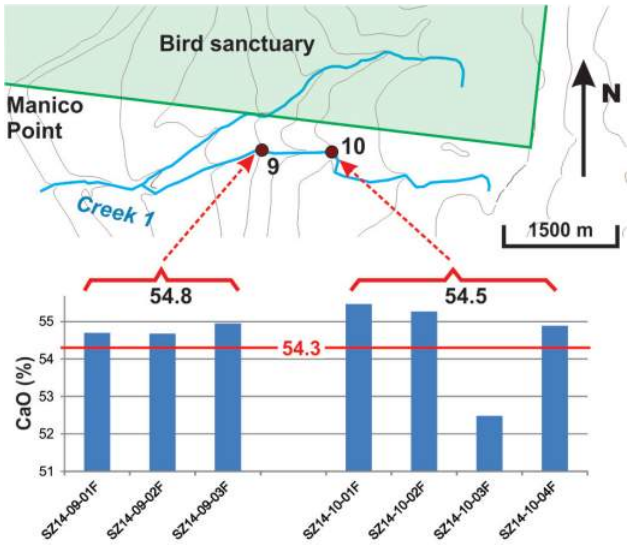

Figure 4. Percentage of CaO in samples collected from localities 9 and 10 along creek 1.

Creek 3

Creek 3 is located approximately 3 km south of creek 2. A total of 22 samples were collected from seven localities (localities 18, 18a, 18b and 19–22) along the creek and two samples were collected from locality 25 on the coast near the mouth of creek 3 (Figure 6). The distribution of high-purity limestone in creek 3 is similar to that in creek 2: approximately 10 m of high-purity limestone and 20 m of very high purity limestone are distributed at elevations between 10 and 20 m (localities 18a and 25) and between 80 and 100 m (localities 21 and 22), respectively. On average, the samples from the two localities at the lower elevations (localities 18a and 25) contain 55 and 55.2% CaO, and those from the two localities at the higher elevations (localities 21 and 22) contain 55.1 and 55.6% CaO (Figure 6).

Creek 4

Creek 4 is approximately 5 km south of Creek 3. Only two outcrops were found along this creek (Figure 7). Two samples were collected from locality 24 at an elevation of approximately 40 m. They contain 55.5% CaO and can be classified as very high purity limestone. A total of eight samples were collected from locality 23 at an elevation of approximately 30 m, which yielded an average of 54.2% CaO, only 0.1% lower than those classified as high purity. Six out of the eight samples, however, contain more than 54.3% CaO (Figure 7); sample SZ14-23-05F contains 50.76% (CaO), which makes the main contribution to the 0.1% difference.

Creek 5

Creek 5 is approximately 5 km south of creek 4. Five outcrops (localities 13–17) were found below an elevation of 80 m along the creek (Figure 7). High- and very high purity limestone was discovered at two localities. Approximately 10 m of strata are exposed at locality 15 at an elevation between 20 and 30 m, where four samples yielded an average of 55.2% CaO. Approximately 5 m of strata are exposed at

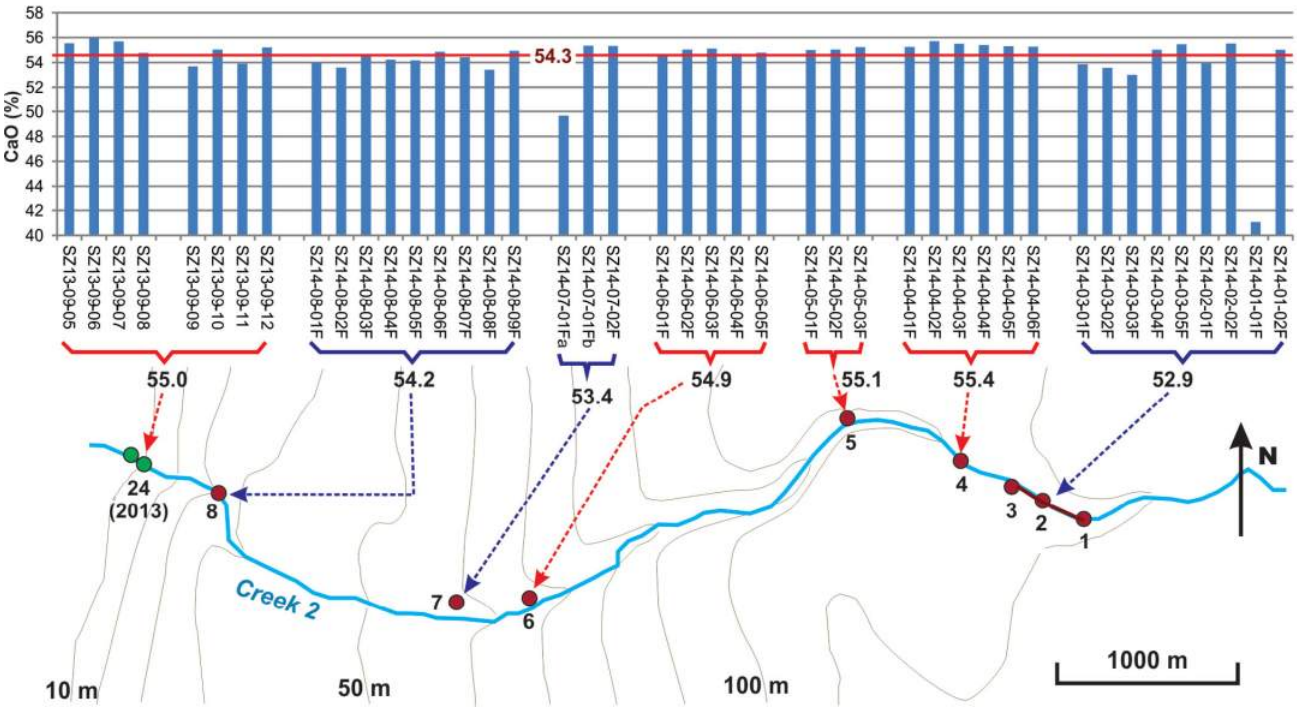

Figure 5. Percentage of CaO in samples collected from localities 1–8 and 24 (2013) along creek 2.

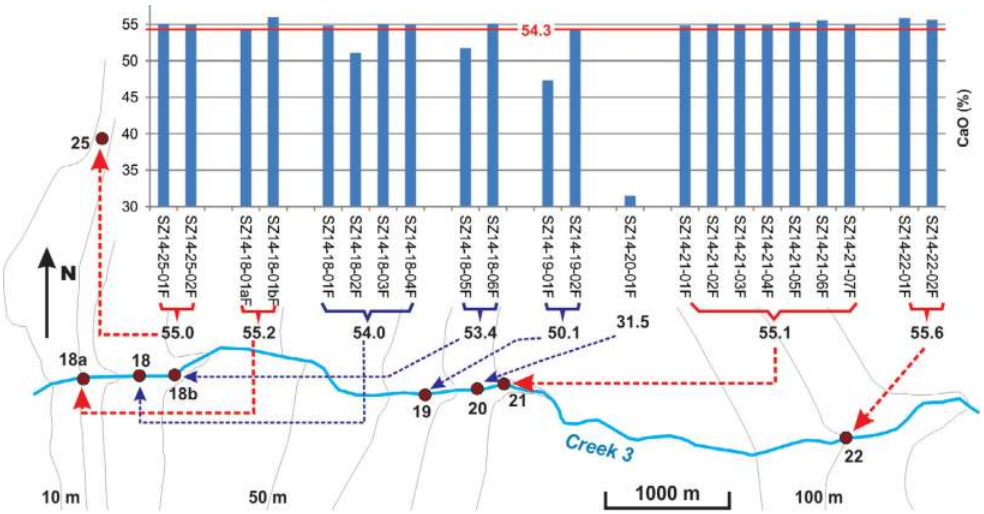

Figure 6. Percentage of CaO in samples collected from localities 18, 18a, 18b, 19–22 and 25 along creek 3.

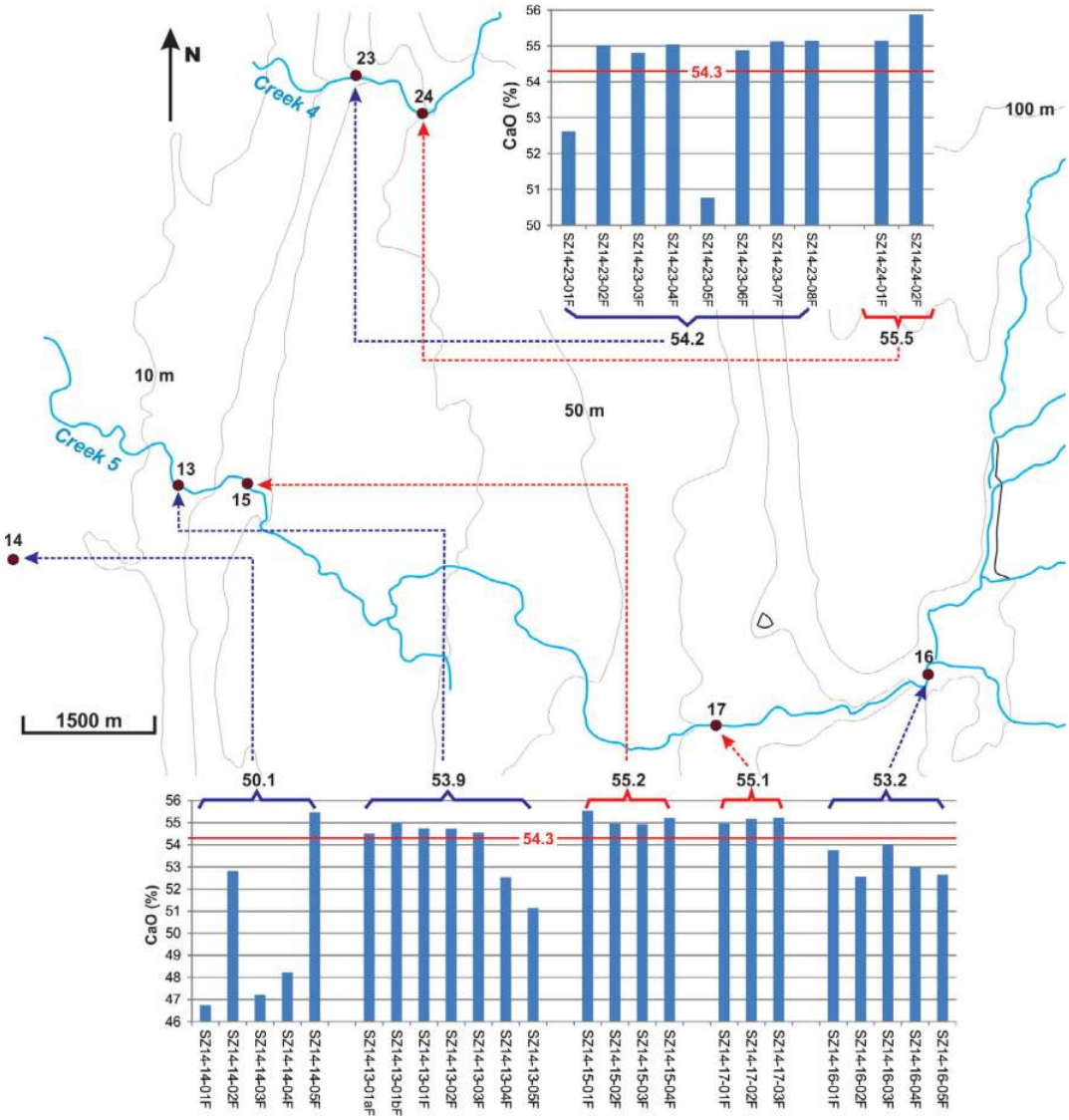

Figure 7. Percentage of CaO in samples collected from localities 23 and 24 along creek 4 and localities 13–17 along creek 5.

locality 17 at an elevation between 60 and 70 m, where three samples contain 55.1% CaO on average.

Creek 6

Creek 6 is located in the southern end of the project area and immediately north of Nalugalaarvik Point. Only two outcrops (localities 11 and 12) were found near the mouth of creek 6 at an elevation below 30 m (Figure 8). No high- or very high purity limestone was discovered from the two localities along creek 6. Four samples were collected from locality 11 and another four from locality 12; on average, they yielded 45.2 (classified as impure) and 48.8% CaO (classified as low purity), respectively.

Impure or low-purity intervals

Figure 9 shows the percentage of CaO, MgO and SiO_2 in all the samples collected from localities 1–25 and locality 2013 (which is locality 24 in Zhang et al. [2014]) along six creeks in the area between Manico Point and Nalugalaarvik Point. It is obvious that the samples yielding <54.3% CaO are related to either high contents of MgO, SiO_2, or both. For example, all eight samples from locality 8 along creek 2 contain an average of 1.84% SiO_2, which decreases the average CaO to 54.2%, slightly below the standard of high purity. The highest SiO_2 contents are in two samples (SZ14-12-01F and SZ14-12-02F) at locality 12 along creek 6, 27.06 and 19.12%, respectively, resulting in 40.15 and 44.4% CaO in these two samples. All four samples from locality 11 along creek 6 yielded an average of 9.23% MgO and 45.2% CaO. In general, high contents of SiO_2 and/or MgO are the main contributors to the impure or low-purity nature of the limestone in the project area.

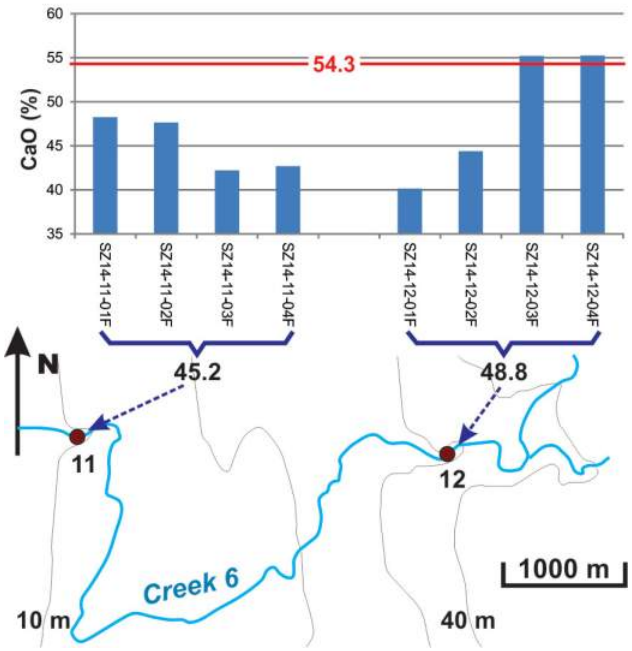

Figure 8. Percentage of CaO in samples collected from localities 11 and 12 along creek 6.

The low-purity or impure intervals are not only recognized by XRF analysis, but also can be easily identified in the field. Normally, the low-purity or impure intervals contain many white-coloured chert or dolomite nodules, or are composed of interbedded dolostone and limestone, or dolomitic limestone, or dolostone (Figure 10a–d). If this area was quarried for pure limestone, the impure or low-purity intervals could be easily avoided.

Map of limestone purity distribution

Based on the compilation and analysis of the results of whole-rock major- and trace-element analysis by XRF, field observations and the distribution pattern of the Paleozoic strata on Southampton Island with reference to elevation, a map of limestone purity distribution was made for the area between Manico Point and Nalugalaarvik Point (Figure 11). Of the 114 samples, 76 (67%), contain >54.3% CaO. These samples represent intervals of high- or very high purity limestone.

Generally, the limestone yielding >54.3% CaO is mainly distributed at elevations between 30 and 100 m (Figure 11); this is based on data from

- localities 9 and 10 at elevations between 50 and 70 m along creek 1,
- localities 4 to 7 at elevations between 65 and 100 m along creek 2,
- localities 21 and 22 at elevations between 75 and 100 m along creek 3,
- locality 24 (2013) with an elevation of approximately 40 m along creek 2, and
- localities 15 and 17 at elevations between 25 and 65 m along creek 5.

Because of lateral facies change within elevations between 30 and 100 m, samples containing <54.3% CaO were found at localities 19 and 20 along creek 3 and locality 16 along creek 5; therefore, a narrow interval of low-purity or impure limestone was recognized at elevations between 70 and 80 m in the middle and southern part of the project area (Figure 11).

A narrow interval of limestone with >54.3% CaO is distributed near the coast in the northern part of the project area, which is based on the data from locality 9 from the 2013 field season (Zhang et al., 2014) near the mouth of creek 2, locality 25 close to the coast and locality 18a close to the mouth of creek 3 (Figure 11).

Limestone with <54.3% CaO is mainly distributed along the coast approximately below an elevation of 30 m, which is supported by the data collected from locality 8 along creek 2, localities 18 and 18b along creek 3, locality 23

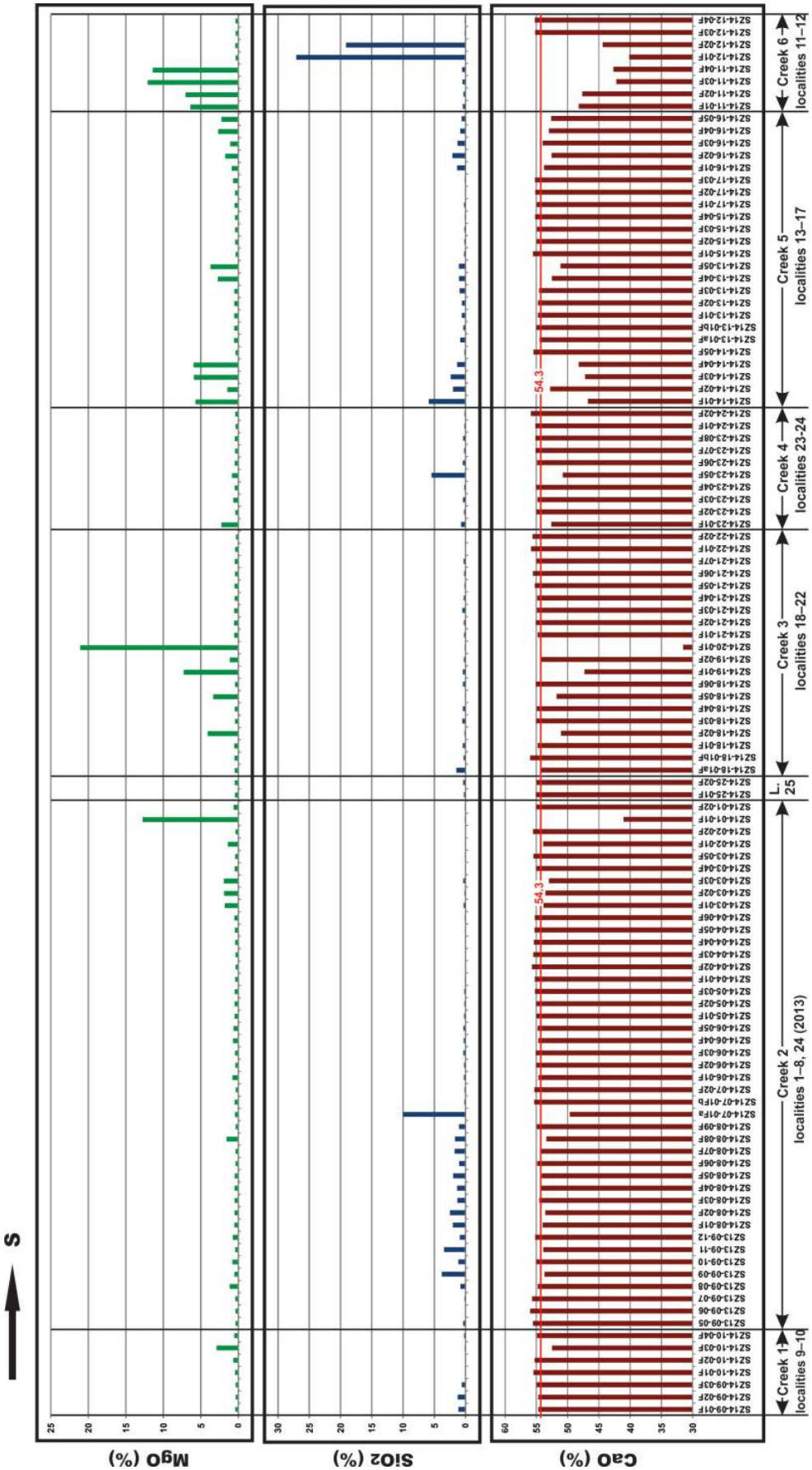

Figure 9. Percentages of CaO, MgO and SiO_2 in all the samples collected from localities 1–25 and 24 (2013) along six creeks in the area between Manico Point and Nalugalaarvik Point.

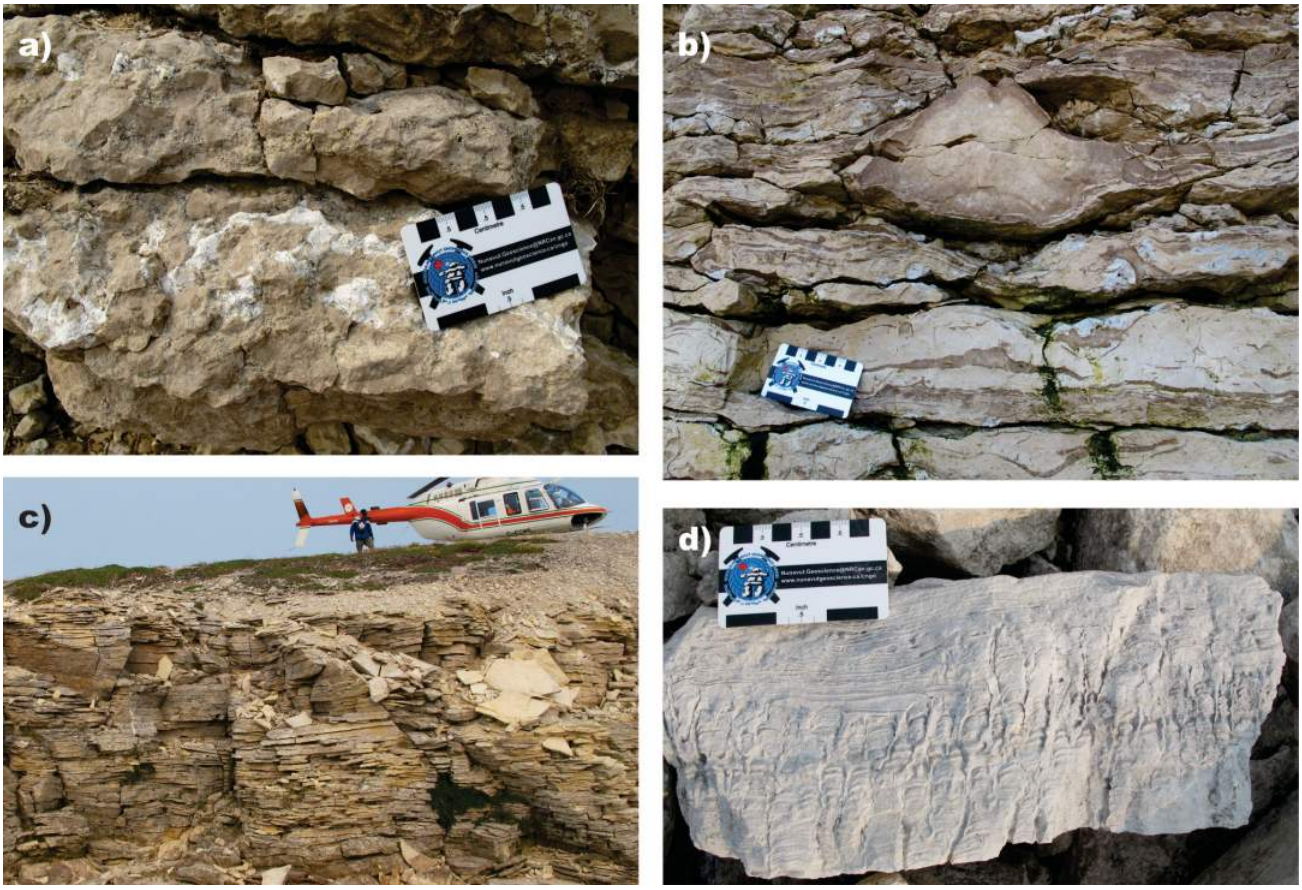

Figure 10. Examples of impure or low-purity samples/intervals in the study area: **a)** chert nodules in sample SZ14-12-01F at locality 12, creek 6; **b)** interbedded limestone and dolostone in sample SZ14-14-04F at locality 14, creek 5; **c)** dolomitic limestone in sample SZ14-11-03F at locality 11, creek 6; **d)** dolostone of sample SZ14-20-01F at locality 20, creek 3.

along creek 4, localities 13 and 14 along creek 5 and localities 11 and 12 along creek 6 (Figure 11).

An interval of limestone with <54.3% CaO is also identified at elevations between 100 and 110 m, which is only supported by the data from localities 1 to 3 in the upper reaches of creek 2 (Figure 11). In the rest of the project area, no outcrops were found at or above this elevation.

Economic considerations

The purpose of the project was to identify high-purity limestone within the Silurian Ekwan River Formation, western Southampton Island. A total of 106 samples plus 8 from the 2013 field season were collected from 28 localities along 6 creeks in the area between Manico Point and Nalugalaarvik Point.

Of the 114 analyzed samples, 67% yielded >54.3% CaO, which is suitable for many industrial purposes. Extensive sampling confirms that a locally mineable high-calcium limestone deposit exists between Manico Point and Nalugalaarvik Point, and it could become an extremely valuable resource for Nunavut and the community of Coral Harbour.

Possible future studies at the Canada-Nunavut Geoscience Office (CNGO)

Another potential area with high- or very high purity limestone lies to the northwest of Manico Point; however, it is located within the Harry Gibbons Migratory Bird Sanctuary (Figure 1). In this area, there are many deeply incised rivers and creeks that expose the rocks better than the current study area. If this area could be studied and sampled, continuous sections of the Ekwan River Formation would likely be found, more detailed data would be collected, the resource of mineable high-calcium limestone deposits on Southampton Island would likely be greatly increased and the boundaries of mineable high-calcium limestone intervals could be defined more accurately than the current study has been able to do.

Acknowledgments

Financial support for this work was provided by the Canada-Nunavut Geoscience Office (CNGO), the Canadian

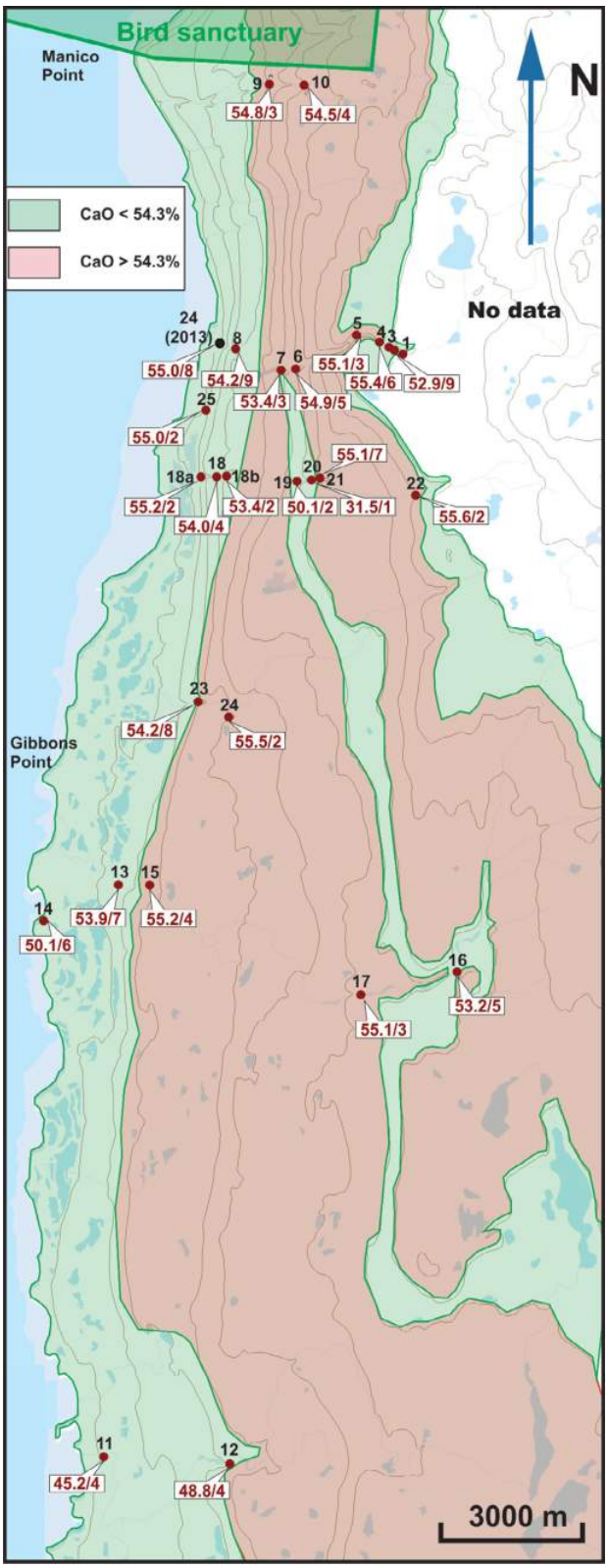

Figure 11. Limestone purity distribution for the area between Manico Point and Nalugalaarvik Point. Red and black dots indicate sample localities (27 represented by red in 2014; 1 by black in 2013), black numbers are locality numbers and the red numbers indicate the average percentage of CaO and the number of samples collected (e.g., 55.5/2 is an average CaO of 55.5% for two samples).

Northern Economic Development Agency's (CanNor) Strategic Investments in Northern Economic Development (SINED) program and the Government of Nunavut (GN). Logistical support was provided by the Polar Continental Shelf Project (PCSP). Special thanks to R. Hinanik and P. Adams for their field assistance and to K. Dewing for acting as a scientific reviewer.

Natural Resources Canada, Earth Science Sector contribution 20150309

References

Cooper, R.A. and Sadler, P.M. 2012: The Ordovician Period; Chapter 20 *in* The Geological Time Scale 2012, F.M. Gradstein, J.G. Ogg, M. Schmitz and G. Ogg (ed.), p. 489–523.

Harrison, D.J., Inglethorpe, S.D.J., Mitchell, C.J., Kemp, S.J., Chaodumrong, P. and Charusribandhu, M. 1998: Procedures for the rapid assessment of limestone resources; British Geological Survey, Technical Report WC/98/1, 120 p.

Heywood, W.W. and Sanford, B.V. 1976: Geology of Southampton, Coats and Mansel Islands, District of Keewatin, Northwest Territories; Geological Survey of Canada, Memoir 382, 35 p.

Melchin, M.J., Sadler, P.M. and Cramer, B.D. 2012: The Silurian Period; Chapter 21 *in* The Geological Time Scale 2012, F.M. Gradstein, J.G. Ogg, M. Schmitz and G. Ogg (ed.), Elsevier B.V., p. 525–558.

Zhang, S. 2008: New insight into Ordovician oil shales in Hudson Bay: their number, stratigraphic position, and petroleum potential; Bulletin of Canadian Petroleum Geology, v. 56, p. 300–324.

Zhang, S. 2011: Late Ordovician conodont biostratigraphy and redefinition of the age of oil shale intervals on Southampton Island; Canadian Journal of Earth Sciences, v. 48, p. 619–643.

Zhang, S. 2015: Field localities and whole rock analysis of limestone samples from the 2014 field season on Southampton Island, Nunavut; Canada-Nunavut Geoscience Office, Geoscience Data Series GDS2015-012, Microsoft® Excel® file.

Zhang, S. and Barnes, C.R. 2007: Late Ordovician–Early Silurian conodont biostratigraphy and thermal maturity, Hudson Bay Basin; Bulletin of Canadian Petroleum Geology, v. 55, p. 179–216.

Zhang, S., Prosh, E.C. and James, D.T. 2011: An assessment of a potential source of industrial limestone on Southampton Island, Nunavut; Geological Survey of Canada, Open File 6827, 30 p.

Zhang, S., Prosh, E. and Mate, D.J. 2014: Resource potential for industrial limestone on Southampton Island, Nunavut: summary of fieldwork and geochemical data; *in* Summary of Activities 2013, Canada-Nunavut Geoscience Office, p. 201–212.

Nunavut Carving Stone Deposit Evaluation Program: 2015 fieldwork at Rankin Inlet, Cumberland Sound and Arctic Bay, Nunavut

M.A. Beauregard[1] and J. Ell[2]

[1]*Minerals and Petroleum Resources, Department of Economic Development and Transportation, Government of Nunavut, Arviat, Nunavut, mbeauregard@gov.nu.ca*

[2]*Winnipeg, Manitoba*

Beauregard, M.A. and Ell, J., 2015: Nunavut Carving Stone Deposit Evaluation Program: 2015 fieldwork at Rankin Inlet, Cumberland Sound and Arctic Bay, Nunavut; *in* Summary of Activities 2015, Canada-Nunavut Geoscience Office, p. 183–192.

Abstract

The Nunavut Carving Stone Deposit Evaluation Program is a collaborative project led by the Government of Nunavut–Department of Economic Development and Transportation and involves the Canada-Nunavut Geoscience Office. This paper summarizes field observations and deposit evaluations of carving stone sites near Rankin Inlet, south of Pangnirtung on the south shore of Cumberland Sound and near Arctic Bay that were carried out in 2015. Highlights include the discovery of two new serpentinite sites near carving stone–impoverished Rankin Inlet and an additional seven sites in four locations near Arctic Bay; these findings more than double the number of skarn marble deposits close to that community. An ultramafic formation of carving stone south of Arctic Bay is a small kimberlite diatreme that was previously unrecognized**.**

This program's focus is the establishment of grade, tonnage and artisan suitability of known traditional carving stone sites and prospective government-mapped soft stone deposits on behalf of Nunavut's arts industry. Including the 2015 results reported herein, 119 carving stone sites have been documented in the vicinity of 23 communities across Nunavut since 2010. As a result of this work, the supply inventory for territorial carving stone resources indicates that 17 of Nunavut's 25 communities have access to local carving stone resources sufficient for their long-term needs.

Résumé

Le Programme d'évaluation des gisements de pierre à sculpter du Nunavut est un projet de nature collaborative dirigé par le ministère du Développement économique et des Transports du gouvernement du Nunavut, et impliquant Le Programme d'évaluation des gisements de pierre à sculpter du Nunavut est un projet de nature collaborative dirigé par le ministère du Développement économique et des Transports du gouvernement du Nunavut, et impliquant le Bureau géoscientifique Canada-Nunavut. Le présent rapport fait état des observations de terrain et des évaluations de gisements de pierre à sculpter réalisées en 2015 à des sites de pierre à sculpter dans la région de Rankin Inlet, au sud de Pangnirtung sur le littoral sud du détroit de Cumberland, et près de la baie Arctic. Parmi les points saillants de l'étude, on remarque la découverte de deux nouveaux gisements de serpentinite dans la région dépourvue de pierre à sculpter de Rankin Inlet et de sept autres gisements à quatre emplacements près de la baie Arctic. Ces découvertes viennent doubler le nombre de gisements de marbre skarnifère situés à proximité de cette collectivité. Une formation ultramafique de pierre à sculpter située au sud de la baie Arctic est en fait un petit diatrème kimberlitique qui n'avait pas été identifié jusqu'à présent.

Le programme met l'accent sur la détermination, en termes de sa valeur artisanale, de la teneur, du grade et de la composition de la pierre des gisements connus de pierre à sculpter traditionnels et de gisements prometteurs de pierre tendre pour lesquels le gouvernement a dressé des cartes à l'intention du secteur de l'économie artistique du Nunavut. Depuis 2010, la présence de 119 sites de pierre à sculpter, comprenant les résultats de 2015 dont fait état le présent rapport, a été relevée à proximité de 23 collectivités dans l'ensemble du Nunavut. Grâce à ces travaux, l'inventaire territorial de l'approvisionnement en pierre à sculpter démontre que 17 des 25 collectivités du Nunavut ont accès à des ressources locales de pierre à sculpter en quantité suffisante pour satisfaire leurs besoins à long terme.

This publication is also available, free of charge, as colour digital files in Adobe Acrobat® PDF format from the Canada-Nunavut Geoscience Office website: http://cngo.ca/summary-of-activities/2015/.

Introduction

The Nunavut Carving Stone Deposit Evaluation Program (NCSDEP) is a multiyear collaborative project that was initiated in 2010. Led by the Government of Nunavut–Department of Economic Development and Transportation (GN-EDT), the program involves collaboration with the Canada-Nunavut Geoscience Office (CNGO) and other agencies, such as Regional Inuit Associations (RIAs), Aboriginal Affairs and Northern Development Canada (AANDC) and Natural Resources Canada (NRCan)–Geological Survey of Canada (GSC; Beauregard and Ell, 2013; Beauregard et al., 2013; Steenkamp et al., 2014; Beauregard and Ell, 2015; Steenkamp et al., 2015). The primary goals of this evaluation program—to assess traditional carving stone sites and to identify new deposits—are based on the rights of Inuit to collect carving stone as set out in Article 19, Part 9 of the Nunavut Land Claims Agreement and carving stone documents prepared by the Government of Nunavut (Government of Canada, 1993; Nunavut Department of Economic Development and Transportation, 2007a, b). The guidance of ongoing fieldwork and reporting of new sites by local carvers from every community in Nunavut is an integral part of the NCSDEP.

In 2015, the NCSDEP evaluated soft stone sites near three localities: Rankin Inlet, a community that has no identifiable or accessible carving stone resources; south of Pangnirtung on the south shore of Cumberland Sound, in conjunction with the Geological Survey of Canada's (GSC) McKeand River bedrock mapping program; and near Arctic Bay, a community noted for its skarn marble carving stone deposits. This paper reports field observations, carving stone characteristics and deposit parameters for 15 sites at 10 locations in the vicinity of 3 communities (Figure 1, Table 1).

Rankin Inlet carving stone resources

Rankin Inlet, a large bay on the west shore of Hudson Bay, is underlain by polydeformed Archean mafic metavolcanic rocks and minor metasedimentary rocks of the Rankin Inlet Group, and minor Paleoproterozoic supracrustal rocks. The Rankin Inlet Group sequence forms an F_1 homocline folded into an aerially spectacular, southeast-plunging F_2 syncline. The greenschist to lower amphibolite metamorphic grade of the Rankin Inlet Group is considered to be Archean. Minor panels of a Paleoproterozoic quartzite-arenite sequence are, for the most part, in tectonic contact with Rankin Inlet Group rocks (Tella, 1994).

Rankin Inlet carvers are badly in need of local carving stone resources. A tiny site in a tidal mud flat on Falstaff Island provides minor amounts of carving stone. All other carving stone is usually imported into the community and sold to carvers (Beauregard and Ell, 2012).

Several large carving stone targets had been identified from prior mining, mineral exploration and government mapping in the Rankin Inlet locale. An occurrence of once-modest proportions is the Siskin Point community quarry, 12 km east of Rankin Inlet, abandoned in the 1970s due to the use of explosives that ruined 500 tonnes of carving stone (Beauregard and Ell, 2012). A second site that falls entirely within municipality boundaries was first reported during the historical operation of a small underground nickel-copper mine, where miners drove drifts across a 60–100 m wide serpentinite sill on two levels to access the ore (Hannah, 1961). This short-lived underground mining operation (1957–1962) employed many Inuit, resulting in the establishment of the Hamlet of Rankin Inlet, which has since become Nunavut's second largest community. The abandoned mine's wasterock pile provided local artists with usable carving stone until the minesite was ultimately reclaimed in 2011. Twenty years after the mine closed, Asamera Minerals Inc. drilled 24 surface exploration holes into soft, competent serpentinite beneath shallow overburden that ranges in thickness from 1 to 16 m along a 1200 m section of the sill (Hassell, 1989). The nickel–copper–platinum group element ore at the base of the east-northeast-trending ultramafic sill has been dated by Re-Os geochronology at 2762 ±90 Ma (Tella, 1994). A potentially massive carving stone resource in the form of a large serpentinite sill occurs beneath the community of Rankin Inlet, but this resource is not available for carving due to intensive municipal development (Beauregard and Ell, 2012).

Two diamond-drill holes from prior exploration work tested the ends of a 1–1.5 km long, northwest-trending electromagnetic conductor in shallow overburden near Melvin Bay, west of Rankin Inlet. Both drillholes plunge 45° to the southwest. Serpentinized ultramafic rock, or 'soapstone', was intersected in both holes, with a 23 m intersection contained in the southeasterly hole (1972-10) and 40 m intersected in the northwesterly hole (1972-9; Harquil, 1973). The collar of the southeasterly hole was rediscovered in 2015, approximately 3 km west of Rankin Inlet (Figures 1, 2a; Table 1). A northwest-trending, 1 m high fault scarp with minor serpentinite slickensides occurs where the south contact of the soft stone formation found in drillhole 1972-10 is projected to surface. Recommendations were provided to the Hamlet of Rankin Inlet for further work at this site with shallow overburden.

Two small sites of medium-hardness (2.5 on Mohs Hardness Scale) carving stone were located in 2015 in a north-trending ultramafic formation near Silent Cove, approximately 6 km west of Rankin Inlet (Figure 1; Table 1; Laporte, 1975). The northern portion of the formation can be accessed by all-terrain-vehicle (ATV) from an ATV trail 0.5 km to the east. The variably altered ultramafic formation, 1 km long and up to 100 m wide, is conformable with surrounding mafic volcanic rocks. The Silent Cove North

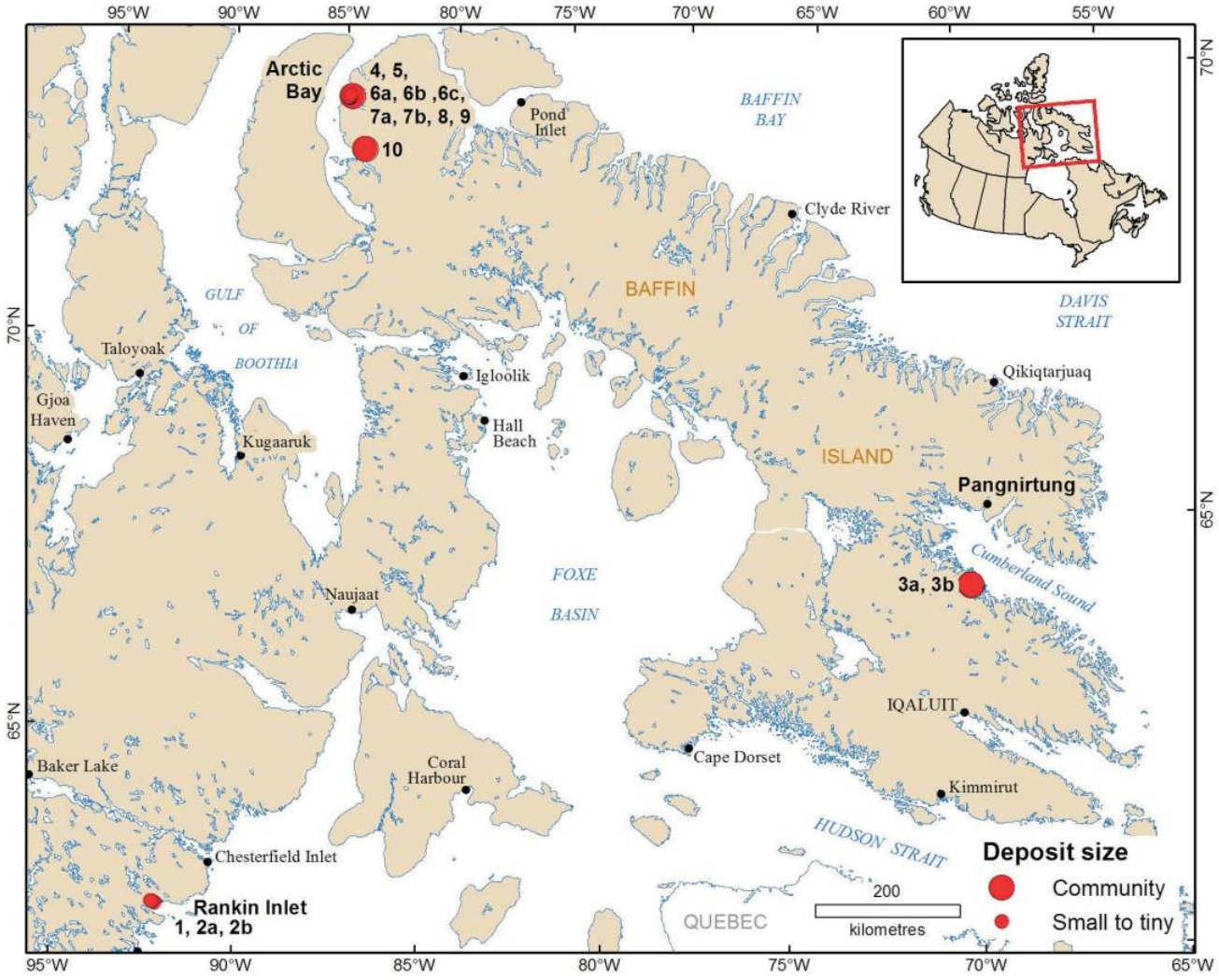

Figure 1: Carving stone sites, quarries and deposits visited or reviewed by the Nunavut Carving Stone Deposit Evaluation Program in 2015 near Rankin Inlet, Pangnirtung and Arctic Bay, Nunavut; numbers correspond to site numbers listed in Table 1.

site is fine-grained, light green serpentinite exposed in a 20 m long by 3 m wide outcrop that is the only exposure in an overburden-covered lineament on the east side of the ultramafic formation (Figure 2b). The Silent Cove South site consists of fine-grained, dark green serpentinite contained in an 8 m wide outcrop on the west side of the ultramafic formation. Stone from either site requires further testing to determine its suitability for artisans. Each site may be of sufficient size to provide up to 100 tonnes of material if the stone is extracted using the plugger-and-feather method.

Cumberland Sound carving stone resources

The south shore of Cumberland Sound on southeastern Baffin Island is underlain by autochthonous metasedimentary rocks of the Lake Harbour Group atop Archean orthogneiss. These rocks have been deformed, metamorphosed and intruded by leucogranite sills and dykes. The Ptarmigan Fiord area, in particular, presents a series of imbricated midcrustal thrusts (Dyck and St-Onge, 2014). Mafic-ultramafic sills and dykes have been reported within the Lake Harbour Group rocks in this area. Additional reported work includes a dataset of geochemical analyses from selected serpentinite quarries and ultramafic sites (Steenkamp, 2015; Steenkamp et al., 2015).

Pangnirtung residents make use of extensive Inuit-Owned Lands (IOL) throughout Cumberland Sound. The bulk of artisan stone used by community carvers is recovered from the Opingivik quarry, 112 km southwest of Pangnirtung (Beauregard and Ell, 2013), although a number of carving stone sites are known in the Cumberland Sound area. Weather conditions limited the 2015 site evaluations to two targets, one that was brought forward by the concurrent GSC mapping program and one from community consultation work. The Opingivik quarry was also revisited in 2015.

The site investigated by the GSC's 2015 McKeand River bedrock mapping program is located west of Chidliak Bay

Table 1: Carving stone sites, quarries and deposits visited or reviewed by the Nunavut Carving Stone Deposit Evaluation Program in 2015 near Rankin Inlet, Pangnirtung and Arctic Bay, Nunavut.

Site no.	Community	Region	Site name	Latitude	Longitude	Size	Quality	Hardness (Mohs scale)
1	Rankin Inlet	Kivalliq	Melvin Bay drillhole 1972-10	62° 48' 37.6"	92° 09' 40.7"	Unknown	Unknown	Unknown
2a	Rankin Inlet	Kivalliq	Silent Cove North	62° 49' 50.7"	92° 15' 34.4"	Small	Fair	Med, 2.5
2b	Rankin Inlet	Kivalliq	Silent Cove South	62° 49' 44.6"	92° 15' 58.9"	Small	Fair	Med, 2.5
3a	Pangnirtung	Qikiqtani	Opingivik community quarry	65° 15' 01.6"	67° 04' 25.2"	Community	Excellent	Soft, 2.0
3b	Pangnirtung	Qikiqtani	Opingivik serpentinite outcrop	65° 15' 59.0"	67 04' 26.0"	Community	Good	Med, 2.5
4	Arctic Bay	Qikiqtani	White Marble quarry	73° 02' 46.4"	85° 06' 38.1"	Community	Excellent	Med, 2.5
5	Arctic Bay	Qikiqtani	Old Main (Banded Marble) quarry	73° 02' 23.7"	85° 13' 56.5"	Small	Excellent	Med, 2.5
6a	Arctic Bay	Qikiqtani	Three-Stone locality, Banded Marble site	73° 01' 47.0"	85° 14' 44.0"	Tiny	Excellent	Hard, 3.0
6b	Arctic Bay	Qikiqtani	Three-Stone locality, Serpentinite site	73° 01' 45.8"	85° 14' 41.4"	Small	Good	Med, 2.5
6c	Arctic Bay	Qikiqtani	Three-Stone locality, Marble Breccia site	73° 01' 45.7"	85° 14' 38.5"	Small	Good	Med, 2.5
7a	Arctic Bay	Qikiqtani	Two-Stone locality, White Marble site	73° 01' 35.2"	85° 13' 41.5"	Small	Good	Hard, 3.0
7b	Arctic Bay	Qikiqtani	Two-Stone locality, Banded Marble site	73° 01' 38.6"	85° 13' 52.6"	Tiny	Good	Hard, 3.0
8	Arctic Bay	Qikiqtani	Rubble Zone Marble	73° 02' 16.4"	85° 15' 51.3"	Small	Good	Hard, 3.0
9	Arctic Bay	Qikiqtani	Victor Bay Marble	73° 03' 26.9"	85° 10' 29.9"	Small	Good	Hard, 3.0
10	Arctic Bay	Qikiqtani	Fabricius Fiord Kimberlite	72° 22' 32.0"	84° 43' 22.6"	Community	Good	Soft, 2.0

and consists of a large, well-foliated to coarse-grained, gabbro-pyroxenite-dunite-peridotite ultramafic intrusive. The northwestern corner of the folded ultramafic formation contains a small area with tiny, white-weathering lenses of soft, fine-grained black serpentinite. No lenses were competent enough to be deemed 'carving stone'. GSC site L121 (located at latitude 64°47'32.9"N, longitude 66°43'43.0"W) was sampled for geochemical and thin-section petrographic analysis (Liikane, 2015).

Ujjuttuuq, the site brought forward from community consultation work, was marked at approximately latitude 65°35'25"N, longitude 68°00'48"W on the west shore of Irvine Inlet. The site was traversed in 2015 with no ultramafic formation or carving stone found.

A talus-covered hillside at the Opingivik site hosts a north-trending, lineament-bounded artisan serpentinite formation exposed in quarry, outcrop and subcrop (Table 1, Figure 3a). The quarry was evaluated in 2011 and the immediate area mapped in 2014 (Beauregard and Ell, 2012; Steenkamp et al., 2015). The ultramafic formation lies within orthopyroxene±biotite monzogranite. The quarry has been active for more than 15 years and it is estimated

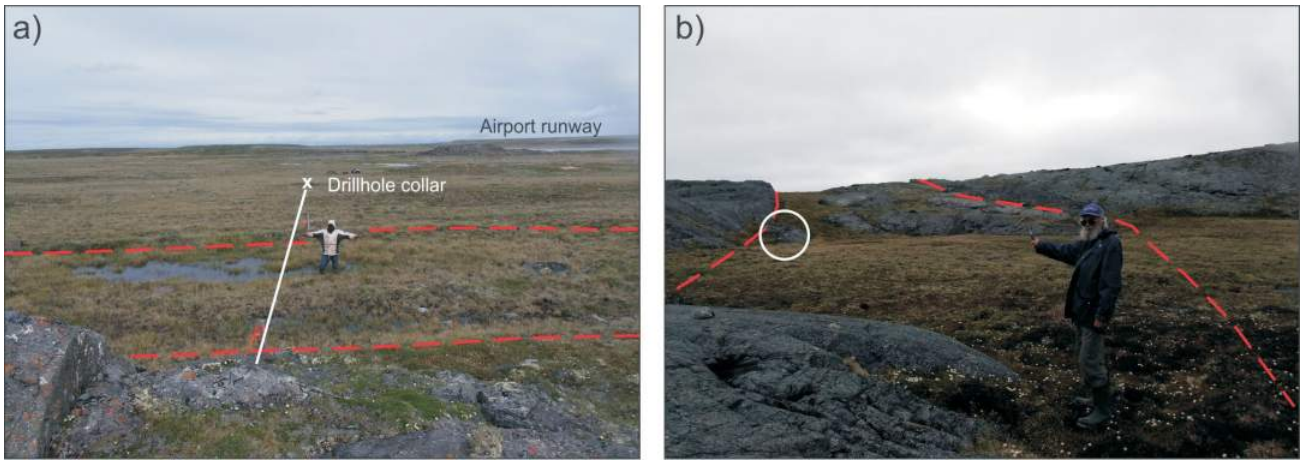

Figure 2: Carving stone sites west of Rankin Inlet, southwestern Nunavut: **a)** Melvin Bay drillhole target, showing fault scarp in left foreground, extent of soft stone formation between dashed red lines, drillhole projected to surface in shallow overburden and drillhole collar (X); northeast-facing view; **b)** Silent Cove North site, showing extent of 75 m wide, variably serpentinized ultramafic formation between dashed red lines and elongated outcrop of light green carving stone within white circle; south-facing view.

that 200 tonnes of material have been excavated by carvers in that time. Much of the carving stone is unusable—wastage is on the order of 60%—due to freeze-and-thaw effects of surface-water drainage. Stone blocks up to 0.6 m in size have been recovered. During the 2015 visit, the quarry was filled with slumped overburden to a depth of 2–3 m; this material is lying atop the community's excellent-quality, medium-soft carving stone (Figure 3b). Several outcrops on the west-central side of the talus slope were confirmed to be competent, good-quality, medium-hard carving stone that can be extracted by the plugger-and-feather method for provision of very large blocks. The largest outcrop is an 8 m high exposure (Figure 3c). Serpentinite subcrop is found in a tectonized 'crush' zone exposed by water erosion; this zone occurs some 125 m downhill from the community quarry. The material in this zone resembles the uppermost layer of rock that was uncovered during the opening of the quarry (J. Ishulutak, pers. comm., 2015). This poorly consolidated subcrop (at latitude 65°14'58.0"N, longitude 67°04'25.0"W) was dug to a depth of 1 m without any observable improvement in competency.

Arctic Bay carving stone resources

The area of interest close to Arctic Bay on northwestern Baffin Island is underlain by Mesoproterozoic metasedimentary rocks of the ca. 1.2 Ga Borden Basin within the tectonically complex Milne Inlet graben (Turner, 2009, 2011). A basal basalt formation, dated at ca. 1267 Ma, is overlain by quartz arenite, shale and dolostone. The dolostone that makes up the formerly named Society Cliffs Formation has subsequently been subdivided into four members that form a west-facing, shallow- to deep-water carbonate ramp with precursor deep-water carbonate mounds. This dolostone formation hosts the abandoned and reclaimed Nanisivik lead-zinc mine that operated from 1977 to 2002. After an initial period of uplift, extensional fracturing and erosion, the basin continued to fill with a stromatolitic limestone reef–bearing shale unit, followed by several vertical kilometres of sandstone divided into three formations. The Borden Basin was intruded by a significant mafic dyke swarm, part of the 723 Ma Franklin magma event. The Proterozoic rocks are capped, in part, by siliciclastic rocks of Cambrian age.

Prior work in this area included unpublished aeromagnetic surveying by mining companies and government bedrock mapping of the area between the Nanisivik minesite and Arctic Bay at 1:100 000 scale (Patterson et al., 2003). All carving stone sites in the Arctic Bay area are marble skarn deposits (with minor serpentinized olivine gabbro occurrences) exposed on the surface and at the contact between the Franklin dykes and fine-grained carbonate rocks of Mesoproterozoic age (Beauregard and Ell, 2013). Arctic Bay carvers prefer to work with altered marble (hardness of 2–2.5) but will utilize competent, fine-grained marble with a hardness of 3. Banded marble, locally referred to as 'argillite', is a finely laminated marble that has been altered and strengthened by fluid interaction. Individual laminations exhibit weak magnetism. Most banding appears to be conformable to otherwise indistinguishable bedding.

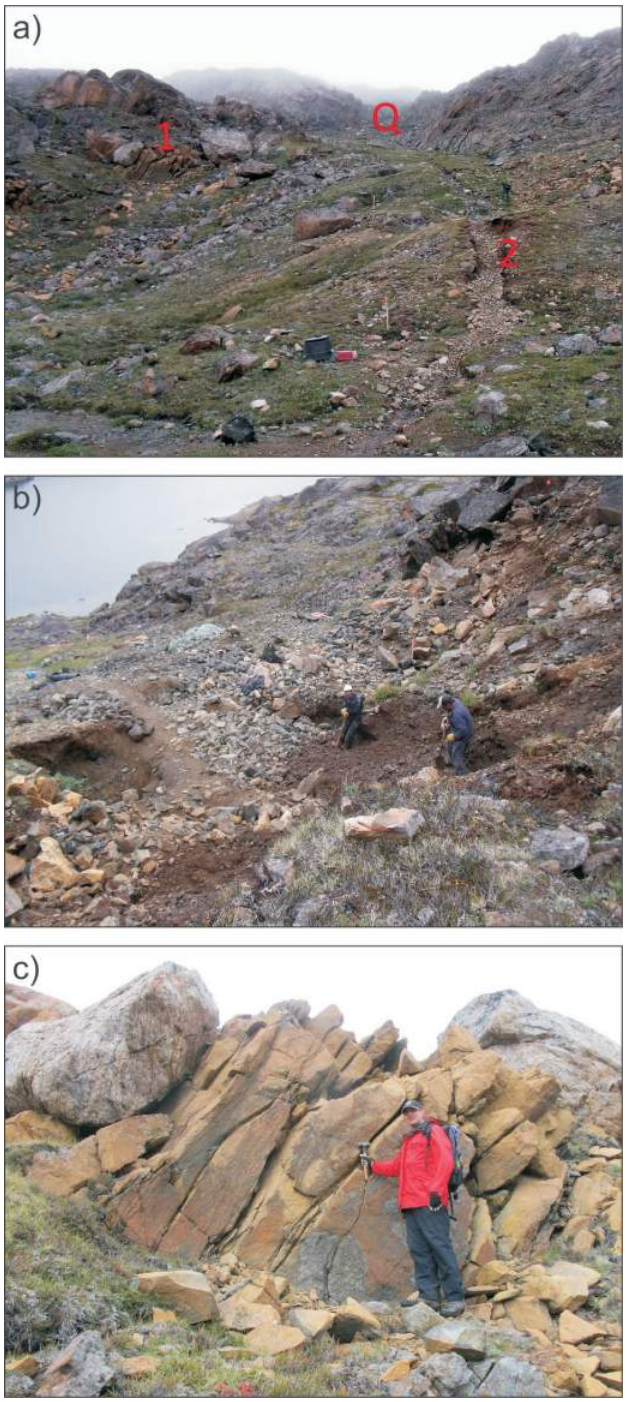

Figure 3: Opingivik community quarry, south shore of Cumberland Sound south of Pangnirtung, southern Baffin Island, Nunavut: **a)** overburden-covered hillside showing exposures of ultramafic formation in quarry (Q), outcrop (1) and subcrop (2); 2014 north-facing view; **b)** quarry and debris pile; 2011 southwest-facing view; **c)** close-up of 8 m high outcrop of competent carving stone on west side of overburden-covered hillside; 2014 north-facing view.

Evaluations were performed on seven skarn marble sites in four locations west, northwest and north of Arctic Bay (Table 1, Figure 4). Not visited was a promising site of white marble southwest of Arctic Bay at the end of an ATV trail discernible on Google™ earth, located at approximately latitude 73°01’04"N, longitude 85°11’18"W. This white marble site is known from carvers who have collected this rock in the past. Small laminated marble skarns were evaluated at the new Argillite site (latitude 73°02’12.7"N, longitude 85°13’44.2"W) and another site, Tagutsalik at latitude 73°02’33.8"N, longitude 85°13’43.9"W, that has been used for making traditional ‘stir-stick’ artifacts. The soft stone at both sites was determined to be not competent enough for use as ‘carving stone’.

In addition to being the first reported site of artisan-suitable ultramafic rock near Arctic Bay, the new Three-Stone locality has excellent-quality laminated marble in large blocks and good-quality marble breccia (Table 1, Figures 4, 5a–c). Fine-grained, competent marble skarns occur at the Two-Marble locality (Figure 5d), the Rubble Zone site (Figure 5e) and the Victor Bay site (Figure 5f). The Two-Marble locality consists of a site of white marble with broad black bands, available in large blocks, and a second site of laminated marble, available in small blocks. Grey marble found in the tidal-flat area at the Victor Bay site is accessible only at low tide.

The inactive Old Main quarry is the largest known resource of excellent-quality laminated marble in the Arctic Bay area (Figure 6a). This site is no longer accessible for collection of stone, as the quarry is filled with debris from decades of collecting. The White Marble quarry pit has doubled in size since the 2012 visit; this deposit’s resource estimate can now be upgraded from small (i.e., individual) scale to community-scale (Figure 6b).

An artisan serpentinite deposit occurs on a south-facing hillside above tidewater on the north shore of Fabricius Fiord, 70 km south of Arctic Bay (Figure 1, Table 1). Samples collected in 2012 were analyzed by scanning electron microscope (SEM) and determined to be typical ilmenite-bearing kimberlite (LeCheminant, unpub. data, no date). The vertically emplaced, 25 m wide ultramafic diatreme in-

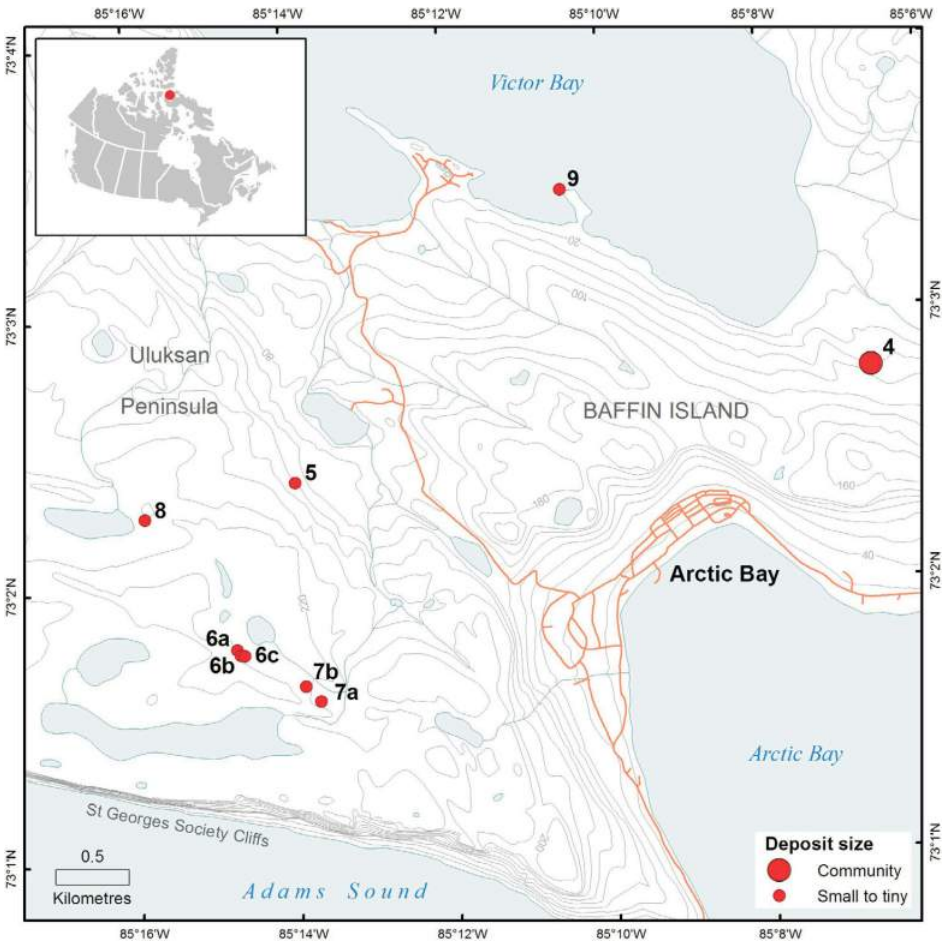

Figure 4: Locations of evaluated quarries and sites 4–9 (see Table 1) in the immediate area of Arctic Bay, northeastern Baffin Island, Nunavut.

Figure 5: Seven additional skarn marble sites in four separate locations near Arctic Bay: **a)** Three-Stone locality, showing the Banded Marble site (1), Serpentinite site (2) and Marble Breccia site (3); note Franklin dyke on right side of photo; southwest-facing view; **b)** detail of excellent quality laminated marble boulders in talus at Banded Marble site; west-facing view; **c)** detail of good-quality artisan ultramafic boulders in talus at Serpentinite site; west-facing view; **d)** Two-Marble locality with part of White Marble site in foreground, Banded Marble site (X) in distance and Franklin dyke on left side of photo; northwest-facing view; **e)** 25 m wide Rubble Zone Marble site (outlined) with Franklin dyke on right side of photo; west-facing view; **f)** underwater Victor Bay Marble site in foreground and onshore west-trending Franklin dyke; south-facing view.

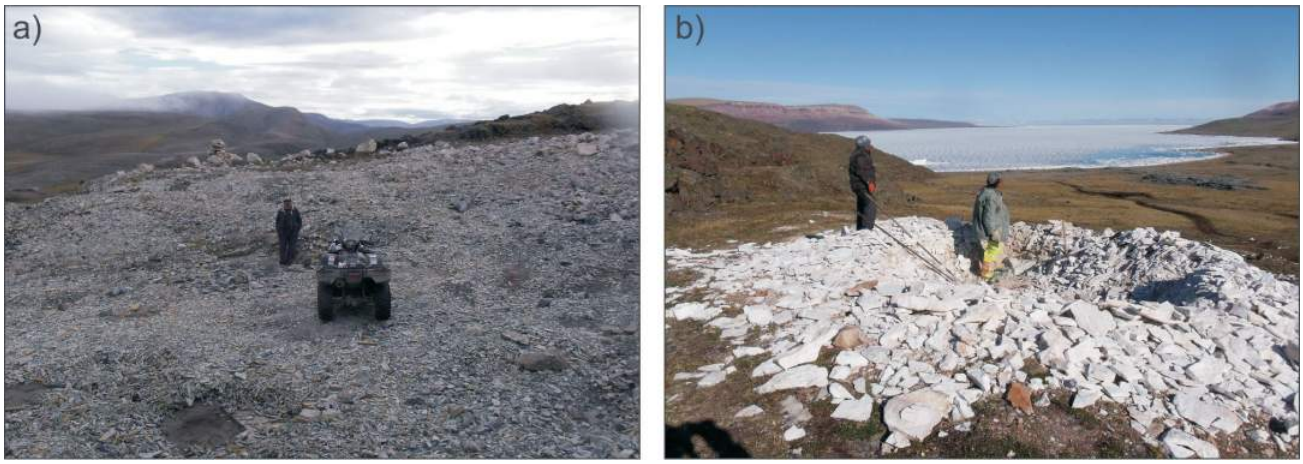

Figure 6: Arctic Bay's quarries: **a)** Old Main quarry; note proximal Franklin dyke behind project carver J. Ell, who is standing on artisan-suitable bedrock in pit floor; southeast-facing view; **b)** active White Marble quarry; note Franklin dyke on left side of photo; 2012 northeast-facing view.

trudes migmatitic gneiss and is exposed in two parts, with a narrow dyke lying above a small, bulbous, downward-tapering diatreme (Figure 7).

Economic considerations

The Rankin Inlet area is highly prospective for carving stone deposits in mafic to ultramafic rocks in the Rankin Inlet Group. Glacially dispersed boulder trains on the order of 10–50 km in length can be expected from large ultramafic deposits. Any discovery of a large to major resource near tidewater in the vicinity of Rankin Inlet would immediately provide stone for the four carving stone–impoverished communities in the south Kivalliq region, as well as provide for the needs of other communities throughout eastern Nunavut.

The south shore of Cumberland Sound is highly prospective for the discovery of carving stone sites close to tidewater. Mapping has shown ultramafic formations to be associated with rocks of the Lake Harbour Group (Steenkamp et al., 2014); these formations deserve further attention to determine if they could be used for carving stone. A particularly promising area identified from community consultation is southern Moodie Island between Neptune Bay and Littlecote Channel, where hunters have found boulders of carving stone from an undetermined source—possibly from traditional soft stone sites used in the past (Beauregard and Ell, 2013; J. Ishulutak, pers. comm., 2015).

Pangnirtung's community quarry at Opingivik is impacted by wasterock debris and colluvium that have fallen in. The provision of wheelbarrows would assist quarries with wasterock management as well as with the gathering of stone. A ground geophysical survey is recommended over the overburden-covered hillside south of the Opingivik quarry. Such a survey would assist in the delineation of ultramafic rock.

Arctic Bay has sufficient artisan marble for long-term local supply as well as marine distribution to the carving stone–impoverished communities of Resolute and Grise Fiord. Additional marble skarn and serpentinite sites in the vicinity of Arctic Bay are known to local carvers (Beauregard and Ell, 2013). Further consultation of carvers by the Hamlet of Arctic Bay is recommended. Detailed stratigraphic mapping, subsequently integrated with unpublished mining-industry aeromagnetic surveys, is recommended over areas wherever Franklin dykes intrude carbonate rock formations. Such exposures are known to occur in the southern portion of Uluksan Peninsula, the Arctic Bay–Victor Bay locale, on English Bay, and in and southeast of the Nanisivik minesite area (Patterson et al., 2003; Turner, 2009). Recommended follow-up mapping and prospecting of selected areas from Arctic Bay to Nanisivik should be performed by teams consisting of a geologist and a local carver.

Figure 7: Outlined kimberlite diatreme of good-quality, soft carving stone at Fabricius Fiord, 70 km south of Arctic Bay, Nunavut; 2012 northeast-facing view.

The newly recognized small kimberlite diatreme south at Fabricius Fiord is a traditional, little-utilized carving stone site. The kimberlite formation is located on Arctic Bay IOL Block 30 and subject to IOL surface rights that are administered by the Qikiqtani Inuit Association. This artisan-suitable deposit of kimberlite altered to serpentinite is on a hillside adjacent to tidewater and is estimated to have 250 tonnes of soft, good-quality green stone.

Conclusions

New resources of carving stone were assessed by the Nunavut Carving Stone Deposit Evaluation Program in 2015 west of Rankin Inlet and in proximity to Arctic Bay. No new resources were found during follow-up work through the GSC's 2015 McKeand River bedrock mapping program on the south shore of Cumberland Sound. Two small sites of new stone near carving stone–impoverished Rankin Inlet require further testing for artisan suitability. Further investigations were recommended to the Hamlet of Rankin Inlet in connection with a 23 m intersection of soft stone in drillcore from a rediscovered mineral exploration drillhole near the community.

Arctic Bay has sufficient resources of excellent-quality skarn marble for both its community carvers and, by marine transport, the carving stone–impoverished small communities of Resolute and Grise Fiord. It was determined that Arctic Bay now has resources at two quarries and seven new sites in four locations, all in proximity to the hamlet. Arctic Bay's closest site of good-quality serpentinite is also included in these new resources. All carving stone sites accessible to Arctic Bay carvers are skarn marble deposits that outcrop at surface, found where ultramafic dykes of the Franklin magmatic event are in contact with fine-grained carbonate rocks. Arctic Bay's active White Marble quarry and inactive Old Main quarry are full of debris from decades of carving stone extraction. A modest amount of cleaning at both sites would result in improved accessibility to these soft stone resources. Additional resources of carving stone can be anticipated from recommended future mapping and prospecting of the Arctic Bay–Nanisivik locale. The little-utilized carving stone site at Fabricius Fiord, south of Arctic Bay, is a small kimberlite diatreme.

Acknowledgments

The authors thank prospector B. Gawor of Rankin Inlet for guidance work; full-time carver J. Ishulutak of Pangnirtung for advice; carvers T. Tatatuapik and P. Oqalluq of Arctic Bay for guidance and artisan-suitability work; and A.N. LeCheminant for SEM analytical results. The authors gratefully acknowledge services provided by Community Economic Development Officer (CEDO) J. Kaludjak of Rankin Inlet; CEDO C. Kines of Arctic Bay; and the supervisors and field crew of the GSC's Geo-mapping for Energy and Minerals (GEM) south Baffin, McKeand River bedrock mapping camp. Additional thanks go to Polar Continental Shelf Program, Universal Helicopters and Bradley Air Services for safe and efficient air transportation. Financial support of this study was provided by the Strategic Investments in Northern Economic Development (SINED) program delivered by the Canadian Northern Economic Development Agency (CanNor). A review of this manuscript by L. Ham is appreciated.

References

Beauregard, M. and Ell, J. 2012: 2010–2012 carving stone results in Kivalliq Region, Nunavut; Mineral and Petroleum Resources, Department of Economic Development and Transportation, Government of Nunavut, unpublished report prepared for hamlets, regional Inuit associations and government agencies, 55 p.

Beauregard, M. and Ell, J. 2013: 2011–2013 carving stone results in Qikiqtaaluk (Baffin) Region, Nunavut; Mineral and Petroleum Resources, Department of Economic Development and Transportation, Government of Nunavut, unpublished report prepared for hamlets, regional Inuit associations and government agencies, 44 p.

Beauregard, M. and Ell, J. 2015: Nunavut Carving Stone Evaluation Program: 2013 and 2014 fieldwork in the Kitikmeot Region, Belcher Islands, Hall Peninsula and Repulse Bay, Nunavut; *in* Summary of Activities 2014, Canada Nunavut Geoscience Office, p. 163–174.

Beauregard, M., Ell, J., Pikor, R.K. and Ham, L.J. 2013: Nunavut Carving Stone Evaluation Program (2010–2013): third year results; *in* Summary of Activities 2012, Canada Nunavut Geoscience Office, p. 151–162.

Dyck, B.J. and St-Onge, M.R. 2014: Dehydration-melting reactions, leucogranite emplacement and the Paleoproterozoic structural evolution of Hall Peninsula; *in* Summary of Activities 2013, Canada Nunavut Geoscience Office, p. 73–84.

Government of Canada 1993 (amendments up to and including 2009): Agreement between the Inuit of the Nunavut Settlement Area and Her Majesty the Queen in right of Canada (Nunavut Land Claims Act); Indian and Northern Affairs Canada, Article 19 (Title to Inuit Owned Lands), Part 9 (Rights to Carving Stone), p. 149–150.

Hannah, G.J.R. 1961: The new North: land of today, North Rankin Nickel mine; Precambrian; December–January 1961, p. 6–20.

Harquil, J.A. 1973: Report on surface diamond drilling program, Rankin (1972) project, Rankin Inlet, NWT; unpublished mineral claim assessment report prepared for Rankin Nickel Syndicate by Surveymin Consultants, Aboriginal Affairs and Northern Development Canada, Assessment Report 060050, 70 p., URL <http://nunavutgeoscience.ca/apps/ref/showDetailedRef.php?rId=927&drNbr=060050> [October 2011].

Hassell, D. 1989: Results of diamond drill program performed by Asamera Minerals Inc., RIP and OFF mineral claims, Rankin Inlet, N.W.T.; Department of Indian Affairs and Northern Development, Yellowknife, NWT, Assessment Report 082704, 184 p, <http://nunavutgeoscience.ca/apps/ref/showDetailedRef.php?rId=1819&drNbr=082704> [October 2015].

Laporte, P.J. 1975: Geology of the Rankin Inlet area, Northwest Territory; M.Sc. thesis, Brock University, St. Catharines, Ontario, 147 p.

Liikane, D.A., Rayner, N.M. and St-Onge, M.R. 2015: Frobisher suite mafic, ultramafic and layered mafic-ultramafic intrusions, western Cumberland Sound, Baffin Island, Nunavut; *in* Summary of Activities 2015, Canada-Nunavut Geoscience Office, p. 21–32.

Nunavut Department of Economic Development and Transportation 2007a: Ukkusiksaqtarvik – the place where we find stone: carving stone supply action plan; Nunavut Department of Economic Development and Transportation, 12 p., URL <http://www.gov.nu.ca/sites/default/files/carving_stone_action_plan_english.pdf> [October 2014].

Nunavut Department of Economic Development and Transportation, 2007b: Sanujgait: a strategy for growth in Nunavut's arts and crafts sector; Nunavut Department of Economic Development and Transportation, 40 p., URL <http://www.gov.nu.ca/sites/default/files/Sanaugait_arts_strategy.pdf> [October 2014].

Patterson, K.M., Powis, K., Sutherland, R.A. and Turner, E.C. 2003: Stratigraphy and structural geology, Nanisivik area, northern Baffin Island, Nunavut; Geological Survey of Canada, Open File 1552, 1:100 000 scale bedrock geology map with descriptive notes.

Steenkamp, H.M. 2015: Data file accompanying "Carving stone and mineral resource potential of the Opingivik deposit, Baffin Island, Nunavut"; Canada-Nunavut Geoscience Office, Geoscience Data Series GDS 2015-005, Microsoft® Excel® file and Esri ArcGIS project, URL <http://cngo.ca/summary-of-activities/2014/> [January 2015].

Steenkamp, H.M., Beauregard, M.A. and Mate, D.J. 2015: Carving stone and mineral resource potential of the Opingivik quarry, southern Baffin Island, Nunavut; *in* Summary of Activities 2014, Canada-Nunavut Geoscience Office, p. 153–162.

Steenkamp, H.M., Bros, E.R. and St-Onge, M.R. 2014: Altered ultramafic and layered mafic-ultramafic intrusions, new economic and carving stone potential on northern Hall Peninsula, Baffin Island, Nunavut; *in* Summary of Activities 2013, Canada-Nunavut Geoscience Office, p. 11–20.

Steenkamp, H.M., Pizzo-Lyall, M., Wallace, C.J., Beauregard, M.A. and Dyck, B.J. 2014: Geology, history and site-management planning of the Kangiqsukutaaq carving stone quarry, south Baffin Island, Nunavut; *in* Summary of Activities 2013, Canada-Nunavut Geoscience Office, p. 193–200.

Tella, S. 1994: Geology, Rankin Inlet (55K/16), Falstaff Island (55J/13) and Quartzite Island (55J/11), District of Keewatin, Northwest Territories; Geological Survey of Canada, Open File 2968, Sheet 1 of 2, 1:50 000 scale bedrock geology map with descriptive notes.

Turner, E.C. 2009: Mesoproterozoic carbonate systems in the Borden Basin, Nunavut; Canadian Journal of Earth Sciences, v. 46, p. 915–938.

Turner, E.C. 2011: Structural and stratigraphic controls on carbonate-hosted base-metal mineralization in the Mesoproterozoic Borden Basin (Nanisivik District); Economic Geology, v. 106, p. 1197–1223.

Characterization of carving stone deposits in Aberdeen Bay, southern Baffin Island, Nunavut

A. Camacho[1], R.K. Pikor[2] and M.A. Beauregard[3]

[1]*Department of Geological Sciences, University of Manitoba, Winnipeg, Manitoba, alfredo.camacho@umanitoba.ca*

[2]*Department of Geological Sciences, University of Manitoba, Winnipeg, Manitoba*

[3]*Minerals and Petroleum Resources, Department Economic Development and Transportation, Government of Nunavut, Arviat, Nunavut*

This work is part of the Hall Peninsula Integrated Geoscience Program (HPIGP), led by the Canada-Nunavut Geoscience Office (CNGO) in collaboration with the Government of Nunavut, Indigenous and Northern Affairs Canada, Dalhousie University, University of Alberta, Université Laval, University of Manitoba, University of Ottawa, University of Saskatchewan, University of New Brunswick, Nunavut Arctic College and the Geological Survey of Canada. It is supported logistically by several local, Inuit-owned businesses and the Polar Continental Shelf Program. The focus is on bedrock and surficial geology mapping (1:100 000 scale). In addition, a range of thematic studies is being conducted, including Archean and Paleoproterozoic tectonics, geochronology, landscape uplift and exhumation, microdiamonds, sedimentary rock xenoliths and permafrost. The goal is to increase the level of geological knowledge and better evaluate the natural resource potential in this frontier area.

Camacho, A., Pikor, R.K. and Beauregard, M.A. 2015: Characterization of carving stone deposits in Aberdeen Bay, southern Baffin Island, Nunavut; *in* Summary of Activities 2015, Canada-Nunavut Geoscience Office, p. 193–200.

Abstract

Two carving stone deposits, one developed and one undeveloped, in Aberdeen Bay, southern Baffin Island, were evaluated during the 2013 summer field season. The Tatsituya deposit, considered to be one of Nunavut's foremost carving stone quarries, is located at the intersection of a steep, east-west–trending, sinistral, strike-slip fault with a marble layer in the middle of the Lake Harbour Group. The fault records several episodes of deformation and fluid flow. The higher proportion of aluminum-rich lizardite rimming lizardite kernels and brucite appears to distinguish good-quality carving stone from excellent-quality carving stone in this deposit. An altered ultramafic unit deformed by the same fault system hosts the Tatsitui Tiniiniya deposit located ~1.25 km northwest of the Tatsituya quarry. The chemistry of alteration minerals and altered rocks is different between the deposits. Higher iron (FeO) and chromium (Cr_2O_3) contents in serpentine from serpentinized ultramafic rock distinguish this rock from serpentinized marble; this can be used to discriminate among source rocks, making exploration for excellent-quality carving stone more efficient.

Résumé

Un gisement de pierre à sculpter exploité et un deuxième encore inexploité dans la région de la baie Aberdeen, dans la partie sud de l'île de Baffin, ont fait l'objet d'une évaluation au cours de la campagne de terrain estivale de 2013. Le gisement Tatsituya, soit la carrière de pierre à sculpter que l'on estime être l'une des plus importantes du Nunavut, se situe à l'intersection d'une faille de coulissage à décrochement senestre très escarpée d'orientation est-ouest et d'une couche de marbre de la partie moyenne du groupe de Lake Harbour d'âge paléoprotérozoïque. La faille témoigne de nombreux épisodes de déformation et de circulation de fluides. Une proportion plus élevée de lizardite riche en aluminium entourant des cœurs de lizardite et de brucite semble être le critère qui permet de distinguer la pierre à sculpter de bonne qualité de la pierre de qualité supérieure au sein de ce gisement. Une unité ultramafique altérée, qui a été déformée suite à l'activité de ce même système de failles, renferme le gisement Tatsitui Tiniiniya, lequel se situe environ 1,25 km au nord-ouest de la carrière Tatsituya. Les réactions chimiques des minéraux d'altération et des roches altérées varient d'un gisement à l'autre. Des teneurs en fer (FeO) et en chrome (Cr_2O_3) plus élevées dans la serpentine provenant de roches ultramafiques serpentinisées aident à distinguer la roche en question du marbre serpentinisé; cette caractéristique peut servir de critère pour établir une différence entre les roches mères, rendant ainsi plus efficaces les méthodes d'exploration utilisées en vue de découvrir des gisements de pierre à sculpter de qualité supérieure.

This publication is also available, free of charge, as colour digital files in Adobe Acrobat® PDF format from the Canada-Nunavut Geoscience Office website: http://cngo.ca/summary-of-activities/2015/.

Introduction

The evaluation and characterization of carving stone deposits throughout Nunavut is a collaborative effort between the Government of Nunavut's Nunavut Carving Stone Deposit Evaluation Program (NCSDEP), the Canada-Nunavut Geoscience Office (CNGO) and the University of Manitoba. The aim of this project is to better understand what comprises artisan serpentinite and to gain insight into the geological processes responsible for the formation of good- to excellent-quality serpentinite carving stone. The evaluation of developed and undeveloped carving stone deposits in southern Baffin Island, as well as those across the territory, is necessary and significant because carving is a source of income for many in Nunavut, and quarries are becoming overworked and local supplies are diminishing as result of traditional carving stone practices.

During the summer of 2013, fieldwork with the NCSDEP was carried out across southern Baffin Island. The carving stone deposits investigated for this study were the Aberdeen Bay quarries (Tatsituya and Tatsitui Tiniiniya) northwest of Kimmirut, the Opingivik quarry southwest of Pangnirtung, the Korok Inlet quarry (Kangiqsukutaaq) east of Cape Dorset, and the undeveloped Hall Peninsula (Ikatuyak) ultramafic deposit southeast of Iqaluit (Figure 1).

Various rock types are used for traditional carving using carving stone: primarily serpentine, marble and soapstone, which occur in many geological settings and environments. Carving stone can be defined as a rock that is soft enough to carve and manipulate with carbide tools (Beauregard et al., 2013). The quarries of interest have been classified by the NCSDEP as containing good- to excellent-quality rock, indicating that the carving stone has a Mohs hardness of 2.0–2.5, has excellent consistency with tough and interlocking minerals, holds fine detail, polishes well with a desirable colour and can be quarried in large blocks. The NCSDEP has determined the Tatsituya quarry in Aberdeen Bay to be a community-sized (~500 tonnes), mature and nearly depleted quarry and the Opingivik quarry to be a community-sized (~200 tonnes), recently opened quarry with the potential to become a large quarry that could produce up to 25 000 tonnes of stone. Steenkamp et al. (2014) estimated that a total of 50 000 tonnes of carving stone has been removed to date from the Korok Inlet quarry and recommends that further carving stone be extracted using mechanized excavation techniques for safety reasons because of the extensive workings. The Hall Peninsula ultramafic deposit discovered in 2014 has not been sufficiently examined to determine its quantities of usable carving stone. The quality of the stone and size of the resource at these four locations indicate that they have the potential to provide significant carving stone resources to several communities for decades (Beauregard et al., 2013).

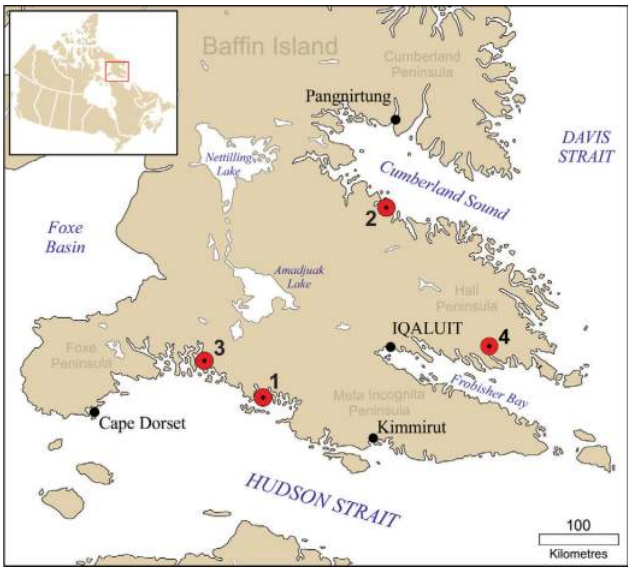

Figure 1: Locations of the evaluated quarries: 1) Aberdeen Bay, 2) Opingivik, 3) Korok Inlet and 4) Hall Peninsula. Figure modified from Beauregard et al. (2013).

The Aberdeen Bay carving stone occurrences (Tatsituya and Tatsitui Tiniiniya) are the focus of this paper and show evidence of metasomatic alteration caused by significant fluid flow. Field observations and detailed sampling of each quarry, critical for the evaluation of each carving stone deposit, show evidence of fluid-flow pathways. Identifying such large-scale conduits such as faults for fluid flow is important in identifying additional carving stone sites.

This study involves integrating laboratory analysis with standard measures of artisanal suitability to classify carving stone deposits in terms of geochemical compositions and microstructural features to determine characteristics of excellent-quality carving stone. Understanding how mineral compositions and structures of carving stone deposits were influenced by metasomatism and fluid flow patterns in the middle and upper crust will provide insight into alteration processes, fluid percolation during major tectonic events and geological settings that are ideal for the formation of carving stone.

Geological setting

The Aberdeen Bay deposits are hosted within the Paleoproterozoic Lake Harbour Group, a continental-margin clastic-carbonate shelf succession that overlies crystalline basement of the Meta-Incognita microcontinent (St-Onge et al., 2007). The crystalline rocks act as the depositional basement for the Lake Harbour Group units and consist of layered orthopyroxene–biotite±hornblende monzogranite and tonalite orthogneiss termed the Ramsay River

orthogneiss (Theriault et al., 2001). The monzogranite gneiss is Archean in age that has, however, undergone significant Paleoproterozoic reworking based on a U-Pb age of 1950 ±6 Ma (Scott et al., 2002).

The clastic-carbonate metasedimentary units of the Lake Harbour Group are interpreted to be a shelf succession deposited along the margin of the Superior craton and later rifted from this margin. The Lake Harbour Group consists of interlayered garnet-rich psammite and pelite with minor quartzite, which are overlain by marble and calcsilicate units. The age of the sedimentary rocks in the Lake Harbour Group is Paleoproterozoic, as detrital zircons from this succession yield ages of 2.2–1.6 Ga and were deposited after 1934 ±2 Ma, the age of the youngest detrital zircon (Scott and Gauthier, 1996). Granulite-facies metamorphism of the Lake Harbour Group at ca. 1840 Ma (Scott, 1997) may be coeval with Paleoproterozoic charnockite (Sanborn-Barrie et al., 2008). Mafic and ultramafic sills of unknown age intrude the Lake Harbour Group and charnockite.

Deposit descriptions

The Tatsituya and Tatsitui Tiniiniya carving stone deposits are located along the northwestern coastline of Aberdeen Bay, approximately 160 km west of the hamlet of Kimmirut, Nunavut (Figure 1). The Tatsituya deposit is considered to be one of Nunavut's foremost carving stone quarries and community carvers have worked this site for more than 50 years (Gustavison, 1999). The Tatsitui Tiniiniya deposit is an undeveloped resource located approximately 1.25 km northwest of the Tatsituya quarry (Beauregard et al., 2013). Along this coast, a marble layer ~15 m by 1 km in the middle of the Lake Harbour Group is intruded by younger Paleoproterozoic felsic rocks, possibly associated with the Cumberland Batholith, and ultramafic rocks.

Tatsituya deposit

The excellent-quality green serpentinite from the Tatsituya deposit is located at the intersection of a steep, east-west–trending, sinistral, strike-slip fault (Figure 2a) with the marble layer in the middle of the Lake Harbour Group.

The marble (sample AB-18) with a white-grey weathered surface is homogeneous and medium to coarse grained. Thin laminations caused by variations in grain size and composition mark the north-striking vertical foliation. Calcsilicate boudins are distributed throughout the marble and typically range from 5 to 30 cm in diameter, but may be as large as 50 cm (Figure 2b). The presence of calcsilicate boudins with marble foliation wrapping around the boudins indicates that the calcsilicate rocks acted competently during deformation. The primary granulite- or amphibolite-facies mineral assemblage within these rocks includes diopside and forsterite within a calcite-dolomite matrix (Camacho et al., 2015)[4].

Partially serpentinized marble (sample AB-12) surrounds the green carving stone deposit. Forsterite and diopside are largely replaced by serpentine and exhibit a typical mesh texture (Figure 3a). Serpentine also fills fractures and rims calcsilicate nodules (Figure 2b). Phlogopite forms clusters and is not extensively altered to serpentine. Magnetite is present in trace amounts and is associated with serpentine that infills internal fractures. The calcsilicate nodules (sample AB-12) consist of diopside and are extensively fractured and partially replaced by serpentine and calcite. Veins of serpentine and chlorite that are several centimetres thick (samples AB-13, -15) appear to be more common in the vicinity of the deposit.

Serpentinite forms the carving stone deposit and is restricted to the zone where the fault intersects the marble. Traditional carvers distinguish between two types of carving stone: the apple-green, fine-grained serpentinite (sample AB-20) is an excellent-quality stone (Beauregard et al., 2013), and the lime-green, coarser grained serpentinite (sample AB-21) is considered to be good quality. Both of these rock types consist of primarily serpentine, brucite and calcite. Serpentine kernels, with mesh texture, are surrounded by radiating crystals of Al-lizardite and brucite (Figure 3b). Clots of brucite, calcite and subhedral chlorite grains appear to fill voids (Figure 3b). Veins filled with perpendicular-layered brucite cut across mesh textures (Figure 3c, d). The higher proportion of Al-lizardite rimming lizardite kernels appears to distinguish good-quality carving stone from excellent-quality carving stone.

The main fault contains evidence for different stages of fluid infiltration and high-strain deformation, and is best observed in the granite (sample AB-11). At least three stages of deformation are observed. The first stage is associated with the infiltration of silica-rich fluids that precipitated quartz along veins and altered biotite to chlorite. These veins are overprinted by thin high-strain zones that brecciate the rock (Figure 3e) and in turn are cut by another stage of quartz veining. The fault also contains graphite but it is uncertain as to which deformation event the graphite is related. In the serpentinite samples affected by the fault (sample AB-19), a similar chronology of events has been not established, as the last stage of deformation extensively altered and fractured the serpentinite (Figure 2a). A vein ~5 cm thick in the fault zone (sample AB-19) is different from other sampled veins as the fault-zone vein contains tremolite and talc.

[4] *CNGO Geoscience Data Series GDS2015-013, containing the data or other information sources used to compile this paper, is available online to download free of charge at http://cngo.ca/summary-of-activities/2015/.*

A second fault system, with an approximate north-south trend, occurs at the marble-granite interface. This fault system is extremely rich in graphite and contains coarse-grained lath-shaped epidote and chlorite.

Tatsitui Tiniiniya deposit

An altered ultramafic unit hosts the Tatsitui Tiniiniya deposit, ~1.25 km northwest of the Tatsituya quarry. This unit has a fabric subparallel to the orientation of the main strike-slip fault exposed in the Tatsituya deposit to the south. Two samples of good-quality stone were collected: a dark-green, almost black serpentinite situated near the shore (sample AB-22) and dark-green, specular serpentinite found on the rock ledge of a tidal flat (sample AB-23).

The primary igneous assemblage of forsterite, phlogopite and Cr-magnetite is common to both samples, and clinoenstatite is present only in sample AB-22 (Camacho et al., 2015). The higher content of phlogopite in sample AB-23 accounts for its specular appearance. Serpentine is the dominant alteration phase, pseudomorphs forsterite and exhibits a typical mesh texture (Figure 4a, b). The rock is extensively fractured, and serpentine and magnetite fill irregular fractures in primary mineral grains and veins (Figure 4a). Chlorite alteration appears to be confined to phlogopite (Figure 4c, d).

Mineral chemistry of alteration minerals

Tatsituya deposit

X-ray diffraction patterns indicate that the serpentine carving stone comprises mainly lizardite-1T and Al-lizardite. In sample AB-21, kernels of lizardite are layered by several generations of Al-lizardite growth with the Al content increasing outward from the edges of the kernels (Figure 3b). Vein serpentine grains contain mainly lizardite and sometimes contain antigorite.

Chlorite (pycnochlorite-ripidolite) in fault rocks derived from the granitoid are relatively low in Mg-Si and high in Al-Fe when compared with chlorite (penninite) in veins in the altered metasedimentary rocks (Camacho et al., 2015). In addition, Cr_2O_3 contents in both the fault rocks and serpentinite are essentially below detection. The chlorite geothermometer of Zang and Fyfe (1995) produces temperature estimates of ~280°C for the fault rocks and ~180°C for the veins.

Brucite, a form of magnesium hydroxide, is essentially pure, contains <1 wt. % FeO and has only been identified in the carving stone samples as clots (samples AB-20, -21). Calcite associated with brucite clots contains essentially no magnesium.

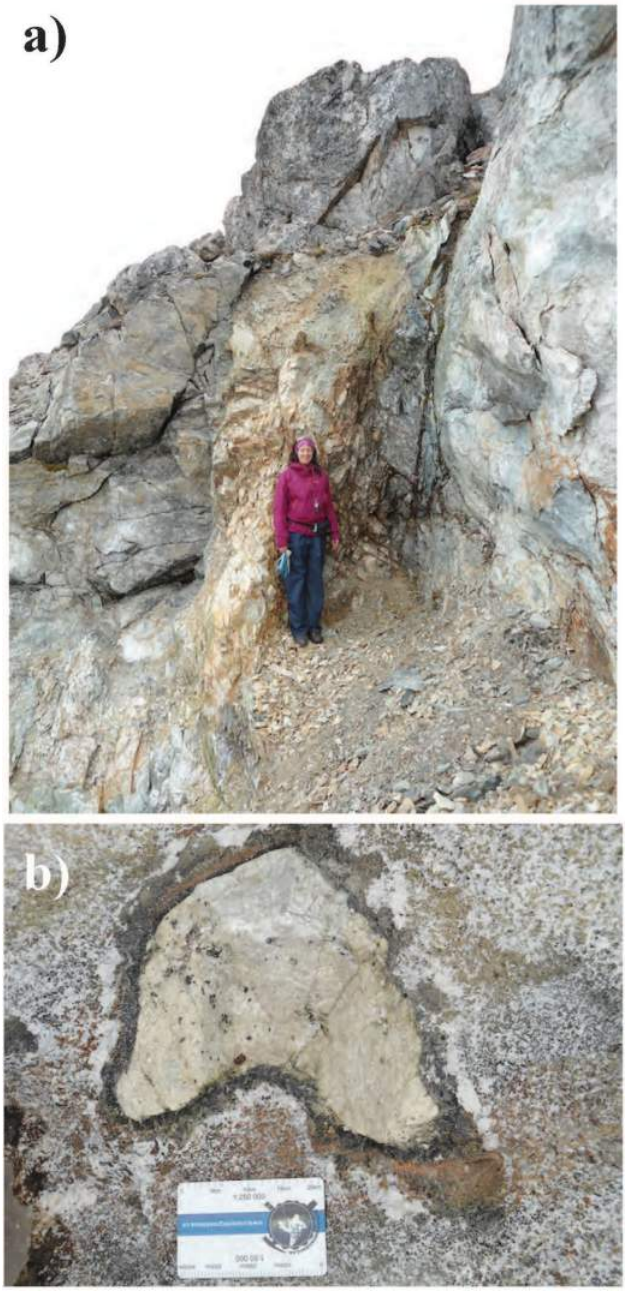

Figure 2: Photographs of the Tatsituya deposit showing a) the fault zone, view to the east and b) a calcsilicate nodule with a rind of serpentinite and calcite in partially serpentinized marble.

Tatsitui Tiniiniya deposit

X-ray diffraction patterns reveal that the serpentines in the two samples from this deposit are different. Sample AB-23 contains antigorite and lizardite-1T, whereas sample AB-22 contains chrysotile-2Mc1. There is no Al-serpentine in either sample. A thin compound vein in sample AB-22 shows that the last fluid event precipitated serpentine that is slightly more aluminous than the first generation (Figure 4c).

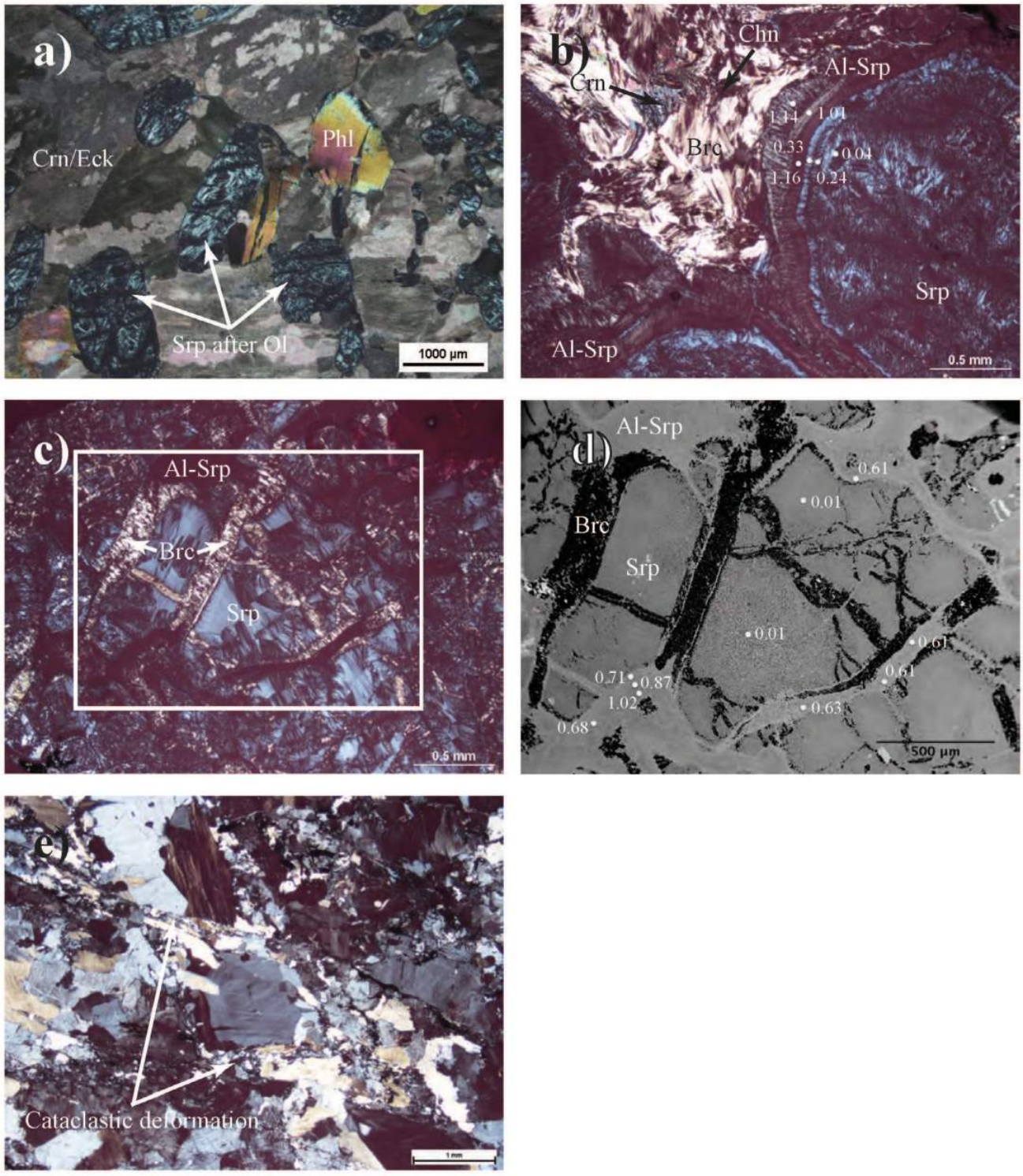

Figure 3: a) Partially serpentinized marble (sample AB-12) showing pseudomorphs of serpentine after olivine, and relatively unaltered carbonate and phlogopite, crossed polars; **b)** excellent-quality serpentinite (sample AB-20) showing partially replaced serpentine along fractures by veins of brucite and Al-serpentine, crossed polars; **c)** backscattered electron image of the centre of the previous image showing the electron microprobe spot analyses, values represent Al content in serpentine; **d)** serpentine kernels (sample AB-21) surrounded by concentric ribbons of fibrous Al-serpentine, brucite, chlorite and calcite fill the interstitial space, values represent Al content in serpentine, crossed polars; **e)** quartz vein in the fault that has been deformed by thin, cataclastic shear bands (sample AB-11), crossed polars. Abbreviations: Al-Srp, aluminum serpentine; Brc, brucite; Chn, chondrodite; Crn, corundum; Eck, eckermannite; Ol, olivine; Phl, phlogopite; Srp, serpentine.

Chlorite (clinochlore) is only found as an alteration product of phlogopite. The chlorite geothermometer of Zang and Fyfe (1995) returns temperature estimates of ~240°C.

The magnetite that infills the fractures (Figure 4a) is another product of serpentinization. It is essentially pure with Cr_2O_3 content below the detection limit.

Although both deposits have similar alteration mineral assemblages, there are some marked differences. The FeO and Cr_2O_3 contents in serpentine are significantly higher in the serpentinized ultramafic rock than in the serpentinized marble. Similarly, chlorite has elevated amounts of Cr_2O_3 in the serpentinized ultramafic rock (Camacho et al., 2015).

Geochemistry of whole-rock samples

The protolith of extensively altered rocks is difficult to determine due to the mass transfer of chemical constituents. Some studies have shown that high-field-strength elements (HFSEs; e.g., Ti and Zr), and transition elements such as Cr and Ni tend to be conserved (i.e., are immobile) during hydrothermal alteration of basaltic rocks at greenschist-facies metamorphism (e.g., Humphris and Thompson, 1978). Nevertheless, in each study area, immobility of element pairs should be tested rather than assumed (MacLean and Barrett, 1993). In this study, element mobility is compared during hydrothermal alteration of marble (Tatsituya) and ultramafic rock (Tatsitui Tiniiniya). Representative chemi-

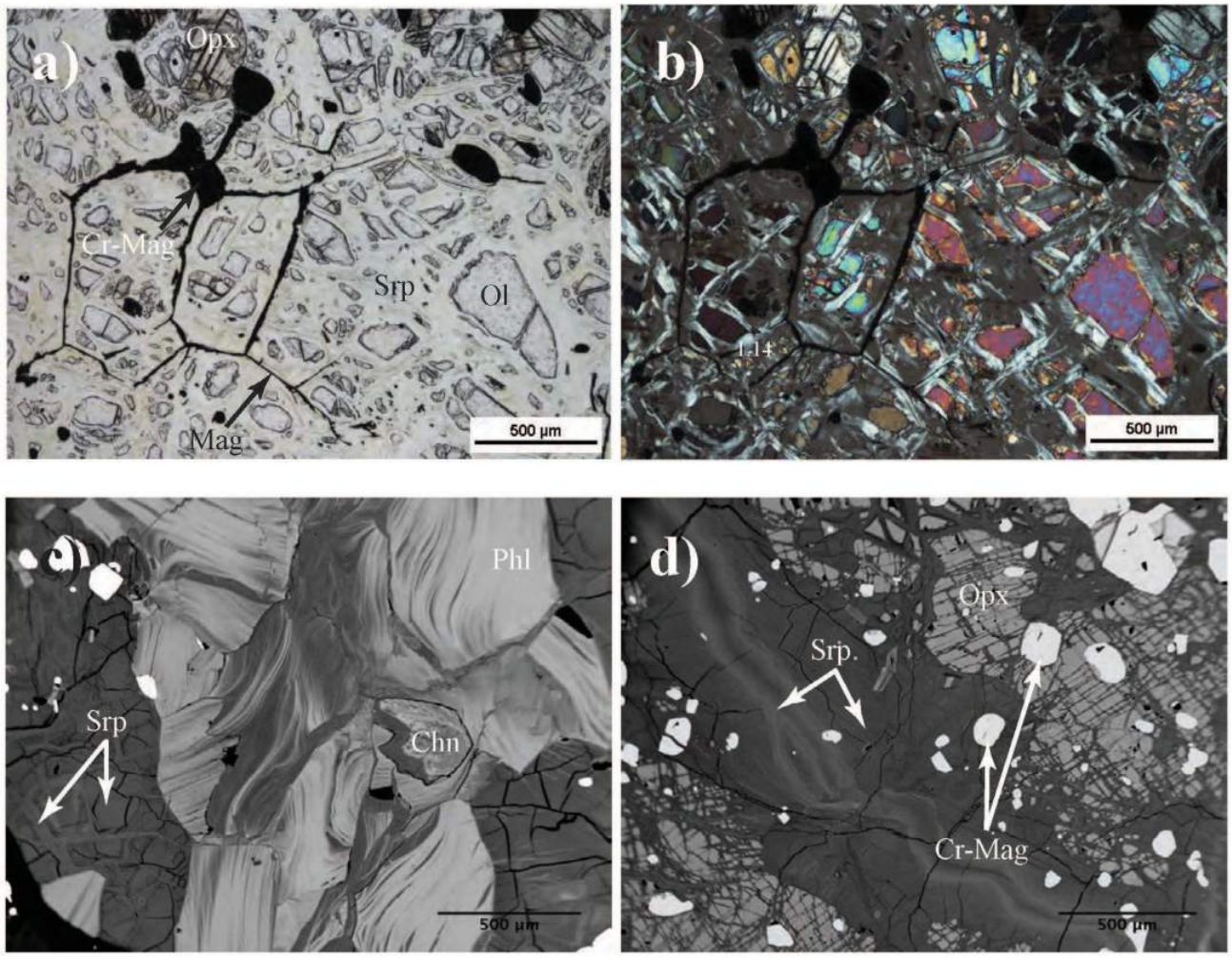

Figure 4: a) Onshore ultramafic unit (sample AB-22) showing grains of olivine (high relief) partly replaced along fractures by veins of serpentine; the image also shows magnetite outlining fracture patterns and possible former grain boundaries, plane-polarized light; **b)** same field of view as a) in crossed polars; **c)** backscattered electron image of a serpentine vein in sample AB-22 showing concentric ribbon texture of subparallel ribbons of fibrous serpentine; clinoenstatite is extensively fractured and filled with veins of serpentine, whereas the chrome spinel appears to have not been affected; **d)** backscattered electron image of phlogopite and mesh texture serpentine in sample AB-23; phlogopite is mainly altered to chlorite. Abbreviations: Chn, chondrodite; Cr-Mag, chromium magnetite; Mag, magnetite; Ol, olivine; Opx, orthopyroxene; Phl, phlogopite; Srp, serpentine.

cal analyses of rocks from Aberdeen Bay are presented in Camacho et al. (2015). Samples from the Tatsituya deposit include unaltered marble (sample AB-18), partially serpentinized marble (sample AB-12) and completely serpentinized marble (samples AB-20, -21); samples from the Tatsitui Tiniiniya deposit include extensively serpentinized ultramafic rock (samples AB-22, -23).

From the Tatsituya deposit, sample AB-18 has 5 wt. % MgO and sample AB-12 has 18.32 wt. % MgO. These values are substantially lower than the ~40 wt. % MgO in the serpentinites. It is difficult to conceive how such rocks reflect the protolith unless there was considerable volume loss and element mobility (especially Ca, C, Si and Mg) during hydrothermal alteration. The alternative is that sample AB-18, the unaltered marble, represents a calcite-rich layer within the mainly dolomitic marble. More work clearly needs to be done to address this issue.

When the chemistry of the serpentinites in the Tatsituya and Tatsitui Tiniiniya deposits are compared, several differences become evident (Camacho et al., 2015). Notably, the contents of transition elements (Cr, Ni and Co) are much higher, and HFSEs, light rare-earth elements, U and Th are lower in the serpentinized ultramafic rock from Tatsitui Tiniiniya deposit than in the serpentinized marble in the Tatsituya deposit.

These differences become significant considering that both sites appear to have been affected by the same fault system with the orientation of the late structures being the same; therefore, the same fluidizing events seem to have affected both sites.

Economic considerations

Understanding the characteristics and features of high-quality carving stone has economic implications for carvers of Nunavut, as those attributes can be used to explore for additional high-quality carving stone resources. The stone should typically show little deformation, as pervasive planes of weakness are detrimental to carving. Geochemical, microstructural and textural features, and isotopic signatures can be used to determine attributes that constitute high-quality stone, allowing for scientific characteristics to add to the carver-derived classifications developed by Beauregard et al. (2013) for potential carving stone quarries. Examining the effects of metasomatism will indicate which geological settings are ideal for the formation of good- to excellent-quality carving stone.

The distribution of carving stone in Aberdeen Bay is patchy, and the deposits occur in sites where specific rock types were extensively hydrated by fluids flowing along fractures. The chemistry of alteration minerals and altered rocks is different between the deposits, and these differences can be used to discriminate among source rocks, making exploration more efficient. The authors plan to further test these findings and this hypothesis on the Opingivik quarry, the Korok Inlet quarry (Kangiqsukutaaq) and the Hall Peninsula ultramafic deposit (Ikatuyak).

Acknowledgments

The authors thank the Nunavut Carving Stone Deposit Evaluation Program, the late E. Prosh, Director of Government of Nunavut, Department of Economic Development and Transportation–Minerals and Petroleum Resources Division (GN, EDT-MPR) and L. Ham, Manager of GN, EDT-MPR for logistical support in and out of the field, and project carver J. Ell (in 2012), and J. Ishulutaq (in 2013). The authors also thank H. Steenkamp for extended fieldwork and T. Stainton for helping with the manuscript. Financial support was provided by the Strategic Investments in Northern Economic Development (SINED) program delivered by the Canadian Northern Economic Development Agency (CanNor).

References

Beauregard, M.A., Ell, J., Pikor, R.K. and Ham, L.J. 2013: Nunavut carving stone deposit evaluation program (2010–2013): third year results; *in* Summary of Activities 2013, Canada-Nunavut Geoscience Office, p. 151–162.

Camacho, A., Pikor, R.K. and Beauregard, M.A. 2015: Data tables accompanying "Characterization of carving stone deposits in Aberdeen Bay, southern Baffin Island, Nunavut"; Canada-Nunavut Geoscience Office, Geoscience Data Series GDS2015-013, Microsoft® Excel® file, URL <http://cngo.ca/summary-of-activities/2015/> [December 2015].

Gustavison, S. 1999: Northern Rock: Contemporary Inuit Stone Sculpture; McMichael Canadian Art Collection, 192 p.

Humphris, S.E. and Thompson, G. 1978: Hydrothermal alteration of oceanic basalts by seawater; Geochimica et Cosmochimica Acta, v. 42, p. 107–125.

Sanborn-Barrie, M., St-Onge, M.R., Young, M.D. and James, D.T. 2008: Bedrock geology of Southwestern Baffin Island, Nunavut: expanding the tectonostratigraphic framework with relevance to mineral resources; Geological Survey of Canada, Current Research 2008-6, 16 p.

Scott, D.J., Stern, R.A., St-Onge, M.R. and McMullen, S.M. 2002: U-Pb geochronology of detrital zircons in metasedimentary rocks from southern Baffin Island: implications for the Paleoproterozoic tectonic evolution of Northeastern Laurentia; Canadian Journal of Earth Sciences, v. 39, p. 611–623.

Scott, D.J. and Gauthier, G. 1996: Comparison of TIMS (U–Pb) and laser ablation microprobe ICP–MS (Pb) techniques for age determination of detrital zircons from Paleoproterozoic metasedimentary rocks from northeastern Laurentia, Canada, with tectonic implications; Chemical Geology, v. 131, p. 127–142.

Scott, D.J. 1997: Geology, U-Pb, and Pb-Pb geochronology of the Lake Harbour area, southern Baffin Island: implications for the Paleoproterozoic tectonic evolution of northeastern Laurentia; Canadian Journal of Earth Sciences, v. 34, p. 140–155.

St-Onge, M.R., Wodicka, N. and Ijewliw, O. 2007: Polymetamorphic evolution of the Trans-Hudson Orogen, Baffin Island, Canada: integration of petrological, structural and geochronological data; Journal of Petrology, v. 48, p. 271–302.

Steenkamp, H.M., Pizzo-Lyall, M., Wallace, C.J., Beauregard, M.A. and Dyck, B.J. 2014: Geology, history and site-management planning of the Kangiqsukutaaq carving stone quarry, southern Baffin Island, Nunavut; *in* Summary of Activities 2013, Canada-Nunavut Geoscience Office, p. 193–200.

Theriault, R.J., St-Onge, M.R. and Scott, D.J. 2001: Nd isotopic and geochemical signatures of the Paleoproterozoic Trans-Hudson Orogen, southern Baffin Island, Canada: implications for evolution of eastern Laurentia; Precambrian Research, v. 108, p. 113–138.

Zang, W. and Fyfe, W.S. 1995: Chloritization of the hydrothermally altered bedrock at the Igarapé Bahia gold deposit, Carajás, Brazil; Mineralium Deposita, v. 30, p. 30–38.

NUMIN: online access to information about mineral showings and exploration-project documents at NunavutGeoscience.ca

A. Markey[1], P. Budkewitsch[2], S.L. Basso[3] and S. Sharpe[2]

[1]*Indigenous and Northern Affairs Canada, Iqaluit, Nunavut, andrea.markey@aandc-aadnc.gc.ca*

[2]*Indigenous and Northern Affairs Canada, Iqaluit, Nunavut*

[3]*Canada-Nunavut Geoscience Office, Iqaluit, Nunavut*

Markey, A., Budkewitsch, P., Basso, S.L. and Sharpe, S. 2015: NUMIN: online access to information about mineral showings and exploration-project documents at NunavutGeoscience.ca; *in* Summary of Activities 2015, Canada-Nunavut Geoscience Office, p. 201–208.

Abstract

NunavutGeoscience.ca is an open-access data portal to public geoscience information available for Nunavut, enabled with search and direct-download capabilities, or indirect downloads through links to partner organizations. This website, initiated in 2006, is a partnership between the Canada-Nunavut Geoscience Office, Indigenous and Northern Affairs Canada, the Government of Nunavut, Natural Resources Canada and Nunavut Tunngavik Incorporated. This paper is a brief synopsis of the collaboration in the development of the NUMIN (NUnavut MINeral showings) database, housed within the NunavutGeoscience.ca website. The NUMIN database originated as part of a relational database for mineral showings and reference metadata, called NORMIN.DB, that was housed within Indigenous and Northern Affairs Canada[4] in Yellowknife.

The NUMIN database contains the metadata for mineral showings and information sources, a NUMIN file system for digital documents, and a set of three web applications (NUMIN Showings, NUMIN References, and Gateway, which are collectively known as NUMIN). These applications allow users to access the contents of the database and to download distributable reports and publications. In 2014–2015, a collaborative effort was initiated by staff from Indigenous and Northern Affairs Canada and the Canada-Nunavut Geoscience Office to update the showings information in NUMIN, with financial support provided from Strategic Investments in Northern Economic Development programming through the Canadian Northern Economic Development Agency.

Résumé

NunavutGeoscience.ca est un portail de données en libre accès, qui permet au public d'accéder aux renseignements de nature géoscientifique portant sur le Nunavut; il possède des capacités de recherche et de téléchargement soit direct, soit indirect en ayant recours à des liens maintenus par des organisations partenaires. Ce site Web, lancé en 2006, découle d'un partenariat impliquant le Bureau géoscientifique Canada-Nunavut, Affaires autochtones et du Nord Canada, le Gouvernement du Nunavut, Ressources naturelles Canada et la Nunavut Tunngavik Incorporated. Le présent article donne un bref aperçu de la collaboration qui a mené à l'élaboration de la base de données NUMIN (NUnavut MINeral showings ou venues minérales du Nunavut), à laquelle on peut accéder à partir du site Web NunavutGeoscience.ca. Initialement, NUMIN faisait partie d'une base de données relationnelle des venues minérales et de métadonnées pour les documents de référence qui portait le nom de NORMIN.DB et qui était gérée par Affaires autochtones et du Nord Canada[5] à Yellowknife.

La base de données NUMIN renferme des métadonnées relatives aux venues minérales et aux sources d'information, un système de fichiers NUMIN servant à gérer les documents numériques et un ensemble de trois applications Web (NUMIN Showings, NUMIN References et Gateway, connues collectivement sous le nom de NUMIN). Ces applications permettent

[4]*As background for the reader, this paper covers a time period in which the same department has been known by three different official names. The current official departmental name of Indigenous and Northern Affairs Canada [INAC] is used throughout this paper, and should be understood to also mean the previous Indian and Northern Affairs Canada, as well as the more recent Aboriginal Affairs and Northern Development Canada.*

[5]*À titre d'information pour le lecteur, cet article couvre une période de temps au cours de laquelle le même ministère a porté trois noms officiels différents. Le nom actuel d'Affaires autochtones et du Nord Canada est utilisé ici, mais il est entendu qu'il peut tout aussi bien pouvoir s'agir de l'ancien ministère des Affaires autochtones et du Nord Canada ou de la plus récente appellation d'Affaires indiennes et développement du Nord Canada.*

This publication is also available, free of charge, as colour digital files in Adobe Acrobat® PDF format from the Canada-Nunavut Geoscience Office website: http://cngo.ca/summary-of-activities/2015/.

aux usagers l'accès au contenu de la base de données ainsi que la possibilité de télécharger les rapports et publications diffusables. En 2014–2015, un effort collectif de la part du personnel d'Affaires autochtones et du Nord Canada et de celui du Bureau géoscientifique Canada-Nunavut a permis de mettre à jour les renseignements afférant aux venues minérales contenus dans NUMIN, ceci grâce au soutien financier fourni par le biais du programme Investissements stratégiques dans le développement économique du Nord géré par l'Agence canadienne de développement économique du Nord.

Introduction

Most of the territory of Nunavut is extremely remote and there are several challenges in carrying out mineral exploration programs. Nunavut lacks a developed transportation infrastructure, so mobilization of personnel and equipment are costly and require extensive logistical planning in support of exploration programs. Added to this, seasonal access beyond the summer becomes increasingly complex due to the reduced hours of daylight and harsh climate during the cold winter months.

To strategically plan any type of exploration in this area, it is essential that exploration personnel gather and analyze all relevant geoscience information available for the area of interest before initiating fieldwork. Such planning includes reviewing all government mapping and research, and data from all previously reported exploration activities, including mapping, trenching, sampling, assaying, drilling and geochemical and geophysical surveys. This latter information is publicly available in assessment reports filed with the federal government. Of particular importance are the location and characterization of mineralized targets or anomalies of any type (i.e., mineral showings) in order to investigate these occurrences and other high priority targets while doing fieldwork.

In the past, conducting this type of planning and research would have involved exploration personnel visiting the government offices where the archives of paper assessment reports documenting work done on Crown lands are stored. Data gathering would have involved copying or retrieving the information of interest to create their own custom maps from the contents of these documents.

Paper copies of reports and maps, however, can now be easily scanned to create digital documents. Currently, digital assessment reports are often submitted by exploration companies to the government. (The Nunavut Mining Regulations now allow for the submission of assessment reports in digital format, thereby reducing any potential quality issues or errors that may be introduced from scanning.) Following the submission of reports, catalogues of metadata about information sources (references) are created in a database so that users can query the catalogue online, using metadata parameters, to find the references needed. Related key information that geoscientists use to identify showings is housed in the same database as the reference metadata, and the two catalogues are linked. In this manner, the Internet is now the main distribution medium for digital data and documents.

This paper is a brief synopsis of the collaboration in the development of the NUMIN (NUnavut MINeral showings) database. This database contains the metadata for mineral showings and information sources, a NUMIN file system for digital documents, and a set of web applications (collectively known as NUMIN) that allows users to access information through the NunavutGeoscience.ca website.

The collaborating organizations for NUMIN and NunavutGeoscience.ca were the Nunavut Regional Office of Indigenous and Northern Affairs Canada (INAC; formerly Indian Affairs and Northern Development Canada [INAC] and also formerly Aboriginal Affairs and Northern Development Canada [AANDC]), the Canada-Nunavut Geoscience Office (CNGO), the Government of Nunavut (GN), Nunavut Tunngavik Incorporated (NTI), Natural Resources Canada (NRCan), the Northwest Territories Geoscience Office (NTGO, now the Northwest Territories Geological Survey) and Indigenous and Northern Affairs Canada–Yellowknife, the latter two located in Yellowknife, Northwest Territories.

The NUMIN database is now being enhanced with a new partnership project funded by the Strategic Investments in Northern Economic Development (SINED) program of the Canadian Northern Economic Development Agency (CanNor), the purpose of which is to update the showings aspects in NUMIN.

Archives of mineral-exploration assessment reports

As fulfilment of regulatory requirements, assessment reports on exploration and technical work are filed by exploration companies with the federal government (INAC). The purpose of filing is to establish exploration expenditures (or credits) that allow exploration companies to maintain tenure rights to tracts (claims, permits or leases) of Crown land. These reports are generally confidential for a period of three years, dependent on tenure type, after being reviewed and approved by District Geologists. Once the confidentiality period is over, the reports are publicly available and are catalogued in a digital database. Many other publications and maps are also housed and catalogued in these archives.

The original impetus for creating the NUMIN database was that the archives of company exploration reports were unpublished and only available in the regional offices through the District Geologists and Mining Recorders. Paper copies of mineral-exploration assessment reports for all of the Northwest Territories (that included Nunavut until 1999) were housed in the Northwest Territories Geoscience Office (NTGO) in Yellowknife.

In the 1990s, INAC in Yellowknife began scanning assessment reports and other documents to make these available digitally. The digital files were organized in a file store to which an Internet application called 'Gateway' provided access for query and download.

History of the NUMIN database

The NUMIN database catalogues metadata about known mineral showings (termed 'Showings' in the database) and information sources (termed 'References'). It originated as part of a relational database for mineral showings and reference metadata called NORMIN.DB, which was housed within INAC in Yellowknife. The NORMIN.DB database was initially populated with shallow showings data and references derived from CANMINDEX (described by Picklyk et al., 1978) and maintained in the Mineral Resources Division Data Centre at the Geological Survey of Canada (GSC) in Ottawa until approximately 1992. This database incorporated information on all showings and exploration activities in the then–Northwest Territories before the creation of Nunavut in 1999; it was maintained intact by staff and contractors in the INAC Yellowknife office until 2005.

The NORMIN.DB database and its associated archive of digital reports have been accessible for querying over the Internet for more than 10 years. The database has four interconnected components that house metadata for Showings, References, Resources/Reserves and Production (Figure 1). In addition to these components, the database contains stored procedures for generating summary tables and web reports that are used by query applications. The Web applications started with both map and query windows for Showings, a query window for References and a Gateway Browser that a user could employ to query and download the data and publications.

Development of NUMIN

With the creation of Nunavut in 1999, INAC staff selected all paper reports and publications pertaining specifically to Nunavut and shipped them to Iqaluit. Reports pertaining to Nunavut in the digital file system were also separated from those dealing with work in Northwest Territories. This was an enormous task that involved thousands of paper documents. Once completed, a project to scan the remaining Nunavut reports, as well as those submitted to Nunavut Tunngavik Incorporated (NTI) for work done on Inuit-Owned Lands, and to input this information into the file system was undertaken in Iqaluit.

Updates to mineral showings in the recent past involved primarily locations in the Northwest Territories, except for significant deposits in Nunavut. As a result, many Nunavut showings in the database remained unchanged from the original CANMINDEX.

In 2005, NTGO separated the Northwest Territories portion of NORMIN.DB into its own database that is still called NORMIN but without the suffix (.DB). The information pertaining to Nunavut became the responsibility of INAC in Nunavut. A committee comprising representatives from INAC in Iqaluit, GN, CNGO and NRCan named the Nunavut database NUMIN. As the Nunavut Regional Office (NRO) of INAC embarked on a project to scan and organize assessment reports, emphasis was placed on keeping the References metadata in NUMIN up-to-date as new assessment reports became public. This updating was the job of the mineral archivist. Additional emphasis was placed on filling in missing information (e.g., National Topographic System [NTS] map area, company name, ac-

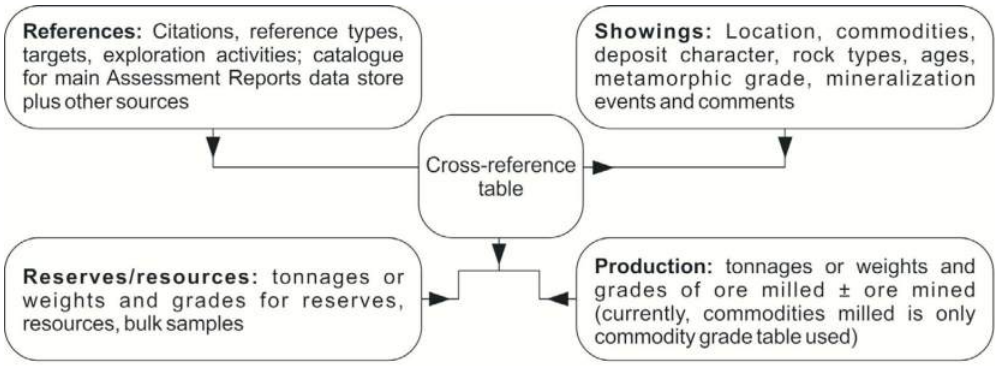

Figure 1. Overview schematic illustrating the organization of the NUMIN database.

tivity and work) in NUMIN References so these attributes could be used to search and filter the database.

Concurrent with the scanning project, geologists at the GSC in Ottawa were compiling showings in the GSC World Minerals Geoscience Database Project system for project use and map preparation (Chorlton et al., 2000; Laramée, 2015). In December 2006, with the help of a contractor and database managers at both INAC and NRCan, the GSC was able to perform a bulk update to the NUMIN Showings database, adding 867 new showings and updating 308 showings. The challenges for this operation and, in fact, for the compilations that preceded this update were to ensure that the indexed references in the GSC source databases were synchronized with NUMIN References being maintained by INAC. Additional challenges involved ensuring that further synchronization to map fields and controlled vocabulary worked cleanly from the GSC systems to the NUMIN system, and to ensure that no existing showings data were eliminated and no showings were duplicated. Many trial runs were evaluated before the final update. To reduce potential data complications, the GSC recommended that, in the future, Showings and References be entered directly into the NUMIN system from Iqaluit.

Evolution of NunavutGeoscience.ca

A website called NunavutGeoscience.ca provided the first online access to NUMIN in 2006. This initial access consisted of applications for querying NUMIN Reference metadata and a Gateway publication-download service similar in function to services offered by the NTGO. This website was also formed as part of the NUMIN evolution and involved the same collaborators. As a result of this work, the mineral archivist in Nunavut no longer had to query the database and package the resulting digital data on media (such as hard drives and DVDs) to be sent by mail in response to data requests from the public.

In February 2007, after intense collaboration by the project manager at CNGO, staff in the Data Management and Dissemination Branch of NRCan and the same contractor, the new NUMIN Showings query and map display application was available online to join the NUMIN References and Gateway.

The NUMIN database was joined on NunavutGeoscience.ca by Exploration Overview—another query and map display application that allows users to query the database by project and company, and to download both the current and previous versions of the yearly Nunavut Exploration Overview, the partnered publication of exploration and mining activities in Nunavut. MIRAGE, an NRCan map-image query portal customized for Nunavut, was also added to the NunavutGeoscience.ca website.

NunavutGeoscience.ca and its applications—NUMIN, Exploration Overview and Mirage—were hosted on an NRCan server until mid-2013, when the server was disconnected by Shared Services Canada due to security issues.

Following the interruption in service, work by CNGO to have NUMIN and/or NunavutGeoscience.ca restored ultimately resulted in the site being supported by a third-party service provider. NunavutGeoscience.ca was reinstated in late 2014, with the NUMIN applications of NUMIN Showings, NUMIN References and Gateway. At the present time, however, the NunavutGeoscience.ca website is not directly connected to the NUMIN database, and neither are the Exploration Overview and Mirage applications functions. An image of the current database is taken and updated at various times to the server. The CNGO and INAC are working together to have these functions restored, as it is recognized by all that the fully functioning NunavutGeoscience.ca portal is an important information service. Although the NUMIN Showings have been updated by staff at INAC since 2006, updates were infrequent. Efforts are underway to provide new information to this part of NunavutGeoscience.ca, as discussed below.

NUMIN online and updates

Three web applications, NUMIN Showings, NUMIN References and Gateway, which are collectively known as NUMIN, allow users to access the contents of the NUMIN database and to download distributable reports and publications. Stored procedures within NUMIN generate summary spreadsheets that these applications use for simple list-style displays, and prepare complete reports for each showing and linked data, such as the individual references. Each application allows the user to filter components of the database by search criteria and to view or download results extracted from the database, or download selected contents from the file archive in the case of Gateway. Gateway can be accessed from both the Showings and Reference query applications.

NUMIN Showings

In 2014–2015, a collaborative effort was initiated by staff from INAC and CNGO to update NUMIN Showings, with financial support provided from the SINED program of CanNor. The project involves examining—'data mining'—assessment reports for undocumented showings and extracting additional information on existing showings where possible. The recent assessment reports come from the three regions of Nunavut—Kitikmeot (west), Kivalliq (central) and Qikiqtaaluk (east)—and were prioritized for this data-mining exercise. Historical mineral occurrences were extracted from the reports, as well as from other reference sources that include reports and papers (predominantly from the GSC), journals, theses, National Instrument (NI) 43-101 industry reports and press releases. To

date, this work has resulted in the addition of 87 showings and updates to 42 showings. This project is ongoing and will continue as the confidentiality period of assessment reports ends and they become public information.

The NUMIN Showings search-and-retrieve function allows a user to view and download a spreadsheet of available mineral occurrences for all of Nunavut or a specific geographic area, or to query the NUMIN Showings database using one to five criteria. This application includes a map window on the left of the screen, with a Layers menu to the right that allows the user to add or hide a number of map layers relevant to geoscience by clicking on icons and using the 'Refresh Map' button. A useful layer in this menu is a simplified point file showing the approximate locations of Exploration Projects, symbolized by a generalized commodity type. The Map Tools menu, to the left of the map window, allows a user to navigate and zoom in and out. The 'Identify' tool allows a user to click on multiple points to view a simple spreadsheet list in a separate tab page labelled 'Identified Showing' in the space below the Layers menu. Below the map window and Layers menu are two tab pages, the left one labelled 'Query' and the right one labelled 'Matching Showing', with the number of showings currently selected in brackets. Users can employ the Query tab to refine their map-based search based on commodity, development stage, hostrock, deposit type, showing name or any combination of these fields (Figure 2). Clicking 'Submit Query' will cause the application to apply the filter(s), and the new number of matching showings will be listed in the label of the second tab page. Highlighting the second tab page will bring the spreadsheet listing of matching showings to the foreground.

The user can check or uncheck individual showings in this listing and can choose to download the checked showings by clicking on the label at the bottom of the tab page. Clicking on the Showing Id in this list (highlighted in blue) will bring up a third tab page showing the complete showing report, including comment fields, resources and production (if any have been entered in the database) and, most importantly, the References that are linked to the showing. The references that are linked to the selected showings can be added to a client's Gateway cart, or downloaded directly from Gateway by clicking on the buttons in the lower right corner of the Matching Showing tab page (see 'NUMIN Gateway' section below).

NUMIN References

NUMIN References (Figure 3) allows a user to filter the References component of the database and to view or download metadata about each reference. What a user is searching for will determine which of the 18 optional search fields are used in the reference query tool. If the user is interested in a broad search of a given area, the recommended search field to use is the NTS map-area field—and options would

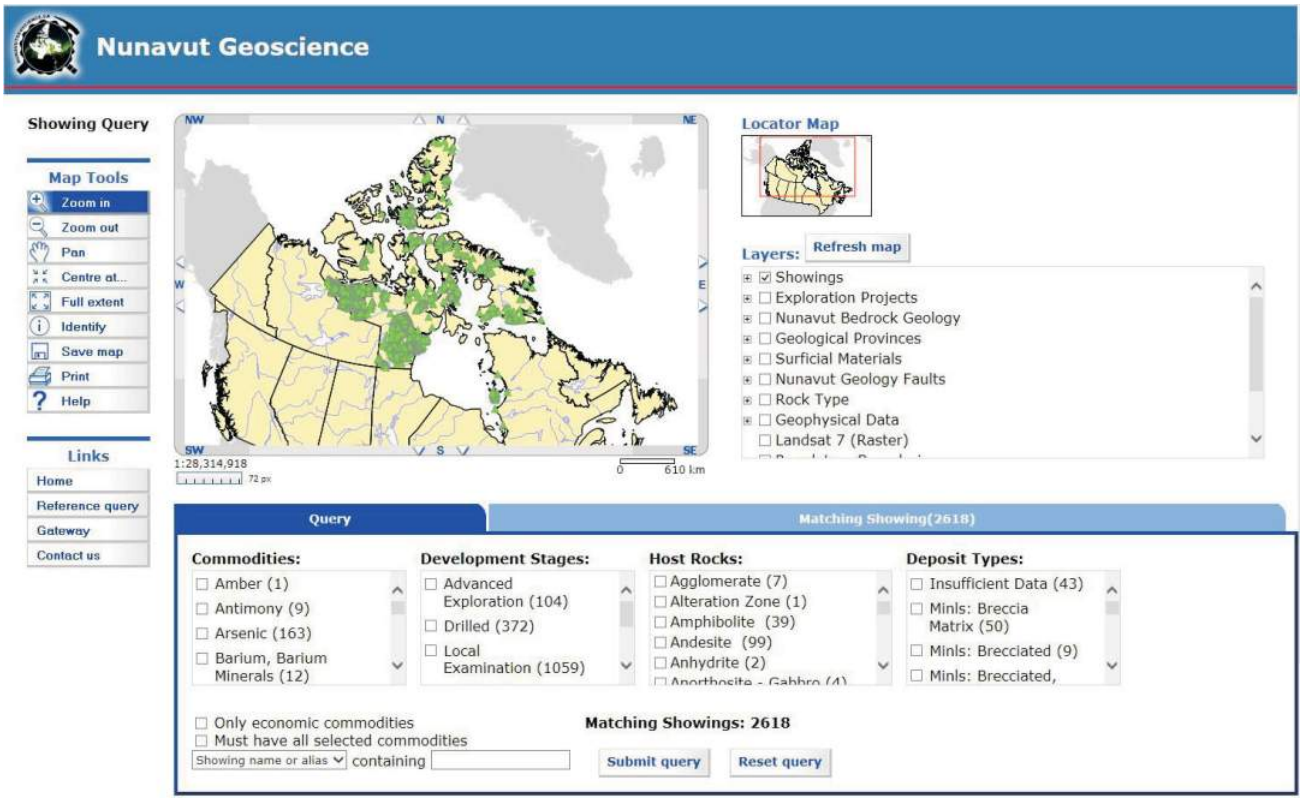

Figure 2: Users can select one or more fields from the Query tab to refine their map-based search of available showings.

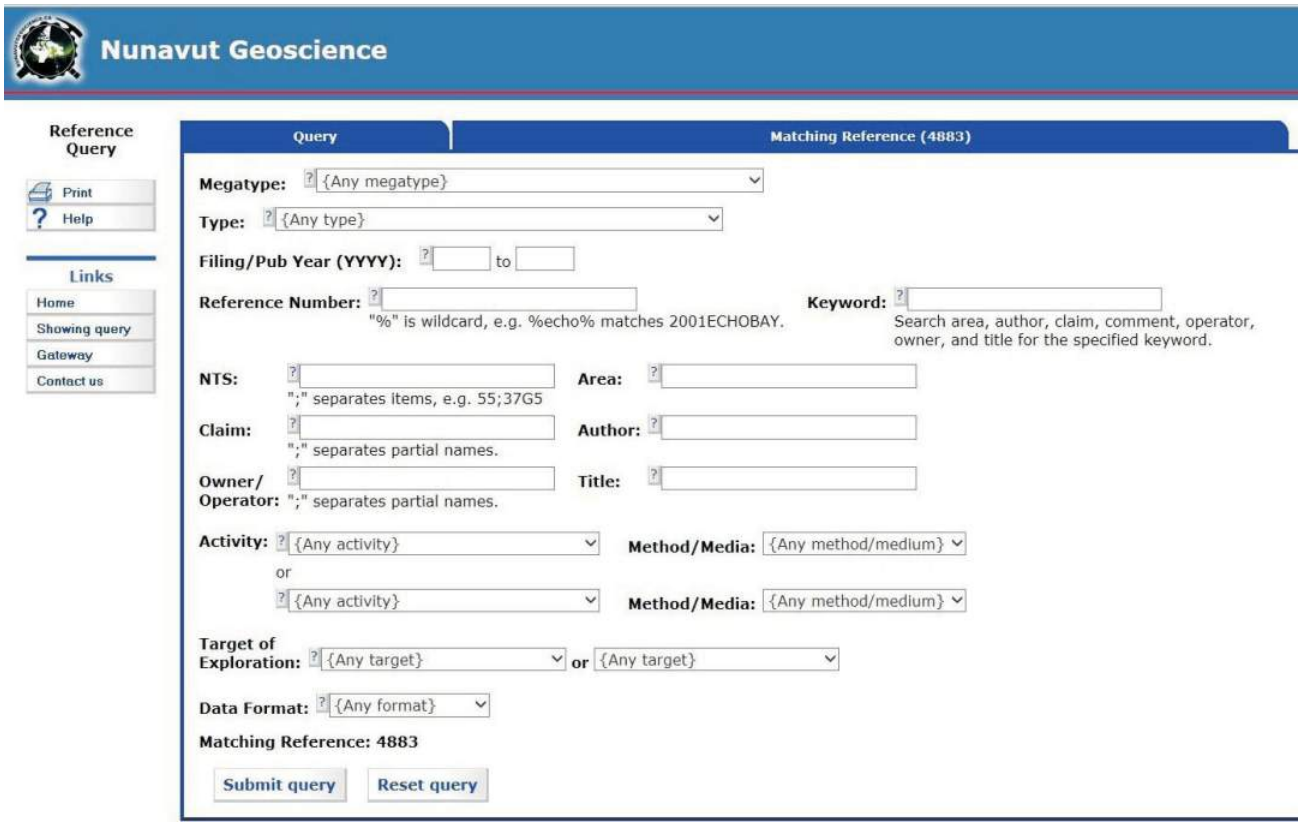

Figure 3: NUMIN Reference allows the user to select up to 18 search fields in the query tool.

be to use the entire map area, the 1:250 000 map area or a 1:50 000 map area (i.e., 37, 37G or 37G/05, respectively). Clicking on the '?' (help) button beside any of the fields will give more information. Help for the NTS field, for example, will provide the user with a map outlining the NTS reference areas for Nunavut (Figure 4). Once criteria have been set, clicking 'Submit query' at the bottom of the page will cause the application to apply the filter to the NUMIN References, and the number of Matching References will appear in brackets to the right of the label on the second tab page. Highlighting that page will bring a summary listing of references to the foreground. As with the Showings, a user can 1) click on the highlighted string in the Number column to view the metadata report; 2) use the buttons at the bottom left to check or uncheck individual records; 3) download a .CSV file of a summary spreadsheet of the checked records; or 4) go to Gateway, using the buttons in the bottom right corner of the tab page, to download files.

NUMIN Gateway

NUMIN Gateway (Figure 5) is the application that allows users to obtain digital reports and other publications organized in the file store. This application is the distribution medium and became critical once the majority of the assessment reports were made digital. Similar to NUMIN References, Gateway depends on the data in the NUMIN References part of the database; therefore, the completeness of References is critical for user access to Gateway contents. The references accessible through Gateway are classified into five broad types (megatypes), and the user can filter further by selecting from subtypes in the dropdown lists beneath each megatype. Clicking on a subtype will bring up a new window with the selected series. A user can simply click on 'Report Search' at the top or 'Search report' at the bottom of the page to start over. If a user wishes to directly download a single reference, clicking on 'Download' below the reference will trigger this direct download. Adding items to a cart, or choosing more than one item, will trigger a login with the user's email address as a username. First-time users with no passwords should register and they will be sent a temporary password by email.

Economic considerations

Innumerable desktop studies have taken place based on information available through NunavutGeoscience.ca. By reviewing up-to-date mineral tenure for the territory (available on the Government of Canada's Open Data Portal) in tandem with information from NUMIN, exploration companies have re-staked known showings that they feel warrant further investigation—some with very promising results.

Conclusions

Nunavut governments and organizations (INAC, CNGO, GN and NTI) have made significant progress in providing convenient Internet access to metadata about mineral-exploration targets, exploration-related and other geoscience references, and source documents that the respective organizations have the right to distribute. INAC is the sole source of the mineral-assessment reports that contain exploration and mapping work; these reports are key documents for anyone undertaking an exploration project in any area of Nunavut. Therefore, the NUMIN and Gateway applications are tremendous public services and hold a wealth of information. In the past, capacity to keep the Showings

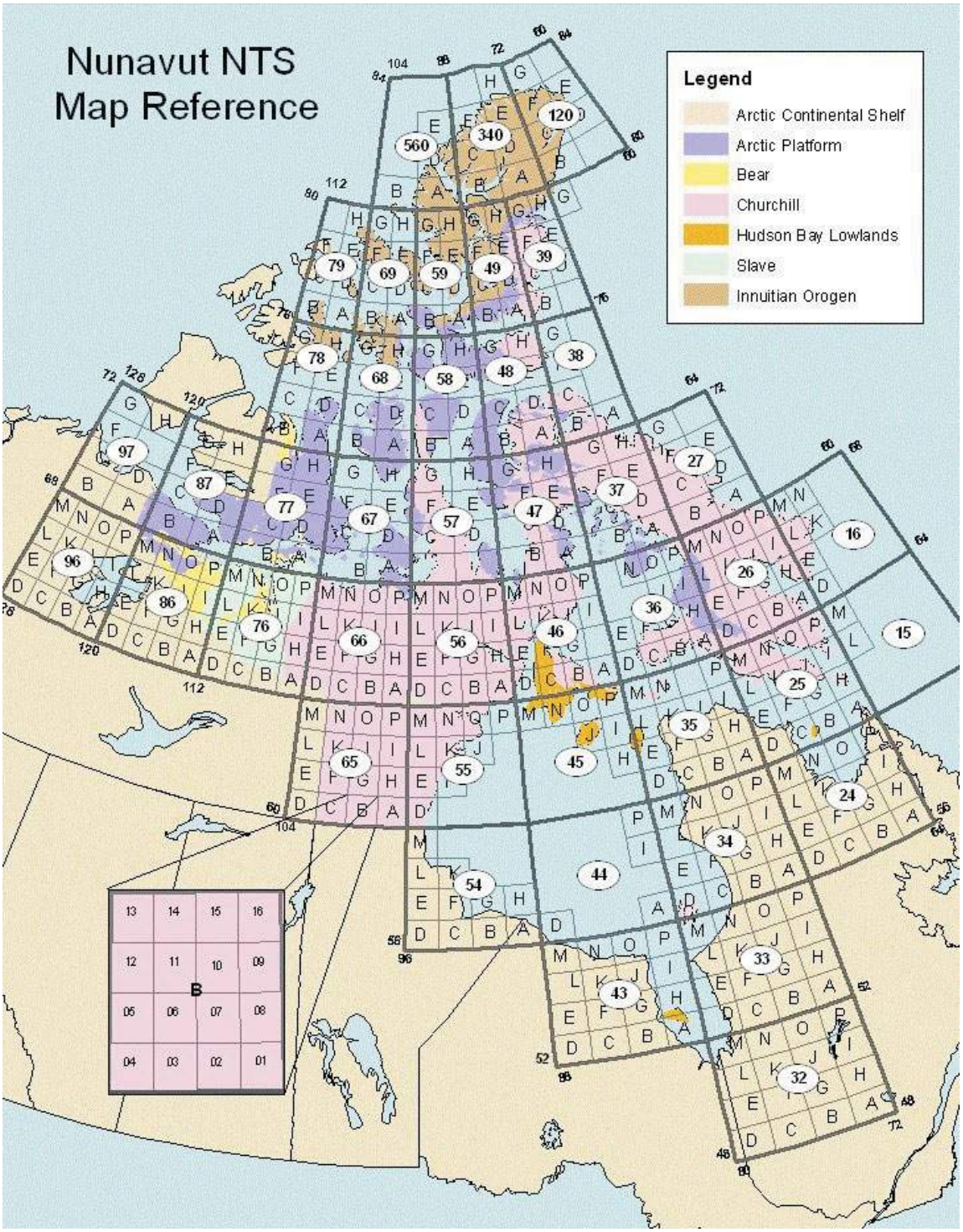

Figure 4: The Help tab on NUMIN Reference provides the user with a map of Nunavut NTS map-area boundaries.

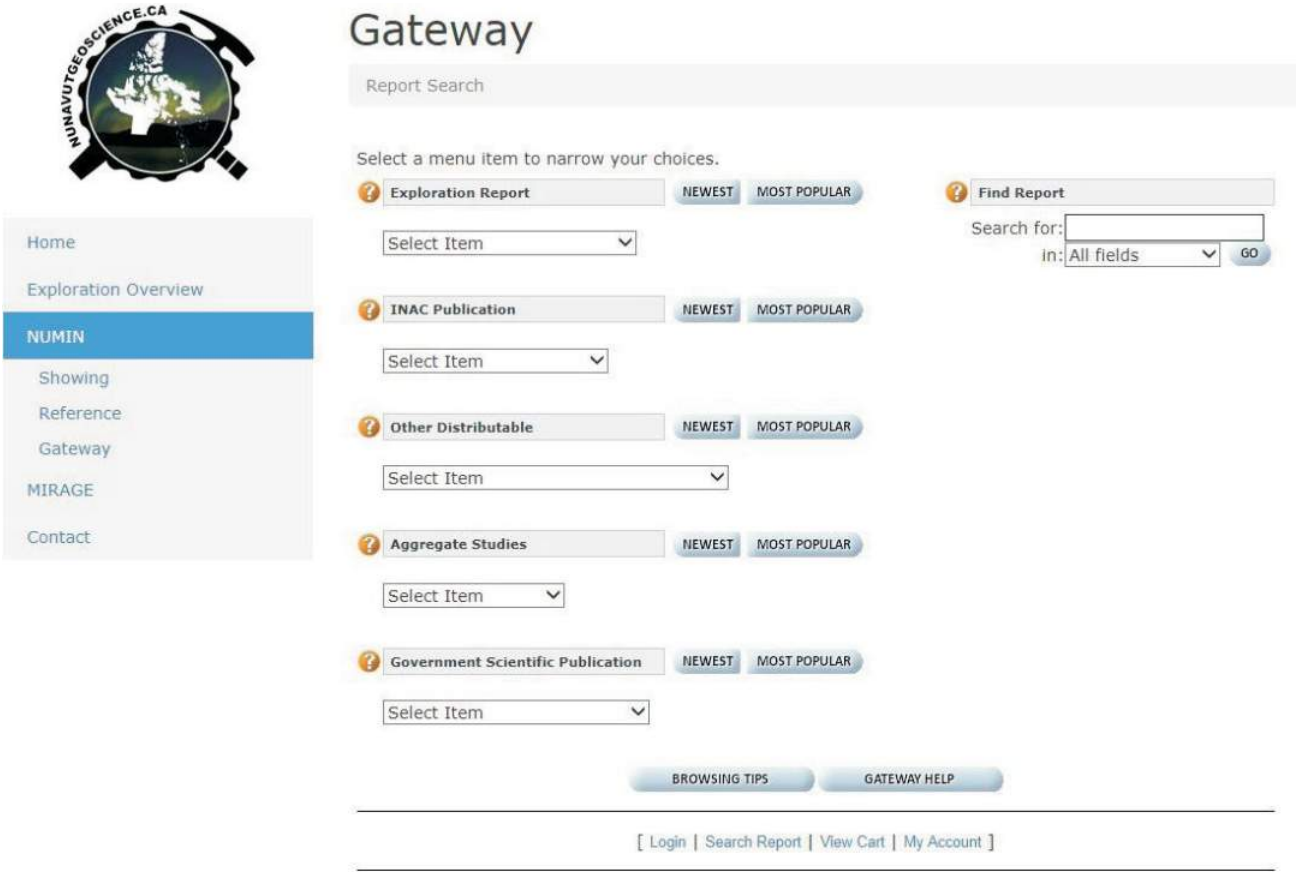

Figure 5: The Gateway application has references classified into five broad types (megatypes).

information up-to-date was limited, so users looking for reports and mineral showings reported in the news were unable to retrieve the necessary information. With this collaborative project of INAC and CNGO, funded by SINED, the ongoing updating of the Showings will eventually close that information gap.

Acknowledgments

Much work has been put into NunavutGeoscience.ca and NUMIN over the years by many people who care deeply about public geoscience information, including K. Brazel, K. Cameron, L. Chorlton, B. Fischer, C. Gilbert, T. Houlahan, D. James, N. Kavanagh, C. Lafferty, B. Lau, B. MacIsaac, D.J. Mate, E. Prosh, J. Rupert, L.L. Tobicoe and A. Udell.

The Strategic Investments in Northern Economic Development (SINED) program of the Canadian Northern Economic Development Agency (CanNor) provided financial support for the recent work on updating the Showings information.

Many thanks go to L. Chorlton and L. Ham for their thorough reviews of and contributions to this paper, and to C. Gilbert for assistance with figures.

References

Chorlton, L., Laramée, R., Sinclair, D. and Hillary, E. 2000: Digital inventory of global bedrock and mineral deposit geology; *in* Deposit Modeling, Mineral Resource Assessment, and their Role in Sustainable Development: a Workshop, K.J. Schulz and J.A. Briskey (ed.), 31st International Geological Congress, Rio de Janeiro, Brazil, 20 p.

Laramée, R.M. 2015: Source code for GlobalDBSystem, data management interfaces for mineral deposit databases, World Minerals Geoscience Database Project; Geological Survey of Canada, Open File 7872, 3 p. doi:10.4095/296953

Picklyk, D.D., Rose, D.G. and R.M. Laramée, R.M. 1978: Canadian Mineral Occurrence Index (CANMINDEX) of the Geological Survey of Canada; Geological Survey of Canada, Paper 78-8, 27 p.

The **Canada-Nunavut Geoscience Office** conducts new geoscience mapping and research, supports geoscience-capacity building, disseminates geoscience information and develops collaborative geoscience partnerships for Nunavut.

www.cngo.ca